Targeting receptor tyrosine kinases in leukemia: from identification of new targets to overcoming mechanisms of resistance

By:

Sunil K. Joshi

A DISSERTATION

Presented to the Department of Physiology & Pharmacology and
the Oregon Health & Science University School of Medicine

in partial fulfillment of
the requirements for the degree of

Doctor of Philosophy

March 2021

School of Medicine

Oregon Health & Science University

CERTIFICATE OF APPROVAL

This is to certify that the PhD dissertation of

Sunil K. Joshi

has been approved

_____
Brian J. Druker, M.D.

_____
Cristina E. Tognon, Ph.D.

_____
Elie Traer, M.D., Ph.D.

_____
Evan Lind, Ph.D.

_____
David Qian, Ph.D.

_____
Robert Duvoisin, Ph.D.

Table of Contents

Acknowledgements

"Don't ask what the world needs. Ask what makes you come alive and go do it. Because what the world needs is more people who have come alive."

— Howard Thurman

I owe my initial interest in science and medicine to my grandfather. He lay in agony with so many tubes protruding from his body that it hurt me to look at him. His lungs were filled with so much fluid that his words were almost unintelligible. He looked helpless, and helpless is exactly how I felt. I remember this very scene as I witnessed him succumb to cancer.

While caring, translating, and advocating for my grandfather for 12 years sparked my interest in science and medicine, it was my time at UC Berkeley and UC San Francisco that transformed my curiosity into a resolute passion. I am extremely thankful to Caroline Kane who has continuously mentored me since I met her in 2007 at UC Berkeley. Her unwavering commitment to my learning and growth as a scientist and, importantly as an individual has been invaluable. I am thankful to Kenneth Downing who introduced me to science. I joined his lab on a work-study job at UC Berkeley to wash glassware and overtime he gave me the opportunity to explore the world of the invisible through microscopy. I am thankful to my undergraduate honors thesis advisor Jean Fréchet for challenging me to think outside the box as I synthesized multiple drug delivery polymers under his mentorship. I am better because of his feedback. I also thank my many mentors and colleagues at the San Francisco VA Medical Center and UCSF who collectively offered me a rich scientific environment that allowed me to develop skills in undertaking independent research. I especially thank Joseph Wong for serving as an inspiring example of a physician-scientist and augmenting my critical thinking skills. I will always cherish his quiet brilliance, positivity, and genuine concern for all his employees and trainees.

I have been fortunate to be surrounded by supportive mentors and friends throughout my training at OHSU. Firstly, I would like to thank my PhD mentor Brian Druker for providing me the opportunity to work under his tutelage. I thank Brian for always seeing the very best in me, providing me genuine advice, feedback, endless opportunities, and most importantly full autonomy over my projects. I also thank him for always being by my side during my times of need. I am equally thankful to my co-mentor Cristina Tognon for her natural leadership style, organization, scientific aptitude, and for always "walking the walk." Whether it's a lab cleanup or someone needing help with an experiment, Cristina was always there for us. I also thank Cristina for helping me gain confidence in myself and for making me recognize my deep-seated passion for developing my own research program. Lastly but not least, I am thankful to my co-mentor Elie Traer for carrying out his promise of always serving as my cheerleader, which truly brought out the best in me. His enthusiasm for science is contagious, and our insightful discussions had a formative impact on fueling my curiosity and passion for science. Elie also taught me to always trust my eyes over a cell counter, which proved to be valuable at every step of the way. While he kept me focused, optimistic, and caffeinated, I very much appreciate his trust in me to pursue my ideas, take risks, and assume a leadership role in his lab.

I also thank Tamilla Nechiporuk and Stephen Kurtz for shaping my work and scientific thought-process, sharing their boundless molecular biology skills, having an unshakable trust in my

abilities, and their friendship. I will forever be grateful for their constant support throughout the COVID-19 pandemic. For helping to ensure a safe work environment during the pandemic in the Knight Cancer Research Building, I thank Elizabeth Gutierrez. I also thank Jeffrey Tyner, Shannon McWeeney, Karin Rodland, Daniel Bottomly, Andy Kaempf, Anupriya Agarwal, Chris Eide, Kevin Yee, Kara Johnson, Sarah Bowden, Raphaela Haessler, Bill Chang, Monika Davare, William Bisson, Julie Haines, and Angelo D'Alessandro for all their support with my science and continuous encouragement. Special thank you to all the folks I had the opportunity to mentor – Ariane Haung, Jack Sumner, Janét Pittsenbarger, Setareh Sharzehi, Jordana Brown, Matthew Newman, and Evan Barnes. I thank them for their contribution to my work and for reminding me that knowing how to lead requires knowing how to follow.

Thank you to my dissertation advisory committee members and Physiology & Pharmacology graduate program, Evan Lind, David Qian, and Robert Duvoisin for their consistent scientific advice and counseling. I owe a debt of gratitude to David Jacoby for his unparalleled mentorship, commitment to my success, and the countless leadership opportunities he has provided me. Science is a team sport – I am very thankful to my friends—Robert Raffai, Kimberly Spaulding, James Frank, Sudarshan Iyer, Chris Evans, Archana Sehrawat, Adam Duvall, Luke Fletcher, Kevin Nusser, Letisha Wyatt, Alexis Young, Yifan Xu, Sarah Carratt, Ted Braun, Kyle Romine, Hsin-Yun Lin, Ali Oyaeli, Olivia Lucero, and Natasha Petrova—for all their insightfulness, momentum, and endless encouragement.

I also thank the National Cancer Institute, ARCS Foundation, and The Paul & Daisy Soros Foundation for providing me monetary support throughout my graduate school training. Your dedication to my success has served as a pillar of strength and motivation.

Lastly, but most importantly, I thank my parents, Neelam and Ramesh, for the years of unrecognized hard work that they poured into their three children so that we had every opportunity to chase our dreams even when they had to forgo their own aspirations. They instilled within me the importance of having strong work ethic, purpose, and character, the very principles that have carried me through my journey thus far.

Abstract

Preponderant genomic sequencing and clinical evidence have revealed the remarkable heterogeneity that underpins leukemia. Such efforts have brought to the forefront new oncogenic alterations and mechanisms of drug resistance. This dissertation is focused on the identification and characterization of intrinsic and extrinsic mechanisms of receptor tyrosine kinase (RTK) activation in the setting of leukemia. An understanding of these mechanisms can be harnessed clinically to facilitate the development of new therapies and, thereby expand the promise of precision medicine.

As for intrinsic activation of RTKs, the work presented in this dissertation demonstrates that point mutations in NTRK2/3, ERBB2, and FLT3, identified via deep sequencing of leukemia patient samples or cell lines, are oncogenic in cell-based assays. Each mutation has a distinct mechanism of activation, which is likely influenced by its location within the respective RTK. All identified mutations showed robust sensitivity to either FDA-approved inhibitors or investigational agents, which may help curtail disease progression.

Beyond intrinsic activation, the second half of the dissertation describes how extrinsic activation of RTKs via the bone marrow microenvironment facilitates the survival of residual leukemia cells, which leads to resistance and then relapse. Specifically, protective factors secreted by marrow stromal cells support the survival of residual cells. These residual cells are characterized by slower cell cycle, metabolic reprogramming, and become uniquely dependent upon Aurora kinase B signaling. This work implicates that disrupting the crosstalk between leukemia cells and the marrow microenvironment could circumvent drug resistance and improve patient outcomes.

PART I:
Introduction

1 Leukemia – an introduction to the unmet challenge

> *"Cancer is an expansionist disease; it invades through tissues, sets up colonies in hostile landscapes, seeking "sanctuary" in one organ and then immigrating to another. It lives desperately, inventively, fiercely, territorially, cannily, and defensively—at times, as if teaching us how to survive. To confront cancer is to encounter a parallel species, one perhaps more adapted to survival than even we are."*
>
> — Siddhartha Mukherjee, *The Emperor of All Maladies*

Hematopoiesis

Hematopoiesis is the lifelong process by which blood cells—red blood cells (RBCs), white blood cells (WBCs) and platelets—are continually replenished[1-3]. On average an adult human generates 4-5 $\times$ 10^{11} hematopoietic cells per day[4]. This process occurs within the bone marrow, a soft, spongy tissue in the center cavity of bones[1]. It should be noted that hematopoiesis mainly occurs in large bones and the axial skeleton for adults. A hierarchical organization exists within the marrow where hematopoietic stem cells (HSCs) sit at the top of the hierarchy[1] (**Figure 1**). These HSCs are nurtured and supported by the surrounding bone marrow microenvironment, often referred to as the stem cell niche. HSCs have the propensity to self-renew and produce various progenitor cells that eventually differentiate into mature blood cells that we define as RBCs, WBCs, and platelets. In contrast to HSCs, committed progenitors have a limited self-renewal ability and differentiation potential. Importantly, the hematopoietic process as a whole is tightly regulated to maintain a balance between HSC self-renewal and differentiation. While excessive differentiation may deplete the HSC pool, unrestricted self-renewal can lead to myeloproliferative diseases or leukemia[1, 2]. This chapter of the dissertation will provide a brief introduction to leukemia.

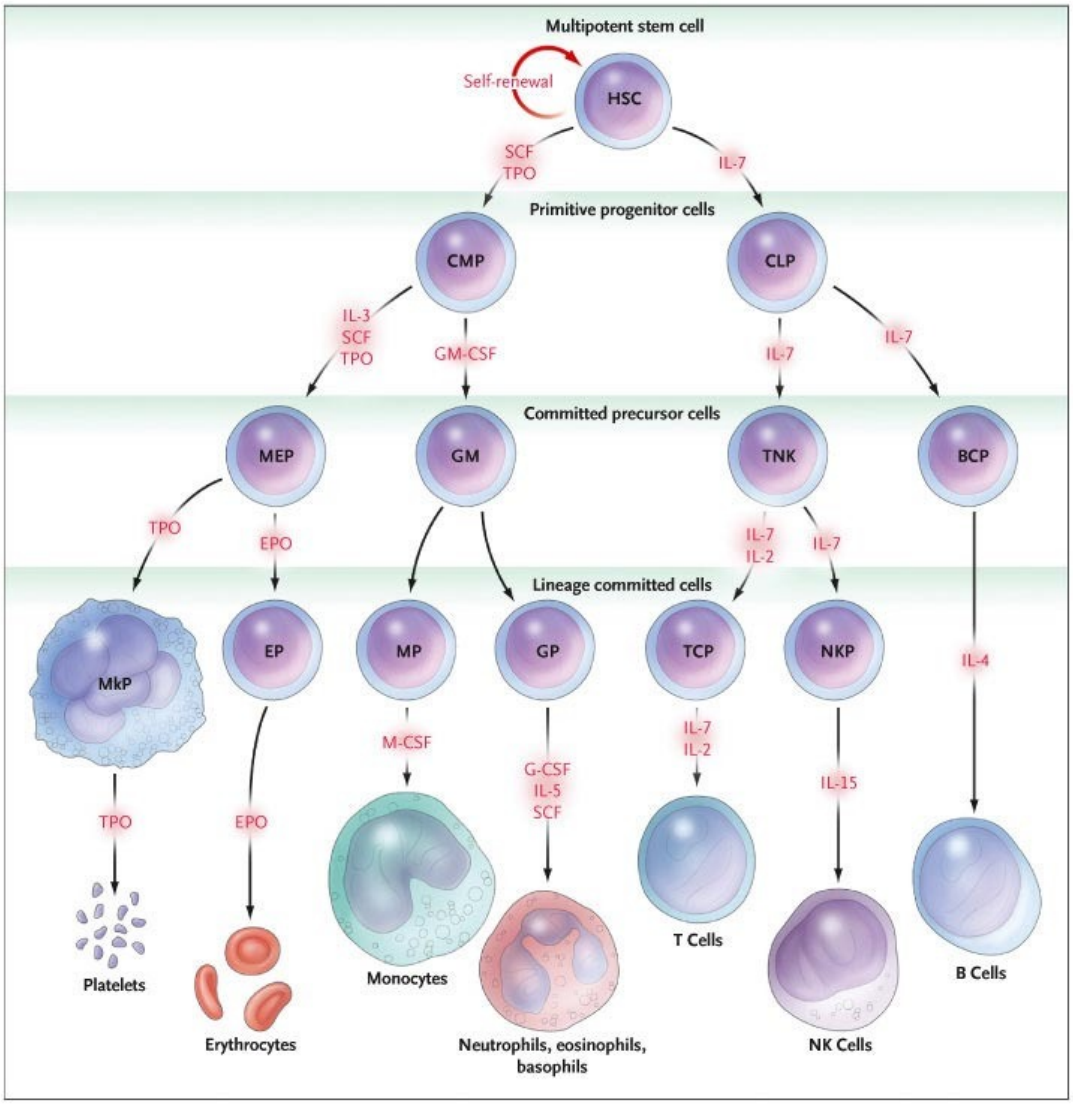

Figure 1: General schematic of hematopoiesis. Hematopoietic stem cells (HSCs) are at the top of the hierarchy. These cells can undergo either self-renewal or differentiation into a multilineage progenitor cells that are either committed to the myeloid or lymphoid lineage. Ultimately, myeloid progenitors give rise to red blood cells, platelets, monocytes, and granulocytes (neutrophils, eosinophils, and basophils). Lymphoid progenitors result in the formation of T, B, and natural killer (NK) cells.

Reproduced with permission from (Kaushansky K. Lineage-specific hematopoietic growth factors. N Engl J Med. 2006 May 11;354(19):2034-45. doi: 10.1056/NEJMra052706. PMID: 16687716.), Copyright Massachusetts Medical Society.

Definition, epidemiology, causes, signs & symptoms, risk factors, and diagnosis

Leukemia is a cancer that arises in the blood and bone marrow and is caused by the proliferation of abnormal white blood cells that are not fully matured, called blasts[5, 6]. The accumulation of blasts disrupts normal hematopoiesis, impairing the marrow's ability to produce red blood cells or platelets. Globally, leukemia is the 15th most commonly diagnosed cancer and the 11th leading cause of cancer deaths[5]. In the United States, leukemia remains as the 10th most common cancer and is the 7th leading cause of cancer-related deaths. In 2019, approximately 62,000 people were diagnosed with leukemia in the United States and approximately 23,000 people died from this malignancy[7]. Men are at a slightly elevated risk relative to women, accounting for an estimated 58% of cases annually[7]. Since 2006, the incidence of leukemia has increased in the United States by an average 0.6% per year.[5] As for age, incidence and mortality rates tend to increase with age[5]. Despite our enhanced understanding of the underlying biology of leukemia and development of targeted therapies, no single cure for leukemia is currently available.

Like any other cancer, there is no specific cause that defines leukemia. However, as in most cases, genetic alterations or some form of damage to DNA can trigger leukemia. Chapter 2 of this dissertation will broadly survey the role and activation of receptor tyrosine kinases (RTKs), which have been implicated as potential drivers of leukemia.

Signs and symptoms of leukemia are often vague, resembling the flu or common cold viruses. Symptoms include bleeding, fatigue, pale skin, fever, weight loss, night sweats, and increased risk of infections, all of which are consistent with a disruption in hematopoiesis[5]. In children, swollen lymph nodes, enlarged spleen (splenomegaly), or liver (hepatomegaly) can also be present[8]. Although the exact causes of leukemia are not fully understood, they remain as an active area of research. Common risk factors include a family history of leukemia, smoking cigarettes, down syndrome, and exposure to high levels of radiation or chemicals (e.g., benzene)[5].

Evaluation for leukemia typically entails a physical exam, blood tests, and bone marrow biopsy. Blood tests can include a complete blood count (CBC), complete metabolite panel (CMP), liver function test (LFT), and coagulation panel. These are usually followed by a peripheral blood smear and bone marrow aspiration and biopsy. The latter being the gold standard. A bone marrow aspiration is used to remove liquid marrow sample while the biopsy removes a small piece of bone filled with marrow. Samples for the aspiration and biopsy are usually taken from the pelvic bone using a long, thin needle[5]. Collected samples are examined under the microscope to detect any morphologic changes. Additional analyses include flow cytometry, immunophenotyping, polymerase chain reaction, karyotyping, and fluorescence in situ hybridization. The culmination of data from these analyses inform the final diagnosis[9].

Classification

Clinically and pathologically, leukemia is often classified by two main factors: the growth pattern or the type of white blood cells that are affected[5]. Chronic leukemias progress more slowly (over a span of months to years), while acute leukemias progress quickly, requiring immediate treatment to prevent spread to other organs. Lymphocytic leukemias refer to the abnormal outgrowth of immature cells that normally develop into T or B lymphocytes and mediate immune responses. By contrast, in myelogenous leukemias, abnormal growth occurs in cells that normally develop into red blood cells, granulocytes, and platelets[6]. There are four broad classifications of leukemia: acute lymphocytic leukemia (ALL), acute myeloid leukemia (AML), chronic lymphocytic leukemia (CLL), and chronic myeloid leukemia (CML).

Brief summary of leukemia subtypes

ALL occurs when immature WBCs from lymphoid progenitors show unrestrained self-renewal, impeding the formation of mature B and T cells[5]. It is the most common leukemia in pediatric patients, accounting for 80% of cases vs. 20% of cases found in adults. While ALL is highly curable in pediatric patients, it is quite deadly in older adults. In contrast to ALL, AML is the most common acute leukemia seen in adults. It is characterized by an uncontrolled proliferation of myeloid blasts. Among these subtypes, AML is the deadliest hematological malignancy, with a large percentage of patients relapsing. This could be attributed to the underlying molecular heterogeneity of AML that has recently become recognized due to the advent of deep-sequencing technologies[10, 11] (**Figure 2**). Of the many genetic alterations driving AML, activating mutations in the class III receptor tyrosine kinase FLT3 occur in approximately one third of all patients[12]. The activation of the FLT3 receptor will be further discussed in Part II and III of this dissertation. CLL is mainly seen in adults between the ages of 60 and 70 and is characterized by a build-up of mature yet dysfunctional lymphocytic cells. Lastly, CML, which mainly occurs in adults, results from an aberrant proliferation of mature myeloid cells (neutrophils, basophils, eosinophils, or macrophages)[5]. The presence of the BCR-ABL1 translocation is required for the diagnosis of CML[13].

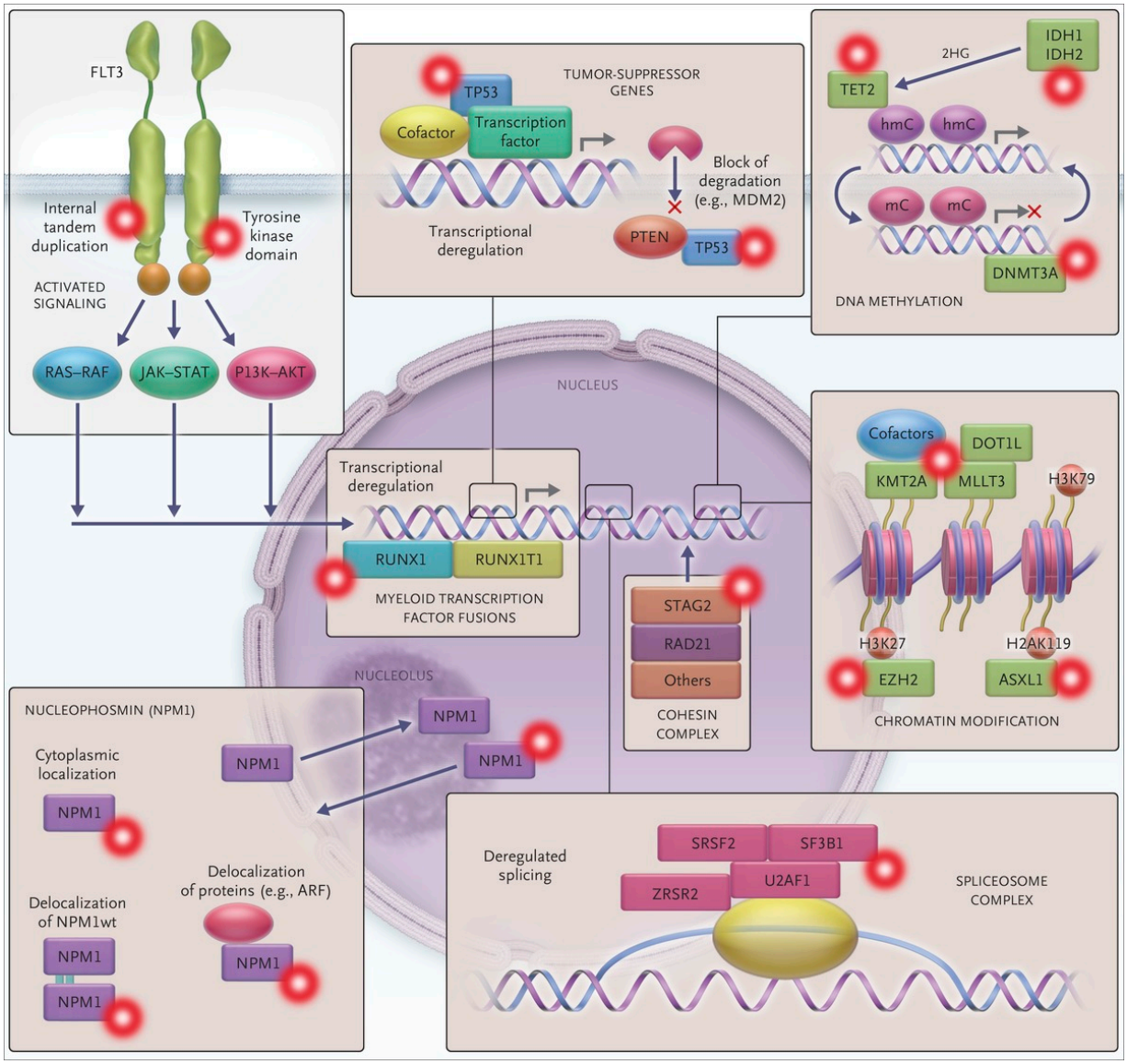

Figure 2: Acute myeloid leukemia is a heterogenous cancer. Mutations in the class III tyrosine kinase receptor gene *FLT3,* myeloid transcription factors, shuttling proteins (NPM1), splicesome-complex genes, and epigenetic regulators confer a proliferative advantage enabling the development of AML.

Reproduced with permission from (Döhner H, Weisdorf DJ, Bloomfield CD. Acute Myeloid Leukemia. N Engl J Med. 2015 Sep 17;373(12):1136-52. doi: 10.1056/NEJMra1406184. PMID: 26376137.), Copyright Massachusetts Medical Society.

Treatment

Treatment for leukemia depends on many factors, which include age, general health of the patient, and type of leukemia.[5] Moreover, treatment may involve a combination of chemotherapy, targeted therapy, and stem cell transplant. Empiric chemotherapy is the first step for the treatment of acute leukemias as it targets fast-dividing cells, preventing their spread to distant organs. If the cancer is more localized to a particular region of the body, radiation therapy can also be used. It involves the use of X-rays and other sources of high energy to damage leukemia cells. Targeted therapies are often preferred in the treatment of chronic leukemias given the slow-growing nature of these cancers. The resounding success of imatinib (Gleevec) for the treatment of CML has ushered an era of precision oncology[13, 14]. Importantly, we learned that a thorough understanding of the biological target can be used to treat that cancer and prevent spread. For the past 20 years, drug discovery efforts have focused on the development of hormone therapies, signal transduction inhibitors, gene expression modulators, apoptosis inhibitors, angiogenesis inhibitors, and immunotherapies[15]. As noted previously, one of the causes of leukemia is the aberrant activation of RTKs. To this end, many small-molecule kinase inhibitors have been developed, many are in clinical trials, and some have been clinically approved. In the following chapter, the activation of RTKs as a driver of tumor growth will be discussed with a focused discussion on kinase inhibitors and their use in cancer treatment.

Lastly, stem cell transplant is also used in the treatment of leukemia. However, a decision to pursue this option is dependent on the health of the patient and whether this option outweighs the associated risks. A stem cell transplant replaces the diseased bone marrow with healthy bone marrow obtained from a donor. Before this procedure, high doses of chemotherapy or radiation are used to destroy all blood-forming cells[5].

2 *Oncogenic activation of receptor tyrosine kinases*

Introduction

Phosphorylation is a fundamental process that cells use to regulate the activity of proteins and protein *kinases* are the key guardians of this process. Kinases transfer the γ-phosphate group of adenosine triphosphate (ATP) onto the hydroxyl group of a tyrosine, serine, or threonine residue of protein substrates[16]. The human proteome contains more than 500 protein kinases[17]. Among the different families of kinase proteins, this discussion will focus on receptor tyrosine kinases (RTKs), a family of cell-surface receptors that play an essential role in mediating cell-to-cell communication, cell growth, differentiation, metabolism, and motility among other normal cellular processes[18-21]. Abnormal activation of these receptors can lead to many pathologies, including cancer, paving the way for the development of small-molecule inhibitors that can block these receptors and forestall disease progression[16, 18].

In the previous chapter on the basics of leukemia, it was stated that one driver of leukemia is aberrant activation of RTKs. In this chapter, an overview on the molecular architecture of RTKs and their role as oncogenes and targets for cancer therapy will be broadly discussed. A more specific description of the intrinsic and extrinsic activation of these receptors and how both modes result in aberrant RTK activity and foster uncontrolled growth and survival of tumor cells will be provided. As will the development of tyrosine kinase inhibitors (TKI) and mechanisms of TKI resistance. Discussion on RTKs will not be limited to leukemia in this chapter but will aim to highlight key studies that have advanced our understanding of how RTKs contribute to tumor

pathogenesis. Part II and III of this dissertation will focus on the intrinsic and extrinsic activation of particular RTKs that were investigated throughout the course of my PhD training.

Overall architecture, domain organization, and function

Of the 90 unique human tyrosine kinases that have been catalogued to date, 58 encode RTKs that can be further divided into 20 subfamilies, and 32 encode cytoplasmic, non-receptor tyrosine kinases that fall into 10 subfamilies[17, 19, 20]. RTKs phosphorylate multiple protein substrates, including themselves. Autophosphorylation of the receptor serves as the basis for signal transduction and engages downstream mediators that propagate essential cellular signaling pathways, whereas aberrant phosphorylation is associated with a variety of disorders. For that reason, the catalytic activity of RTKs is tightly regulated via corresponding phosphatases and built-in autoinhibitory receptor mechanisms (cis-autoinhibition) that will be briefly discussed below.

All RTKs consist of an extracellular domain for ligand binding, a single transmembrane helix, and a cytoplasmic region that contains the juxtamembrane domain, tyrosine kinase domain, and carboxy-terminal tail region[18] (**Figure 1**). In the absence of ligand binding, RTKs can reside as monomers or oligomers. For example, members of the insulin receptor subfamily, which includes the insulin-like growth factor 1 (IGF1) receptor, are expressed on the cell surface as disulfide-linked $(\alpha\beta)_2$ dimers in the inactive state[22]. Studies have also shown that the epidermal growth factor receptor (EGFR/ErbB1) can exist as an inactive predimers and in higher oligomeric states[23, 24].

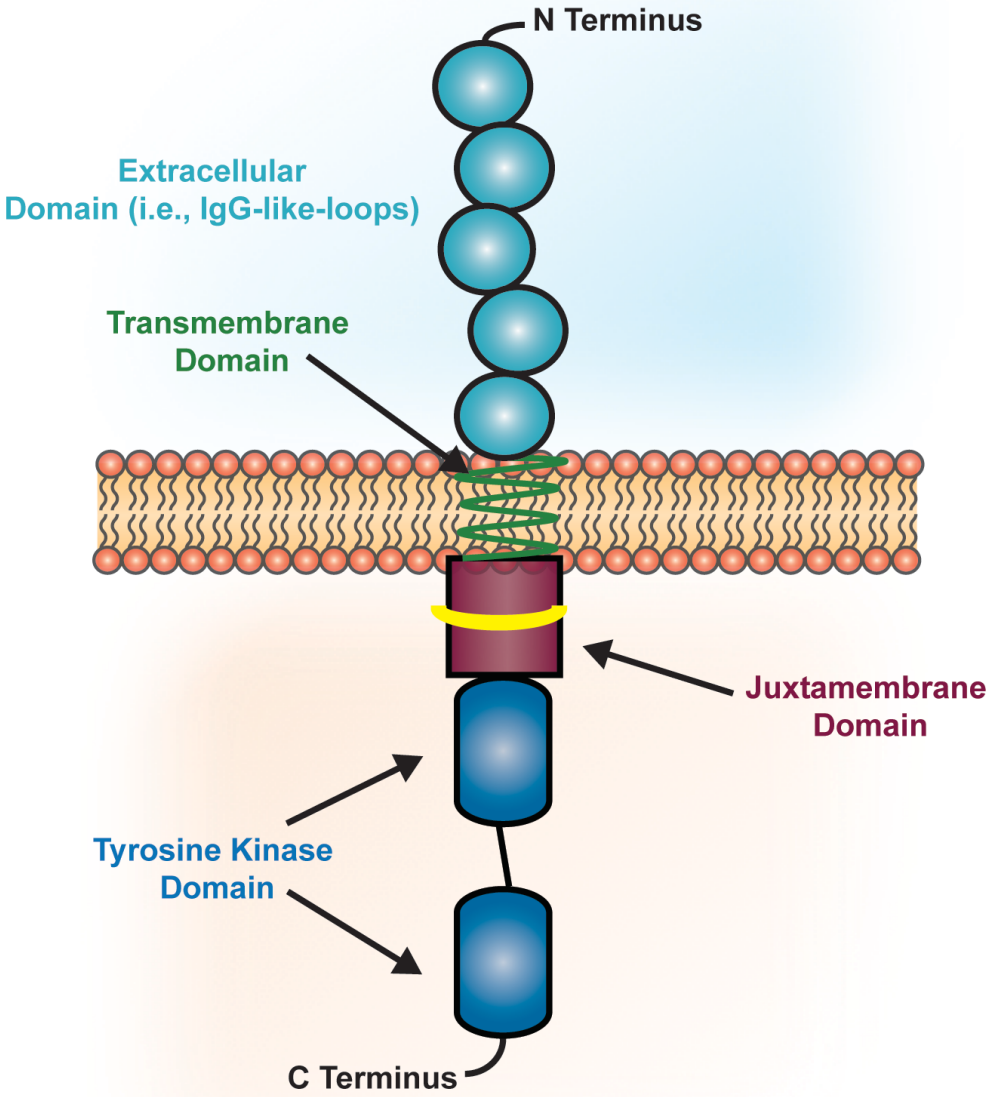

Figure 1: Basic anatomy of receptor tyrosine kinases (RTKs). Here the FLT3 receptor is used as an example. All RTKs consist of an extracellular domain for ligand binding and oligomerization, a single-pass transmembrane domain, regulatory juxtamembrane domain, and an intracellular tyrosine kinase domain.

It should also be noted that the extracellular domain of RTKs is not uniform across the receptor subfamilies[25]. It can consist of an array of structural motifs from immunoglobulin (Ig)-like loops, cysteine-rich sequence repeats, leucine-rich repeats, glycosylation sites, fibronectin type III-like domains, to EGF-like domains[21, 25, 26]. While the complete functional significance of these motifs is unknown, it is speculated that these regions may facilitate ligand binding and/or prevent unwarranted receptor activity in the absence of ligand stimulation[21, 27, 28].

The transmembrane domain mainly anchors the receptor to the plasma membrane. However, previous studies have shown that mutations in the transmembrane domain could stabilize the RTK (e.g., increase retention of receptor at cell surface) and induce aberrant kinase activity[29-32].

In contrast to the extracellular domain, the cytoplasmic region of RTKs is more uniform. The juxtamembrane domain is a flexible region consisting of 40 or more residues that link the C-terminus of the transmembrane domain with the tyrosine kinase domain[33]. It has a dual function of both promoting and inhibiting catalytic activity[33]. Once the tyrosine residues of the domain are phosphorylated, they serve as recruitment sites for downstream adapter proteins that further amplify signaling. As for its inhibitory function, this is still an active area of study. Previous studies have shown that the N-terminal end of the juxtamembrane domain contains basic, positively charged residues at positions 1 to 5 that interact with negatively charged lipid headgroups (e.g., phosphatidylinositol-4,5-biphosphate, PIP_2) found in the lipid bilayer[34, 35]. This interaction is key to maintain the RTK at its basal, low-activity state. An alteration of this interaction can lead to unwarranted RTK activation. Specifically, arginine and lysine residues of the juxtamembrane domain mediate this interaction in all 58 human receptor tyrosine kinases[34]. As a proof of concept, a recent computational study using a near complete EphA2 receptor described a suggestive role for receptor-lipid interactions in the regulation of EphA2 receptor activity[36]. Crystallization of the FMS-like tyrosine kinase 3 (FLT3)[37] and KIT[38] receptors have also provided insight on the autoinhibitory function of the juxtamembrane domain in the context of AML, which is likely utilized by other members of this subfamily[37]. These studies show that regions of the juxtamembrane

domain make direct contact with parts of the tyrosine kinase domain (particularly the activation loop) to stabilize an inactive receptor conformation. Mutations that disrupt the autoinhibitory function of the juxtamembrane domain lead to constitutive RTK activation[37].

The tyrosine kinase domain is the most conserved region of all RTKs[18]. It comprises of a small, mainly β-stranded N-lobe that is connected by a short hinge region to a larger C-lobe that is predominantly α-helical in secondary structure[39]. Key structural regions of the N and C lobes participate in the catalytic reaction, including the hinge region, phosphate loop, activation loop, catalytic loop, and α-helix (**Figure 2**). These regions are briefly discussed below.

ATP binds in the cleft formed between the N- and C-lobes where the adenine group of ATP forms hydrogen bonds to the hinge region[39]. The ATP binding site consists of a lysine residue, which is a conserved structural motif for all RTKs. A gatekeeper residue is also found deep in the ATP binding pocket. Mutations in the gatekeeper residue result in constitutive kinase activity[18, 40, 41]. In addition to five β-sheets (β1-5), the N-lobe also contains a single α-helix (the C-helix, αC) and a glycine-rich loop (also referred to as the P- or G-loop)[42]. Importantly, the glutamic acid residue of the α-helix forms a salt bridge with the lysine residue found at the ATP binding site of the N-lobe in β3. This interaction anchors and orients the ATP for the catalytic reaction. Likewise, the primary function of the P-loop is to also anchor the β-phosphate of ATP so that the γ-phosphate is in position for its transfer[39, 42, 43]. The C-lobe of the kinase domain consists of the catalytic loop and activation loop (also known as the A-loop), both of which interact with the α-helix of the N-lobe to facilitate the catalytic reaction[39]. The A-loop is defined by two conserved tripeptide motifs (DFG…APE) and controls access to the active site[44]. It is the tyrosine residue found in the A-loop that becomes phosphorylated, resulting in activation of the RTK. Once the tyrosine is phosphorylated the A-loop adopts an open conformation, where the DFG motif faces inwards (DFG-in) and the A-loop is displaced outwards. In the active (DFG-in) state, the aspartic acid residue points into the active site to coordinate the ATP. In the inactive state, the DFG motif

faces outwards (DFG-out, with the phenylalanine pointing into the active site) and the A-loop is displaced inwards[44]. Similar to the juxtamembrane domain, the tyrosine kinase domain also has a built-in autoinhibitory mechanism, which is well-characterized for the insulin, IGF1, and FGFR1 receptors[18, 33, 45]. In all cases, the activation loop interacts directly with the active site of the kinase in *cis* conformation and impedes access of ATP. However, once the respective ligand binds, the loop is reoriented (allows for ATP binding) and enables RTK activation, which is discussed in more detail below.

The carboxy-terminal region of RTKs vastly differs between receptors. This region provides another mode of regulation to minimize basal RTK activity in the absence of ligand stimulation. Similar to the juxtamembrane domain, the carboxy-terminal tail interacts with the ATP binding site, stabilizing the inactive receptor conformation. This is particularly notable in the Tie2 receptor involved in angiogenesis and vasculature maintenance[46].

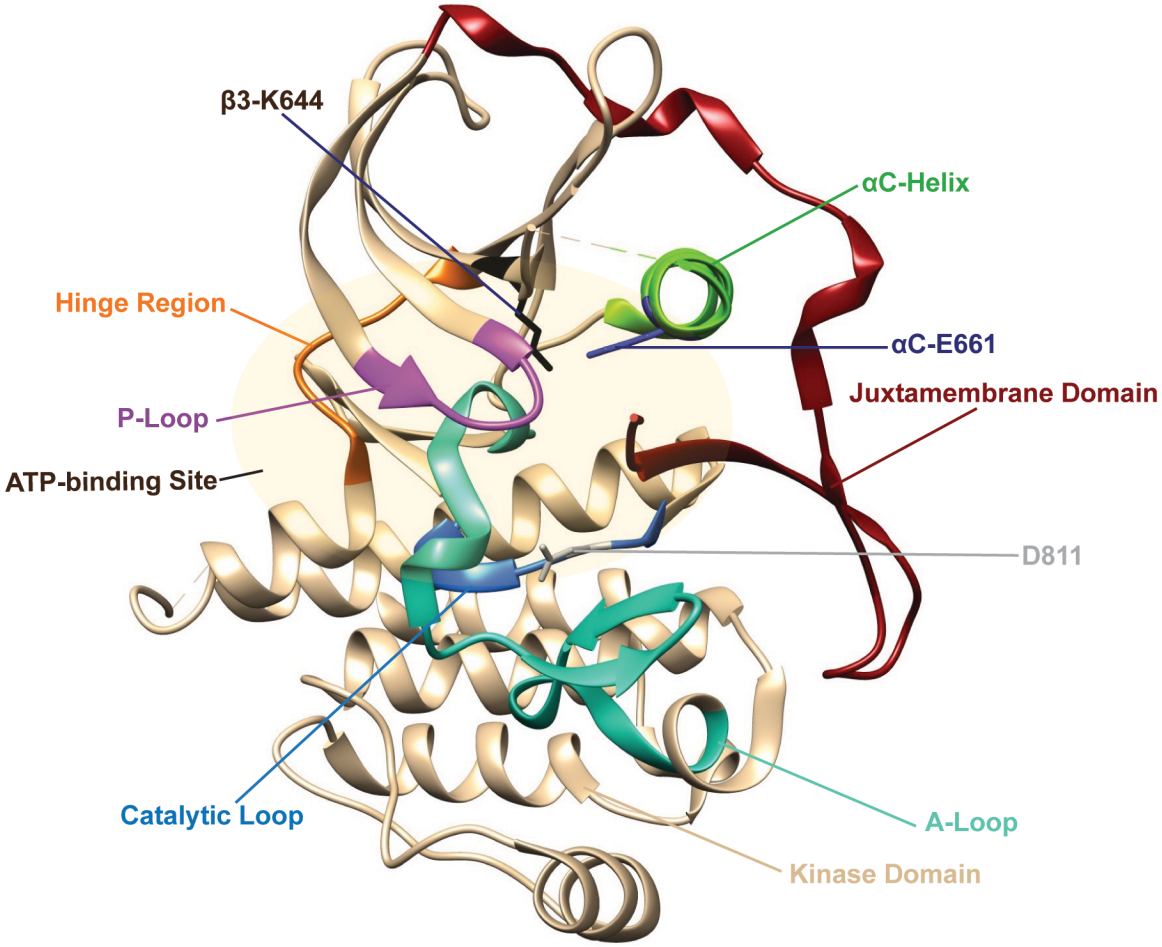

Figure 2: Ribbon diagram highlighting the catalytic components of receptor tyrosine kinases. Here the tyrosine kinase domain of the FLT3 receptor is being used to illustrate the key conserved structural elements required for kinase catalytic activity[47]. The hinge region connects the N and C lobes and hydrogen bonds with the adenine ring of ATP. The P-loop anchors the β-phosphate of ATP, allowing for the transfer of the γ-phosphate. The catalytic loop plays a structural and catalytic role. Specifically, residue D811 is the proton acceptor (abstracts protein substrate proton) and residue N816 chelates Mg^{2+}. Residue K644 of β3 in the N lobe forms a salt bridge with residue E661 of the αC-Helix, which allows proper receptor orientation for the catalytic reaction. Residue K644 also forms a salt bridge with the α and β phosphates of ATP. K644 is also known as the ATP binding site. The juxtamembrane domain is also labeled for reference. Diagram was adapted from PDB 1RJB[37] and visualized with the UCSF Chimera software[48].

Mechanism of receptor activation

RTKs are activated through the binding of their cognate protein ligand (growth factor or cytokine), which induces receptor dimerization that is followed by transphosphorylation of key tyrosine residues in the A-loop[25]. The number of tyrosine residues in the A-loop varies between one and three. This initial phosphorylation event activates the kinase and triggers phosphorylation in other regions of the cytoplasmic domain that serve as docking sites for downstream signaling effector proteins. These signaling proteins contain phosphotyrosine-recognition domains, such as the Src homology 2 (SH2) domain or the phosphotyrosine-binding (PTB) domain that directly engage with phosphorylated tyrosines of the RTK[25, 49]. This interaction leads to the activation of canonical signaling through the Ras/Raf mitogen-activated protein kinase (MAPK), phosphoinositide-3-kinase (PI3K)/AKT, phospholipase C-γ, and JAK/STAT pathways. Activation of these pathways results in cellular differentiation, proliferation, and survival[49] (**Figure 3**). Due to their critical role in signal transduction, RTKs are tightly regulated in normal cells. Examples of regulation include phosphatases[50], autoinhibitory mechanisms of the RTK as discussed above, transcription of negative regulators[51], receptor endocytosis, ubiquitylation, and heterodimerization with kinase-dead receptors[18].

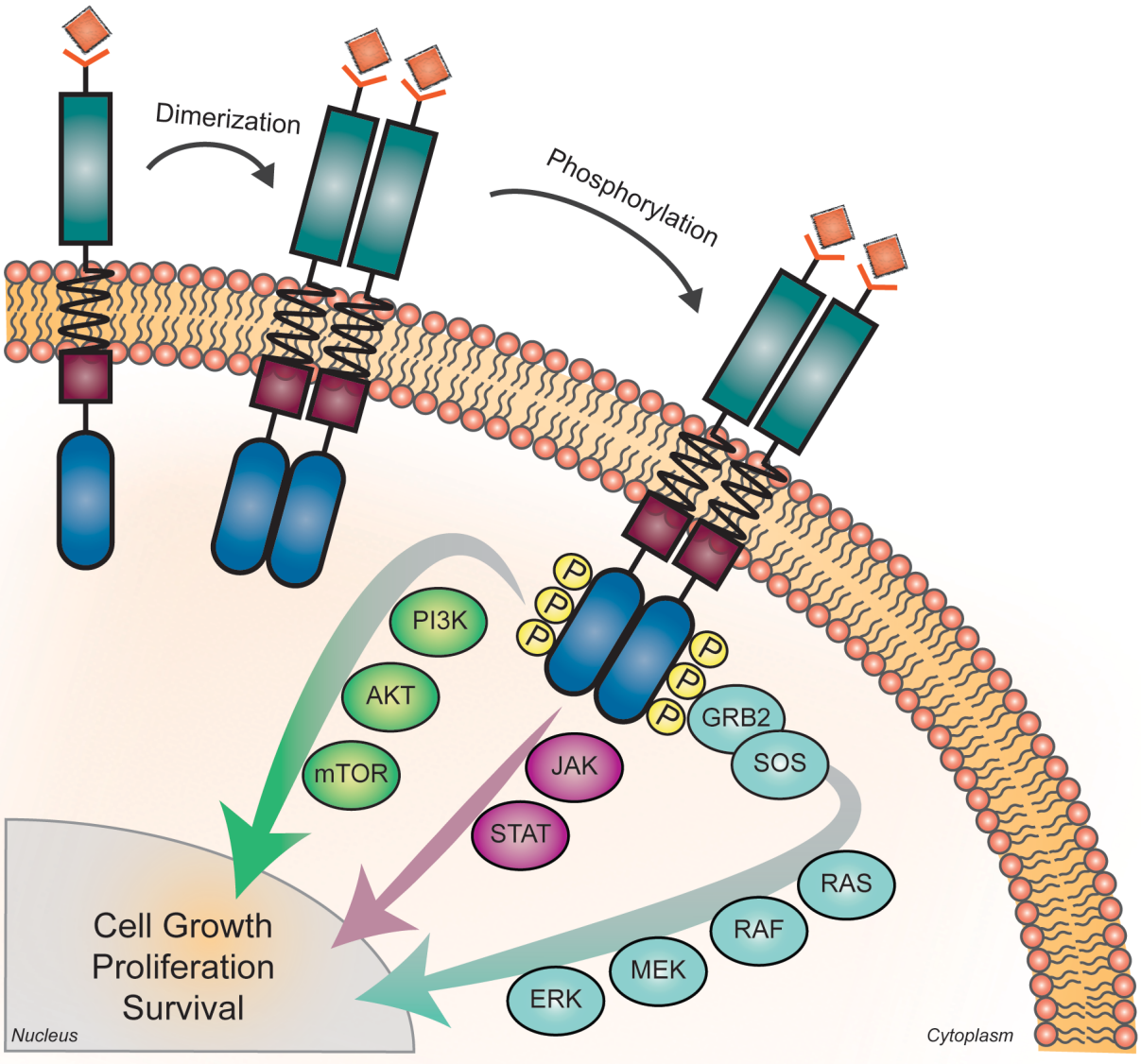

Figure 3: Activation of receptor tyrosine kinases results in activation of downstream signaling pathways that promote cell growth, proliferation, and survival. The MAPK pathway is depicted in aqua, JAK/STAT pathway in pink, and AKT/mTOR pathway in green. For simplicity, only phosphorylation of the kinase domain is shown in the figure. However, it should be noted that RTK activation triggers phosphorylation of tyrosine's in the juxtamembrane, tyrosine kinase, and c-terminal domains of the receptor. For example, in the case of the FLT3 receptor, 10 tyrosine residues undergo phosphorylation, though the order of phosphorylation has not been determined[47].

Oncogenic activation of RTKs – intrinsic and extrinsic mechanisms

RTKs can become constitutively activated in the setting of cancer via different mechanisms, serving as oncogenes[52, 53]. These activation mechanisms can be broadly categorized into intrinsic and extrinsic. Intrinsic mechanisms mainly involve alterations to the RTK itself, while extrinsic mechanisms often implicate crosstalk with the tumor microenvironment (**Figure 4**).

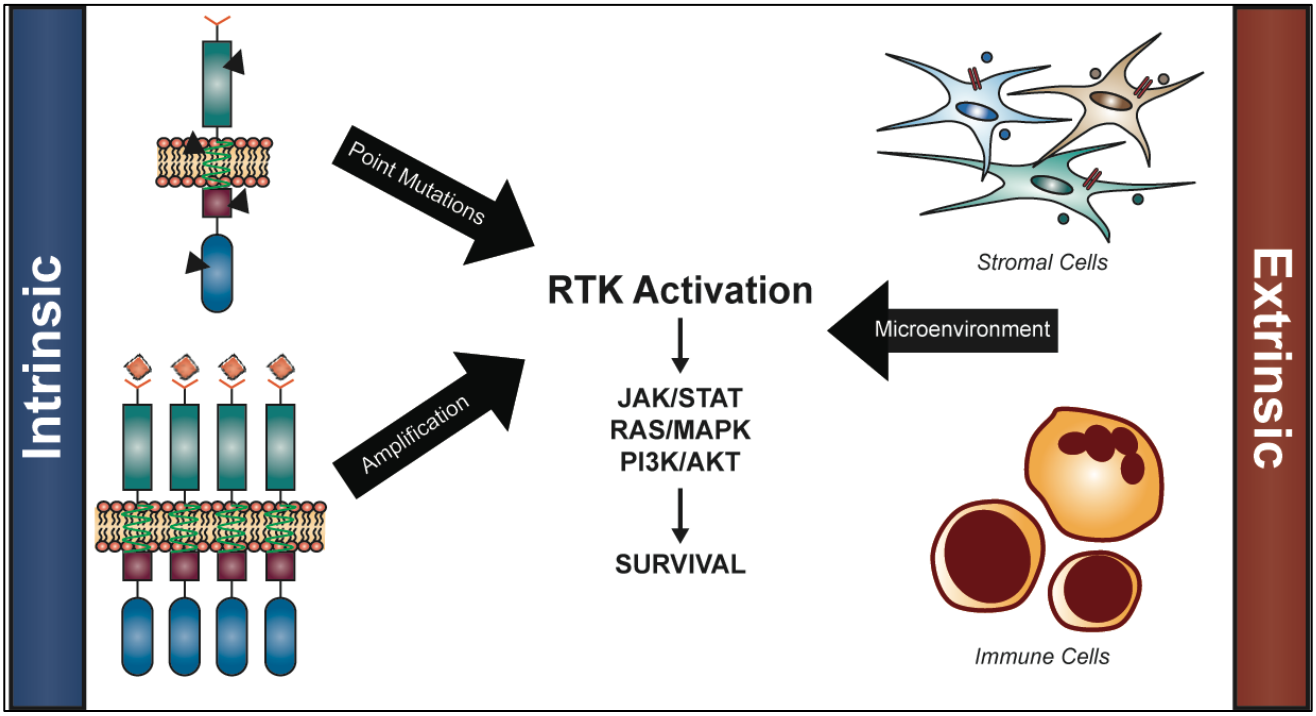

Figure 4: Receptor tyrosine kinases can be activated by intrinsic and extrinsic mechanisms.

Intrinsic mechanisms

Given the advent of next generation sequencing platforms, the mutational landscape of common forms of human cancers have become well-defined[11, 54, 55]. These studies have revealed that the most common intrinsic mechanism underlying cancer is the accrual of pathogenic genetic alterations, which include point mutations, amplification events, and chromosomal rearrangements/translocations. As for point mutations in RTKs, these often consist of gain-of-function mutations that drive uncontrolled RTK activation in the absence of ligand binding. While these mutations can occur in any part of the RTK, they often cluster around evolutionally conserved residues near the activation loop, ATP binding site, or gatekeeper region. In many cases, these mutations serve as primary drivers, causing cancer cells to be "addicted" to them[56, 57]. Point mutations in the EGFR receptor were among the first to be described as oncogenic in 1984[58]. Since then mechanistic studies focused on EGFR signaling in non-small cell lung cancer[59, 60], breast cancer[61], and glioblastoma demonstrate that mutations near the ATP-binding pocket and/or activation loop can hyperactivate kinase signaling and induce tumorigenesis. A similar pattern is also evident with mutated-FLT3 in AML[62]. Activating mutations KIT^{V560G} and $PDGFRA^{V561D}$ in gastrointestinal stromal tumors interfere with the juxtamembrane domain's autoinhibitory function, conferring oncogenic behavior[63].

Overexpression or gene amplification is another mode of intrinsic activation of RTKs. Overexpression increases the local concentration of RTKs such that inherit regulatory mechanisms fall short of correcting for the underlying alteration. The ErbB family of RTKs provide a notable example, where their overexpression correlates with poor prognosis in a variety of solid malignancies[64]. Gene amplification leads to an increase in copy number of a specific region of the genome[65]. Amplification of RTKs has been described in many cancers, including EGFR in gliomas[66], ERBB2 in breast, ovarian, and gastric cancers[67], and FGFR1 in lung[68] and breast[69] cancers.

Oncofusions resulting from chromosomal rearrangements can also lead to aberrant RTK signaling and have been well characterized in cancer. The first tyrosine kinase fusion was identified in 1960 by Peter Nowell and David Hungerford using karyotype testing in the setting of chronic myeloid leukemia (CML)[70]. With the development of chromosomal-banding techniques, Janet Rowley confirmed this acrocentric chromosomal finding as being a translocation between chromosomes 9 and 22[71, 72]. This translocation event, t(9;22)(q34;q11), gave rise to what is now known as the BCR-ABL1 fusion, where the ABL1 tyrosine kinase on chromosome 9 fuses with the BCR gene on chromosome 22. The fusion results in constitutive ABL1 kinase activity, which imparts the malignant phenotype observed in CML[73, 74]. The discovery of the BCR-ABL1 fusion has spurred interest in the identification of other oncofusions that are associated with various solid and hematologic malignancies[75-78]. RET, ALK, ROS1, and TRK rearrangements have been well-documented in human cancers[78-81]. In fact, fusions involving the Trk family of RTKs have been identified across 9 or more tumor types, including both solid and liquid tumors[79, 82]. Despite the diversity in oncofusion structure and upstream partners, the tyrosine kinase domain is preserved in all cases.

Increased local concentration of ligand (autocrine activation) is another mode of activation that subsequently hyperactivates the respective RTK. This is best exemplified by the autocrine loop that exists between the stem cell factor and c-KIT receptor (SCF-KIT), which has been reported in the proliferation of small cell lung[83] and pancreatic[84] cancers. It should be noted that autocrine activation of RTKs differs from paracrine activation, which often results from the communication between cancer cells and cells of the tumor microenvironment as discussed below.

Lastly, the downstream program of activated RTKs can be supported by the loss of negative regulators. Most notably, a mutation in the tumor suppressor gene, phosphatase and tensin homolog (PTEN) is observed in many human cancers[85]. PTEN typically acts by down-regulating mitogenic signaling through dephosphorylation of phosphatidylinositol (3,4,5)-triphosphate (PIP_3)

to PIP_2, which inhibits activation of the AKT signaling pathway. However, loss of PTEN enables cells to continue dividing uncontrollably, a hallmark of cancer.

Extrinsic mechanisms

While understanding the intrinsic biology of cancer cells themselves is imperative, it overlooks the contribution of extrinsic factors that can also activate RTKs and drive the cancer program. The dynamic interplay of intrinsic and extrinsic factors in the pathogenesis of cancer was first hinted by the English surgeon and pathologist, Stephen Paget in 1889[86]. He coined the "seed and soil" hypothesis of cancer progression and metastasis after examining the autopsy records of 735 patients with terminal breast cancer[86]. This hypothesis suggested that a plant sends out multiple seeds in the hope that one will germinate on fertile soil[87]. This same idea also holds true for cancer cells. Not all cancer cells can proliferate, migrate, and metastasize into new areas of the body. A corollary to this idea is that examining the tumor microenvironment is equally important as it nurtures the malignant seed cells.

A growing body of evidence has revealed how the underlying crosstalk between the tumor microenvironment and cancer cells results in RTK activation, supporting sustained cancer progression[88, 89]. The tumor-permissive microenvironment consists of a collection of various cells often broadly referred to as the stroma, which include fibroblasts, endothelial cells, mesenchymal stromal cells, immune cells, or a combination of all. These cells can secrete growth factors, cytokines, chemokines, extracellular vesicles that communicate with the tumor cell (paracrine activation). Beyond biochemical cues from the microenvironment, physical cues and spatial communication between cells of the microenvironment and tumor cells greatly contribute to the progression and dissemination of the tumor program[88]. Interaction between tumor stroma and cancer cells has led to increased Eph RTK signaling and metastasis in the setting of breast,

prostate, non-small cell lung, and colon cancers[90]. SCF released by stromal cells upregulates c-KIT in prostate cancer cell lines (paracrine activation), favoring activation of the RTK complex and bone metastasis[91]. VEGFR1-mediated angiogenic signaling has been reported to provide a permissive niche for proliferation of lung and melanoma cancer cells in the tumor microenvironment[92]. Release of platelet-derived growth factor (PDGF) from cancer-associated fibroblasts stimulates PDGFR-mediated lung cancer growth[93] among other cancers[94]. Autocrine and/or paracrine signals expressed by stromal and immune cells—such as IL-1[95-97], IL-6[98, 99], PKCβ/IL-8[100, 101], GM-CSF[98, 99], TNFα[102, 103], FLT-3 ligand[104, 105], FGFs[106, 107], SDF-1α[108-110], TGFβ-1[109], WNTs[111], NF-κB[112], ENT1[113], Sonic Hedgehog[114, 115], and galectins[116, 117]—have been shown to enable persistence of AML cells within the leukemic microenvironment and contribute to disease relapse.

Of the many cells that create the AML microenvironment niche, part III of this dissertation will focus on mesenchymal stromal cells, the critical support cells of the marrow microenvironment that protect leukemia cells. In 2006, the International Society for Cellular Therapy (ISCT) issued the minimal criteria for defining mesenchymal stromal cells[118]. These criteria include adherence of stromal cells to plastic under standard culturing conditions, expression of defined surface markers (CD73, CD90, and CD105), and ability to differentiate along the classical tri-lineage pathways of adipogenesis, osteogenesis, and chondrogenesis. Mesenchymal stromal cells are essential for human hematopoiesis[119] and can be reprogramed to support leukemia cells[120-122]. Leukemia-associated stromal cells differ functionally and molecularly from healthy stromal cells in that they exhibit a decreased capacity to proliferate, reduced differentiation potential, and altered DNA methylation patterns[123].

Tyrosine kinase inhibitors (TKIs)

Given that aberrant activation of RTKs can perpetuate various malignancies independent of tissue origin, these signaling receptors have become principal targets for cancer therapy. Several small molecule inhibitors and monoclonal antibodies have been developed to target RTKs and downstream kinase-driven signaling pathways. Imatinib, the first small-molecule inhibitor that received approval from the US Food and Drug Administration (FDA) in 2001, targets the chimeric BCR-ABL1 oncofusion that constitutively activates the ABL kinase, leading to the development of CML[13, 14, 124] (**Figure 5**). Its success pioneered the era of precision oncology. Importantly, it lends credence to the idea of genomic-driven therapy that results in fewer adverse effects than conventional chemotherapy.

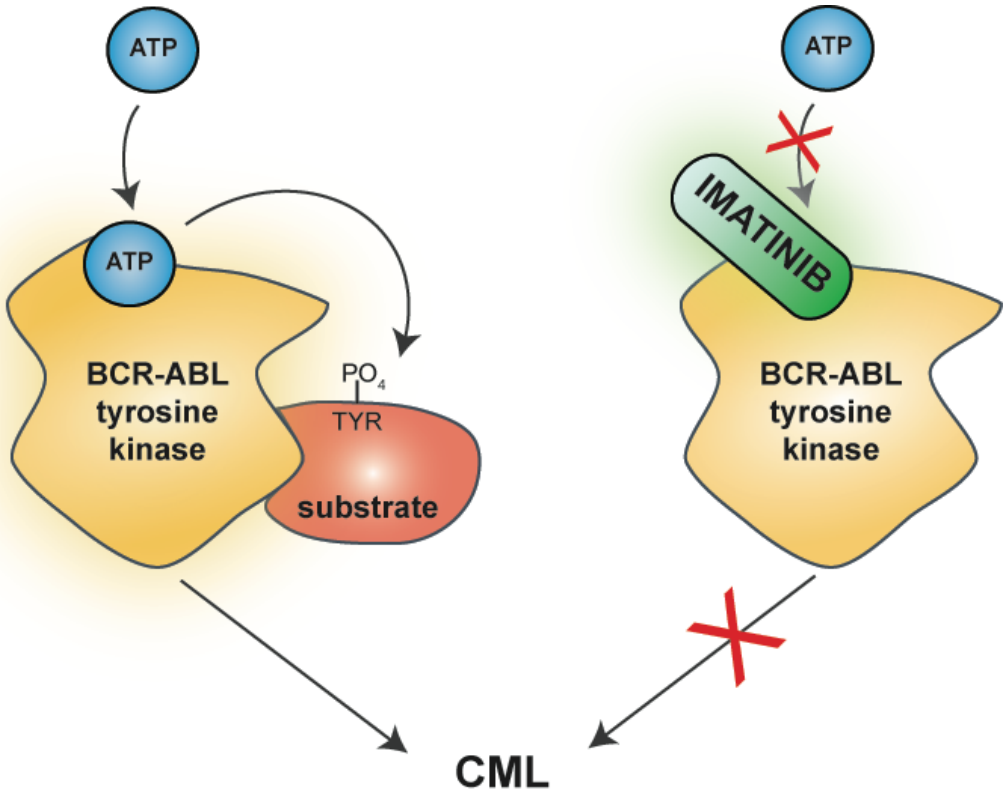

Figure 5: Imatinib serves as the "magic bullet" for the treatment of chronic myeloid leukemia. The oncogene BCR-ABL1 induces constitutive activation of the ABL kinase. Binding of imatinib prevents the growth of CML cells[125].

To date, the FDA has approved a total of 52 small-molecule protein kinase inhibitors of which 28 target RTKs[16]. Most of these inhibitors perturb ATP binding as they bind the ATP-binding pocket in the kinase domain of the receptor. A small number of inhibitors bind the allosteric site. The Dar and Shokat classification system (type I-III) is widely used to categorize these inhibitors[126]. Over the years, this classification system has been further revised to subclassify allosteric inhibitors as type III and IV[127]. Type I inhibitors are canonical ATP competitors and bind the ATP-binding site when the receptor is in the active conformation (**Figure 6A**). Type II inhibitors interact with the hydrophobic region immediately adjacent to the ATP-binding site that is only accessible when the receptor adopts the inactive conformation (**Figure 6B**). As discussed earlier in the chapter, the active and inactive conformation are defined by the orientation of the DFG structural motif and the displacement of the activation loop[126]. Active conformation is synonymous to the DFG motif facing inwards and the activation loop being displaced outwards (open/extended conformation). Specifically, the aspartate of the DFG motif points towards the ATP-binding site and coordinates two Mg^{2+} ions in the active conformation[128]. In the inactive conformation, the DFG is facing outwards owing to the movement of aspartate away from the ATP-binding site and the activation loop is closed and collapsed onto the surface of the kinase domain[128]. In this case, the phenylalanine faces the active site. The structural movement of the DGF motif in the active and inactive conformation explains why type I and II inhibitors bind those respective conformations (**Figure 6C-E**). Particularly, the steric hindrance offered by the phenylalanine sidechain explains the preferential underlying binding of type I and II inhibitors (**Figure 6D-E**, see inset panels). Type III inhibitors bind an allosteric site opposite to the ATP binding site (often called the “back pocket”), while Type IV inhibitors bind an allosteric site distant from the ATP-binding pocket[127]. An understanding of the inhibitor and its preferred binding conformation can be leveraged when targeting resistance mutations that cause a switch in inhibitor class. For example, mutations in residues G667 and G696 of NTRK1 and NTRK3, respectively confer resistance to type I Trk inhibitors as they stabilize the inactive conformation of the kinase[129]. Yet, these same mutations

show sensitivity to type II Trk inhibitors, emphasizing the importance to not only understand structural changes induced by mutations but also the binding engagement of inhibitors. Such insight could be harnessed clinically to mitigate drug resistance.

In addition to small-molecule kinase inhibitors, the FDA has also approved many monoclonal antibodies that impede RTK activation. Trastuzumab (Herceptin) in the treatment of $HER2^+$ breast cancer provides a notable example as the first monoclonal antibody to prolong survival in patients with this malignancy[130]. However, not all patients respond to trastuzumab, which led to the discovery of pertuzumab[131]. Pertuzumab inhibits the dimerization of HER2, offering further therapeutic benefit that is unattainable with trastuzumab. Apart from monoclonal antibodies in the treatment of breast cancer, the FDA has also approved cetuximab in lung cancer[132], panitumumab in colon cancer[133], and cetuximab in head and neck cancer[134].

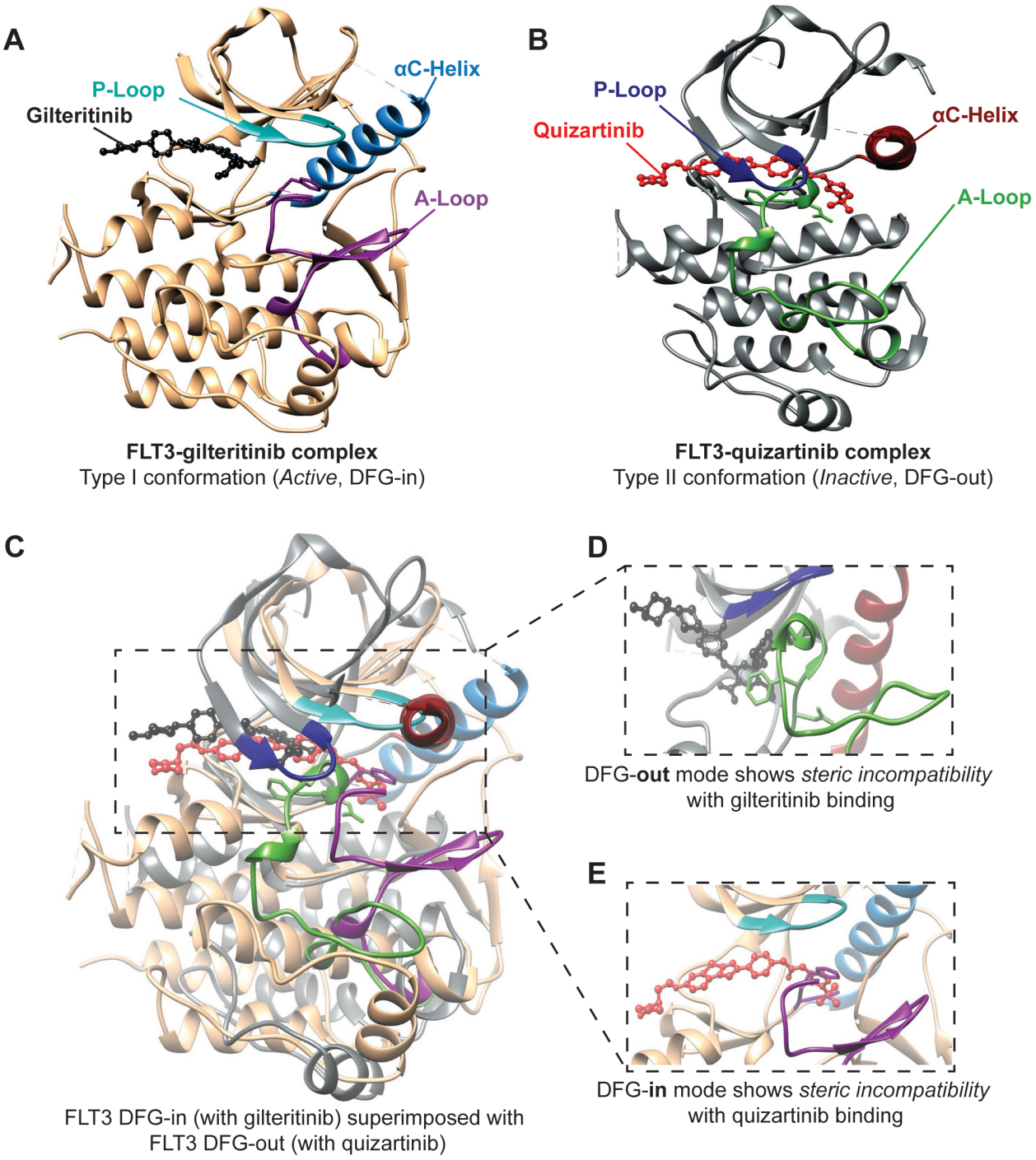

Figure 6: Type I and II binding modes of receptor tyrosine kinases. To highlight the differences between the binding of type I and type II inhibitors, FLT3 inhibitors, gilteritinib (type I inhibitor) and quizartinib (type II), were used as examples. **A.** Gilteritinib preferentially binds FLT3 in the active conformation (DFG-in). The A-loop is in an open/extended conformation and the aspartate (D) residue of DFG is positioned to chelate Mg^{2+}. **B.** Quizartinib binds FLT3 in the inactive conformation (DFG-out). The A-loop is displaced inwards, residing on the surface of the

kinase domain. The phenylalanine (F) residue of DFG sterically hinders the binding of ATP. **C.** FLT3 DFG-in (with gilteritinib) was superimposed with FLT3 DFG-out (with quizartinib). **D-E.** The inset panels illustrate the unfeasibility of type I and II inhibitors to bind the inactive conformation (**D**) and active conformations (**E**), respectively. Ribbon diagrams were adapted from PDB 4RT7[62] and PDB 6JQR[135] and visualized with the UCSF Chimera software[48]. MatchMaker analysis from Chimera was used for overlaying receptors in **C**. The visualization utilized by this figure was adapted from Drilon *et al.* who focus on the receptor tyrosine kinase ROS1[81].

Resistance to TKI therapy

While TKIs show impressive activity upfront, their durability is limited due to the development of drug resistance, culminating in eventual disease relapse. Understanding and combatting mechanisms of TKI resistance is a vital step in extending the durability of these potent inhibitors. Clinically, resistance to cancer therapies can be classified as primary (innate) or secondary (acquired) resistance. Primary resistance corresponds to tumors that show no response to treatment. By contrast, secondary resistance refers to tumors that recur following a period of clinical response. It is important to note that tools to assess clinical response and tumor pathology are constantly evolving, making this classification open to interpretation[136]. Similar to RTK activation, in this section, the framework of intrinsic (genetic alterations) and extrinsic (tumor microenvironment) is used to highlight common mechanisms of TKI resistance. This section begins by briefly commenting on the common modes of resistance and then discussing mechanisms of resistance for FLT3 inhibitors given their relevance to part III of this dissertation.

Intrinsic resistance mechanisms

Given the strong selective pressure resulting from TKI treatment, cancer cells can acquire genetic alterations that abrogate inhibitor binding and provide tumor cells an avenue to evade death. Notably, mutations in the gatekeeper residue of RTKs, a conserved hydrophobic residue

in active site, can disrupt TKI binding and, thereby promote resistance[62, 137-139]. The classic example being the T315I gatekeeper mutation in BCR-ABL1 that impedes imatinib binding by introducing a steric clash that prevents imatinib from forming a hydrogen bond at the active site[41]. A similar steric interference mechanism has been reported with gatekeeper mutations $FLT3^{F691L}$, $NTRK1^{F589L}$, $NTRK2^{F633L}$, $NTRK3^{F617L}$, ALK^{L1196M}, and $ROS1^{L2026M}$, which hinder the binding of respective TKIs[62, 140]. In contrast, the gatekeeper mutation T790M in EGFR increases the receptor's affinity for ATP, effectively weakening its affinity for TKIs[141, 142]. In other cases, resistance mutations can cause kinases to switch conformations, rendering them unresponsive to the inhibitor[129, 143]. Amplification of MET or HER2 can also confer resistance to TKI therapy in EGFR-mediated lung cancers[144]. Studies focused on resistance to BCL-2 inhibitor venetoclax in AML have brought forward three other mechanisms of resistance – bypass pathway signaling, changes in tumor metabolism, and in cellular differentiation status. Genome-wide CRISPR/Cas9 screening of venetoclax-sensitive AML cells revealed that a loss of the TP53 network induces resistance due to an acquired dependency upon TRK signaling, which serves as a bypass pathway in this setting[145]. Studies performed on leukemia stem cells (LSCs) from AML patients following relapse to venetoclax and azacitidine treatment show that changes in metabolism confer resistance[146, 147]. Lastly, more differentiated LSCs were also resistant to venetoclax[148, 149].

Extrinsic resistance mechanisms

While TKIs are able to eradicate most of the initial tumor, residual tumor cells are able to persist within the tumor microenvironment. Advances in our understanding of the tumor microenvironment have revealed that microenvironmental factors protect these cells from initial TKI treatment until more complex acquired drug resistance phenotypes can develop[107, 150-152]. These cells are often referred to as "persister cells," or "drug-tolerant persisters" and remain understudied as they go undetected due to their low abundance and lack of known biomarkers

for classification[153]. In general, these cells display no genetic alteration, slow proliferation, epigenetic modifications, and altered metabolism[153]. Seminal studies in lung[154-156], gliloblastoma[157], and breast[158, 159] cancers have begun to characterize these reservoirs of malignant cells that inexorably culminate in disease relapse.

Apart from the tumor cells, the microenvironment is also dynamically undergoing remodeling throughout the disease course due to continuous crosstalk between tumor cells and cells of the microenvironment. For example, in chronic lymphocytic leukemia (CLL) and AML, extracellular vesicles released from leukemia cells can reshape the microenvironment by downregulating growth factors that support hematopoietic stem cells[160] or hindering the function of natural killer cells[161].

Mechanisms underlying resistance to FLT3 inhibitors in AML

FLT3 inhibitors can primarily be classified as type I or II inhibitors. Despite their initial clinical efficacy, resistance to single agents develops after months of therapy, which limits their use in the clinic. Mechanisms of FLT3 inhibitor resistance differ with respect to inhibitor class, but broadly can be subdivided into cell intrinsic and extrinsic mechanisms. Tumor intrinsic mechanisms involve (i) emergence or expansion of secondary point mutations in the FLT3 receptor (on-target resistance) and (ii) activation of alternative (bypass or parallel) signaling pathways (off-target resistance). Extrinsic mechanisms involve crosstalk between leukemia cells and cells of the bone marrow microenvironment that modulate FLT3 inhibitor response.

Intrinsic resistance mechanisms

Portions of the text below are adapted from:

Fletcher L, Joshi SK, Traer E. Profile of Quizartinib for the Treatment of Adult Patients with Relapsed/Refractory FLT3-ITD-Positive Acute Myeloid Leukemia: Evidence to Date. Cancer Manag Res. 2020 Jan 8;12:151-163. doi: 10.2147/CMAR.S196568. PMID: 32021432; PMCID: PMC6955578.

The most common tumor intrinsic mechanism is the emergence of secondary point mutations in the TKD of FLT3 that confer resistance to FLT3 inhibitors. TKD mutations particularly at the D835 residue, are a common cause of clinical resistance to type II FLT3i, which bind the inactive kinase conformation[40, 62, 162]. These mutations destabilize the inactive conformation of FLT3 that is required for the binding of type II inhibitors quizartinib[40] and sorafenib[162]. Type I inhibitors were subsequently developed to overcome these mutations, as they can bind the active kinase conformation. In contrast to type II inhibitors, bypass pathway alterations confer resistance to the type I inhibitor, midostaurin[163] (RAS/MAPK signaling), crenolanib[137] (RAS/MAPK signaling, TET2, IDH1/2) and gilteritinib[164] (RAS/MAPK signaling). Noncanonical extracellular domain (K429E) and TKD resistance mutations (Y693C/N, G697S) have also been reported with crenolanib[137] and gilteritinib[165], respectively. Infrequently, mutations in the gatekeeper residue (F691) have also been identified in patients following relapse to type I or II FLT3 inhibitors[40, 137, 164].

To date the most extensive clinical and laboratory characterization of resistance-causing mutations in FLT3 have been performed with quizartinib. As such, I discuss in detail our understanding of how secondary point mutations in FLT3 propel resistance using quizartinib as a prime example. In 2012, shortly after the release of the interim analysis for the phase 2 trial of quizartinib monotherapy of 53 patients with relapsed/refractory FLT3 internal tandem duplication (ITD) AML, point mutations at three residues within the kinase domain of the FLT3 receptor were reported to confer resistance to quizartinib[40]. These residues consist of the ‘gatekeeper’ residue (i.e., F691) and residues within the activation loop of FLT3 (i.e., D835, Y842). The binding of quizartinib to the crystal structure of the FLT3 kinase domain was modeled and suggested that

substitutions of F691 with non-aromatic residues could hinder the π-π stacking interaction needed to stabilize the benzo-imidazol-thiazol ring of quizartinib[40]. In contrast, replacement of residues D835 or Y842 resulted in a loss of hydrogen bonding between these residues and S838, which is critical to maintain the inactive conformation of FLT3 needed for quizartinib to bind to FLT3[40].

These observations were further confirmed with the first cocrystal structure of quizartinib bound to the FLT3 kinase domain. Importantly, this structure demonstrated that quizartinib binding to FLT3 relies on edge-to-face aromatic interactions mediated by the gatekeeper residue, F691 and activation loop residues[62]. Only disruptions that strongly hinder this interaction enabled quizartinib resistance[62]. A more recent study that performed extensive atomistic molecular dynamics simulations of the FLT3-quizartinib complex further suggests that once the active state of FLT3 is adopted due to the TKD mutations, the transition to the FLT3 inactive state is less likely due to the reaction kinetics[166]. In a follow up study, it was reported that not all D835 mutations facilitate quizartinib resistance[167]. Specifically, bulky hydrophobic substitutions (i.e., D835Y/V/I/F) at this residue produced a resistant phenotype as these mutations prohibited hydrogen bonding between the activation loop and the S838 region of FLT3 and sterically hindered the binding of quizartinib[167]. In aggregate, these early studies demonstrated that TKD mutations provide a survival mechanism by enabling the FLT3 receptor to shift from an inactive to active conformation, precluding the binding of quizartinib. Likewise, these mutations also promote resistance to type II FLT3 inhibitors such as sorafenib and ponatinib[167].

More recently, single-cell analysis of FLT3-ITD primary AML cells suggests that mutational resistance to quizartinib is more complex than initially thought[168]. While FLT3-ITD AML cells can acquire de novo FLT3 TKD mutations following treatment with quizartinib, this model alone does not accurately depict what is observed clinically. In an analysis of 15 patients treated with quizartinib, FLT3 TKD mutations were detected in 14 patients at resistance. Interestingly, the FLT3 TKD mutations were often found on the native FLT3 allele rather than the FLT3-ITD allele, and there were subpopulations that were resistant to quizartinib that did not contain FLT3 TKD

mutations[168]. Thus, in some patients, both FLT3-dependent and -independent resistant mechanisms can coexist, highlighting the underlying clonal heterogeneity that contributes to development of quizartinib resistance.

Apart from resistance mutations in the FLT3 receptor, upregulation of receptor tyrosine kinase AXL provides another route to quizartinib resistance. Previous studies have shown that increased expression of AXL is associated with worse progression-free and overall survival for patients with AML[169-171]. AXL activates downstream PI3K/AKT, MAPK, NF-kB, and JAK/STAT pathways. Mechanistically, upregulation of AXL has been shown to mediate phosphorylation of FLT3[172]. Inhibition of AXL via inhibitor or siRNA suppresses cell growth, induces apoptosis, and restores myeloid differentiation *in vivo*[172]. Upon treatment with quizartinib, it was shown that expression of AXL increases in AML cell lines and in patients after treatment with quizartinib, supporting the idea that AXL upregulation may enable quizartinib resistance in the setting of leukemia[173]. Inhibition of AXL with a small-molecule inhibitor TP-0903 restored sensitivity to quizartinib, corroborating its role in mediating resistance. The FLT3 inhibitor gilteritinib is also an AXL inhibitor[174], and it has been suggested that AXL inhibition delays development of resistance. Apart from AXL's role in promoting tumor-intrinsic resistance, a recent study has shown that marrow stromal cells support increased phosphorylation of STAT5, which in turn leads to increased AXL activity that drives quizartinib resistance both *in vitro* and *in vivo*[175]. The study showed that the hypoxic marrow microenvironment further contributed to increased Axl activity, and thereby, supports quizartinib resistance[175]. Upregulation of the MYC network, which enhances SIRT1 protein expression, has also been shown to promote quizartinib resistance[176, 177]. **Table 1** summarizes intrinsic mechanisms of resistance for type I and II FLT3 inhibitors.

Table 1				
FLT3 Inhibitor	**Type I or II**	**On-Target Resistance**	**Off-Target Resistance**	**Citations**
Midostaurin	I	**FLT3 TKD mutations:** A627P, ITD672E, N676K/D/I/S, F691L, G697R	**MAPK signaling (KRAS)**	Heidel *et al.*, Blood, 2006. Sato *et al.*, Blood, 2011. Rosenberg *et al.,* Oncotarget, 2020.
Quizartinib	II	**FLT3 TKD mutations:** A627P, F691L, D835H/V/Y/F, D839V, Y842C/H/N	**FGF2-FGFR1 accessory pathway** **MAPK signaling (KRAS)** **MYC network** **Gas6/AXL**	Sato *et al.*, Blood, 2011. Smith *et al.*, Nature, 2012. Ben-Batalla *et al.*, Blood, 2013. Fiskus *et al.*, Mol Cancer Ther., 2014. Li *et al.*, Cell Stem Cell, 2014. Traer *et al.*, Cancer Res., 2016. Hou *et al.*, Cancer Res., 2017. Javidi-Sharifi *et al.,* Elife, 2019.
Sorafenib	II	**FLT3 TKD mutations:** D835H/V/Y/F	**MAPK signaling (LZTR1)**	Sato *et al.*, Blood, 2011. Man *et al.*, Blood, 2012. Baker *et al.*, Clin Cancer Res., 2013. Damnernsawad *et al.*, Haematologica, 2020.
Crenolanib	I	**FLT3 TKD mutations:** F691L **FLT3 Extracellular Domain Mutation:** K429E	**MAPK signaling** **TET2 & IDH1/2**	Zimmerman *et al.*, Blood, 2013. Smith *et al.*, PNAS, 2014. Zhang *et al.*, Nature Commun., 2019.
Gilteritinib	I	**FLT3 TKD mutations:** F691L, Y693C/N, G697S	**MAPK signaling (NRAS)**	McMahon *et al.*, Cancer Discov., 2019. Tarver *et al.*, Blood Adv., 2020.

Table 1: Summary of intrinsic mechanisms of resistance to FTL3 inhibitors. On-target mechanisms include secondary point mutations in FLT3[40, 137, 162, 165, 178-182]. Off-target mechanisms include bypass pathways that are activated in the setting of resistance[106, 137, 163, 164, 176, 177, 183-186].

Given that MAPK signaling is a common mode of resistance for FLT3 inhibitors, there is great interest in targeting this pathway, also known as the RAS-RAF-MEK-ERK pathway[187]. Hyperactivation of the MAPK pathway is seen in approximately 30-40% of human cancers, including ~70% of advanced melanoma that is driven by mutations in BRAF, NRAS, and NF1[188]. This pathway can be targeted at various levels from the most proximal member, RAS or the most distal member, ERK1/2. A major challenge in the successful deployment of MAPK inhibitors in combination with TKIs is toxicity and the precipitation of common side-effects of therapy[188]. However, this remains as an active area of research as new inhibitors are in development[189].

Extrinsic resistance mechanisms

Many studies[108, 190-194], including our own[96, 97, 106], have shown that the bone marrow microenvironment contributes significantly to the development of drug resistance in the setting of AML. Leukemia cells circulating in the peripheral blood are rapidly cleared by FLT3 inhibitors while leukemia cells within the microenvironment respond more slowly and a small number of leukemia cells persist despite treatment[104, 108, 195]. Survival of these residual cells leads to the development of resistance and eventual relapse[196, 197]. This tumor-permissive microenvironment consists of a collection of mesenchymal stromal cells, immune cells, and hematopoietic cells that signal to residual leukemia cells.

Marrow stromal cells produce a number of growth factors, cytokines, and adhesion molecules within the AML microenvironment that provide the necessary cues for leukemia cells to survive initial therapy and eventually become resistant[96, 106, 108, 190]. One such factor is FLT3 ligand (FL), which is secreted by stromal cells[198]. FL binds to the FLT3 receptor and in turn leads to restoration of FLT3 and downstream MAPK signaling, allowing FLT3 ITD AML cells to survive[199]. Addition of exogenous FL to leukemia cell lines *in vitro* protects cells and increases the IC_{50} for FLT3 inhibition[104]. In agreement with this model, FL expression also increases in patients treated with FLT3 inhibitors[104, 179]. Addition of a MAPK inhibitor is able to abrogate stromal-mediated resistance and restore sensitivity to quizartinib[104]. Other groups have found that AKT is also activated by marrow stromal cells. AKT inhibitors have been shown to have synergy with quizartinib and lead to increased cell death in FLT3 ITD+ cell lines such as MOLM14 and M4V-11, and overcomes the protective effects of bone marrow stromal cells *in vitro*[200].

Previous work from our laboratory has shown that fibroblast growth factor 2 (FGF2) is secreted by marrow stromal cells and can protect FLT3 ITD AML cells from quizartinib[106, 185] (**Figure 7**). Addition of FGF2 leads to increased survival of FLT3 ITD AML cell lines and primary cells *in vitro.* In patients treated with quizartinib, expression of FGF2 in marrow stromal cells increased

significantly during treatment and peaked just prior to resistance. FGF2 binds FGFR1 on AML cells, leading to downstream RAS/MAPK signaling and quizartinib resistance, which eventually leads to relapse. Combined inhibition of FLT3 and FGFR signaling overcame FGF2-mediated protection of these AML cells[106, 185]. In comparison to FL resistance, FGF2 activates an accessory pathway through FGFR for survival, yet both ligand-mediated resistance mechanisms converge on the downstream RAS/MAPK pathway to drive resistance. In a separate but similar finding, a genome-wide CRISPR screen identified that loss of SPRY3, an intracellular inhibitor of FGF signaling, and GSK3, a canonical Wnt signaling antagonist, can also induce quizartinib resistance[184]. Deletion of these genes in the FLT3 ITD AML cell line MV4-11, conferred quizartinib resistance as evidenced by increased cell viability and increased downstream RAS/MAPK and Wnt signaling[184]. These findings were further confirmed in quizartinib-resistant AML patient samples.

Although discussed separately, it should be noted that extrinsic and intrinsic resistance mechanisms are not distinct, but interrelated. As previously mentioned, AXL expression can be increased in AML cells during treatment with quizartinib through intrinsic and extrinsic mechanisms, and others have shown increased GAS6 expression in the marrow microenvironment (ligand for AXL) may also influence resistance[183]. Likewise, FL- or FGF2-mediated resistance to quizartinib can lead to acquisition of resistance mutations over time in FLT3-ITD AML cell lines and patients treated with quizartinib, suggesting that extrinsic mechanisms of resistance mediate early resistance, which then leads to acquisition and outgrowth of intrinsic resistance mutations[54]. In addition, further characterization of the unique features of the leukemia microenvironment may define targets in the microenvironment for future clinical trials. For example, the finding that increased FGF2 expression in leukemia stromal cells can be blocked by FGFR inhibitors suggests a strategy to target the leukemia-permissive microenvironment that protects leukemia cells[53].

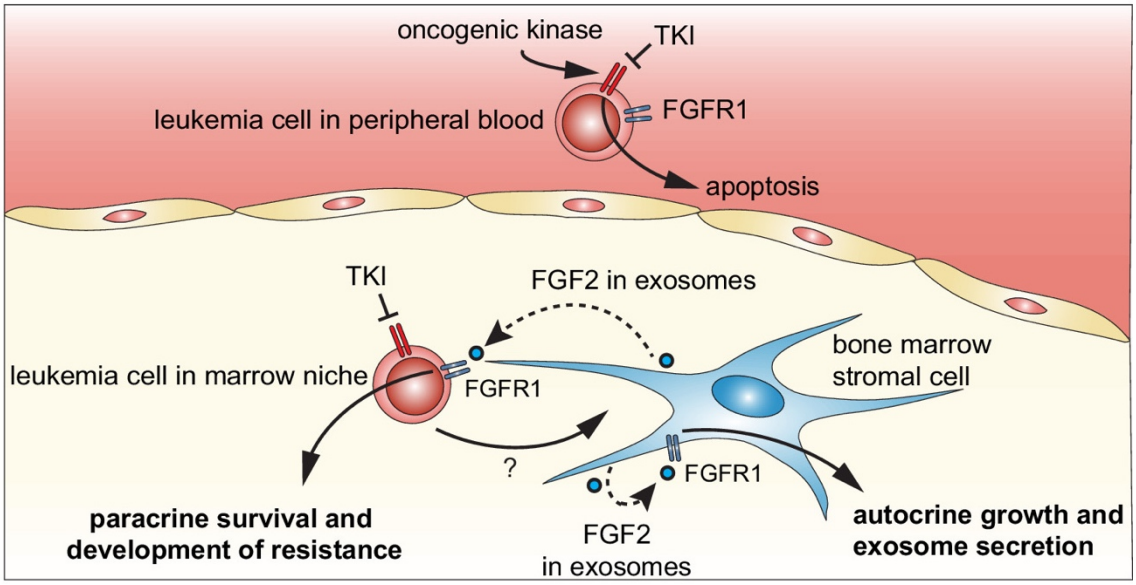

Figure 7: Model of bone marrow stromal FGF2 autocrine signaling and paracrine protection of leukemia cells by FGF2-containing exosomes[185]. This work is further discussed in Chapter 7 of this dissertation.

Reproduced with permission from Javidi-Sharifi N, Martinez J, English I, Joshi SK, Scopim-Ribeiro R, Viola SK, Edwards DK 5th, Agarwal A, Lopez C, Jorgens D, Tyner JW, Druker BJ, Traer E. FGF2-FGFR1 signaling regulates release of Leukemia-Protective exosomes from bone marrow stromal cells. Elife. 2019 Feb 5;8:e40033. doi: 10.7554/eLife.40033. Erratum in: Elife. 2019 Mar 29;8: PMID: 30720426; PMCID: PMC6363389.

Objective of dissertation

In part II of the dissertation focused on ***intrinsic*** activation of RTKs, I will discuss my findings on the discovery and characterization of novel NTRK, ERBB2, and FLT3 point mutations that enable oncogenic growth in leukemia. Given the resurgence of interest in Trk signaling owing to the development and approval of Trk inhibitors, in the beginning of part II, I discuss our current understanding of Trk activation in the setting of hematological malignancies and then discuss my findings. In part III focused on ***extrinsic*** activation, I will describe how protective factors secreted by marrow stromal cells promote oncogenic signaling in AML cells and confer resistance to the

FLT3 inhibitors quizartinib and gilteritinib. In part IV, I will summarize our major findings from the previous chapters, discuss themes and concepts that emerged from our work, and finally suggest future work.

PART II: *Intrinsic Activation of Trk, ErbB2, & FLT3 receptors*

Abstract

NTRK fusions are dominant oncogenic drivers found in rare solid tumors. These fusions have also been identified in more common cancers, such as lung and colorectal carcinomas, albeit at low frequencies. Patients harboring these fusions demonstrate significant clinical response to inhibitors such as entrectinib and larotrectinib. Although current trials have focused entirely on solid tumors, there is evidence supporting the use of these drugs for patients with leukemia. To assess the broader applicability for Trk inhibitors in hematological malignancies, this review describes the current state of knowledge about alterations in the NTRK family in these disorders. We present these findings in relation to the discovery and therapeutic targeting of BCR-ABL1 in chronic myeloid leukemia.

The advent of deep sequencing technologies has shown that NTRK fusions and somatic mutations are present in a variety of hematologic malignancies. Efficacy of Trk inhibitors has been demonstrated in NTRK-fusion positive human leukemia cell lines and patient-derived xenograft studies, highlighting the potential clinical utility of these inhibitors for a subset of leukemia patients.

Introduction

Advances in technologies from chromosomal banding to massively parallel sequencing have enabled the identification of oncogenic mutations, and enhanced our understanding of the biology contributing to malignant phenotypes. A seminal example is the identification of the BCR-ABL1 fusion protein in chronic myeloid leukemia (CML)[71-74]. Studies of BCR-ABL1 have not only shaped our understanding of the tumorigenic process but also provided insight into how cancer can be treated. The discovery and success of imatinib, the first FDA-approved tyrosine kinase inhibitor against BCR-ABL1, has revolutionized how we approach the treatment of cancer[124, 201]. Importantly, this paved the way for precision oncology, wherein development of selective, molecularly-guided therapeutic modalities have shown significant improvements in patient outcomes, as compared to non-selective chemotherapeutics. This principle has also been shown to be effective in the treatment of several solid and liquid tumors[202-204], underscoring the broad value of using drugs that precisely target cancer driving lesions.

Recently, the FDA granted accelerated approval to larotrectinib (also commonly referred to as LOXO-101 or Vitrakvi™), the first selective neurotrophic tyrosine receptor kinase (NTRK) inhibitor for patients of all ages with advanced solid tumors harboring NTRK gene fusions, regardless of tumor histology[205, 206]. The efficacy and safety profile of larotrectinib were confirmed in three independent trials with patients ranging from all ages (the youngest being a one-month-old)[206-208]. Interestingly, NTRK gene fusions occur at higher frequency (up to 90%) in patients with rare cancers, such as infantile fibrosarcoma, secretory breast carcinoma, mammary analogue secretory carcinoma, and cellular or mixed congenital mesoblastic nephroma, but are less prevalent in common adult tumors[82]. With an overall response rate of >75%, a median duration of response not reached following 18 months, and minimal adverse effects, larotrectinib's efficacy parallels that of imatinib, and marks another milestone for the field of precision oncology[207]. Even more recently, entrectinib, a pan-Trk, ROS1, ALK inhibitor also received accelerated FDA

approval[209]. Similar to imatinib, the approval of larotrectinib and entrectinib remind us of the importance of understanding the biological target as a stringently vetted response biomarker, and the need to continue screening for other actionable targets by harnessing the rapidly amassing 'omics data.

Moreover, with the approval of larotrectinib and entrectinib, the Trk family of cell surface tyrosine kinase receptors have drawn considerable attention. NTRK1, 2 and 3 genes encode TrkA, TrkB and TrkC receptors, respectively. These receptors signal through JAK/STAT, PI3K/AKT, and MEK/ERK to promote proliferation, differentiation, and survival[210, 211]. Although much of the literature has focused on the importance of these receptors in central and peripheral nervous system development and function[212], alterations in the NTRK family have been described in colon[213], thyroid[214, 215], lung[216], glial[217], and breast[218] cancers. These alterations are found at relatively low frequencies (<1%) within each of these individual solid tumors but collectively, when considering all tissues, NTRK-driven cancers constitute a significant number of patients, making them an important therapeutic target[216, 219-222]. Notably, NTRK fusions are pathognomonic for several rare solid tumor malignancies[218, 220, 223-227]. A number of excellent reviews have summarized recent work on Trk signaling in solid tumors[78, 82, 210, 228]. Despite the emerging success of NTRK inhibition in solid tumors, the role of these receptors in hematologic malignancies remains under investigated. Therefore, this review provides a comprehensive overview of our current understanding of NTRK-mediated tumorigenesis in hematological malignancies and links recent successes in NTRK-targeted therapy to historical milestones achieved by the targeting of BCR-ABL1 in CML.

NTRK receptor alterations and their role in cancer development

To date the BCR-ABL1 fusion remains the most prevalent mechanism of oncogenic ABL activation. In contrast activation of NTRK receptors can result from a wider range of molecular

events such as chromosomal rearrangements, deletions/truncations, point mutations, and changes in mRNA and protein expression. Among these mechanisms, oncofusions involving NTRK receptors are the most common mechanism of activation.

NTRK oncofusions

In 1986, shortly after the confirmation of BCR-ABL1 in CML[72], the first gene fusion involving an NTRK receptor was identified in a patient with colorectal cancer (**Figure 1**). This oncogenic translocation, TPM3-TRK, resulted from the fusion of the tropomyosin 3 gene amino terminus with the transmembrane and kinase domains of NTRK1[213], a finding that has since been confirmed[229]. Over the past few years, several NTRK fusions have been reported in solid tumors[78, 79, 228, 230].

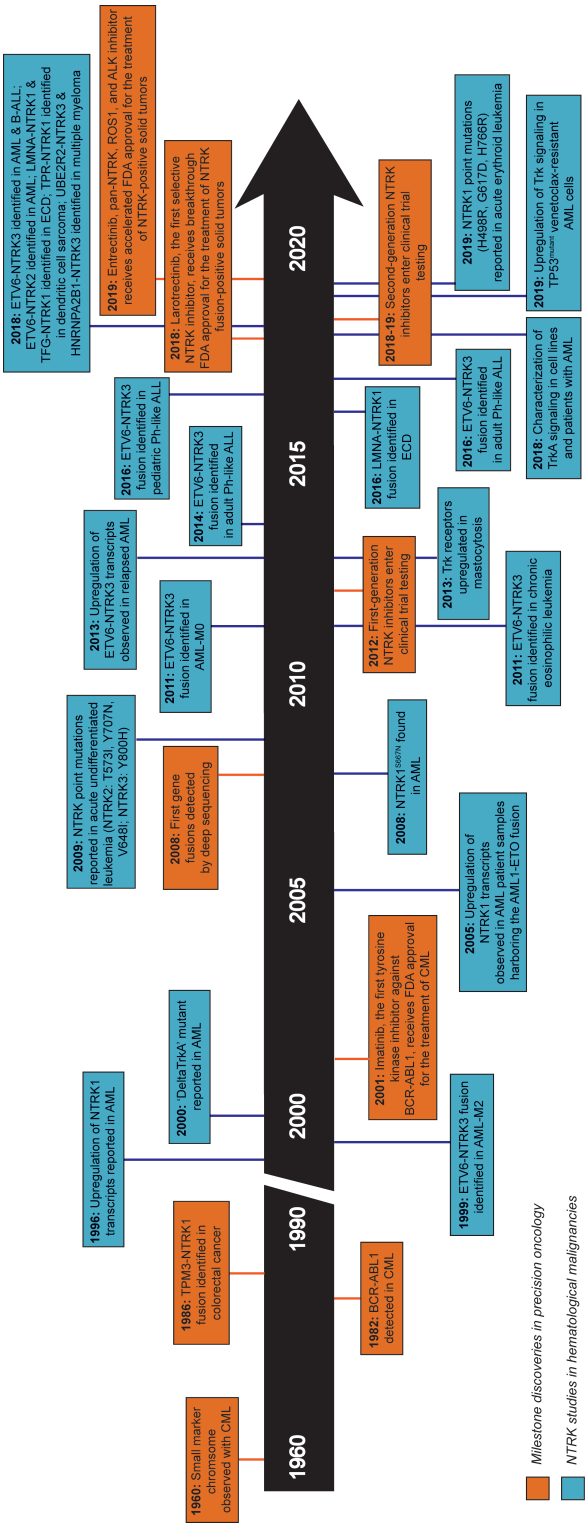

Figure 1: This timeline highlights the discovery of NTRK-related alterations in a variety of hematologic malignancies in relation to milestone studies that ushered an era of precision oncology. The growing number of NTRK alterations found in hematologic malignancies over the years suggests that these alterations have profound clinical implications that warrant further investigation.

Many of these Trk fusions involve the transcription factor, E26 transformation-specific variant 6 (ETV6, also known as TEL) located on chromosome 12p13. Specifically, ETV6-NTRK3 fusions (EN; t(12;15) (p13;q25)) have been previously characterized in the setting of secretory breast carcinoma[218, 231], congenital fibrosarcoma[232], thyroid carcinoma[233], and pontine gliomas[217]. Interestingly, the EN fusion is the first oncogenic fusion to be identified in cancers that are derived from all three cell lineages[228]. In the most common version of the EN fusion, the amino terminus of the ETV6 transcription factor, containing the helix-loop-helix (HLH) domain (exons 1-5; also commonly referred to as the sterile alpha motif (SAM) or pointed (PNT) domain), fuses with the kinase domain of the partnering protein resulting in constitutive kinase activity[234, 235]. The ETV6 HLH domain has been shown to be essential for mediating protein activity of the EN fusion. Its deletion results in the loss of dimer formation and ability to transform mutant cells[236]. Substituting the ETV6 HLH domain with an inducible FK506 binding protein (FKBP) dimerization domain does not inhibit catalytic activation of the fusion, but abrogates its transformative capacity. These data suggested that the ETV6 HLH domain provides specific signaling or polymerization capabilities required for full activation of the fusion protein[237-239].

Although other, non-NTRK ETV6-based fusions have been long reported to play a role in leukemogenesis[234, 240-243], an EN fusion was first reported in 1999 by Eguchi *et al.*[244, 245] in a 59-year-old female with AML-M2 using fluorescence in situ hybridization (FISH, **Figure 1**). They identified two variants of the fusion with FISH (**Figure 2A**). In each case, exons 1-4 of the ETV6 HLH domain were fused in-frame with exons 13-18 of NTRK3 that encoded the protein-tyrosine kinase (PTK) domain. These fusions differed from the EN fusions described in solid tumors as only the first four exons of ETV6 were fused with the kinase domain of NTRK3. Moreover, one fusion included the entire PTK domain (encoding a 52 kD protein) while the other variant involved a truncated PTK domain (encoding a 38 kD protein). However, both of these chimeric proteins lack a 42-base-pair exon near the C-terminus of the NTRK3 protein that was reported thereafter in the EN oncofusion found in cases of congenital fibrosarcoma[244].

In addition to the 42-base-pair stretch, the fusion found in congenital fibrosarcoma contains ETV6 exons 1-5 versus 1-4 that are seen in EN fusions found in AML. When these differing EN fusions (± ETV6 exon 5) were expressed in mice, only the variant without exon 5 produced leukemia, suggesting the importance of the ETV6 exon number in determining the disease phenotype[246].

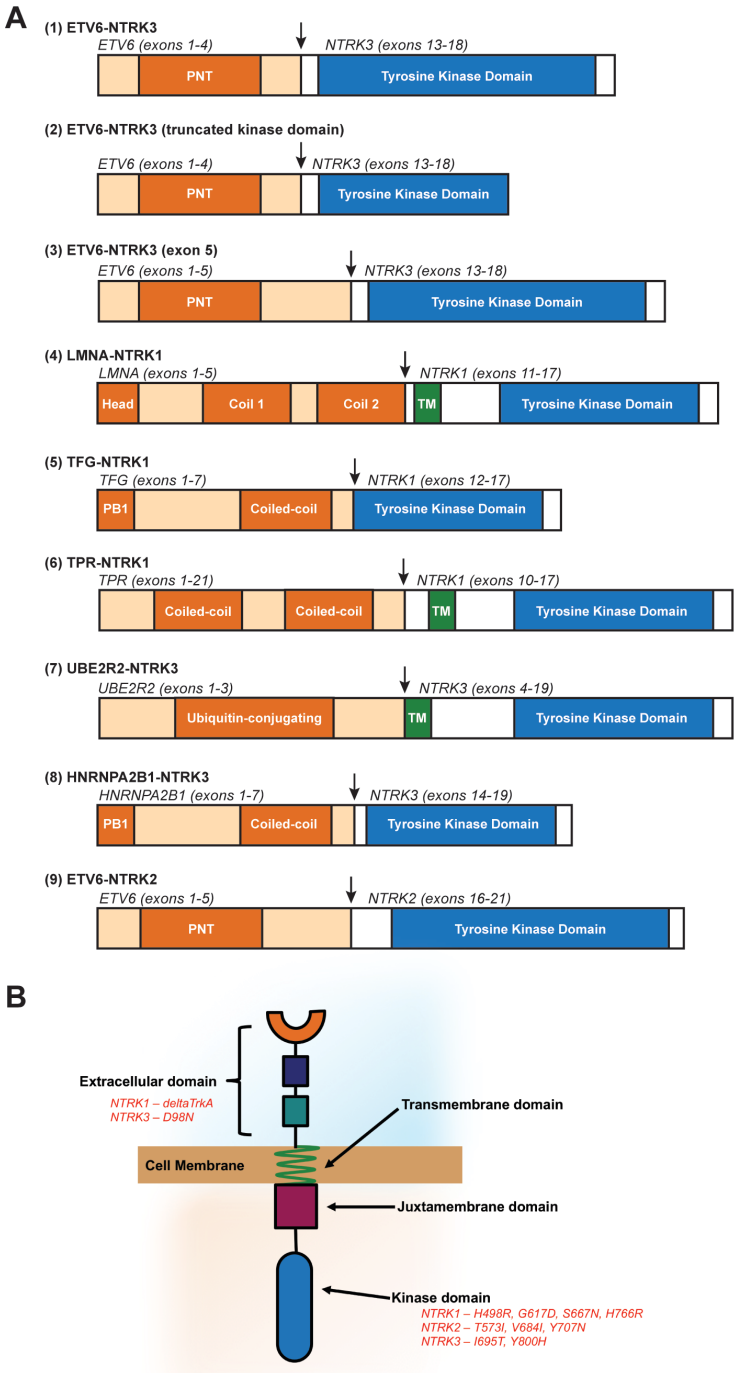

Figure 2: A. Diagram of the unique Trk fusions identified in various hematological malignancies[244, 247, 248]. For each fusion, the carboxy-terminal kinase domain of the Trk protein is fused in-frame with the upstream amino-terminal binding partner. All relevant domains that contribute to the final chimeric fusion are shown. Vertical arrows indicate the breakpoint. PNT, pointed domain; TM, transmembrane domain. Fusions are numbered in the order they are discussed throughout the text. **B.** Representative Trk receptor indicating location of known deletions[28] and point mutations[249-251].

Differences in structural make-up of these EN oncofusions may also affect downstream signaling. Subsequent mechanistic studies described that the peptide encoded by the 42-base-pair moiety decreases tyrosine kinase activity and impairs downstream signaling mediated by SHC and PLCγ[252, 253]. In other words, robust kinase activity and signaling through PLCγ was observed only in the setting of AML, resulting from the EN fusion. These data suggest a necessary role for activation of PLC-regulated pathways, including protein kinase C and/or calcium flux mediated signaling, in myeloid leukemogenesis.

Twelve years after the first report of EN in AML, the EN fusion was identified in an 82-year-old female who developed chronic eosinophilic leukemia following pancreatic carcinoma[254]. That same year, a different variant of the EN fusion transcript was identified in a 55-year-old male patient with AML-M0 [247]. Analysis of this variant suggested that the first five exons of ETV6 fused with the kinase domain of NTRK3 (**Figure 2A**). This was in contrast to the oncofusion described by Eguchi *et al.*[244], where only the first four exons of ETV6 were fused to NTRK3.

In studying samples from patients with AML, Pemovska *et al.* (2013) saw an abundant EN transcript in a 37-year-old AML patient with a recurrent t(11;19)(q23;p13.1) translocation corresponding to the MLL-ELL fusion gene[255]. This patient had relapsed from three previous rounds of conventional chemotherapy. While a decrease in bone marrow blast count following treatment with dasatinib, sunitinib, and temsirolimus was observed, this response was short-lived. Resistance had developed due to the upregulation of EN and STRN-ALK fusions, which provided these tumor cells a bypass mechanism to evade death[255].

In 2014, Roberts *et al.* were the first to describe the EN fusion in a case of Philadelphia chromosome-like Acute Lymphoblastic Leukemia (Ph-like ALL) through genomic analyses[256]. They went on to characterize this fusion via a conditional knock-in mouse model, and noted the development of aggressive lymphoid leukemia with complete penetrance and a median latency of 38 days, recapitulating human B-ALL[257]. Treatment with PLX7486 or larotrectinib for twelve weeks decreased tumor burden and splenic weight.

Another case of the EN fusion in adult Ph-like ALL has also been reported [258]. After performing cytogenetic, FISH, and whole-genome single-nucleotide polymorphism (SNP) analysis on 60 ALL cases, an EN fusion was identified in a 9-year-old boy with B-ALL[259]. SNP analysis revealed a breakpoint within intron 5 of ETV6 that fused with the breakpoint in the C-terminal of NTRK3, resulting in the formation of the EN oncofusion. Interestingly, their finding contradicts an earlier report from Alessandri *et al.* (2001) who found the presence of no EN transcripts in pediatric AML and ALL patients via qPCR analysis[260]. However, this discrepancy could suggest the need for a more integrative approach when screening for the presence of such fusions.

Apart from EN fusions, in recent years other NTRK fusions have been described and functionally evaluated in hematological malignancies. An LMNA-NTRK1 fusion was identified in a 27-year-old patient with Erdheim-Chester disease (ECD, **Figure 2A**)[261]. This fusion resulted in the activation of MAPK and PI3K/AKT signaling. In addition to the LMNA-NTRK1 and EN fusions, other NTRK fusions in patients with ECD, AML, and multiple myeloma were recently reported[248].

Specifically, after performing targeted RNA sequencing on 7,311 patients with hematologic malignancies, Taylor *et al.* discovered eight patients harboring NTRK oncofusions[248] (**Figure 2A**). They identified a TFG-NTRK1 fusion in a 2-month-old patient with ECD, a TPR-NTRK1 fusion in a 20-year-old patient with interdigitating dendritic cell sarcoma, and UBE2R2-NTRK3 and HNRNPA2B1-NTRK3 fusions in 53- and 76-year-old patients with multiple myeloma. Between the two fusions discovered in multiple myeloma, only the UBE2R2-NTRK3 fusion was able to transform Ba/F3 cells. This could result from the differing number of NTRK3 exons present in the final oncofusion. Regardless of transformation capacity, all fusions identified were sensitive to Trk inhibition as assessed via mouse colony formation and cell viability assays.

In the same study, they also identified a previously unreported NTRK2 fusion (ETV6-NTRK2) in a 77-year-old male with AML and studied its transforming potential and downstream signaling

in a cytokine-dependent murine hematopoietic cell line (Ba/F3 cells) and in a patient-derived xenograft model[248] (**Figure 2A**). This fusion demonstrated robust PI3K-AKT signaling that was attenuated upon treatment with larotrectinib both *in vitro* and *in vivo*. Surprisingly, this patient also had a co-occurring KRAS Q61P mutation. The presence of co-occurring mutations with driver tyrosine kinase alterations has rarely been reported[262, 263]. Nonetheless, this scenario warrants that co-occurring mutations with NTRK alterations should be considered as they may pose a resistance liability and limit durability of the response.

A recent study investigating the contribution of NTRK fusions in neuroendocrine tumors reported six cases, originating from various anatomic sites that include the pancreas, uterus, and lung[263]. Interestingly, in three patients, the NTRK fragment was 5' to its fusion partner. Although it is unusual for NTRK to be the upstream binding partner, this finding potentially implicates an unknown function of the 5' region of NTRK that should be further studied. Thus far, no such NTRK fusions have been described in hematological malignancies.

While there was a lag in the identification of NTRK fusions in hematologic malignancies since the first case reported by Eguchi *et al.,*[244] the advent of deep sequencing technologies[264] in 2008 accelerated the detection of such fusions (**Figure 1**). In fact, due to such technological advances, we have learned that NTRK fusions (and that of orthologues, ROS1 and ALK), irrespective of tumor histology, are more common than previously speculated[79].

Deletions & truncations

A deleted form of NTRK1 (named 'deltaTrkA') that lacks 75 amino acids in the extracellular domain (including the ligand-binding Ig2 domain) and four glycosylation sites adjacent to the transmembrane domain was reported in 2000 in an AML patient[28] (**Figure 2B**). The in-frame deletion of these amino acids resulted in constitutive tyrosine kinase activity. This aberrant activity could partly be explained by the loss of glycosylation, which is known to inhibit kinase activity in

TrkA[265] and by the loss of cysteine residues that affect the overall tertiary structure of the receptor[266]. Expression of deltaTrkA in cells resulted in activation of Ras/MAPK and PI3K/AKT signaling and transformation of fibroblasts, epithelial, and myeloid cells *in vitro*[28]. A later study reported that mice transplanted with myeloid 32D cells engineered to express deltaTrkA developed polyclonal AML that was mediated by PI3K and mTOR-raptor signaling[267].

These initial studies with deltaTrkA suggested that the extracellular domain contained a 'regulatory switch' that, when lost, resulted in constitutive kinase activation. Parallel studies in other tumor models also validated the regulatory function of the extracellular domain (i.e., Ig1 and 2 subdomains) in preventing spontaneous dimerization and kinase activation[268, 269]. Specifically, deletion of exons 6, 7, and 9 and of the functional IG-C1 and N-glycosylation subdomains of TrkA, resulting in TrkAIII splice variant, promoted neuroblastoma[270].

The importance of the extracellular domain in serving as a mediator of Trk activation could also explain why constitutive kinase activity is seen with Trk oncofusions. It may be the case that loss of the extracellular domain (that encompasses the autoinhibitory subdomains) in addition to the HLH domain[239] of the upstream binding partner enables constitutive kinase activation.

Point mutations

After performing high-throughput resequencing of the kinase domain of 26 tyrosine kinase genes, a mutation in the kinase domain of NTRK1^{S667N} was reported in four patients with AML of 188 tested[249] (**Figure 2B**). A year later, sequencing of leukemic cells in another study revealed four novel previously unreported point mutations in NTRK receptors of four patients (NTRK2: T573I, V684I, and Y707N; NTRK3: Y800H)[250]. Point mutations in the NTRK3 receptor—D98N and I695T—have also been reported in patients with B-cell lymphoma and myeloid leukemia, respectively (The Cancer Genome Atlas). Functional characterization of the aforementioned point mutations has yet to be reported.

More recently, NTRK1 point mutations were observed in three patients with acute erythroid leukemia (AEL) from a cohort of 159 patients that were sequenced[251]. These mutations—H498R, G617D, and H766R—were located in the kinase domain of the receptor. To assess the leukemogenic potential of these NTRK1 mutations, wildtype and mutated NTRK1 were expressed in lineage-negative hematopoietic stem and progenitor cells from wildtype or TP53 mutated mice. The co-expression of mutated NTRK1$^{H498R/\ G617D/H766R}$ with TP53^{R172H} culminated in an extremely penetrant form of erythroid leukemia[251]. However, a single NTRK1 mutation in the absence of mutated TP53 had no effect on the overall survival of these animals. Likewise, a single TP53 mutation resulted in a mild form of disease, implicating that the co-occurrence of TP53 and NTRK1 mutations explains the underlying oncogenicity.

Changes in mRNA and protein expression

In 1996, Kaebisch *et al.* reported the association of Trk expression and leukemia[271]. After evaluating gene expression in 59 patients with acute myeloid leukemia (AML), they observed up-regulation of NTRK1 transcripts in 44% of the patients in the cohort. Following this initial study, a series of studies reported a role of Trk receptors and their respective ligands in various stages of hematopoiesis[272, 273]. Trk receptors promote proliferation and survival of erythroblasts, dendritic cells, lymphocytes, monocytes, and macrophages[274]. Specifically, NTRK2 is highly expressed in immature thymocytes and its expression progressively declines throughout the T cell maturation process[275]. Despite these studies, the functional role of Trk receptors in hematopoiesis is not completely understood.

Since then, many studies have reported overexpression of NTRK receptors in a variety of hematological malignancies. Overexpression of NTRK1 was observed in AML patient samples harboring the AML1-ETO fusion protein, generated by t(8;21)[276]. While it is uncertain what provides these AML1-ETO-expressing leukemia cells a growth advantage, one hypothesis is their

crosstalk with bone marrow stromal cells that express nerve growth factor (NGF). NGF binds to its cognate receptor, TrkA and may therefore drive leukemia.

In a prospective study of 94 adult patients with de novo or secondary AML, acute lymphoblastic leukemia (ALL), or acute undifferentiated leukemia, expression of at least one NTRK receptor was seen in 55% of the analyzed cases[250]. While coexpression of two or more NTRK receptors was observed on AML blasts, ALL blasts exclusively expressed NTRK2.

After mining large publicly available datasets (e.g., Microarray Innovations in Leukemia (MILE) study), Herbrich *et al.* (2018) reported that expression of NTRK1 was significantly higher in a combined group of 456 patients with AML when compared to normal $CD34^+$ bone marrow cells[277]. Separating AML samples by cytogenetic subtypes, they saw the highest expression of NTRK1 mRNA in patients with t(8;21) and inv(16)/t(16;16). The increase in NTRK1 mRNA that they observed in patients with t(8;21) was in line with Mulloy *et al.*, who observed a similar trend after analyzing 262 primary AML patient samples[276].

Recent work from our laboratory has uncovered a critical dependency on Trk signaling in $TP53^{mutant}$ venetoclax-resistant AML cells[145]. To identify essential target genes and pathways contributing to venetoclax resistance in AML, we performed a genome-wide CRISPR/Cas9 screen on a patient-derived AML cell line. We identified TP53, BAX, and PMAIP1 as key genes whose inactivation conferred resistance to venetoclax. Moreover, TP53 knockout cells were found to gain sensitivity to a panel of Trk inhibitors, suggesting a dependency on Trk-mediated activation for the survival of TP53 mutant cells. We saw a similar correlation in TP53-mutant AML patient samples. Our findings were in line with the work of Iacobucci *et al.* who recently demonstrated that the co-occurrence of NTRK1 and TP53 mutations promoted the development of an aggressive erythroid leukemia[251]. Our collective findings highlight a new potential clinical utility of Trk inhibitors in leukemia harboring TP53 mutations.

Up-regulation of the Trk receptors has also been reported in mastocytosis, a subcategory of myeloid neoplasms. Peng *et al.* (2013) were the first to show elevated expression of TrkB and

TrkC receptors on the mast cells of patients with mastocytosis[278]. Thereafter, Yang *et al.* (2014) demonstrated that activation of TrkB by BDNF in murine hematopoietic stem and progenitor cells induces a disease phenotype that mimics the clinical presentation of mastocytosis[279]. More recently, they showed that activation of the TrkA receptor triggers the onset of mastocytosis in mice and confers drug resistance[280].

While NTRK receptors can be activated via multiple mechanisms, proliferation and survival of cells harboring NTRK alterations is dependent on similar downstream signaling cascades as those activated by BCR-ABL1 in CML (i.e., MAPK, PI3K/AKT, and JAK/STAT)[211, 218, 223, 277, 281-283]. Such patterns of signaling contribute to the observed phenotype.

NTRK and EN fusion expressing cell line models

Despite the identification of NTRK mutations and fusions in leukemic patients, there are a limited number of cell culture models available to study the role of Trk receptors in leukemogenesis and validate potential inhibitors. Based on mRNA and protein expression analysis, Kaebisch *et al.* (1996) reported that the following myeloid leukemia cell lines—HEL, K562, and KG-1—expressed NTRK3[271]. Moreover, they found that treating the human promyelocytic cell line, HL-60, with tetradecanoylphorbol 13-actetate induced expression of NTRK3 in these cells. After performing a comprehensive and systematic review of TrkA signaling in leukemia, another study has identified 11 cell lines that have detectable levels of NTRK1 transcripts[277]. The highest expression was observed in megakaryoblastic (i.e., CMK), erythroleukemic (i.e., TF-1), and chronic myeloid leukemia (i.e., K562) cell lines[277].

Three main AML cell lines have been cited in the literature to study EN fusions: IMS-M2, M0-91, and AP-1060[244, 284, 285]. Bone marrow cells taken from an EN-positive AML-M2 patient gave rise to the IMS-M2 cell line[244]. After screening over 40 AML cell lines with mass spectrometry and sequencing, Gu *et al.* (2007) identified M0-91 as an EN-expressing cell line with

increased phosphorylation of TrkB and TrkC. siRNA-mediated knockdown of the EN fusion in these cells decreased their growth and viability, suggesting that the EN fusion was essential for the growth and survival of M0-91 cells[284]. Treatment of M0-91 cells with an IGF1R inhibitor also promotes degradation of the endogenous fusion protein[286]. These results suggest that the M0-91 EN fusion possesses signaling and regulatory properties similar to those observed in other engineered cell line models. Using genomic and transcriptomic microarray-based profiling, Chen *et al.* (2018) have recently shown the presence of the EN fusion in an acute promyelocytic leukemia (APML) cell line, called AP-1060[285].

NTRK inhibition in hematological malignancies

The discovery of imatinib for the treatment of CML has shifted the paradigm of cancer treatment towards precision oncology[13, 14, 201]. It was the first small-molecule protein-kinase inhibitor that was designed to target a specific kinase fusion, BCR-ABL1. Its success has paved the way for development of other kinase-specific inhibitors and curtailed the use of empiric chemotherapy for CML patients. Among these inhibitors, Trk inhibitors have attracted considerable attention over the past few years owing to their remarkable efficacy in patients harboring NTRK fusions in early clinical trials[207, 221]. As mentioned earlier, the presence of the EN fusion is pathognomonic for several rare solid tumor malignancies[218, 220, 223-225], further underscoring the need for Trk inhibitors. Despite the rarity of NTRK-mediated clinical cases reported in leukemias, the positive clinical evidence observed in solid tumors provides an impetus to investigate the efficacy of such inhibitors in these tumors. The available preclinical and clinical studies that have investigated the potency of these inhibitors in hematologic malignancies are summarized below (**Table 1**).

Table 1 - Summary of inhibitors targeting NTRK in hematological malignancies			
Drug Name	**Malignancy**	**PMID**	**Publication Year**
AG-879	AML	19059881	2009
AZ-23	APML	29119387	2018
AZD-1480	AML	31048320	2019
Belizatinib (TSR-011)	AML	29237803	2017
BMS-754807	AML	24056683	2013
		29903916	2018
Crizotinib	AML	23811600	2013
	Ph-like B-ALL	25207766	2014
	AML	29237803	2017
	Ph-like B-ALL	29880614	2018
	AML	31048320	2019
Entrectinib	Mastocytosis	29088753	2017
	AML	29237803	2017
	AML	31048320	2019
Foretinib	AML	31048320	2019
GW-2580	AML	31048320	2019
K252a	AML	19059881	2009
Larotrectinib	Ph-like B-ALL	29880614	2018
	AML	29920189	2018
	AML	29920189	2018
	ECD	29920189	2018
	Multiple Myeloma	29920189	2018
	Multiple Myeloma	29920189	2018
	AEL	30926971	2019
	AML	31048320	2019
Midostaurin (PKC412)	AML	23131561	2012
PLX7486	Ph-like B-ALL	29880614	2018

Table 1: This table provides a summary of inhibitors targeting NTRK receptors in hematological malignancies that have been investigated in pre-clinical and clinical studies.

In 2009, Li *et al.* evaluated apoptosis in cultured leukemic cells obtained from four patients with AML[250]. These cells were exposed for approximately 18 hours to varying concentrations (100-400 nM) of K252a, a previously validated non-selective Trk inhibitor (indolocarbazole analogue)[287], resulting in a 65% reduction of viable cells and dephosphorylation of NTRK

receptors. Using an AML patient-derived mouse xenograft, they also saw enhanced survival of mice following treatment with AG879, a TrkA inhibitor[250].

Minimal response to standard chemotherapy seen in two AML patients[245, 247] harboring the EN fusion prompted Chi *et al.* (2012) to consider evaluating midostaurin, a broad spectrum kinase inhibitor[288-290]. Treatment with 100 nM of midostaurin inhibited EN activity in AML cell lines (i.e., IMS-M2, M0-91) carrying the fusion and Ba/F3 cells stably expressing the fusion. Following eight hours of treatment, phosphorylation of STAT5, AKT, and MAPK was suppressed and apoptosis was induced. This was the first study to show that small-molecule kinase inhibitors could serve as a promising avenue to treat NTRK-driven leukemias.

Although initially approved against ALK fusions in patients with non-small cell lung cancer (NSCLC)[291], crizotinib, another small-molecule kinase inhibitor was evaluated on NTRK-mediated cancers with the first case being a patient with NSCLC harboring the MPRIP-NTRK1 fusion[216]. When tested on IMS-M2 and M0-91 AML cell lines, crizotinib blocked proliferation of EN-dependent tumor cells, decreased phosphorylation of downstream signaling, and impacted growth of tumor xenografts[292]. Three additional inhibitors (imatinib, ponatinib, and NVP-TAE684) were also considered but only crizotinib demonstrated nanomolar potency in the cell-based assay.

Similarly, the EN fusion of a patient with Ph-like ALL was sensitive to crizotinib[256]. This study also assessed the efficacy of crizotinib in a xenograft model in which EN^+ cells from the Ph-like ALL patient were engrafted into immunodeficient mice. *Ex vivo* cytotoxicity assay data from these mice showed sensitivity to crizotinib whereas imatinib had no effect.

In another case, a 37-year-old relapsed-AML patient with an abundance of EN transcripts was sensitive to BMS-754807, an IGF-IR/TrkC inhibitor[255]. This inhibitor was also effective in blocking EN-mediated transformation in cell lines models[293] as well as inhibiting viability of M0-91 cells[286]. Interestingly, an EN fusion found within a cell culture model of acute promyelocytic leukemia,[285] a subtype of AML, was hypersensitive to AZ-23, a selective NTRK inhibitor that has been previously validated in a Trk-expressing xenograft model of neuroblastoma[294].

Results from basket trials performed on entrectinib (RXDX-101), a selective pan-Trk, ROS1, and ALK inhibitor have garnered much attention. Entrectinib demonstrated robust antitumor activity across a broad range of solid tumors regardless of histology[221, 295]. It was well tolerated, with mainly Grade 1 and 2 adverse events that were reversible with dose modification. Given entrectinib's therapeutic profile, Yang *et al.* (2017) showed that treatment with entrectinib decreased activation of TrkA in mast cell lines (HMC-1, HMC-1.2), primary mast cells from patients with systemic mastocytosis, and in mice xenotransplanted with HMC-1 cells. Moreover, they showed that inhibition of Trk signaling via entrectinib restored sensitivity to KIT inhibition in their *in vitro* and *in vivo* studies[280].

Another study reported that entrectinib inhibited cell proliferation, at sub-nanomolar concentrations, of IMS-M2 and M0-91 cells (0.47 and 0.65 nM, respectively) and induced apoptosis[296]. Entrectinib was 6 to 158-fold more potent than other tested Trk inhibitors (i.e., crizotinib, larotrectinib, and belizatinib (TSR-011)). Phosphorylation of the EN fusion and downstream signaling mediators was inhibited by entrectinib in a dose-dependent manner. Lastly, in animal models (mice and zebrafish), entrectinib treatment resulted in tumor regression. In August 2019, entrectinib received accelerated FDA approval for adults and pediatric patients with solid tumors harboring NTRK mutations[209].

Likewise, in a cohort of 17 tumor types, larotrectinib, the most selective pan-Trk inhibitor, blocked Trk signaling with an overall response rate of 80% in patients. Based on these data, in November 2018 larotrectinib received Breakthrough Therapy FDA approval for adult and pediatric patients with solid tumors bearing NTRK fusions[207]. Given the efficacy of larotrectinib in solid tumors, its ability to inhibit the EN fusion in a murine xenograft model of Ph-like B-ALL and Ba/F3 cell assay was evaluated[257]. In all cases, treatment with larotrectinib reduced the tumor burden, splenic weight, and decreased phosphorylation of ERK1/2, STAT3, and STAT5 with robust response seen following 24 hours. Similar trends were seen with PLX7486, a NTRK, CSF1R, and AURK inhibitor. However, larotrectinib was much more efficacious. In comparison to crizotinib,

within their Ba/F3-EN model, larotrectinib was approximately 12 times more potent (17 nM vs. 205 nM, respectively)[257].

Taylor *et al.* (2018) also evaluated larotrectinib's activity on Trk fusions found in patients with AML, histiocytosis, and multiple myeloma in a cell-based proliferation assay and on an AML patient-derived xenograft containing ETV6-NTRK2 cells. In all cases, larotrectinib reduced expression and Trk activity[248]. Based upon the xenograft model results, larotrectinib was given twice daily to a 77-year-old man with refractory secondary AML possessing an ETV6-NTRK2 fusion. The patient achieved a partial remission with changes in ETV6-NTRK2 fusion abundance mirroring clinical response[248]. Although these results are from a single case report, they suggest a potential clinical utility of Trk inhibition in hematological malignancies harboring Trk fusions and highlight a previously unrecognized role of the ETV6-NTRK2 fusion. Due to the inherent differences in biology between solid and liquid tumors, a tailored basket trial or other unique clinical trial designs may be required specifically for Trk fusion positive leukemias and lymphomas.

Our recent work in a venetoclax-resistant cell line model system uncovered a role for NTRK in TP53 null cells[145]. TP53 knockout cell lines were found to be highly sensitive to a number of Trk inhibitors such as entrectinib, larotrectinib, GW-2580, crizotinib, AZD 1480, and foretinib. These results, along with confirmatory western blots in cell lines and primary patient samples identified upregulation of Trk protein in the context of TP53 loss of function and a concomitant gain of sensitivity to Trk inhibitors. Similar to our work, mice harboring NTRK1 and TP53 co-mutations developed a highly aggressive erythroid leukemia that was very responsive to larotrectinib, further highlighting the relevance of Trk inhibitors for clinical trials in patients with hematological malignancies[251].

Apart from the aforementioned inhibitors, many others have been validated in solid tumors bearing NTRK fusions or mutations. These include cabozantinib[297], foretinib[297], merestinib[298], and nintedanib[297] among others. Moreover, IGF1R/IR pathway inhibitors, in particular, have shown to

be effective at blocking EN activity by initiating a process that results in the ubiquitylation and proteasomal degradation of the fusion protein itself[286].

Amino acid substitutions involving the solvent front, activation loop DFG motif, or gatekeeper residues have conferred resistance to a variety of tyrosine kinase inhibitors[299-301]. In CML, the classic gatekeeper mutation, BCR-ABL^{T315I} interferes with imatinib's ability to bind the ABL kinase, rendering it ineffective[281, 300]. Similar mechanisms of resistance have been recently reported for entrectinib and larotrectinib in the setting of colorectal[302] and MASC[220] tumors. As such, second generation NTRK inhibitors that overcome this acquired resistance are currently in development. These inhibitors include LOXO-195[303] and repotrectinib (TPX-0005)[304]. Advancements in molecular profiling and the occurrence of NTRK mutations in liquid tumors, calls for the validation of these inhibitors in hematologic malignancies.

Conclusion

The success of imatinib not only improved the prognosis for patients with CML but ushered an era of precision oncology—where knowledge of the underlying biology is key to efficient drug development. Though Trk oncofusions were among the first oncogenes to be identified following BCR-ABL1, they often went unnoticed due to their low prevalence among various solid cancers. However, this is no longer the case. Recent advances in deep sequencing technologies and immunohistochemical techniques provide promising avenues to identify Trk alterations[207, 221, 305, 306]. In many ways, such methods have negated the notion that alterations in Trk receptors are uncommon. Mechanistic studies have further shown the importance of Trk signaling in driving leukemia. The success of early clinical trials with larotrectinib and entrectinib as well as the different studies discussed above suggest that oncogenic Trk aberrations are amenable to targeted inhibition and hold the promise of providing clinical benefit in a variety of hematologic malignancies. While it is difficult to predict the efficacy of Trk inhibition in patients, our work, and

that of others provide a rationale for the need to initiate trials focused on Trk inhibition in liquid tumors.

Acknowledgements

We apologize to all the authors whose work could not be included in this manuscript owing to space constraints.

4 *Discovery and characterization of targetable NTRK point mutations in hematologic neoplasms*

Sunil K. Joshi, Kristin Qian, William H. Bisson, Kevin Watanabe-Smith, Ariane Huang, Daniel Bottomly, Elie Traer, Jeffrey W. Tyner, Shannon K. McWeeney, Monika A. Davare, Brian J. Druker, Cristina E. Tognon

This manuscript was published in *Blood*, Volume 135(24), Pages 2159-2170, June 11, 2020. https://doi.org/10.1182/blood.2019003691

Key Points

We identified and characterized four oncogenic NTRK point mutations in patients with hematologic neoplasms that are amenable to FDA-approved Trk inhibitors.

Abstract

Much of what is known about the neurotrophic receptor tyrosine kinase (NTRK) genes in cancer is through the identification and characterization of activating Trk fusions across many tumor types. A resurgence of interest in these receptors has emerged owing to the realization that they are promising therapeutic targets. The remarkable efficacy of the pan-Trk inhibitors, larotrectinib and entrectinib, in clinical trials led to their accelerated, tissue agnostic FDA approval for adult and pediatric patients with Trk-driven solid tumors. Despite our enhanced understanding of Trk biology in solid tumors, the importance of Trk signaling in hematological malignancies is underexplored and warrants further investigation. Herein, we describe mutations in NTRK2 and NTRK3 that were identified via deep sequencing of 185 patients with hematological malignancies. Ten patients contained a point mutation in NTRK2 or NTRK3. Among these patients, we identified nine unique point mutations. Of these nine mutations, four were oncogenic—NTRK2^{A203T}, NTRK2^{R458G}, NTRK3^{E176D}, and NTRK3^{L449F}—as determined via cytokine-independent cellular assays. Our data demonstrate that these mutations have transformative potential to promote downstream survival signaling and leukemogenesis. Specifically, the three mutations located within the extracellular (i.e., NTRK2^{A203T} and NTRK3^{E176D}) and transmembrane (i.e., NTRK3^{L449F}) domains increased receptor dimerization and cell-surface abundance. The fourth mutation, NTRK2^{R458G}, residing in the juxtamembrane domain, activates TrkB via non-canonical mechanisms that may involve altered interactions between the mutant receptor and lipids in the surrounding environment. Importantly, these four activating mutations can be clinically targeted

using entrectinib. Our findings contribute to ongoing efforts focused on defining the mutational landscape that drives hematological malignancies and underscore the utility of FDA-approved Trk inhibitors for patients with aggressive Trk-driven leukemias.

Introduction

The neurotrophic receptor tyrosine kinases (NTRKs) are a family of genes—NTRK1, NTRK2, and NTRK3—that encode TrkA, TrkB, and TrkC receptors, respectively[210]. These surface receptors consist of an extracellular domain for ligand binding, a single-pass transmembrane domain, and intracellular juxtamembrane and kinase domains. Upon ligand binding, these receptors homodimerize, which in turn leads to trans-phosphorylation of key tyrosine residues in the intracellular domain that further activate several downstream pathways including JAK/STAT, PI3K/AKT, and RAS/MAPK to promote proliferation, differentiation, and survival[228].

Apart from the seminal role these receptors play in the central and peripheral nervous system[307-311], oncofusions containing NTRKs have been implicated in pediatric and adult cancers, with the first fusion (i.e., TPM3-NTRK1) reported in 1986 in a patient with colorectal cancer[210, 213, 228, 312]. Since then, fusions with NTRKs have been identified and characterized in many solid tumors, including congenital fibrosarcoma[232], secretory breast carcinoma[218], papillary thyroid carcinoma[214], and glioblastoma[217] among others[79]. The resultant chimeric Trk oncoproteins promote ectopic expression and constitutive kinase activity. Of the fusions identified, the ETV6-NTRK3 fusion, which juxtaposes the helix-loop-helix domain of transcription factor ETV6 and the kinase domain of NTRK3, has been intensively studied as a defining driver and diagnostic marker for many rare solid tumor malignancies[82, 211, 218, 232].

Although Trk-mediated cancers are rare (<1%), alterations in these receptors have recently emerged as promising therapeutic targets in solid tumors owing to the development of highly selective and durable inhibitors[207, 221, 295, 304, 313]. Regardless of age or tumor origin, larotrectinib, a selective pan-Trk inhibitor, demonstrated robust antitumor activity with an overall response rate of 80%, culminating in its breakthrough FDA approval[207]. Entrectinib, a pan-Trk, ROS1, and ALK inhibitor, has also shown efficacy against a broad range of histologies, including in patients with

primary or secondary central nervous system disease[221]. Its clinical utility resulted in its recent accelerated FDA approval[313].

The tolerability and effectiveness of entrectinib and larotrectinib for Trk-positive solid tumors have sparked our interest in assessing the role of NTRKs in hematological malignancies. Studies thus far have primarily focused on ETV6-NTRK3 fusions in patients with acute myeloid leukemia (AML)[244, 247], chronic eosinophilic leukemia[254], and Philadelphia chromosome-like acute lymphoblastic leukemia[256, 258]. In animal models of AML, entrectinib treatment resulted in tumor regression and elimination of residual ETV6-NTRK3^{+} cancer cells from the marrow[296]. More recently, after evaluating Trk fusions across 7,311 patients with hematologic malignancies, Taylor *et al.*, identified four previously unrecognized Trk oncofusions in patients that were sensitive to larotrectinib[248]. They also reported partial remission in a patient with AML who harbored an ETV6-NTRK2 fusion following treatment with larotrectinib. Despite these and other studies[255, 259], the significance of Trk signaling in leukemia largely remains unrecognized[80].

While Trk fusions represent the primary genetic alteration that confer oncogenic behavior in Trk-driven liquid tumors, point mutations in NTRK genes may also contribute to the tumorigenic process; however, this has not been rigorously investigated to date. Point mutations in the kinase domain of the NTRK genes have been previously reported in hematologic malignancies,[249, 250] although their functional significance remains uncertain. We recently sequenced primary samples from patients with hematologic malignancies and identified nine novel point mutations in the NTRK2 or NTRK3 genes, many of which were found outside the kinase domain. Of the nine unique mutations we identified and tested, here, we show that four mutations are oncogenic drivers and cells transformed by these mutations are amenable to Trk inhibition. We also suggest a potential mechanism that drives the activation of these NTRK mutants and highlight major trends revealed through our functional genomics screens involving small-molecule inhibitors and siRNA perturbation that were conducted on leukemia cells from patients that harbored the specific NTRK mutations we report herein.

Results

Identification of oncogenic NTRK point mutations in leukemia patient samples

Deep sequencing using a custom capture library consisting of 1,862 kinase and kinase-associated genes in 185 leukemia samples revealed NTRK point mutations in ten patients (5.4%) diagnosed with hematologic malignancies (**Figure 1A**). NTRK2^{R458G} was identified in two patients.

To assess the oncogenic capacity of these mutations, we stably expressed them in Ba/F3 cells, a murine IL-3 dependent pro-B cell line that provides a well-established transformation model[314]. Certain oncogenes transform Ba/F3 cells by permitting sustained proliferation in the absence of IL-3. Of the nine unique mutations we identified and tested, four mutations—NTRK2^{A203T}, NTRK2^{R458G}, NTRK3^{E176D}, and NTRK3^{L449F}—conferred IL-3 independent growth. Going forward, these four mutants were prioritized for further characterization. Ba/F3 cells expressing wildtype (WT) NTRK2, NTRK3, and empty vector (pMX-puro) were unable to grow without IL-3 (**Figure 1B**). Similarly, mutants NTRK2^{S167Y}, NTRK2^{H245Y}, NTRK3^{T261I}, NTRK3^{L378V}, and NTRK3^{R645C} did not exhibit oncogenic capacity (**Supplemental Figure 1**).

Independent of the Ba/F3 model, NTRK WT and prioritized mutants were transiently transfected into HEK 293T/17 cells. We observed robust Trk phosphorylation with NTRK mutant cells compared to WT following serum starvation (**Supplemental Figure 2**).

We confirmed the presence of NTRK2^{A203T}, NTRK2^{R458G}, NTRK3^{E176D}, and NTRK3^{L449F} in patient samples via Sanger sequencing of genomic DNA (**Figure 1C-F**) and immunoblotting (**Figure 1G**). Protein lysates from available clinical samples indicated expression and phosphorylation of TrkB or TrkC in patients with the NTRK2^{A203T}, NTRK2^{R458G}, and NTRK3^{L449F} mutations. Protein lysate for the patient with NTRK3^{E176D} was unavailable.

NTRK2^{A203T} was found in a patient with primary myelofibrosis and resides within the extracellular domain. NTRK2^{R458G}, located within the juxtamembrane domain, was observed in two patients, one with chronic myeloid leukemia (CML) and the other with atypical CML (**Figure**

1H). NTRK3^{E176D} was observed in a patient with NPM1-mutated AML and found within the extracellular domain. NTRK3^{L449F} was seen in a patient with T-cell ALL and is located within the transmembrane domain (**Figure 1H**). Available information about patient variant allele frequency and co-occurring mutations is provided in **Supplemental Table 3**. It should be noted that the capture library is focused on kinase-associated genes, and there may, therefore, be other mutations present in other gene families now known to be prevalent in leukemia that were not assessed using this platform.

Analysis of sequence alignment of NTRK2 genes from different species suggests that the R458 residue is a highly conserved residue throughout evolution whereas A203 was conserved only among mammals (**Supplemental Figure 3**). Sequence alignment of multiple NTRK3 homologues show that both E176 and L449 are also highly conserved throughout evolution (**Supplemental Figure 4**). These alignment studies suggest that these residues may contribute to the structure and biologic function of the TrkB and TrkC receptors, implicating that mutations in such residues may have functional consequences. In our analysis of cBioPortal, The Cancer Genome Atlas, PeCan, and COSMIC, we saw that our transforming mutants fell in regions of the NTRK genes where similar mutations have been identified in other cancers, further supporting our hypothesis that these mutants may contribute to leukemogenesis (**Supplemental Figure 5**).

A

Gene	Amino Acid Change	VAF	Location of Mutation	Patient Specimen ID	Diagnosis	Specific Diagnosis
NTRK2	H245Y	0.27	Extracellular	10-00440	AML	AML, NOS
NTRK2	S167Y	0.47	Extracellular	08-00423	MPN	CML, BCR-ABL1^{+}
NTRK2	A203T	0.48	Extracellular	12-00171	MPN	Primary Myelofibrosis
NTRK2	R458G	0.46	Juxtamembrane	12-00337	MPN	CML, BCR-ABL1^{+}
NTRK2	R458G	0.53	Juxtamembrane	13-00187	MPN	aCML, BCR-ABL1^{-}
NTRK3	L449F	0.26	Transmembrane	10-00828	ALL	T-ALL
NTRK3	T261I	0.62	Extracellular	10-00669	AML	AML with mutated NPM1
NTRK3	R645C	0.49	Kinase	11-00366	AML	AML with mutated NPM1
NTRK3	L378V	0.41	Extracellular	12-00035	AML	AML with mutated NPM1
NTRK3	E176D	0.48	Extracellular	12-00165	AML	AML with mutated NPM1

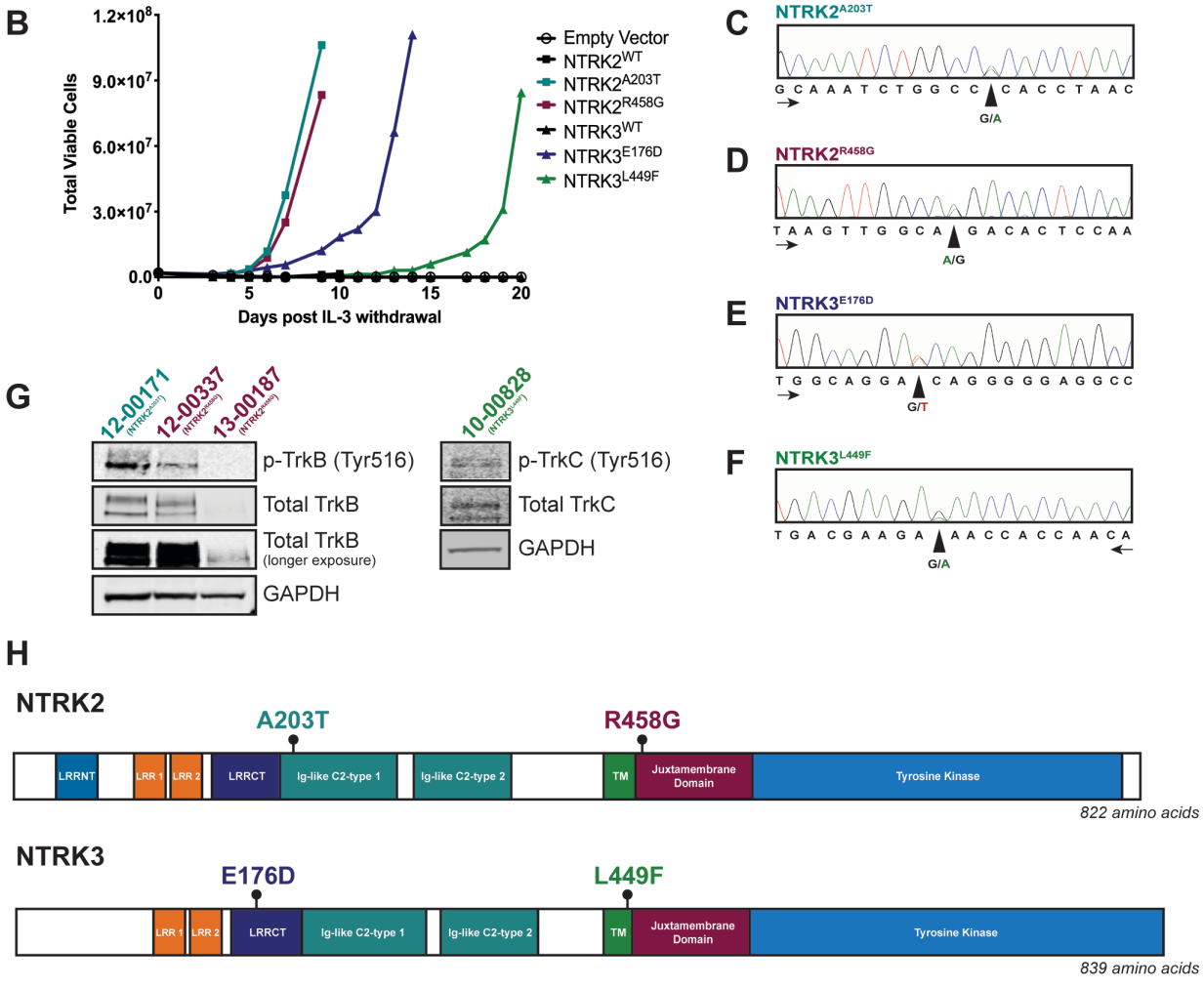

Figure 1: Identification of four oncogenic NTRK point mutations in leukemia patient samples. A. Among the 185 patient samples sequenced using a custom capture library consisting of 1,862 kinase and kinase-associated genes, ten patients harbored a mutation in one of the NTRK genes. The NTRK2^{R458G} mutation was found in two patients. Mutations are organized by gene and diagnosis. Patient Specimen ID is also provided. VAF, Variant Allele Frequency. **B.** NTRK2^{A203T}, NTRK2^{R458G}, NTRK3^{E176D}, and NTRK3^{L449F} mutations transform the murine Ba/F3

pro-B cell line and enable IL-3 independent growth. No growth was observed in Ba/F3 cells harboring an empty vector (pMX-puro) or wildtype (WT) NTRK2 or NTRK3. Total viable cells are plotted over time and cell growth was measured after the withdrawal of IL-3. This experiment was repeated at least twice with consistent results. Additional validation studies are found in Supplemental Figure 2. **C-F.** Electropherograms from sanger sequencing of patient genomic DNA confirm the presence of $NTRK2^{A203T}$, $NTRK2^{R458G}$, $NTRK3^{E176D}$, and $NTRK3^{L449F}$ mutations. Peaks correspond to the following nucleotides: A (green), T (red), C (blue), and G (black). Arrows indicate direction of sequencing. **G.** Immunoblot analysis of total and phosphorylated TrkB and TrkC on patient samples with known $NTRK^{A203T}$ (12-00171), $NTRK^{R458G}$ (12-00337 & 13-00187), and $NTRK3^{L449F}$ (10-00828) mutations. **H.** Gene schematics depict the location of the NTRK2 and NTRK3 point mutations. The location of the following domains is included: LRRNT (NTRK2-specific), LRR 1, LRR 2, LRRCT, Ig-like C2-type 1, Ig-like C2-type 2, transmembrane (TM), juxtamembrane, and tyrosine kinase. Daniel Bottomly assisted with VAF assessment (A) and Cristina E. Tognon assisted with Ba/F3 IL-3 withdrawal studies (B).

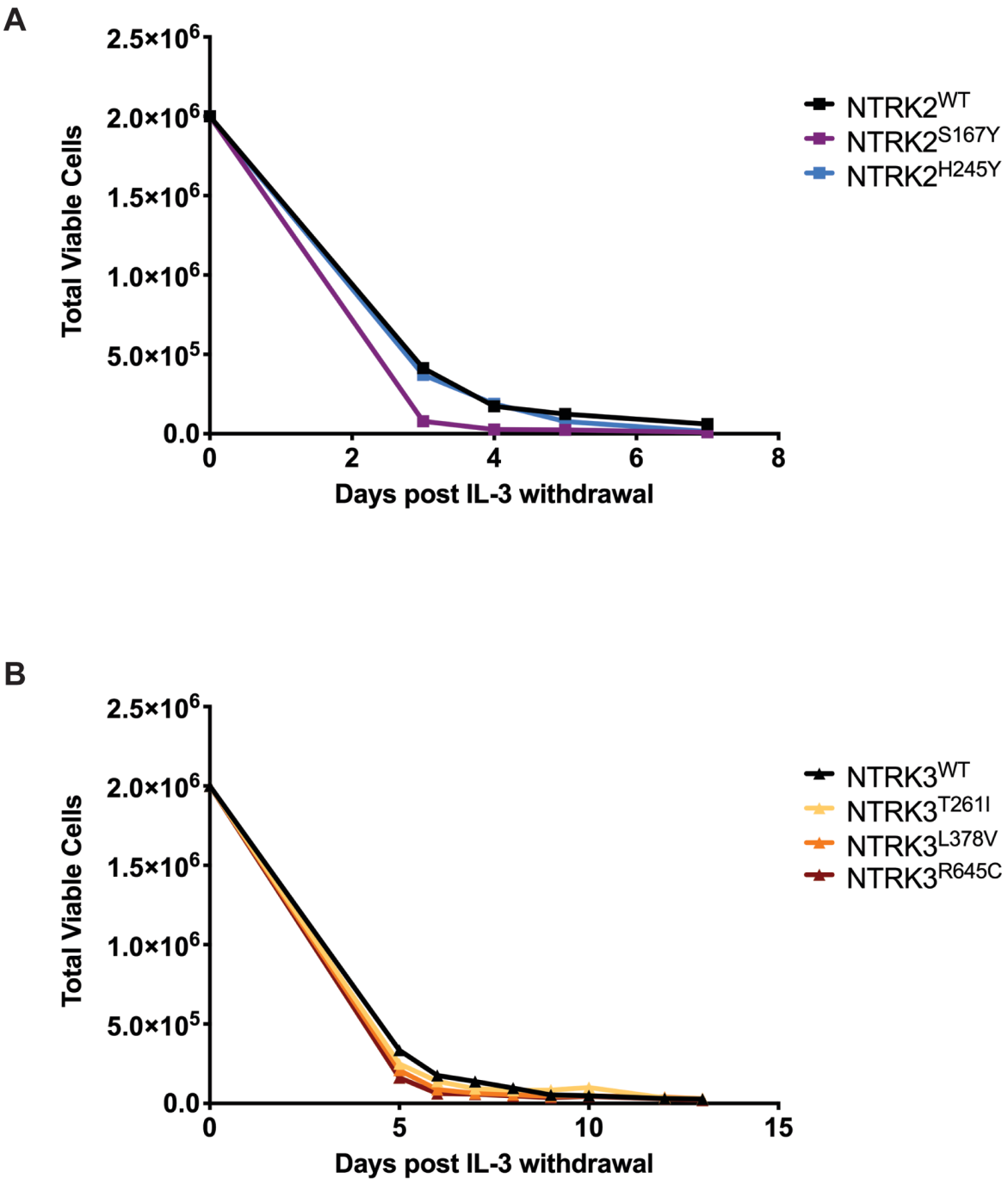

Supplemental Figure 1: NTRK2^{S167Y}, NTRK2^{H245Y}, NTRK3^{T261I}, NTRK3^{L378V}, and NTRK3^{R645C} mutations do not transform the murine Ba/F3 pro-B cell line to cytokine-independent growth. Total viable cells are plotted over time and cell growth was measured after the withdrawal of IL-3. Cristina E. Tognon performed Ba/F3 studies shown in A and B.

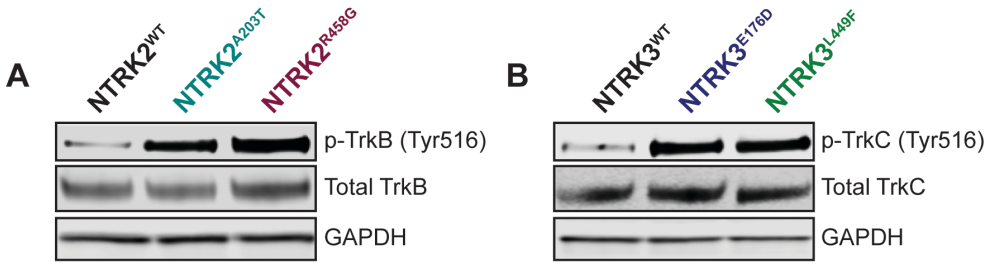

Supplemental Figure 2: Transient transfection of NTRK mutants shows robust phosphorylation of TrkB and C receptor, respectively. A-B. 2 µg of NTRK WT, mutant, or empty vectors were transiently expressed in HEK293T/17 cells. Following 48 hours, cells were serum starved for 4 hours in 0.1% BSA DMEM and lysed for immunoblotting. In comparison to cells transfected with WT NTRK2 or NTRK3 vectors, cells expressing mutant vectors show increased phosphorylation of TrkB and C receptor, respectively.

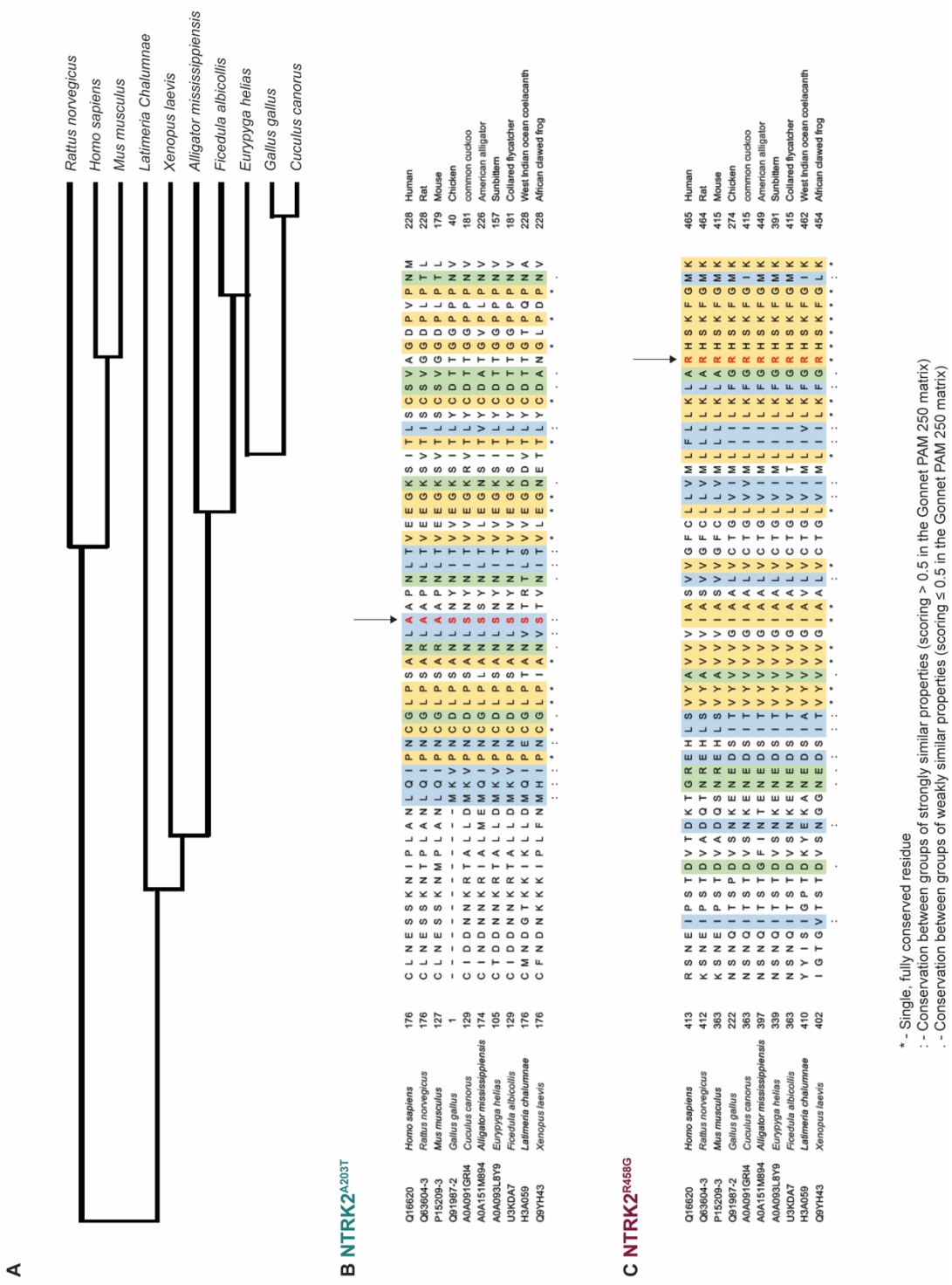

Supplemental Figure 3: R458 is a highly conserved residue in NTRK2 homologues. A. Taxonomic distribution of species used for multiple sequence alignment. **B-C.** Multiple sequence alignment for NTRK2 residues A203 and R458 among homologues. A203 is conserved among mammals while R458G is conserved among all species. Alignment performed using CLUSTALO, 11.71% of positions were identical across all species.

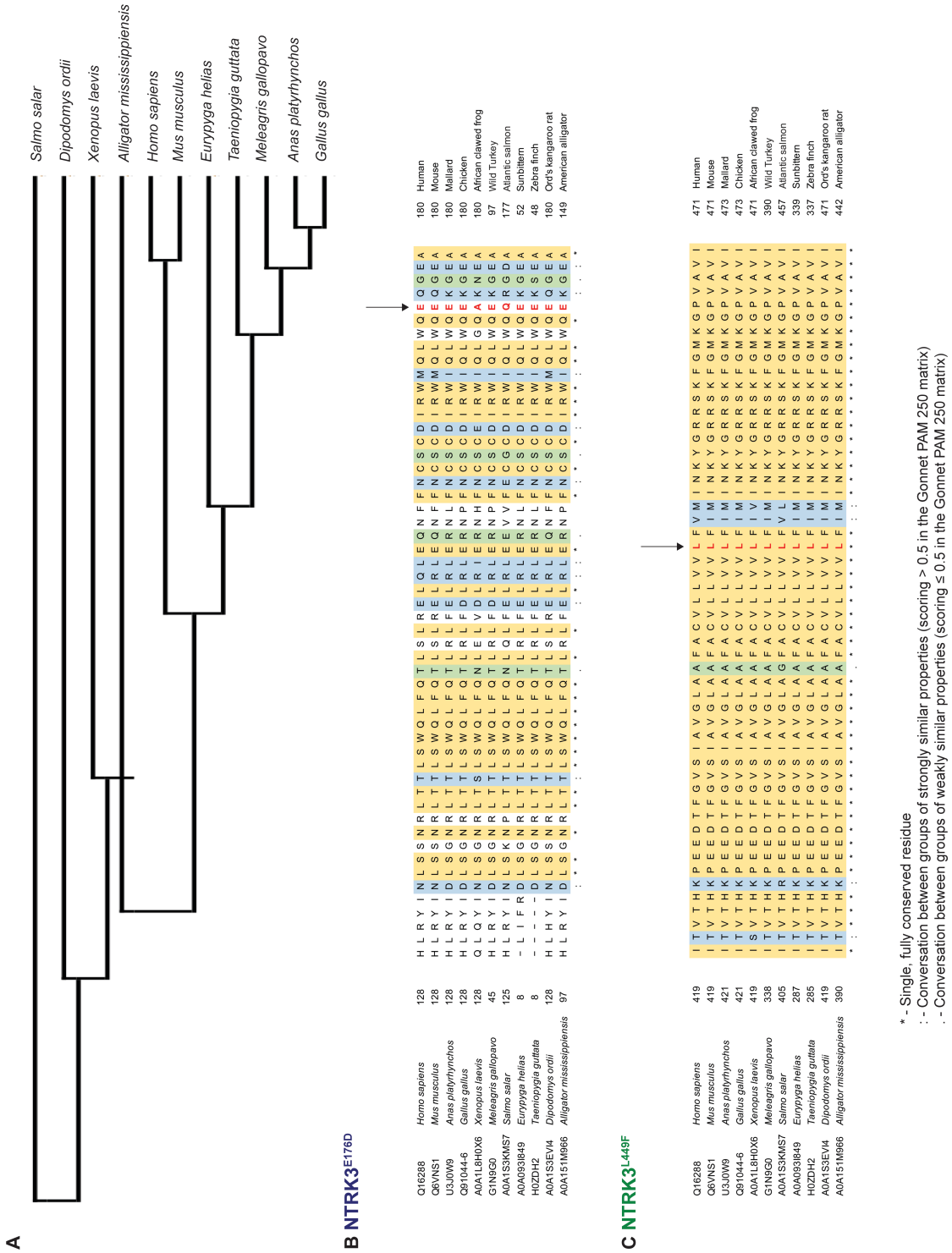

Supplemental Figure 4: Both NTRK3 mutations affect residues that are highly conserved throughout evolution. A. Taxonomic distribution of species used for multiple sequence alignment. **B-C.** Multiple sequence alignment for NTRK3 residues E176 and L449 among homologues. Alignment performed using CLUSTALO, 22.555% of positions were identical across all species.

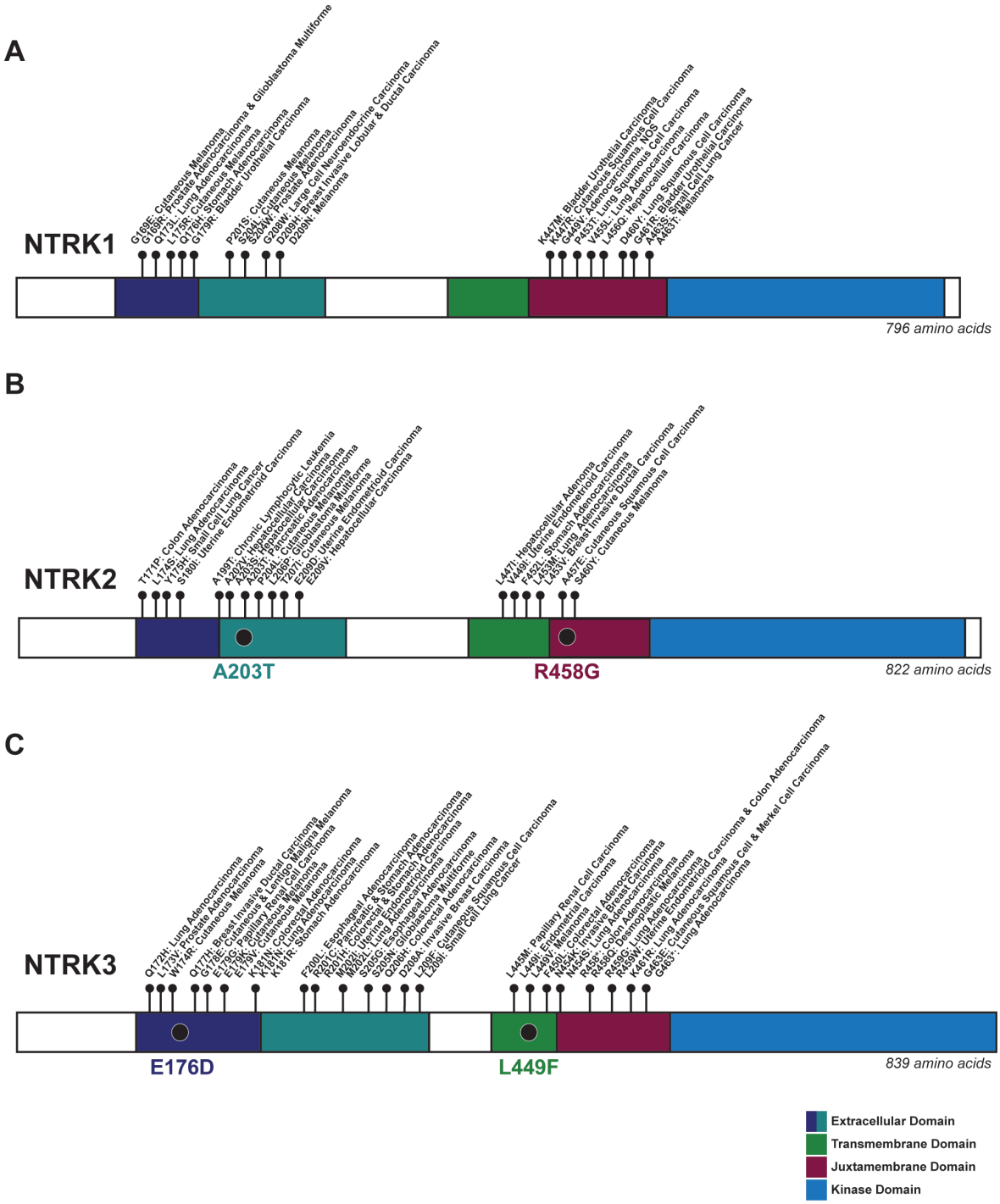

Supplemental Figure 5: NTRK2^{A203T}, NTRK2^{R458G}, NTRK3^{E176D}, and NTRK3^{L449F} mutations are found in regions of the NTRK genes that have been identified in other cancers. A-C. NTRK gene schematics annotating mutation information compiled from cBioPortal, The Cancer Genome Atlas, PeCan, and COSMIC. While this data may reflect elevated mutation accumulation in these areas of the NTRK receptors, the biological relevance of these mutations in solid and liquid tumors is not completely understood.

Prioritized NTRK mutants exhibit increased Trk signaling and confer entrectinib sensitivity

Immunoblot analysis revealed increased phosphorylation of TrkB (Tyr516) or TrkC (Tyr516) in mutant-transformed Ba/F3 cells relative to parental Ba/F3 cells or cells transfected with WT NTRK or empty vectors (pMX-puro) (**Figure 2A-B**). Furthermore, NTRK2 and NTRK3 mutant-driven cells exhibited enhanced phosphorylation of AKT (Ser473), and ERK (Thr202/Tyr204) compared to WT cells, suggesting the importance of MAPK and PI3K/AKT signaling in promoting the survival of these oncogenic cells. While phosphorylation of STAT3 (Tyr705) was significantly increased in Ba/F3 cells transfected with both NTRK3 mutants, it was increased only in one of the NTRK2 mutants (A203T). Upregulation of SRC phosphorylation (Tyr527) was observed only with Ba/F3 cells transfected with NTRK2 mutants. No significant difference was seen with phosphorylation of STAT5 (Tyr694) between WT and mutant NTRK2 or NTRK3 Ba/F3 cells (**Figure 2A-B**).

We next sought to identify inhibitors that could abrogate Trk signaling with the following tyrosine kinase inhibitors - BGJ398, cabozantinib, crenolanib, crizotinib, entrectinib, foretinib, imatinib, and ponatinib (**Supplemental Figure 6A**). Of these, cabozantinib[297], crizotinib[256, 292, 296], entrectinib[296], and foretinib[145] have been previously reported to have activity against NTRK and its orthologues, ROS1 and ALK. Apart from BGJ398 (pan-FGFR inhibitor) and imatinib (BCR-ABL1 inhibitor), which served as negative controls, all other tested inhibitors reduced the growth and viability of our mutant-transformed NTRK Ba/F3 cells to varying degrees (**Supplemental Figure 6A & Supplemental Table 4**). Entrectinib was the most potent inhibitor with an IC_{50} of 1.644 nM for $NTRK2^{A203T}$, 1.566 nM for $NTRK2^{R458G}$, 0.9794 nM for $NTRK3^{E176D}$, and 1.015 nM for $NTRK3^{L449F}$ Ba/F3 cells (**Figure 2C**). With the recent accelerated FDA approval of larotrectinib for NTRK-positive solid tumors, we also tested the sensitivity of larotrectinib on our mutant Ba/F3 cell lines[205, 207]. Larotrectinib inhibited cell growth with an IC_{50} of 12.91 nM for $NTRK2^{A203T}$, 13.42 nM for $NTRK2^{R458G}$, 11.46 nM for $NTRK3^{E176D}$, and 12.97 nM for $NTRK3^{L449F}$ Ba/F3 cells (**Figure**

2D). These data suggest that our four NTRK point mutations are highly sensitive to selective NTRK inhibitors. In all cases, WT NTRK Ba/F3 cells grown in IL-3 supplemented media were completely insensitive to all inhibitors.

As a consequence of entrectinib's potency in our mutant-transformed Ba/F3 cell lines, we further characterized its cytotoxicity and specificity. We saw increased apoptosis following 48 and 72 hours of entrectinib treatment in all mutant-driven Ba/F3 cells (**Figure 2E**). Entrectinib did not induce apoptosis in Ba/F3 cells harboring the BCR-ABL1 oncogene or empty vector (pMX-puro), indicating that the cell death we observed in NTRK-transformed Ba/F3 cells is not due to entrectinib's off-target toxicity but due to its specificity for NTRK (**Supplemental Figure 6B-C**).

Upon treating our NTRK mutant-transformed Ba/F3 cells with entrectinib (0, 5, 25, 75, 100, and 250 nM), we observed a decrease in expression of total and phosphorylated TrkB and TrkC in all mutants (**Figure 2F**). However, we saw a varying degree of inhibition of STAT3, AKT, and ERK phosphorylation, suggesting some variability in downstream signaling among the mutants.

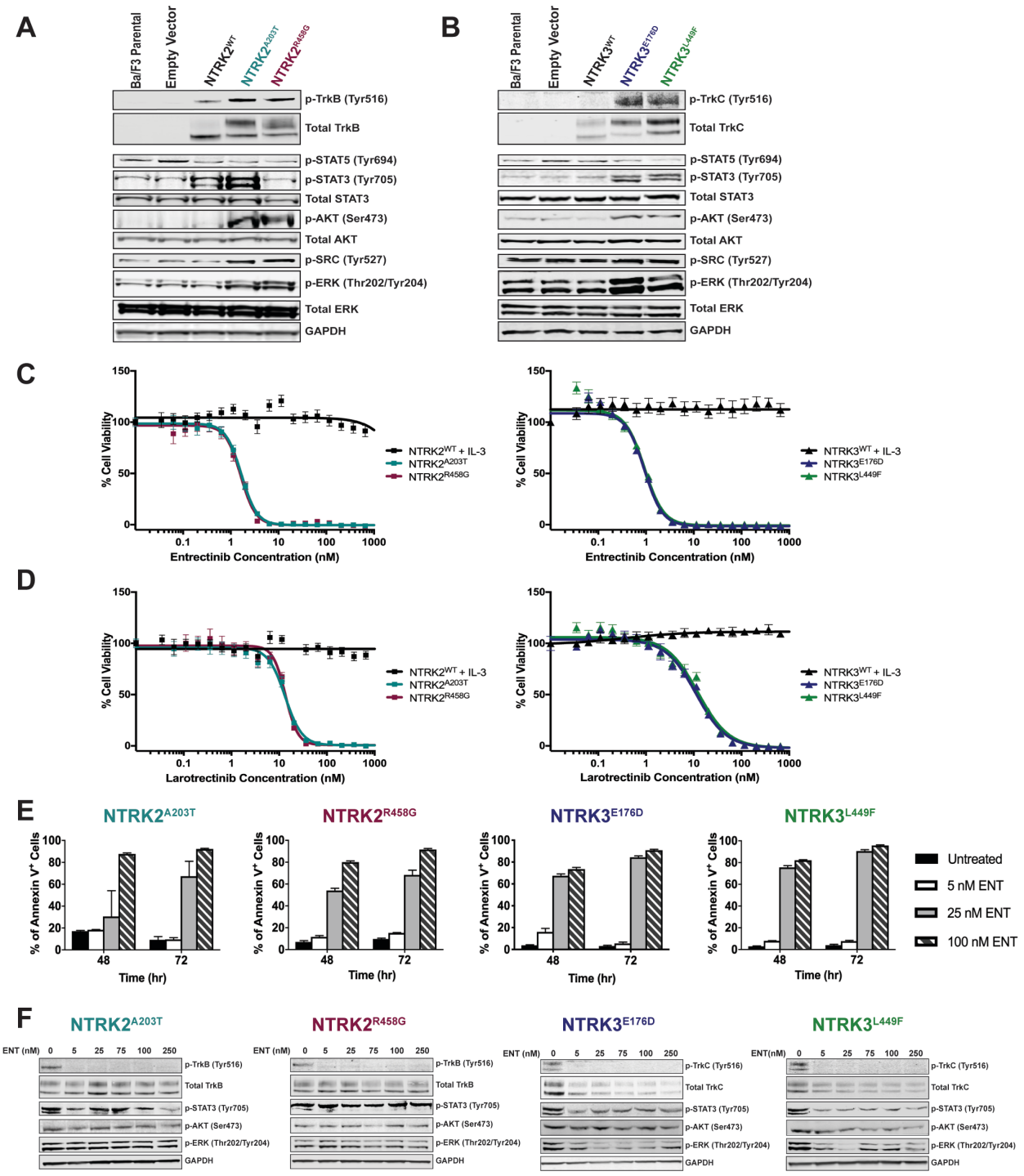

Figure 2: NTRK2 and NTRK3 mutants are constitutively phosphorylated and sensitive to Trk inhibition. A-B. Expression of total and phosphorylated TrkB and TrkC is increased in mutant-transformed Ba/F3 cells relative to WT cells. All mutants phosphorylate canonical downstream effectors – AKT and ERK. STAT3 phosphorylation was not evident in NTRK2^{R458G}.

Both NTRK2 mutants result in increased SRC phosphorylation. GAPDH served as a loading control. Prior to lysis, WT cells were grown in IL-3 supplemented media and all lines were starved overnight in 0.1% BSA RPMI. **C-D.** NTRK mutants are sensitive to entrectinib and larotrectinib. Six replicates of WT and mutant NTRK2 and NTRK3 Ba/F3 cells were plated with varying concentrations of entrectinib and larotrectinib for 72 hrs. $NTRK2^{WT}$ and $NTRK3^{WT}$ cells were plated in media supplemented with IL-3. Cell viability was determined using a tetrazolamine-based viability assay. Viability is represented as a percentage of the untreated control. The average mean ± SEM is shown. Additional validation studies are found in Supplemental Figure 6B. **E.** Mutant-transformed Ba/F3 cells were starved overnight in 0.1% BSA RPMI and then treated with increasing concentrations of entrectinib (ENT) for approximately 16 hours and immunoblotted for Trk and downstream effectors. **F.** ENT induces apoptosis in mutant-transformed Ba/F3 cells following 48 and 72 hours. Annexin V staining was performed in triplicate. The average mean ± SEM is shown. Validation studies in Supplemental Figure 6C. Kristin Qian performed annexin V staining (F).

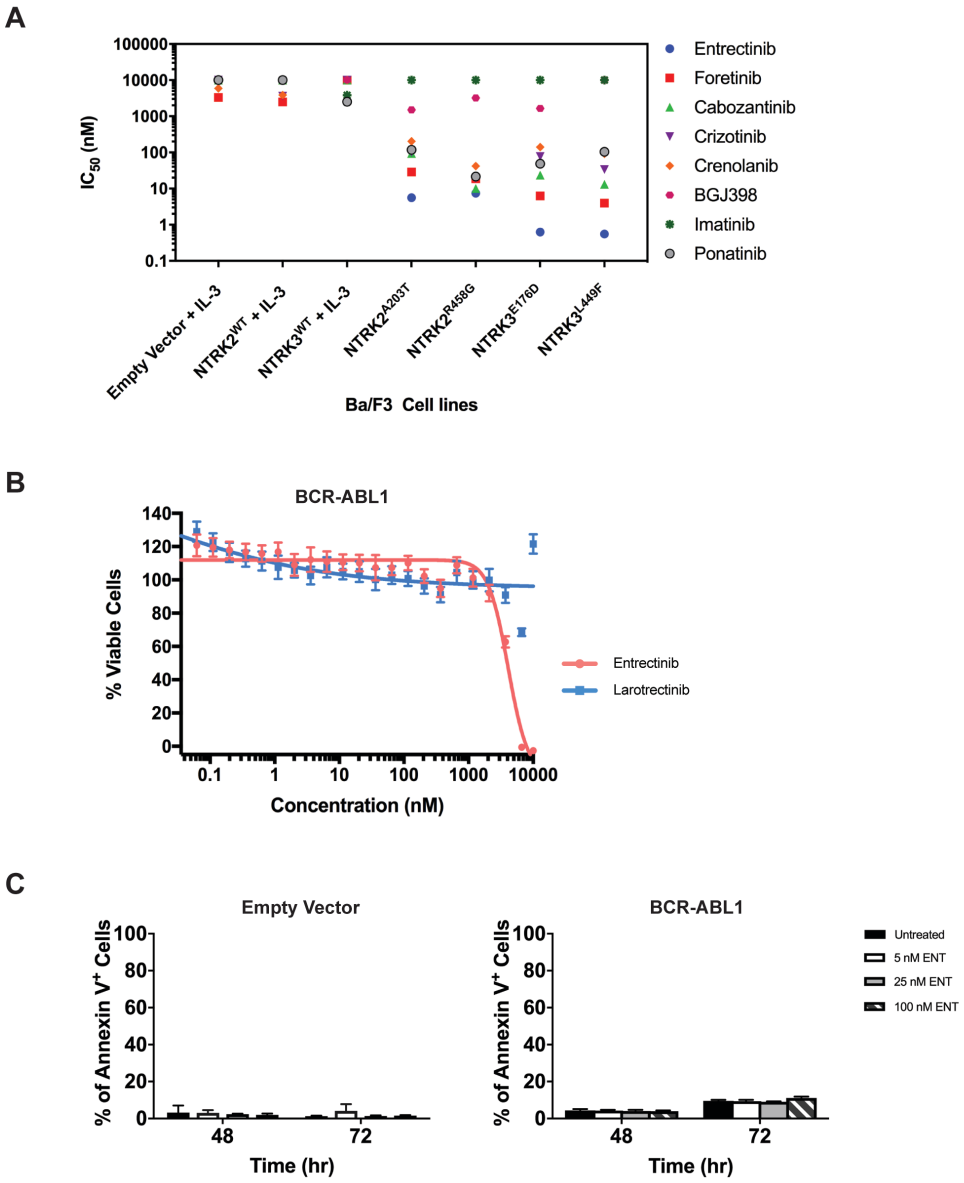

Supplemental Figure 6: Entrectinib selectively inhibits NTRK with minimal toxicity. A. Of the small-molecule inhibitors we considered, NTRK mutants were most sensitive to entrectinib as evident by the plotted IC_{50} values. WT and mutant NTRK Ba/F3 cells were plated in triplicate and exposed to small-molecule inhibitors for 72 hrs. WT cells were grown in media supplemented with IL-3. Cell viability was determined using a tetrazolamine-based viability assay. The average mean ± SEM is shown. **B.** Entrectinib and larotrectinib are selective for NTRK. Ba/F3 cells harboring a BCR-ABL1 construct were used as a negative control to account for non-specific inhibition. Six replicates of BCR-ABL1 Ba/F3 cells were plated. Cell viability was determined as in A. Viability is represented as a percentage of the untreated control. The average mean ± SEM is shown. **C.** Entrectinib induction of apoptosis is NTRK-specific. Annexin V staining was performed in triplicate. The average mean ± SEM is shown. Monika A. Davare performed inhibitor screening (A) and Kristin Qian performed annexin V staining (C).

Increased cell surface abundance of Trk receptors seen with mutants NTRK2^{A203T}, NTRK2^{E176D}, and NTRK3^{L449F}

To begin to understand how our NTRK mutants lead to kinase activation, we modeled the impact of the amino acid change to the secondary structure of the Trk receptors using a previously published protein prediction model, Phyre[2] (Protein Homology/analogY Recognition Engine V 2.0)[315]. While NTRK2^{A203T} was predicted to result in a partial loss of the beta-pleated sheet, NTRK2^{R458G} was predicted to shift the stretch of amino acids that contribute to the transmembrane domain alpha helix and increase the helix by one amino acid (**Supplemental Figure 7A-B**). In the case of NTRK3, both mutations were predicted to replace beta-pleated sheets found in the WT receptor with alpha helices (**Supplemental Figure 8A-B**).

These predicted changes in secondary structure led us to hypothesize that our NTRK mutants may alter cell surface localization and retention of the TrkB and TrkC receptors. To test our hypothesis, we measured cell surface localization and retention via flow cytometry using APC-conjugated anti-TrkB or anti-TrkC antibodies. These flow antibodies were validated on human glioblastoma cell lines that endogenously express TrkB or TrkC (**Supplemental Figure 9A-B**). NTRK2^{A203T} resulted in approximately a two-fold increase in the abundance of TrkB receptor on the cell surface relative to WT ($p=0.002$, **Figure 3A**). No significant difference in TrkB receptor localization was observed between NTRK2^{R458G} and WT receptor ($p=0.6436$, **Figure 3A**). While both NTRK3 mutations resulted in increased receptor localization statistically compared to the WT receptor ($p<0.0001$), the biological significance of this finding is uncertain as evident by the small increase observed (**Figure 3B** and **Supplemental Figure 9E-F**).

To evaluate alterations in protein retention at the cell surface, we performed a time course experiment (12 and 24 hours) by treating serum-starved WT and mutant NTRK2 and NTRK3 Ba/F3 cell lines with 100 µg/mL of cycloheximide followed by flow staining for cell surface expression of TrkB and TrkC. Following 12 hours of cycloheximide treatment of Ba/F3 cells

expressing the NTRK2 mutants or WT, NTRK2^{A203T} possessed a decreased half-life relative to WT TrkB receptor (p=0.0410, **Figure 3C**). At 24 hours, no difference in protein retention at the cell surface was observed between the NTRK2 mutants or WT Ba/F3 cells. Both NTRK3 mutants were less stable than WT TrkC receptor following 12 hours of cycloheximide, with the difference between WT and NTRK3^{E176D} resulting in statistical significance (p=0.0481**,** **Figure 3D**). After 24 hours of cycloheximide treatment, both NTRK3 mutants were found at lower levels at the surface relative to NTRK3^{WT} (p=0.0007 for NTRK3^{E176D} and p=0.0012 for NTRK^{L449F}, **Figure 3D**). Despite higher surface expression of NTRK2^{A203T} and NTRK3$^{E176D/L449F}$ (**Figure 3A-B**), this was not due to an increase in protein retention at the cell surface, and in fact the mutated isoforms had shorter cell surface half-lives.

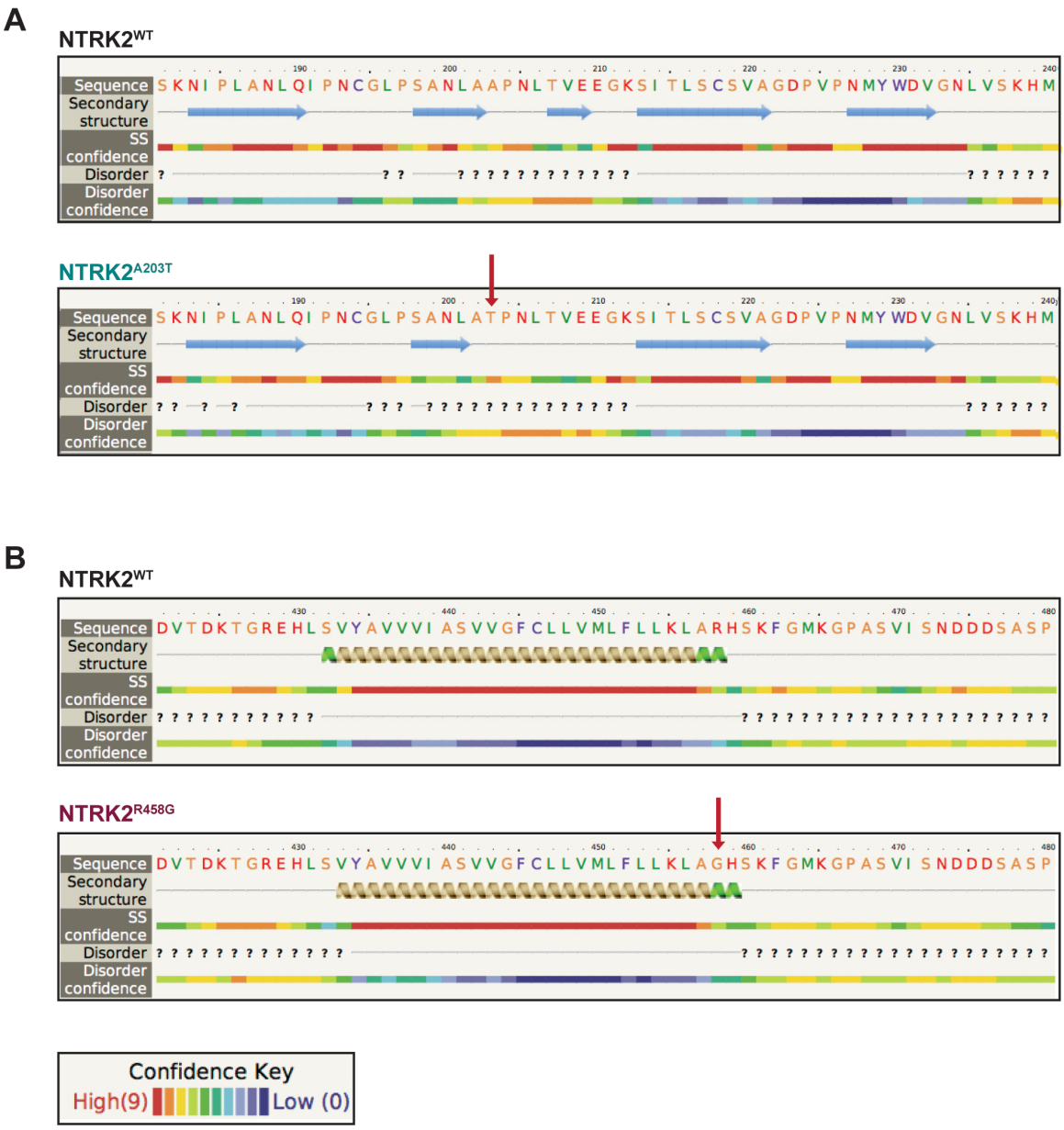

Supplemental Figure 7: NTRK2 mutants change the secondary structure of the TrkB receptor. A. A203T mutation results in partial loss of a beta-pleated sheet. **B.** R458G shifts the amino acid sequence that contributes to the formation of the transmembrane domain alpha helix and increased the helix by one amino acid. Brown represents transmembrane domain helix. Green represents alpha helix.

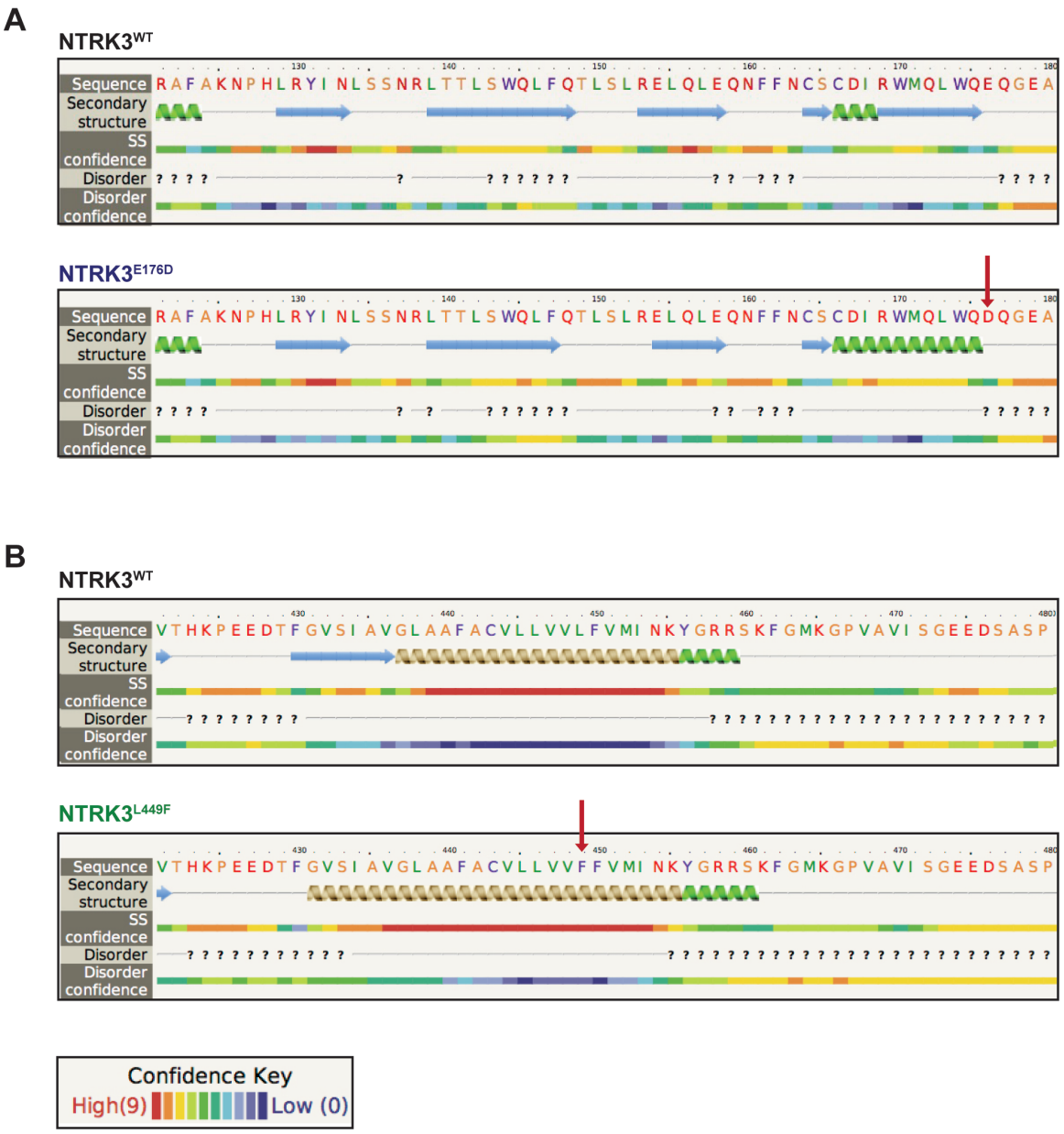

Supplemental Figure 8: Point mutations in NTRK3 result in the loss of beta-pleated sheets. **A-B.** According to the Phyre[2] prediction model, mutations E176D and L449F shift the secondary structure from beta-pleated sheets to alpha helices at both mutation sites of NTRK3.

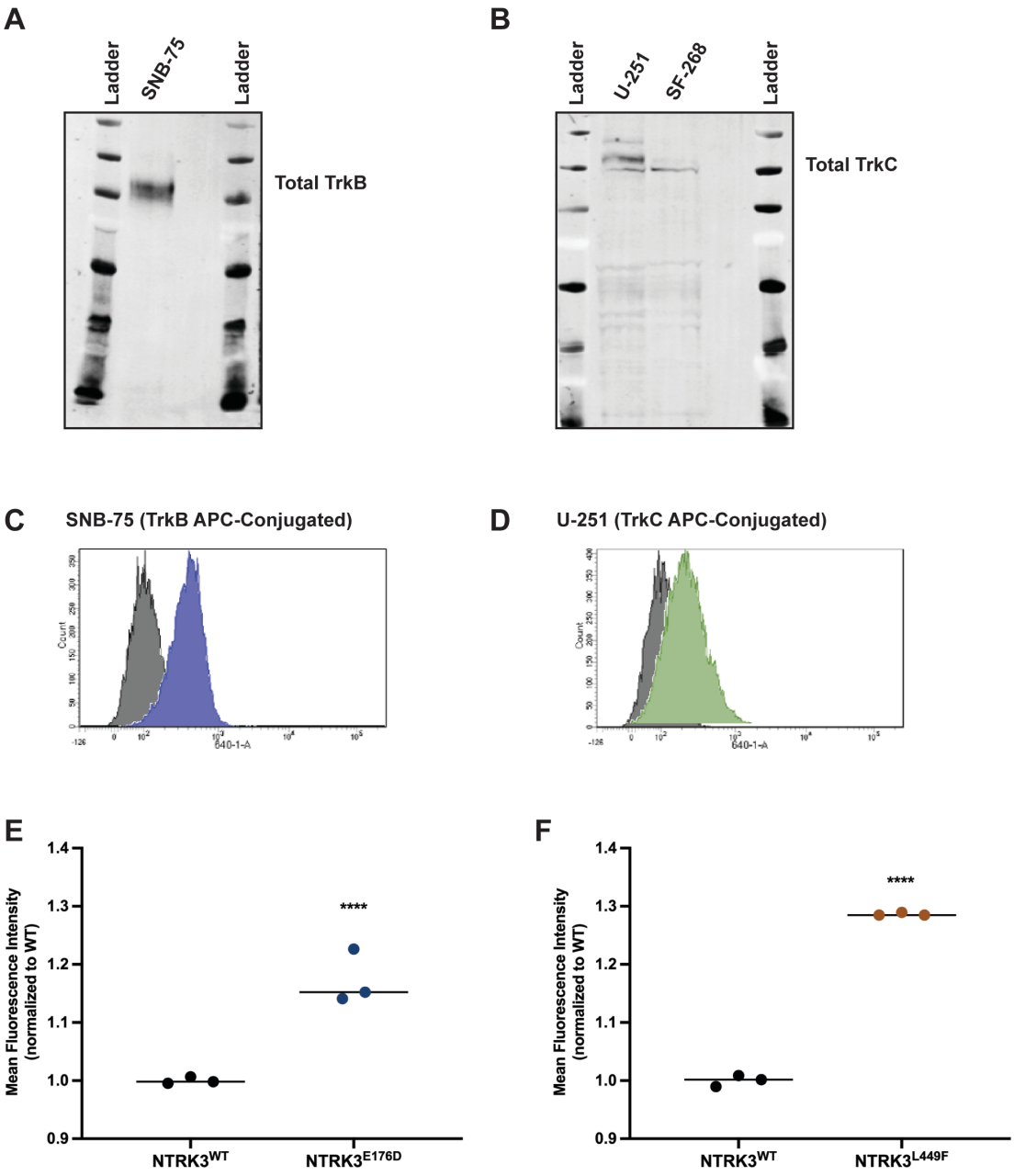

Supplemental Figure 9: APC-conjugated TrkB and TrkC antibodies are target-specific in our Ba/F3 model. A-B. SNB-75 and U-251, human glioblastoma cell lines endogenously express TrkB and TrkC, respectively. Minimal expression of TrkC was observed with SF-268, a human astrocytoma cell line. **C-D.** SNB-75 and U-251 were stained with APC-conjugated anti-TrkB or anti-TrkC antibodies (Supplemental Table 2) and analyzed by flow cytometry. These cell lines served as positive controls for all flow experiments. **E-F.** Flow staining to assess cell surface localization of $NTRK3^{E176D}$ and $NTRK3^{L449F}$ with their respective WT samples was performed on separate days. The data presented in Figure 3D are shown here as separate plots.

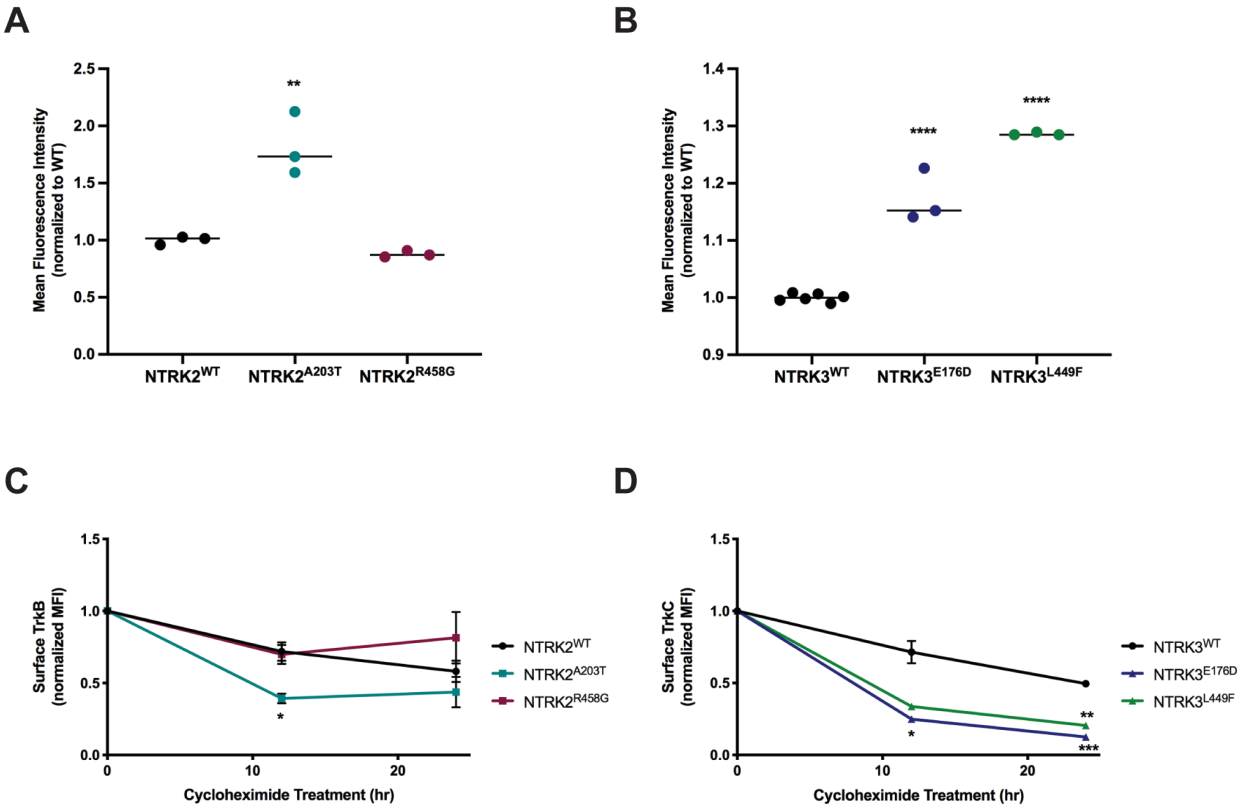

Figure 3: Mutants NTRK2^{A203T}, NTRK3^{E176D}, and NTRK3^{L449F} increase Trk cell surface localization but not retention. A-B. In order to assess differences in mutant receptor localization, WT and mutant Ba/F3 cells were stained with APC-conjugated anti-TrkB or anti-TrkC antibodies and analyzed by flow cytometry. A significantly higher localization of Trk receptors was observed with NTRK2^{A203T}, NTRK3^{E176D}, and NTRK3^{L449F} mutants relative to their respective WT receptor. Validation of APC-conjugated Trk flow antibodies is shown in Supplemental Figure 9C-D. **C-D.** To assess receptor retention at the cell surface, WT and mutant NTRK2 and NTRK3 Ba/F3 cells were treated with 100 µg/mL of cycloheximide for 12 or 24 hours, stained with APC-conjugated anti-TrkB or anti-TrkC antibodies, and analyzed via flow cytometry. Following 12 hours, NTRK2^{A203T} was less stable than NTRK2^{WT}. Both NTRK3 mutants were less stable than NTRK3^{WT} after 12 and 24 hours of cycloheximide treatment. Normalized mean fluorescence intensity (MFI) is shown over time. For all experiments, WT Ba/F3 cells were grown in IL-3 supplemented media and all lines were starved overnight in 0.1% BSA RPMI. Staining was performed in triplicate. Statistical significance was assessed by a one-way or two-way ANOVA followed by a Tukey's multiple comparison test. All statistical comparisons shown are between WT and mutant receptors. The average mean ± SEM is shown. *, *p<0.05*, **, *p<0.01*, ***, *p<0.001*, ****, *p<0.0001*

NTRK2^{A203T}, NTRK3^{E176D}, and NTRK3^{L449F} mutants increase receptor dimerization

Another possible explanation for increased concentration of NTRK2^{A203T}, NTRK3^{E176D}, and NTRK3^{L449F} at the cell surface despite decreased cell surface retention (**Figure 3**) is increased receptor dimerization. To this end, we created and co-transfected C-terminal FLAG- and HA-tagged vectors for all WT and NTRK mutants in HEK 293/T17 cells. Dimerization was measured by immunoprecipitating the FLAG-tagged construct followed by immunoblotting for HA (**Figure 4A**). A higher ratio of HA to FLAG immunoprecipitation was indicative of increased receptor dimerization.

We saw an approximate two-fold increase in dimerization with NTRK2^{A203T} relative to NTRK2^{WT} ($p=0.0405$, **Figure 4B-C**). NTRK2^{R458G} exhibited no increase in dimerization ($p=0.6751$, **Figure 4B-C**). Both NTRK3 mutants had a statistically significant increase in dimerization relative to WT NTRK3 (four-fold increase, $p=0.0002$ for NTRK3^{E176D} and three-fold increase, $p=0.0013$ for NTRK3^{L449F}, **Figure 4D-E**).

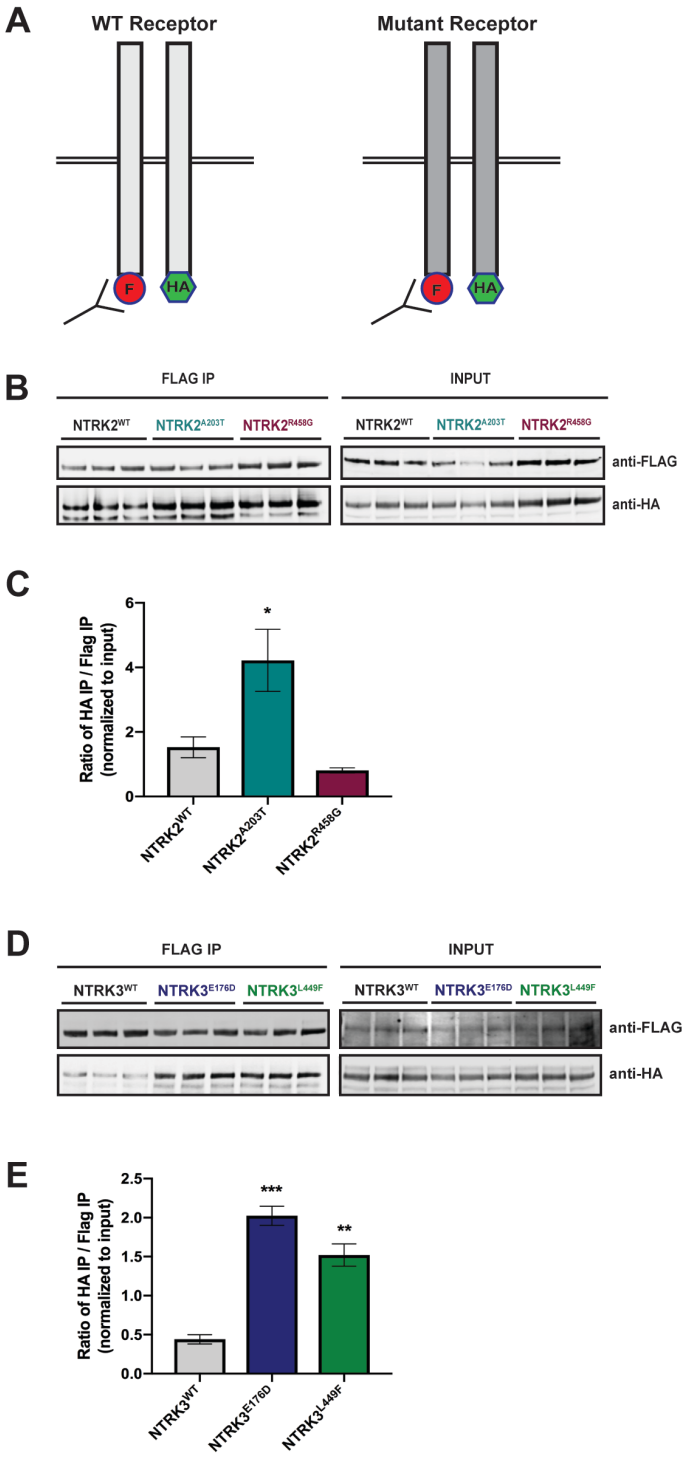

Figure 4: NTRK2^{A203T}, NTRK3^{E176D}, and NTRK3^{L449F} exhibit increased receptor dimerization in comparison to their respective WT receptor. A. Schematic of NTRK dimerization studies. 0.5 µg of FLAG- and HA-tagged NTRK WT or mutant constructs were co-transfected into HEK293T/17 cells and immunoprecipitated using anti-FLAG beads. FLAG immunoprecipitates were then probed with an anti-HA antibody to detect the co-immunoprecipitating receptor,

suggestive of receptor dimerization. The level of HA and FLAG co-immunoprecipitation was quantified using ImageJ and normalized to input. A higher ratio of HA to FLAG immunoprecipitation was indicative of increased receptor dimerization. **B-C.** Immunoblot analysis and quantification of WT and mutant NTRK2 constructs suggest that the NTRK2^{A203T} mutation caused increased receptor dimerization. **D-E.** Increased receptor dimerization was seen with both NTRK3 mutants relative to WT as evident by immunoblot and quantification analysis. For all experiments, statistical significance was assessed by a one-way ANOVA followed by a Tukey's multiple comparison test. All statistical comparisons shown are between WT and mutant receptors. Three biological replicates were performed for each condition. Each experiment was performed at least twice with consistent results. The average mean ± SEM is shown. *, *p<0.05*, **, *p<0.01*, ***, *p<0.001*

TrkB and TrkC are expressed in patients with leukemia and sensitive to small-molecule inhibitors and siRNAs

To identify functional targets in primary patient samples, peripheral mononuclear white blood cells from patients carrying the NTRK2^{A203T} (12-00171; **Figure 5A**), NTRK2^{R458G} (12-00337; **Figure 5B**), and NTRK3^{L449F} (10-00828; **Figure 5C**) mutations were assayed ex vivo against panels of small-molecule inhibitors or small interfering RNA (siRNAs)[316, 317]. Among the various small-molecule drug families, we saw an increased sensitivity to PI3K/AKT/mTOR and Type III RTK/VEGF inhibitors in the patient harboring the NTRK2^{A203T} mutation (**Figure 5A**). As for the patient with the NTRK2^{R458G} mutation, among the tested inhibitors, this patient sample showed enhanced sensitivity to an NF- kB activation inhibitor, crizotinib (an inhibitor of Trk/ALK/ROS1), and LY294002 (a PI3K inhibitor) (**Figure 5B**). It should be noted that entrectinib and larotrectinib had not been developed at the time of patient sample accrual. Since *ex vivo* inhibitor testing can only be done on fresh samples at the time of sample procurement, we cannot comment on how these patients would respond to these two inhibitors. Reduced cell viability in the presence of siRNA targeting NTRK2 and NTRK3 was observed with the patient containing the NTRK3^{L449F} mutation, suggesting that these cells may exhibit dependence on NTRK2 and NTRK3 for cell survival. The knockdown of NTRK2 significantly altered cell viability (**Figure 5C**).

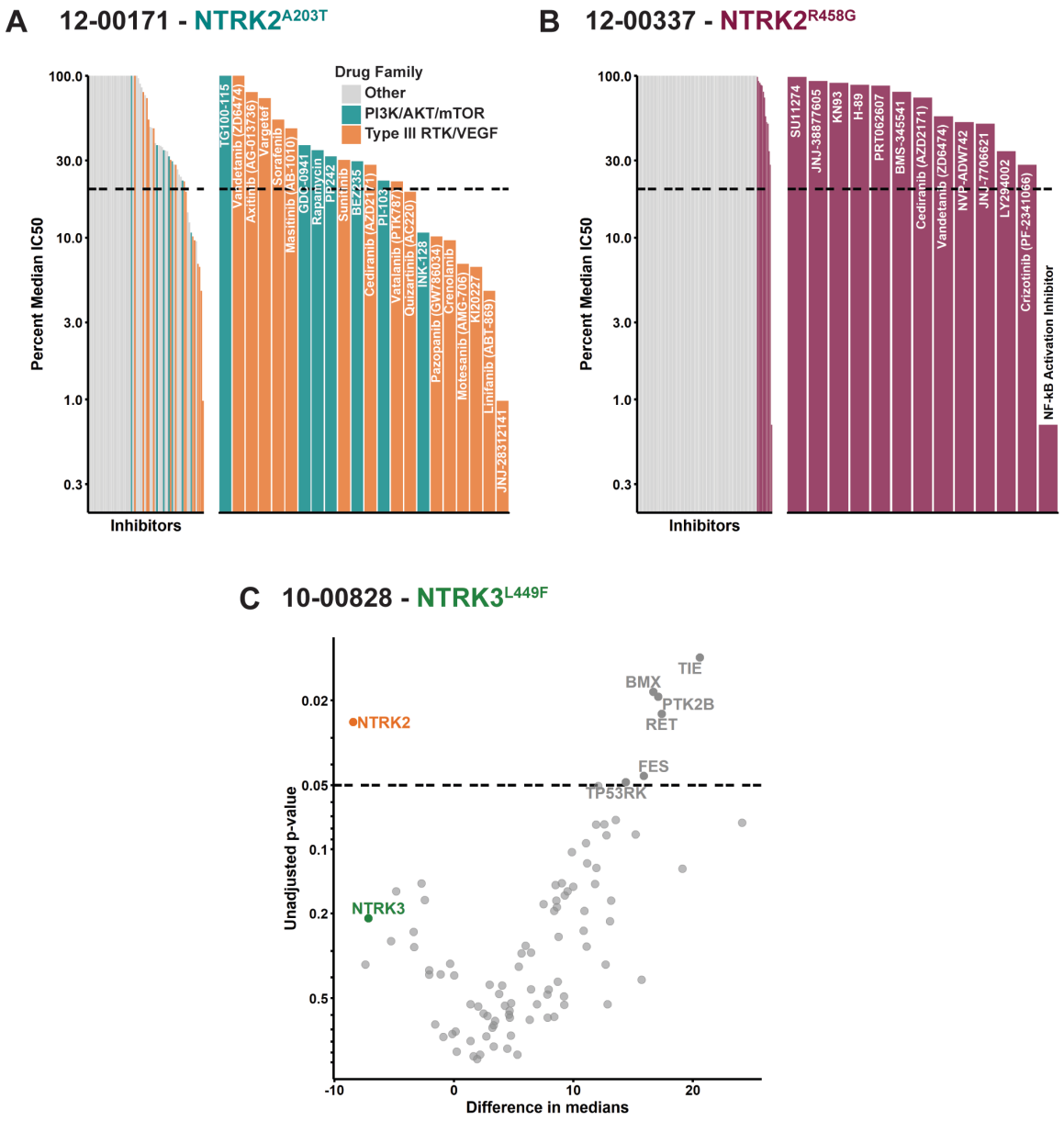

Figure 5: Patients with leukemia harboring NTRK mutations show altered sensitivity to small-molecule inhibitors of various signaling pathways. A. Inhibitor profile for patient 12-00171, with the IC_{50} response to each inhibitor shown on a $\log_{10}$-scale relative to the median IC_{50} of all primary samples tested to-date. Dotted line indicates 20% of the median IC_{50}, which has historically been a marker for patient samples remarkably sensitive to a screened inhibitor[317, 318]. Inhibitors targeting the indicated families are colored, and then emphasized with the breakout panel on the right (drugs targeting other families are removed from the chart). **B.** Inhibitor profile for patient 12-00337, all drugs with IC_{50} responses less than the median IC_{50} are shown in the breakout panel on the right and labeled. **C.** siRNA screen targeting tyrosine kinases in patient 10-00828. Targets are compared against non-targeting control, with unadjusted p-values derived

from a Student's two-tailed T-test (n=3 for each target) shown on the y-axis (negative $\log_{10}$ scale), and effect size shown as difference in median viability on the x-axis. NTRK2 and NTRK3 knockdown resulted in reduced cell viability. The data shown in A-C are available in our lab's Beat AML repository and were visualized with the assistance of Kevin Watanabe-Smith and Daniel Bottomly.

Discussion

Inhibitors targeting Trk oncofusions have shown dramatic and durable responses in pediatric and adult patients with solid tumors regardless of histology[207, 208, 221, 295, 313]. The success of these inhibitors has reinvigorated interest in delineating the contribution of Trk signaling in hematologic tumors. Similar to FLT3, KIT, CSF1R, CSF2Rβ, CSF3R, and PDGFRβ, previous studies have suggested that Trk receptors and their respective ligands also contribute to different stages of hematopoiesis[30, 272, 274, 319]. Trk receptors are expressed on hematopoietic cells and mesenchymal stromal cells found within the bone marrow microenvironment[276]. They promote proliferation and survival of dendritic cells, lymphocytes, macrophages, and monocytes[274]. In particular, TrkB is highly expressed on immature thymocytes and its expression declines as T cells differentiate[275]. Marrow stromal cells secrete nerve growth factor that binds to TrkA on hematopoietic cells[276]. However, apart from these studies, a clear functional role of Trk signaling in normal hematopoiesis remains undefined.

There is increasing evidence highlighting Trk receptors in leukemogenesis[80]. Differing from the activation of ABL1 that is predominantly driven by the BCR-ABL1 fusion, Trks can be activated by much broader mechanisms, including oncogenic fusions[244, 248, 256], deletion/truncation events[28, 267], transcriptional upregulation[145, 271, 277], and point mutations[249, 250] in leukemia.

In this study, we identified and characterized four novel oncogenic NTRK point mutations in patients with leukemia: two in NTRK2 (A203T, R458G) and two in NTRK3 (E176D, L449F) (**Figure 1H**). Stable expression of these mutations in IL-3-dependent Ba/F3 cells provided a proliferative advantage (**Figure 1B**) and increased downstream signaling (**Figure 2A-B**), further underscoring that NTRKs can serve as an oncogene. Upon further evaluation, we saw that a majority of these point mutations facilitate increased receptor dimerization with the exception of $NTRK2^{R458G}$ (**Figure 4**). Selective inhibition of NTRK2 and NTRK3 with entrectinib, a well-validated NTRK inhibitor currently in clinical trials for NTRK-fusion positive cancers[221, 295], can

inhibit proliferation and induce apoptosis of NTRK mutant-transformed Ba/F3 cells (**Figure 2C-E**). Collectively, our data in combination with others, accentuate a previously underestimated role of NTRK point mutations in a subset of patients with leukemia and propel the need to consider Trk inhibitors for such patients clinically.

Although rare, the few NTRK point mutations—NTRK1^{S667N}, NTRK2$^{T573I/V684I}$, and NTRK3^{Y800H}—previously reported in patients with acute leukemias were identified in the kinase domain of the Trk receptor[249, 250]. Their functional characterization and potential contribution to leukemogenesis has yet to be reported. More recently, a study identified point mutations—H498R, G617D, and H766R—in the kinase of domain of NTRK1 in patients with acute erythroid leukemia[251]. Interestingly, co-occurrence of these mutations with TP53^{R172H} induced an aggressive form of erythroid leukemia[251]. A single NTRK1 mutation in the absence of mutated TP53 did not generate such a phenotype. Of the nine mutations we identified, only one, R645C, was found in the kinase domain of NTRK3. However, this mutation did not confer IL-3-independent growth. Among the four transforming mutations we identified, two reside in the extracellular domain of the TrkB and TrkC receptors (A203T and E176D, respectively), one within the transmembrane domain of TrkC (L449F), and one within the juxtamembrane domain of TrkB (R458G). While similar point mutations have been reported in solid tumors (**Supplemental Figure 5**), to our knowledge, we are the first to study and characterize these mutations in hematological malignancies. Due to the unavailability of a matched skin biopsy, we were unable to confirm if these mutations are somatic or germline. While they are not found in the COSMIC database, it should be noted that the NTRK2^{A203T} mutation has been reported in ExAC, albeit at a very low allele frequency[320] (**Supplemental Table 3**). The location of these point mutations may be indicative of the activating mechanism, which we discuss below.

We saw that point mutations, A203T and E176D in the extracellular domain of TrkB and TrkC receptors, respectively, transformed Ba/F3 cells and led to increased phosphorylation of the Trk receptor and its downstream effectors, RAS/MAPK, PI3K/AKT, and JAK/STAT signaling. Both

point mutations also exhibited increased receptor dimerization (**Figure 4**). Our data is in agreement with the deltaTrkA mutation that was found in a patient with AML[28]. This in-frame mutation contains a 75-amino acid deletion in the extracellular domain of the TrkA receptor that resulted in constitutive kinase activity, activation of downstream signaling, transformation of fibroblasts *in vitro*, and polyclonal AML in mice transplanted with deltaTrkA^{+} cells[28, 267]. Deletion of the 75 amino acids likely alters the tertiary structure of the receptor and results in the removal of key glycosylation sites which prevent spontaneous receptor-receptor interactions (i.e., dimerization)[265]. Previous work from our lab has also shown that a point mutation in the colony-stimulating factor 3 receptor (CSF3R)—T618I—abrogates an O-glycosylation event, which in turn increases receptor dimerization[321]. As evident by both studies, the extracellular domain, particularly glycosylation sites within this domain could serve as a regulatory switch that prevent spontaneous dimerization and kinase activation.

In line with these findings, we speculate that NTRK2^{A203T} and NTRK3^{E176D} disrupt nearby N-glycosylation sites at residues 205 of TrkB and 163 of TrkC, enabling receptor dimerization (**Figure 4**) and, thus supporting the aberrant kinase activity we observed (**Figure 2A-B**). NTRK3^{E176D} could also disrupt disulfide bond formation between cysteines at residues 166 and 207 and, thereby distort the receptor's tertiary structure leading to aberrant signaling. The increase in NTRK2^{A203T} and NTRK3^{E176D} receptor molecules at the cell surface and decrease in cell surface retention (**Figure 3A & 3C**) further reinforce that receptor dimerization is possibly the predominant mechanism of activation for these mutants. It is likely that increased abundance of cell surface receptor molecules could facilitate increased dimerization events, culminating in increased receptor internalization, which is further supported by the decrease we saw in surface retention of the mutant receptors.

We also saw an increased propensity to dimerize with our transmembrane domain mutant, NTRK3^{L449F} (**Figure 4C-D**). Transmembrane domain mutations have been shown to cause constitutive receptor activation through receptor stabilization, which increases kinase activity and

downstream oncogenic signaling[30-32]. For example, previous work from our lab has shown that a transmembrane domain mutation in the colony-stimulating factor 2 receptor beta (CSFR2β), R461C, resulted in prolonged surface retention of the mutant receptor relative to the WT receptor in a patient with T-ALL[30]. A very similar finding was seen with activating mutations in the interleukin 7 receptor again in patients with T-ALL[32]. Receptor stability, in both studies, stemmed from the formation of disulfide bonds between cysteine residues that were introduced by the respective point mutations. Although we saw a similar downstream signaling profile for the NTRK3^{L449F} mutant, in our case, disulfide bond formation was not the underlying activation mechanism. Increased dimerization exhibited by NTRK3^{L449F} could potentially be explained by the change in secondary protein structure. Our Phyre^2 modeling predicted that a leucine to phenylalanine alteration results in a shift from a beta-pleated sheet to an alpha helix (**Supplemental Figure 8B**). The alpha helix is possibly more conducive for receptor dimerization.

Unlike the extracellular and transmembrane domain NTRK mutants, NTRK2^{R458G} did not induce increased receptor dimerization (**Figure 4A-B**). Nonetheless, we saw robust kinase activation (**Figure 2A**) and oncogenicity (**Figure 1B**), signifying that dimerization may not serve as the underlying activation mechanism. It should be noted that the arginine residue at position 458 is conserved in all three NTRK genes and, therefore may play an important function in Trk regulation (**Supplemental Figure 10A**).

Given the proximity of the R458 residue to the TrkB transmembrane domain, we examined whether NTRK2^{R458G} altered the transmembrane domain and if this change influenced receptor-receptor interactions or interactions between the juxtamembrane and transmembrane domains[35]. Based on our analysis of the transmembrane domain using previously validated prediction models[30, 322-332], NTRK2^{R458G} did not significantly alter the stretch of amino acids that typically delineate the transmembrane domain (**Supplemental Figure 10B-C**).

A

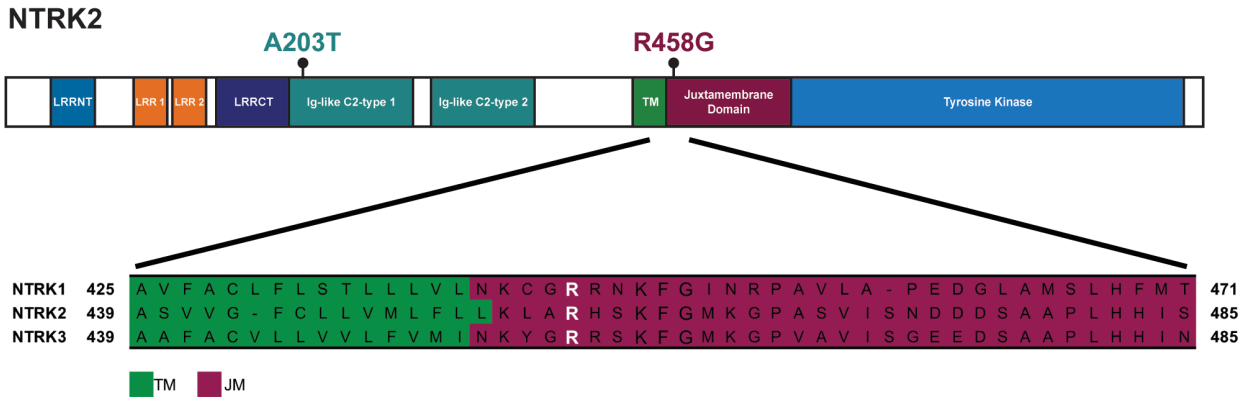

B

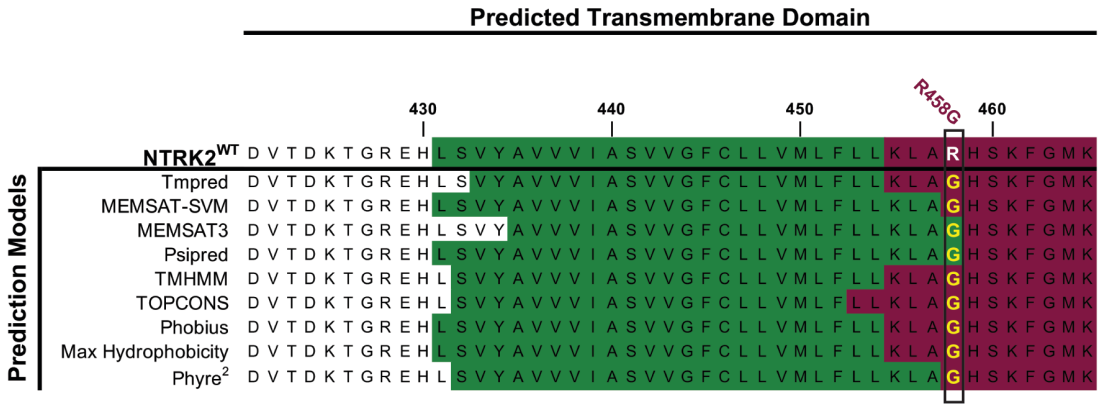

C

Prediction Model	Website	Predicted TM Domain WT	Predicted TM Domain R458G
Uniprot	https://www.uniprot.org/uniprot/Q16620	431-454	n/a
Tmpred	https://embnet.vital-it.ch/software/TMPRED_form.html	433-452	433-454
MEMSAT-SVM	http://bioinf.cs.ucl.ac.uk/psipred/	431-458	431-457
MEMSAT3	http://bioinf.cs.ucl.ac.uk/psipred/	435-458	435-458
Psipred	http://bioinf.cs.ucl.ac.uk/psipred/	431-458	431-458
TMHMM	http://www.cbs.dtu.dk/services/TMHMM/	432-454	432-454
TOPCONS	http://topcons.cbr.su.se	432-452	432-452
Phobius	http://phobius.sbc.su.se	431-454	431-454
Max Hydrophobicity	http://www.tulane.edu/~biochem/WW/PepDraw/	431-454	431-454
Phyre^2	http://www.sbg.bio.ic.ac.uk/phyre2/html/page.cgi?id=index	433-456	432-457

Supplemental Figure 10: Multiple prediction models suggest that residue R458 does not lie within the transmembrane domain of NTRK2. A. Arginine (R) is a conserved residue among all three NTRK genes. **B.** A series of transmembrane prediction models show that a loss of a positively charged arginine residue does not heavily change the composition of the NTRK2 transmembrane domain. Predicted domain is labeled in mustard and residue 458 is bolded. In

very few models is residue R458 included within the transmembrane domain of NTRK2. Sequence of WT NTRK2 is based on uniprot.org. **C.** The chart provides information on each prediction model used and the corresponding sequence differences observed between $NTRK2^{WT}$ and $NTRK2^{R458G}$.

It may be the case that the $NTRK2^{R458G}$ mutant modifies the structure of the juxtamembrane domain and the manner by which this domain interacts with lipids in its immediate environment. To date, multi-scale molecular dynamics receptor simulation studies have shown the importance of the interaction between anionic lipids found within the membrane and juxtamembrane domains of epidermal growth factor and ephrin receptors[34, 36]. Both of these studies highlight that basic, positively charged residues at the N-terminus of the juxtamembrane domain interact with negatively charged phosphatidylinositol-4,5-biphosphate (PIP_2) headgroups, driving the formation of lipid nanoclusters in the membrane. Specifically, arginine and lysine are key residues that mediate this interaction with PIP_2 in all 58 human receptor tyrosine kinases (RTKs), implicating the importance of this interaction for the structure and function of these receptors[34]. Studies suggest that these lipid nanoclusters around the juxtamembrane domain may maintain an autoinhibitory function that prevents unwarranted receptor activation in normal physiologic conditions[37, 333, 334]. Loss of this autoinhibitory function may enable constitutive receptor activation and downstream signaling that facilitates cancer growth and progression. We believe this phenomenon is analogous to what is observed in a subset of RTKs, such as FLT3 and PDGFRβ, where key residues in the juxtamembrane domain of the receptor maintain basal receptor activity[33]. As such, we postulate that loss of the positively charged arginine in the R458G mutant could alter these lipid-protein interactions, resulting in a functionally active TrkB receptor that encourages upregulation of downstream signaling and leukemogenesis.

Based on a previously reported course-grain molecular dynamics simulation study, we prepared the homology model of human NTRK2 WT and colored each protein residue by the mean number of contacts with PIP_2 (**Supplemental Figure 11A**)[34]. Two significant changes

observed following the mutation of an arginine to a glycine were the change in polarity (i.e., decrease in the positively charged blue area) and a decrease in the shape of the molecular surface due to the loss of a bulky side chain (**Supplemental Figure 11B-C**). We, therefore predict that the R458G mutation changes the way PIP_2 lipid molecules are recruited and how they nanocluster around the juxtamembrane domain.

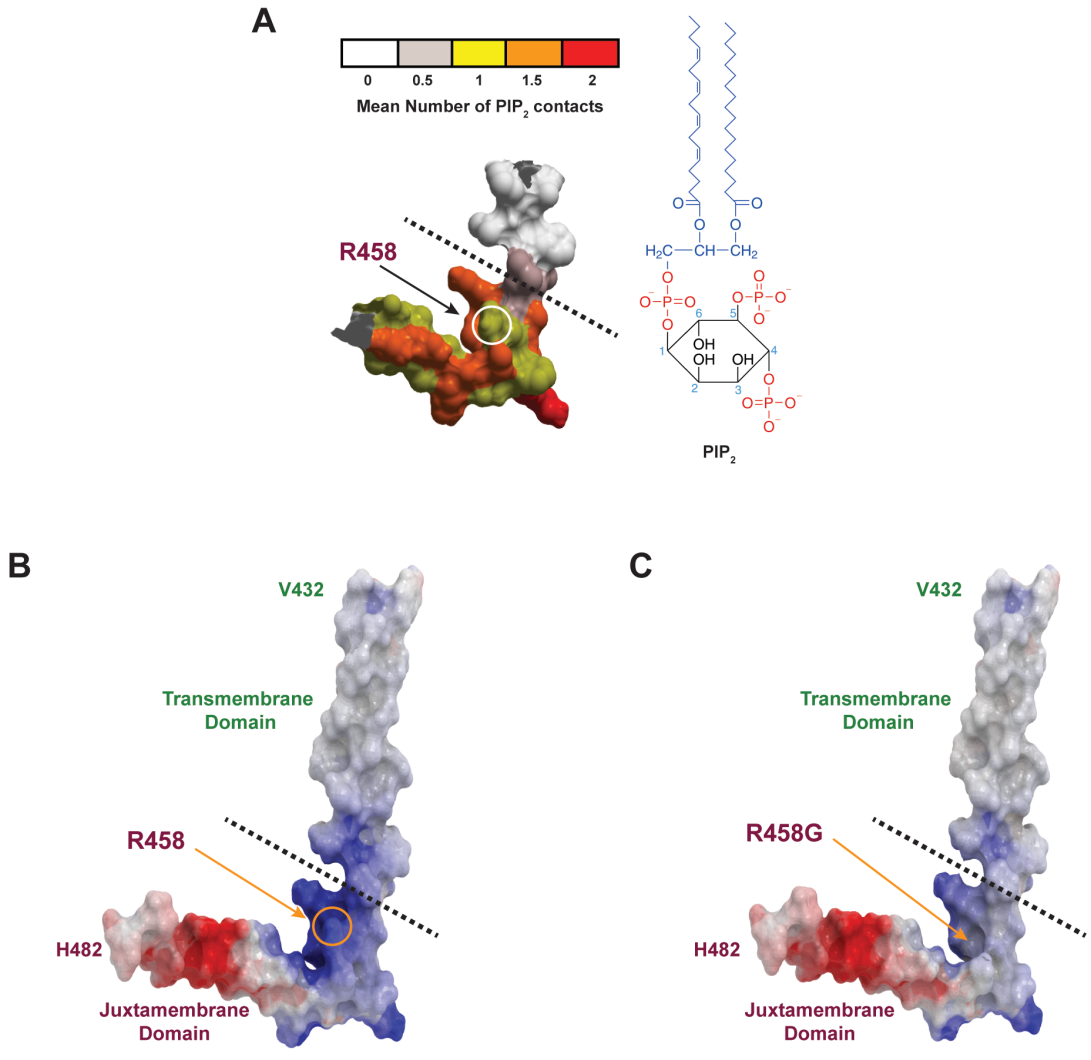

Supplemental Figure 11: Loss of a positively-charged, basic amino acid residue may explain the activation of the NTRK2^{R458G} mutant. A. PIP_2 interactions in human NTRK2 (L448-TM-JM-D474). Each protein residue is colored by the mean number of contacts with the phosphoryl group attached to the glycerol moiety of the PIP_2 headgroup per course-grain

simulation frame, as previously reported[34]. **B.** Homology model of human WT NTRK2 (V432-TM-JM-H482). The protein is displayed as molecular surface and colored according to electric potential (basic residues in blue; anionic residues in red). **C.** Homology model of human NTRK2^{R458G} mutant (V432-TM-JM-H482). The protein is displayed as molecular surface and is also colored according electric potential. Transmembrane Domain, TM; Juxtamembrane Domain, JM. Molecular dynamic simulation modeling was performed in collaboration with William Bisson of the Oregon State University.

The lack of a crystallized structure that engages the flexible Trk juxtamembrane domain prevents us from fully understanding how the NTRK2^{R458G} mutation alters the lipid-juxtamembrane domain interactions relative to the WT receptor. Despite this limitation, our data suggest that the loss of arginine, a conserved residue among all three Trk receptors, is crucial to the regulatory function of the TrkB receptor. Future studies will consider the use of cryo electron microscopy to study the molecular interactions by which the juxtamembrane domain controls Trk function and activity.

Irrespective of the underlying activation mechanism, we saw decreased phosphorylation of TrkB and TrkC in our mutant-transformed Ba/F3 cells following treatment with entrectinib. We also observed a dose-dependent increase in apoptosis in our mutant cells following entrectinib treatment. Our findings were in line with Smith *et al.*, who reported that *in vitro* entrectinib treatment potently inhibits cellular proliferation, Trk activation, and induces apoptosis in ETV6-NTRK3^{+} AML cell lines and in a xenograft study[296]. Akin to their study, we found entrectinib to be more potent than larotrectinib, a selective pan-Trk inhibitor, in our Ba/F3 model.

Assays performed on freshly isolated clinical material from patients with NTRK$^{A230T/R458G}$ mutations, allowed us to observe altered sensitivities to small-molecule inhibitors of various signaling pathways (**Figure 5A-B**). Importantly, we saw sensitivity to Trk and PI3K/AKT inhibitors based on IC_{50} values. These findings correlate with the increased Trk activation and downstream PI3K/AKT signaling we observed in our mutant-transformed cells (**Figure 2A**). It should be noted

that both patients with the NTRK2^{R458G} mutation, had either a co-occurring mutation in BCR-ABL1^{T315I} or CSF3R^{T640N} (**Supplemental Table 3**). Despite these known oncogenes, the NTRK2^{R458G} mutation may play an important role in mediating resistance. According to our small-molecule inhibitor screen, the patient (i.e., 12-00337) with the BCR-ABL1^{T315I} was resistant to ponatinib, an FDA-approved inhibitor against BCR-ABL1^{T315I} mutations seen in CML. We also saw no response to other known CML tyrosine kinase inhibitors such as imatinib, dasatinib, and nilotinib (**Supplemental Table 5**). Here, the NTRK2^{R458G} may serve as a bypass resistance pathway for these leukemia cells. Whether the NTRK mutation is an early event or a secondary mutation is outside the scope of this current work but will be considered in future studies. As for the patient (i.e., 13-00187) harboring NTRK2^{R458G} with an accompanying functional CSF3R^{T640N} co-mutation, we are unable to comment on which mutation is driving leukemogenesis[335]. It may be the case that both mutations contribute to the overall phenotype.

Taken together, we identified and characterized four oncogenic NTRK point mutations in the setting of leukemia. These mutations bear functional consequence. Their response to FDA-approved inhibitors—entrectinib and larotrectinib—is striking and warrants investigation of other rare, yet targetable NTRK mutations in hematological malignancies. In an era of personalized cancer therapy, where understanding a patient's mutational landscape is imperative for treatment, our study paves the way for therapeutic targeting of Trk signaling in hematological malignancies. Similar to basket trials focused on solid tumors harboring Trk mutations, a parallel systematic approach is necessary to assess the efficacy of Trk inhibitors in patients with liquid tumors.

Materials & Methods

Sequencing of patient samples

All clinical specimens were collected with informed consent from patients with hematologic malignancies according to a protocol approved by the Oregon Health and Science University (OHSU) institutional review board (IRB 4422; NCT01728402). A total of 185 patient samples were collected and sequenced, including 96 acute myeloid leukemia (AML), 51 acute lymphoblastic leukemia (ALL), and 38 myeloproliferative neoplasms (MPN).

Peripheral blood and bone marrow aspirates from these patients were processed by Ficoll gradient centrifugation followed by red blood cell lysis. Cell pellets for subsequent genomic and protein studies were snap-frozen in liquid nitrogen. DNA was extracted using the Qiagen DNeasy Blood & Tissue kit (Qiagen Inc., Germantown, MD) according to the manufacturer's protocol.

Deep sequencing was performed on 1,862 kinase and kinase-associated genes as described previously[318, 336]. In brief, the final purified libraries were sequenced on a HiSeq 2000 sequencer (Illumina Inc., San Diego, CA) followed by FASTQ assembly using the CASAVA pipeline (Illumina)[318]. Sequence capture, library preparation, and deep sequencing were performed by the OHSU Massively Parallel Sequencing Shared Resource. Raw sequencing files are available upon request. Variant allele frequencies (VAF) were determined based on GATK v3.3 as reported previously[11].

NTRK mutations were confirmed by PCR amplification of NTRK exons using the primers listed in **Supplemental Table 1a**. Sanger sequencing with M13 forward (5'—GTAAAACGACGGCCAGT—3') and M13 reverse (5'—CAGGAAACAGCT-ATGACC—3') primers was used to confirm the presence of NTRK point mutations in patient genomic DNA. Sequencing was performed using Eurofins MWG Operon (Louisville, KY) and analyzed using Sequencher and DNASTAR software. Additional sequencing was performed by GeneWiz Inc. (South Plainfield, NJ).

Cloning

NTRK2 cDNA (NM_006180), NTRK3 cDNA (NM_001012338), and gateway-compatible entry clones (pDONR223 and pENTR223) were purchased from Arizona State University. All NTRK mutations were introduced by site-directed mutagenesis using the QuikChange II XL kit (Agilent Technologies Inc., Santa Clara, CA) and primers listed in **Supplemental Table 1b**. Mutagenesis primers were designed using the QuikChange Primer Design Program available through Agilent and purchased from Eurofins. Mutated cDNAs were then transferred into a Gateway-compatible pMX retroviral vector using a Gateway LR Clonase kit (Life Technologies Inc., Carlsbad, CA). Constructs were verified by Sanger sequencing.

Cell culture and retroviral production

HEK 293T/17 cells (ATCC, Manassas, VA) were cultured in DMEM (Life Technologies Inc.) supplemented with 10% FBS (Atlanta Biologicals, Flowery Branch, GA), 2% L-glutamine, 1% penicillin/streptomycin (Life Technologies Inc.), and 0.1% amphotericin B (HyClone, South Logan, UT). To produce murine retrovirus, HEK 293T/17 cells were co-transfected with FuGENE 6 (Promega, Madison, WI), EcoPac helper packaging plasmid, and pMX NTRK constructs (wild-type (WT) or mutant). pMX-puro was used as an empty vector control. Retroviral supernatants were harvested 48 hours after transfection.

Ba/F3 cells were grown in RPMI (Life Technologies Inc.) supplemented with 10% FBS, 2% L-glutamine, 1% penicillin/streptomycin, 0.1% amphotericin B as stated above, and 15% WEHI conditioned medium (a source of IL-3). Stable Ba/F3 NTRK2^{WT}, NTRK3^{WT}, and mutant cell lines were generated by infection of 3 x 10^6 cells with 1 mL of retroviral supernatant followed by spinoculation with polybrene at 2500 rpm for 90 minutes[30]. Ba/F3 cells infected with the pMX empty, WT NTRK and mutant vectors were then selected using 2 µg/mL puromycin (ThermoFisher Scientific, Waltham, MA) selection.

Ba/F3 transformation assay (IL-3 withdrawal)

Parental Ba/F3 cells and cells expressing empty vector, $NTRK2^{WT}$, $NTRK3^{WT}$, and mutants were washed three times in RPMI medium with 10% FBS (to remove all traces of IL-3-containing WEHI conditioned medium). Cells were then suspended at a density of 5×10^5 cells per mL and counted on a Guava personal flow cytometer (Millipore Inc., Burlington, MA) every other day and divided as necessary[30, 336].

Transient transfection studies

2 µg of NTRK WT, mutant, or empty vector constructs were transfected into HEK 293T/17 cells using FuGENE 6. Following 48 hours, cells were serum starved (0.1% BSA) for 4 hours and prepared for immunoblotting as described below.

Immunoblotting

Following overnight serum starvation in 0.1% BSA RPMI media, 10-15 million parental, empty vector, NTRK WT, and mutant Ba/F3 cells were spun down and lysed with 150 µL of Cell Lysis Buffer (Cell Signaling Technologies Inc., Danvers, MA) containing a Complete Mini Protease Inhibitor Cocktail Tablet, Phosphatase Inhibitor Cocktail 2, and Phenylmethanesulfonyl Fluoride (PMSF) solution (Sigma-Aldrich Inc., St Louis, MO) and clarified by centrifugation at 14,000 *g*, 4 °C for 15 minutes. Cell pellets from available clinical samples were lysed in 30-40 µL of lysis buffer. Protein was quantified using a bicinchoninic acid (BCA) assay (ThermoFisher Scientific Inc.). 50 µg of each protein lysate was loaded on NuPAGE 4-12% Bis-Tris gradient gels (Thermo Fisher Scientific Inc.), transferred on Immobilon-FL PVDF membranes (Millipore Inc.), and blocked for 1 hour. Following overnight incubation with primary antibody (**Supplemental Table 2**) at 4 °C, the membranes were washed and probed with fluorescent IRDye 800CW goat anti-rabbit IgG and IRDye 680RD Goat anti-mouse IgG antibodies (1:15,000; LI-COR

Biosciences, Lincoln, NE). The membranes were then imaged with the Odyssey Infrared Imaging System (LI-COR Biosciences).

Inhibitor studies

Small-molecule inhibitors, purchased from LC Laboratories Inc. (Woburn, MA), MedChemExpress (Monmouth Junction, NJ), and Selleck Chemicals (Houston, TX) were reconstituted in DMSO and stored at -80°C. In this study, the following small-molecule inhibitors were used - BGJ398, cabozantinib, crenolanib, crizotinib, entrectinib, foretinib, imatinib, larotrectinib, and ponatinib. Cells were seeded into 384-well assay plates using a Multidrop™ Combi Reagent Dispenser (ThermoFisher Scientific Inc.) at a density of 1,000 cells/well in 50 µL of RPMI media supplemented with 10% fetal bovine serum, 2% L-glutamine, 1% penicillin-streptomycin, and 0.1% amphotericin B. Inhibitors were dispensed into the plates with an HP D300e Digital Dispenser (Tecan, Mannedorf, Switzerland) at increasing concentrations. The final concentration of DMSO was ≤0.1% in all wells. All conditions were plated with six replicates. After three days of culture at 37°C in 5% CO_2, cell viability was measured using a methanethiosulfonate (MTS)-based assay (CellTiter96 Aqueous One Solution; Promega) and absorbance (490 nm) was read at four hours after adding MTS reagent using a BioTek Synergy 2 plate reader (BioTek, Winooski, VT). MTS absorbances of inhibitor-treated wells were normalized to those of untreated cells as previously described[145]. Regression curve fit analysis of the normalized data to determine IC_{50} values was performed using GraphPad Prism software.

Annexin staining

To detect apoptosis of cells, the Guava Nexin Annexin V Assay (Millipore Inc.) was used according to the manufacturer's protocol and cells were counted using Guava personal flow cytometer following 48 and 72 hours of entrectinib treatment. The assay uses two dyes: Annexin V-PE to detect phosphatidylserine (PS) on the external membrane of early apoptotic cells and 7-

AAD, a cell impermeant dye, to identify cells in late-stage apoptosis and dead cells. All experiments were performed in triplicate.

Cell surface localization and protein retention studies

For cell surface localization and protein stability studies, all Ba/F3 cell lines were serum starved overnight (~16-18 hours) in 0.1% BSA RPMI media. For localization studies, 1 million cells per Ba/F3 cell line (WT or mutant), were stained with APC-conjugated anti-TrkB or anti-TrkC antibodies (**Supplemental Table 2**; Novus Biologicals, Centennial, CO) for 1 hour, washed in PBS with 0.5% BSA, and analyzed by flow cytometry (BD FACSAria IIIu and BD LSR II) for mean fluorescence intensity (MFI) and normalized to WT samples. The experiment was performed in triplicate (n=3 per cell line).

For protein retention studies, Ba/F3 cells (WT and mutant) were treated with 100 µg/ml of cycloheximide in DMSO or DMSO (control) for 12 and 24 hours, washed with 1X PBS, and stained with APC-conjugated anti-TrkB or anti-TrkC antibodies as described above. Cells were analyzed by flow cytometry for MFI and normalized to untreated DMSO controls. The experiment was performed in triplicate (n=3 per condition).

Taxonomy studies

Alignment was performed using the Clustal Omega program available via UniProt.

Protein secondary structure and transmembrane domain prediction modeling

To understand the structural impact of the NTRK point mutations, we utilized a prediction model, Phyre[2] (http://www.sbg.bio.ic.ac.uk/~phyre2/html/page.cgi?id=index) to study changes in protein secondary structure, that has been previously validated[315, 337, 338].

For transmembrane domain analysis, consensus coding sequences for WT and NTRK2^{R458G} were analyzed by the indicated transmembrane modeling programs in **Supplemental Figure 9**

as previously described[30]. Top predictions that maintained a single transmembrane domain and type-I orientation are listed.

Receptor dimerization studies

FLAG and HA-tagged NTRK WT and mutant constructs were created using the In-Fusion HD Cloning Plus kit and pCMV-FLAG and HA vector sets (Takara Bio Inc., Mountain View, CA) according to the manufacturer's instructions. FLAG and HA vectors were linearized by restriction digestion with EcoR1 HF (NEB Inc., Ipswich, MA) and fused with PCR-generated NTRK WT and mutant inserts using the Takara In-Fusion Enzyme. All PCR primers were designed with the on-line Takara Primer Design tool and are listed in **Supplemental Table 1c**.

Dimerization studies were performed using a previously validated protocol[321, 335]. Briefly, 0.5 µg of FLAG and HA-tagged NTRK WT or mutant constructs were co-transfected into HEK 293T/17 cells. Following 48 hours, cells were lysed with cell lysis buffer as described above and incubated overnight with anti-FLAG M2 Affinity Gel beads (Sigma-Aldrich Inc.). Immunoprecipitates were then collected by brief centrifugation for 30 seconds and washed by spinning through cell lysis buffer containing 15% sucrose. Bound protein was eluted by boiling immunoprecipitates with electrophoresis 4X sample LDS loading buffer and 10X reducing buffer (Life Technologies Inc.) at 95 °C for 10 minutes and loaded onto NuPAGE 4-12% Bis-Tris gradient gels as described above. Blots were probed using anti-FLAG and anti-HA antibodies (**Supplemental Table 2**). Immunoprecipitations were normalized to the starting input using ImageJ quantification.

siRNA and kinase inhibitor assays

Mononuclear cells isolated from fresh primary patient samples were screened in triplicate on an siRNA panel targeting the tyrosine kinome as previously described[316]. Following normalization by row, column, and plate, viability following knockdown of each target was compared to non-

targeting control siRNA using a Student's two-tailed T-test to determine significance. Unadjusted p-values are compared against difference in median viability between each target and the non-targeting control in a volcano plot with points of interest labeled.

Patient samples, processed as above, were screened on multiple inhibitor panels containing individual targeted agents in four-point or seven-point dose curves with cellular viability measured 72 hours later, as previously described[11, 317]. It should be noted that larotrectinib and entrectinib had not been developed at the time of patient sample accrual. Since ex vivo inhibitor testing can only be done on fresh samples at the time of sample procurement, we cannot comment on how these patients would respond to larotrectinib or entrectinib.

Relative viability readouts were constrained between 0 and 100% viability, fitted with a probit regression curve, and the concentration corresponding to 50% relative viability (IC_{50}) was interpolated. When a response curve never reached 50% viability, the IC_{50} is reported as the highest tested dose. IC_{50} values were converted into percent of median IC_{50}, where the median IC_{50} is the median response of all primary leukemic patient samples (n = 2,395) screened on the same inhibitor compound. Drug families of inhibitors are derived from prior work[11] and manually simplified into larger subcategories. Analysis and visualization were performed using R version 3.5.1, Rstudio version 1.1.463, the tidyverse packages, as well as ggrepel, readxl, janitor, extrafont, scales, and patchwork[339-347].

In silico molecular modeling

The homology models of human WT and NTRK2^{R458G} (V432-TM-JM-H482) were built using the 3D-coordinates of human EGFR TM-JM-A segments[348] and energetically refined in the internal coordinate space[349]. The protein skin representing the molecular surface was colored according to the electrostatic potential calculated by the Rapid Exact-Boundary Electrostatics (REBEL) method (hydrogen atoms were ignored). The energy calculated by this method consists

of the Coulomb energy and the solvation energy. Areas colored blue represent positive areas and red represents negative areas (Molsoft ICM v3.8).

Statistical analysis

Mean ± SEM are shown unless otherwise stated. One-way or two-way ANOVA with Tukey's multiple comparison test were used to determine statistical significance. Statistical analysis was conducted using GraphPad Prism version 8.0. *P* values less than 0.05 were deemed significant. Asterisks in figures and in their corresponding legends denote level of statistical significance.

Data Sharing Statement

Raw sequencing files are available upon request.

Supplemental Tables

Table 1a: Exon Sequencing Primers

Gene	Amino Acid Change	Exon Number	Forward Primer Sequence (5'→3')	Tm (°C)	Reverse Primer Sequence (5'→3')	Tm (°C)
NTRK2	A203T	6	gtaaaacgacggctgtctggtagagg	71.9	caggaaacagctatttgttcaggatg	71.3
	R458G	11	gtaaaacgacggcattatcatcgtca	71	caggaaacagctaccttctttagtgg	71.2
NTRK3	E176D	5	gtaaaacgacggcctggatttctttt	71.5	caggaaacagctaggtgtgatgagaa	71.2
	L449F	11	gtaaaacgacggcagaacattcaatc	72.6	caggaaacagctagcataagcccttc	71.3

Table 1b: Site-Directed Mutagenesis Primers

Gene	Amino Acid Change	Forward Primer Sequence (5'→3')	Tm (°C)	Reverse Primer Sequence (5'→3')	Tm (°C)
NTRK2	H245Y	cttaaggagccctgtgtagcttgtttcattcatatgt	78.45	acatatgaatgaaacaagctacacacagggctccttaag	78.45
	A203T	catctgcaaatctggccacacctaacctcactgtg	80.44	cacagtgaggttaggtgtggccagatttgcagatg	80.44
	R458G	ttctgcttaagttggcaggacactccaagtttggc	78.1	gccaaacttggagtgtcctgccaacttaagcagaa	78.1
	S167Y	actctccaagaggctaaatacagtccagacactca	78.1	tgagtgtctggactgtatttagcctcttggagagt	78.1
NTRK3	L449F	ctgtgtcctgttggtggtttttcttcgtcatgatca	78.1	tgatcatgacgaagaaaaccaccaacaggacacag	78.1
	E176D	gctctggcaggatcaggggggaggcc	80.02	ggcctcccctgatcctgccagagc	80.02
	T261I	cagaccaatctgaactggatcaatgttcatgccatcaac	79.5	gttgatggcatgaacattgatccagttcagattggtctg	79.5
	L378V	aacaatggcaactatacccgtcattgccaaaaacccac	78.28	gtgggtttttggcaatgacggtataagttgccattgtt	78.28
	R645C	ccttgtggatggacagccatgccaggccaa	80.27	ttggcctggcatggctgtccatccacaagg	80.27

Table 1c: In-Fusion Cloning Primers

Gene	Forward Primer Sequence (5'→3')	Tm (°C)	Reverse Primer Sequence (5'→3')	Tm (°C)
NTRK2	gcccaggcccgaattcatgtcgtcctggataaggtggc	64.2	tcggtcgaccgaattcggcctagaatgtccaggtagacc	63.9
NTRK3	gcccaggcccgaattcatggatgtctcttgcccagc	64.9	tcggtcgaccgaattcggccaagaatgtccaggtagattg	63.4

Supplemental Table 1: List of primers used for exon-sequencing **(A)**, site-directed mutagenesis **(B)**, and in-fusion cloning **(C).**

Supplemental Table 2: A list of all antibodies used in this study.

Table 2: Antibodies used in this study						
Target	**Antibody Product #**	**Vendor**	**Clone**	**Species**	**Antibody Dilution**	**Predicted Size (kDa)**
Phospho-Akt (Ser473)	9271	Cell Signaling		Rb	1:1000	60
Akt	9272	Cell Signaling		Rb	1:1000	60
Phospho-p44/42 MAPK (Erk1/2) (Thr202/Tyr204)	9101	Cell Signaling		Rb	1:1000	42, 44
p44/42 MAPK (Erk1/2)	9102	Cell Signaling		Rb	1:1000	42, 44
Phospho-SRC (Tyr416)	2101	Cell Signaling		Rb	1:1000	60
Phospho-Stat3 (Tyr705)	9131	Cell Signaling		Rb	1:500	79, 86
Total-Stat3	9139	Cell Signaling	124H6	Ms	1:1000	79, 86
Phospho-Stat5 (Tyr694)	9351	Cell Signaling		Rb	1:250	90
Phospho-TrkA (Tyr490)/TrkB (Tyr516)	4619	Cell Signaling	C35G9	Rb	1:500	140
TrkB	4603	Cell Signaling	80E3	Rb	1:1000	140, 90
Phospho-TrkC (Tyr516)	PA5-40271	Thermo Fisher		Rb	1:250	140
Pan-Trk	92991	Cell Signaling	A7H6R	Rb	1:500	120-140
GAPDH	AM4300	Thermo Fisher	6C5	Ms	1:5000	39
FLAG	F1804	Sigma Aldrich	M2	Ms	1:10000	-
HA	3724	Cell Signaling	C29F4	Rb	1:10000	-
IRDye 800CW Goat anti-Rabbit IgG	926-32211	LiCOR		Rb	1:15000	-
IRDye 680RD Goat anti-Mouse IgG	926-68070	LiCOR		Ms	1:15000	-
TrkB (APC-conjugated)	NBP2-52523AF647	Novus	8D2E8	Ms	1:50	-
TrkC (APC-conjugated)	FAB3731R	Novus	75213	Ms	1:50	-

Table 3: Available Patient & Mutation Information										
Diagnosis	**Specific Diagnosis**	**Age**	**Sex**	**Gene**	**Nucleotide Change**	**Amino Acid Change**	**Variant Allele Frequency**	**ExAC Frequency**	**COSMIC Status**	**Other Genetic Alterations**
MPN	Primary Myelofibrosis	N/A	N/A	NTRK2	G607A	A203T	0.48	0.0002142	Not Found	$JAK2^{-}$
MPN	$BCR\text{-}ABL1^{+}$ CML	N/A	F	NTRK2	A1372G	R458G	0.57	0	Not Found	$BCR\text{-}ABL1^{T315I}$
MPN	Atypical CML	N/A	M	NTRK2	A1372G	R458G	0.48	0	Not Found	$CSF3R^{T640N}$; $SETBP1^{G870S}$
AML	$NPM1^{+}$ AML	48	F	NTRK3	G528T	E176D	0.48	0	Not Found	N/A
ALL	T-ALL	N/A	M	NTRK3	C1345T	L449F	0.26	0	Not Found	N/A

Supplemental Table 3: List of NTRK point mutation variant allele frequencies and co-occurring mutations. These point mutations were checked in COSMIC and ExAC to determine if they were previously reported. VAF, Variant Allele Frequency

Table 4:				
Inhibitors	IC_{50} (nM)			
	$NTRK2^{A203T}$	$NTRK2^{R458G}$	$NTRK3^{E176D}$	$NTRK3^{L449F}$
BGJ398	1506	3218	1654	10000
Cabozantinib	93.37	10.05	23.45	13.10
Crenolanib	202	41.99	140.10	91.75
Crizotinib	101.20	19.09	77.25	33.71
Entrectinib	1.644	1.566	0.9794	1.015
Foretinib	28.730	18.730	6.245	3.491
Imatinib	10000	10000	10000	10000
Larotrectinib	12.91	13.42	11.46	12.97
Ponatinib	117.50	21.51	48.88	104.40

Supplemental Table 4: Summary of IC_{50} values for inhibition of NTRK mutant-transformed Ba/F3 cell growth by small-molecule inhibitors calculated from data presented in Figure 2C, 2D, and Supplemental Figure 6A.

Supplemental Table 5 and 6 are available at https://doi.org/10.1182/blood.2019003691

Supplemental Table 5: Tabular form of analyzed inhibitor response data for patients 12-00171 ($NTRK2^{A203T}$) and 12-00337 ($NTRK2^{R458G}$). Data corresponds to waterfall plots shown in Figure 5A and 5B.

Supplemental Table 6: Tabular form of normalized siRNA data for patient 10-00828 ($NTRK3^{L449F}$) that was utilized for statistical analysis and to create the volcano plot shown in Figure 5C.

Acknowledgements

We are extremely thankful to our patients for their time and precious tissue samples. We also thank the Oregon Health & Science University Massively Parallel Sequencing Shared Resource and Flow Cytometry Core for technical support, Nicola Long and Beth Wilmot for analytical support, and Stephen Kurtz for critical review of our manuscript. Funding for this project was provided by the Howard Hughes Medical Institute, Leukemia & Lymphoma Society, and the National Cancer Institute grant (1R01CA214428) awarded to B.J.D. B.J.D. is also supported by the following grants from the National Cancer Institute (1U01CA217862, 5U01CA214116, and 1U54CA224019). S. K.J. is supported by the ARCS Scholar Foundation, The Paul & Daisy Soros Fellowship, and National Cancer Institute (1F30CA239335-01). E.T. is supported by grants from the Leukemia & Lymphoma Society (LLS SCOR 7005-11), Lamfrom funds, American Cancer Society (MRSG-17-040-01-LIB), and National Cancer Institute (1U54CA224019). J.W.T. received grants from the V Foundation for Cancer Research, Gabrielle's Angel Foundation for Cancer Research, and National Cancer Institute (1R01CA183947,1U01CA217862, 1U54CA224019, and 3P30CA069533).

Authorship Contributions

Study supervision: B.J. Druker, C.E. Tognon

Conception and design: S.K. Joshi, W.H. Bisson, M.A. Davare, B.J. Druker, C.E. Tognon

Development of methodology: S.K. Joshi, W.H. Bisson, K. Watanabe-Smith, S.K. McWeeney, M.A. Davare, B.J. Druker, C.E. Tognon

Acquisition of data: S.K. Joshi, K. Qian, W.H. Bisson, K. Watanabe-Smith, A. Huang

Analysis and interpretation of data (e.g., statistical analysis, biostatistics, computational analysis): S.K. Joshi, K. Qian, W.H. Bisson, K. Watanabe-Smith, D. Bottomly, E. Traer, J.W. Tyner, M.A. Davare, S.K. McWeeney, B.J. Druker, C.E. Tognon

Writing, review, & editing of the manuscript: S.K. Joshi, K. Qian, W.H. Bisson, K. Watanabe-Smith, A. Huang, D. Bottomly, E. Traer, J.W. Tyner, M.A. Davare, S.K. McWeeney, B.J. Druker, C.E. Tognon

Development of prioritization framework to assist in rigor and reproducibility: S.K. McWeeney

5 *ERBB2/HER2 mutations are transforming and therapeutically targetable in leukemia*

Sunil K. Joshi*, Jamie M. Keck*, Christopher A. Eide, Daniel Bottomly, Elie Traer, Jeffrey W. Tyner, Shannon K. McWeeney, Cristina E. Tognon, Brian J. Druker

***These authors equally contributed to this work.**

This manuscript was published in *Leukemia*, Volume 34(10), Pages 2798-2804, May 4, 2020. https://doi.org/10.1038/s41375-020-0844-7

Abstract

The ErbB/HER family of receptor tyrosine kinases is among the most studied receptor families in cell signaling owing to its role in oncogenesis. In addition to receptor amplification or overexpression, studies in solid tumors, particularly in breast and non-small cell lung cancers, have shown that activating point mutations in ErbB/HER receptors similarly contribute to the tumorigenic phenotype and drug resistance. Nonetheless, very little is known about aberrant ErbB signaling in hematological malignancies. We recently performed deep sequencing on 185 patients with acute myeloid leukemia, acute lymphoblastic leukemia, or myeloproliferative neoplasms and identified point mutations within the extracellular domain (i.e., R188C and P489L) and the intracellular C-terminal region (i.e., L1157R) of the ErbB2/HER2 receptor in three patients. Here, we report that these point mutations are oncogenic. Stable expression of these mutations in Ba/F3 cells led to cytokine-independent growth and in NIH 3T3 fibroblasts exhibited a transformed morphological phenotype. Survival of Ba/F3 cells expressing ERBB2 mutants was inhibited by treatment with irreversible ErbB inhibitors, many of which are FDA-approved in solid tumor malignancies. Although the identification of ERBB2/HER2 mutations is unexpected in leukemia, our results highlight a unique therapeutic opportunity for a subset of patients with acute leukemia harboring ERBB mutations and urge the need to further consider such mutations in the setting of hematological malignancies.

Introduction

The ErbB/HER family of receptor tyrosine kinases consists of four cell surface glycoproteins: epidermal growth factor 1 (EGFR or ErbB1), ErbB2 (c-Neu or human EGF receptor 2 [HER2]), ErbB3, and ErbB4[350]. Each receptor contains an extracellular ligand binding domain, a single-pass transmembrane region, and a cytoplasmic tyrosine kinase domain[350]. Binding of the soluble ligand to its cognate ErbB receptor induces formation of homo- or heterodimer complexes, which activates receptor tyrosine kinase activity, leading to increased downstream RAS/MAPK, PI3K/AKT, and JAK/STAT signaling[351]. It should be noted that ErbB2 is always in an active conformation, requiring no ligand binding. For that reason, it is the preferred heterodimerization co-receptor for all other ErbB family members[351].

These receptors play a fundamental role in the development, proliferation, and differentiation of epithelial, mesenchymal, and neuronal tissues; however overexpression, amplification, and activating point mutations of these receptors promote oncogenesis[350, 351]. Amplification or overexpression of ErbB2 is classically observed in approximately 25 to 30% of breast cancers[352, 353] and is associated with an aggressive clinical phenotype. This oncogenic behavior of ErbB2 can be attributed to its ligand-independent activation and propensity to readily heterodimerize with other ErbB receptors as noted above. Specifically, data gleaned from *in vitro* studies has shown that the ErbB2/ErbB3 heterodimer acts as an oncogenic unit to induce breast cancer cell proliferation via PI3K/AKT signaling[354, 355]. Moreover, activating point mutations such as $ERBB2^{L755P}$ and $ERBB2^{L869R}$ enable ErbB2/ErbB3 dimerization, oncogenic signaling, and cell growth while the gatekeeper mutation $ERBB2^{T798I}$ confers resistance[138, 356].

Analysis of HER2 status by immunohistochemistry, *in situ* hybridization, and Sanger sequencing has shown that HER2 is also overexpressed and/or amplified in approximately 7 to 34% of gastric tumors[357], 30% of salivary duct carcinomas[358], and 20% of non-small-cell lung cancer (NSCLC)[350, 359] cases. Activating mutations in the kinase domain of EGFR have also been

reported in NSCLC[360, 361]. Similar to HER2-mediated breast cancer, EGFR dimerizes with ErbB3 in NSCLC, culminating in up-regulation of PI3K/AKT signaling and aberrant cell proliferation[362].

With advances in precision oncology, blocking antibodies that bind the extracellular domain of EGFR and ErbB2 alongside small-molecule inhibitors that inhibit their intracellular kinase activity have been developed clinically. Most notably, the FDA approval of the monoclonal antibody trastuzumab (Herceptin) has revolutionized the treatment of $HER2^+$ breast cancer and improved clinical outcomes[363]. More recently, neratinib, an irreversible tyrosine kinase inhibitor of ErbB2/HER2 and EGFR was FDA-approved for adjuvant treatment of adult patients with early stage $HER2^+$ breast cancer and holds the potential to reduce breast cancer relapse rate[364]. Emerging data has suggested that afatinib, another irreversible inhibitor approved for the treatment of NSCLC, is also effective against $HER2^+$ breast cancer[365]. The development of these and numerous other ErbB inhibitors reinforce the importance of these receptors in tumorigenesis.

However, despite the well-studied role of ErbB receptors in solid tumors and paralleled advances in their therapeutic targeting, the potential of deregulated ErbB signaling to contribute to leukemia is largely unknown. We recently performed deep sequencing on primary samples from patients with a range of hematologic malignancies and discovered point mutations in the ErbB2 receptor in a small subset of patients. Here, we show that these mutations are oncogenic and cells transformed by these mutations are sensitive to several irreversible ErbB inhibitors and trastuzumab.

Results

Identification of ERBB2 point mutations in patients with acute leukemia

Point mutations in the ERBB2 gene were uncovered and characterized in three of 185 patients with hematologic malignancies following deep sequencing using a custom capture library consisting of 1,862 kinase and kinase-associated genes. The cohort of 185 included patients with acute myeloid leukemia (AML; n = 96), acute lymphoid leukemia (ALL; n = 51), and myeloproliferative neoplasms (MPN; n = 38). The three ERBB2 mutations were prioritized by the HitWalker algorithm[366], which uses *ex vivo* functional drug screening data collected in parallel to rank mutations that may be associated with critical survival pathways in a given patient sample (**Supplemental Figure 1**). It should be noted that the capture library is focused on kinase and kinase-associated genes, and so there may be other mutations present that were not assessed using this platform.

Two mutations, ERBB2^{R188C} and ERBB2^{P489L} were found in pediatric patients with AML and ALL, respectively. Both mutations lie within the extracellular domain of the ErbB2 receptor. Specifically, R188C mutation resides within the Furin-Like Cysteine Rich Region (FLCRR, domain II) and P489L is located in between the Receptor L Domain (RLD, domain III) and the Growth Factor Receptor Domain (GRRD4, domain IV). Another mutation discovered in an adult patient with AML, ERBB2^{L1157R}, is located near the C-terminus (**Figure 1A, Supplemental Figure 2**). The presence of all three mutations was confirmed via Sanger sequencing (**Figure 1B**)**.** While P489L has been previously reported in patients with breast[367] and lung squamous cell carcinoma[368], to our knowledge, R188C and L1157R have not yet been reported. Due to the unavailability of a matched skin biopsy, we were unable to confirm if these mutations are somatic or germline. Information about patient variant allele frequency (VAF) and HitWalker ranking[366] is provided in **Supplemental Table 1**. Of note, the higher disease burden in the bone marrow for all three patients (ranging from 72-100% blasts) makes it difficult to determine whether the 52% VAF for

P489L and the 46% VAF for L1157R are heterozygous somatic or germline mutations. The R188C mutation, with a 29% VAF, is most likely somatic and potentially a prominent subclone within the leukemia, with approximately 60% of the 91% blasts harboring a heterozygous variant (**Supplemental Table 1**).

Given that very little is known about ERBB2 in hematopoiesis and leukemia, we sought to measure the expression of ERBB2 in available patient samples harboring the specific mutations discussed above. While no clinical material was available for the adult patient with AML harboring $ERBB2^{L1157R}$, we found that ERBB2 is expressed at the RNA level in both pediatric patients with $ERBB2^{R188C}$ and $ERBB2^{P489L}$ mutations via Affymetrix exon microarray analysis[369] (**Supplemental Figure 3A-B**). Expression was determined using the probeset detected above background (PSDABG) metric, which measures whether a given ERBB2 exon probeset signal was detected at significantly higher intensity than background regions with similar GC content[369]. Our analysis suggests that a majority of the ERBB2 exons are expressed above background for these samples.

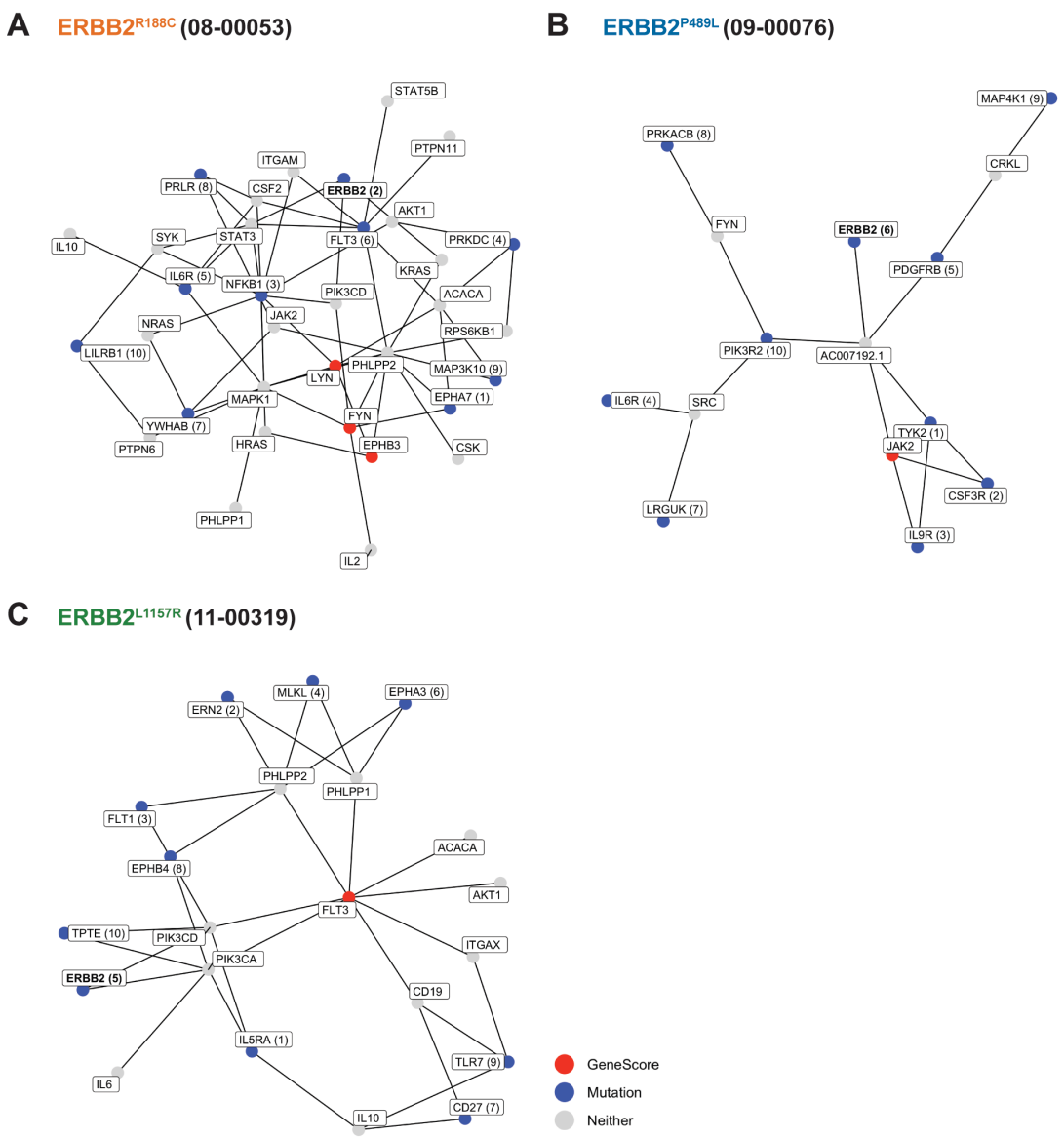

Supplemental Figure 1: ERBB2 point mutations represent important targets in leukemia using the HitWalker algorithm that integrates deep sequencing data with functional screening. Hitwalker diagrams are shown for patient: 08-00053 expressing ERBB2^{R188C} (**A**), 09-00076 expressing ERBB2^{P489L} (**B**), 11-00319 expressing ERBB2^{L1157R} (**C**). The functional targets (acquired from inhibitor screening data) are shown in red, and mutated genes are shown in blue. Each mutated gene is assigned a rank based on predicted association with one or more putative drug targets. Networks are drawn using a Steiner Tree approximation[370] with the seed genes in this context being the union of the functional targets and mutations. HitWalker diagrams were provided by Daniel Bottomly.

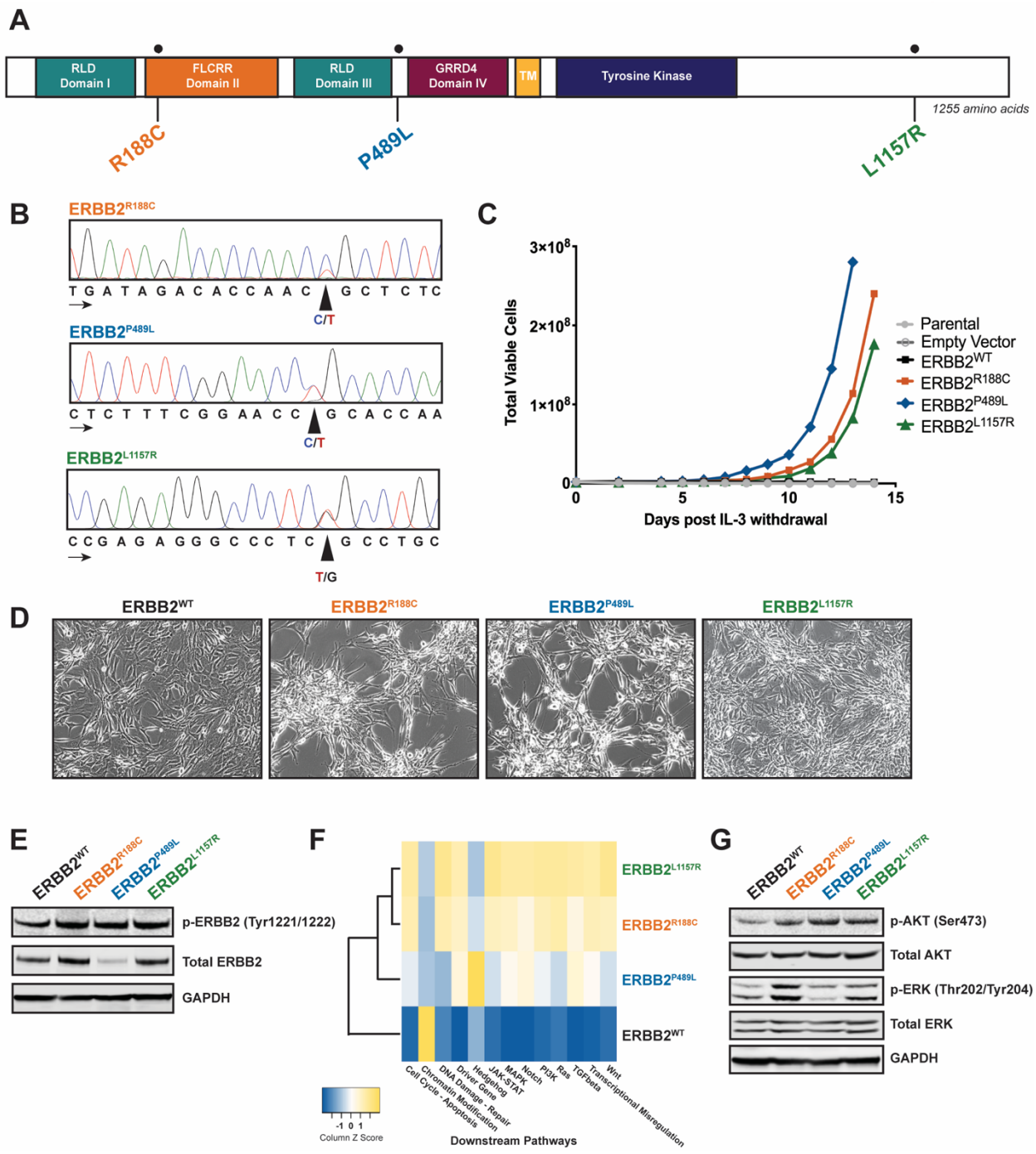

Figure 1: ERBB2 point mutations found in leukemia samples are oncogenic, enable cytokine-independent proliferation, and downstream activation. A. ERBB2 gene schematic with location of point mutations depicted. The location of the following domains is included: Receptor L Domain (RLD, domain I and III), Furin-Like Cysteine Rich Region (FLCRR, domain II), Growth Factor Receptor Domain (GRRD4, domain IV), transmembrane domain (TM), and tyrosine kinase domain. **B.** Sanger sequencing chromatograms of patient genomic DNA confirms the presence of $ERBB2^{R188C}$, $ERBB2^{P489L}$, and $ERBB2^{L1157R}$ mutations. Peaks correspond to the

following nucleotides: A (green), T (red), C (blue), and G (black). Arrows indicate direction of sequencing. **C.** ERBB2^{R188C}, ERBB2^{P489L}, and ERBB2^{L1157R} mutations transform the murine Ba/F3 pro-B cell line to IL-3-independent growth. No growth was observed in parental Ba/F3 cells or cells harboring an empty vector or wildtype (WT) ERBB2. All engineered Ba/F3 cell lines were flow sorted for low, equivalent GFP expression prior to the IL-3 withdrawal assay. Total viable cells are plotted over time after the withdrawal of IL-3. This experiment was repeated at least twice with consistent results. **D.** Stable expression of ERBB2 mutants in NIH 3T3 fibroblasts exhibited spontaneous foci formation in monolayers independent of cell plating density. 3T3 cells transduced with ERBB2^{WT} lack this phenotype but exhibit an increased rate of cell growth. **E.** Immunoblot analysis of ERBB2-transformed Ba/F3 cells shows increased phosphorylation of ErbB2 with all three mutants compared to ERBB2^{WT}. GAPDH served as a loading control. Prior to lysis, WT cells were grown in IL-3 supplemented media and all lines were starved overnight in 0.1% BSA RPMI. **F.** In comparison to Ba/F3 cells expressing ERBB2^{WT}, changes in gene expression were observed in mutant-transformed Ba/F3 cells. Most notably, all mutants resulted in an increase in expression of MAPK signaling. Prior to RNA isolation, WT cells were grown in IL-3 supplemented media and all lines were starved overnight in 0.1% BSA RPMI. Expression analysis was performed in triplicate. **G.** Expression of phosphorylated AKT is increased in mutant-transformed Ba/F3 cells relative to WT cells. ERK phosphorylation was evident only in Ba/F3 expressing ERBB2^{R188C} and ERBB2^{L1157R}. GAPDH served as a loading control. As noted above, all cell lines were starved overnight in 0.1% BSA RPMI. NIH 3T3 experiments were performed by Jamie M. Keck.

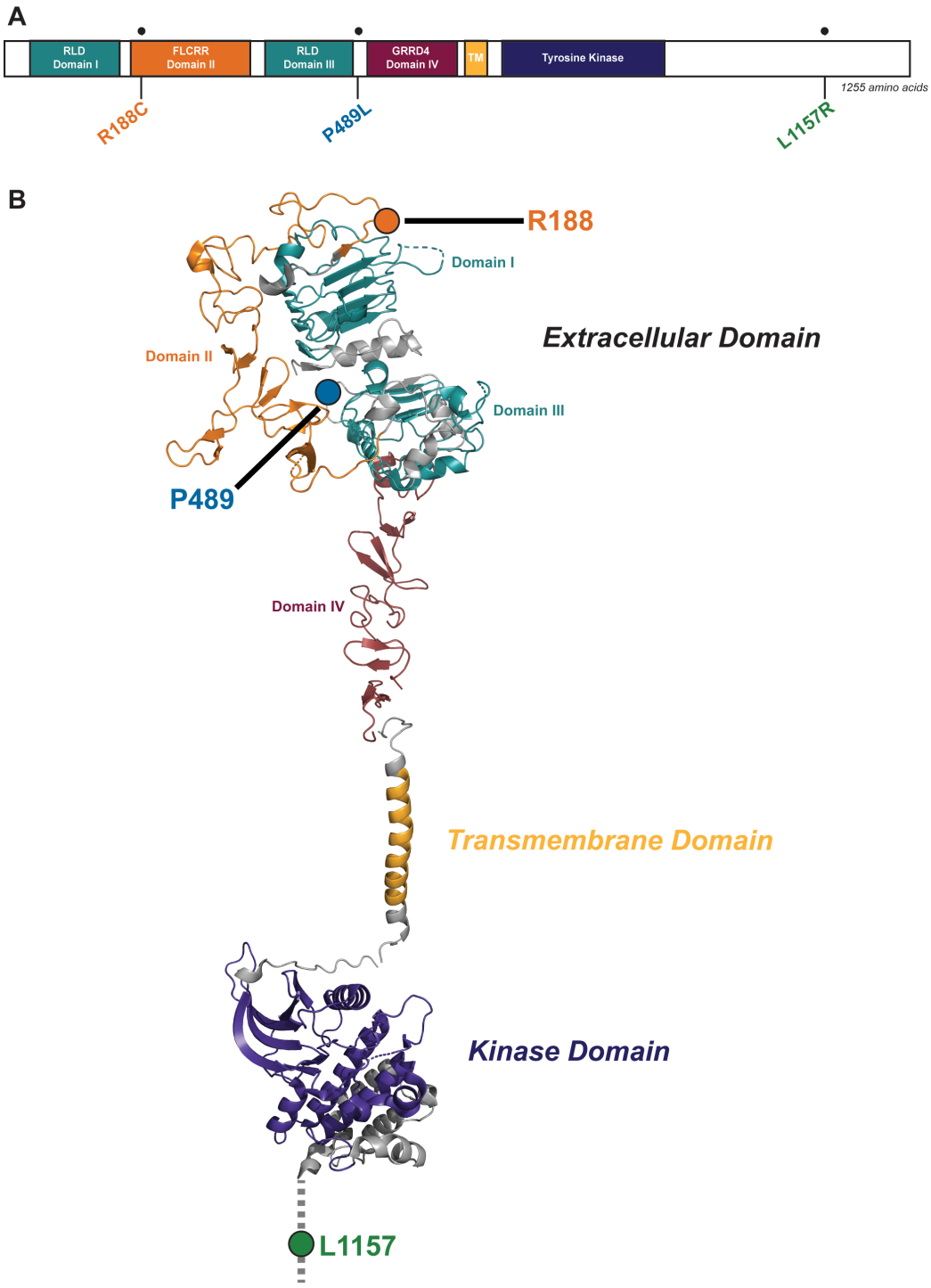

Supplemental Figure 2: 3D mapping of ERBB2 point mutations. A. Gene schematic of ERBB2 with location of point mutations indicated. **B.** Relative positions of native ERBB2 amino acids (i.e., R188, P489, and L1157) for the mutations studied are highlighted using PyMOL. Since the ERBB2 receptor is not fully crystallized, the location of L1157 is approximated.

A **08-00053 (ERBB2^{R188C})**

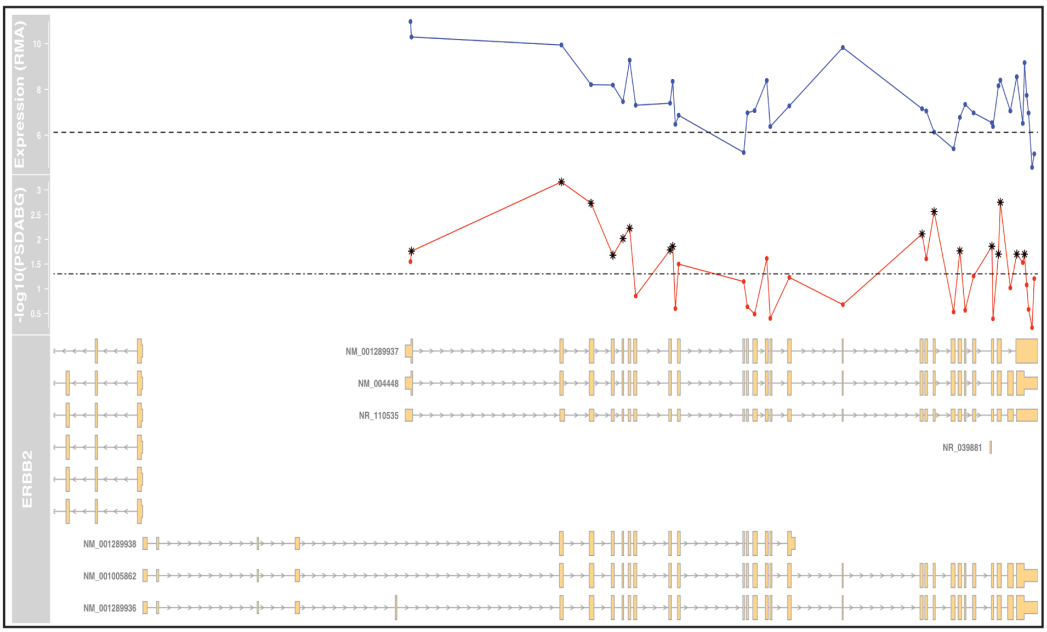

B **09-00076 (ERBB2^{P489L})**

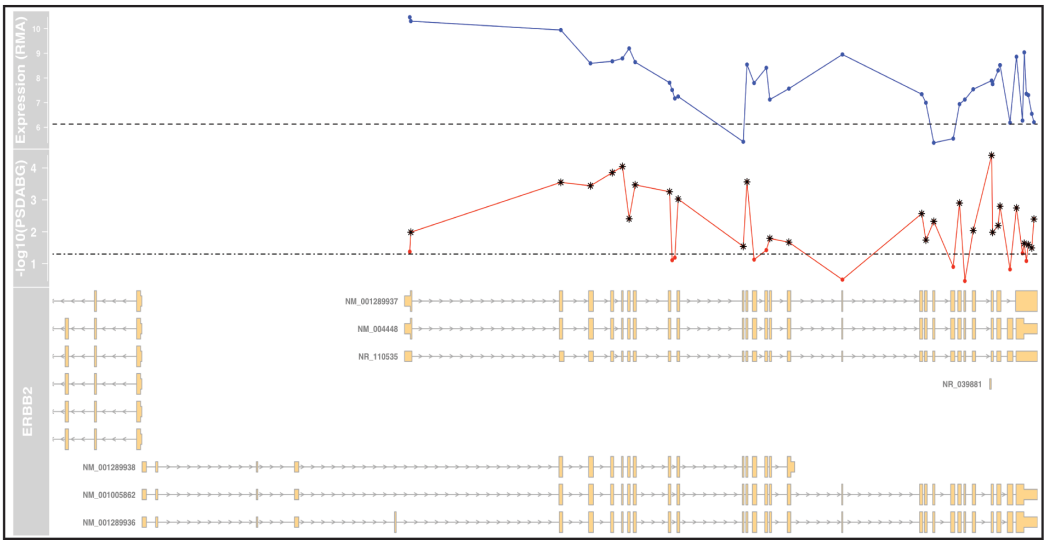

Supplemental Figure 3: Summary of Affymetrix exon microarray expression for ERRB2. A-B. Expression was determined using the probeset detected above background (PSDABG) metric, which measures whether a given ERBB2 exon probeset signal was detected at significantly higher intensity than background regions with similar GC content[369]. Our analysis suggests that a majority of the ERBB2 exons are expressed above background for these samples. The RefSeq gene models for ERRB2 are provided relative to hg19 (bottom track). Each high-confidence probeset was tested for whether its expression was greater than background. A red line tracing the -log10(P-values) from this test is plotted in the middle track with the dot-dash line indicating

the nominal 0.05 p-value threshold. If the given probesets would still be significant after FDR correction they are indicated by an '*'. The top track shows the probeset-level robust multi-array average (RMA) expression values with the dashed line indicating the median across all probesets for that sample. Only the high-confidence probesets are displayed here for clarity. Exon microarray data was analyzed and visualized by Daniel Bottomly and Shannon McWeeney.

ERBB2 point mutations are transforming and upregulate receptor signaling activity

To determine if the identified ERBB2 mutations induce oncogenic transformation, we stably expressed each of them in Ba/F3 cells, a murine IL-3-dependent pro-B cell line that provides a well-established model to study kinase mutations[314]. Oncogenes expressed in Ba/F3 cells enable IL-3 independent growth. Since it is known that overexpression of wildtype (WT) ERBB2 itself confers some transforming activity[356], we sorted all ERBB2 Ba/F3 cell lines for equivalent, low GFP-positive expression prior to performing the IL-3 withdrawal assay. At low expression, all three ERBB2 mutations enabled IL-3-independent growth and proliferation, whereas parental Ba/F3 cells or cells expressing empty vector or WT ERBB2 were unable to grow without IL-3 (**Figure 1C**). Retroviral transduction of ERBB2 constructs into murine NIH 3T3 fibroblast cells further showed a transformed morphological phenotype and increased ability to spontaneously form foci when grown to confluence for ERBB2 mutant-expressing NIH 3T3 cells compared to those expressing ERBB2 WT or empty vector controls (**Figure 1D**).

Using western blotting, we validated the expression of total and phosphorylated ErbB2 in our ERBB2-mutant transformed Ba/F3 cell lines and found that all three mutants resulted in increased autophosphorylation of the ErbB2 receptor at Tyr1221/1222 in comparison to Ba/F3 cells that expressed WT ERBB2 (**Figure 1E**). We also used these stable Ba/F3 cell lines to assess downstream signal transduction pathways that could contribute to the tumorigenic phenotype. With NanoString's nCounter technology, we saw that ERBB2^{R188C} and ERBB2^{L1157R} resulted in an

upregulation in gene expression of several pathways relative to ERBB2^{WT} cells, including JAK/STAT, PI3K/AKT, RAS/MAPK, and WNT signaling. Notably, with the ERBB2^{P489L} mutant, we saw an increase in hedgehog signaling (**Figure 1F**). Similar to our NanoString data, we saw variability in downstream signaling among the mutants via western blotting (**Figure 1G**). Together, these data indicate that these mutations in ERBB2 result in hyperactivation of the receptor with pursuant cellular transformation.

ERBB2 point mutants are sensitive to irreversible ErbB inhibitors

Given the factor-independent growth and heightened receptor signaling activation of the ERBB2 mutants in Ba/F3 cells, we assessed the *ex vivo* sensitivity of primary patient samples harboring ERBB2 R188C, P489L, and L1157R mutations to a panel of clinically relevant ErbB inhibitors that were available at the time of patient sample accrual. Our panel consisted of reversible ErbB family inhibitors (i.e., erlotinib, gefitinib, and lapatinib) and two investigational irreversible inhibitors (i.e., canertinib and pelitinib). Among the reversible inhibitors, erlotinib and gefitinib are currently FDA-approved for the treatment of NSCLC harboring exon-19 deletions and activating EGFR mutations, and lapatinib is approved for metastatic HER2^{+} breast cancer[371]. However, only lapatinib targets cancers that overexpress ERBB2/HER2; erlotinib and gefitinib act in cancers with mutated or overactive EGFR[371]. Upon patient sample procurement, leukemia cells were assayed for cell survival after incubation with one of four graded concentrations of a given drug and a 3rd order polynomial curve was fit per sample and inhibitor. An IC_{50} value was calculated for each inhibitor and compared with the median of the inhibitor IC_{50}s for the overall patient sample cohort of similar 4-point dose-responses. Inhibitors for which the IC_{50} value was less than 20% of the cohort median were considered effective given historical inhibitor screening data[317, 318]. Considering only members of the cohort with similar diagnoses (i.e., acute myeloid or

acute lymphoid leukemias) did not change the result. On the whole, we saw little to no sensitivity to these reversible ErbB inhibitors in our primary patient samples (**Figure 2A**). While this result may be expected for the EGFR inhibitors erlotinib and gefitinib, it was surprising to observe a minimal response with lapatinib.

Our ErbB2 mutant-transformed Ba/F3 cell lines were also insensitive to erlotinib and gefitinib (**Supplemental Figure 4A, Supplemental Table 2**). However, we saw some activity of lapatinib. Of the three mutants, $ERBB2^{P489L}$-transformed Ba/F3 cells showed modest sensitivity to lapatinib with an IC_{50} of 27.1 nM followed by $ERBB2^{R188C}$ and $ERBB2^{L1157R}$-transformed cells with an IC_{50} of 38.0 nM and of 53.8 nM, respectively (**Supplemental Figure 4A, Supplemental Table 2**). In each case, $ERBB2^{WT}$ Ba/F3 cells grown in IL3-supplemented media were insensitive to all inhibitors.

We observed a trend towards increased sensitivity in patient samples to pelitinib and canertinib, especially against the $ERBB2^{L1157R}$ mutation with an IC_{50} of 0.6 μM and 2.2 μM respectively. The patient with $ERBB2^{R188C}$ showed higher sensitivity to canertinib with an IC_{50} of 2.9 μM in comparison to the patient with $ERBB2^{P489L}$. However, on the whole, the response to these inhibitors in patient samples was limited in comparison to their response observed with ERBB2 mutant-expressing Ba/F3 cell lines. All ERBB2 mutant-expressing Ba/F3 cell lines were sensitive to irreversible ErbB inhibitors. Pelitinib potently inhibited the proliferation of the ERBB2 mutant expressing Ba/F3 lines with IC_{50} values of 18.7, 10.9, and 19.3 nM for $ERBB2^{R188C}$, $ERBB2^{P489L}$, and $ERBB2^{L1157R}$, respectively. Mutant lines exhibited even greater sensitivity canertinib, with IC_{50} values ranging from 3.3 to 8.4 nM (**Supplemental Figure 4B, Supplemental Table 2**).

The differences in sensitivity observed between the primary samples and cell line models is likely due to additional mutations. We observed that the pediatric patient with $ERBB2^{R188C}$ had a $MAP3K10^{P168Q}$ co-mutation while the pediatric patient with $ERBB2^{P489L}$ harbored additional mutations in $MAP4K1^{P422L}$ and $CSF3R^{M696T}$. A $FLT1^{I623V}$ mutation was found in the patient with

ERBB2^{L1157R} (**Supplemental Figure 1**). While the functional significance of these mutations is undetermined, MAP3K10 and MAP4K1 lead to activation of the JNK pathway, which could contribute to leukemia cell growth downstream of ERBB2[372, 373]. Similarly, CSF3R and FLT1 could activate downstream MAPK and JAK/STAT signaling, further facilitating leukemogenesis[318, 374]. Additionally, the possible subclonal status of the ERBB2^{R188C} mutation with a VAF of 29% with a disease burden of 91% blasts within the marrow may also explain the limited sensitivity observed to ErbB inhibitors.

Given the increased potency observed for the investigational irreversible ERBB2 inhibitors pelitinib and canertinib, we expanded drug profiling to evaluate the response of our ErbB2 mutant-transformed Ba/F3 lines to the current FDA-approved irreversible ErbB inhibitors afatinib and neratinib. These second-generation inhibitors irreversibly inhibit both EGFR and ErbB2 and have shown potency against HER2^{+} breast cancer[364, 365, 371]. Neratinib is also particularly well-suited to target the EGFR^{T790M} gatekeeper mutation that mediates resistance in NSCLC[371]. Treatment of mutant-transformed ERBB2 Ba/F3 cells with either afatinib or neratinib potently inhibited cell growth with IC_{50} values ranging 1.6 to 3.2 nM and 0.8 to 1.8 nM, respectively (**Figure 2C**). Additionally, a recent pan-cancer analysis revealed that poziotinib, an irreversible pan-ErbB family inhibitor, has broad antitumor effects in multiple ERBB2 mutant cancer types independent of the mutation location[375]. This compound was equally robust in inhibiting growth in our Ba/F3 lines with an IC_{50} of 1.1 nM for ERBB2^{R188C}, 1.9 nM for ERBB2^{P489L}, and 0.7 nM for ERBB2^{L1157R} (**Figure 2C**, **Supplemental Table 2**). Since *ex vivo* small-molecule inhibitor screening requires the use of fresh patient samples, we cannot comment on how patients with ERBB2 R188C, P489L, or L1157R would respond to afatinib, neratinib, and poziotinib. Nonetheless, our small-molecule inhibitor data in Ba/F3 cells show that our ERBB2 point mutants are generally sensitive to irreversible ErbB inhibitors in the nanomolar range. These findings are in line with previous studies that also show increased efficacy of irreversible over reversible inhibitors against ERBB2 point mutations[356, 375].

Lastly, we evaluated the efficacy of trastuzumab in our mutant-transformed Ba/F3 cell lines. Compared to the cytoplasmic mutant ERBB2^{L1157R}, both extracellular domain mutants, ERBB2^{R188C} and ERBB2^{P489L}, demonstrated higher sensitivity to trastuzumab with an IC_{50} of 1.2 nM and 0.6 nM, respectively. However, neither mutant reached an IC_{90} following treatment with trastuzumab. The trastuzumab antibody binds ERBB2 at the extracellular domain IV where it interacts with its partnering ErbB receptors, and therefore it would not be expected to effectively inhibit the cytoplasmic mutant, ERBB2^{L1157R}, which plateaued after reaching its IC_{50} of 8.7 nM (**Supplemental Figure 4C**, **Supplemental Table 2**).

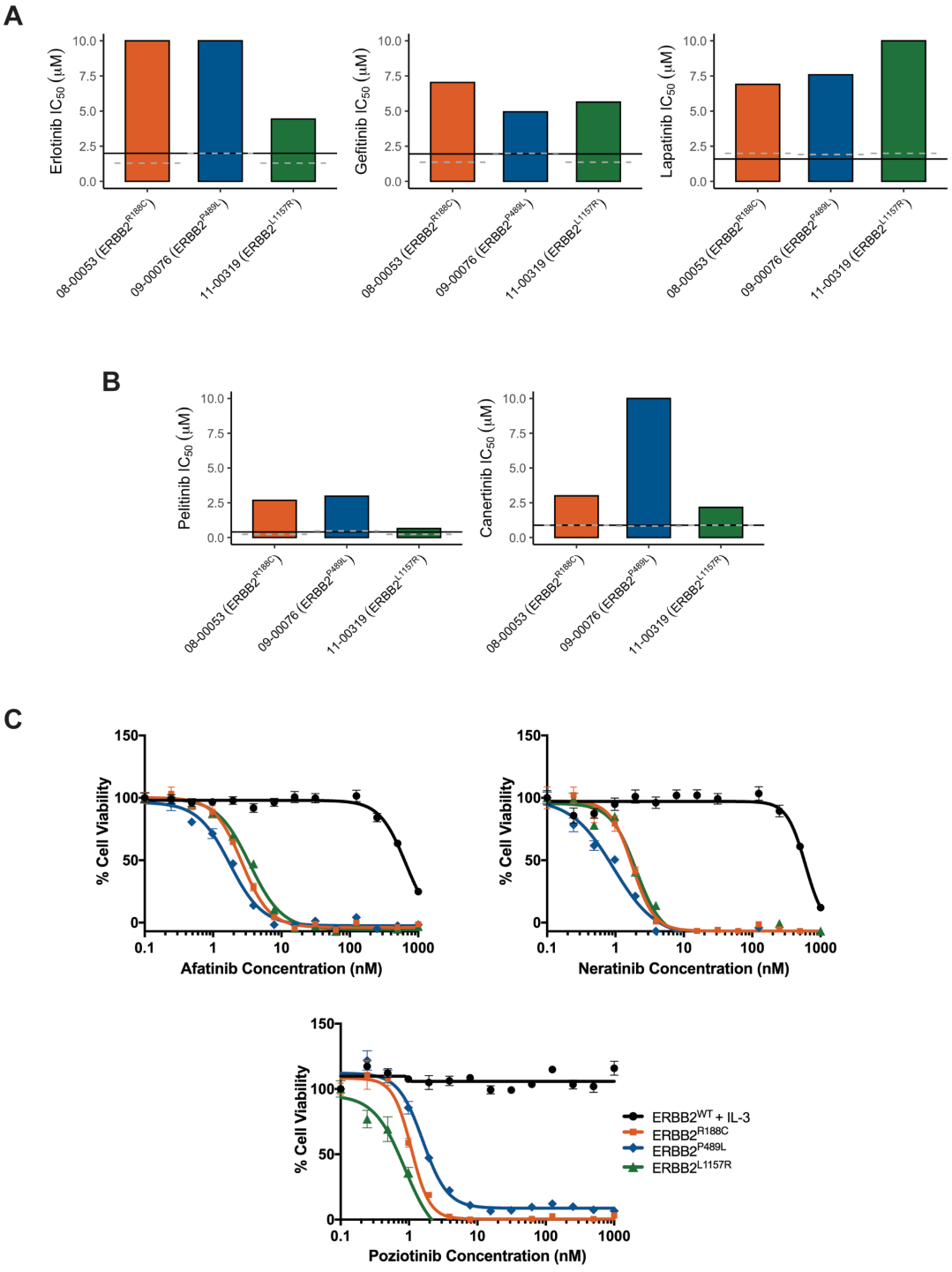

Figure 2: ERBB2 point mutations confer sensitivity to irreversible ErbB inhibitors. A-B. *Ex vivo* inhibitor profiles for patients 08-00053 ($ERBB2^{R188C}$), 09-00076 ($ERBB2^{P489L}$), and 13-00319 ($ERBB2^{L1157R}$) with the IC_{50} measure of response to each reversible (**A**; erlotinib, gefitinib, and lapatinib) and irreversible (**B**; pelitinib and canertinib) inhibitor shown on the Y axis. Sensitivity is determined by % median IC50 which has historically been a marker for patient samples

remarkably sensitive to a screened inhibitor[317, 318].Solid black lines indicates 20% of median IC_{50} for the overall cohort while the grey dotted line indicates 20% of the median IC_{50} for samples with similar diagnoses (i.e., acute myeloid leukemia or acute lymphoid leukemia). **C.** ERBB2 mutant-transformed Ba/F3 cells are sensitive to irreversible inhibitors. Five replicates of WT and mutant ERBB2 Ba/F3 cells were plated with varying concentrations of afatinib, neratinib, and poziotinib for 72 hrs. $ERBB2^{WT}$ cells were plated in media supplemented with IL-3. Cell viability was determined using a tetrazolamine-based viability assay. Viability is represented as a percentage of the untreated control. The average mean ± SEM is shown.

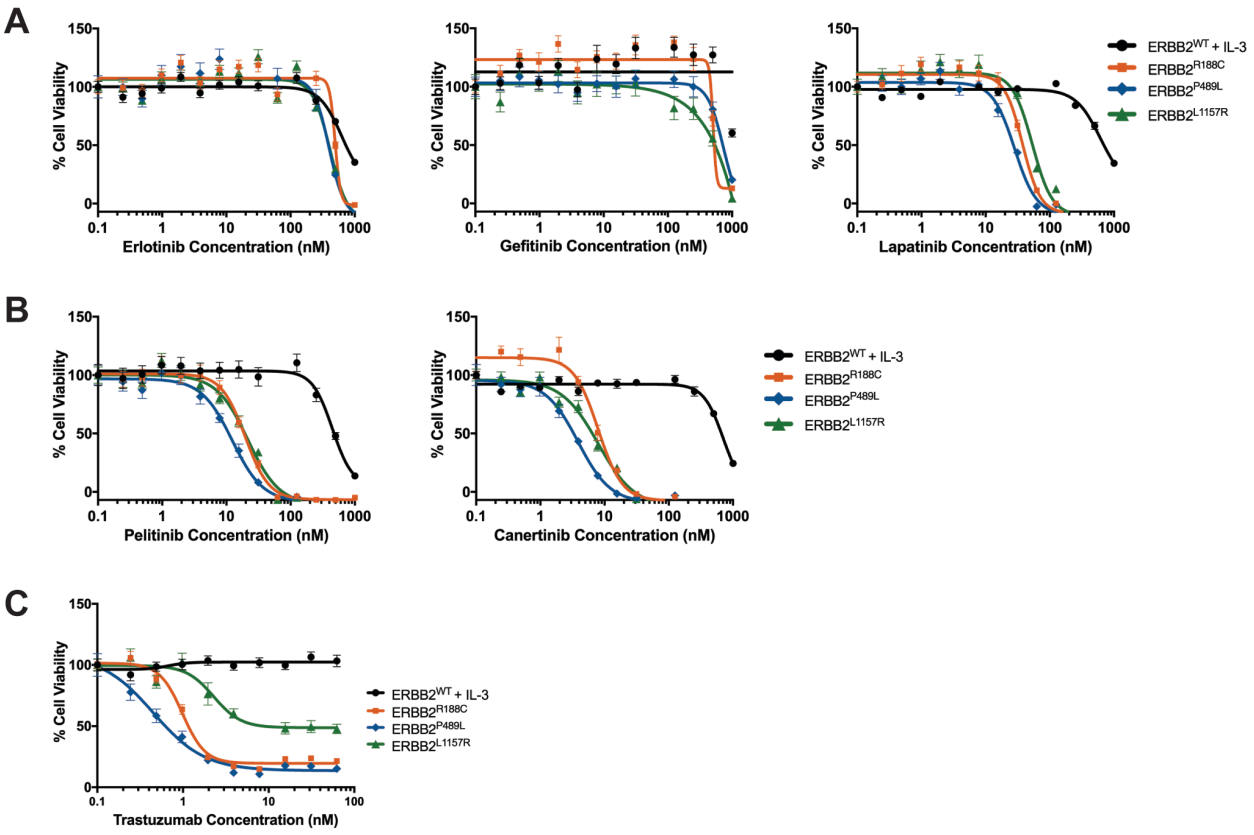

Supplemental Figure 4: ERBB2 mutant-transformed Ba/F3 cell lines display minimal sensitivity to reversible ErbB inhibitors. A. FDA-approved reversible ErbB inhibitors erlotinib, gefitinib, and lapatinib were tested. Lapatinib showed modest sensitivity against ERBB2 mutations. **B.** All ERBB2-transformed Ba/F3 cells were sensitive to irreversible inhibitors pelitinib and canertinib at low nanomolar concentrations. Higher sensitivity was observed with canertinib. **C.** Both extracellular domain ERBB2 mutants, R188C and P489L, demonstrated an increased response to trastuzumab. The trastuzumab antibody binds ERBB2 at the extracellular domain IV where it interacts with its partnering ErbB receptors, and therefore it would not be expected to effectively inhibit the cytoplasmic mutant, $ERBB2^{L1157R}$, which plateaued after reaching its IC_{50} of 8.7 nM. Cell viability was determined using a tetrazolamine-based viability assay. Viability is represented as a percentage of the untreated control. The mean of five replicates is plotted, along with the SEM.

Discussion

The advent of next-generation sequencing technologies has enabled the identification of ERBB2/HER2 point mutations in various cancers. However, their functional characterization and oncogenic potential has yet to be rigorously investigated. Despite the paucity of ERBB2 expression in hematopoietic tissues, in this study, we discovered three oncogenic ERBB2 point mutations—R188C, P489L, and L1157R—in patients with acute leukemia. Stable expression of these mutations in Ba/F3 cells provided a proliferative advantage and enabled increased activation of ErbB2. $ERBB2^{R188C}$ is located within subdomain II of the extracellular domain, a region that is characterized by 11 disulfide bonds. Based upon data from previously reported mutations in ERBB2 (C311R and C334S) and CSF2Rβ (R1461C), we speculate that R188C induces constitutive receptor activation via formation of disulfide bonds between cysteine residues that stabilize the mutant receptor[30, 376]. In the case of mutations P489L and L1157R, these mutations may destabilize the inactive receptor, similar to the $EGFR^{L858R}$ in lung cancer[377], culminating in active receptor molecules that contribute to the underlying leukemia. Particularly, the loss of proline with mutant P489L could introduce flexibility into the protein that destabilizes the receptor and enables it to readily adopt the activated form. This could explain why it predominately resides in the phosphorylated form as evident from our immunoblot results.

Selective inhibition of ErbB2 with irreversible ErbB inhibitors attenuated proliferation and induced cell death of our mutant-transformed ERBB2 Ba/F3 cells. It should be noted that the current clinical indication for the approved ERBB2 inhibitors afatinib, lapatinib, and neratinib is limited to cancers with ERBB2 amplification and overexpression. No small-molecule inhibitor is currently approved for cancers harboring oncogenic ERBB2 point mutations.

In aggregate, we report three functional ERBB2 mutants in the setting of leukemia that are highly sensitive to irreversible ErbB inhibitors in our cytokine-independent cellular assay. Whether these mutations drive leukemia or mediate secondary resistance is currently unknown.

Nonetheless, our data suggest that these mutations have the potential to contribute to leukemogenesis and highlight the importance of investigating rare, yet clinically targetable mutations, as such studies further our ability to develop precise and individualized treatment regimens for a subset of patients with leukemia.

Materials & Methods

Sequencing of patient samples

Clinical specimens were collected with informed consent from patients according to a biorepository research protocol approved by the Oregon Health & Science University institutional review board (IRB 4422; NCT01728402). Deep sequencing was performed on 1,862 kinase and kinase-associated genes using a custom capture library as described previously[318, 336]. A total of 185 patient samples were sequenced: 96 acute myeloid leukemia (AML), 51 acute lymphoblastic leukemia (ALL), and 38 myeloproliferative neoplasms (MPNs). It should be noted that the capture library is focused on kinase and kinase-associated genes, and so there may be other mutations present that were not assessed using this platform.

ERBB2 mutations were confirmed via Sanger sequencing genomic DNA using the following primers: $ERBB2^{R188C}$ Forward 5'—GCCCCAAGGGAAGCAGAAGGTG—3', Reverse 5'—CCCCAGAGATGAAGAGGCACAGGG—3'; $ERBB2^{P489L}$ Forward 5'—CCTGTGGGAAGCTTTGGGCCTG—3', Reverse 5'—GACGGGCAGTCTGCACAAGTCC—3'; $ERBB2^{L1157R}$ Forward 5'—AGCGGTACAGTGAGGACCCCAC—3', Reverse 5'—TTCCCCTCTCAGGCCAGCTTCC—3'.

Functional drug screening-guided variant prioritization

Primary patient mononuclear cells were screened ex vivo using an established panel of small-molecule inhibitors as previously described[11]. Genomic variants were prioritized based on the HitWalker algorithm, which integrates genomic information with functional screening (i.e., ex vivo small-molecule inhibitor screening) to identify oncogenic targets as described previously[366, 378]. First scores were assigned to genes based on the small-molecule inhibitor profiles in relation to putative gene-targets[317]. Based on the distribution of these gene scores, the top genes were chosen as 'seeds'. A network propagation approach was used to rank genes in the STRING[379]

network with respect to seed proximity. Using their relative ranks, the top ten putative gene mutations were chosen for further inspection.

Affymetrix exon microarray

cDNA was prepared from available patient RNA. Samples were amplified and labeled using the Affymetrix WT Terminal Labeling kit (ThermoFisher Scientific Inc.) per manufacturer instructions.

The exon microarray data was processed using the 'oligo' package[380]. Expression values for the 'core' probesets were computed using the robust-multiarray average (RMA) method[381]. The probeset detected above background (PSDABG) approach was used to calculate a p-value indicating whether a given probeset (roughly an exon) was more expressed than background. In practice this was done by computing p-values for each probe and sample using the DABG approach[369] with the resulting p-values summarized to the probeset level using Fisher's method. These data are available from GEO (GSE42731).

Cell culture

Ba/F3 cells were maintained in RPMI (Life Technologies Inc.) supplemented with 10% FBS, 2% L-glutamine, 1% penicillin/streptomycin, 0.1% amphotericin B and 15% WEHI-3B-conditioned medium (a source of IL-3). NIH 3T3 cells (ATCC) were grown in DMEM (Life Technologies Inc.) supplemented with 10% calf serum (Atlanta Biologicals).

Retroviral transduction & downstream assays

Wild-type and mutant ERBB2 cDNA constructs were ectopically expressed in Ba/F3 and NIH 3T3 cells using a Gateway-modified pMX-IRES-GFP puro retroviral vector (Cell BioLabs Inc.)[30, 336]. All ERBB2 mutations were introduced by site-directed mutagenesis using the QuikChange II

XL kit (Agilent Technologies Inc.). The following primers were used for mutagenesis: ERBB2^{R188C} Forward 5'—GCAGGCCCGAGAGCAGTTGGTGTCTATCA—3', Reverse 5'—TGATAGACACCAACTGCTCTCGGGCCTGC—3'; ERBB2^{P489L} Forward 5'—GCAGAGCTTGGTGCAGGTTCCGAAAGAGC—3', Reverse 5'—GCTCTTTCGGAACCTGCACCAAGCTCTGC—3'; ERBB2^{L1157R} Forward 5'—GGGCAGCAGGCCGAGGGCCCTCT—3', Reverse 5'—AGAGGGCCCTCGGCCTGCTGCCC—3'.

Cells were then sorted using a FACSAria flow cytometer (BD Biosciences Inc.) for equivalent, low levels of GFP expression to avoid the known transformative effects of highly overexpressed ErbB2 levels. Ba/F3 cell culture model provides a well-established model to study kinase mutations[314]. For IL-3 withdrawal studies, Ba/F3 cell lines were seeded at a density of 5 x 10^5 cells/mL, monitored by Guava Viacount assay (Millipore Inc.) and expanded as described previously[30, 336]. NIH 3T3 lines expressing ERBB2 constructs were grown as a monolayer until confluence, and images were obtained using a Leica DM IL LED microscope (Leica Microsystems Inc.). All were experiments were performed twice with consistent results.

Immunoblotting

Immunoblot analysis was performed on serum starved (0.1% BSA RPMI) Ba/F3 cells as described previously[318]. Following overnight serum starvation, 10-15 million WT and ERBB2 mutant Ba/F3 cells were spun down and lysed with 200 μL of Cell Lysis Buffer (Cell Signaling Technologies Inc.) containing a Complete Mini Protease Inhibitor Cocktail Tablet, Phosphatase Inhibitor Cocktail 2, and Phenylmethanesulfonyl Fluoride (PMSF) solution (Sigma-Aldrich Inc.) and clarified by centrifugation at 14,000 *g*, 4 °C for 15 minutes. 50 μg of each protein lysate was loaded on NuPAGE 4-12% Bis-Tris gradient gels (Thermo Fisher Scientific Inc.), transferred on Immobilon-FL PVDF membranes (Millipore Inc.), blocked for 1 hour, and

incubated with primary antibody overnight. The primary antibodies used were rabbit anti-ErbB2 (Cell Signaling Technology; #2242), anti-phospho-ErbB2 (#2243) and mouse anti-GAPDH (ThermoFisher; #AM4300). Following overnight incubation with primary antibody at 4 °C, the membranes were washed and probed with fluorescent IRDye 800CW goat anti-rabbit IgG and IRDye 680RD Goat anti-mouse IgG antibodies (1:15,000; LI-COR Biosciences). The membranes were then imaged with the Odyssey Infrared Imaging System (LI-COR Biosciences).

Gene expression profiling

Isolated RNA (Qiagen) from serum starved ERBB2-expressing Ba/F3 cell lines (n=3 per cell line) was evaluated for nCounter analysis using the Pan-Cancer Human Pathways codeset (Nanostring Technologies Inc.).

Inhibitor studies

Ba/F3 cell lines or primary leukemia cells were seeded in 384-well plates, incubated with the indicated concentrations of inhibitor for 72 hours, and assessed for cell survival using a methanethiosulfonate (MTS)-based assay (Promega) as previously described[11, 317]. The final concentration of DMSO was ≤0.1% in all wells. Five technical replicates were plated for all Ba/F3 cell lines. Small-molecule inhibitors were purchased from LC Laboratories Inc. and Selleck Chemicals. Herceptin was purchased from MedChemExpress. Analysis for the cell line was completed via GraphPad Prism version 8.0. For the primary leukemia cells, raw absorbance values were first adjusted to a reference blank and then normalized to untreated control wells to form a measure of normalized viability expressed as a percentage. The concentration values were log transformed and curves were fit to these data using a 3rd degree polynomial. The IC_{50} was defined as the estimated concentration where the normalized viability was equal to 50%. An IC_{50} value was calculated for each inhibitor and compared with the median of the inhibitor IC_{50}s for the overall patient sample cohort of similar 4-point dose-responses. Inhibitors for which the IC_{50} value

was less than 20% of the cohort median were considered effective given historical inhibitor screening data[318]. It should be noted that *ex vivo* inhibitor testing can only be done on fresh patient samples at the time of sample procurement. Frozen samples have compromised viability, which confounds interpretation of the results.

Supplemental Tables

Table 1: Available Patient & Mutation Information										
Specimen ID	**Diagnosis**	**Specific Diagnosis**	**Sex**	**Pediatric/Adult (Age)**	**Blast %**	**ERBB2 Mutation**	**BM VAF**	**COSMIC Status**	**ExAC Frequency**	**HitWalker Ranking**
08-00053	AML	AMML with MLL rearrangement	F	Pediatric (5)	PB: 59 BM: 91	R188C	0.29	No	0.00003298	2
09-00076	ALL	B-ALL, CRLF2^{+}	M	Pediatric (unknown)	PB: 75 BM: 100	P489L	0.52	Yes	0.0007738	6
11-00319	AML	NPM1^{+}, FLT3-ITD^{+}	F	Adult (66)	PB: 45 BM: 72	L1157R	0.46	No	0.00007937	5

PB, Peripheral Blood; BM, Bone Marrow; VAF, Variant Allele Frequency
CRLF2, Cytokine Receptor-like Factor 2

Supplemental Table 1: Available clinical and mutation information on patients harboring ERBB2 point mutations. VAF from patient bone marrow aspirate is provided. These point mutations were checked in COSMIC and ExAC to determine if they were previously reported. Hitwalker ranking is provided. Of note, the higher disease burden in the bone marrow for all three patients (ranging from 72-100% blasts) makes it difficult to determine whether the 52% VAF for P489L and the 46% VAF for L1157R are heterozygous somatic or germline mutations. The R188C mutation, with a 29% VAF, is most likely somatic and potentially a prominent subclone within the leukemia, with approximately 60% of the 91% blasts harboring a heterozygous variant. PB, Peripheral Blood; BM, Bone Marrow; VAF, Variant Allele Frequency; CRLF2, Cytokine Receptor-like Factor 2.

Table 2: Summary of inhibitor screening on mutant-transformed Ba/F3 cell lines				
Inhibitors	**IC_{50} (nM)**			
	$ERBB2^{WT}$	**$ERBB2^{R188C}$**	**$ERBB2^{P489L}$**	**$ERBB2^{L1157R}$**
Erlotinib	727.4	500.0	390.6	396.3
Gefitinib	>1000	526.4	717.8	~ 539.0
Lapatinib	694.1	38.0	27.1	53.8
Afatinib	628.6	2.6	1.6	3.2
Canertinib	661.3	8.4	3.3	6.4
Neratinib	573.9	1.7	0.8	1.8
Pelitinib	474.1	18.7	10.9	19.3
Poziotinib	>1000	1.1	1.9	0.7
Trastuzumab	>1000	1.2	0.6	8.7

Supplemental Table 2: Summary of IC_{50} values for inhibition of ERBB2 mutant-transformed Ba/F3 cell growth by small-molecule inhibitors calculated from data presented in Figure 2C and Supplemental Figure 4.

Acknowledgements

We are extremely thankful to our patients for their time and precious tissue samples. We also thank the Oregon Health & Science University Massively Parallel Sequencing Shared Resource and Flow Cytometry Core for technical support, Nicola Long, Kevin Watanabe-Smith, and Beth Wilmot for analytical support, Elitza Koutleva for help with NanoStrings analysis, and Kevin Yee for critical review of our manuscript. Funding for this project was provided by the Howard Hughes Medical Institute (HHMI), Leukemia & Lymphoma Society, and the National Cancer Institute grant (1R01CA214428) awarded to B.J.D. B.J.D. is also supported by the following grants from the National Cancer Institute (1U01CA217862, 5U01CA214116, 1U54CA224019). S.K.J. is supported by the ARCS Scholar Foundation, The Paul & Daisy Soros Fellowship, and National Cancer Institute (1F30CA239335-01). E.T. is supported by grants from the Leukemia & Lymphoma Society (LLS SCOR 7005-11), American Cancer Society (MRSG-17-040-01-LIB), and National Cancer Institute (1U54CA224019). J.W.T. received grants from the V Foundation for Cancer Research, The Mark Foundation, Gabrielle's Angel Foundation for Cancer Research, and National Cancer Institute (1R01CA183947,1U01CA217862, 1U54CA224019, 3P30CA069533).

Author Contributions

Conception and design: S.K. Joshi, J.M. Keck, C.E. Tognon, B.J. Druker

Development of methodology: S.K. Joshi, J.M. Keck, C.E. Tognon, B.J. Druker

Acquisition of data: S.K. Joshi, J.M. Keck, D. Bottomly, C.E. Tognon, B.J. Druker

Analysis and interpretation of data (e.g., statistical analysis, biostatistics, computational analysis): S.K. Joshi, J.M. Keck, C.A. Eide, D. Bottomly, E. Traer, J.W. Tyner, S.K. McWeeney, C.E. Tognon, B.J. Druker

Writing, review & editing of the manuscript: S.K. Joshi, J.M. Keck, C.A. Eide, D. Bottomly, E. Traer, J.W. Tyner, S.K. McWeeney, C.E. Tognon, B.J. Druker

Study supervision: C.E. Tognon, B.J. Druker

Other (development of prioritization framework to assist in rigor and reproducibility): S.K. McWeeney

6 *A noncanonical FLT3 gatekeeper mutation disrupts gilteritinib binding and confers resistance*

Sunil K. Joshi, Setareh Sharzehi, Janét Pittsenbarger, Daniel Bottomly, Cristina E. Tognon, Shannon K. McWeeney, Brian J. Druker, Elie Traer

This manuscript is currently under review at *Blood Advances.*

Introduction

Acute myeloid leukemia (AML) is a genetically heterogenous disease with approximately 20,000 new cases per year in the United States[11, 382]. Patients with AML have a 5-year survival of <25%, and intense efforts are underway to develop new treatments to improve survival[382]. Mutations in the FMS-like tyrosine kinase-3 (FLT3) gene are among the most common genomic aberrations in AML. Internal tandem duplication (ITD) in the juxtamembrane domain of FLT3 are present in approximately 20% of patients with AML. These mutations cause constitutive kinase activity, and lead to an increased risk of relapse and reduced survival. Another set of mutations in the tyrosine kinase domain (TKD) of FLT3 occur in 5-10% of AML patients. In contrast to FLT3-ITD, FLT3 TKD mutations result in less activation of FLT3 and do not increase the risk of relapse[37].

Multiple FLT3 tyrosine kinase inhibitors have been developed and can be separated into two classes. Type I inhibitors are canonical ATP competitors that bind the ATP binding site of FLT3 in the active conformation and are effective against both ITD and TKD mutations. By contrast, type II inhibitors bind the hydrophobic region adjacent to the ATP binding domain in the inactive conformation. Type II inhibitors are effective against FLT3-ITD, but do not inhibit FLT3 TKD mutations. Quizartinib, a type II inhibitor, has potent activity against FLT3, KIT, and RET. Despite high response rates as a monotherapy in patients with relapsed/refractory AML, the duration of response to quizartinib is approximately 4 months, and resistance via FLT3 TKD mutations is common[12, 40, 165]. These mutations occur frequently at the activation loop residue D835 and less commonly at F691 which represents the “gatekeeper” position in FLT3[40].

Gilteritinib is second-generation inhibitor that targets FLT3 and AXL[383]. As a type I inhibitor, it is active against TKD mutations that impart quizartinib resistance. It was approved as monotherapy in relapsed/refractory patients with AML based upon the randomized phase 3 clinical study (ADMIRAL) which compared gilteritinib with chemotherapy[383]. Despite the significant survival benefit in the gilteritinib arm, monotherapy is limited by the development of resistance,

which typically occurs after 6-7 months. Resistance to gilteritinib most commonly occurs through acquisition/expansion of NRAS mutations, however a minority of patients with F691L gatekeeper mutations were also identified[164]. To search for additional resistance mutations to gilteritinib, Tarver *et al.* used a well-established ENU mutagenesis assay and identified Y693C/N and G697S as mutations that confer resistance *in vitro*[165]. These mutations appear to function similar to the gatekeeper mutation by blocking gilteritinib binding to FLT3, but have not been reported in patients.

Results & Discussion

To more broadly investigate mechanisms of resistance to gilteritinib, we developed a two-step model of resistance that recapitulates the role of the marrow microenvironment (**Figure 1A**). In the first stage of resistance, or early resistance, the FLT3-mutated AML cell lines MOLM14 and MV4;11 are cultured with exogenous ligands, fibroblast growth factor 2 (FGF2) and FLT3 ligand (FL), that are normally supplied by marrow stromal cells. These culture conditions allow the cells to become resistant to gilteritinib without the need for resistance mutations[106]. When ligands are removed, the cells regain sensitivity to gilteritinib, but ultimately become resistant, which we term late resistance. At this point, intrinsic resistance mutations were identified in all of the cultures via whole exome sequencing. Similar to clinical data[383], we found that the most common mutations are activating mutations in NRAS (submitted for publication). One late resistant culture had an $FLT3^{F691L}$ gatekeeper mutation, and 3 cultures had an $FLT3^{N701K}$ mutation, which has not previously been reported (**Figure 1B**). Given its proximity to F691L (**Figure 1C-D**), we hypothesized that this mutation might also disrupt gilteritinib binding to FLT3.

To determine whether the $FLT3^{N701K}$ mutation has oncogenic capacity, we evaluated this mutation in the Ba/F3 transformation assay. Ba/F3 cells are normally IL-3 dependent but the presence of certain oncogenes transforms them to grow indefinitely in the absence of IL-3[314]. The $FLT3^{N701K}$ mutation, similar to $FLT3^{ITD}$ and $FLT3^{D835Y}$, is an activating mutation and promoted growth of Ba/F3 cells in the absence of IL-3, whereas the parental, empty vector, FLT3 wild type ($FLT3^{WT}$), or $FLT3^{F691L}$ did not confer IL-3-independent growth (**Figure 1E**).

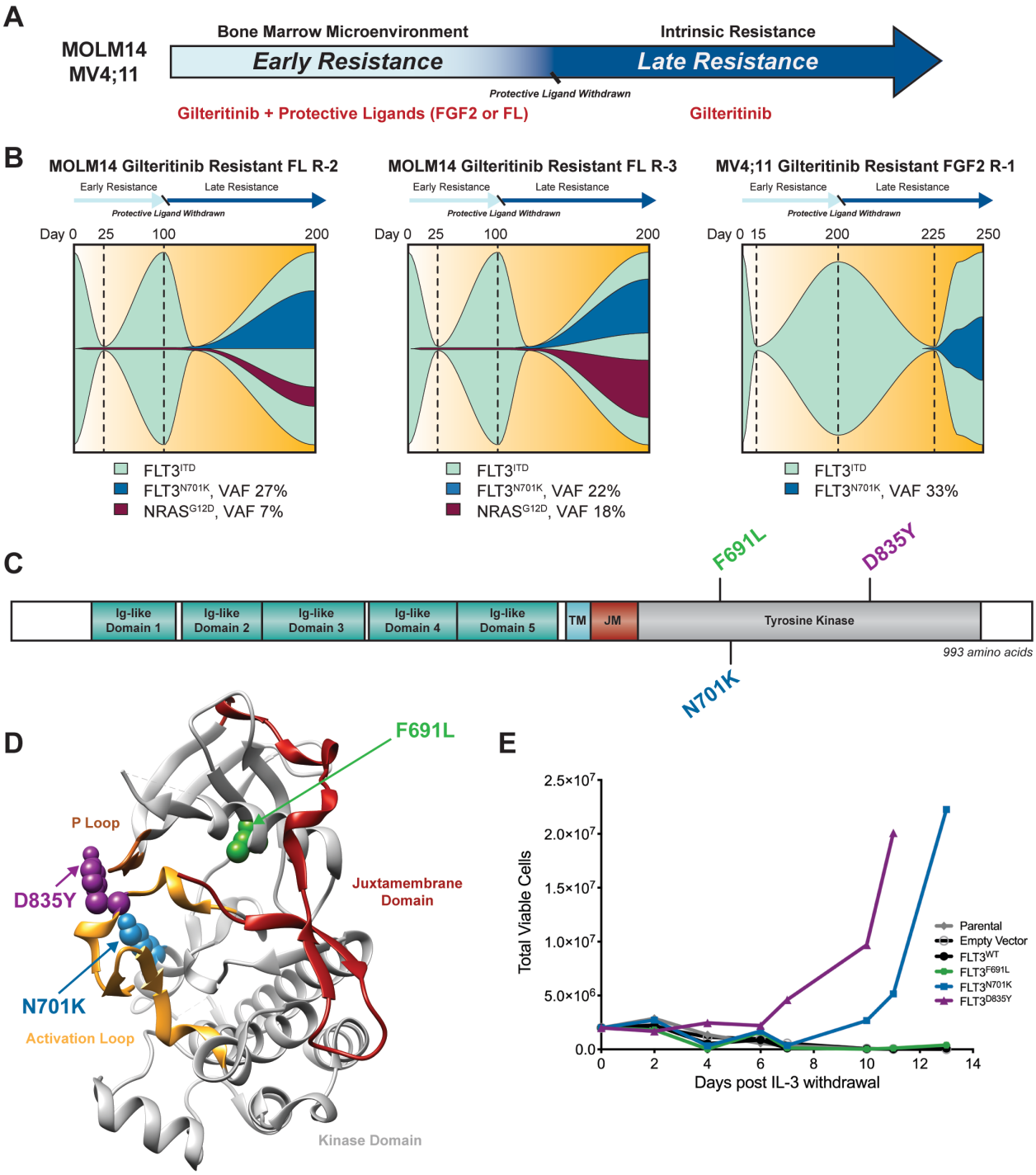

Figure 1: FLT3^{N701K} is an oncogenic mutation. A. Model of early and late gilteritinib resistance. MOLM14 (N = 8) and MV4;11 (N = 8) cultures were continuously treated with gilteritinib and exogenous microenvironmental ligands (FGF2 or FL, 10 ng/mL) to recapitulate the role of the marrow microenvironment in the development of early resistance. Following ligand withdrawal, cultures become transiently sensitive to gilteritinib again, but eventually become resistant with the outgrowth of NRAS and FLT3 resistance mutations that drive late resistance. **B.** Potential clonal

evolution paths resulting in the outgrowth of the $FLT3^{N701K}$ mutation in three cultures. Mutations were identified by whole exome sequencing and displayed via fishplots[384]. All mutations were confirmed by Sanger sequencing. **C.** Gene schematic depicts location of the $FLT3^{N701K}$ point mutation relative to FLT3 gatekeeper (F691L) and activating loop (D835Y) mutations. The location of the following domains is included: immunoglobulin (Ig)-like loops, transmembrane (TM), juxtamembrane (JM), and tyrosine kinase. **D.** Ribbon diagram mapping the location of $FLT3^{N701K}$ onto the crystal structure of the FLT3 kinase domain. Diagram was adapted from PDB 1RJB[37] and visualized with the UCSF Chimera software[48]. **E.** $FLT3^{N701K}$ transforms the murine Ba/F3 pro-B cell line and enables IL-3 independent growth. No growth was observed in parental Ba/F3 cells or cells harboring an empty vector (pMX-puro), wildtype (WT) FLT3, or $FLT3^{F691L}$. Total viable cells are plotted over time and cell growth was measured after the withdrawal of IL-3. This experiment was repeated at least twice with consistent results. Janét Pittsenbarger assisted with Ba/F3 withdrawal studies.

In contrast to Ba/F3 cells expressing $FLT3^{D835Y}$, Ba/F3 cells with $FLT3^{N701K}$ were much less sensitive to gilteritinib with an approximate 8.5-fold increase in IC_{50} (**Figure 2A**). To test whether $FLT3^{N701K}$ also promoted resistance to gilteritinib in the presence of $FLT3^{ITD}$ mutations (**Figure 1B**), we generated $FLT3^{ITD + N701K}$ and $FLT3^{ITD + F691L}$ double mutants and expressed them in Ba/F3 cells. Concordant with previous studies[40], the $FLT3^{ITD + F691L}$ mutant demonstrated an approximate 11-fold increase in IC_{50} to gilteritinib compared to FLT3-ITD alone. $FLT3^{ITD+N701K}$ Ba/F3 cells were nearly identical to $FLT3^{ITD + F691L}$ cells in their resistance to gilteritinib (**Figure 2B**). As a control, $FLT3^{WT}$ Ba/F3 cells grown with IL-3 were insensitive to gilteritinib at comparable doses.

Next, we assessed the impact of $FLT3^{N701K}$ mutations on downstream FLT3 signaling pathways. Ba/F3 cells transformed with $FLT3^{N701K}$, $FLT3^{ITD}$, $FLT3^{ITD + F691L}$, and $FLT3^{ITD + N701K}$ all resulted in phosphorylation of FLT3 (Y589/591) and STAT5 (Y694), AKT (S473), and ERK (T202/Y204) (**Figure 2C**). However, only $FLT3^{ITD + N701K}$ or $FLT3^{ITD + F691L}$ showed sustained phospho-FLT3 with increasing concentrations of gilteritinib (**Figure 2D**), indicating that both of these mutations prevent gilteritinib inhibition of FLT3, particularly at lower doses. The FLT3 kinase activity as reflected by FLT3 phosphorylation mirrored the viability assays in **Figure 2B**.

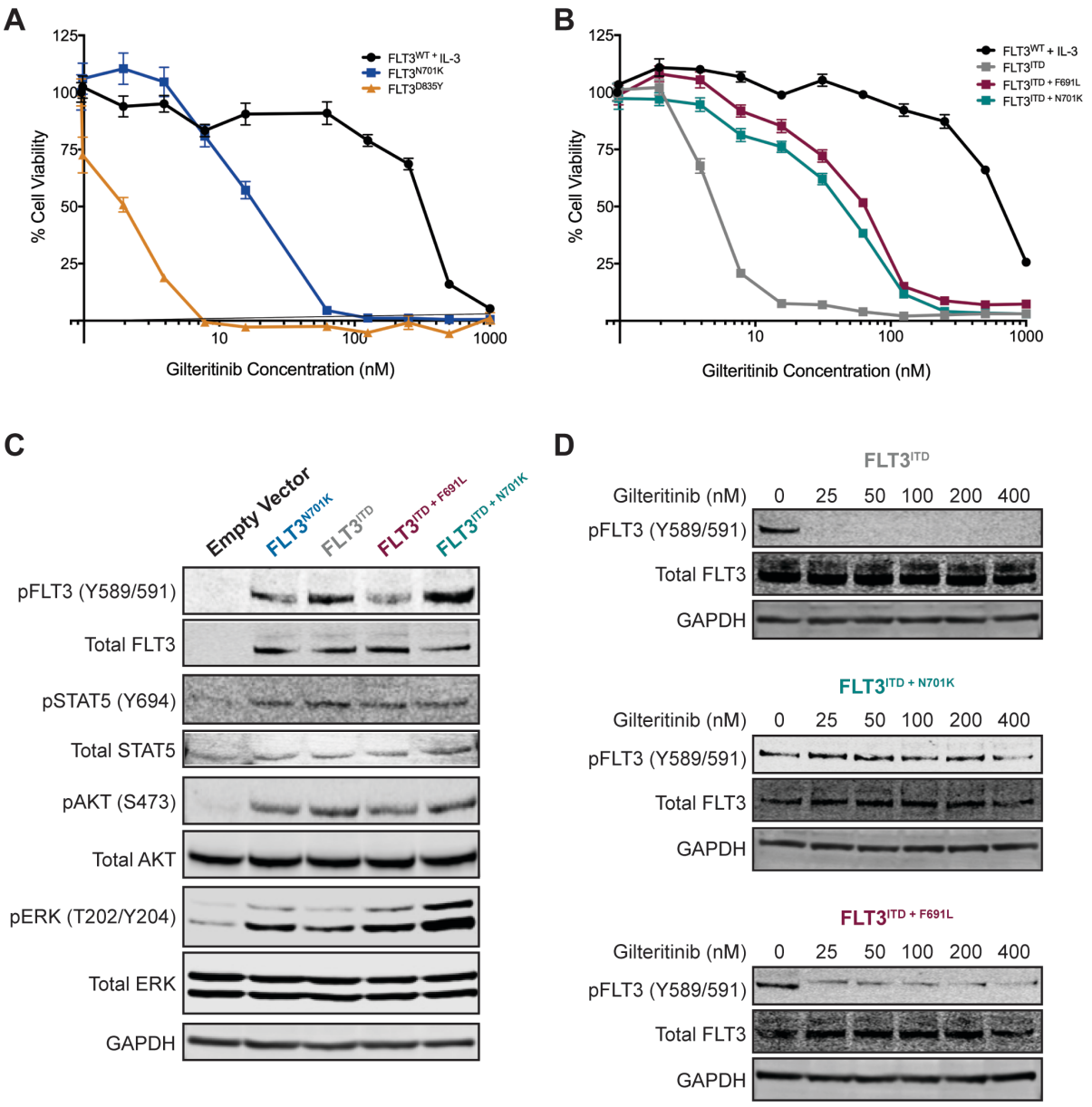

Figure 2: FLT3^{N701K} confers resistance to gilteritinib. A-B. Ba/F3 cells expressing FLT3^{N701K} and FLT3$^{ITD+N701K}$ demonstrate reduced gilteritinib sensitivity. FLT3^{D835Y} and FLT3$^{ITD+F691L}$ were used as historical controls. Six replicates of WT and mutant FLT3 Ba/F3 cells were plated with a dose gradient of gilteritinib (0 – 1000 nM) for 72 hrs. FLT3^{WT} cells were plated in media supplemented with IL-3. Cell viability was determined using a tetrazolamine-based viability assay. Viability is represented as a percentage of the untreated control. The average mean ± SEM is shown. **C.** Expression of total and phosphorylated FLT3 is increased in mutant-transformed Ba/F3 cells relative to cells harboring empty vector. All mutants phosphorylate canonical downstream effectors – STAT5, AKT, and ERK. GAPDH served as a loading control. Prior to lysis, empty vector cells were grown in IL-3 supplemented media and all lines were starved overnight in 0.1%

BSA RPMI. **D.** FLT3 activity is sustained with mutations in N701K and F691L. Ba/F3 cells harboring $FLT3^{ITD}$, $FLT3^{ITD+F701K}$, and $FLT3^{ITD+F691L}$ were treated with gilteritinib (0 – 400 nM) for 90 minutes and lysed for immunoblot analysis[40, 165]. Setareh Sharzehi assisted with western blotting experiments (D).

Since F691L gatekeeper mutations are known to drive resistance to multiple FLT3 inhibitors[40, 62, 137, 164], we treated $FLT3^{ITD}$, $FLT3^{ITD + N701K}$ and $FLT3^{ITD + F691L}$ Ba/F3 cells with midostaurin, crenolanib, and quizartinib. Although $FLT3^{ITD + F691L}$ and $FLT3^{ITD + N701K}$ were largely insensitive to type I inhibitors midostaurin and crenolanib, cells with $FLT3^{ITD + N701K}$ were notably more sensitive to the type II inhibitor quizartinib (**Supplemental Figure 1**), suggesting that N701K blocks gilteritinib binding of type I inhibitors more effectively than type II. This was further apparent from our modeling of the $FLT3^{N701K}$ mutation. While the $FLT3^{N701K}$ mutation may sterically interfere with the binding of gilteritinib, quizartinib binding does not appear to be affected (**Supplemental Figure 2**).

Through our studies, we identified the novel $FLT3^{N701K}$ mutation in addition to the $FLT3^{F691L}$ gatekeeper mutation. We used the Ba/F3 system to demonstrate that N701K blocks gilteritinib binding to FLT3, similar to the gatekeeper F691L, and promotes resistance to gilteritinib. Our data fit nicely with recent data from a mutagenesis screen of Ba/F3 cells with FLT3-ITD that identified F691L in addition to D698N, G697S, and Y693C/N as mutations that drive resistance to gilteritinib[165]. Modeling of these mutations indicates that they cause the loss of hydrogen bonding that accommodates the FLT3 side chain, leading to a steric clash between the tetrahydropyran ring of gilteritinib and FLT3[165]. Given the proximity of N701K to these mutations, we speculate that the mechanism of resistance to gilteritinib imparted by this mutation is similar (**Supplemental Figure 2**). Importantly, these complementary methods identify a common hotspot for gilteritinib resistance mutations (**Supplemental Figure 3**). Given the increasing use of gilteritinib in the clinic, we anticipate that additional resistance mutations will likely be identified in patients. Of note, the N701K mutation appears to be more resistant to type I inhibitors but retains sensitivity to type

II inhibitors such as quizartinib (**Supplemental Figure 1**). This knowledge can be used to help rationally sequence FLT3 inhibitors upon development of resistance.

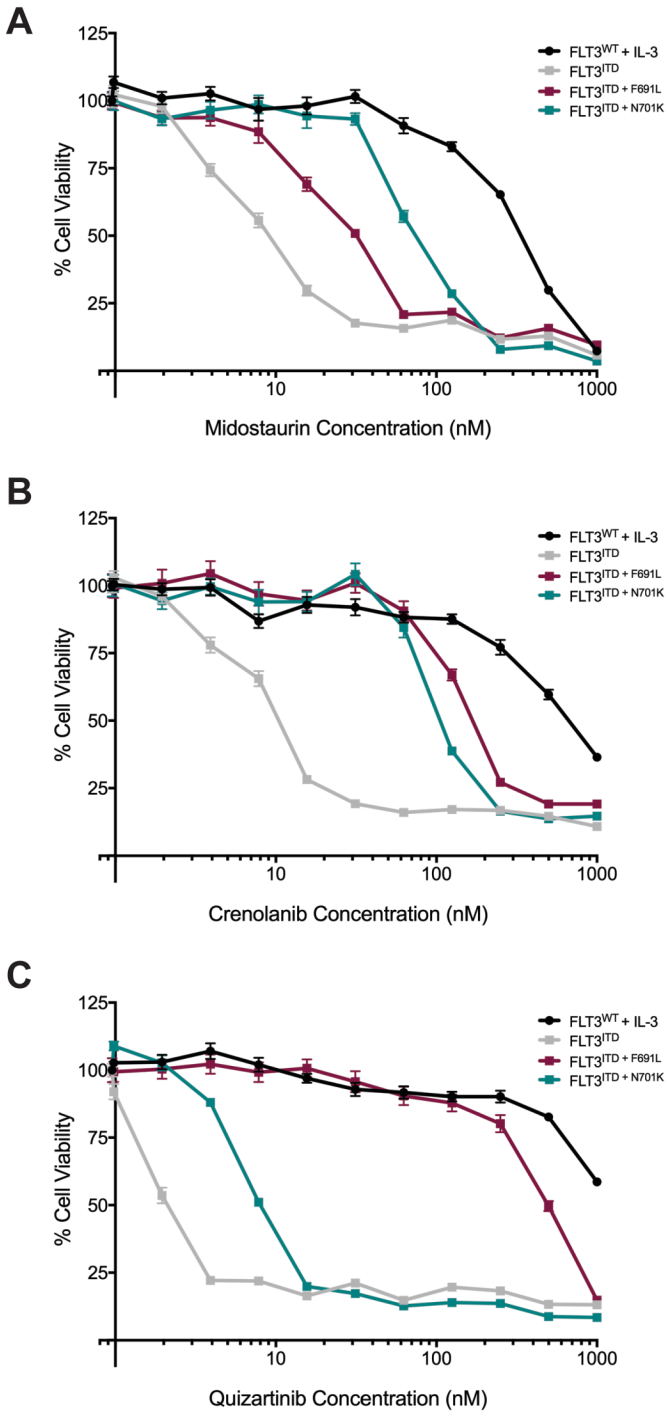

Supplemental Figure 1: FLT3^{N701K} is resistant to type I inhibitors, midostaurin and crenolanib but relatively sensitive to type II inhibitor, quizartinib. A-C. Six replicates of FLT3^{WT}, FLT3^{ITD}, FLT3$^{ITD+F701K}$, and FLT3$^{ITD+F691L}$ Ba/F3 cells were plated with a dose gradient (0 – 1000 nM) of type I and II inhibitors, midostaurin (A, type I), crenolanib (B, type I), and quizartinib (C, type II) for 72 hrs. FLT3^{WT} cells were plated in media supplemented with IL-3. Cell viability was determined using a tetrazolamine-based viability assay. Viability is represented as a percentage of the untreated control. The average mean ± SEM is shown.

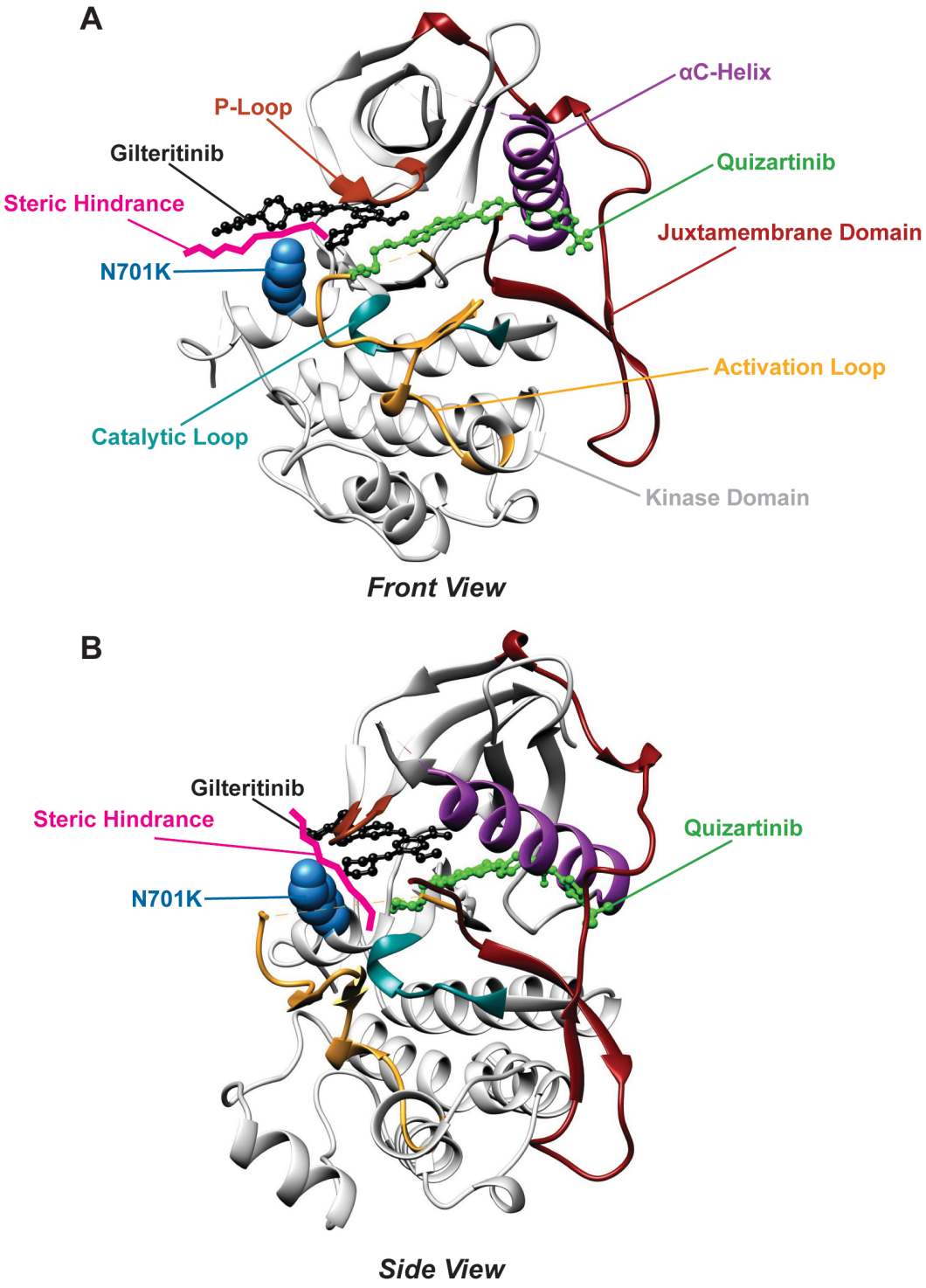

Supplemental Figure 2: FLT3^{N701K} sterically hinders binding of type I inhibitor gilteritinib (black). Binding of type II inhibitor quizartinib (green) is not affected by FLT3^{N701K}. This modeling correlates with the drug sensitivity results presented in Supplemental Figure 1. **A.** Front view. **B.** Side view. Ribbon diagrams were adapted from PDB 4RT7[62] (quizartinib) and PDB 6JQR[135] (FLT3 and gilteritinib) and visualized with the UCSF Chimera software[48].

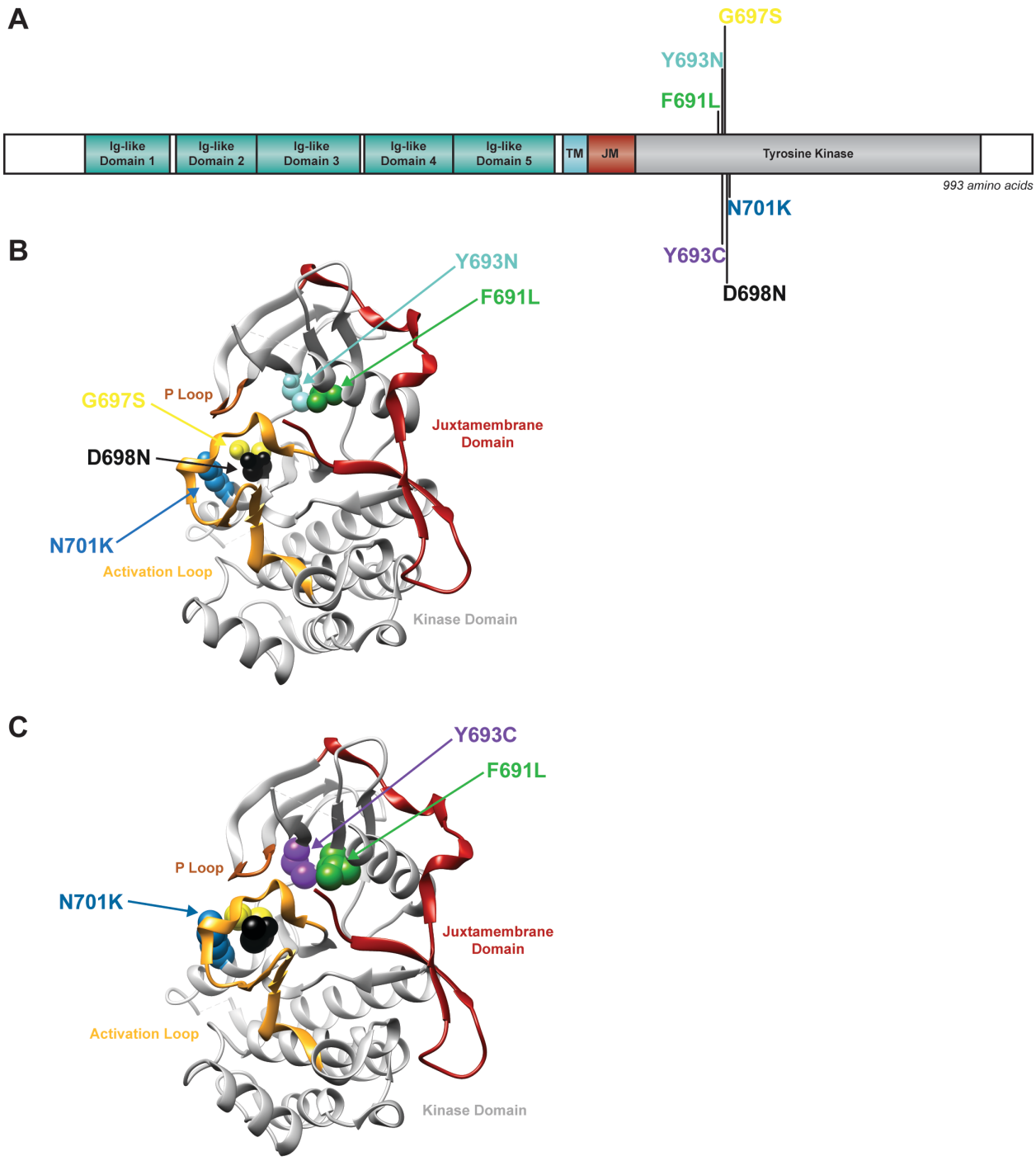

Supplemental Figure 3: FLT3^{N701K} is found in a region where multiple noncanonical mutations that confer gilteritinib resistance reside. A. Gene schematic depicts location of all noncanonical gilteritinib-resistant mutations[165]. **B-C.** Noncanonical mutations mapped onto the crystal structure of the FLT3 kinase domain. FLT3^{N701K} is in close proximity to these mutations. Diagram was adapted from PDB 1RJB[37] and visualized with the UCSF Chimera software[48].

Materials & Methods

Generation of early (ligand-dependent) and late (ligand-independent) gilteritinib resistant cultures

Human MOLM14 cells were generously provided by Dr. Yoshinobu Matsuo (Fujisaki Cell Center, Hayashibara Biochemical Labs, Okayama, Japan). Human MV4;11 cells were purchased from ATCC (Manassas, VA). Both cell lines were grown in RPMI (Life Technologies Inc., Carlsbad, CA) supplemented with 10% FBS (Atlanta Biologicals, Flowery Branch, GA), 2% L-glutamine, 1% penicillin/streptomycin (Life Technologies Inc.), and 0.1% amphotericin B (HyClone, South Logan, UT). Authentication was performed on all cell lines used in this study at the OHSU DNA Services Core facility.

To establish resistant cultures, 10 million MOLM14 or MV4;11 cells were treated with 100 nM of gilteritinib (Selleck Chemicals, Houston, TX) in media alone (N = 4) or in media supplemented with 10 ng/mL of FGF2 (N = 4) or FLT3 ligand (N = 4, FL; PeproTech Inc., Rocky Hill, NJ). All cultures were maintained in 10 mL of media. Every 2 or 3 days, recombinant ligands and gilteritinib were replaced and cell viability was evaluated using the Guava personal flow cytometer (Millipore Inc., Burlington, MA). Following ligand withdrawal, gilteritinib and media were similarly replenished and viability was monitored every 2 to 3 days. All cell lines were tested for mycoplasma on a monthly schedule.

Whole Exome Sequencing

Genomic DNA for all cell lines was extracted using the DNeasy Blood & Tissue Kit (Qiagen Inc., Germantown, MD) according to the manufacturer's protocol. High throughput sequencing was performed on all MOLM14 and MV4;11 parental and late/ligand-independent gilteritinib resistant cell lines. Paired-end 100 base reads were generated using the Illumina HiSeq 2500

(Illumina Inc., San Diego, CA) for parental and gilteritinib resistant cell lines after capture with the Nextera DNA Exome kit v1.2. Each sample was pre-processed using GATK 4.1[385] including alignment to build 37 (GRCh37) of the human genome using BWA[386]. Raw mutations were called for all replicates relative to the parental cell lines using MuTect2. The mutations were annotated using the Variant Effect Predictor v99.1[387]. The final set of mutations were: selected after limiting to those that passed filter, predicted to have a non-synonymous change or indel, seen in less than 1% of GNOMAD[388], and had at least 5 reads with a tumor variant allele frequency (VAF) of greater than 8%. All NRAS and FLT3 mutations were confirmed by Sanger sequencing as previously described (manuscript in review). Sequencing was performed using Eurofins (Louisville, KY) and analyzed using Sequencher and DNASTAR software.

Site-Directed Mutagenesis

All FLT3 (F691L, N701K, D835Y) mutations were introduced by site-directed mutagenesis to $FLT3^{WT}$ vector (Addgene, #23895) using the QuikChange II XL kit (Agilent Technologies Inc., Santa Clara, CA) and primers listed in **Supplemental Table 1a**. Mutagenesis primers were designed using the QuikChange Primer Design Program available through Agilent and purchased from Eurofins. Mutated cDNAs were then transferred into a Gateway-modified pBABE-IRES-GFP puro retroviral vector (Cell BioLabs Inc., San Diego, CA) using a Gateway LR Clonase kit (Life Technologies Inc.). Constructs were verified by Sanger sequencing with primers listed in **Supplemental Table 1b**. $FLT3^{D835Y}$ was verified using the M13R primer (5'-caggaaacagctatgacc-3') available via Eurofins.

Retroviral production, Ba/F3 transduction, and IL-3 withdrawal assay

HEK 293T/17 cells (ATCC) were cultured in DMEM (Life Technologies Inc.) supplemented with 10% FBS (Atlanta Biologicals), 2% L-glutamine, 1% penicillin/streptomycin (Life Technologies Inc.), and 0.1% amphotericin B (HyClone). To produce murine retrovirus, HEK

293T/17 cells were co-transfected with FuGENE 6 (Promega, Madison, WI), EcoPac helper packaging plasmid, and pBABE FLT3 constructs (wild-type (WT) or mutant). pBABE-IRES-GFP puro was used as an empty vector control. Retroviral supernatants were harvested 48 hours after transfection.

Ba/F3 cells were grown in RPMI (Life Technologies Inc.) supplemented with 10% FBS, 2% L-glutamine, 1% penicillin/streptomycin, 0.1% amphotericin B as stated above, and 15% WEHI conditioned medium (a source of IL-3). Stable Ba/F3 $FLT3^{WT}$ and mutant cell lines were generated by infection of 3 x 10^6 cells with 1 mL of retroviral supernatant followed by spinoculation with polybrene at 2500 rpm for 90 minutes. Ba/F3 cells infected with pBABE empty, $FLT3^{WT}$, and mutant vectors were then selected using 2 µg/mL puromycin (ThermoFisher Scientific) selection.

Parental Ba/F3 cells and cells expressing empty vector, $FLT3^{WT}$, and mutants were washed three times in RPMI medium with 10% FBS (to remove all traces of IL-3-containing WEHI conditioned medium). Cells were then suspended at a density of 5 x 10^5 cells per mL and counted on a Guava personal flow cytometer every other day and divided as necessary.

Small molecule inhibitor studies

Ba/F3 cell lines were seeded in 384-well plates, incubated with the indicated concentrations of inhibitor for 72 hours, and assessed for cell survival using a methanethiosulfonate (MTS)-based assay (Promega) as previously described[11, 317]. The final concentration of DMSO was ≤0.1% in all wells. Six technical replicates were plated for all Ba/F3 cell lines. Small-molecule inhibitors were purchased from LC Laboratories Inc. and Selleck Chemicals. GraphPad Prism 8 was used to model dose-specific, normalized cell viability values with 4-parameter logistic regression curves to determine IC_{50}s.

Immunoblotting

Following overnight serum starvation in 0.1% BSA RPMI media, 10-15 million parental, empty vector, and FLT3 mutant Ba/F3 cells were spun down and lysed with 150 μL of Cell Lysis Buffer (Cell Signaling Technologies Inc., Danvers, MA) containing a Complete Mini Protease Inhibitor Cocktail Tablet, Phosphatase Inhibitor Cocktail 2, and Phenylmethanesulfonyl Fluoride (PMSF) solution (Sigma-Aldrich Inc., St Louis, MO) and clarified by centrifugation at 14,000 *g*, 4 °C for 15 minutes. Protein was quantified using a bicinchoninic acid (BCA) assay (ThermoFisher Scientific Inc., Waltham, MA). 50 μg of each protein lysate was loaded on NuPAGE 4-12% Bis-Tris gradient gels (ThermoFisher Scientific Inc.), transferred on Immobilon-FL PVDF membranes (Millipore Inc.), and blocked for 1 hour. Following overnight incubation with primary antibody (**Supplemental Table 2**) at 4 °C, the membranes were washed and probed with fluorescent IRDye 800CW goat anti-rabbit IgG and IRDye 680RD Goat anti-mouse IgG antibodies (1:15,000; LI-COR Biosciences, Lincoln, NE). The membranes were then imaged with the Odyssey Infrared Imaging System (LI-COR Biosciences).

Supplemental Tables

Table 1a: Site-Directed Mutagenesis Primers					
Gene	**Amino Acid Change**	**Forward Primer Sequence (5'→3')**	**Tm (°C)**	**Reverse Primer Sequence (5'→3')**	**Tm (°C)**
FLT3	F691L	CCATAGCAACAGTATTCYAAAATCAAG TAAATTGGTCCTGACAGTGT	79.84	ACACTGTCAGGACCAATTTACTTGATTT TRGAATACTGTTGCTATGG	79.84
	N701K	TTTTCTCTTTTACTTCTTAGATACTTGA GAAGATCACCATAGCAACA	78.10	TGTTGCTATGGTGATCTTCTCAAGTATC TAAGAAGTAAAAGAGAAAA	78.10
	D835Y	GTTGGAATCACTCATGATATATCGAGC CAATCCAAAGTCAC	79.60	GTGACTTTGGATTGGCTCGATATATCAT GAGTGATTCCAAC	79.60

Table 1b: Sanger Sequencing Primers					
Gene	**Mutation**	**Forward Primer Sequence (5'→3')**	**Tm (°C)**	**Reverse Primer Sequence (5'→3')**	**Tm (°C)**
FLT3	F691L/N701K	ACCCACAGACTTCACGGTGCCT	62.13	TCAGCAGAGAACCAAGCCCTCC	60.31

Supplemental Table 1: List of all site-directed mutagenesis (**a**) and Sanger sequencing (**b**) primers used in this study.

Table 2: Antibodies used in this study						
Target	**Antibody Product #**	**Vendor**	**Clone**	**Species**	**Antibody Dilution**	**Predicted Size (kDa)**
Phospho-Akt (Ser473)	9271	Cell Signaling		Rb	1:1000	60
Akt	9272	Cell Signaling		Rb	1:1000	60
Phospho-p44/42 MAPK (Erk1/2) (Thr202/Tyr204)	9101	Cell Signaling		Rb	1:1000	42, 44
p44/42 MAPK (Erk1/2)	9102	Cell Signaling		Rb	1:1000	42, 44
Phospho-Stat5 (Tyr694)	9351	Cell Signaling		Rb	1:250	90
Total Stat5	25656	Cell Signaling	D3N2B	Rb	1:1000	90
Phospho-FLT3 (Tyr589/591)	3464	Cell Signaling	30D4	Rb	1:1000	160
Total FLT3	3462	Cell Signaling	8F2	Rb	1:1000	130, 160
GAPDH	AM4300	Thermo Fisher	6C5	Ms	1:5000	39
IRDye 800CW Goat anti-Rabbit IgG	926-32211	LiCOR		Rb	1:15000	-
IRDye 680RD Goat anti-Mouse IgG	926-68070	LiCOR		Ms	1:15000	-

Supplemental Table 2: List of all antibodies used in this study.

Acknowledgements

We are extremely thankful to the Massively Parallel Sequencing Shared Resource for technical support. We thank Sudarshan Iyer for assistance with UCSF Chimera. This work was supported by the American Cancer Society (MRSG-17-040-01-LIB) to E.T., the Drug Sensitivity and Resistance Network (DRSN; U54CA224019) to B.J.D, S.K.M, and E.T, and Cancer Center Support grant (5P30CA069533-22) to B.J.D. Additional funding was provided by the Howard Hughes Medical Institute, and The Leukemia & Lymphoma Society to E.T. and B.J.D. S.K.J. is supported by the ARCS Scholar Foundation, The Paul & Daisy Soros Fellowship, and the National Cancer Institute (F30CA239335). E.T. is supported by grants from the Leukemia & Lymphoma Society, Hildegard Lamfrom Physician Scientist Award, American Cancer Society, and Cancer Early Detection Advanced Research Center. C.T., D.B., S.K.M., B.J.D, and E.T. were all supported by National Cancer Institute (U54CA224019).

Author Contributions

Study supervision: E. Traer

Conception and design: S.K. Joshi, E. Traer

Development of methodology: S.K. Joshi, E. Traer

Acquisition of data: S.K. Joshi, S. Sharzehi, J. Pittsenbarger

Analysis and interpretation of data (e.g., statistical analysis, biostatistics, computational analysis): S.K. Joshi, S. Sharzehi, J. Pittsenbarger, D. Bottomly, C.E. Tognon, S.K. McWeeney, B.J. Druker, E. Traer

Writing, review, & editing of the manuscript: S.K. Joshi, J. Pittsenbarger, S. Sharzehi, D. Bottomly, C.E. Tognon, S.K. McWeeney, B.J. Druker, E. Traer

Development of prioritization framework to assist in rigor and reproducibility: D. Bottomly, S.K. McWeeney

PART III: *Extrinsic Activation of the FLT3 receptor*

7 *FGF2-FGFR1 signaling regulates release of leukemia-protective exosomes from bone marrow stromal cells*

Nathalie Javidi-Sharifi*, Jacqueline Martinez*, Isabel English, **Sunil K. Joshi**, Renata Scopim-Ribeiro, Shelton K. Viola, David K. Edwards 5th, Anupriya Agarwal, Claudia Lopez, Danielle Jorgens, Jeffrey W. Tyner, Brian J. Druker, Elie Traer

*These authors equally contributed to this work.

This manuscript was published in *Elife*, February 5, 2019.

https://doi.org/10.7554/eLife.40033.001

This paper was submitted for publication shortly after I joined the laboratory. I became a co-author during the revision process. My main contribution to this work included optimizing and performing western blots on primary human and mouse bone marrow stroma to show microvesicles contained FGF2. I also performed trilineage differentiation assays on cultured primary human bone marrow stroma. Lastly, I assisted in performing several inhibitor studies to test protection of FGF2 and FL in other cell line models, not all of this data was included in the final manuscript. The work presented in this chapter provided the context for our investigation of gilteritinib resistance in chapter 8, especially given the fact that gilteritinib and quizartinib serve as two unique prototypical examples of type I and II FLT3 inhibitors, respectively.

Abstract

Protective signaling from the leukemia microenvironment leads to leukemia cell persistence, development of resistance, and disease relapse. Here, we demonstrate that fibroblast growth factor 2 (FGF2) from bone marrow stromal cells is secreted in exosomes, which are subsequently endocytosed by leukemia cells, and protect leukemia cells from tyrosine kinase inhibitors (TKIs). Expression of FGF2 and its receptor, FGFR1, are both increased in a subset of stromal cell lines and primary AML stroma; and increased FGF2/FGFR1 signaling is associated with increased exosome secretion. FGFR inhibition (or gene silencing) interrupts stromal autocrine growth and significantly decreases secretion of FGF2-containing exosomes, resulting in less stromal protection of leukemia cells. Likewise, *Fgf2* -/- mice transplanted with retroviral BCR-ABL leukemia survive significantly longer than their +/+ counterparts when treated with TKI. Thus, inhibition of FGFR can modulate stromal function, reduce exosome secretion, and may be a therapeutic option to overcome resistance to TKIs.

Introduction

TKIs have revolutionized the treatment of CML and have shown promise in AML, however development of resistance remains a problem. In CML, resistance develops in a minority of patients, and is most often caused by resistance mutations. However, some patients still develop resistance in the absence of known resistance mutations. In contrast, development of resistance in AML is the norm. Inhibitors of mutated FLT3, present in about 30% of AML patients, are initially quite efficacious[40]. However, resistance to FLT3 kinase inhibitors in AML typically develops within a few months. In some cases, resistance is cell-intrinsic and due to secondary mutations in the activating loop of FLT3 that prevent drug binding[389], however, resistance still develops in the absence of these mutations. Within the marrow microenvironment, leukemia cell survival can be mediated by extrinsic ligands that activate alternative survival pathways[150, 168, 199] and over time can lead to development of intrinsic resistance mutations[150, 390].

Bone marrow stromal cells provide a supportive structure and secrete cytokines that contribute to the normal hematopoietic stem cell niche, but can also protect leukemic cells from therapy[196, 391]. Initial studies into the mechanisms of resistance utilized normal marrow stroma[392], but the stroma can be altered by leukemia, in a manner similar to development of cancer associated fibroblasts in solid tumors[393-395]. We found that fibroblast growth factor 2 (FGF2) expression is increased in marrow stromal cells during tyrosine kinase inhibitor (TKI) therapy and protects leukemia cells[106, 107, 152, 396]. FGF2 has also been shown to be essential for stress hematopoiesis after chemotherapy[397, 398], suggesting that leukemia cells can hijack a normal marrow stress response for their own survival.

Despite its important roles in physiology and pathology, several aspects of FGF2 biology remain poorly understood. FGF2 does not have a signal peptide and is not secreted through the canonical secretory pathway. Alternative mechanisms for secretion have been proposed, but how FGF2 is conveyed between two cells remains unclear[399, 400]. Additionally, while recombinant FGF2

directly stimulates myeloid colony formation[401], there are also reports suggesting that FGF2 can indirectly regulate hematopoiesis by stimulating stromal cells to produce cytokines[402].

We discovered that FGF2 is largely secreted in extracellular vesicles (ECVs) and exosomes from bone marrow stromal cells. ECVs are able to protect leukemia cells from the effects of TKI therapy. Furthermore, autocrine FGF2-FGFR1 activation in marrow stromal cells increases the secretion of FGF2-laden exosomes, indicating that exosome secretion is regulated in part by FGF2-FGFR1 signaling. Inhibition of FGFR1 can reverse this protective stroma-leukemia interaction and restore leukemia cell TKI sensitivity in the marrow niche.

Results

Stromal cell ECVs protect leukemia cells from TKI therapy

The human stromal cell line HS-5 expresses abundant FGF2, in addition to other soluble cytokines such as IL-5, IL-8 and HGF[403], and conditioned media (CM) from HS-5 is highly protective of leukemia cell lines. HS-5 CM was ultracentrifuged at 100,000g to separate soluble proteins (supernatant, S100) from ECVs and larger macromolecules (pellet, P100). We compared the protective effect of unfractionated CM, S100, and P100 fractions on the viability of two leukemia cell lines: MOLM14 (FLT3 ITD$^+$ AML) and K562 (CML), in the presence of their respective TKIs, quizartinib (AC220, a highly selective and potent inhibitor[404]) and imatinib (**Figures 1A and 1B**). The protective capacity of the S100 fraction was less than unfractionated CM, and protection was enriched in the concentrated P100 ECV fraction (**Figure 1**), indicating that a substantial protective component of HS-5 CM is mediated by ECVs. A more extensive profiling of protection is also shown in **Supplemental Figure 1**.

To determine if ECVs produced by HS-5 cells are internalized by K562 and MOLM14 leukemia cells, K562 and MOLM14 cells were stained with a green lipophilic tracer (DiO) and incubated with HS-5 ECVs stained with a red lipophilic tracer (DiI). Analysis by confocal microscopy showed that ECVs are indeed internalized by leukemia cells, although the exact mechanism of internalization is still under investigation (**Figure 1C and Figure 1 – video 1 and 2**).

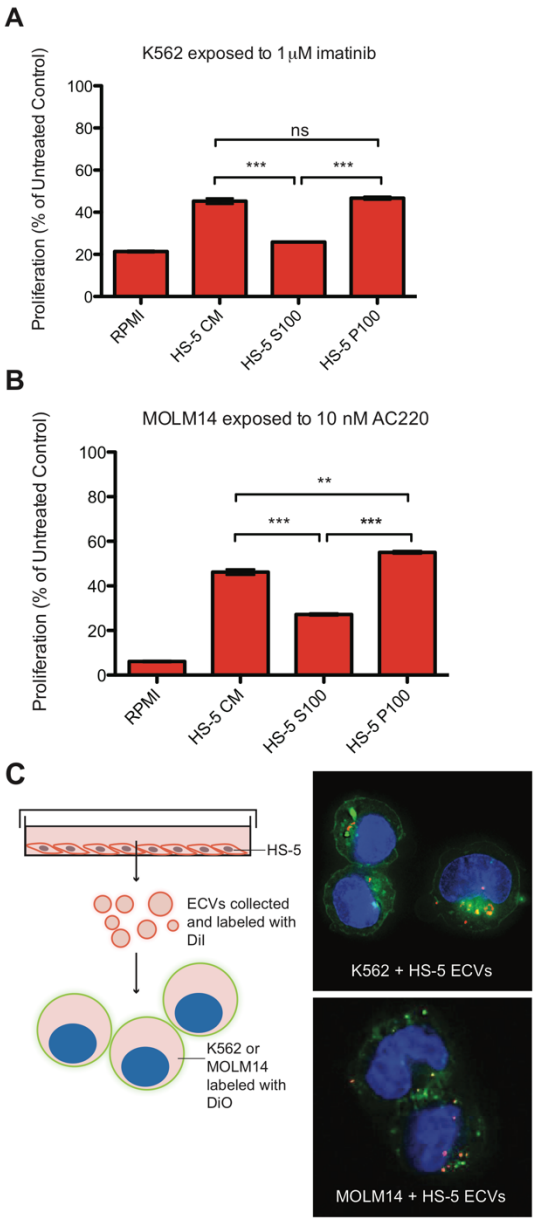

Figure 1: Extracellular vesicles (ECVs) secreted by HS-5 cells are internalized by MOLM14 and K562 cells and protect from treatment with AC220 or imatinib, respectively. HS-5 conditioned media (CM) was collected and separated by ultracentrifugation at 100,000g into a supernatant (S100) and pellet (P100) fraction containing ECVs. These fractions were incubated with **A.** K562 cells +/- 1 μM imatinib, or **B.** MOLM14 cells +/- 10 nM AC220, and viability measured by MTS assay after 48 hours. Values were normalized to respective untreated condition. All wells were plated in triplicate and error bars indicate standard deviation. RPMI is the media control. p values are indicated by *<0.05, **<0.005, and ***=0.0007. **C.,** MOLM14 and K562 cells were stained with DiO (green) tracer, washed, and immobilized on Poly-D-lysine coated chamber slides. HS-5 P100 fraction was stained with DiI (red) tracer and added to the cells for a 24-hour incubation. Slides were stained with DAPI (blue) and imaged by confocal fluorescent microscopy. A movie of the z-stack images is included in Supplemental data.

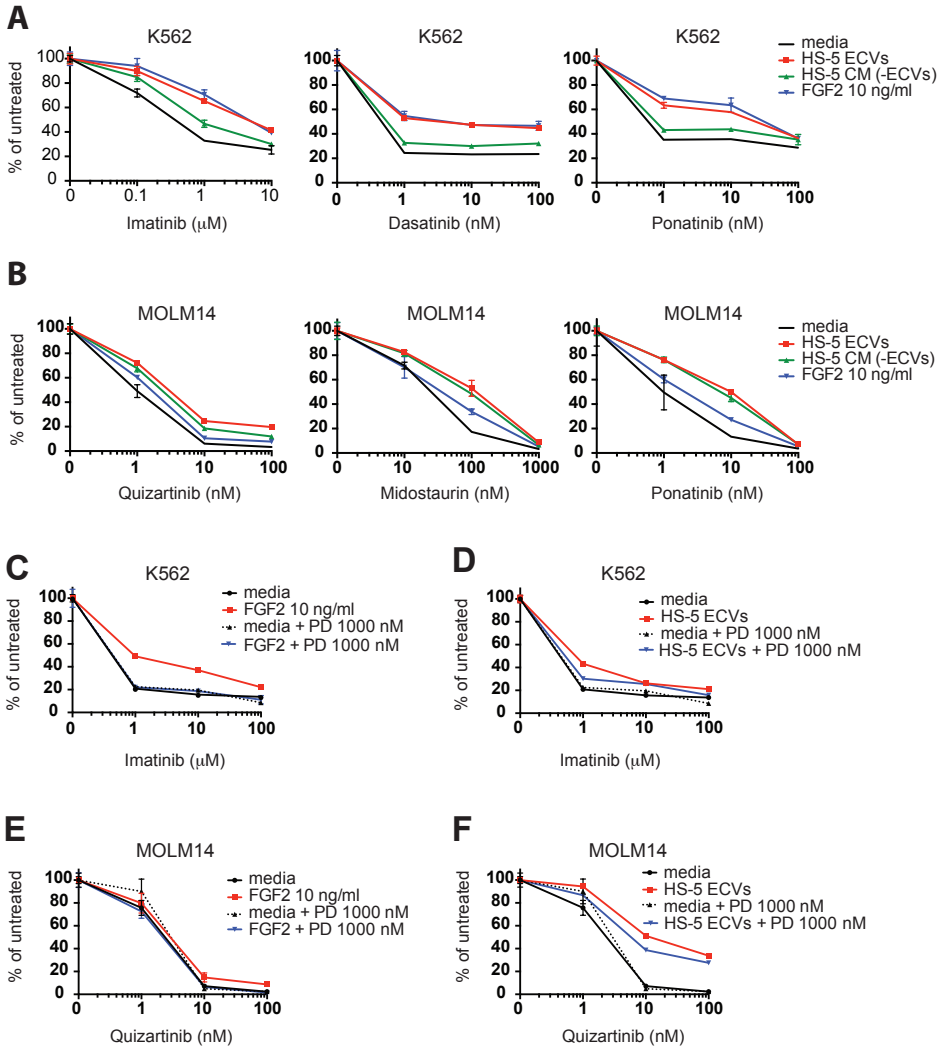

Supplemental Figure 1: Comparison of protection from recombinant FGF2, HS-5 ECVs, and CM after ECV depletion (-ECV) in both K562 and MOLM14 cells. HS-5 conditioned media (CM) was collected and separated by ultracentrifugation at 100,000g into ECVs and CM without ECVs (-ECV). These fractions and RPMI media +/- 10 ng/ml recombinant FGF2 were incubated with **A.** K562 cells, or **B.** MOLM14 cells with the concentrations of inhibitors as shown, and viability measured by MTS assay after 48 hours. Values were normalized to respective untreated condition. Ponatinib inhibits FGFRs around 100 nM and midostaurin inhibits FGFRs around 200 nM, and this activity blocks the protection of recombinant FGF2 completely (consistent with our previous work) and also blocks a portion of the protection of ECVs, which contain FGF2 as well as other proteins. K562 cells were incubated with media, **C.** recombinant FGF2 10 ng/ml or **D.** HS-5 ECVs and then treated with the indicated inhibitors +/- 1000 nM PD173074 (PD). Viability was measured by MTS assay after 48 hours and normalized to respective untreated condition. MOLM14 cells were incubated with media, **E)** recombinant FGF2 10 ng/ml or **F)** HS-5 ECVs and then treated with the indicated inhibitors +/- 1000 nM PD173074 (PD). Viability was measured by MTS assay after 48 hours and normalized to respective untreated condition. In both cases,

addition of PD has no effect with just media, but blocks protection by FGF2. PD also partially blocks protection by HS-5 ECVs, which contain FGF2. Wells were plated in triplicate and error bars indicate standard deviation.

Figure 1 – Video 1: HS-5 ECVs were stained with DiI (red) and K562 cells were stained with DiO (green) and incubated for 24 hours at 37°C as described in Materials and methods. Cells were washed, placed on poly-D-lysine coated chamber slides, and DAPI-stained. Z-stack imaging was performed on an Olympus IX71 inverted microscope. Video is available online, https://doi.org/10.7554/eLife.40033

Figure 1 – Video 2: HS-5 ECVs were stained with DiI (red) and MOLM14 cells were stained with DiO (green) and incubated for 24 hours at 37°C as described in Materials and methods. Cells were washed, placed on poly-D-lysine coated chamber slides, and DAPI-stained. Z-stack imaging was performed on an Olympus IX71 inverted microscope. Video is available online, https://doi.org/10.7554/eLife.40033

FGF2 is contained in stromal cell ECVs and exosomes

FGF2 is highly expressed in the HS-5 stromal cell line but the related HS-27 expresses little FGF2 (**Figure 2A**[106]). We analyzed FGF2 in S100 and P100 fractions of both HS-5 and HS-27 by immunoblot (**Figure 2B**). Little FGF2 was detected in the soluble protein fraction (S100), but FGF2 was enriched in ECVs (P100). Washing the ultracentrifuge tube with detergent liberated even more FGF2 (detergent wash P100), due to ECVs adhering to the ultracentrifuge tube. To compare FGF2 to other soluble cytokines, HS-5 CM was ultracentrifuged into S100 and ECVs, cytokines quantified by Luminex multiplex assay, and normalized to unfractionated CM (**Figure 2C**). Pelleted ECVs were resuspended in 10% of the original CM volume, and the P100 bars in **Figure 2B** thus represent a 10-fold enrichment, although as shown in **Figure 2B** not all ECVs can be liberated from the ultracentrifuge tube. FGF2 was uniquely enriched in ECVs, whereas soluble cytokines such as stem cell factor, interleukin (IL)-6, IL-8, etc. were found primarily in the S100 fraction.

HS-5 ECVs were further separated into microvesicles, exosomes, and insoluble extracellular matrix proteins (ECM) using a sucrose step-gradient to separate by density. FGF2 and cell compartment-specific molecular markers were probed by immunoblot (**Figure 2D**). FGF2 was most highly enriched in the 15-30% sucrose interface, which also contained the exosome-specific markers CD9 and tsg101. Markers of nuclear (lamin A/C), endoplasmic reticulum (calreticulin) and mitochondria (Bcl-XL) were located in the 45-60% interface containing larger microvesicles and apoptotic bodies.

To determine if FGF2 was bound to the outside of ECVS, or contained within ECVs, proteinase K was used to digest proteins not enclosed by lipid membrane. Recombinant FGF2, HS-5 or HS-27 ECVs, and intact HS-5 cells were incubated with proteinase K and probed for FGF2 by immunoblot (**Figure 2E**). Recombinant FGF2 was completely degraded by proteinase K (* indicates degraded fragments) but intact FGF2 was detected in both HS-5 ECVs and control

HS-5 cells. We repeated this experiment using purified HS-5 exosomes and again observed that a fraction of FGF2 was protected from digestion (**Figure 2F**). Addition of 0.1% Triton X-100 disrupted the lipid membrane and resulted in complete digestion of all protein. We found a similar digestion pattern with the exosomal transmembrane proteins CD9 and tsg101. We conclude that FGF2 is contained within ECVs and exosomes, however we cannot exclude that FGF2 may also be on the surface since partial FGF2 degradation was noted in intact HS-5 cells, ECVs and purified exosomes (**Figures 2E-F**).

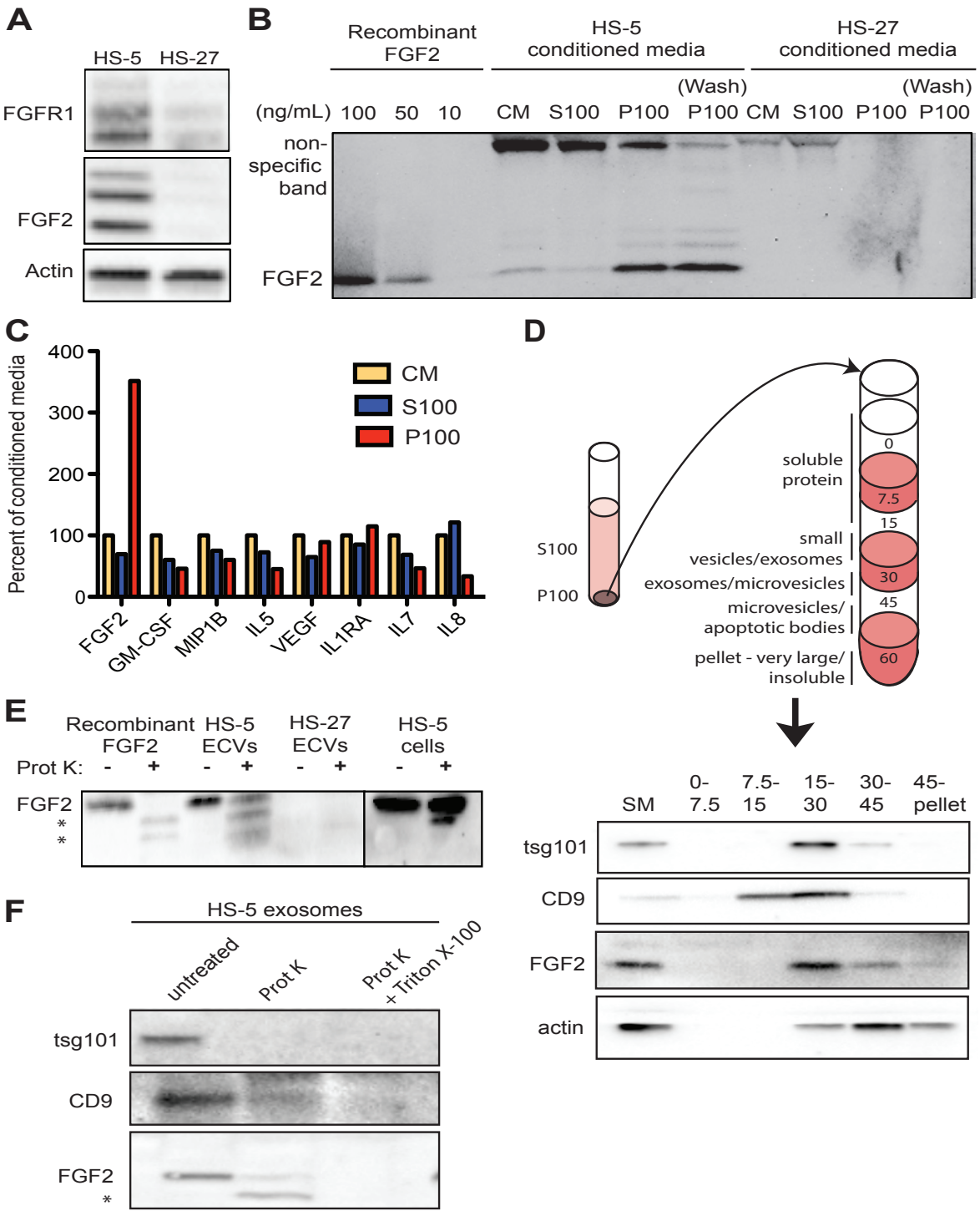

Figure 2: FGF2 is enriched in exosomes from HS-5 bone marrow stromal cells. A. Immunoblot of FGFR1, FGF2 and actin in HS-5 and HS-27 whole cell lysates. **B.** HS-5 and HS-27 CM was ultracentrifuged at 100,000g for 2 hours at 4 degrees C. CM, soluble protein (S100), and ECV (P100) fractions were collected and analyzed by immunoblot, using 10, 50, and 100 ng/ml recombinant FGF2 for comparison. The ultracentrifuge tube was also washed with

detergent to remove adherent ECVs and material (detergent wash P100). **C.** HS-5 CM, S100 and P100 fractions (concentrated ~10 fold compared to HS-5 CM) were solubilized in 0.1% NP-40 and analyzed by cytokine multiplex ELISA (Luminex). The S100 and P100 fractions were normalized to CM. **D.** The HS-5 P100 fraction (starting material, or SM) was further fractionated on a sucrose step-gradient. Sucrose layer interfaces (0-7.5%, 7.5-15%, 15-30%, 30-45%, and 45%-pellet) were collected, lysed and analyzed by immunoblot with antibodies against the exosomal markers CD9 and tsg101; FGF2; and cytoplasmic marker actin. **E.** HS-5 and HS-27 ECVs (P100), recombinant FGF2, and HS-5 cells were exposed to proteinase K and analyzed by immunoblot (top panel). **F.** HS-5 exosomes were isolated by sucrose step-gradient (see panel D) and then exposed to proteinase K with or without detergent (0.1% Triton X-100, used to dissolve the lipid membrane). Samples were subjected to immunoblot analysis using antibodies against tsg101, CD9 and FGF2. The * indicates degraded FGF2 after partial proteinase K digestion.

HS-5 stromal cells overproduce ECVs

Since HS-5 CM is more protective than HS-27 CM[98, 106, 392], we suspected that ECVs may be more numerous in HS-5 CM. We chose several orthogonal methods to quantify vesicles in CM. First, we used nanoparticle tracking analysis to quantify and compare HS-5 and HS-27 ECVs (**Figure 3A**). In parallel, we employed the Virocyt Virus Counter, a flow cytometry-based technique developed to detect viruses, which also works well to quantify ECVs (**Figure 3B**). As a gold standard, negative stain transmission electron microscopy of purified HS-5 and HS-27 exosomes was also used to image and quantify exosomes by counting (30-100 nm diameter with cup-shape appearance characteristic for exosomes, **Figure 3C**). Finally, we used sucrose step-gradient fractionation of HS-5 and HS-27 ECVs to compare cell compartment and exosome-specific markers by immunoblot (**Figure 3D**). Exosomes layer primarily at the 15-30% sucrose interface as indicated by exosomal markers CD9 and tsg-101, and are increased in HS-5 cells compared to HS-27. Interestingly the receptor for FGF2, FGFR1, was also found to localize preferentially with HS-5 exosomes. With all methods, we consistently observed greater than two-fold excess of vesicles produced by HS-5 compared to HS-27 cells (**Supplemental Figure 2** for additional data).

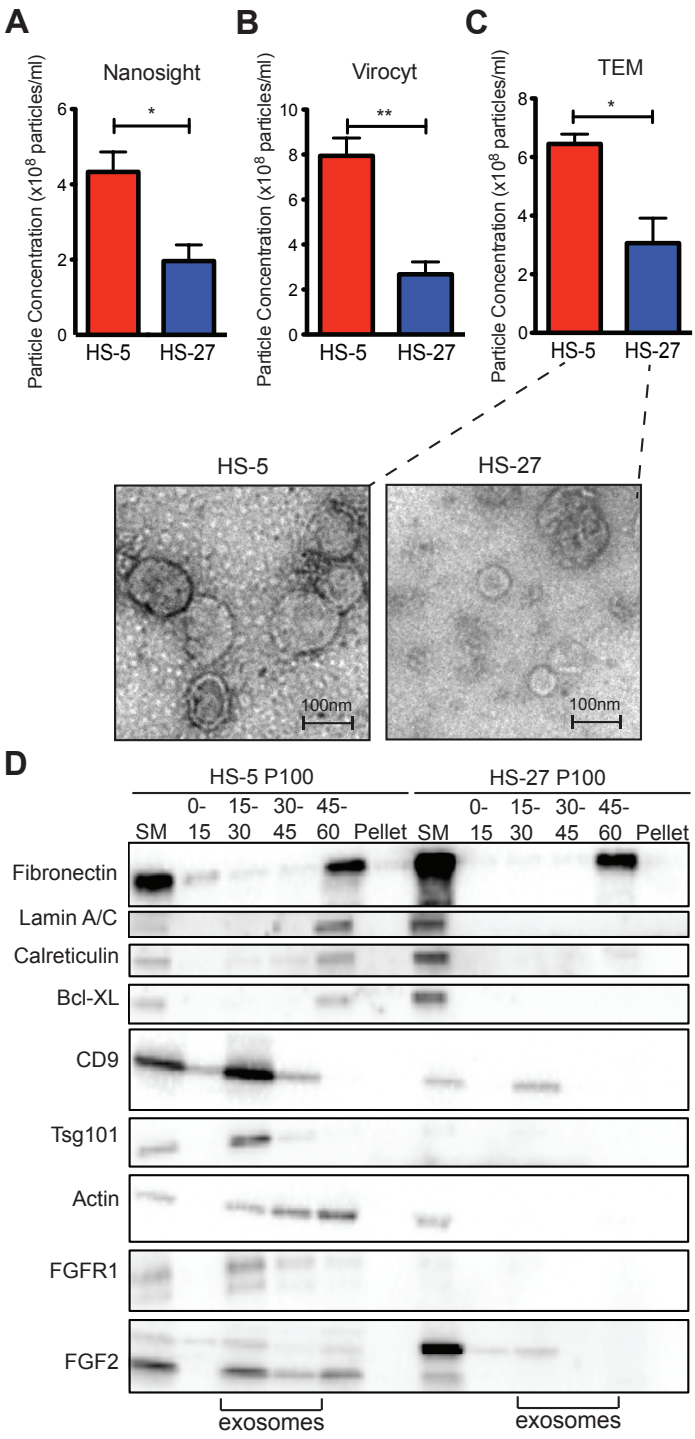

Figure 3: HS-5 cells secrete more exosomes than HS-27 cells. Equal numbers of HS-5 and HS-27 cells were plated in RPMI with exosome-depleted FBS for 24 hours. The ECVs were pelleted by ultracentrifugation at 100,000g for 2 hours at 4 degrees C and resuspended in PBS. ECVs were quantified by **A.** Nanosight, a nanovesicle tracking analysis, **B.** Virocyt Virus Counter, a proprietary flow cytometry using fluorescent dyes that stain both nucleic acid and protein, or **C.**

transmission electron microscopy. **D.** HS-5 and HS-27 exosomes were collected by sucrose-step gradient and analyzed by transmission electron microscopy. Vesicles were quantified by counting in three 2x2μm areas per sample. All experiments were done in triplicate, error bars represent standard deviation, p values are indicated by *<0.05, **<0.005. HS-5 and HS-27 ECVs (P100) were obtained by ultracentrifugation (starting material, or SM), and the exosome fraction was further purified by a sucrose step-gradient. Sucrose layer interfaces (0-7.5%, 7.5-15%, 15-30%, 30-45%, and 45%-pellet) were collected, lysed and analyzed by immunoblot. Blots were probed with antibodies against exosomal markers CD9 and tsg101; cell compartment markers: fibronectin, lamin A/C, BCL-XL; as well as FGFR1 and FGF2. The lanes with highest enrichment for CD9 and tsg-101, indicating exosomes, are marked below.

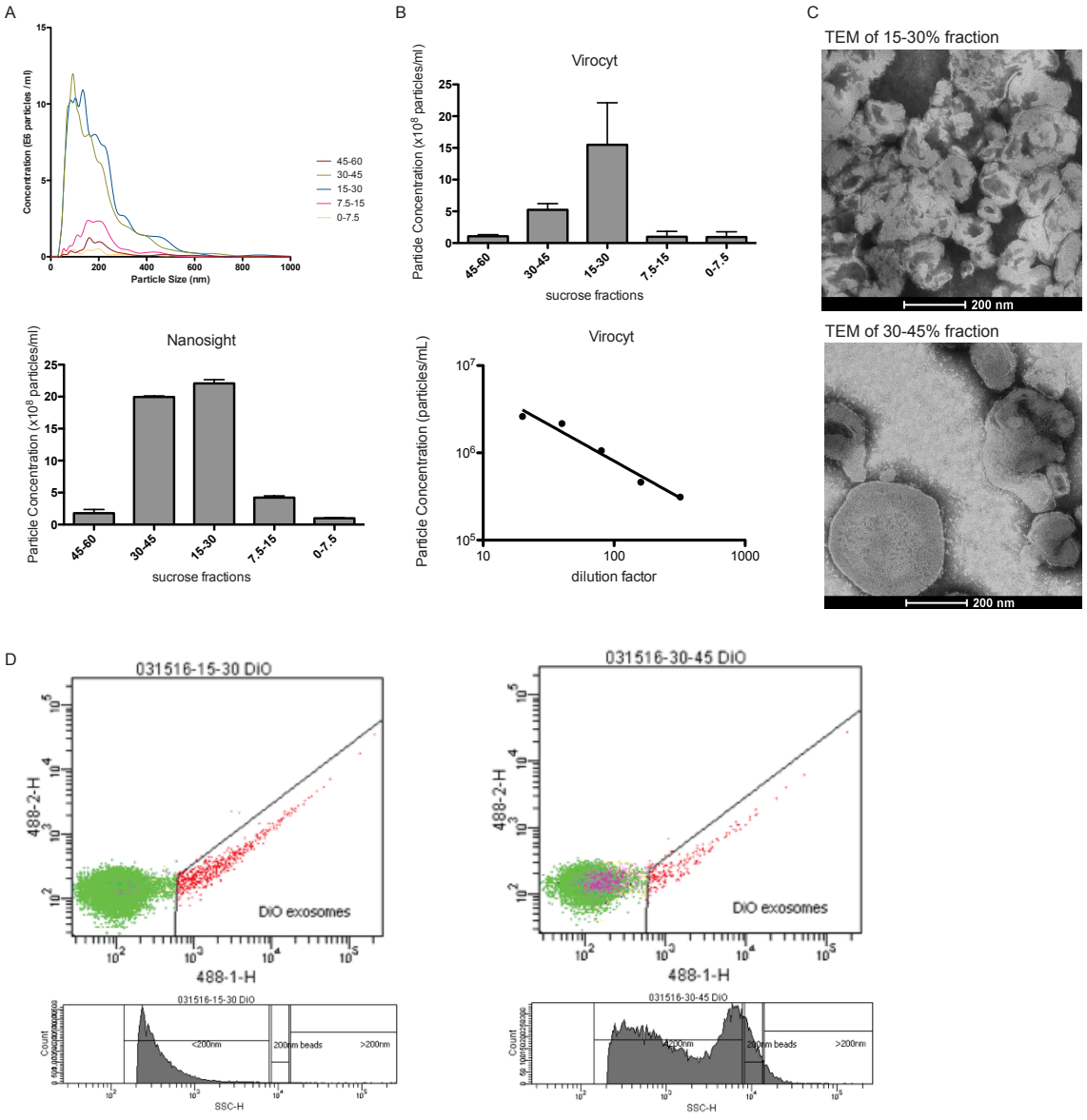

Supplemental Figure 2: Methods for exosome quantification and further evaluation of microvesicle populations. **A.** CM fractionated by sucrose density gradient assessed for microvesicles by nanoparticle tracking analysis (Nanosight). **B.** Fractions assessed by flow cytometry optimized for virus particles (Virocyt). **C.** Transmission electron microscopy of sucrose fractions showing microvesicle size difference between 15-30% and 30-45% fractions. **D.** Fractions dyed with fluorescent tracer and analyzed by flow cytometry. Size distribution of two different fractions shown relative to 200nm beads.

FGF2-FGFR1 signaling promotes stromal growth and paracrine protection of leukemia

FGF2 is an autocrine signaling protein for stroma, but recombinant FGF2 also mediates paracrine protection of leukemia cells[106, 107]. Thus, there are two potential mechanisms by which FGFR inhibition can attenuate protection of leukemia cells in the marrow microenvironment: 1) FGFR inhibitors block FGF2-mediated paracrine protection at the leukemia cells; and/or 2) FGFR inhibitors interrupt stromal FGF2-FGFR1 autocrine signaling to reduce secretion of protective FGF2-containing exosomes. To compare the relative effect of FGFR inhibition on autocrine and paracrine signaling, HS-5 cells were pre-treated with the FGFR inhibitor PD173074[405, 406] for one week prior to collection of CM. CM collected from HS-5 cells pre-treated with PD173074 was significantly less protective than CM from an equal number of untreated HS-5 cells (**Figure 4A**), providing evidence that interruption of FGF2-FGFR1 signaling affects subsequent protection of leukemia cells. In contrast, addition of PD173074 to untreated HS-5 CM only modestly attenuated protection of MOLM14 cells. We found similar results with K562 cells exposed to imatinib (**Supplemental Figure 3**). Purified ECVs from HS-5 CM, which are enriched in FGF2, were more sensitive to FGFR inhibition (**Supplemental Figure 1**), however pre-treatment of HS-5 cells with PD173074 still had the greatest absolute reduction in protection. These results indicate that FGFR inhibitors overcome protection of leukemia cells primarily by directly altering secretion of FGF2-expressing stromal cells, making them significantly less protective.

To further evaluate the effects of FGFR inhibition in stromal cells, HS-5 cells were evaluated for viability, morphology, and growth using HS-27 cells as comparison (low FGF2). HS-5 or HS-27 cells had little reduction in cell viability after 72-hour treatment with PD173074 (**Figure 4B**), however HS-5 growth slowed dramatically over 15 days (**Figure 4C**). HS-5 cells exposed to PD173074 changed morphology and became less refractile, larger, and more adherent (**Figure 4D**). Cell size was quantified using CellProfiler software and PD173074 significantly increased HS-5 cell size (**Figure 4E**).

To evaluate FGF2 and FGFR1 expression in primary leukemia stroma, bone marrow aspirates from a series of leukemia patients were cultured *ex vivo* and FGF2 and FGFR1-4 expression quantified by RT-PCR (**Figure 4F**). FGFR1 and FGF2 transcripts were the most highly expressed in primary stroma, and there was a strong positive correlation between FGFR1 and FGF2 expression (**Figure 4G**, $r^2 = 0.5683$ and $p<0.0001$ on nonparametric correlation). This indicates that FGF2 and FGFR1 expression are coordinately regulated in primary marrow stromal cells consistent with activation of an FGF2-FGFR1 autocrine loop. There were 9 stromal cultures from AML patients with FLT3 ITD (indicated with red dots), but most of them were newly diagnosed, and based upon our previous data we would not expect increased expression of FGF2[106]. Similar to our observations in cell lines described above, we also detected FGFR1 and FGF2 in ECVs derived from primary marrow stromal cultures (**Supplemental Figure 4**). However, primary marrow stromal cells grow slowly and produce smaller amounts of ECVs, so we were unable to evaluate the effect of FGFR inhibitors on cell morphology, growth, and ECV production with primary marrow stromal cells. Additional characterization of primary stromal cultures is contained in **Supplemental Figure 5**.

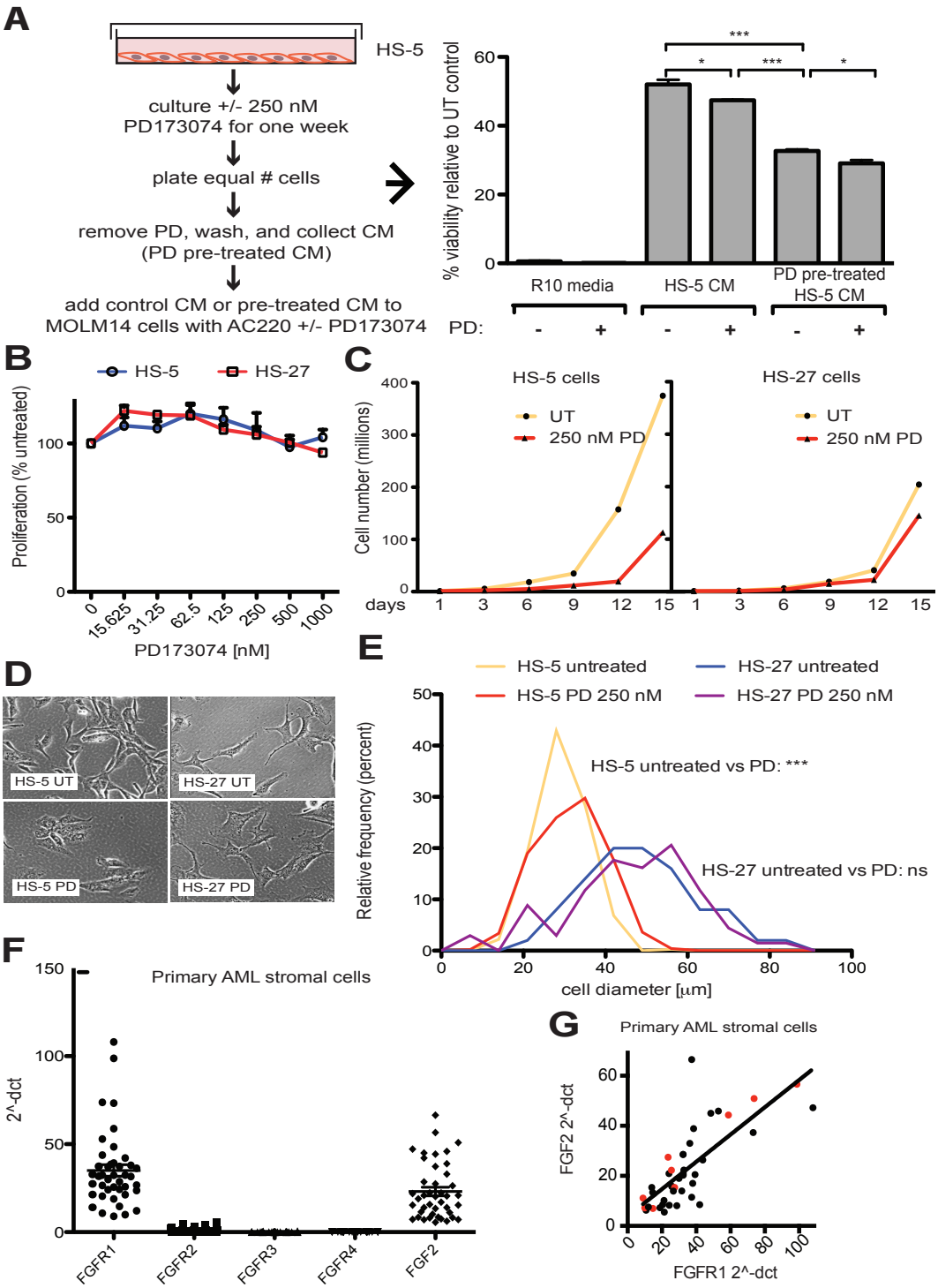

Figure 4: FGF2 is an autocrine growth factor in bone marrow stromal cells, and FGFR inhibition attenuates growth. A. HS-5 cells were cultured in media +/- 250 nM PD173074 for one week and then equal numbers of cells were replated for comparison. After adhesion, the cells cultured in PD173074 were washed and fresh media added to collect CM. MOLM14 cells were resuspended in media, untreated HS-5 CM, and PD pre-treated HS-5 CM and treated with +/- 10 nM AC220 and +/- 250 nM PD173074. Viability was measured by MTS assay after 72 hours and

values were normalized to the relevant UT control. Error bars represent standard deviation, p values are indicated by *<0.05, **<0.005, and ***=0.0007. **B.** HS-5 and HS-27 cells were plated in triplicate on 96 well plates in a gradient of FGFR inhibitor PD173074. Proliferation was measured using MTS reagent after 72 hours. Error bars indicate standard deviation. **C.** HS-5 and HS-27 cells were incubated media +/- 250 nM PD173074 (PD). The number of viable cells was measured with Guava ViaCount every 3 days over a 15-day period. Fresh media and PD173074 was added every 3 days. **D.** HS-5 and HS-27 cells were incubated in media +/- 1 μM PD173074 for 1 week. Brightfield microscopy images were obtained using a 10X objective. **E.** HS-5 cells were incubated in 4-well glass chamber slides in media +/- 250 nM PD173074 (PD). Cells were stained with lipophilic tracer DiI for 24 hours, fixed, then nuclei stained with DAPI. Immunofluorescent images were analyzed with CellProfiler software to determine cell size (μm^2) and number of cells for each size range was binned and graphically displayed. PD173074 had no effect on HS-27 growth, morphology or size (CellProfiler data not shown), consistent with an on-target FGFR effect. **F.** Ex vivo cultured primary bone marrow stromal cells from a series of leukemia patients (n=42) were lysed for RNA extraction and cDNA synthesis. Taqman qPCR analysis was performed using FGFR1, FGFR2, FGFR3, FGFR4, and FGF2 Taqman primer assays and expression plotted (n=42 for each except FGFR4 which is n=41 due to failed PCR for one sample). **G.** FGFR1 and FGF2 qPCR values (2^-ΔCT) were plotted against each other. There were 9 AML patients with FLT3 ITD (most newly diagnosed) and these patients are indicated with red dots. Linear regression produced a line fit with r^2=0.5683 and slope significantly non-zero with p<0.0001.

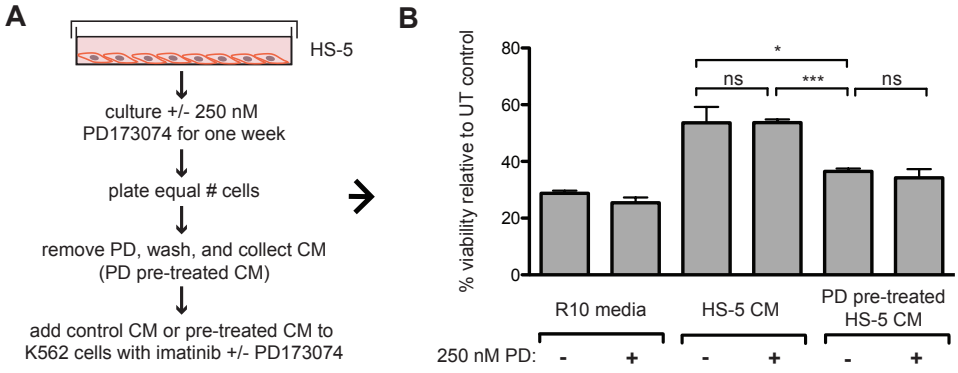

Supplemental Figure 3: Pre-treatment of HS-5 stromal cells with FGFR inhibitor reduces protective properties of HS-5 CM when added to K562 cells exposed to imatinib. A. HS-5 cells were cultured in media +/- 250 nM PD173074 for one week and then equal numbers of cells were replated for comparison. After adhesion, the cells cultured in PD173074 were washed and fresh media added to collect CM. K562 cells were resuspended in media, untreated HS-5 CM, and PD pre-treated HS-5 CM and treated with +/- 1 uM imatinib and +/- 250 nM PD173074. **B.** Viability was measured by MTS assay after 72 hours and values were normalized to the relevant UT control. Error bars represent standard deviation, p values are indicated by *<0.05, **<0.005, and ***=0.0007.

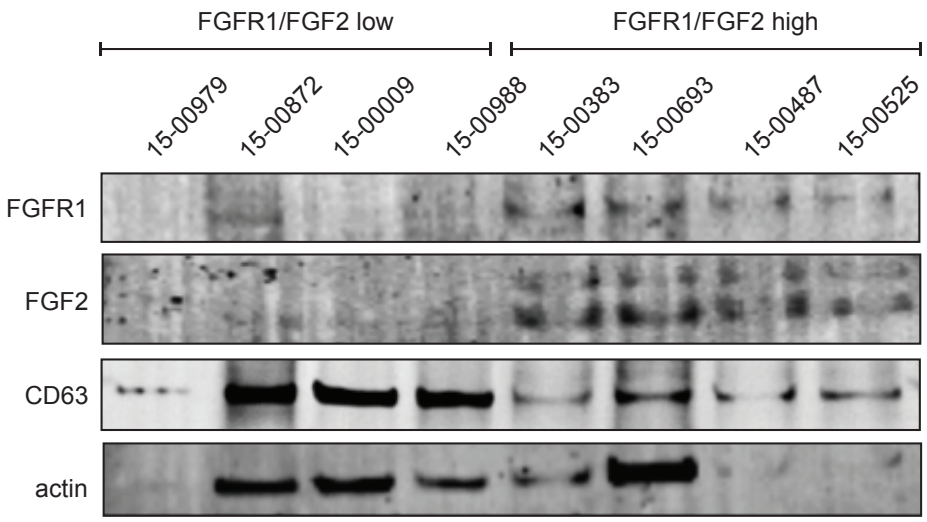

Supplemental Figure 4: Cultures of primary human and mouse bone marrow stroma produce microvesicles containing FGF2. Conditioned medium was collected from cultured human bone marrow stroma. Samples were ultracentrifuged and pellets were lysed with 78 μL of Cell Lysis Buffer (Cell Signaling Technologies Inc., Danvers, MA) containing a Complete Mini Protease Inhibitor Cocktail Tablet, Phosphatase Inhibitor Cocktail 2, and Phenylmethanesulfonyl Fluoride (PMSF) solution (Sigma-Aldrich Inc., St Louis, MO) and clarified by centrifugation at 14,000 g, 4°C for 15 minutes. All samples were loaded on NuPAGE 4-12% Bis-Tris gradient gels, ran in MES buffer (Thermo Fisher Scientific Inc., Waltham, MA), transferred on Immobilon-FL PVDF membranes (Millipore Inc., Billerica, MA), and blocked overnight at 4°C. Following overnight incubation, membranes were incubated with the following primary antibodies: anti-FGFR1, anti-FGF2, anti-CD63, anti-CD9, and anti-actin (Supplemental File) overnight at 4°C. The following day membranes were washed and probed with fluorescent IRDye 800CW goat anti-rabbit IgG and IRDye 680RD Goat anti-mouse IgG antibodies (Supplemental File). The membranes were imaged with the Odyssey Infrared Imaging System (LI-COR Biosciences).

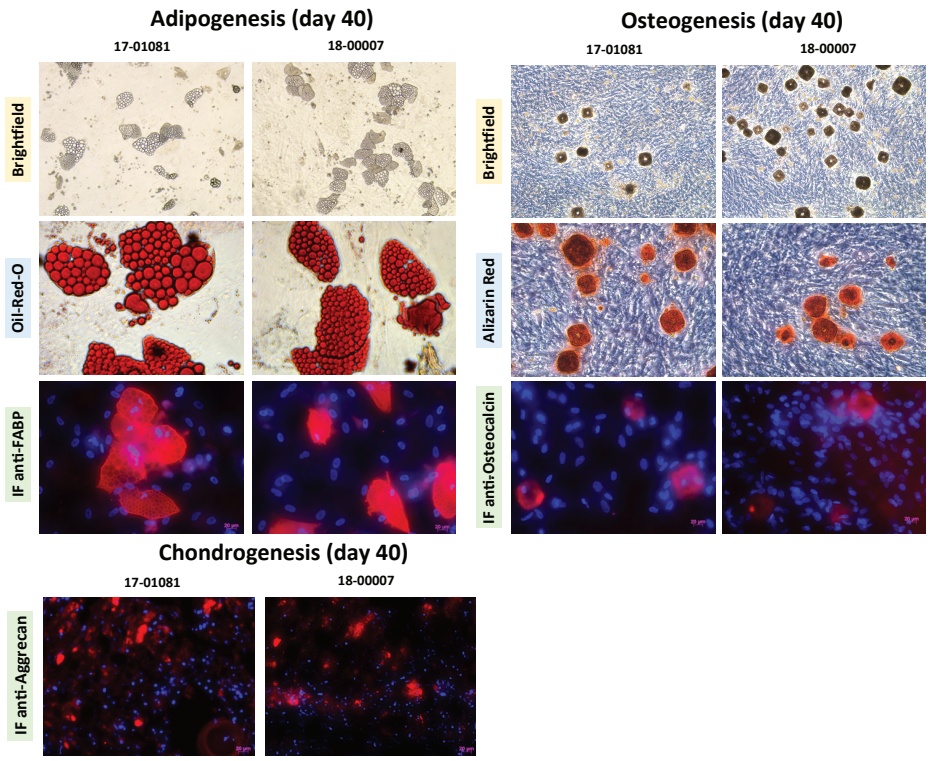

Supplemental Figure 5: Cultured primary human bone marrow stroma exhibits trilineage differentiation. Mesenchymal stromal cells at passage 4 were differentiated into adipocytes, osteocytes, and chondrocytes using the Human Mesenchymal Stem Cell Functional Identification Kit (R&D Systems Inc., Minneapolis, MN) according to the manufacturer's instructions. Cells were cultured for 40 days with induction medium replaced every three days. On day 40 of induction, the cultures were washed with PBS and fixed for 20 min in 4% buffered paraformaldehyde at room temperature. The presence of adipogenic cells was confirmed with oil-red-o staining and immunofluorescence staining for fatty acid binding protein (FABP). Osteogenesis was assessed with alizarin red staining and immunofluorescence staining for osteocalcin. For chondrogenic pellets, upon fixing, pellets were cryosectioned at a thickness of 5μm and stained for aggrecan using immunofluorescence.

FGFR inhibition decreases stromal cell production of exosomes

Since FGFR inhibition attenuates HS-5 growth and morphology, we hypothesized that it might also reduce secretion of ECVs. HS-5 cells exposed to graded concentrations of PD173074 and BGJ398 had a dose-dependent decrease in ECVs measured by Virocyt Virus Counter (**Figure 5A – B**). Notably, there was a significant decrease in vesicle number as early as 6 hours after drug exposure (**Supplemental Figure 6**), suggesting that FGFR inhibition directly affects vesicle production or release. ECVs were also collected from HS-5 and HS-27 cells exposed to PD173074 and analyzed by immunoblot. PD173074 reduced the exosome markers tsg101 and CD9 (and FGF2) but had no effect on ECV production from HS-27 cells (**Figure 5C**, similar results with BGJ398 shown in **Supplemental Figure 6**). Scanning electron microscopy of HS-5 cells revealed abundant budding membrane, whereas the surface of PD173074-exposed cells was smoother, implicating a change in membrane dynamics (**Supplemental Figure 7**). To evaluate exosome secretion specifically, sucrose step-gradient fractionation was performed on ECVs from untreated and PD173074 treated HS-5 cells. PD173074 reduced exosomal markers CD9, tsg101, and FGF2 in the expected 15-30% interface fraction (**Figure 5D**).

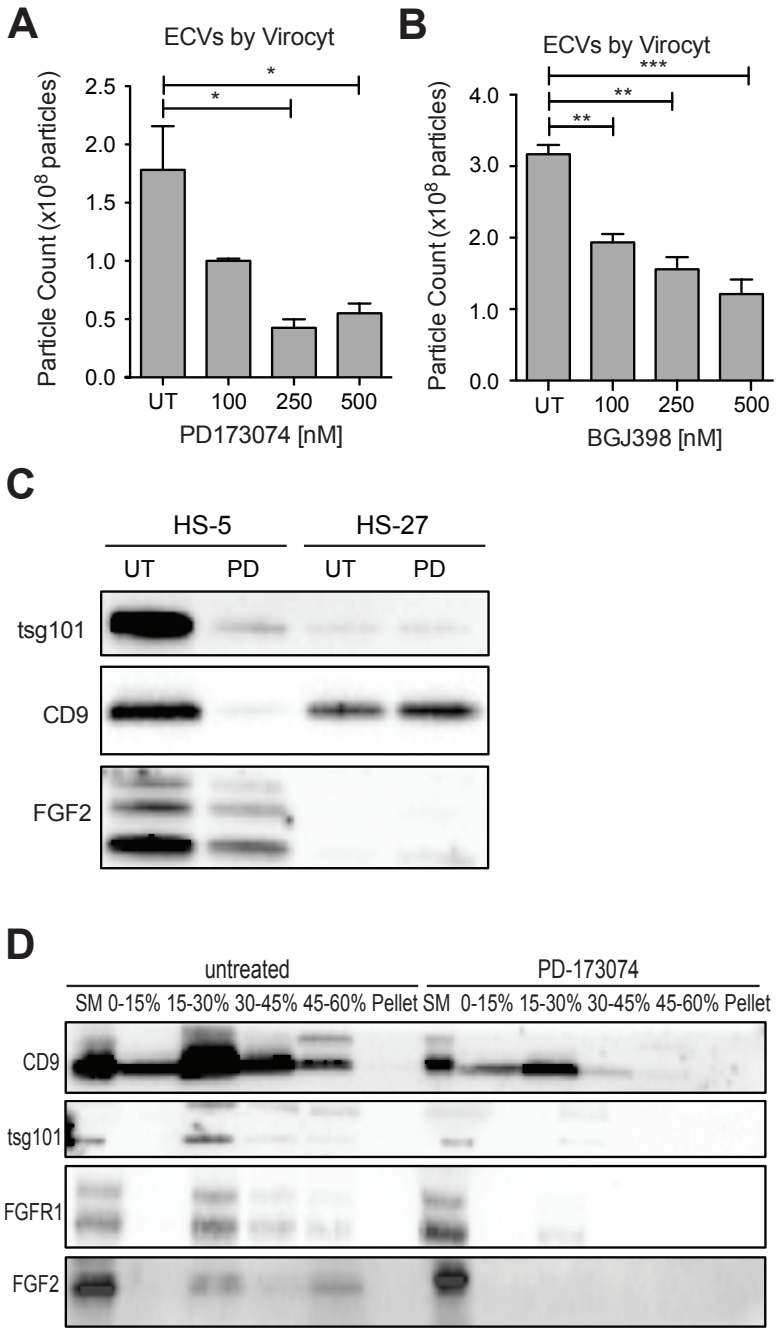

Figure 5: FGFR inhibition decreases exosome production in FGF2-expressing stroma. HS-5 cells were exposed to a gradient of the FGFR inhibitors **A.** PD173074 and **B.** BGJ-398 for 48 hours prior to collecting CM. ECVs were pelleted by ultracentrifugation at 100,000g and quantified by Virocyt Virus Counter. Error bars indicate standard deviation and p values are indicated by *<0.05. **C.** HS-5 and HS-27 cells were incubated in media +/- 1 μM PD173074 for 72 hours prior to collecting ECVs. ECVs were analyzed by immunoblot for FGF2. The exosome markers CD9 and tsg101 are also shown. **D.** HS-5 cells were plated in media +/- 1 μM PD173074 for 72 hours. P100 fractions were obtained by ultracentrifugation, and further fractionated on a sucrose step-gradient. The interfaces (0-7.5%, 7.5-15%, 15-30%, 30-45%, and 45%-pellet) were collected,

lysed and processed by immunoblot with antibodies against the exosomal markers CD9 and tsg101 as well as FGFR1 and FGF2.

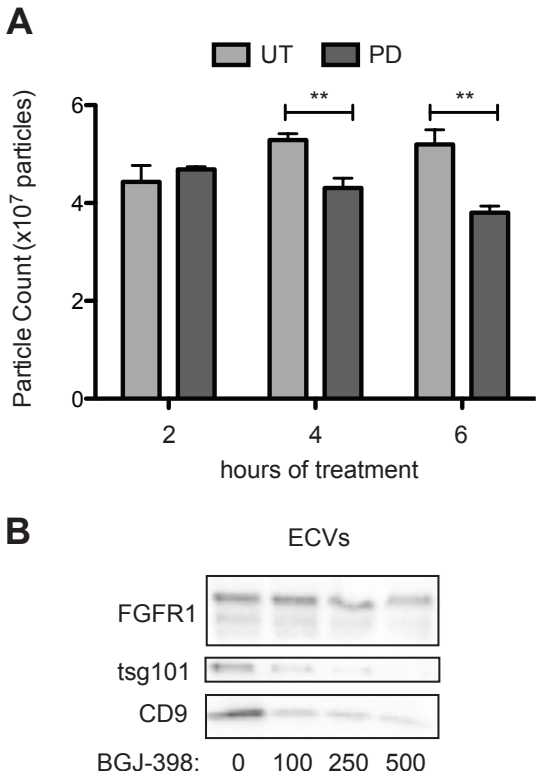

Supplemental Figure 6: FGFR inhibition reduces HS-5 cell exosome secretion. A. HS-5 cells were exposed to 500 nM PD173074 (PD) for 2, 4 and 6 hours before collection of CM and ECVs as previously described. ECVs were quantified by Virocyt. Results obtained in triplicate. Error bars indicates standard deviation. ** $p<0.005$ **B.** HS-5 cells were exposed to a gradient of BGJ-398 for 72 hours before isolation of ECVs from CM. ECVs were lysed and run on immunoblot to demonstrate reduction in exosome markers (CD9 and tsg-101).

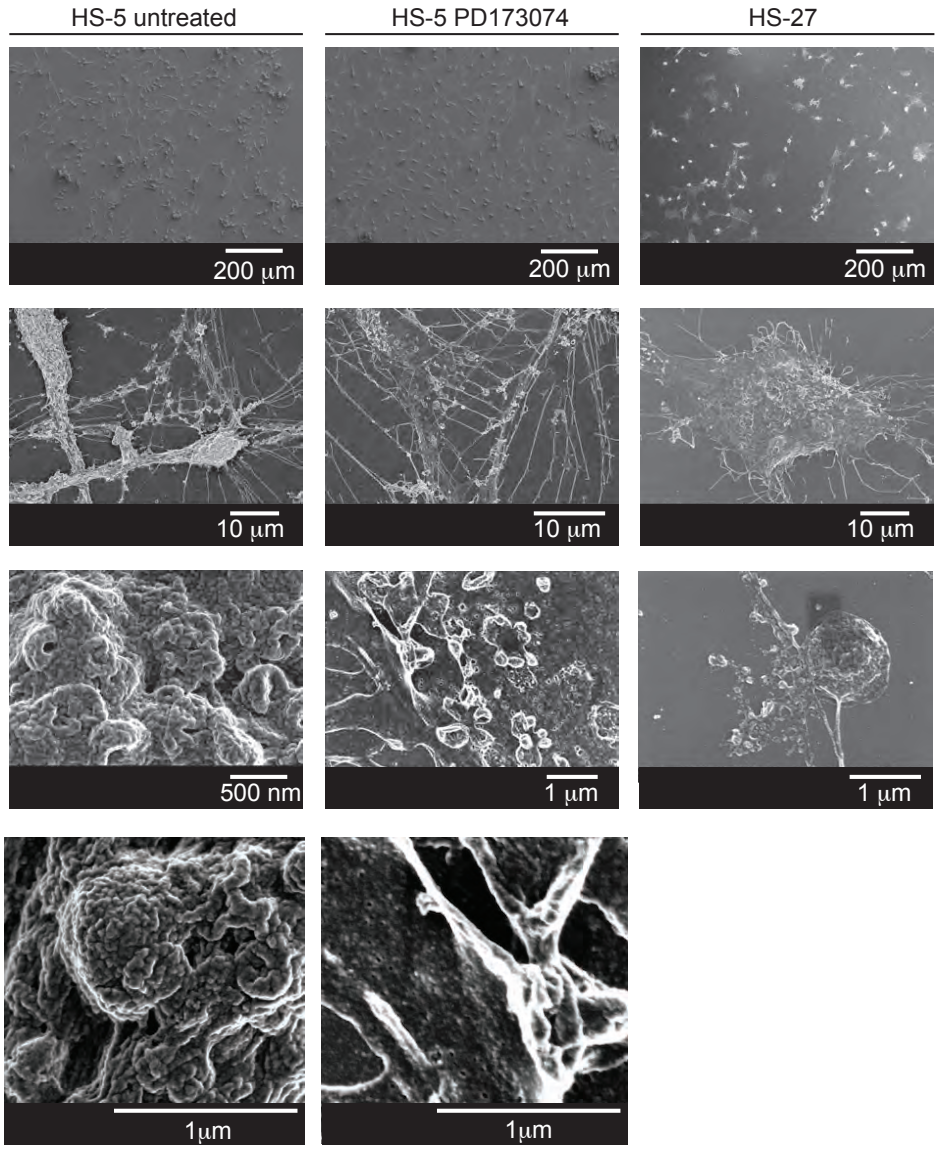

Supplemental Figure 7: Scanning electron microscopy of HS-5 cells shows altered membrane dynamics after FGFR inhibition. Cells grown on coverslips were fixed with 2% paraformaldehyde and 1% glutaraldehyde (Ted Pella Inc., Redding, CA, USA) in phosphate buffered saline for at least one hour. Following three rinses in phosphate buffered saline, the samples were immersed in 1% osmium tetroxide in phosphate buffered saline for one hour at room temperature. Following three buffer rinses, the samples were rinsed once in ddH2O before entering an ascending ethanol gradient, incubating for ten minutes in each mixture of ethanol:ddH2O (50%, 75%, to 95% ethanol). After two incubations in 100% ethanol the samples were critical point dried (Tousimis Samdri CPD, Rockville, MD, USA). Dried coverslips were mounted on aluminum stubs with carbon tape and silver paint and then sputter coated with 6-10 nm of gold-palladium (Hummer Sputter System, Anatech USA, Hayward, CA, USA). The samples were imaged on a FEI Helios Nanolab 660 (FEI Inc., Hillsboro, OR). Images were collected with the Elstar in-lens TLD detector or the Everhart-Thornley Detector at 1 kV accelerating voltage.

Genetic knock-down of FGFR1 or FGF2 attenuates exosome production

To confirm that decreased exosome secretion is specific for FGFR1 inhibition, HS-5 cells were stably transfected with either a GFP-expressing lentivirus control vector (GIPZ), or doxycycline-induced shRNA targeting FGFR1. FGFR1 silencing led to a significant reduction in ECVs (**Figure 6C**). Similar results were obtained with siRNA targeting FGFR1 (**Supplemental Figure 8**). siRNA and shRNA constructs targeting FGF2 did not achieve reliable silencing of FGF2. HS-5 CRISPR/Cas9 knockout of FGFR1 and FGF2 in HS-5 cells were generated, however genetic silencing prevented continued growth. Multiple attempts to make stable deleted cell lines were unsuccessful, likely due to the importance of FGF2-FGFR1 signaling for HS-5 self-renewal and growth[407-409]. That being said, ECVs collected shortly after CRISPR/CAS9 treatment, which resulted in partial silencing of FGF2 or FGFR1, both demonstrated decreased ECVs by immunoblot and reduced protection of MOLM14 cells (**Supplemental Figure 9**). To test the role of FGF2 in ECV production in primary cells, equal numbers of murine stromal cells from *Fgf2* +/+ and -/- mice (*Fgf2tm1Doe*[104]) were treated with PD173074 and ECVs quantified by Virocyt (**Figure 6D**). *Fgf2* +/+ stromal cells secreted significantly more ECVs than -/-, and PD173074 only reduced ECV secretion in +/+ stroma. ECVs from *Fgf2* +/+ and -/- mice were also analyzed by immunoblot with similar reduction in ECV proteins from *Fgf2* -/- stroma (**Figure 6E**).

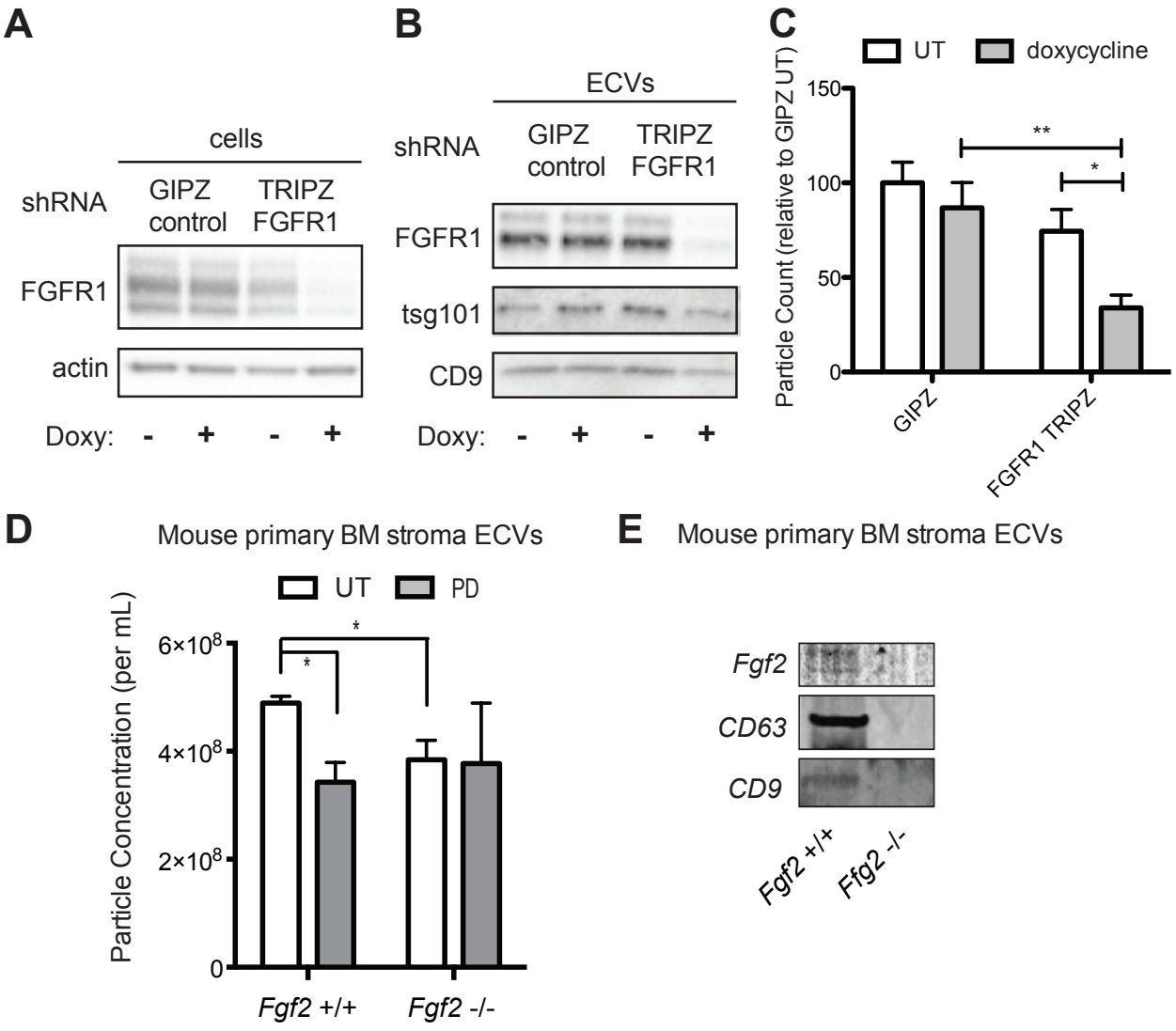

Figure 6: Genetic silencing of FGFR1 or deletion of FGF2 attenuates exosome secretion. A doxycycline-inducible lentiviral shRNA targeting FGFR1 was used to create a stable HS-5 cell line. The cells were then treated with doxycycline to induce FGFR1 silencing and compared to a GIPZ lentiviral control. **A.** Silencing of FGFR1 expression is shown by immunoblot of cell lysates. ECVs from doxycycline-treated cells were analyzed by **B.** immunoblot or **C.** Virocyt Virus Counter. *p<0.05. **D.** Bone marrow was isolated from *Fgf2* +/+ and -/- mice and cultured *ex vivo* to grow adherent marrow stroma. Equal numbers of cells were then plated, CM collected for 72 hours, and then ultracentrifuged to collect ECVs. The ECVs were quantified by Virocyt. *p<0.05. **E.** Equal number of cultured marrow cells from *Fgf2* +/+ and -/- mice were plated and then ECVs collected by ultracentrifugation and analyzed by immunoblot.

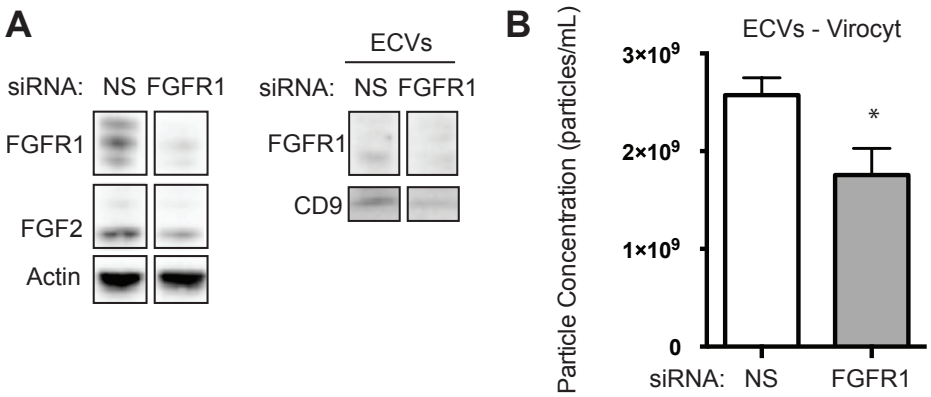

Supplemental Figure 8: Genetic silencing of FGFR1 by siRNA reduces exosome secretion and protection capacity of HS-5 stromal cells. FGFR1 siRNA pool was purchased from Thermo Fisher Scientific Dharmacon RNAi Technologies (Waltham, MA, USA). HS-5 cells were transfected with siRNAs using Lipofectamine 2000 reagent purchased from Thermo Fisher Scientific (Grand Island, NY, USA), according to manufacturer's protocol. After 72 hours, cells were harvested, and cells and CM collected for analysis. siRNA effectively silences of FGFR1 in cells and leads to reduction in ECVs by **A.** immunoblot and **B.** Virocyt analysis.

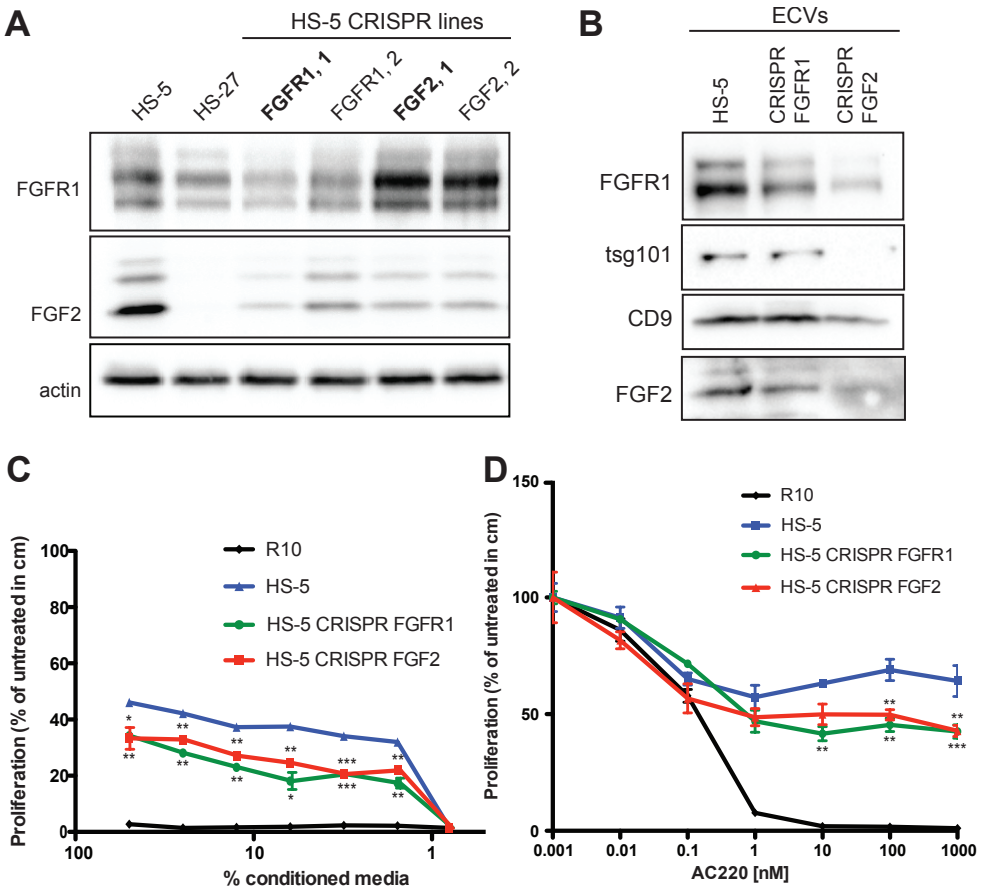

Supplemental Figure 9: Genetic silencing of FGFR1 by CRISPR/CAS9 reduces exosome secretion and protection capacity of HS-5 stromal cells. A. FGFR1 and FGF2 genes were knocked out in HS-5 cells by lentiviral CRISPR-Cas9 genome editing. Each gene was targeted with two single guide RNA sequences (labeled 1, 2 and whole cell lysates were analyzed by immunoblot to demonstrate gene silencing. However, once FGF2 and FGFR1 were genetically mutated, the HS-5 cells were unable to continue to grow, so we were only able to analyze the cell lines for a short time after CRISPR/CAS9 treatment, which initially results in a partial genetic silencing as demonstrated in panel A. Constructs selected for subsequent experiments are indicated in bold. **B.** ECVs from control HS-5 cells and CRISPR/Cas9 HS-5 cells were analyzed by immunoblot with antibodies against FGFR1, tsg101, CD9, FGF2, and actin. **C.** CM was harvested from HS-5 cells, FGFR1 CRISPR/Cas9 HS-5 cells, and FGF2 CRISPR/Cas9 HS-5 cells after 72 hours. MOLM14 cells were plated in 96 well plates in 10nM AC220 and media alone or with serial dilutions of CM. Proliferation was measured using MTS reagent after 48 hours. **D.** CM was harvested from HS-5 cells, FGFR1 CRISPR/Cas9 HS-5 cells, and FGF2 CRISPR/Cas9 HS-5 cells after 72 hours. MOLM14 cells were plated in 96 well plates in media alone or CM and then graded concentrations of quizartinib (AC220). Proliferation was measured using MTS reagent after 48 hours. Error bars indicate standard deviation. All experiments were done in triplicate and p values are indicated by *<0.05, **<0.005, ***=0.0007.

Fgf2 -/- stroma produces fewer exosomes and is less protective of BCR-ABL leukemia

To test the role of stromal *Fgf2* in an *in vivo* leukemia model, bone marrow from *Fgf2* +/+ mice was retrovirally transfected with BCR-ABL containing GFP as a marker[390] and used to transplant lethally irradiated FGF2 +/+ and -/- mice. This induces a very aggressive disease in mice that is more akin to AML than CML, and TKIs are only effective for a limited duration. Mice were treated with nilotinib 75 mg/kg/day by oral gavage starting on day 14 post-transplant. Mice that were found to have aplastic marrow (unsuccessful transplantation) were excluded from analysis since their death was not related to leukemia (4 mice in the *Fgf2* +/+ untreated group, 1 mouse in the *Fgf2* -/- untreated group, 2 mice in the *Fgf2* +/+ nilotinib group, and 2 mice in the *Fgf2* -/- nilotinib group). The survival curves of the remaining mice are shown in **Figure 7A**. The cohorts of untreated *Fgf2* +/+ and -/- both died rapidly from disease, as expected. Nilotinib significantly increased survival of *Fgf2* +/+ and -/- mice compared to untreated mice, but the survival of the nilotinib-treated *Fgf2* -/- was also significantly longer than their *Fgf2* +/+ counterparts. To ensure equal engraftment of disease in both backgrounds, the blood and bone marrow was analyzed for GFP and found to be similar in both *Fgf2* +/+ and -/- mice at time of death (**Figure 7B and Supplemental Figure 10**), suggesting that nilotinib was more effective at attenuating disease progression of BCR-ABL leukemia cells in an *Fgf2* -/- microenvironment. To directly evaluate the protective effect of ECVs on leukemia progenitor cells, ECVs were isolated from equal numbers of +/+ and -/- primary marrow stromal cells cultured with and without PD173074 treatment. Then, bone marrow from +/+ mice was retrovirally transfected with BCR-ABL and incubated with the ECVs overnight. The cells were washed, plated in methylcellulose with and without imatinib, and colonies counted after 8 days. Imatinib significantly reduced colony formation without ECVs, but ECVs from +/+ stroma almost completely reversed the inhibitory effects of imatinib (**Figure 7C**). ECVs from PD173074-treated +/+ stroma or -/- stroma were not as protective, suggesting that *Fgf2* +/+ stroma more effectively protects BCR-ABL leukemia cells from the effects of kinase

inhibition through secretion of protective exosomes. We confirmed the presence of *Fgf2* in microvesicles isolated from cultured *Fgf2* +/+ mouse stroma (**Figure 6**). To confirm that ECVs can be endocytosed by primary cells, lineage-negative hematopoietic progenitor cells were isolated from *Fgf2* +/+ mice and stained with a green lipophilic tracer (DiO) and incubated with ECVs from *Fgf2* +/+ or *Fgf2* -/- stromal cells stained with a red lipophilic tracer (DiI). Confocal microscopy confirmed internalization of fluorescently labeled primary stromal ECVs by murine progenitor cells (**Figure 7D and Figure 7 – Videos 1 and 2**).

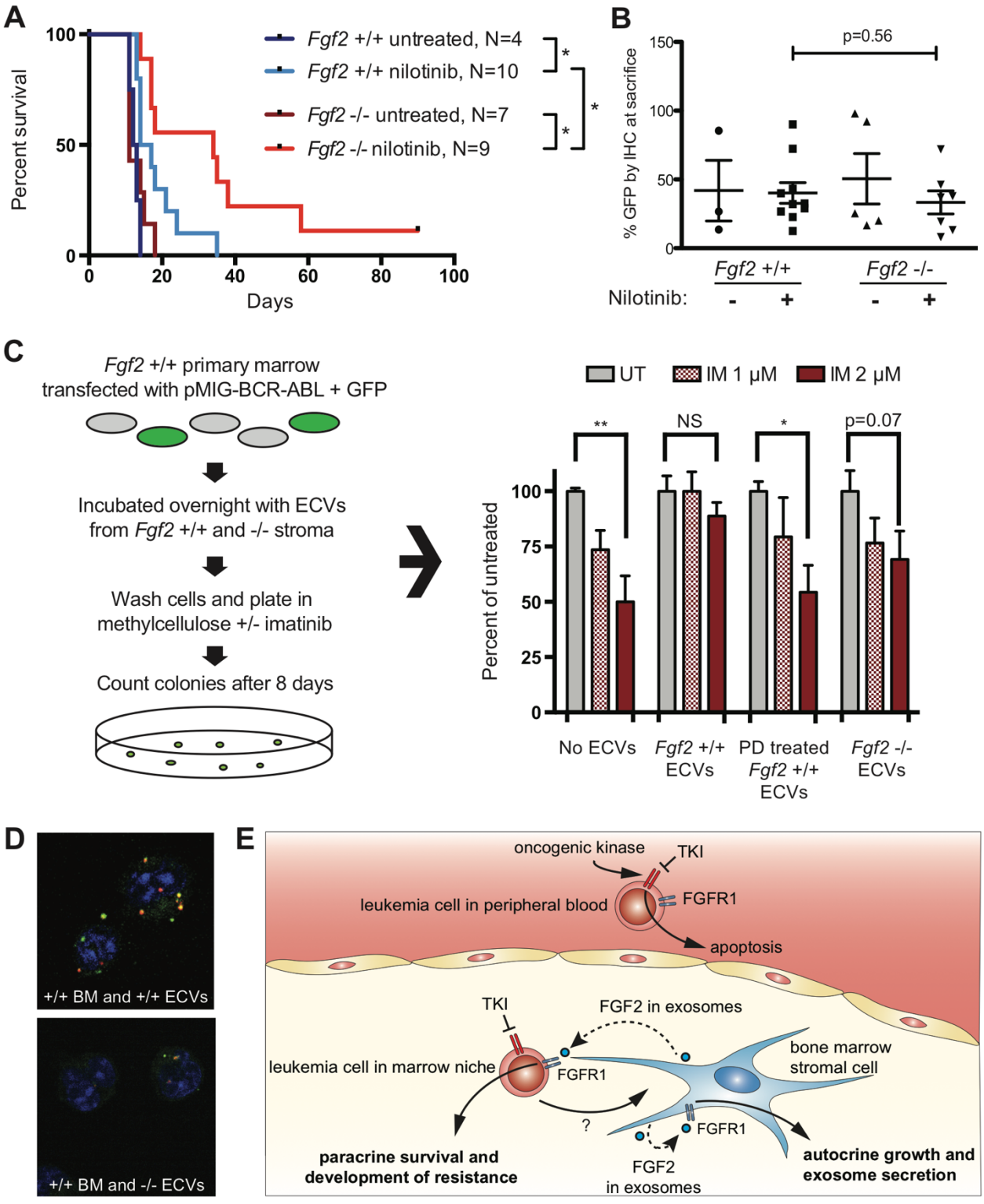

Figure 7: *Fgf2* -/- mice survive significantly longer with TKI therapy in a murine BCR-ABL leukemia model. *Fgf2* +/+ bone marrow was removed from donor mice and spinoculated with pMIG BCR-ABL retrovirus containing an IRES-GFP marker. The transfected bone marrow was

then transplanted into lethally irradiated *Fgf2* +/+ or -/- recipients. Mice were treated with 75 mg/kg/day nilotinib by oral gavage starting on day 11 of transplant. **A.** Survival curves of untreated and nilotinib-treated *Fgf2* +/+ and -/- mice. **B.** GFP in peripheral blood was evaluated weekly and at time of euthanasia to quantify disease burden. The average GFP (percent of nucleated cells) is shown and did not differ significantly between groups indicating that all animals developed similar disease burden. Error bars indicate standard deviation. **C.** Bone marrow cells from *Fgf2* +/+ mice were spinoculated with pMIG BCR-ABL retrovirus containing GFP-IRES. The cells were then incubated with ECVs obtained from *Fgf2* +/+ and -/- primary stroma cultured alone or with 500 nM PD173074. The next day the incubated cells were washed three times to remove cytokines and exosomes and plated in cytokine-free methylcellulose +/- imatinib. After 8 days, colonies were counted and normalized to untreated condition. Graph shown on right. Error bars indicate standard error of the mean. *$p<0.5$ and **$p<0.05$. **D.** Lineage-negative bone marrow cells were isolated from *Fgf2* +/+ mice and cells were stained with DiO (green) tracer, washed, and immobilized on Poly-D-lysine coated chamber slides. ECVs from bone marrow stroma of *Fgf2* +/+ or -/- mice were stained with DiI (red) tracer and added to the cells for a 24-hour incubation. Slides were stained with DAPI (blue) and imaged by confocal fluorescent microscopy. Movie of the z-stack images are included as Figure 7-video 1 and 2. **E.** Model of bone marrow stromal FGF2 autocrine signaling and paracrine protection of leukemia cells by FGF2-containing exosomes.

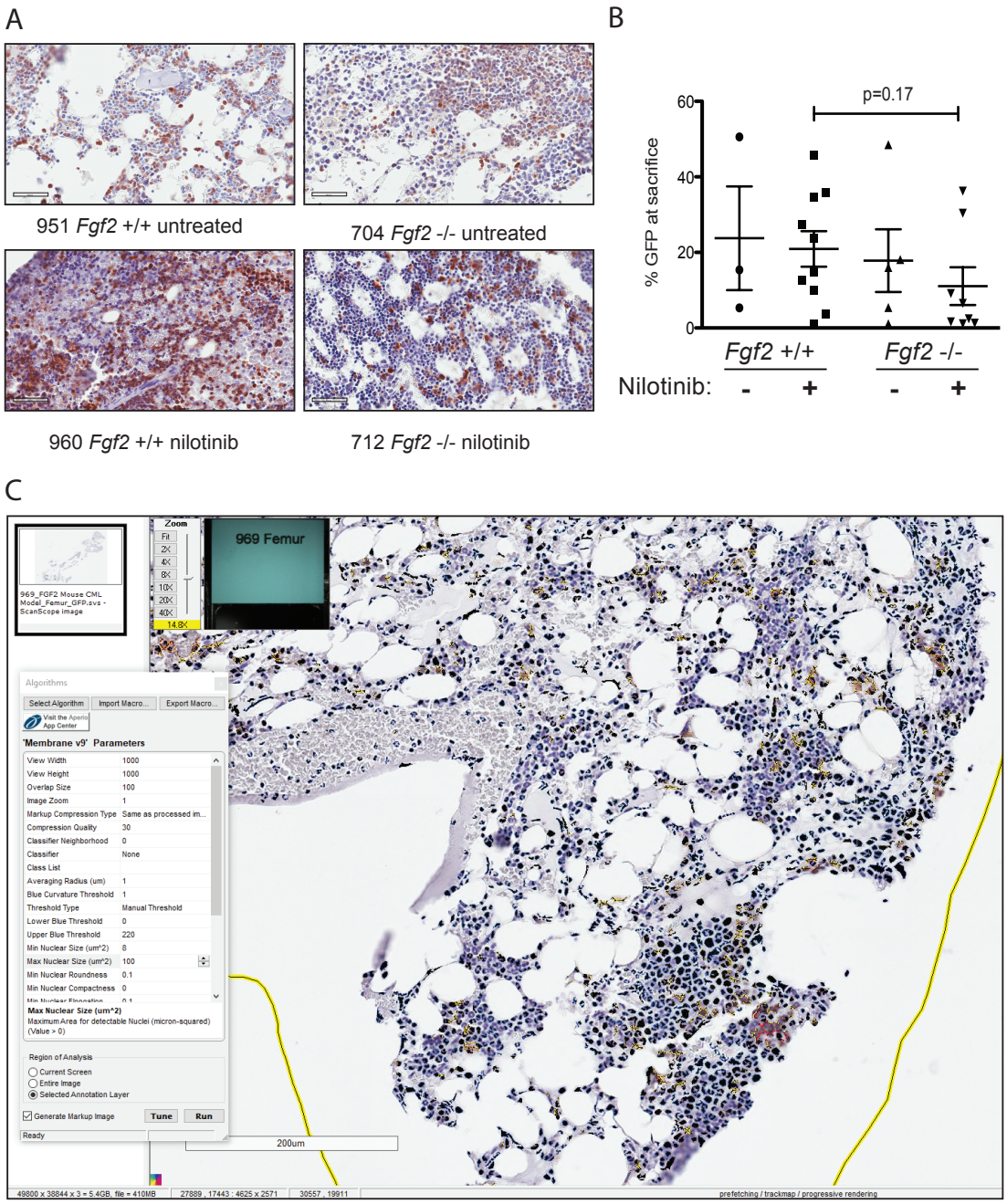

Supplemental Figure 10: *Fgf2* +/+ and -/- mice demonstrate engraftment of leukemia by immunohistochemistry (IHC) of GFP. *Fgf2* +/+ marrow was removed from donor mice and spinoculated with pMIG BCR-ABL retrovirus containing an IRES-GFP marker. The transfected marrow was then transplanted into lethally irradiated *Fgf2* +/+ or -/- recipients. Mice were treated with 75 mg/kg/day nilotinib by oral gavage starting on day 11 of transplant. Lungs, spleens, and femurs were collected for analysis by hematoxylin and eosin staining and IHC for GFP as previously described[106, 107]. **A)** IHC of GFP in marrows of representative mice to demonstrate engraftment of leukemia. **B)** GFP in peripheral blood was evaluated weekly and at time of euthanasia to quantify disease burden. The average GFP (percent of nucleated cells) at time of

euthanasia is shown and did not differ significantly between groups indicating that all animals developed similar disease burden prior to death. Error bars indicate standard deviation. **C)** Illustration of patient tissue analysis using the Aperio ScanScope CS Slide Scanner. Bone marrow tissue selected for analysis showing results of analysis using the membrane-v9 algorithm.

Figure 7 – Video 1: ECVs collected from *Fgf2* +/+ primary marrow stromal cell cultures were stained with DiI (red) and lineage-depleted hematopoietic cells from *Fgf2* +/+ marrow were stained with DiO (green) and incubated for 24 hours at 37°C as described in Materials and methods. Cells were washed, placed on poly-D-lysine coated chamber slides, and DAPI-stained. Z-stack imaging was performed on an Olympus IX71 inverted microscope. Video is available online, https://doi.org/10.7554/eLife.40033

Figure 7 – Video 2: ECVs collected from *Fgf2* -/- primary marrow stromal cell cultures were stained with DiI (red) and lineage-depleted hematopoietic cells from *Fgf2* +/+ marrow were stained with DiO (green) and incubated for 24 hours at 37°C as described in Materials and methods. Cells were washed, placed on poly-D-lysine coated chamber slides, and DAPI-stained. Z-stack imaging was performed on an Olympus IX71 inverted microscope. Video is available online, https://doi.org/10.7554/eLife.40033

Discussion

The normal hematopoietic microenvironment is altered by leukemia, and can protect leukemia cells from the effects of both chemotherapy and targeted kinase inhibitors[104, 106, 107, 410]. Until recently, stromal protection of leukemia cells was thought to be largely mediated by secreted cytokines or through direct contact (review[395]). Here, we show that exosomes from bone marrow stromal cells are transferred to leukemia cells, and protect them from kinase inhibitors. Exosomes have previously been identified as important mediators of malignancy, including recent reports of leukemia exosomes modulating marrow stroma[393, 411-413]. We found that the reciprocal transfer also occurs, and that marrow stromal exosomes efficiently protect leukemia cells from targeted kinase inhibitors. Along with recent reports that entire mitochondria are transferred between stromal cells and leukemia cells during therapy[414, 415], our data adds to an increasingly complex and intimate relationship between marrow stromal cells and leukemia cells. Indeed, it is almost hard to imagine the leukemia cell in the niche as a separate entity given the direct exchange of organelles, ECVS, cell-cell signaling, and secreted cytokine signaling between stromal and leukemia cells. A better understanding of this relationship is important to develop better ways to eradicate leukemia cells and cure more patients.

Isolated reports have previously suggested that FGF2 is contained in ECVs[415, 416], but FGF2 has also been reported to self-assemble into a pore-like structure on the cell membrane and mediate its own translocation with the help of extracellular heparan sulfate[399, 417]. Compared to other soluble secreted cytokines, FGF2 was uniquely enriched in ECVs and exosomes (**Figure 2**), suggesting that from marrow stromal cells secretion in ECVs is the primary mechanism of FGF2 paracrine signaling. Since FGFR1 is also found on exosomes (**Figure 3D**), the FGF2-FGFR1 interaction on exosomes may play a direct role in loading FGF2 in exosomes and/or regulate secretion. FGFR inhibitors also increase the amount of FGFR1 protein in stromal cells

as measured by immunoblot, consistent with a role in receptor cycling and/or reduced secretion in exosomes.

Similar to our observations, epidermal growth factor receptor has been shown to be secreted on ECVs, and secretion is increased after ligand stimulation[418, 419]. Likewise, overexpression of oncogenic HER2 in breast cancer cell lines resulted in qualitative differences in microvesicle content[420], suggesting a role for activated receptor tyrosine kinases in exosome production and secretion. Receptor-mediated endocytosis is the first step of exosome biogenesis[421], suggesting that inhibitors of receptor tyrosine kinases may act at this step. How FGFR1 is positioned in the exosome membrane (inside or out), how FGF2 binds FGFR1 in exosomes, and how exosomal FGF2 activates FGFR1 in leukemia cells, are areas of active investigation.

FGF2 has been previously implicated in hematologic malignancy progression and development of resistance[422, 423]. Elevated levels of FGF2 have previously been measured in the serum of CML and AML patients[424, 425], as well as in the bone marrow of AML patients, where it was reported to function as an autocrine promotor of proliferation[426]. We found that FGF2 expression was increased in CML and AML stroma during the development of resistance to kinase inhibitors, indicating that FGF2 expression is a regulated autocrine growth factor for stroma[106]. This is consistent with the role of FGF2-FGFR1 autocrine expansion of stroma in stress-induced hematopoiesis[397, 398] and suggests that leukemia cells are able to hijack the FGF2 stress response for survival. The regulation of FGF2-FGFR1 signaling is also supported by the positive correlation in expression of both FGF2 and FGFR1 in a subset of primary AML marrow samples (**Figure 4G**), indicating that this pathway can be selectively activated. FGFR inhibitors not only inhibit autocrine growth of stroma, but reduce exosome secretion and significantly alter the protective ability of stromal cells (**Figures 4A and 7**). Since exosomes contain a complex mixture of proteins, cytokines, lipids and microRNAs (all of which potentially contribute to leukemia cell protection), inhibiting secretion of exosomes is a promising approach to blunting this complex mechanism of resistance.

In summary, FGF2 is a regulated autocrine growth factor for marrow stroma that is important in reprogramming the marrow stroma during development of resistance to TKIs. FGF2-FGFR1 activation in marrow stroma leads to increased secretion of exosomes, which are protective of leukemia cells in both *in vitro* and *in vivo* models. Given the inevitable development of clinical resistance to TKIs (FLT3 ITD AML in particular), addition of FGFR inhibitors to directly modulate the leukemia niche is a promising approach to improve the durability of response.

Materials & Methods

Key Resources Table

Reagent type (species) or resource	Designation	Source or reference	Identifiers	Additional information
gene (homo sapiens)	FGF2	NA		
gene (mus musculus)	*Fgf2*	NA		
gene (homo sapiens)	FGFR1	NA		
gene (mus musculus)	*Fgfr1*	NA		
strain, strain background (mus musculus)	*Fgf2*^{tm1Doe}/J *Fgf2* +/+ and -/- mice	Jackson Laboratory	RRID:MGI:2679603	
genetic reagent (homo sapiens)	FGF2	Thermo Scientific		shRNA in TRIPZ lentiviral vector
genetic reagent (homo sapiens)	FGFR1	Thermo Scientific		shRNA in TRIPZ lentiviral vector
genetic reagent (homo sapiens)		AddGene		GeCKO lentiCRISPRv2 hSpCas9 and guide RNA
genetic reagent (homo sapiens)	FGF2-1	GenScript		CRISPR/Cas 9 guide RNA design
genetic reagent (homo sapiens)	FGF2-2	GenScript		CRISPR/Cas 9 guide RNA design
genetic reagent (homo sapiens)	FGFR1-1	GenScript		CRISPR/Cas 9 guide RNA design

genetic reagent (homo sapiens)	FGFR1-2	GenScript		CRISPR/Cas 9 guide RNA design
genetic reagent (mus musculus)	pMIG with BCR-ABL and GFP			murine retrovirus
cell line (homo sapiens)	MOLM14	Dr. Yoshinobu Matsuo	RRID:CVCL_7916	
cell line (homo sapiens)	K562	American Type Culture Collection	RRID:CVCL_0004	
cell line (homo sapiens)	HS-5	Dr. Beverly Torok-Storb	RRID:CVCL_3720	
cell line (homo sapiens)	HS-27	Dr. Beverly Torok-Storb	RRID:CVCL_0335	
antibody	Mouse monoclonal anti-FGFR1	Cell Signaling	9740	Dilution 1:1000
antibody	Rabbit polyclonal anti-FGF2	Santa Cruz	Sc-79	Dilution 1:500
antibody	Rabbit monoclonal anti-CD63	ABCAM	ab134045	Dilution 1:1000
antibody	Rabbit polyclona anti-CD9	Santa Cruz	Sc-9148	Dilution 1:200
antibody	Mouse monoclonal anti-tsg-101	Santa Cruz	Sc-7964	Dilution 1:200
antibody	Mouse monoclonal anti-actin	Millipore	MAB1501	Dilution 1:5000
peptide, recombinant protein	FGF2 (human)	Peprotech		
commercial assay or kit	Thermo Scientific lentiviral transfection kit			
chemical compound, drug	quizartinib (AC220)	LC labs		
chemical compound, drug	imatinib	LC labs		
chemical compound, drug	nilotinib	SelleckChem		
chemical compound, drug	PD173074	SelleckChem		
chemical compound, drug	BGJ-398	SelleckChem		
chemical compound, drug	doxycycline	Fisher		
software, algorithm	CellProfiler	Cell area		

Cell lines

The human cell line MOLM14 was generously provided by Dr. Yoshinobu Matsuo (Fujisaki Cell Center, Hayashibara Biochemical Labs, Okayama, Japan). The human cell line K562 was obtained from the American Type Culture Collection (Manassas, VA, USA). The human stromal cell lines HS-5 and HS-27a were kindly provided by Dr. Beverly Torok-Storb (Fred Hutchinson Cancer Research Center, Seattle, WA). Cells were maintained in RPMI1640 media supplemented with 10% fetal bovine serum (FBS), 100 U/mL penicillin/100 µg/mL streptomycin, 2 mM L-glutamine, and 0.25 µg/mL fungizone (referred to as **R10**) at 37°C in 5% CO_2. Exosome-depleted FBS was pre-cleared by ultracentrifugation at 100,000g for 2hrs at 4°C. Cell lines were validated by genetic and functional analysis based upon previous reported characteristics. Cell lines were tested monthly for mycoplasma infection and discarded if found to be infected.

ECV isolation

HS-5 cells grown to 90-100% confluence in 15 cm dishes were washed in 8 ml PBS, and incubated in 12 ml exosome-depleted R10 overnight. The media was collected, cleared of debris (2X 2000g spin, 10 min), and ultracentrifuged at 100,000g for 2 hr at 4°C. The resulting supernatant (S100) was poured off, and 100 µL PBS was added to the ECV pellet (P100). This was shaken for 4 hr at 4°C at 2000 rpm. P100 was used fresh or stored at -80°C with 10% DMSO.

Sucrose density step-gradient

Layers of sucrose (60%, 45%, 30%, 15%, 7.5%, and 0%) were carefully pipetted into ultracentrifuge tubes. ECVs were added on top, and the tube ultracentrifuged at 100,000g for 90 min at 4°C. The sucrose interfaces (45-60, 30-45, 15-30, 7.5-15, 0-7.5) were collected with a micropipette, washed in PBS, and pelleted at 100,000g for 2 hr at 4°C.

ECV quantitation

ECVs were quantified by Nanosight LM10 or by Virocyt Virus Counter 3100, following manufacturers' protocols.

Inhibitors and cytokines

Quizartinib (AC220) was purchased from LC labs (Woburn, MA, USA). Nilotinib, PD173074 and BGJ-398 were purchased from SelleckChem (Houston, TX, USA). Imatinib was purchased from LC labs (Woburn, MA, USA). Recombinant FGF2 was purchased from Peprotech (Rocky Hill, NJ, USA).

Viability assays

Viability was assessed with MTS reagent, CellTiter 96 AQueous One Solution Proliferation Assay from Promega Corporation (Madison, WI, USA) or by Guava ViaCount flow cytometer assay (Millipore, Burlington, MA, USA).

Immunoblot analysis

Treated cells were washed in PBS before adding lysis buffer (Cell Signaling, Danvers, MA, USA) supplemented with Complete protease inhibitor (Roche, Indianapolis, IN, USA) and phosphatase inhibitor cocktail-2 (Sigma-Aldrich, St. Louis, MO, USA). Proteins were fractionated on 4-15% Tris-glycine polyacrylamide gels (Criterion gels, Bio-Rad), transferred to PVDF membranes, and probed with antibodies: FGFR1, fibronectin (Cell Signaling, Danvers, MA, USA); CD9, FGF2, calreticulin, tsg101 (Santa Cruz Biotechnology, Dallas, TX, USA), CD63 (Abcam, Boston, MA, USA), and actin (MAB1501, Millipore, Burlington, MA, USA).

Stromal cell cytokine ELISA

Stromal CM, S100 and ECVs were lysed with 0.1% NP-40 for 30 min, centrifuged 3,000 rpm for 10 mins, and 50 µL supernatant was incubated with the magnetic beads overnight and assayed

as per manufacturer's instructions (Luminex Multiplex magnetic beads 30-plex Assay, Life Technologies).

Primary bone marrow stromal cultures

Bone marrow aspirates were obtained from AML patients after informed consent under the OHSU Institutional Research Board protocol IRB0004422, and were processed as previously described[23]. After Ficoll, the red cell pellets were incubated with ACK for 30 minutes on ice to lyse red cells, and plated on 15 cm dishes in MEM-α supplemented with 20% fetal bovine serum (FBS), 100 U/mL penicillin/100 µg/mL streptomycin, 2 mM L-glutamine, and 0.25 µg/mL fungizone at 37°C in 5% CO_2. After 48h, non-adherent cells were removed and new media was added. This step was repeated after an additional 24h. Cells were then incubated for 1-3 weeks with media changes every 7 days, until patchy proliferation became apparent. Cells were trypsinized and replated to facilitate homogenous growth. Cells were expanded over a maximum of 3 passages before use in experiments. Murine primary stroma was isolated from harvested femur marrow without ACK treatment and then cultured as above. Primary stromal samples were analyzed after >2 weeks growth.

Transmission electron microscopy

Stromal cell exosomes were isolated by sucrose step-gradient then washed in 0.22 µm filtered PBS. 10 µL was deposited onto glow discharged carbon formvar 400 mesh copper grids (Ted Pella 01822-F) for 3 min, rinsed 15 secs in water, wicked on Whatman filter paper 1, stained for 45 secs in filtered 1.33% (w/v) uranyl acetate, wicked and air dried. Samples were imaged at 120kV on a FEI Tecnai Spirit TEM system. Images were acquired as 2048x2048 pixel, 16-bit gray scale files using the FEI's TEM Imaging & Analysis (TIA) interface on an Eagle 2K CCD multiscan camera.

Fluorescent confocal microscopy

MOLM14 and K562 cells were stained with DiO (Thermo Fisher) according to manufacturer's protocol. HS-5 ECVs were stained with DiI (Thermo Fisher), washed with PBS, and collected by ultracentrifugation. For experiments using mouse bone marrow, cells were isolated from femurs and tibias, RBCs were lysed using ACK buffer (0.8% NH_4Cl and 0.1 mM EDTA in $KHCO_3$ buffer; pH 7.2-7.6), and lineage-negative cells were isolated by MACS cell separation with the human lineage cell depletion kit (Milteny Biotec). Cells were incubated with a cytokine mix (IL-3, IL-6, SCF) in addition to DiO. DiO-stained cells were combined with DiI-stained ECVs and incubated for 24 hours at 37°C. Cells were washed, placed on poly-D-lysine coated chamber slides, and DAPI-stained. Z-stack imaging was performed on an Olympus IX71 inverted microscope. Images were processed using the Fiji software package[427].

Proteinase K digestion

ECVs, or exosomes isolated by sucrose step-gradient, were resuspended in proteinase K buffer (Tris-HCl pH8, 10 mM CaCl2) and then incubated with 200 µg/ml proteinase K at room temp for 30 min. 5 µL 0.1 M PMSF and SDS loading buffer was added and samples were incubated at 98°C for 5 min to stop reaction prior to immunoblots.

Cell morphology analysis

HS-5 and HS-27 cells were grown to 90% confluence in 4-well chamber microscope slides in R10 +/- 250 nM PD173074. Cells were stained with lipophilic tracer DiI, washed, and stained with DAPI. Cells were imaged with Zeiss Axio Observer fluorescent microscope at 10X using AxioVision software. Images were uploaded into CellProfiler software and analyzed for cell size. Cell diameter was determined as $diameter\ [\mu m] = \sqrt{pixels \times 0.394\ \mu m^2/pixel}$.

shRNA

TRIPZ inducible lentiviral FGF2 and FGFR1 shRNA were purchased from Thermo Fisher Scientific Dharmacon RNAi Technologies (Waltham, MA, USA), along with Dharmacon's trans-lentiviral shRNA packaging kit with calcium phosphate transfection reagent and HEK293T cells. HS-5 and HS-27 cells were transfected with GIPZ control or FGFR1 TRIPZ, per manufacturer's protocol. TurboRFP/shRNA expression was induced with 1 µg/mL doxycycline (Fisher) for 48 hours, cells were washed in PBS, and then media replaced with exosome-depleted R10 + 1 µg/mL doxycycline. Cells and CM were collected after 72 hours for analysis.

CRISPR/Cas9 targeted genome editing

The vector GeCKO lentiCRISPRv2 was obtained from Addgene. This plasmid contains two expression cassettes, hSpCas9 and the chimeric guide RNA. Guide RNA sequences were obtained from GenScript[428], and oligos with 5' overhang for cloning into lentiCRISPRv2 were manufactured by Fisher Scientific. The vector was digested with BsmBI and dephosphorylated, the plasmid was gel-purified, and oligonucleotides were ligated after annealing and phosphorylation. Plasmid was amplified in Stbl3 bacteria, purified, and lentivirus was generated in HEK293T cells. Transduced HS-5 cells were selected in puromycin for 5 days, and cultured an additional 5 days before assessing knockout.

Murine BCR-ABL leukemia experiments

Animal studies were approved by the OHSU Institutional Animal Care and Use Committee. *Fgf2*^{tm1Doe}/J were purchased from Jackson Laboratory to breed homozygous +/+ and -/- littermates. Bone marrow from 5-FU treated *Fgf2* +/+ donors was spinoculated with pMIG containing BCR-ABL and IRES-GFP reporter as previously described[390, 429] and 2x10^6 cells were retro-orbitally injected into lethally irradiated (2x 450 cGy administered 4 hours apart) *Fgf2* +/+ and -/- recipients. 75 mg/kg/day nilotinib was administered by oral gavage and mice were

monitored weekly with cell blood counts and FACS analysis of GFP in peripheral blood. Diseased mice were subjected to detailed histopathologic analysis. For colony assays, ECVs were isolated (as above) from equal numbers of *Fgf2* +/+ and -/- primary stromal cells cultured on 10 cm plates for 3 days, with and without 500 nM PD173074 (3-day pre-treatment and 3 days during ECV collection). Bone marrow from FGF2 +/+ mice was spinoculated with pMIG containing BCR-ABL and IRES-GFP reporter as above, incubated with ECVs overnight and washed 3x the next day. 3% of cells were GFP positive by FACS, and $4x10^3$ cells were then plated in 1 ml of MethoCult® M3234 Methylcellulose Medium for Mouse Cells without cytokines (Stemcell Technologies) in triplicate. Mouse bone marrow colonies larger than 50 cells were counted after 8 days.

Statistical methods

Graphical and statistical data were generated with Microsoft Excel or GraphPad Prism (GraphPad Software, La Jolla, CA, USA). *P* value <0.05 was considered significant.

Acknowledgements

We would like to thank Cristina Tognon and Kara Johnson for administrative assistance, and Angie Rofelty for assistance with primary bone marrow stromal cultures. Electron microscopy was performed at the Multiscale Microscopy Core (MMC) with technical support from the Oregon Health & Science University (OHSU)-FEI Living Lab and the OHSU Center for Spatial Systems Biomedicine (OCSSB).

Author Contributions

Nathalie Javidi-Sharifi, Conceptualization, Data curation, Formal analysis, Funding acquisition, Investigation, Visualization, Methodology, Writing—original draft, Writing—review and editing; Jacqueline Martinez, Data curation, Formal analysis, Validation, Investigation, Visualization, Methodology, Writing—original draft; Isabel English, Data curation, Formal analysis, Investigation, Methodology, Writing—original draft; Sunil K Joshi, Data curation, Formal analysis, Investigation, Visualization, Writing—review and editing; Renata Scopim-Ribeiro, Data curation, Investigation, Visualization; Shelton K Viola, Data curation, Investigation; David K Edwards V, Anupriya Agarwal, Claudia Lopez, Danielle Jorgens, Resources, Investigation; Jeffrey W Tyner, Resources, Writing—review and editing; Brian J Druker, Resources, Supervision, Writing—review and editing; Elie Traer, Conceptualization, Data curation, Formal analysis, Supervision, Funding acquisition, Validation, Investigation, Visualization, Methodology, Writing—original draft, Project administration, Writing—review and editing

8 *The AML microenvironment catalyzes a step-wise evolution to gilteritinib resistance*

Sunil K. Joshi, Tamilla Nechiporuk, Daniel Bottomly, Paul D. Piehowski, Julie A. Reisz, Janét Pittsenbarger, Andy Kaempf, Sara J. C. Gosline, Yi-Ting Wang, Joshua R. Hansen, Marina A. Gritsenko, Chelsea Hutchinson, Karl K. Weitz, Jamie Moon, Thomas L. Fillmore, Chia-Feng Tsai, Athena A. Schepmoes, Tujin Shi, Osama A. Arshad, Jason E. McDermott, Ozgun Babur, Kevin Watanabe-Smith, Emek Demir, Angelo D'Alessandro, Tao Liu, Cristina E. Tognon, Jeffrey W. Tyner, Shannon K. McWeeney, Karin D. Rodland, Brian J. Druker, Elie Traer

This manuscript is currently in the revision phase at *Cancer Cell.*

Abstract

Our study details the stepwise evolution of gilteritinib resistance in FLT3-mutated acute myeloid leukemia (AML). Early resistance is mediated by the bone marrow microenvironment, which protects residual leukemia cells. Removing these supportive extrinsic ligands drives evolution of late, intrinsic resistance. Whole exome sequencing, CRISPR/Cas, metabolomics, proteomics, and pharmacologic approaches were used to mechanistically define both early and late resistance. Early resistant cells undergo metabolic reprogramming, grow more slowly, and are dependent upon Aurora kinase B (AURKB). Late resistant cells are characterized by expansion of pre-existing NRAS mutant subclones and continued metabolic reprogramming. Our model closely mirrors the timing and mutations of AML patients treated with gilteritinib. Pharmacological inhibition of AURKB resensitized both early resistant cell cultures and primary leukemia cells from gilteritinib-treated AML patients. These findings support a combinatorial strategy to target early resistant AML cells with AURKB inhibitors and gilteritinib before the expansion of pre-existing resistance mutations occurs.

Graphical Abstract

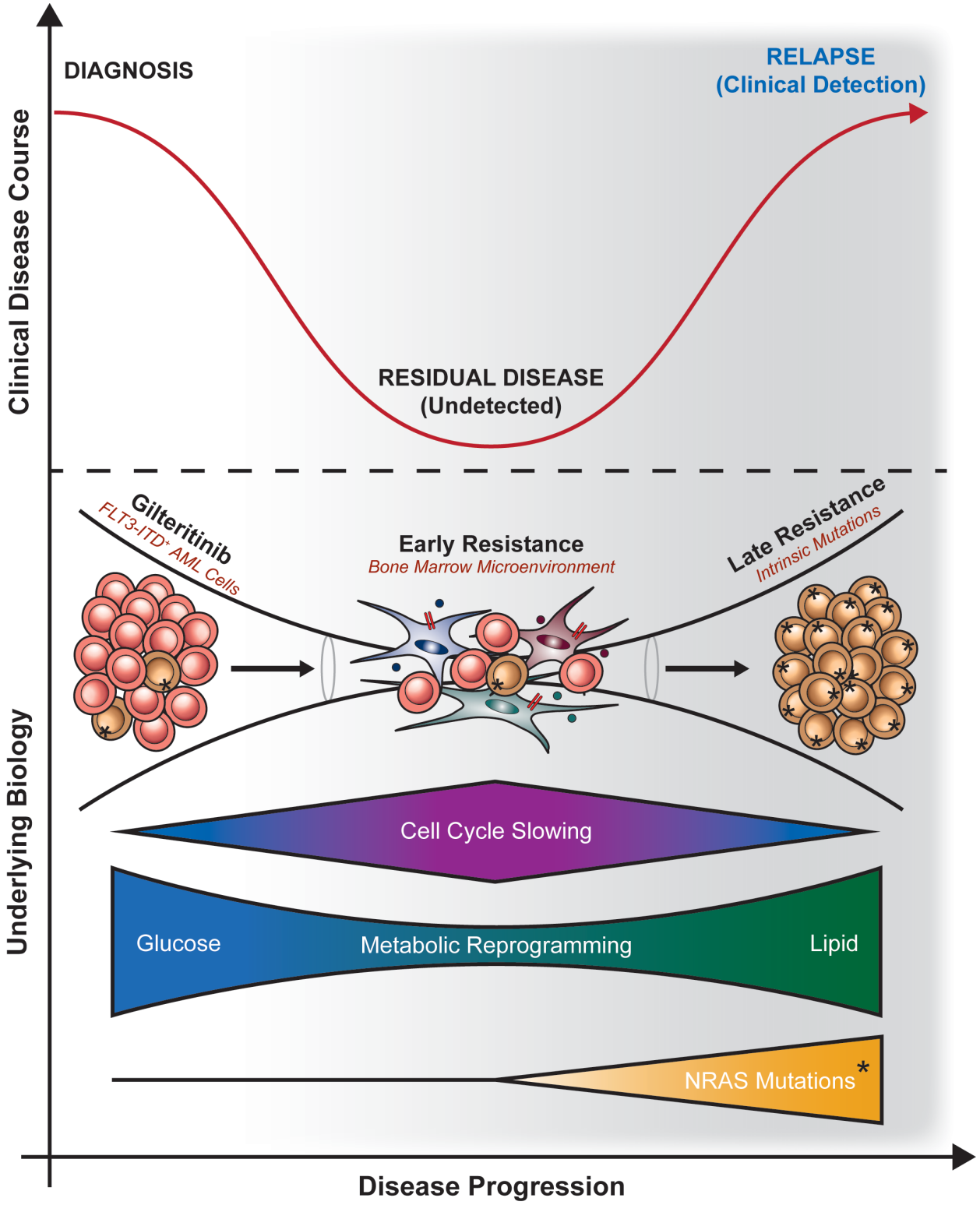

Introduction

Acute myeloid leukemia (AML) is an aggressive hematologic malignancy that disproportionately affects older adults. It is characterized by an aberrant proliferation of immature myeloblasts that infiltrate the bone marrow and impair normal hematopoiesis. Among recurrent genetic alterations, driver mutations in the fms related receptor tyrosine kinase 3 (FLT3) are among the most common and occur in > 30% of all patients with AML[12, 198]. FLT3 mutations predominantly consist of internal tandem duplication (ITD) events within the receptor juxtamembrane domain and, to a lesser extent, point mutations in the tyrosine kinase domain (TKD), resulting in constitutive FLT3 activation, pro-survival downstream signaling, and expansion of leukemic cells[198]. FLT3-ITD mutations particularly portend a poor prognosis with increased risk of relapse, providing impetus for the development of several generations of FLT3 inhibitors (FLT3i).

While FLT3i rapidly clear peripheral leukemic cells in circulation, residual AML cells persist in the bone marrow microenvironment[104, 108, 195] where their survival and expansion lead to disease relapse. Importantly, residual cells are dependent upon growth factors and cytokines within the AML microenvironment for survival, which confer early resistance, also known as disease persistance[96, 106, 117, 179, 185, 190, 430-434]. However, due to the small number of residual cells available for study, very little is understood about their biology and the mechanisms that keep these cells alive. For that reason, drug resistance is most often studied after relapse, which we call late resistance, and is usually defined by the outgrowth of resistance mutations[40, 137, 168]. Pre-clinical studies have shown that these mutations can often be predicted via well-established *in vitro* mutagenesis and transformation assays[40, 165, 167, 181]. However, a fundamental understanding of the adaptations that foster early resistance and how these changes contribute to late resistance, and/or differ from late resistance, have yet to be thoroughly investigated.

Gilteritinib is a potent FLT3i that was recently FDA-approved for relapsed/refractory AML[383, 435]. In this study, we comprehensively analyze the temporal evolution of early to late gilteritinib resistance by integrating whole exome sequencing, CRISPR/Cas9 screening, metabolomics, proteomics, phosphoproteomics, and small-molecule inhibitor screening. To recapitulate microenvironmental-driven resistance, AML cells were cultured with exogenous protective proteins that are normally secreted by bone marrow stromal cells, which promoted ligand-dependent early resistance after a few months of culture. Removal of these ligands transiently restored sensitivity to gilteritinib but eventually led to the expansion of activating mutations in ligand-independent late resistance. Multiple orthogonal approaches showed that late resistance to gilteritinib is primarily driven by clonal selection of NRAS activating mutations and hyperactivation of downstream MAPK signaling, consistent with frequent NRAS mutations found in gilteritinib-treated AML patients at relapse[164]. In contrast, early resistance was not dependent upon NRAS signaling but exhibited metabolic reprogramming, slower growth, and reliance upon Aurora kinase B signaling (AURKB). These experimental observations were corroborated in gilteritinib-treated AML patient samples, which displayed slower cell growth, alterations in metabolism, and profound sensitivity to the combination of gilteritinib and AURKB inhibition. Together, our work defines mechanisms of both early and late gilteritinib resistance and brings forward a novel approach to understand the unique biology of early resistant AML cells, and develop novel combination strategies to block expansion of late resistant cells.

Results

Microenvironmental factors promote development of early gilteritinib resistance

To model microenvironmental protection in gilteritinib resistance, we used exogenous fibroblast growth factor 2 (FGF2) and FLT3 ligand (FL). These proteins were shown to be secreted by marrow stromal cells and can protect FLT3 AML cell lines and primary AML cells from other FLT3i[106, 179, 185]. We treated MOLM14 cells, a human AML FLT3-ITD$^+$ cell line, with increasing concentrations of gilteritinib (0 to 100 nM) +/- 10 ng/mL of FGF2 or FL for 72 hours (**Figure 1A**). Both FGF2 and FL provided protection against gilteritinib in this short-term assay. To mimic prolonged gilteritinib exposure within the protective bone marrow microenvironment that occurs in patients, we cultured MOLM14 with 100 nM of gilteritinib in media alone (N = 4), or media supplemented with 10 ng/mL of FGF2 (N = 4) or FL (N = 4) for approximately 4 months (**Figure 1B**). Media, gilteritinib, and exogenous ligands were replaced every 2-3 days. MOLM14 parental cells treated with gilteritinib without protective ligands never resumed growth (**Figure 1B**, yellow line). However, all cultures supplemented with FGF2 or FL eventually resumed growth, highlighting the importance of extrinsic survival factors in facilitating early resistance to gilteritinib (**Figure 1B,** solid teal and maroon lines). After approximately 4 months in extended culture, we put selective pressure on the ligand-dependent, early resistant cultures by removing FGF2 and FL. While this temporarily restored sensitivity to gilteritinib, the cultures eventually resumed exponential growth after approximately two months, defining evolvement to ligand-independent, late resistance (**Figure 1B,** dotted lines). Immunoblot analysis of FLT3, MAPK, and PI3K/AKT pathways in ligand-dependent early resistant cultures demonstrated that FL partially restored FLT3 activity, and FGF2 reactivated MAPK and AKT through activation of FGFR (**Figure 1C-D**). In contrast, in the late resistant ligand-independent cultures, FLT3 itself remained inactive, but there was clear reactivation of downstream MAPK and PI3K/AKT signaling (**Figure 1C-D**). We also created a parallel gilteritinib resistance model with the human AML FLT3-ITD$^+$ cell line,

MV4;11 and found with this second independent cell culture model a similar biphasic pattern of resistance (**Supplemental Figure 1A**). **Supplemental Table 1** provides a list of all gilteritinib resistant cultures generated and used in downstream analyses. To understand the mechanisms of early and late gilteritinib resistance, we utilized five distinct but complementary approaches: whole exome sequencing (WES), genome-wide CRISPR/Cas screening, metabolomics, proteomics and phosphoproteomics, and small-molecule inhibitor screening (**Figure 1E**).

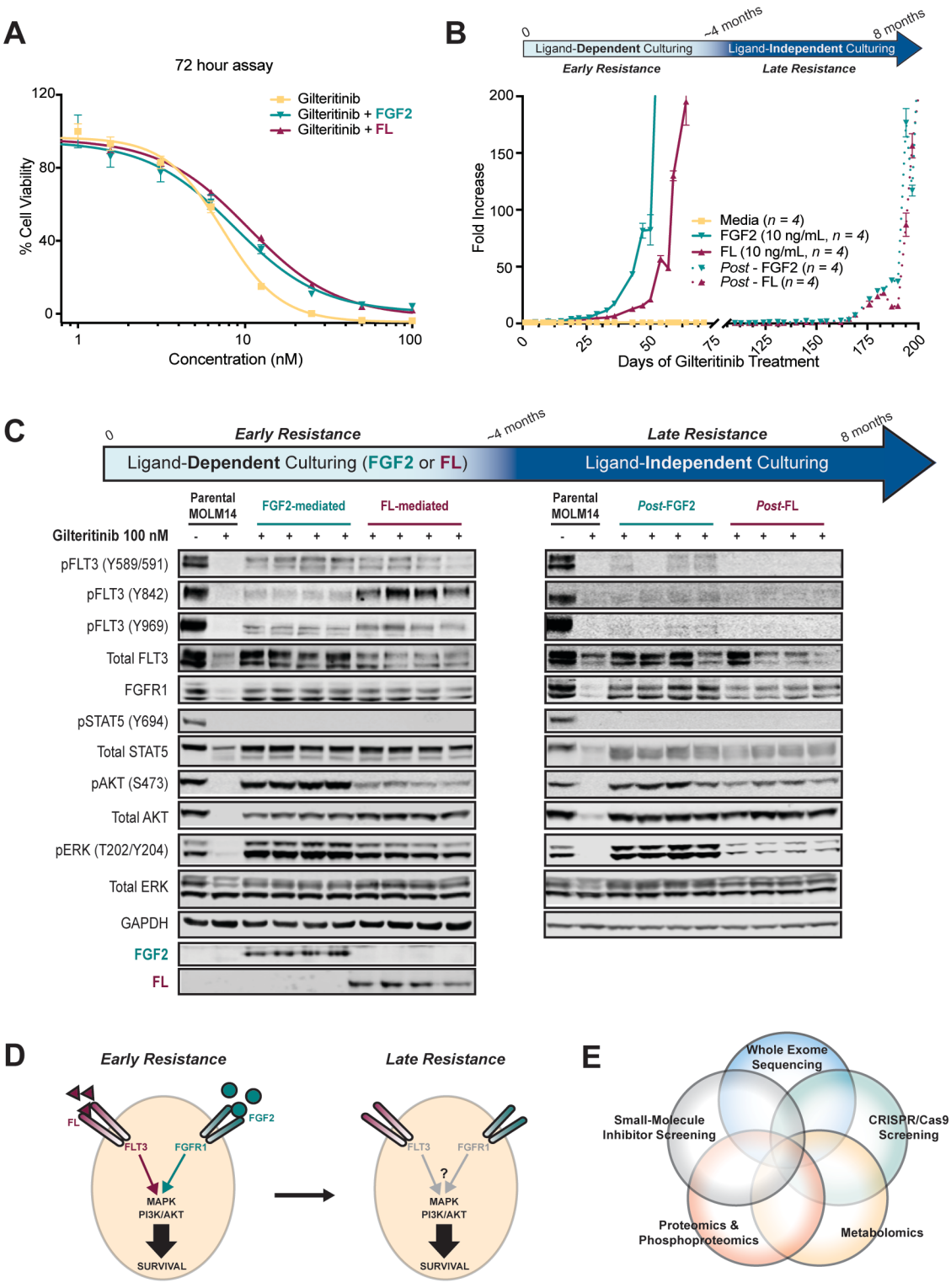

Figure 1: Emergence of early and late gilteritinib resistant cultures. A. MOLM14 parental cells were treated with a gradient of gilteritinib ± recombinant FGF2 or FL (10 ng/mL). Viability was measured after 72 hours and normalized to untreated cells. The mean of five replicates ±

standard error are shown. **B.** MOLM14 cells were cultured continuously with 100 nM gilteritinib ± FGF2 or FL (10 ng/mL; N = 4 for each). Presence of protective ligands facilitated early resistance (ligand-dependent phase). Removal of ligand enabled late resistance (ligand-independent phase). Fresh media, gilteritinib, and recombinant ligands were replaced every two to three days. Mean fold increase in viable cells is plotted ± standard error. **C.** Immunoblot blot analyses of MOLM14 parental cells treated for 48 hours with 100 nM gilteritinib or DMSO (first two lanes of each panel) compared with early (left panel, lanes 3 – 10) and late (right panel, lanes 3 – 10) extended gilteritinib resistant MOLM14 cultures. **D.** Graphic summary of immunoblot results from early and late gilteritinib resistant cultures. **E.** Schematic of approach to study the evolution of gilteritinib resistance.

NRAS mutations are dominant during late resistance, but not required in early resistance

We performed WES analysis of late gilteritinib resistant MOLM14 and MV4;11 cultures and discovered activating NRAS point mutations in 13 of the 15 cultures, although the mutations were not always identical (**Figure 2A**). These results are consistent with clinical data reporting that mutant NRAS is commonly found at relapse in FLT3-mutated AML patients treated with gilteritinib[164] (**Supplemental Figure 1B**). One late resistant culture had a $FLT3^{F691L}$ gatekeeper mutation, which has also been shown to promote resistance to gilteritinib[164], as well as other FLT3i[40, 137, 164]. In three other cultures, we detected a novel $FLT3^{N701K}$ mutation, which we found also drives resistance to gilteritinib in a manner similar to the F691L gatekeeper mutation (manuscript submitted). All mutations detected by WES analyses in late gilteritinib resistant MOLM14 and MV4;11 cultures were confirmed by Sanger sequencing (**Figure 2B, Supplemental Figure 1C, 2, 3**) and FLT3-ITD^{+} status was maintained, as confirmed by Pindel software[436]. We then assessed the time at which these mutations arose during long-term culture. Sanger sequencing revealed that these mutations were undetectable in the presence of ligand in MOLM14 early resistant cultures for up to 4 months (**Figure 2B, Supplemental Figure 2**), however they were detectable in early resistant MV4;11 cultures after 5 months (**Supplemental Figure 1C & 3**).

To test whether low-level NRAS mutations were present prior to development of resistance or arose *de novo* in the MOLM14 gilteritinib resistance model, we optimized a droplet digital PCR (ddPCR) assay to quantify the variant allele frequency (VAF) of NRAS G12S and G12D in parental MOLM14 cells, early resistant cultures, and late resistant cultures. The higher sensitivity of ddPCR enabled us to detect NRAS G12S/D at very low levels in MOLM14 parental cells (< 0.1 %), indicating that these mutations did not arise *de novo*. The VAF increased slightly in early resistant cultures (≤ 0.15%), and then expanded rapidly once protective ligands were removed in late resistance (**Figure 2C**). These data suggest that NRAS mutations are not required in the presence of ligand, but become dominant upon ligand removal. In view of this hypothesis, we sought to test whether NRAS mutations were sufficient to drive gilteritinib resistance in the absence of ligand. We created MOLM14 cell lines that stably express $NRAS^{WT}$ and NRAS G12S/D mutations and assessed their growth in the presence and absence of gilteritinib. In the absence of FLT3 inhibition by gilteritinib, we observed no differences in cell proliferation in NRAS mutant cell lines relative to MOLM14 parental and $NRAS^{WT}$ cells (**Figure 2D**). Treatment with 100 nM of gilteritinib significantly inhibited growth of control and mutant cell lines after 1 week (**Figure 2E-F**), indicating that NRAS mutations alone are insufficient to immediately confer resistance. Eventually MOLM14 cells engineered with $NRAS^{G12S}$ or $NRAS^{G12D}$ alleles developed resistance to gilteritinib without the presence of ligand (**Figure 2E-F**, dotted lines). However, culturing these cells with FGF2 or FL significantly accelerated the onset of resistance, highlighting the ability of the microenvironment to catalyze development of resistance even in the presence of NRAS mutations (**Figure 2E-F**, solid lines).

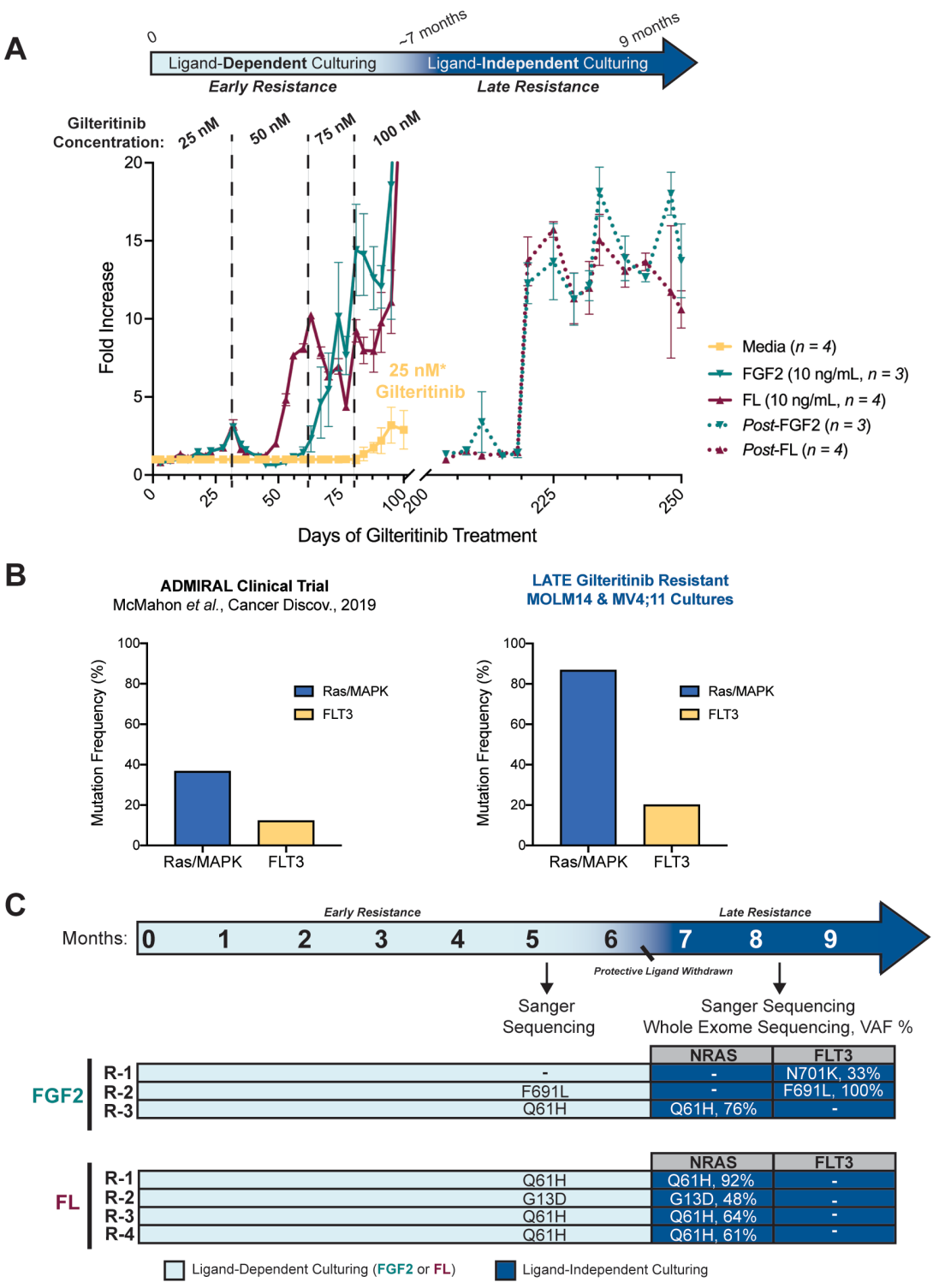

Supplemental Figure 1: Early and late gilteritinib resistance in MV4;11 cells parallels MOLM14 model. A. MV4;11 cells are very sensitive to gilteritinib, so early gilteritinib resistant MV4;11 cultures were derived using stepwise dose escalation (25 to 100 nM) of gilteritinib over a span of 75 days with continuous exposure to FGF2 or FL (10 ng/mL). Vertical dotted lines indicate

changes in gilteritinib concentration. MV4;11 cells cultured in the absence of protective ligands were continually maintained in 25 nM of gilteritinib due to lack of growth. Ligand removal initiated late gilteritinib resistant phase. For all cells, fresh media, gilteritinib, and recombinant ligands were replaced every two to three days. Cell viability was assessed with Guava ViaCount. Mean fold increase in cell number of biological replicates (N = 3 – 4) ± standard error are plotted. **B.** Consistency in NRAS and FLT3 mutations detected in AML patients on ADMIRAL trial and late resistant MOLM14 and MV4;11 cultures. **C.** Schematic of overlap between WES analyses and mutation confirmation by Sanger sequencing. The timepoints at which WES or Sanger sequencing were performed is indicated by arrows. If a mutation could not be detected, it is indicated with "-". Sanger sequencing confirms presence of NRAS mutations in early and late gilteritinib resistant MV4;11 cells. FLT3 gatekeeper mutation, F691L and N701K were also detected in late gilteritinib resistant MV4;11 cells. However, $FLT3^{N701K}$ was not detected in early resistant MV4;11 cells.

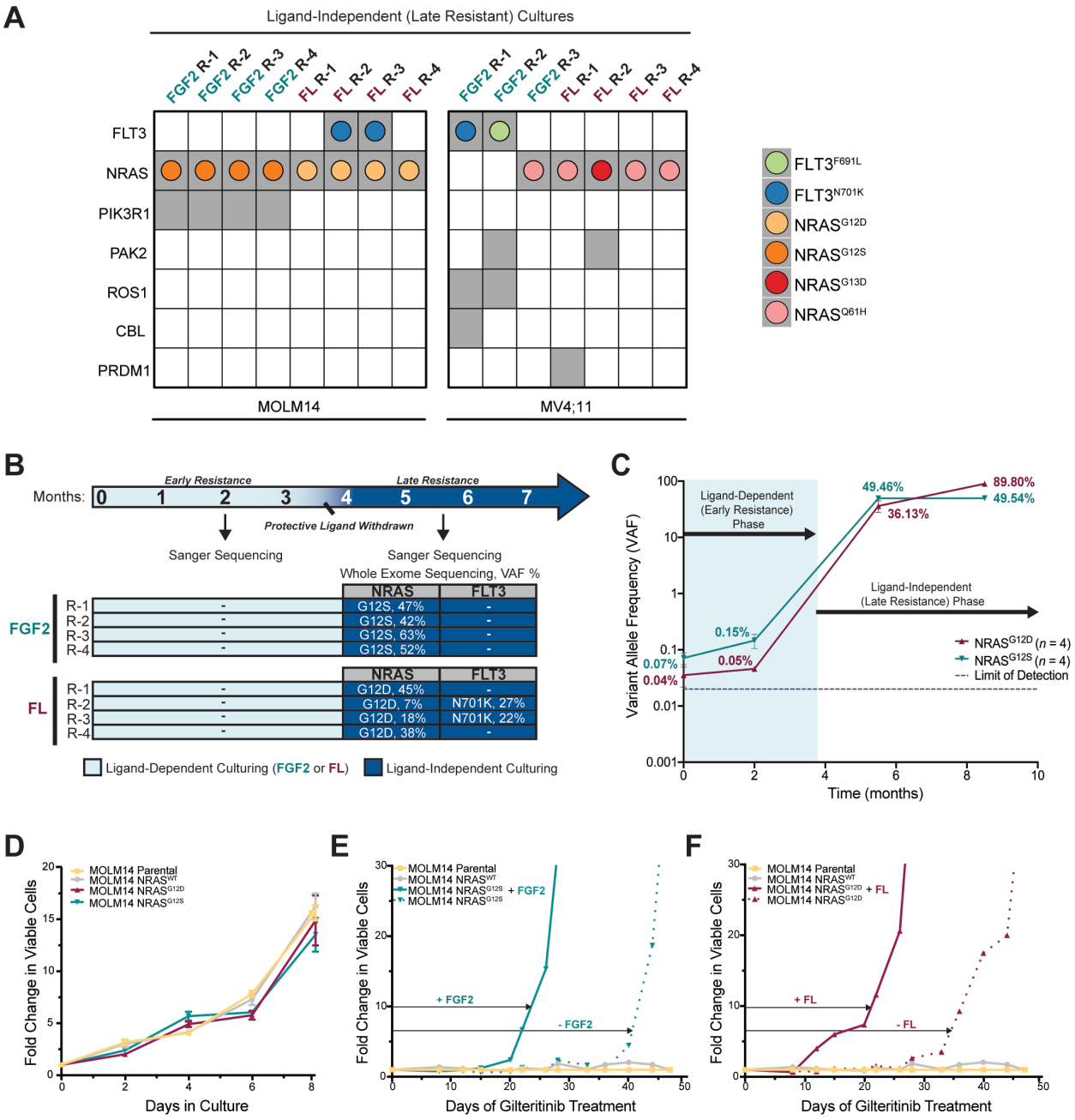

Figure 2: NRAS mutations are enriched in late but not early resistance. A. Mutations (gray squares) identified by WES in late gilteritinib resistant MOLM14 and MV4;11 replicate cultures. AML drivers or genes in common cancer pathways are shown. Colored dots within the gray squares represent specific FLT3 or NRAS mutations. **B.** Overlap between WES analyses and mutation confirmation by Sanger sequencing. Arrows indicate timepoints at which WES or Sanger sequencing were performed. Mutations not detected are indicated with "-". VAF = Variant Allele Frequency. **C.** ddPCR analyses for detection of NRAS G12S/D mutations in parental, ligand-dependent, and independent MOLM14 cultures over time. Mean of 4 biological replicates ± standard error are shown. **D.** NRAS G12S/D mutations provide no growth advantage relative to MOLM14 parental or NRAS^{WT} cells in the absence of gilteritinib. Fold change in number of viable

cells relative to day 0 is plotted. Mean of triplicates ± standard error are shown. **E-F.** NRAS mutant cell lines develop resistance to 100 nM gilteritinib treatment after one month in culture, whereas MOLM14 parental and $NRAS^{WT}$ do not. FGF2 or FL (10ng/mL), accelerate development of resistance (solid vs. dotted lines). WES sequencing analysis and VAF determination was performed by Daniel Bottomly. Janét Pittsenbarger assisted with ddPCR experiments.

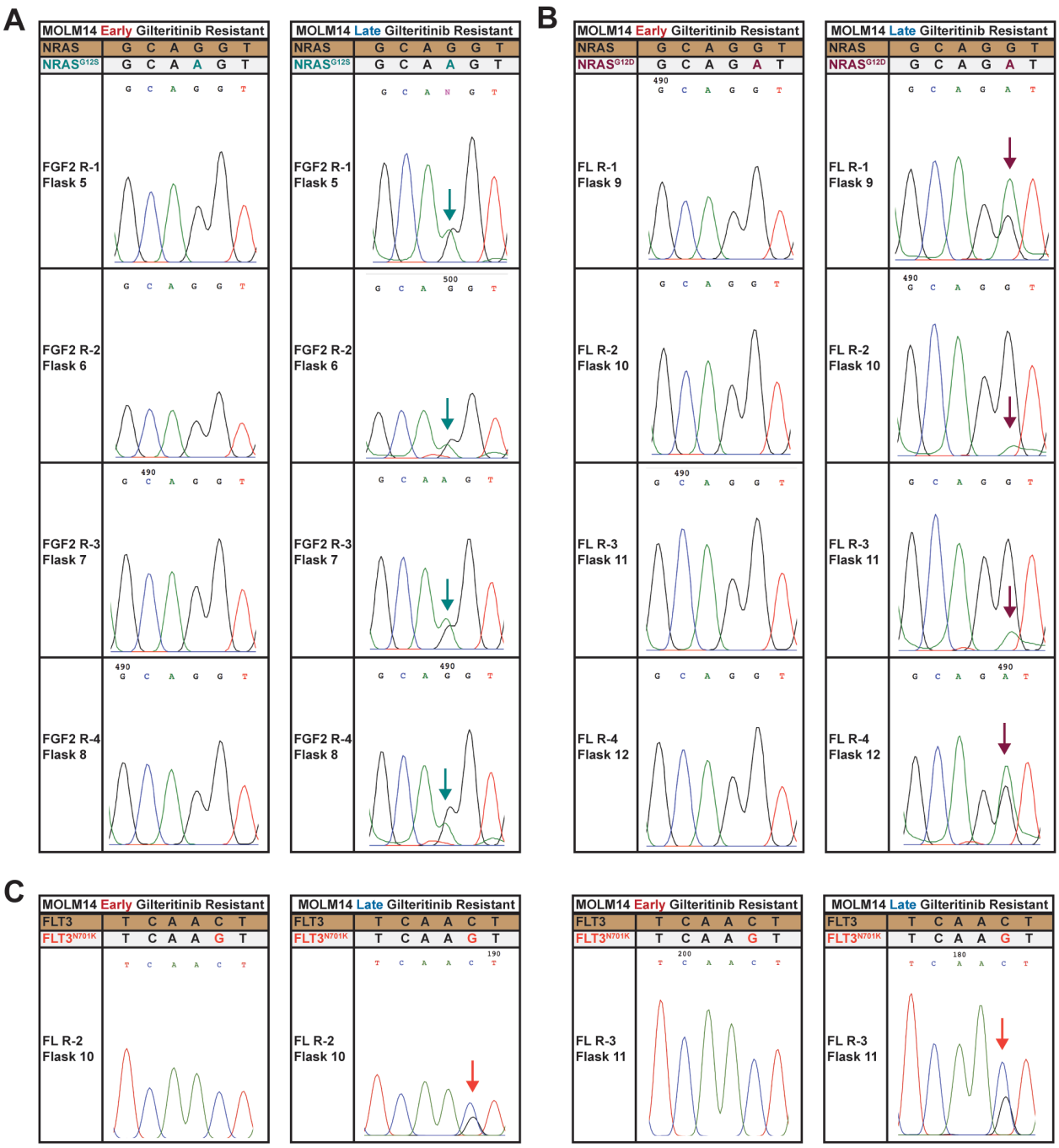

Supplemental Figure 2: Electropherograms from Sanger sequencing of NRAS (A, B) and FLT3 (C) point mutations detected in WES of late gilteritinib resistant MOLM14 cell lines. Sanger sequencing was also utilized to detect the presence of these mutations in early resistant cell lines. PCR amplification and sequencing primers are listed in Supplemental Table 2. Peaks correspond to the following nucleotides: A (green), T (red), C (blue), and G (black).

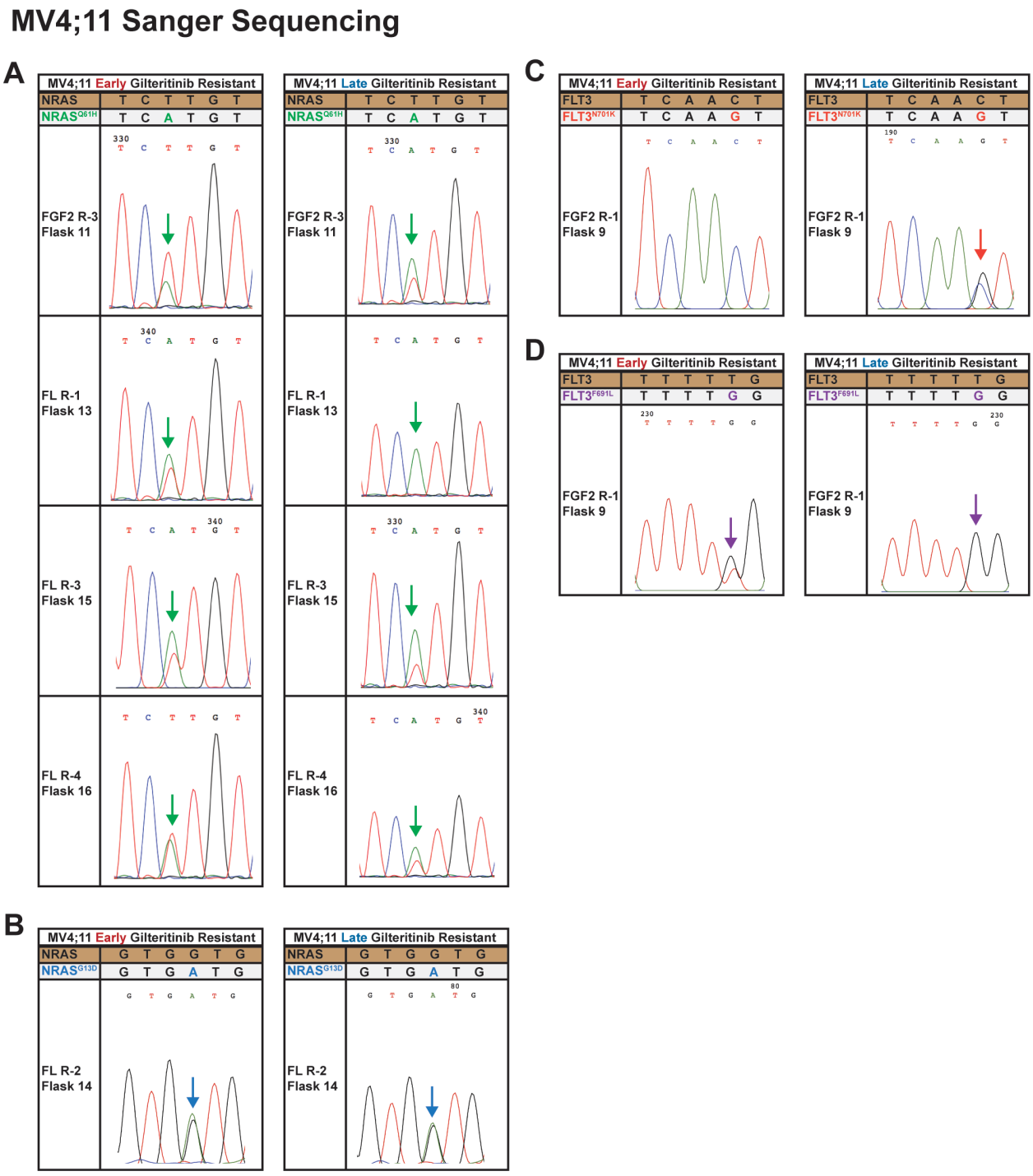

Supplemental Figure 3: Electropherograms from Sanger sequencing of NRAS (A, B) and FLT3 (C, D) point mutations detected in WES of late gilteritinib resistant MV4;11 cell lines. Sanger sequencing was also utilized to detect the presence of these mutations in early resistant cell lines. PCR amplification and sequencing primers are listed in Supplemental Table 2. Peaks correspond to the following nucleotides: A (green), T (red), C (blue), and G (black).

Genome-wide CRISPR screens reveal that early resistance is more complex than late resistance

To genetically interrogate signaling pathways that drive resistance, we performed genome-wide CRISPR resensitization screens in representative FGF2- and FL-dependent (early) and independent (late) gilteritinib resistant MOLM14 cultures (**Figure 3A**). CRISPR analysis of FGF2 and FL early ligand-dependent cultures did not identify a single gene responsible for early gilteritinib resistance, but rather revealed numerous genes involved in cell cycle progression, lipid metabolism, and PI3K/MAPK signaling pathways (**Figure 3B**), underscoring the multifaceted character of early resistance. Validation of significant FGF2 early CRISPR screen hits found that deletion of cell cycle regulators, cyclin D1 (CCND1) and postmeiotic segregation increased 1 (PMS1), improved sensitivity to gilteritinib among other hits (**Supplemental Figure 4**). Parallel validation of top candidates from FL early gilteritinib resistant cells identified the mitotic spindle checkpoint genes, NIMA-related kinase 6 (NEK6) and STIL centriolar assembly protein (STIL), and deletion of these genes also partially restored gilteritinib sensitivity (**Supplemental Figure 5**). Inactivation of sphingolipid metabolism genes, serine incorporator 4 (SERINC4) and sphingosine 1-phosphate lyase 1 (SGPL1) partially restored sensitivity to gilteritinib in FGF2 early cells (**Supplemental Figure 4**) and deficiency of ethanolamine kinase 2 (ETNK2), an important factor in glycerophospholipid biosynthesis, resensitized FL early cells to gilteritinib (**Supplemental Figure 5**).

In contrast to the early resistance screens, NRAS was by far the most significant hit in the late resistant cultures (**Figure 3C**). We used a meta-analysis approach for comparing ranked gene-lists with Robust Rank Aggregation (RRA)[437] to identify overlap between the FGF2 and FL late resistant screens and found that NRAS (FDR < 0.002) was the main regulator of late gilteritinib resistance (**Figure 3C**). Confirmatory CRISPR/Cas deletion of NRAS restored sensitivity to gilteritinib in both late resistance cultures, although incompletely, demonstrating strong

dependency on NRAS/MAPK signaling for survival (**Figure 3D**). The concordance of NRAS dependency uncovered by WES and CRISPR screening (**Figure 3E**) prompted us to test small-molecule inhibitors[11] of the downstream MAPK and PI3K/AKT signaling pathways (**Figure 3F**). Two MEK inhibitors, selumetinib and trametinib, and a PIK3CA inhibitor, taselisib, were also able to partially restore sensitivity to gilteritinib (**Figure 3G-J**, **Supplemental Figure 6, Supplemental Table 2**), reinforcing the importance of NRAS signaling in late resistance.

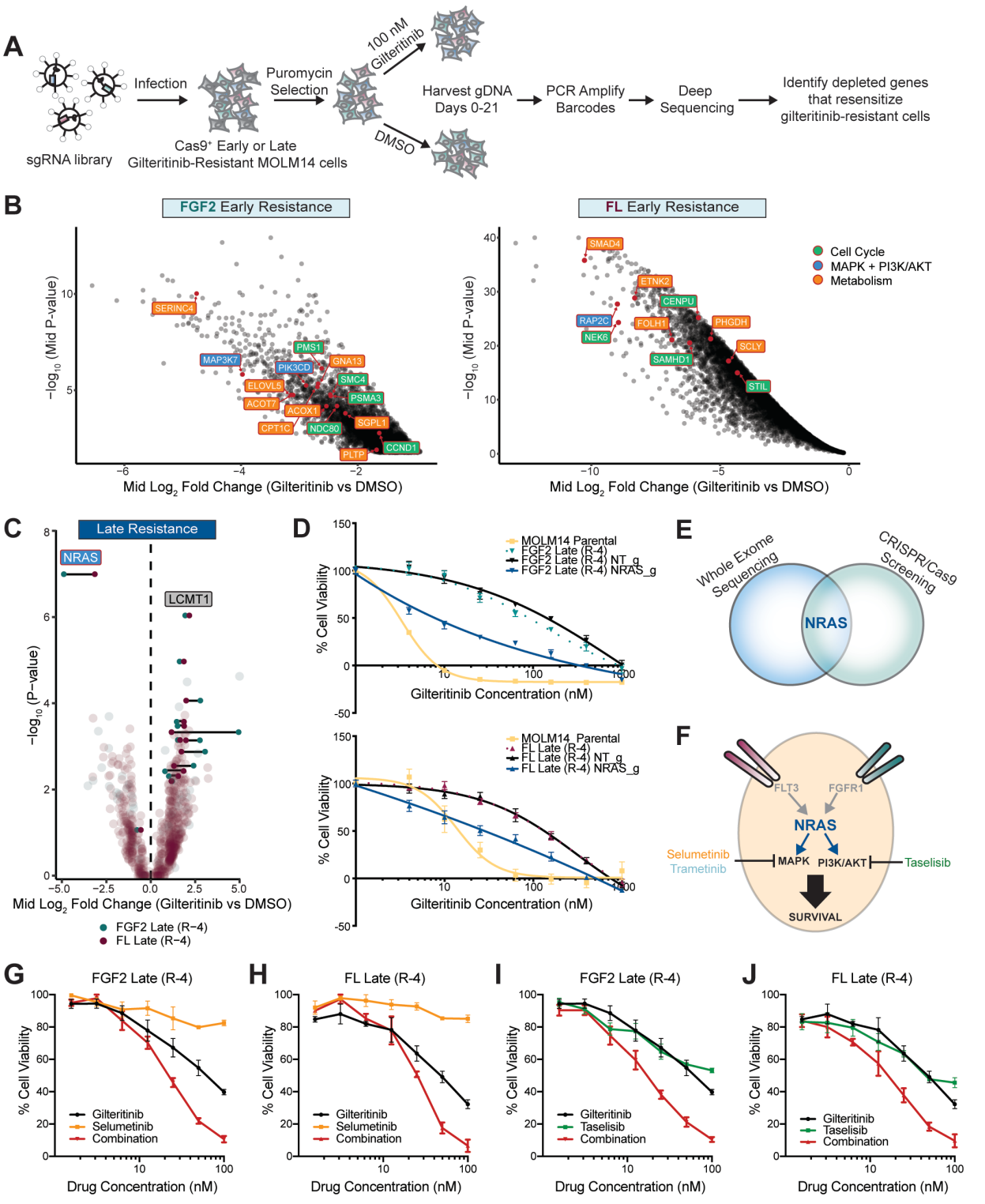

Figure 3: Early gilteritinib resistance is multifactorial while late resistance exhibits dependency on NRAS. A. Genome-wide CRISPR resensitization screen workflow. Cas9^{+} late gilteritinib resistant MOLM14 cell cultures (FGF2 & FL Late R-4) were transduced with a library of

sgRNAs and selected with puromycin for 5 days to enable virus integration. DNA was collected at 0, 7, 14, and 21 days from cells exposed to 100 nM gilteritinib or vehicle (DMSO). PCR-amplified sgRNA barcodes were subjected to deep sequencing to analyze gene depletion in gilteritinib-treated samples relative to DMSO. **B.** Volcano plots display results from CRISPR resensitization screens performed on FGF2 (left) and FL (right) early gilteritinib resistant (R-4) MOLM14 cells. Mid Log_2 fold change is shown per genes. Only sgRNAs that significantly decrease in gilteritinib-treated cells relative to DMSO-treated cells ($p < 0.05$) are shown. **C.** Volcano plot combining results from two independent CRISPR resensitization screens performed with FGF2 and FL late gilteritinib resistant (R-4) MOLM14 cells. Mid Log_2 fold change versus P-values(-Log(RRA P-value)) are plotted[437]. Horizontal lines connect genes of highest significance in both screens. **D.** Growth curves of NRAS knockout single clones in FGF2 (top) and FL (bottom) late cells following treatment with gilteritinib. Viability of gilteritinib-treated cells was measured after 72 hours and normalized to untreated cells. Mean ± standard error are shown. **E.** WES and CRISPR/Cas implicate importance of NRAS in late resistance. **F.** Schematic of NRAS signaling, downstream effectors, and pertinent small-molecule inhibitors. **G-J.** FGF2 (G, I) or FL (H, J) late cells were treated with MEK (selumetinib) or PI3K (taselisib) inhibitors alone or in combination with gilteritinib. Viability was measured after 72 hours and normalized to untreated cells. Mean of triplicates ± standard error are shown. CRISPR/Cas9 screening, analysis, and validation was performed under the supervision and assistance of Tamilla Nechiporuk and Daniel Bottomly (A-D).

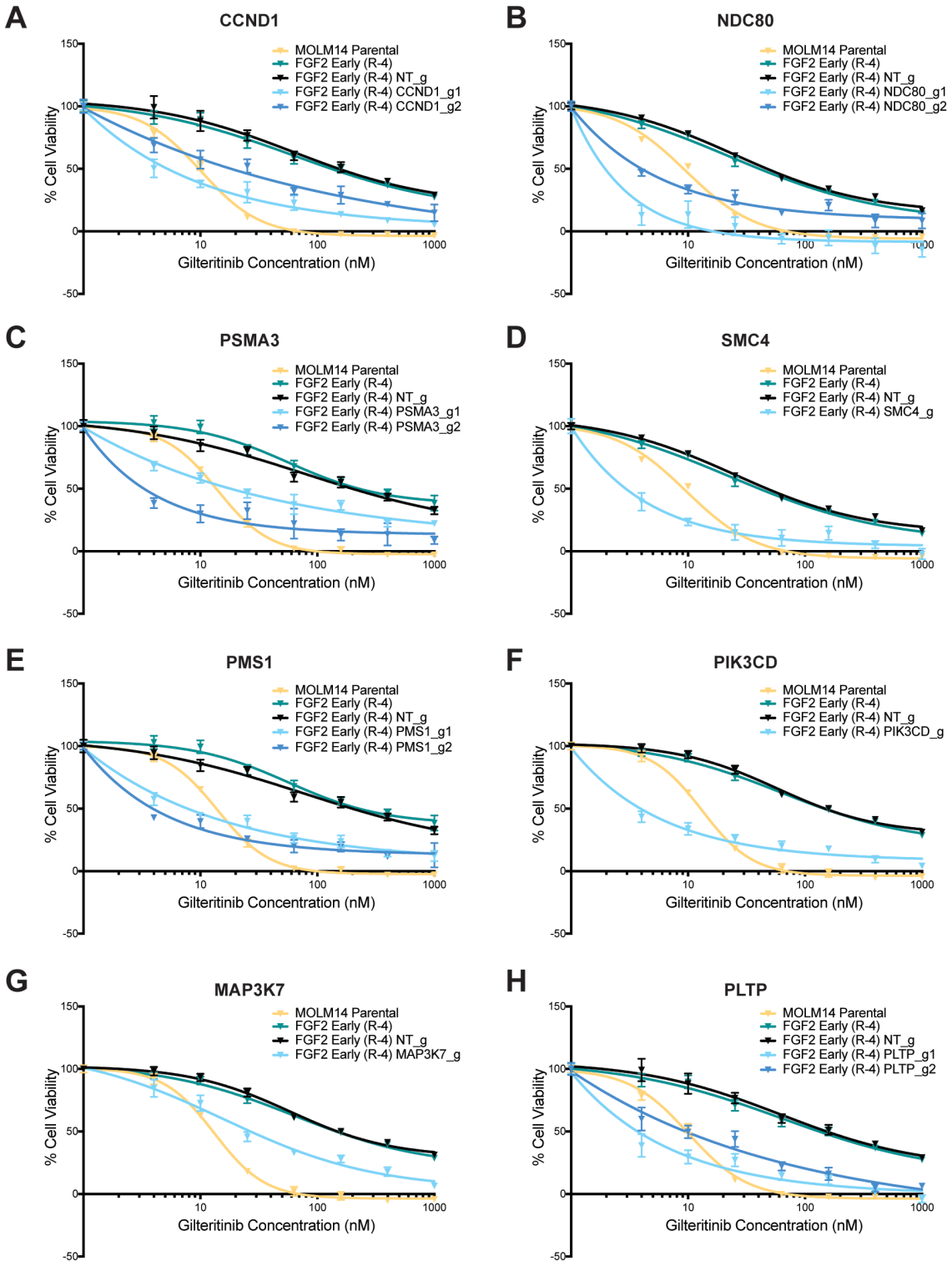
A
CCND1
MOLM14 Parental
FGF2 Early (R-4)
FGF2 Early (R-4) NT_g
FGF2 Early (R-4) CCND1_g1
FGF2 Early (R-4) CCND1_g2
% Cell Viability
Gilteritinib Concentration (nM)
B
NDC80
MOLM14 Parental
FGF2 Early (R-4)
FGF2 Early (R-4) NT_g
FGF2 Early (R-4) NDC80_g1
FGF2 Early (R-4) NDC80_g2
% Cell Viability
Gilteritinib Concentration (nM)
C
PSMA3
MOLM14 Parental
FGF2 Early (R-4)
FGF2 Early (R-4) NT_g
FGF2 Early (R-4) PSMA3_g1
FGF2 Early (R-4) PSMA3_g2
% Cell Viability
Gilteritinib Concentration (nM)
D
SMC4
MOLM14 Parental
FGF2 Early (R-4)
FGF2 Early (R-4) NT_g
FGF2 Early (R-4) SMC4_g
% Cell Viability
Gilteritinib Concentration (nM)
E
PMS1
MOLM14 Parental
FGF2 Early (R-4)
FGF2 Early (R-4) NT_g
FGF2 Early (R-4) PMS1_g1
FGF2 Early (R-4) PMS1_g2
% Cell Viability
Gilteritinib Concentration (nM)
F
PIK3CD
MOLM14 Parental
FGF2 Early (R-4)
FGF2 Early (R-4) NT_g
FGF2 Early (R-4) PIK3CD_g
% Cell Viability
Gilteritinib Concentration (nM)
G
MAP3K7
MOLM14 Parental
FGF2 Early (R-4)
FGF2 Early (R-4) NT_g
FGF2 Early (R-4) MAP3K7_g
% Cell Viability
Gilteritinib Concentration (nM)
H
PLTP
MOLM14 Parental
FGF2 Early (R-4)
FGF2 Early (R-4) NT_g
FGF2 Early (R-4) PLTP_g1
FGF2 Early (R-4) PLTP_g2
% Cell Viability
Gilteritinib Concentration (nM)

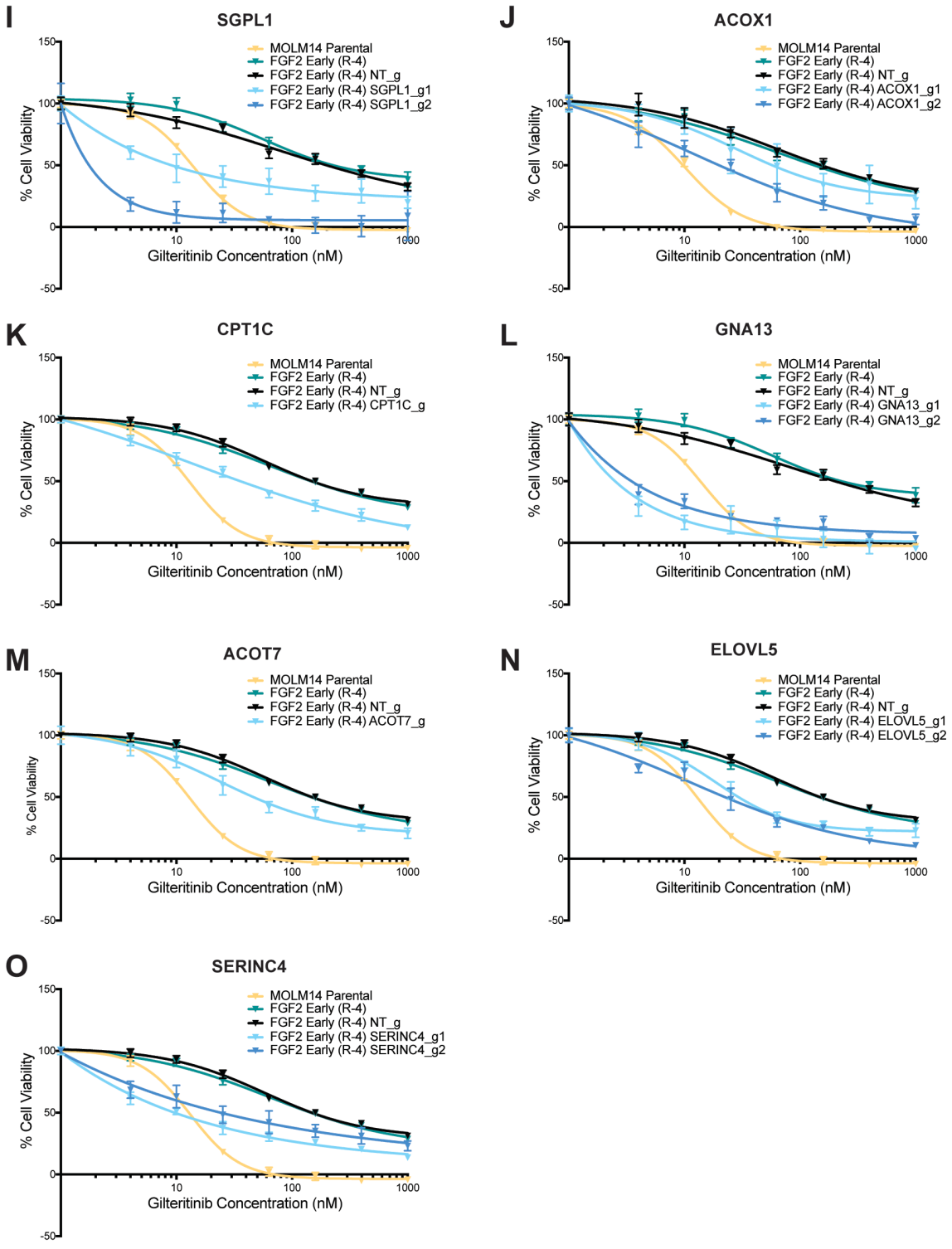

Supplemental Figure 4: Validation of candidate genes prioritized from FGF2 early CRISPR screen partially restores gilteritinib sensitivity. A-O. FGF2 early gilteritinib resistant (R-4)

MOLM14 cells were transduced with lentiviruses carrying single sgRNA/Cas9 constructs targeting CCND1 (A), NDC80 (B), PSMA3 (C), SMC4 (D), PMS1 (E), PIK3CD (F), MAP3K7 (G), PLTP (H), SGPL1 (I), ACOX1 (J), CPT1C (K), GNA13 (L), ACOT7 (M), ELOVL5 (N), SERINC4 (O), or nontargeting (NT) control. Two weeks after transduction, gilteritinib sensitivity was measured in triplicate using MTS viability assay. A 7-point concentration range of gilteritinib from 0.004 – 1 μM was utilized. Viability was measured after 72 hours and normalized to untreated cells. Mean ± standard error are depicted in each individual plot.

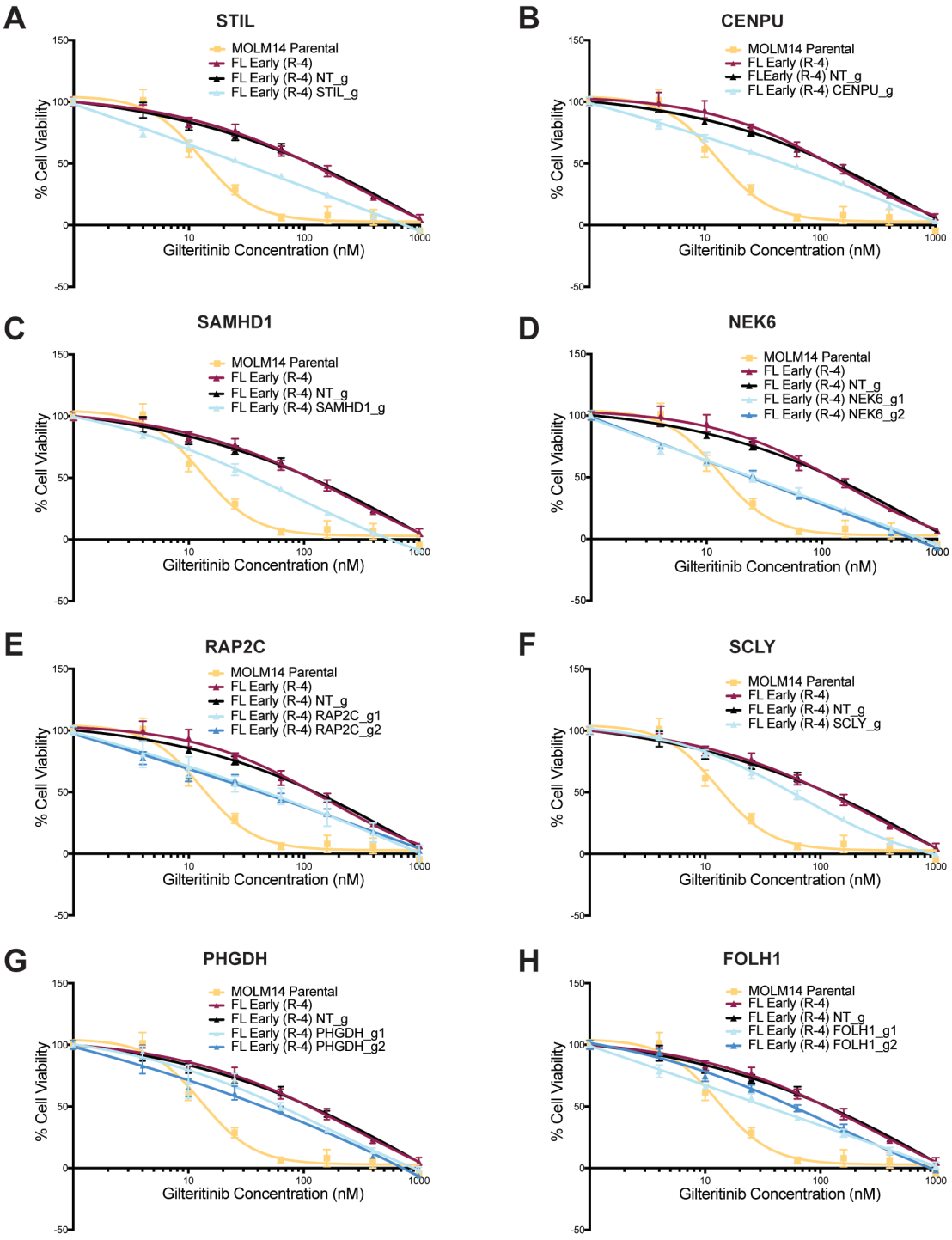
A
STIL
MOLM14 Parental
FL Early (R-4)
FL Early (R-4) NT_g
FL Early (R-4) STIL_g
% Cell Viability
Gilteritinib Concentration (nM)
B
CENPU
MOLM14 Parental
FL Early (R-4)
FLEarly (R-4) NT_g
FL Early (R-4) CENPU_g
% Cell Viability
Gilteritinib Concentration (nM)
C
SAMHD1
MOLM14 Parental
FL Early (R-4)
FL Early (R-4) NT_g
FL Early (R-4) SAMHD1_g
% Cell Viability
Gilteritinib Concentration (nM)
D
NEK6
MOLM14 Parental
FL Early (R-4)
FL Early (R-4) NT_g
FL Early (R-4) NEK6_g1
FL Early (R-4) NEK6_g2
% Cell Viability
Gilteritinib Concentration (nM)
E
RAP2C
MOLM14 Parental
FL Early (R-4)
FL Early (R-4) NT_g
FL Early (R-4) RAP2C_g1
FL Early (R-4) RAP2C_g2
% Cell Viability
Gilteritinib Concentration (nM)
F
SCLY
MOLM14 Parental
FL Early (R-4)
FL Early (R-4) NT_g
FL Early (R-4) SCLY_g
% Cell Viability
Gilteritinib Concentration (nM)
G
PHGDH
MOLM14 Parental
FL Early (R-4)
FL Early (R-4) NT_g
FL Early (R-4) PHGDH_g1
FL Early (R-4) PHGDH_g2
% Cell Viability
Gilteritinib Concentration (nM)
H
FOLH1
MOLM14 Parental
FL Early (R-4)
FL Early (R-4) NT_g
FL Early (R-4) FOLH1_g1
FL Early (R-4) FOLH1_g2
% Cell Viability
Gilteritinib Concentration (nM)

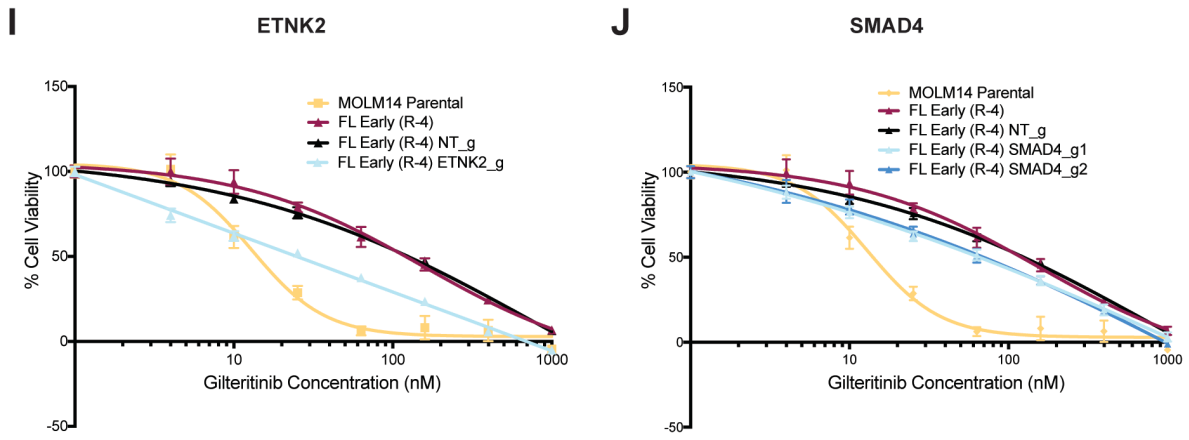

Supplemental Figure 5: Validation of candidate genes prioritized from FL early CRISPR screen partially restores gilteritinib sensitivity. A-J. FL early gilteritinib resistant (R-4) MOLM14 cells were transduced with lentiviruses carrying single sgRNA/Cas9 constructs targeting STIL (A), CENPU (B), SAMHD1 (C), NEK6 (D), RAP2C (E), SCLY (F), PHGDH (G), FOLH1 (H), ETNK2 (I), SMAD4 (J), or nontargeting (NT) control. Two weeks after transduction, gilteritinib sensitivity was measured in triplicate using MTS viability assay. A 7-point concentration range of gilteritinib from 0.004 – 1 μM was utilized. Viability was measured after 72 hours and normalized to untreated cells. Mean ± SE are depicted in each individual plot.

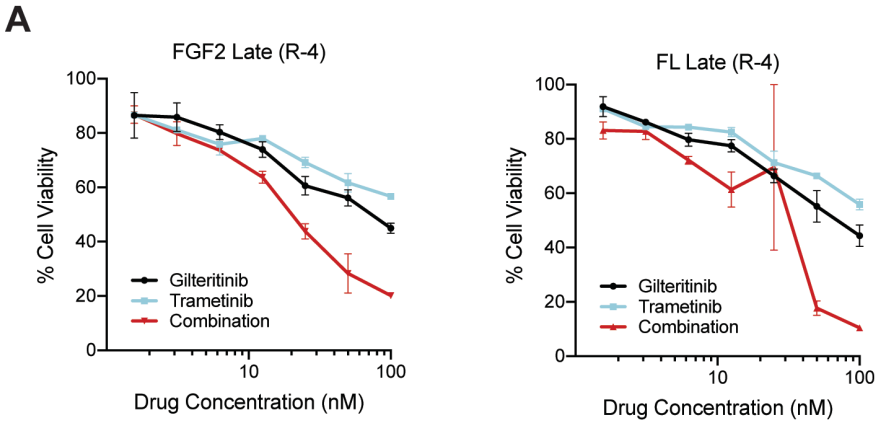

Supplemental Figure 6: Inhibition of MEK enhances efficacy of gilteritinib. A. Equimolar gilteritinib and trametinib (MEK1/2 inhibitor) combination treatment inhibits growth of FGF2 (left panel) and FL (right panel) late resistant MOLM14 cell lines. Viability was measured in triplicate by MTS reagent following 72 hours and normalized to untreated cells. Mean ± SE are plotted.

Metabolic reprogramming starts with early resistance and continues into late resistance

Multiple hits from the FGF2 and FL early CRISPR screens hinted that perturbations in metabolism may contribute to early resistance (**Figure 3B & 4A**), which prompted us to perform global metabolic profiling. As a control, we first analyzed the effect of 48-hour gilteritinib treatment on the metabolome of MOLM14 parental cells (N = 4) relative to untreated cells (N = 4; **Supplemental Figure 7-8, Supplemental Table 3**). Close examination of metabolite clusters indicated that gilteritinib rapidly decreased central energy metabolism and altered glycerophospholipid metabolism (**Supplemental Figure 7A & 8**). These effects were modestly dampened by the addition of FGF2 (N = 4) and FL (N = 4) over 48 hours.

Examination of metabolites in early and late gilteritinib resistant cultures suggested that long-term FLT3 inhibition resulted in a broad metabolomic reprogramming (**Figure 4B, Supplemental Figure 9**). Partial least squares-discriminant analysis (PLS-DA) revealed dramatic differences in the metabolome of early and late gilteritinib resistant MOLM14 cell lines relative to parental cells (**Figure 4C**). Consistent with CRISPR screen results of FGF2-dependent early resistant cells (**Figure 4A**), metabolic profiling of these cells (N = 4) confirmed a trend towards increased sphingolipid/phospholipid metabolites relative to MOLM14 parental cells (N = 4). Unexpectedly, changes to sphingolipid/phospholipid metabolism became even more pronounced in late resistance, with significant enrichment of sphingosine 1-phosphate (p = 0.0118), sphinganine 1-phosphate (p = 0.0006), and ethanolamine phosphate (p < 0.0001) in FGF2 late gilteritinib resistant cells (N = 4) relative to parental (**Figure 4D, Supplemental Table 3**). All metabolite comparisons were Sidak adjusted. These data, in conjunction with CRISPR resensitization screens, implicate an initial dependency on sphingolipid/phospholipid metabolism in FGF2 early resistant cells that becomes even more pronounced in late resistance.

FL-derived gilteritinib resistant cultures, on the other hand, demonstrate increased fatty acid/carnitine metabolism. While acylcarnitine levels in FL early cells (N = 4) were similar to

untreated parental cells, they became significantly higher in FL late resistant cells (N = 4; **Figure 4E, Supplemental Table 3**), similar to the trend observed with sphingolipid signaling in FGF2-derived resistant cultures. To assess the functional relevance of fatty acid catabolism in FL early and late cultures, we measured changes in oxidative phosphorylation (OXPHOS) activity using the Seahorse assay (**Figure 4G-I**). Administration of etomoxir (ETO), an inhibitor of carnitine palmitoyltransferase 1 (CPT1, **Figure 4F**), decreased OXPHOS activity the most in late FL resistant cultures (**Figure 4I**, revealed by decreased maximal respiration between the FCCP and Rotenone/Antimycin A dotted lines). This suggests dependence on acylcarnitines for energy despite abundant glucose over time**.** In line with our metabolomics and Seahorse analyses, CRISPR/Cas inactivation of CPT1A and CPT2 (**Supplemental Figure 10**) led to increased sensitivity to gilteritinib in FL early and late resistant cultures, further supporting dependence on carnitine metabolism in FL-derived cultures.

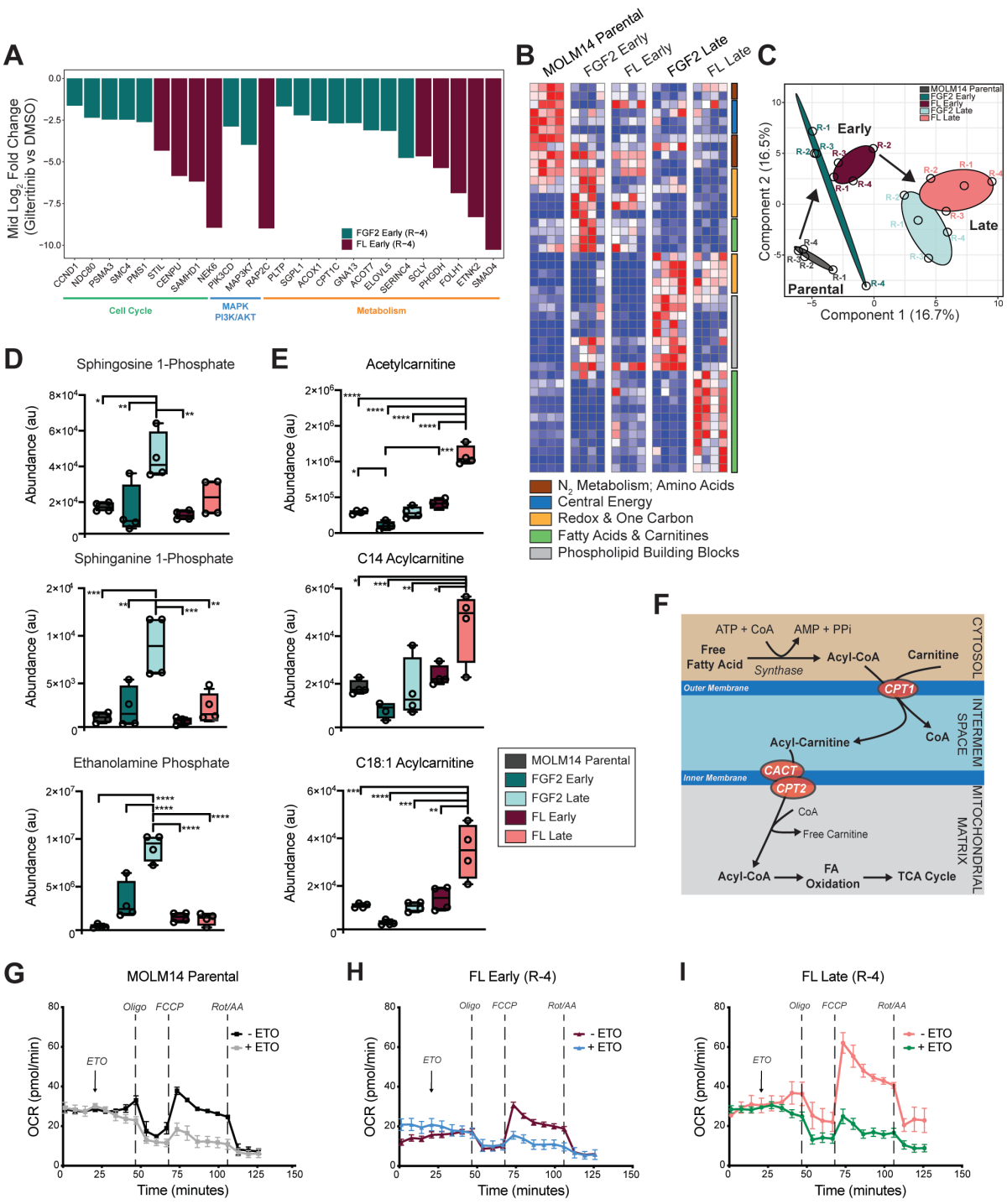

Figure 4: Early and late gilteritinib resistant cells exhibit unique metabolic dependencies. **A.** Plot summarizes major pathways important in early gilteritinib resistance as identified by CRISPR resensitization screens in Figure 3B. **B.** Heat map of hierarchical clustering analysis of significantly changed metabolites (ANOVA; $p < 0.05$) in early and late gilteritinib resistant cultures relative to MOLM14 parental cells. **C.** Partial least squares-discriminant analysis of normalized data from 4B reveals the progression of acquired gilteritinib resistance. **D-E.** Comparison of

selected metabolite abundance (au) in early and late gilteritinib resistant MOLM14 cultures relative to parental cells. Statistical significance was assessed by one-way ANOVA followed by SIDAK correction. *$p < 0.05$, **$p < 0.01$, ***$p < 0.001$, ****$p < 0.0001$ **F.** Overview of carnitine shuttle. CPT1, Carnitine palmitoyltransferase I; CACT, Carnitine-acylcarnitine translocase; CPT2, Carnitine palmitoyltransferase 2 **G-I.** Oxygen consumption rate (OCR) for MOLM14 parental cells (G), FL early (H), and FL late (I) following inhibition of CPT1 activity with etomoxir (ETO, arrow). Each data point has at least three technical replicates; mean ± SE are shown. Vertical dotted lines show inhibitor injection times used in the Seahorse assay. Metabolomics and corresponding analyses were performed under the supervision of Julie A. Reisz and Angelo D'Alessandro of University of Colorado (B-E). Seahorse studies were performed in collaboration with Tamilla Nechiporuk.

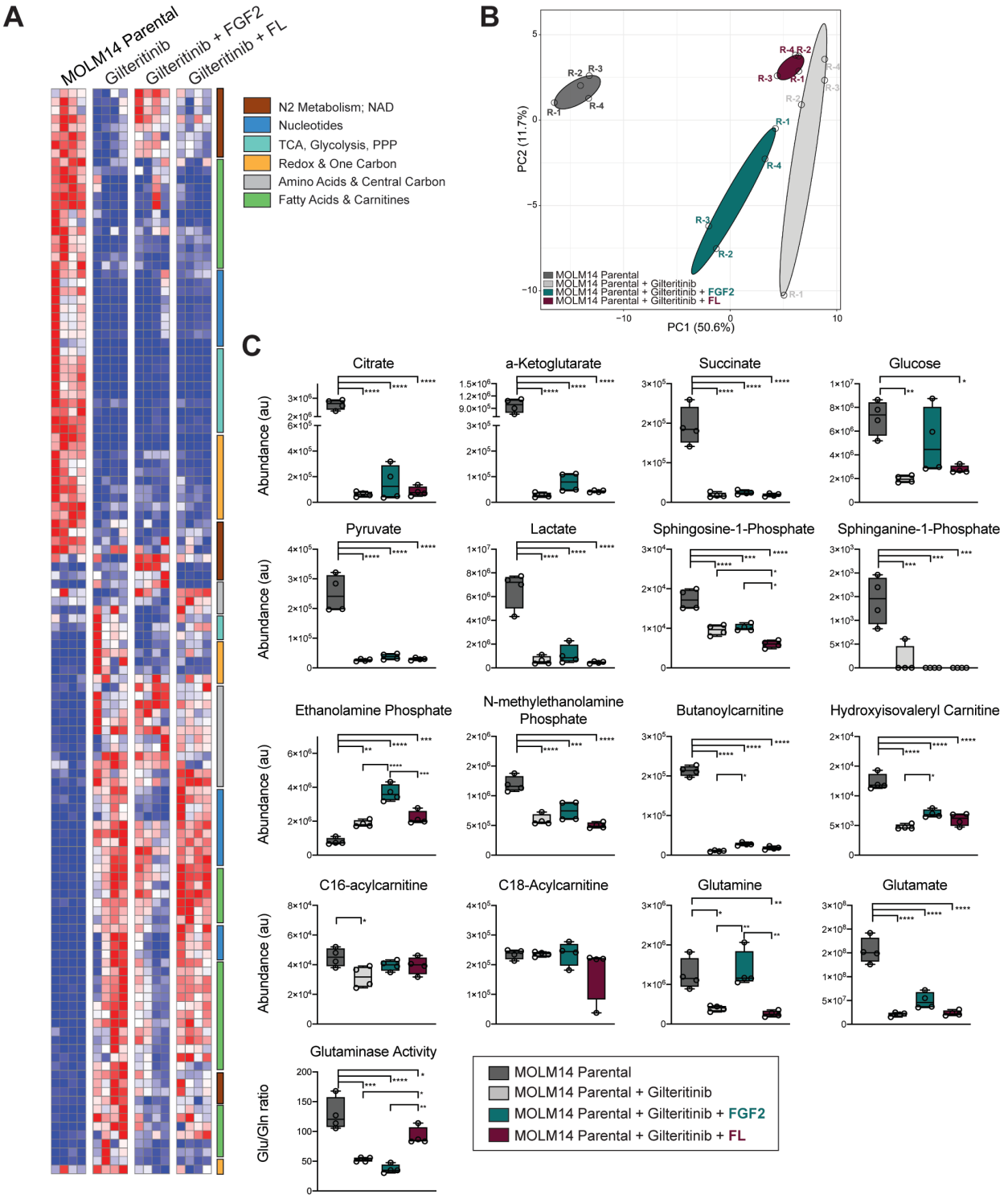

Supplemental Figure 7: Short-term FLT3 inhibition causes broad metabolic changes in MOLM14 parental cells that are dampened with protective ligands. A. Hierarchical clustering analysis of significantly changed metabolites (ANOVA, $p<0.05$). **B.** Principal component analysis of normalized data reveals the effect of gilteritinib treatment along PC1, which is partially

diminished by FGF2 or FL ligands. Ligand-treated groups clustered as intermediates between gilteritinib-treated and untreated MOLM14 parental cells. **C.** Relative abundance (au) of metabolites involved in central carbon and nitrogen metabolism, redox metabolism, one carbon metabolism, and glycerophospholipid metabolism are shown. Metabolites in the Krebs cycle, that generate the majority of cellular ATP, were profoundly decreased along with mitochondrial bound fatty acids (i.e., acylcarnitines) in all gilteritinib-treated samples. Statistical significance was assessed by one-way ANOVA followed by SIDAK correction. *$p < 0.05$, **$p < 0.01$, ***$p < 0.001$, ****$p < 0.0001$. Metabolomics and corresponding analyses were performed under the supervision of Julie A. Reisz and Angelo D'Alessandro of University of Colorado (A-C).

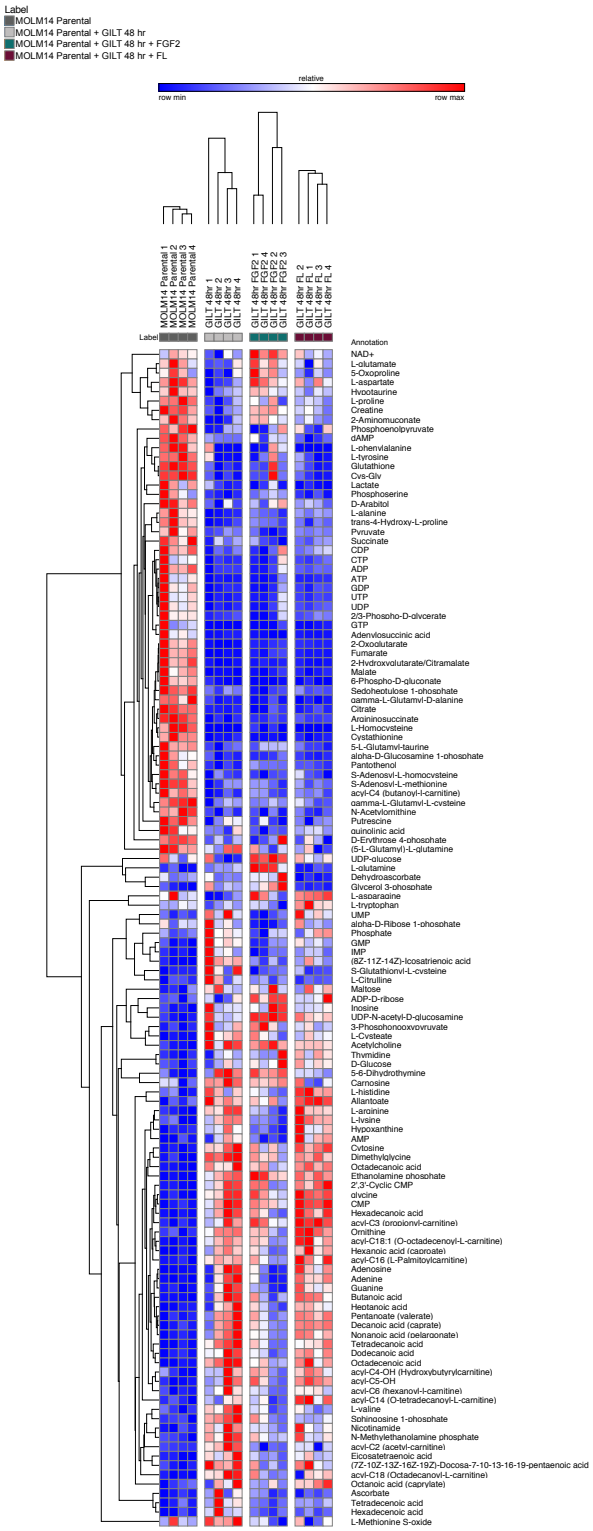

Supplemental Figure 8: Heat map presented in Supplemental Figure 7A with full name of metabolites provided. Metabolite data was analyzed using MetaboAnalyst 4.0 and heat maps were generated using GENE-E (Broad Institute). Supplemental Table 3 contains full summary of individual metabolites.

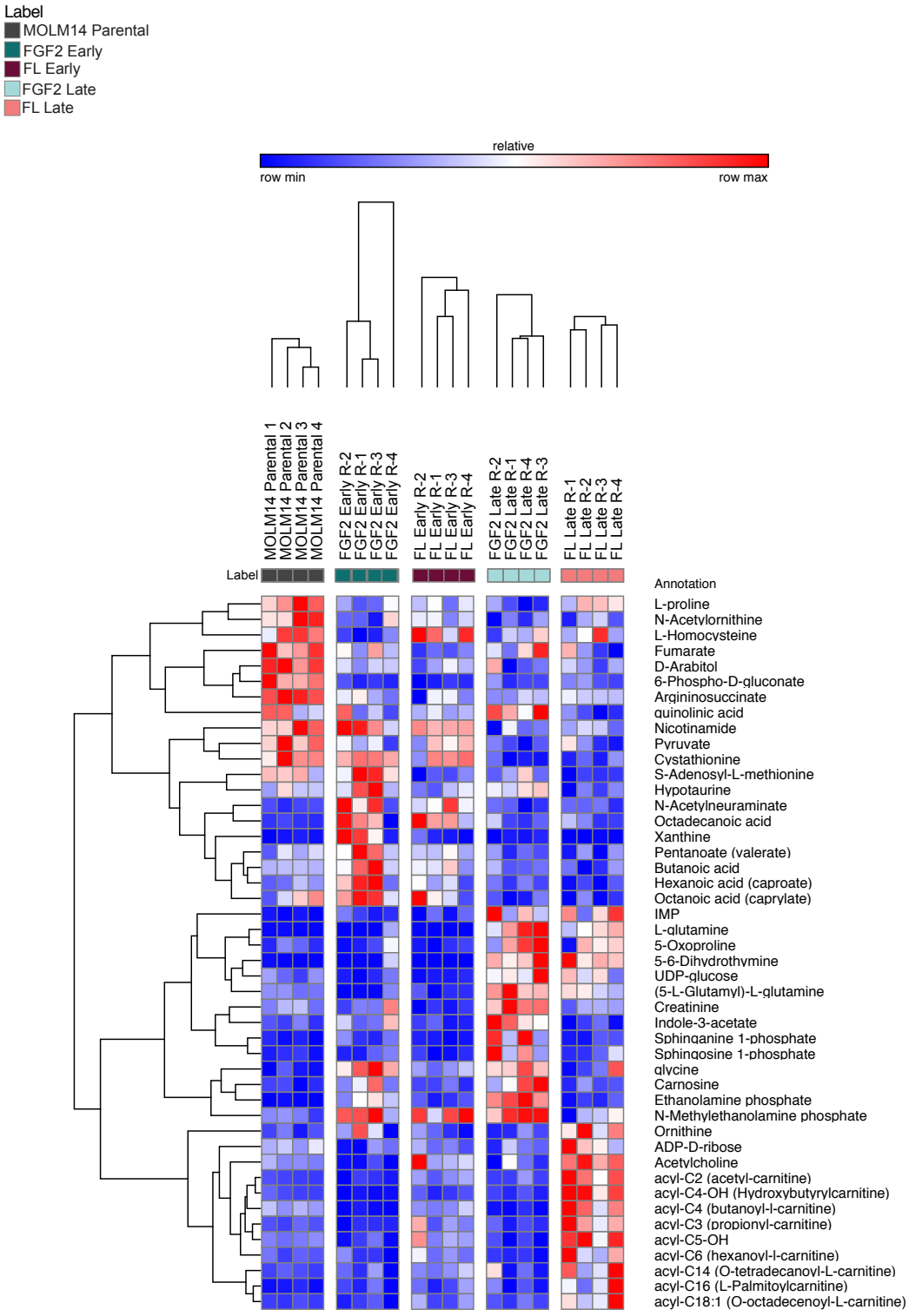

Supplemental Figure 9: Heat map presented in Figure 4B with full name of metabolites provided. Metabolite data was analyzed using MetaboAnalyst 4.0 and heat maps were generated using GENE-E (Broad Institute). Supplemental Table 3 contains full summary of individual metabolites.

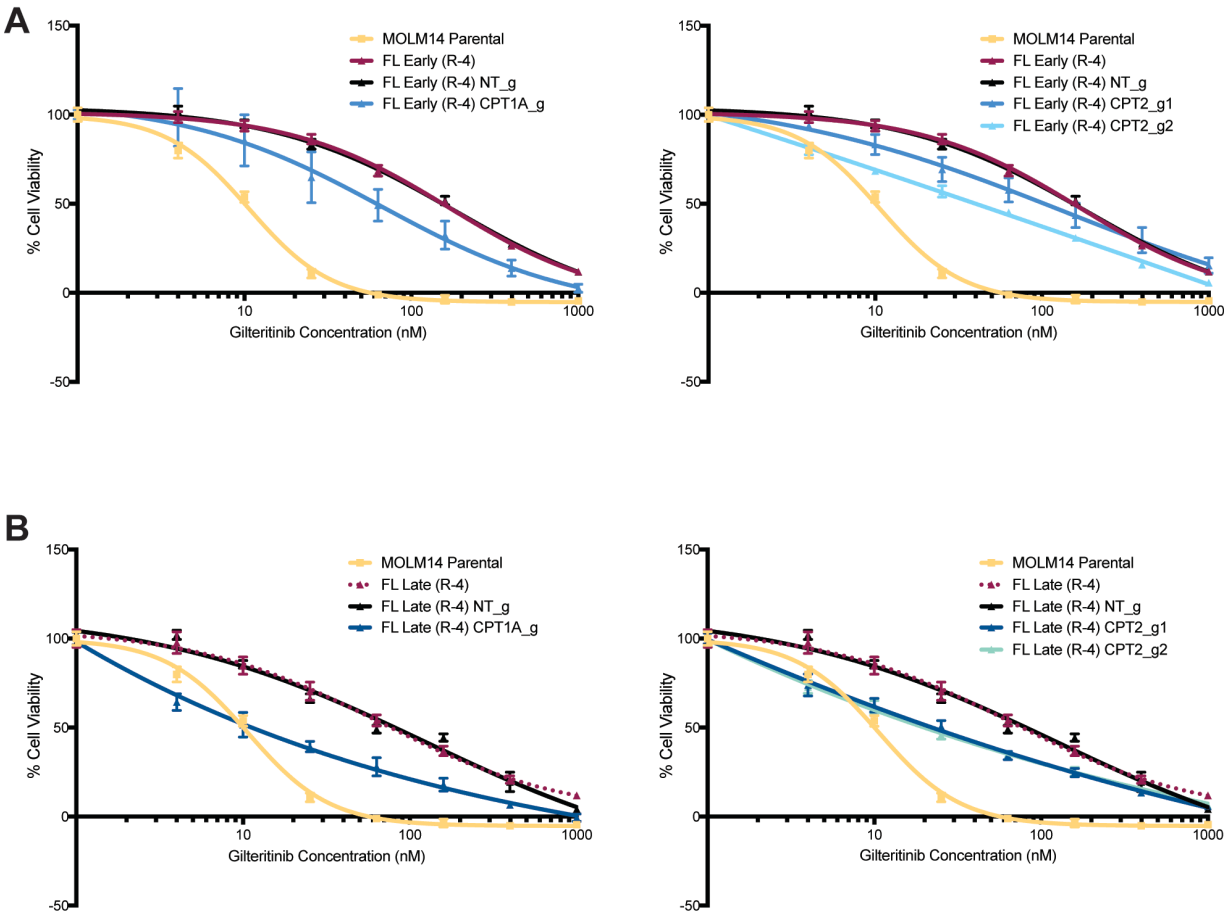

Supplemental Figure 10: FL-derived gilteritinib resistant cells display unique dependence on acylcarnitines for energy metabolism. A-B. Inactivation of CPT1A and CPT2 via CRISPR/Cas9 resensitized FL early (A) and late (B) cells to gilteritinib treatment. The effect was much stronger in late resistant cells. FL-derived gilteritinib resistant cells were transduced with single sgRNAs targeting CPT1A, CPT2, or nontargeting (NT) control. Two weeks after transduction, gilteritinib sensitivity was measured in triplicate using MTS viability assay. A 7-point concentration range of gilteritinib from 0.004 – 1 μM was utilized. Viability was measured after 72 hours and normalized to untreated cells. Mean ± SE are depicted in each individual plot.

Distinct proteomes define early and late gilteritinib resistant cells

Although metabolic reprogramming was evident in early resistant cultures, we discovered an even greater degree of metabolic rewiring in FGF2- and FL late resistant cultures. Interestingly, expansion of NRAS mutations (**Figure 2C**) does not revert late resistant cells to mimic the metabolic profile of MOLM14 parental cells, but rather seems to cement unique metabolic dependencies initiated in early resistance. To further explore the unique features of early resistance, we performed proteomics and phosphoproteomics as a complementary biochemical approach through the Clinical Proteomics Tumor Analysis Consortium (CPTAC). Protein lysates from parental, early, and late gilteritinib resistant MOLM14 and MV4;11 cells were digested and analyzed by mass spectrometry using an isobaric labeling-based, integrated analysis approach[438, 439] (**Figure 5A**). Proteomics and phosphoproteomics analyses identified a total of 7,694 proteins and 36,004 phosphopeptides, respectively. PCA visualization of proteomics and phosphoproteomics demonstrated a clear separation among MOLM14 parental (N = 4), early resistant (N = 4/FGF2, 4/FL), and late (N = 8) resistant cultures. A distinct clustering by ligand, FGF2 or FL, was also apparent within the early and late resistant cells (**Figure 5B**), similar to the metabolic profiles (**Figure 4C**). We also analyzed the proteome and phosphoproteomes of gilteritinib resistant MV4;11 cells, and observed similar differences between early and late resistance, although not as clearly pronounced in the MV4;11 model, likely corresponding to the earlier appearance of NRAS mutations during ligand supplementation (**Supplemental Figure 11A and 1B**).

We evaluated the proteomes of resistant cultures as they evolved from parental to early resistance and then again to late resistance. For the initial analysis, FGF2 and FL early and late resistant MOLM14 cultures (N = 8 early and N = 8 late cultures) were analyzed together. Since phosphorylation modulates multiple cellular processes, kinase-substrate enrichment analysis (KSEA) was used to infer changes in the activity of kinases by evaluating modifications to the

phosphorylation levels of their respective substrates[440, 441]. In early gilteritinib resistant MOLM14 cells, KSEA analysis indicated a significant decrease ($p < 0.05$) in activity of proteins facilitating cell cycle progression (CDK 1, 2, 4, 5, 6, 7 and 9; **Figure 5C**), and a complementary increase in activity of cell cycle checkpoint (PRKCA, CSNK2A1) and DNA damage response (DDR) modulators (ATM; **Figure 5C, Supplemental Figure 12**). Early resistant MV4;11 cells showed a similar pattern, including increased activity of additional mitotic checkpoint proteins AURKB, AURKA, and DDR proteins ATM and ATR, many of which were also found in MOLM14 resistant cultures when FGF2 and FL-derived cultures were considered separately (**Supplemental Figure 11B, 12, 13**). Notably, these cell cycle alterations were largely reversed in late resistant MOLM14 and MV4;11 cells as evident by the significant increase in CDK phosphorylation from early to late resistance (**Figure 5C, Supplemental Figure 11B**). While FGF2 and FL contributed to MAPK and PI3K signaling in early resistant cultures relative to parental cells, these pathways were more prominently increased in late, ligand-independent resistant MOLM14 and MV4;11 cells after expansion of NRAS mutant subclones (**Figure 2B, 5C**, **Supplemental Figure 1B, 11B, 12, 13**).

We also utilized CausalPath, a computational method that uses curated signaling pathway data from Pathway Commons to infer causal relationships between differential proteomic and phosphoproteomic readouts[442]. In agreement with KSEA, CausalPath suggested early resistance is predominantly characterized by a decrease in cell cycle progression as evident by decreased CDK1, CDK2, MYC, and cyclin D3 signaling in early resistant MOLM14 cultures (**Figure 5D**). Early resistance network diagrams also highlighted proteins associated with lipid metabolism, including CPT1A, NRF1, CAPNS1, and SPAST, consistent with the metabolic remodeling that begins in early gilteritinib resistance (**Figure 5D, Supplemental Figure 11C**). Activity of CDKs and MAPK, reflected in their phosphorylation, were then increased in late MOLM14 and MV4;11 resistant lines after acquisition of NRAS mutations (**Figure 5E, Supplemental Figure 11D-E**). Collectively, proteomic and phosphoproteomic profiling of early and late gilteritinib resistant MOLM14 and MV4;11 cultures independently validated many of the genes and pathways

identified by WES, CRISPR/Cas9, and metabolomic analyses, as well as implicating additional signaling pathways.

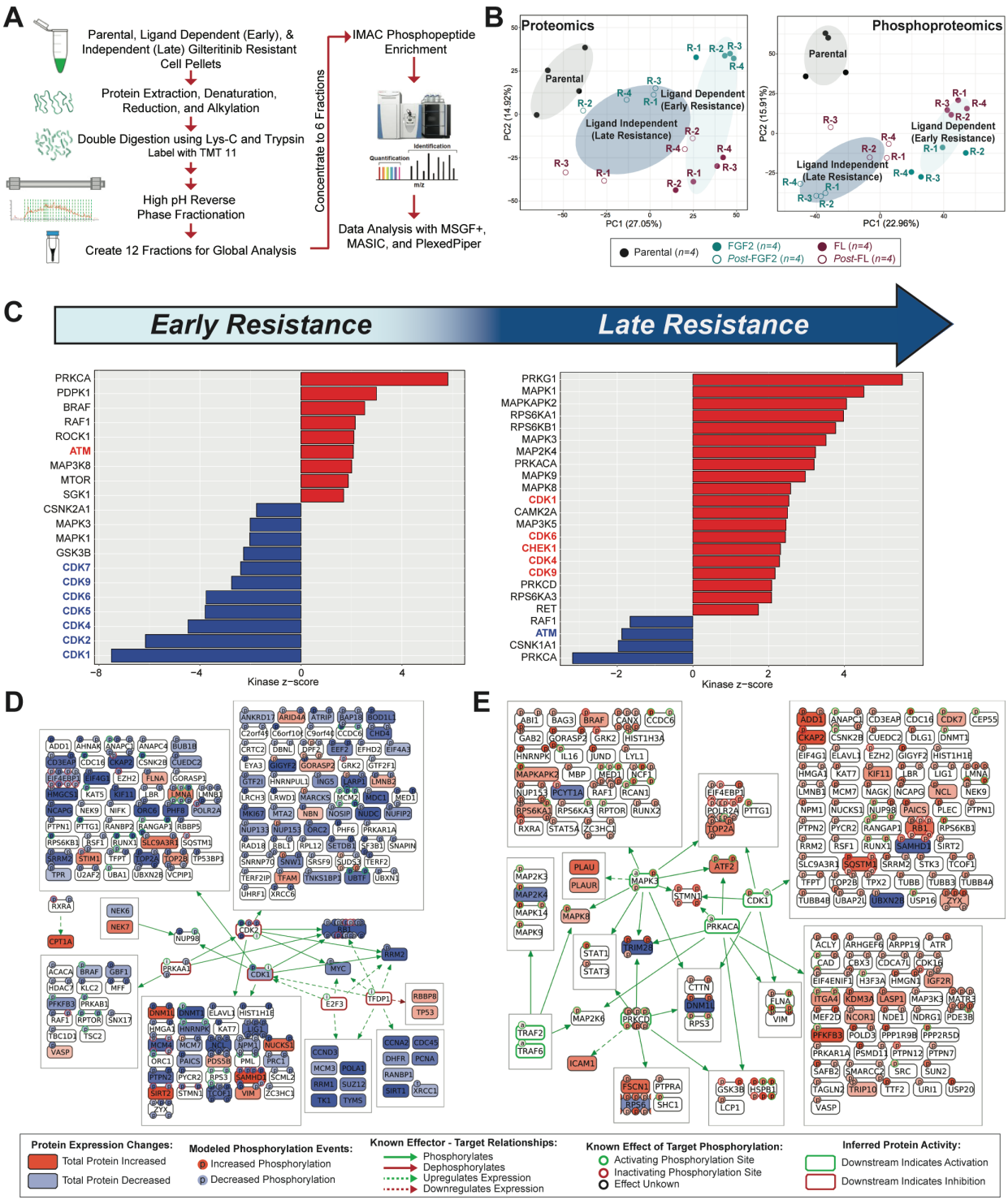

Figure 5: Early and late gilteritinib resistant cultures have distinct proteomic profiles, and early resistance has significantly reduced cell cycle protein activity. A. Overview of integrated proteomics and phosphoproteomics workflow. **B.** Visualization of proteomic (left) and

phosphoproteomic (right) profiling by PCA shows clear separation among parental, early, and late resistant MOLM14 cultures. **C.** KSEA infers changes in kinase activity ($p < 0.05$) throughout the development of gilteritinib resistance from parental to early resistance (left plot) and then early to late resistance (right plot). Higher Z scores correspond to increased activity of a given kinase and vice versa (MOLM14 FGF2 and FL resistant cultures analyzed together). **D-E.** Pathway and causality analysis using CausalPath (FDR < 0.1), visualized by ChiBE. Protein-protein network diagram in D shows proteins dynamically regulated in early resistant cells relative to MOLM14 parental and E shows protein activity altered in late resistant cells relative to early cells (FGF2 and FL resistant cultures analyzed together). Proteomics and phosphoproteomics were performed and analyzed in collaboration with the Pacific Northwest National Laboratory (PNNL) under the supervision of Karin D. Rodland and Paul Piehowski. KSEA analyses were performed by Sara J.C. Gosline. CausalPath diagrams were created by Ozgun Babur.

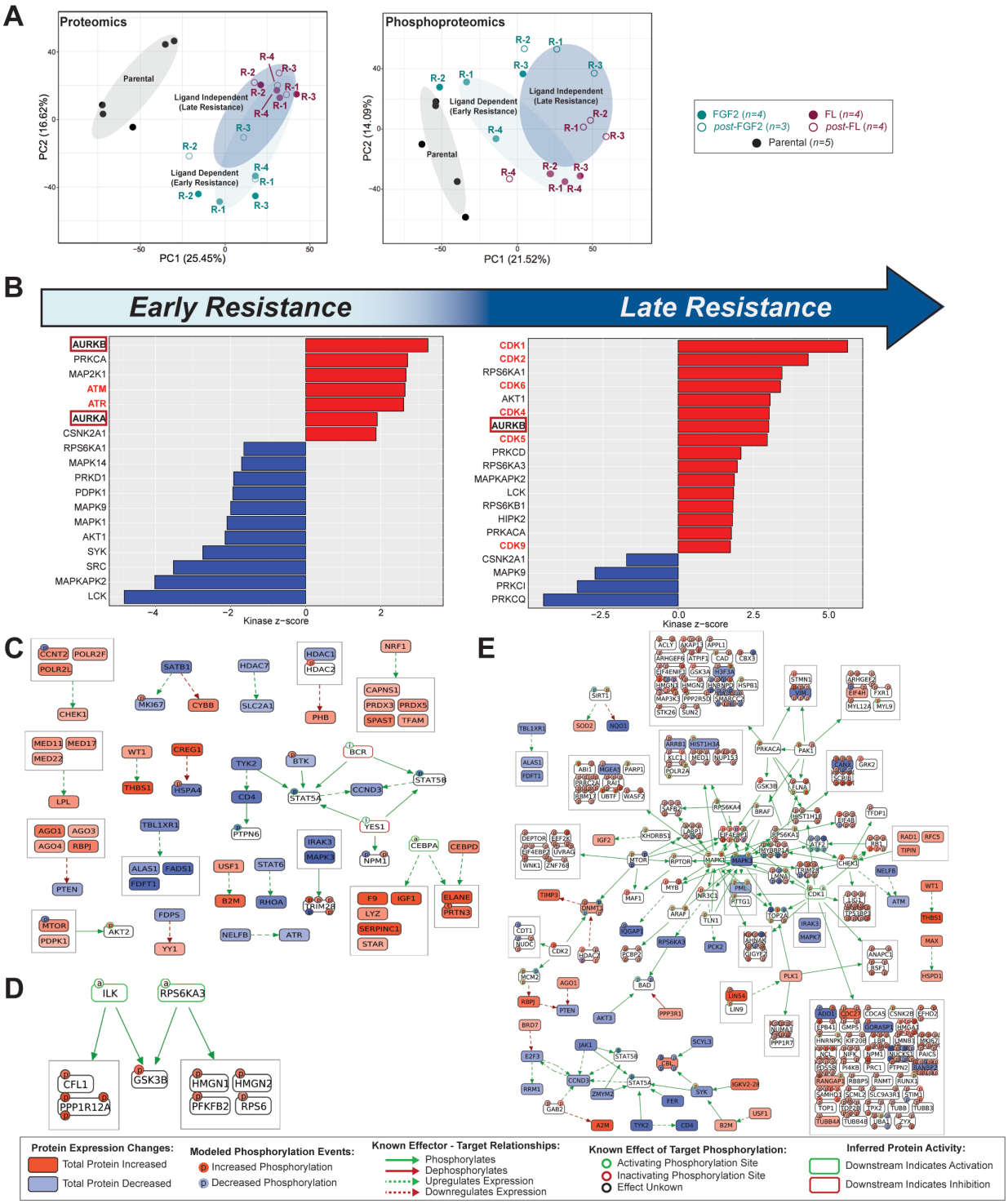

Supplemental Figure 11: Proteomic profiling of early and late gilteritinib resistant MV4;11 cell lines. A. Principal component analysis of proteomics (left) and phosphoproteomics (right) data. PCA plots were created using all proteins (phosphopeptides for phospho) with abundance ratios measured across all samples in the dataset. **B.** Kinase-substrate enrichment analysis

(KSEA) of FGF2 and FL resistant cultures together. Bar plots show that activity of many kinases significantly ($p < 0.05$) changed between MV4;11 parental and early resistant cell lines (left plot) and between early and late resistant cell lines (right plot). Increase in cell cycle mitotic checkpoint and DNA damage response is observed in early resistance, indicative of aberrations in cell cycle progression. Cell cycle progression is restored in late resistance alongside increase AKT and MAPK signaling. **C-E.** CausalPath analyses (0.1 FDR threshold) as visualized by ChiBE. Node colors indicate the relative intensity of the protein, where red and blue denote increased or decreased expression, respectively. Protein phosphorylation sites are shown with smaller "p" circles, where the green border indicates an activating site and red border indicates an inactivating site. The background color of phosphorylation sites indicates their differential measurement from the data, red indicating an increase and blue indicating a decrease. Relative to MV4;11 parental cells, early resistant cells show upregulation of checkpoint proteins and downregulation of transcription (C). Relative to early resistant cells, late resistant cells show an increase in cell proliferation, motility, and protein synthesis (D). In comparison to MV4;11 parental cells, late resistant MV4;11 cells show marked MAPK and PI3K signaling (E). Proteomics and phosphoproteomics were performed and analyzed in collaboration with the Pacific Northwest National Laboratory (PNNL) under the supervision of Karin D. Rodland and Paul Piehowski. KSEA analyses were performed by Sara J.C. Gosline. CausalPath diagrams were created by Ozgun Babur.

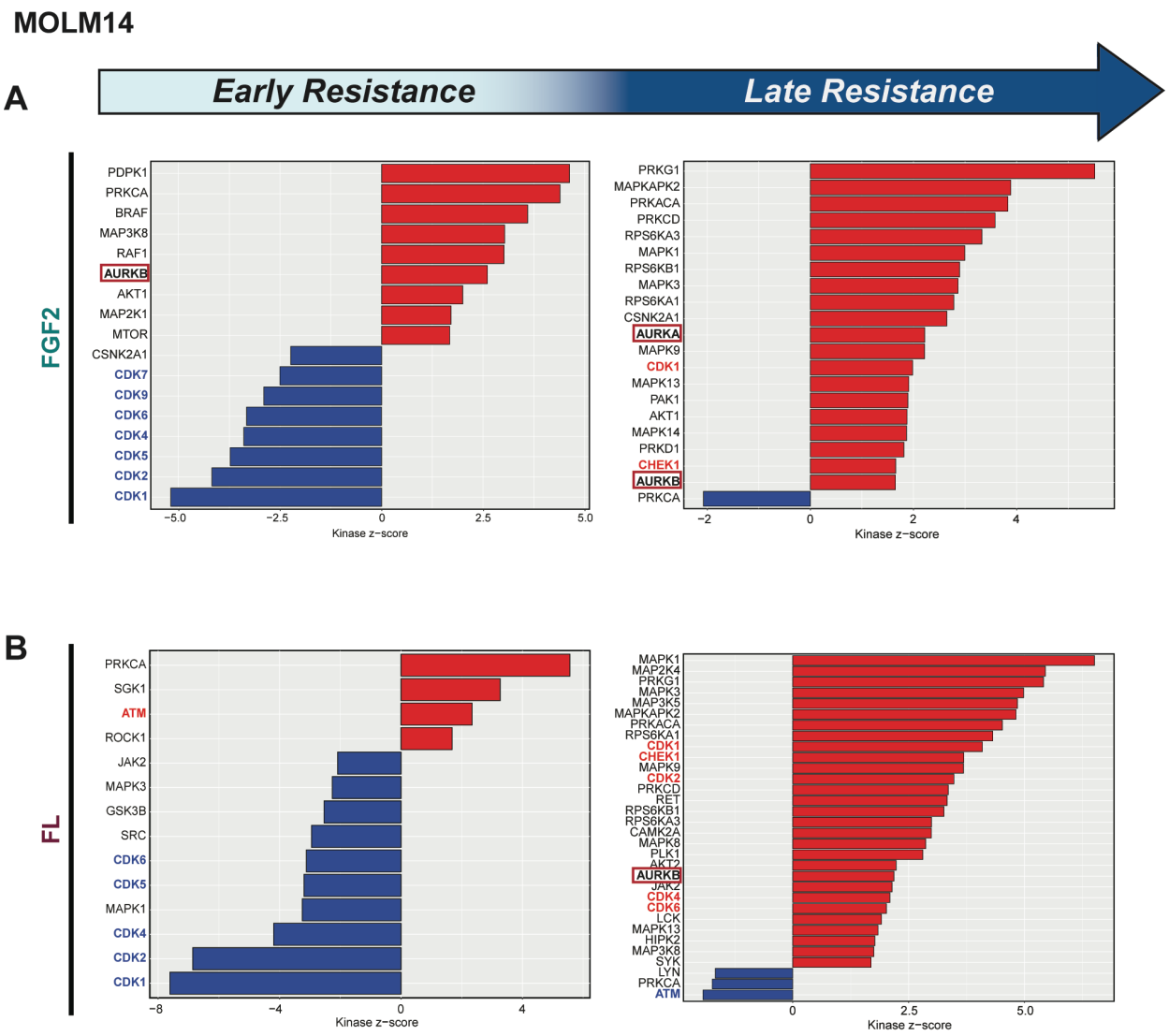

Supplemental Figure 12: Kinase-substrate enrichment analysis (KSEA) on MOLM14 gilteritinib resistant cell lines separated by ligand. A. KSEA ($p < 0.05$) on FGF2 early and late resistant cell lines. Bar plot of FGF2 early cells (left plot) shows definitive decrease in CDK phosphorylation (blue) and increase in AURKB (boxed). Late FGF2 cells (right plot) exhibit recovery in CDK phosphorylation (red) and increased MAPK signaling. **B.** KSEA ($p < 0.05$) on FL early and late cell lines. Similar to FGF2 early cells, FL early cells (left plot) show a decrease in CDK phosphorylation. An increase in ATM (red) activation, transducer of DNA damage response, is also noted. CDK phosphorylation is increased in late FL cells with a parallel decrease in DNA damage response (i.e., ATM, right plot). Proteomics and phosphoproteomics were performed and analyzed in collaboration with the Pacific Northwest National Laboratory (PNNL) under the supervision of Karin D. Rodland and Paul Piehowski. KSEA analyses were performed by Sara J.C. Gosline.

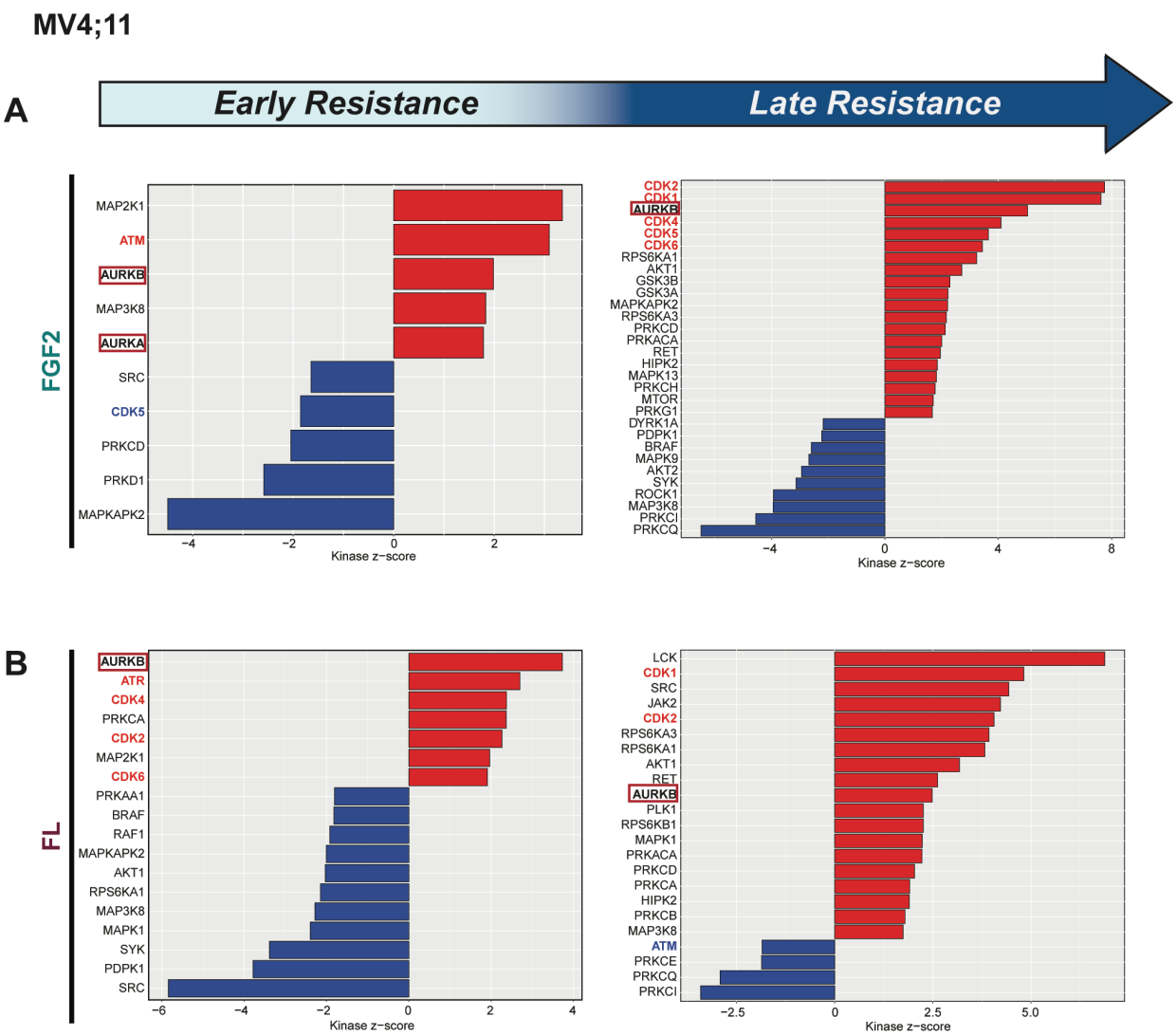

Supplemental Figure 13: Kinase-substrate enrichment analysis (KSEA) on MV4;11 gilteritinib resistant cell lines separated by ligand. A. KSEA ($p < 0.05$) on FGF2 early and late resistant cell lines. Bar plot of FGF2 early cells (left plot) shows decrease in CDK phosphorylation (blue) and increase in AURKB and AURKA (boxed). Late FGF2 cells (right plot) exhibit recovery in CDK phosphorylation (red) and increased MAPK and PI3K signaling. **B.** KSEA ($p < 0.05$) on FL early and late cell lines. FL early cells (left plot) show an increase in CDK (red) phosphorylation with a coinciding activation of ATR (red), transducer of DNA damage response. CDK phosphorylation (red) is more pronounced in late FL cells with a decrease in DNA damage response (i.e., ATM; right plot). Proteomics and phosphoproteomics were performed and analyzed in collaboration with the Pacific Northwest National Laboratory (PNNL) under the supervision of Karin D. Rodland and Paul Piehowski. KSEA analyses were performed by Sara J.C. Gosline.

Early gilteritinib resistance is dependent upon Aurora kinase B for cell cycle regulation

Our phosphoproteomic data strongly implicated that alterations in cell cycle contribute to early gilteritinib resistance. Accordingly, we analyzed the cell cycle profile of MOLM14 parental and early and late gilteritinib resistant cultures using propidium iodide (PI) staining of DNA content. As expected, short-term gilteritinib treatment for 24 or 48 hours essentially halts cell cycle (S and G_2/M) of MOLM14 parental cells (**Figure 6A**). Cell cycle analyses of FGF2 and FL early gilteritinib resistant MOLM14 cultures revealed a decrease in the number of cells entering S phase relative to untreated parental cells (**Figure 6A, C**), consistent with decreased activity of CDK2, 4, and 6 in phosphoproteomic profiling (**Figure 5C-D**). At the same time, the number of cells in G_2/M were relatively unchanged, suggesting an overall decrease in cell cycle progression (**Figure 6A, C**). To further distinguish actively cycling cells from non-cycling cells in G_0, cells were co-labelled with PI (x-axis) and Ki67 (y-axis), a marker of proliferating cells. Early resistant cultures had the highest percentage of non-cycling cells (**Figure 6B-C**). In contrast, late resistant cultures had a similar cell cycle profile to untreated parental MOLM14s (**Figure 6A, C**), despite their divergence in metabolic profile (**Figure 4D-E**). These data corroborate the predicted changes in cell cycle by phosphoproteomics analysis (**Figure 5C-D**).

The reduction of cell cycle in early resistant cultures suggested regulation by checkpoint molecules. We noted robust upregulation of Aurora kinases, which are key mitotic regulatory serine/threonine kinases, in both MOLM14 and MV4;11 resistant cultures, and Aurora kinase B (AURKB) activity in particular was significantly increased by KSEA analysis (**Supplemental Figures 11B, 12, 13**). We tested a specific AURKB inhibitor, AZD2811, in the FGF2 and FL early gilteritinib resistant MOLM14 cultures and found that these cultures were uniquely sensitive to AZD2811 alone, and in combination with gilteritinib (**Figure 6D-E, Supplemental Table 4**). AURKB is a critical component of the chromosomal passenger complex, which regulates spindle assembly and cytokinesis[443]. In comparison, pharmacologic inhibition of AURKA and AURKC

showed little activity in early resistance cultures, suggesting that early gilteritinib resistance is AURKB dependent (**Supplemental Figure 14A-H, Supplemental Table 4**). To confirm the specificity for AURKB, CRISPR-mediated knockout of AURKB was found to enhance sensitivity to gilteritinib in early resistant cell lines (**Figure 6F-G**), whereas CRISPR-mediated inactivation of AURKA or AURKC did not restore sensitivity to gilteritinib (**Supplemental Figure 14I-L**). As further confirmation, genetic deletion of AURKB by CRISPR rendered them insensitive to further inhibition by AZD2811, confirming the specificity of AZD2811 for AURKB (**Supplemental Figure 14M**).

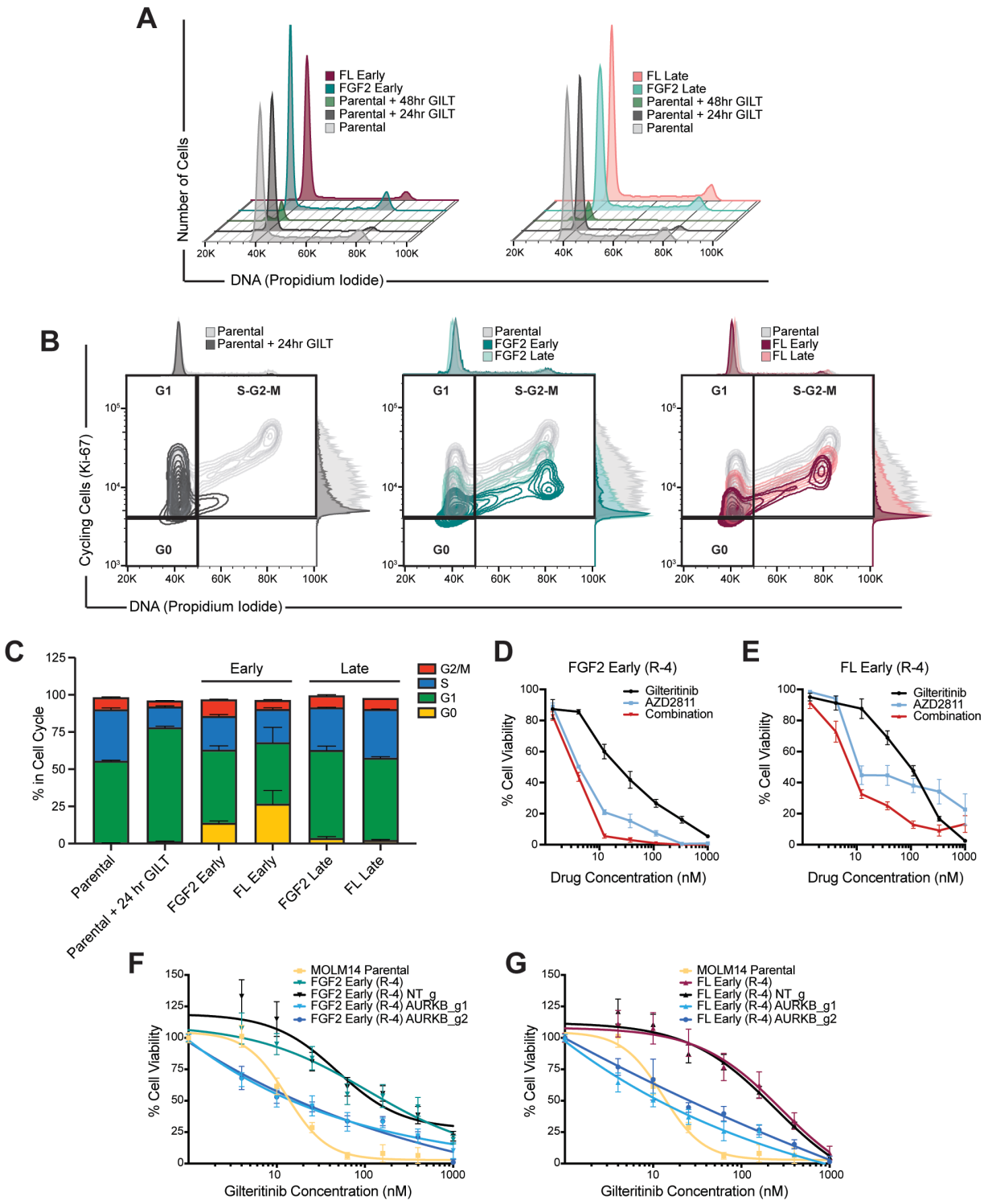

Figure 6: Early resistant cultures have a slower cell cycle and inhibition of AURKB resensitizes early resistant MOLM14 cells to gilteritinib. A. Representative cell cycle analysis profile of MOLM14 parental, treated with 100 nM gilteritinib for 24 and 48 hours, early, and late

resistant cultures maintained with 100 nM gilteritinib. Analyses were performed in triplicate using PI staining and flow cytometry. **B.** Representative contour plots are shown. Cell cycle (PI) plotted against proliferation (Ki-67) to determine G_0 vs G_1. **C.** Quantification of cell cycle profile shown in A and B. Percent of cells per phase ± standard deviation. **D-E.** FGF2 (D) and FL (E) early gilteritinib resistant MOLM14 cell lines were treated with the AURKB inhibitor, AZD2811, and gilteritinib as single agents or in combination. Viability was measured after 72 hours and normalized to untreated cells. Experiments were performed in triplicate. Mean ± standard error are plotted. **F-G.** CRISPR/Cas9 knockout of AURKB in FGF2 (H) and FL (I) early resistant MOLM14 cells restored gilteritinib sensitivity. Viability was measured in triplicate as stated above. Mean ± standard error are plotted.

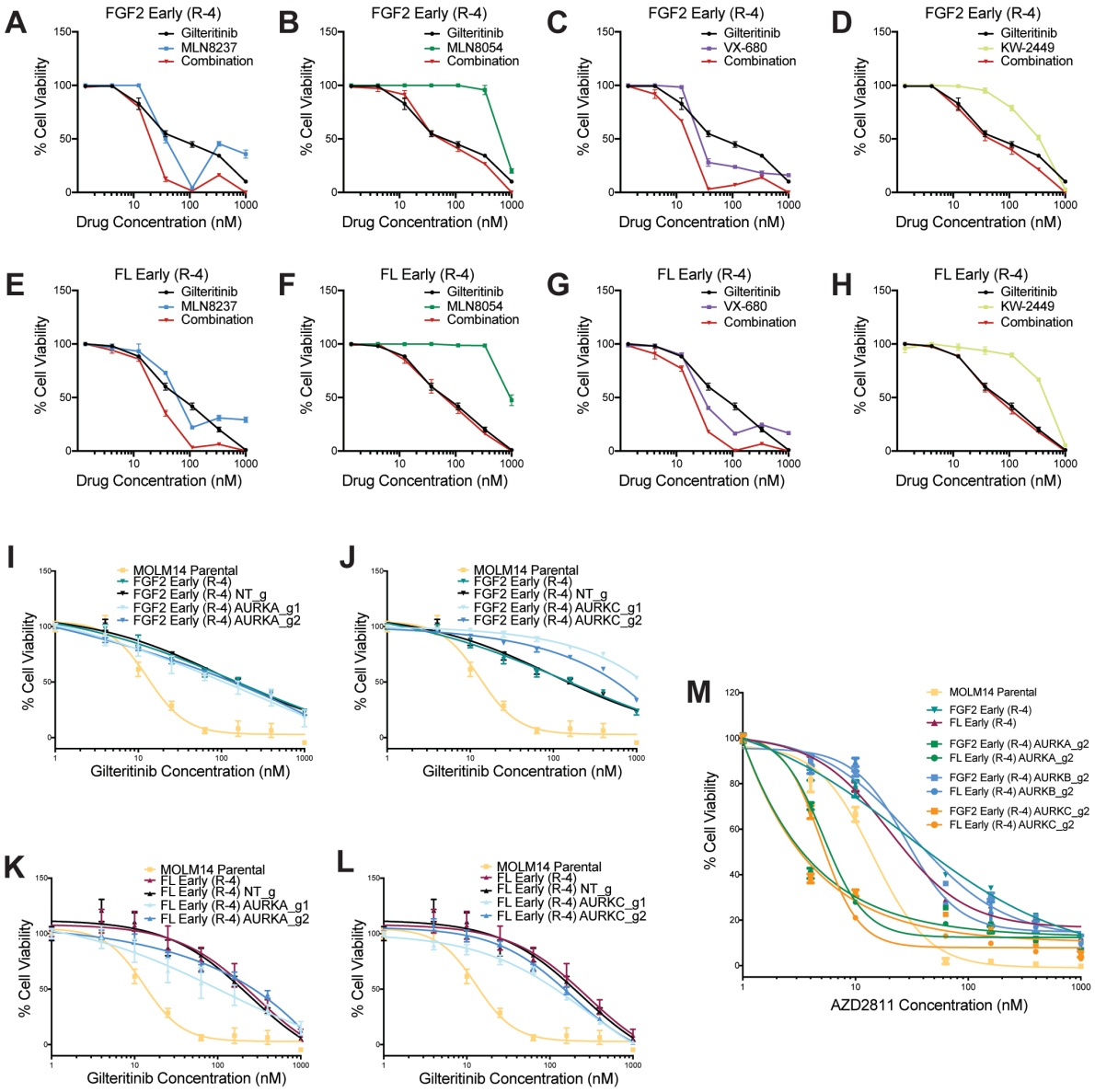

Supplemental Figure 14: Early gilteritinib resistant MOLM14 cells show selective AURKB dependency. A-H. Pharmacologic inhibition of AURKA (MLN8237, MLN8054, VX-680) and AURKC (KW-2449) does not enhance efficacy of gilteritinib (dark red line, 0 – 1000 nM) in FGF2 or FL early gilteritinib resistant (R-4) MOLM14 cell lines. Viability was measured after 72 hours by MTS assay. Inhibitor-treated wells were normalized to those of untreated cells. Experiments were performed in triplicate. Mean ± standard error are plotted. **I-L.** Similar to small-molecule inhibition of AURKA and C, inactivation via CRISPR/Cas9 gene editing, shows no enhancement in gilteritinib efficacy in early resistant MOLM14 cultures. Viability was assessed in triplicate and measured as described above. **M.** CRISPR/Cas9 inactivation of AURKB desensitized cells to AURKB small molecule inhibitor, AZD2811, demonstrating specificity of AZD2811 to AURKB. AURKA and AURKC inactivated cells were sensitive to AZD2811. Viability was assessed in triplicate and measured as described above. No gilteritinib was added in this experiment. Janét Pittsenbarger assisted in the small-molecule inhibitor experiments (A-H).

Model of early and late gilteritinib resistance is recapitulated in human disease

Clinically, early resistance to gilteritinib is characterized by low-level residual disease confined to the bone marrow, and late resistance by increasing leukemic burden and disease relapse. McMahon *et al.* have shown that NRAS mutations and activation of RAS/MAPK signaling is a frequent occurrence in patients with relapsed/refractory AML[164], which is recapitulated by the expansion of NRAS mutations in our late resistant cultures. To evaluate the clinical relevance of our early resistant cultures, we used primary cells from AML patients treated with gilteritinib on the Leukemia & Lymphoma Society supported Beat AML clinical trial (NCT03013998). We selected 12 patients who had both pre-treatment samples and paired samples after 1 or 2 months of gilteritinib. After gilteritinib, most patients still had detectable leukemia cells by flow cytometry, but the percentage of leukemia cells was often low (**Supplemental Table 5**). Given the limited number of patient cells, we developed a targeted proteomics panel of 123 proteins prioritized from our proteomic profiling of MOLM14 and MV4;11 resistant cultures (**Figure 5, Supplemental Figure 11, Supplemental Table 6**). This analysis was completed through the CPTAC.

Primary AML cells were enriched using $CD33^+$ and $CD34^+$ magnetic bead selection and analyzed by targeted proteomics. One patient sample was omitted due to low protein yield. Principal component analysis demonstrated a clear discrimination between the remaining 11 pre-treatment (PT) and early resistant (ER) samples (**Figure 7A**). Of the 123 proteins surveyed with targeted proteomics (**Supplemental Table 6**), 52 proteins were significantly altered between PT and ER samples ($q < 0.05$). Unsupervised hierarchical clustering analysis revealed significant alterations in three major signaling processes relative to PT samples: a prominent decrease in abundance of proteins that regulate cell cycle progression, including CDK1, CDK2, CDK4, and CDK9, an increase in MAPK signaling proteins, and an increase in proteins involved in fatty acid metabolism (**Figure 7B-C**).

Given the overlap in proteome signatures between early gilteritinib resistant cultures and patient samples, we hypothesized that AURKB inhibition could similarly re-sensitize patient AML cells to gilteritinib *ex vivo*. To this end, primary AML cells were selected from paired PT and ER patient samples (N = 4) as noted above, plated in HS-5 stromal cell conditioned media to mimic the marrow microenvironment[106, 185], and treated with gilteritinib and AZD2811 alone and in combination. Cell viability was evaluated after 3 days. Pre-treatment samples were relatively insensitive to gilteritinib or AZD2811 in the presence of HS-5 conditioned media. However, early resistant samples were strikingly sensitive to the combination of gilteritinib and AZD2811 (**Figure 7D**), mirroring results of early resistant cell cultures (**Figure 6D-E**).

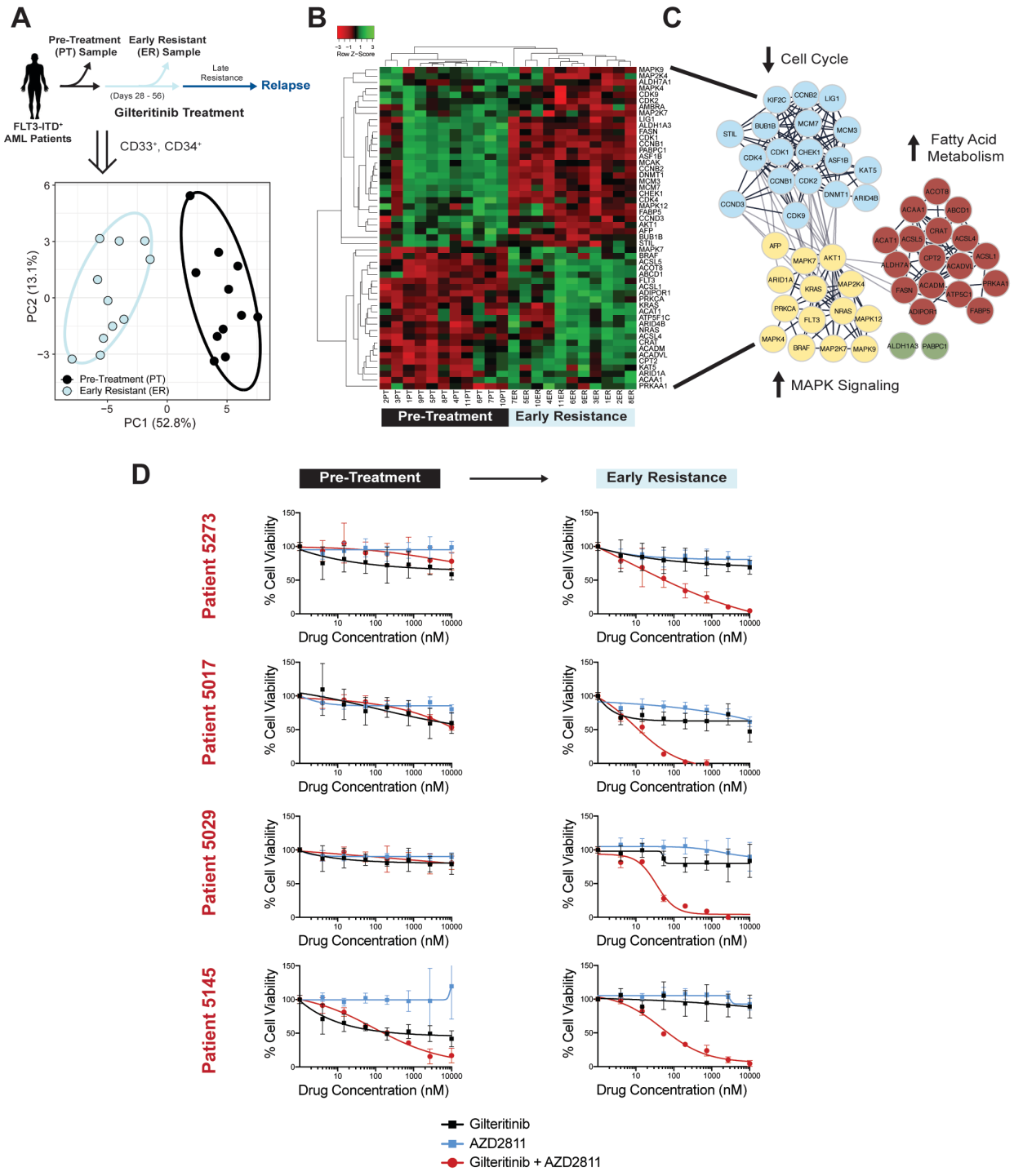

Figure 7: Targeted proteomics of primary early resistant AML samples shows reduced cell cycle proteins, increase in lipid metabolism proteins, and alterations in MAPK signaling proteins. *Ex vivo* treatment confirms AURKB vulnerability in early resistance. A. Pre-treatment (PT) and early resistant (ER) AML patient samples (N = 11) were enriched for leukemia cells by $CD33^{+}/CD34^{+}$ selection and underwent targeted proteomic analysis. PCA of normalized

peak intensity ratios shows clear segregation between PT and ER samples. **B.** Heatmap of unsupervised hierarchical clustering analysis of differentially-expressed proteins between PT and ER samples (N = 52, $q < 0.05$). **C.** Network cluster analyses of differentially-expressed proteins shows significantly altered clusters of proteins involved in cell cycle, fatty acid metabolism, and MAPK signaling. Glay (undirected)[444] was used to perform clustering analysis using STRING interactions[445] within the cytoscape interface[446]. **D.** AML cells from paired PT and ER patient samples (N = 4) were enriched with $CD33^+/CD34^+$ selection and treated with AURKB inhibitor, AZD2811 and gilteritinib as single agents or in combination. Viability was measured after 72 hours and normalized to untreated cells. Mean of triplicates ± standard deviation are shown. Targeted proteomics were performed and analyzed in collaboration with the Pacific Northwest National Laboratory (PNNL) under the supervision of Karin D. Rodland and Tao Liu (A-C). Elie Traer assisted with the selection of patient samples.

Discussion

Genetic alterations resulting in constitutively active receptor tyrosine kinases (ABL, EGFR, FLT3, HER2, TRK, etc.) often promote dependence upon these oncoproteins and their signaling pathways, a process known as "oncogene addiction"[57, 447]. This signaling addiction can be exploited therapeutically with targeted small-molecule kinase inhibitors. However, for most cancers, residual cells persist despite kinase inhibitor therapy and these early resistant cells are the seeds for eventual outgrowth of resistant clones and disease relapse. Mutations that either interfere with kinase inhibition or that activate accessory pathways are well defined and frequently found in late resistant cells. In contrast, the mechanisms that facilitate initial disease *persistence* are less well understood due to the paucity of early resistant cells and their relatively slow growth rate. Recent studies of other malignancies have shown that a subpopulation of "drug tolerant persister" cells are intrinsically more resilient to cancer drugs[154, 155, 157, 448, 449]. While the term persistent implies that the cells are merely static, our data show otherwise. We demonstrate that these cells are uniquely dependent upon survival factors in the AML microenvironment, grow more slowly, and rely on dynamic changes in lipid metabolism with increased sphingolipid/phospholipid and/or fatty acid/carnitine metabolism to survive. Therefore, we prefer the term early resistance to describe this active process. The adaptability of early resistant cells allows them time to evolve mechanisms that free them from their dependency on the marrow microenvironment, either by acquiring new resistance mutations or selecting for pre-existing variant alleles, a process which ultimately culminates in disease relapse. Targeting this reservoir of early resistant cells could yield a useful strategy to improve the durability of gilteritinib response.

Cell line models of resistance most commonly reproduce tumor-intrinsic changes, such as mutations[40, 137, 181, 450], rather than extrinsically-mediated, non-genetic adaptations that define early resistance in patients. By exposing AML cells to the microenvironmental ligands FGF2 and FL, we created a two-step model that captured unique features of early resistance, as well as the

evolution to late resistance (**Figure 1B**). Furthermore, it allows us to consider not only the features of early and late gilteritinib resistance as discrete events, but also as a continuous evolutionary process. Although the marrow microenvironment expresses a number of growth factors and cytokines that affect leukemia cells, FGF2 and FL reproduce two fundamental paradigms of resistance in FLT3 AML. FGF2 activates FGFR1 and downstream MAPK/AKT signaling in a classic accessory resistance pathway in AML[106, 150, 185], as well as other kinase-driven malignancies[107, 151, 152]. Conversely, FL leads to partial re-activation of FLT3 and downstream signaling of MAPK/AKT[106, 179]. Convergence of extrinsic signaling on the MAPK pathway serves as a critical feature of leukemia cells in the marrow microenvironment[104, 117]. Expression levels of both FGF2 and FL increase during development of resistance, indicating that the microenvironment is also dynamic during treatment[106, 107].

Our model shows that initial resistance to gilteritinib does not rely on activating NRAS mutations, in spite of their presence at low levels in early resistant cells (**Figure 2C**). Likewise, the introduction of activating NRAS mutations into MOLM14 cells (**Figure 2E-F**) did not immediately confer resistance, indicating that NRAS mutations alone are insufficient. Despite NRAS mutations in every cell, it took over a month for these cells to become fully resistant to gilteritinib. However, supplementation with FGF2 or FL greatly accelerated development of resistance, emphasizing that non-mutational, metabolic, and phenotypic adaptations during early resistance lay the groundwork for growth of late resistant cells. Although, McMahon *et al.* show that activating NRAS mutations are sufficient to confer gilteritinib resistance in MOLM14 cells, this may result from their use of 25 nM gilteritinib[164] as opposed our use of 100 nM. Our stepwise model also faithfully recapitulates the timing and dynamic changes that occur in AML patients on gilteritinib (**Figure 7B-C**). NRAS mutations are frequently found at relapse in AML, typically after 6 months of treatment[164, 383]. Indeed, we noted that an expansion of NRAS clones in late resistant MOLM14 and MV4;11 cultures (**Figure 2A-C, Supplemental Figure 1B**) occurred in an analogous timeframe to that observed in AML patients. Data from our CRISPR/Cas and proteomic

profiling further underscored the significance of NRAS/MAPK signaling in late resistance (**Figure 3C-D, 5E**). Mutations in the gatekeeper region (FLT3^{F691L} in particular) were also identified in some resistant cultures, which have also been shown to promote resistance in a subpopulation of patients[40, 137, 164, 383]. Taken together, our data support a scenario in which gilteritinib resistance follows a predictable, non-stochastic pattern: a non-mutational, early resistance phase that precedes an NRAS-driven late resistance phase.

Early gilteritinib resistant cells evolve a unique metabolic profile compared to parental MOLM14 cells (**Figure 4B-E**). Prior studies demonstrated that treatment with FLT3i quizartinib has an immediate effect on the metabolism of AML cells[451-453] and we confirm that this also applies to gilteritinib (**Supplemental Figure 7**). However, rescuing these cells with either FGF2 or FL did not restore the metabolome to that of the pre-treatment state. Rather, they induced distinct adaptations, indicating that the microenvironment has a strong influence on metabolism[454, 455] (**Figure 4**). CRISPR/Cas interrogation revealed that early resistant cells do not rely on a single metabolic pathway, suggesting a certain amount of metabolic flexibility (**Figure 3B, 4A).** Proteomic profiling of AML patient samples after gilteritinib treatment further corroborated alterations in metabolism in early resistance (**Figure 7B-C**). In contrast, the metabolome of late resistant cells diverged significantly further from parental MOLM14 cells (**Figure 4B**). FGF2 late resistant cultures had significant alterations in sphingolipid metabolism whereas FL late cultures preferentially utilized carnitine/fatty acid metabolism (**Figure 4D-I**). While these particular metabolic pathways were present in early resistance, they became more essential with the expansion of NRAS mutations in late resistance. How this metabolic memory is retained from early to late resistance warrants further investigation. Many previous studies have also shown that metabolic dependencies of cancer cells evolve to contribute to drug resistance. In particular, while leukemia stem cells (LSCs) rely on OXPHOS[456, 457], the source of energy varies in the setting of drug resistance[146-148]. Similarly, findings from our study bring to light the evolution of a unique metabolic program that parallels development of gilteritinib resistance.

Of note, LSCs also have a slower cell cycle[456], which is similar to what we discovered with our early resistant cultures (**Figure 6A-C**). A slower cell cycle may provide time for metabolic rewiring. Proteomic and phosphoproteomic analyses revealed both a profound decrease in cell cycle proteins during early resistance (**Figure 5C**) and validated many of the metabolic pathways identified by CRISPR/Cas and metabolomics. Remarkably, the protein alterations associated with a slower cell cycle and lipid metabolism in early resistant cells were reproduced by primary AML cells after gilteritinib treatment (**Figure 7B-C**). More in-depth analysis of proteomics revealed that activity of Aurora kinases, in particular AURKB, increased during early resistance (**Supplemental Figures 11-13**). Inhibition of AURKB activity with AZD2811 restored gilteritinib sensitivity in early resistant cell cultures and even more impressively in early resistant primary patient samples (**Figure 6D-E, 7D**). Pre-treatment leukemia cells from patients were minimally responsive to AURKB inhibition (**Figure 7D**), underscoring that AURKB dependency becomes a liability during early resistance. A similar process has been described in non-small cell lung cancer in which EGFR inhibitors induced activation of AURKA[156] and AURKB[443] during acquired resistance. In line with our early and late resistance model, Shah *et al.* demonstrated that AURKA activation maintains residual disease (tolerant phase) that then establishes a path to a mature resistance phenotype (acquired resistance phase)[156]. Collectively, these findings and those from our study support a conserved pathway of cell cycle regulation by the Aurora kinase family during early resistance.

AML patients usually respond to FLT3i initially, but residual disease in the marrow microenvironment eventually leads to development of drug resistance[12, 137, 168]. Recent studies have shown that resistant cells gain new sensitivities following initial therapy, a concept called collateral sensitivity[458] or antagonistic pleiotropy[459]. These new sensitivities can be exploited in combination therapy to enhance the efficacy of the initial agent. Of relevance, the expansion of NRAS mutations in late resistance offers one potential approach for combination therapy to overcome gilteritinib resistance. Both MEK and PI3K inhibitors partially restored gilteritinib efficacy

in late resistance (**Figure 3F-J**). These combinations have been proposed in AML[106, 137, 149, 164] and other cancers[460-462] to prevent resistance. However, it is unclear if the addition of these inhibitors would forestall the expansion of NRAS mutations or rather drive early resistant cells to adopt alternative resistance mechanisms. Only a third of patients treated with gilteritinib develop NRAS or KRAS mutations, which means that these genomic alterations are not the only mode of resistance[383]. For that reason, results from our study suggest that targeting early resistance may be more effective. Our multipronged approach demonstrates that the microenvironment drives both metabolic and cell cycle changes in early resistance that lay the foundation for late resistance. While targeting metabolic dependencies of early resistant cells is a promising strategy, the plasticity seen in our model and that of others[146-148, 463, 464] suggests that this may be challenging to target. This approach is also limited due to the lack of effective small-molecule inhibitors of metabolism. In contrast, irrespective of their unique metabolic profiles, our resistant cultures and primary early resistant AML cells were exquisitely sensitive to the combination of AZD2811 and gilteritinib (**Figure 7D**). Exploiting this unique vulnerability of early resistance may therefore thwart multiple mechanisms of late resistance and improve the durability of response to gilteritinib.

In conclusion, our stepwise, non-stochastic model of gilteritinib resistance recapitulates clinical resistance and provides a novel framework to interpret the evolution of resistance. The comprehensive cataloging of genomic, metabolomic, proteomic, and pharmacologic data provides a rich resource for further investigations of the complex evolution of drug resistance in AML. Our study also suggests that a more thorough understanding of how the marrow microenvironment contributes to early resistance will identify new treatment strategies to increase the depth and durability of FLT3i response.

Materials & Methods

Generation of ligand-dependent (early) and -independent (late) gilteritinib resistant cell lines

Human MOLM14 cells were generously provided by Dr. Yoshinobu Matsuo (Fujisaki Cell Center, Hayashibara Biochemical Labs, Okayama, Japan). Human MV4;11 cells were purchased from ATCC (Manassas, VA). Both cell lines were grown in RPMI (Life Technologies Inc., Carlsbad, CA) supplemented with 10% FBS (Atlanta Biologicals, Flowery Branch, GA), 2% L-glutamine, 1% penicillin/streptomycin (Life Technologies Inc.), and 0.1% amphotericin B (HyClone, South Logan, UT). Authentication was performed on all cell lines used in this study at the OHSU DNA Services Core facility.

To establish resistant cultures, 10 million MOLM14 or MV4;11 cells were treated with 100 nM of gilteritinib (Selleck Chemicals, Houston, TX) in media alone (N = 4) or in media supplemented with 10 ng/mL of FGF2 (N = 4) or FLT3 ligand (N = 4, FL; PeproTech Inc., Rocky Hill, NJ). All cultures were maintained in 10 mL of media. Every 2 or 3 days, recombinant ligands and gilteritinib were replaced and cell viability was evaluated using the Guava personal flow cytometer (Millipore Inc., Burlington, MA). Following ligand withdrawal, gilteritinib and media were similarly replenished and viability was monitored every 2 to 3 days. A list of all generated resistant cell lines is available in **Supplemental Table 1**. All cell lines were tested for mycoplasma on a monthly schedule.

Immunoblotting

Ten million from MOLM14 parental and gilteritinib resistant cell lines were spun down and lysed with 50 µL of Cell Lysis Buffer (Cell Signaling Technologies Inc., Danvers, MA) containing a Complete Mini Protease Inhibitor Cocktail Tablet, Phosphatase Inhibitor Cocktail 2, and phenylmethanesulfonyl fluoride (PMSF) solution (Sigma-Aldrich Inc., St Louis, MO) and clarified by centrifugation at 14,000 *g*, 4 °C for 15 minutes. Protein was quantified using a bicinchoninic

acid (BCA) assay (ThermoFisher Scientific Inc., Waltham, MA). 50 µg of each protein lysate was loaded on NuPAGE 4-12% Bis-Tris gradient gels (ThermoFisher Scientific Inc.), transferred on Immobilon-FL PVDF membranes (Millipore Inc.), and blocked for 1 hour. Following overnight incubation with primary antibody (**Supplemental Table 8**) at 4 °C, the membranes were washed and probed with fluorescent IRDye 800CW goat anti-rabbit IgG and IRDye 680RD Goat anti-mouse IgG antibodies (1:15,000; LI-COR Biosciences, Lincoln, NE). The membranes were then imaged with the Odyssey Infrared Imaging System (LI-COR Biosciences).

Whole Exome Sequencing

Genomic DNA for all cell lines was extracted using the DNeasy Blood & Tissue Kit (Qiagen Inc., Germantown, MD) according to the manufacturer's protocol. High throughput sequencing was performed on all MOLM14 and MV4;11 parental and late/ligand-independent gilteritinib resistant cell lines. Paired-end 100 base reads were generated using the Illumina HiSeq 2500 (Illumina Inc., San Diego, CA) for parental and gilteritinib resistant cell lines after capture with the Nextera DNA Exome kit v1.2. These data are publicly available at the Short Read Archive (PRJNA666471). Each sample was pre-processed using GATK 4.1[385] including alignment to build 37 (GRCh37) of the human genome using BWA[386]. Raw mutations were called for all replicates relative to the parental cell lines using MuTect2. The mutations were annotated using the Variant Effect Predictor v99.1[387]. The final set of mutations were: selected after limiting to those that passed filter, predicted to have a non-synonymous change or indel, seen in less than 1% of GNOMAD[388], and had at least 5 reads with a tumor variant allele frequency (VAF) of greater than 8%. Mutations were further manually curated excluding known problematic genes/mutations and adding back in a low frequency (VAF: 0.067) NRAS p.G12D for sample MOLM14 FL Late (R-2). All NRAS and FLT3 mutations were confirmed by Sanger sequencing with primers listed in **Supplemental Table 7**. Sequencing was performed using Eurofins (Louisville, KY) and analyzed using Sequencher and DNASTAR software.

Droplet Digital PCR

Digital Droplet PCR (ddPCR) reactions (20 µL) were prepared with 2X dUTP-free ddPCR supermix (Bio-Rad Laboratories Inc., Hercules, CA), 20X NRAS mutant (FAM) and wildtype (HEX) primer/probe set, and purified genomic DNA that contained approximately 60,000 copies (~200 ng) of NRAS. The following commercially available assays were validated and utilized: $NRAS^{G12D}$ (dHsaMDV2010095) and $NRAS^{G12S}$ (dHsaMDV2010093). To determine the limit of detection, known mutant $NRAS^{G12D}$ or $NRAS^{G12S}$ plasmids were titrated with $NRAS^{WT}$ plasmid. For all MOLM14 parental (N = 3) and resistant cell lines (N = 4 for FGF2-derived, N = 4 for FL-derived), genomic DNA was isolated at 0, 2, 5.5, and 8.5 months. The ddPCR reaction mixture and droplet generation oil were transferred to the Droplet Generator DG8 Cartridge (Bio-Rad Laboratories Inc.) and droplets were generated with QX200 ddPCR Droplet Generator (Bio-Rad Laboratories Inc.). Droplets were transferred to a 96-well PCR plate, heat-sealed, and placed in the C1000 Touch™Thermo Cycler (Bio-Rad Laboratories). Cycling conditions were as follows: 95°C for 10 min, 40 cycles of 94°C for 30 sec, 55°C for 1 min followed by 98°C for 10 min (ramp rate 2°C/sec). Results were analyzed and visualized by QuantaSoft™ software to determine variant allele frequency. All biological replicates were merged in downstream analysis.

Site-Directed Mutagenesis

All NRAS (G12D and G12S) mutations were introduced by site-directed mutagenesis using the QuikChange II XL kit (Agilent Technologies Inc., Santa Clara, CA) and primers listed in **Supplemental Table 2**. Mutagenesis primers were designed using the QuikChange Primer Design Program available through Agilent and purchased from Eurofins. Constructs were verified by Sanger sequencing with primers listed in **Supplemental Table 7**.

Lentivirus production and transduction

HEK 293T/17 cells were transfected using Lipofectamine-2000 (Life Technologies Inc.) with single transfer vectors in combination with packaging plasmids, psPAX2 (Addgene, #12260) and VSVG (Life Technologies Inc.). The following transfer vectors were obtained from Addgene: pLenti CMV GFP DEST 736-1 (#19732) and pLentiCRISPRv2 (#52961). NRAS WT, G12D, and G12S plasmids were made with the CMV GFP backbone. Viral supernatants were collected, filtered through 0.45 μM filters, and used for transduction as previously described[145]. Briefly, 0.5-1 mL of supernatant was spinoculated with $1x10^6$ cells in 2 mL of growth media in the presence of 10 mM Hepes (ThermoFisher Scientific Inc.) and 8 μg/ml of Polybrene (Santa Cruz Biotechnology, Dallas, TX.) using a six-well format. Centrifugation was carried out at 2600 rpm for 2 hrs at 35°C. Infected cells from either library or single guide RNAs were selected with appropriate antibiotics, (puromycin, 2 μg/ml or blasticidin, 10 μg/ml), for 5-7 days to achieve stable integration. Cells were used for downstream assays following 2-3 weeks post-transduction.

CRISPR/Cas9 resensitization screening & single gene inactivation by individual sgRNAs

Early and late gilteritinib resistant Cas9-expressing cells were generated using lentiCas9-Blast (Addgene, #52962). Loss-of-function screens were performed using the Kosuke Yusa[465] human genome-wide sgRNA library purchased from Addgene (#67989), as described[145], targeting 18,010 genes with 90,709 sgRNAs (average of 5 guides per gene). High titer lentivirus was generated using standard calcium phosphate precipitation procedures in HEK 293T/17 cells. Viral supernatant was concentrated and the titer was determined using a viral titration kit (ABM good, Canada).

100 million cells were used for viral transduction at MOI 0.3 using the above spinoculation protocol, selected with puromycin for 5-7 days to ensure stable viral integration. 5 million cells were collected to ensure library representation and overall cultures were grown to 120 million. 30 million transduced cells were separated in individual flasks and treated with DMSO or 100 nM of gilteritinib, in duplicate, for 14-21 days. For screens on early gilteritinib resistant Cas9-expressing

cells, screen cultures were maintained in 10 ng/mL of FGF2 or FL, respectively. 20-30 million cells were collected at each time point from each sample to ensure 300X representation of the library. Early and Late CRISPR PCR-amplified barcode libraries were generated as previously described[145] and deep sequencing was performed on the NovaSeq and HiSeq 2500, respectively (Illumina Inc.). These data are available at GEO (GSE158717).

The 100 base reads were trimmed leaving only the sgRNA sequences using cutadapt[466]. Alignments were performed with Bowtie2 relative to the database of sgRNA sequences requiring unique matches[467]. Read counts were then generated per sgRNA using MaGeCK count[468]. EdgeR was run after first filtering out lowly-represented sgRNAs (those not seen in the plasmid or those with ≤ 100 counts per million in more than half the samples of the comparison) generating log2 fold changes (gilteritinib treatment vs DMSO) and 2-sided P-values per sgRNA. The sgRNA-level statistics were summarized to gene-level by selecting the sgRNA with the middle P-value as a representative. Robust Rank Aggregation (RRA) was performed for both early and late gilteritinib resensitization screens after ranking genes by their mid P-value[437]. For the early CRISPR screens, as no overlapping genes were found, genes were prioritized using constituent sgRNA significance (median p value < 0.05) and average log fold change focusing on genes involved in metabolism, cell cycle alterations, MAPK or PI3K/AKT pathways.

Inactivation of individual genes was carried out by cloning sgRNAs into plentiCRISPRv2 (Addgene, #52961) per manufacturer's suggestion. All sgRNAs used in this study are provided in **Supplemental Table 9**. GraphPad Prism 8 was used to model dose-specific, normalized cell viability values with 4-parameter logistic regression curves to determine IC_{50}s.

Small-molecule inhibitor screening and analysis pipeline

Small-molecule inhibitors, purchased from LC Laboratories Inc. (Woburn, MA), MedChemExpress (Monmouth Junction, NJ), and Selleck Chemicals (Houston, TX) were reconstituted in DMSO and stored at -80°C. Cells were seeded into 384-well assay plates using

a Multidrop™ Combi Reagent Dispenser (ThermoFisher Scientific Inc.) at a density of 1,000 cells/well in 50 µL of RPMI media supplemented with 10% fetal bovine serum, 2% L-glutamine, 1% penicillin-streptomycin, and 0.1% amphotericin B. For inhibitor screening with early resistance cell lines, the media was supplemented with 10 ng/mL of FGF2 or FL, respectively. Inhibitors were dispensed into the plates with an HP D300e Digital Dispenser (Tecan, Mannedorf, Switzerland). A 7-point inhibitor dilution series was utilized with 2-fold or 3-fold concentration increments between adjacent doses. The final concentration of DMSO was ≤ 0.1% in all wells. All conditions were plated with at least three replicates. Each plate also included at least 32 “no cell” media-only wells as a negative control and 10 untreated wells utilized as a positive control. After three days of culture at 37°C in 5% CO_2, cell viability was inferred using a methanethiosulfonate (MTS)-based assay (CellTiter96 Aqueous One Solution; Promega) and absorbance (490 nm) was read between 3 to 24 hours after adding MTS reagent using a BioTek Synergy 2 plate reader (BioTek, Winooski, VT). MTS absorbances of inhibitor-treated wells were normalized to those of untreated cells.

For experiments with multiple MTS read times, the following quality control (QC) metrics were considered in choosing the optimal read time for analysis: positive to negative control well ratio, percentage of inhibitor wells with an absorbance value less than the negative control average, percentage of inhibitor wells with an absorbance value greater than the positive control average, and the median inhibitor- and dose-specific coefficient of variation (CV) computed on same-plate replicates. To enhance reliability of results, an inhibitor tested on a specific plate was excluded if had a raw absorbance median CV (across the 7 doses) greater than 10%. Entire experiments were discarded before inhibitor efficacy analysis and subsequently rerun if pre-MTS microscopic plate inspection or post-MTS QC parameters (including the above-mentioned metrics as well as the average difference in absorbance between positive and negative control wells and the negative control well CV) were deemed unreliable.

To allow inhibitor efficacy comparisons across plates and experiments, raw absorbance values in inhibitor wells were normalized to a plate's negative and positive controls (specifically, by subtracting the plate's average absorbance value for media-only wells, dividing by the plate's average absorbance value for untreated wells not on the plate edge, multiplying by 100, and bounding the resulting percentage at 0 and 100). These cell viability percentages were then averaged across the same-plate replicates at the inhibitor-specific dose level with standard errors of the mean computed for graphical display. Linear interpolation between observed dose-response values (i.e., $\log_{10}$-concentration on x-axis and normalized, replicate-averaged cell viability on y-axis) was employed to fit a line to each 7-point small-molecule inhibitor profile. The half-maximal inhibitory concentration (IC_{50}) and area under the curve (AUC) were derived from this line and used to quantify inhibitor effect. Fitted lines that did not intersect 50% cell viability were given an IC_{50} equal to the minimum or maximum drug concentration depending on if the entire line was below or above 50%, respectively. Since concentration ranges and dilution increments could vary by inhibitor, raw AUC values were transformed to percentages of the maximum possible AUC to improve interpretability. Summary of small-molecule inhibitor screening results is available in **Supplemental Tables 2** and **4**.

Metabolomics

High throughput metabolomics analysis was performed on frozen cell pellets from MOLM14 parental, short-term treated (48 hour), early, and late gilteritinib resistant cell lines at the University of Colorado School of Medicine Metabolomics Facility, a shared resource of the University of Colorado Cancer Center. Metabolites from frozen pellets were extracted at 2e6 cells per mL using ice cold 5:3:2 methanol:acetonitrile:water (v/v/v) with vigorous vortexing at 4°C followed by centrifugation as described[469]. Clarified supernatants were analyzed (10 µL per injection) by ultra-high-pressure liquid chromatography coupled to mass spectrometry on a Vanquish UHPLC (ThermoFisher Scientific Inc.) coupled to a Q Exactive mass spectrometer (ThermoFisher

Scientific Inc.) in positive and negative ion modes (separate runs). The UHPLC utilized a 5 min C18 gradient at 450 µL/min; eluate was introduced to the MS via electrospray ionization as previously described in detail[470]. Profiling of acylcarnitines was performed using a 15 min positive ESI method as described[471]. Data analysis and quality control measures were performed as described[469, 472]. Resulting data was analyzed using MetaboAnalyst 4.0, heat maps generated using GENE-E (Broad Institute), and individual metabolites plotted using GraphPad Prism 8.0. For PLS-DA shown in Figure 4C, data was first normalized to a pooled sample from the parental group and autoscaled in MetaboAnalyst 4.0. Data from Principal Component Analysis (PCA) in Supplemental Figure 8B was first normalized to median and autoscaled in MetaboAnalyst 4.0. Complete metabolite data is presented in **Supplemental Table 3**.

Seahorse assays

To measure changes in OXPHOS following etomoxir treatment, we used the Seahorse XF Long Chain Fatty Acid Oxidation Stress Test Kit (Agilent Technologies Inc., 103672-100) according to the manufacturer's protocol. MOLM14 parental and gilteritinib resistant cell lines were cultured in substrate-limited growth media (with final concentrations of 0.5 mM carnitine, 0.5 mM glucose, 1 mM glutamine, and 1% fetal bovine serum) overnight before performing assay.

Proteomics & phosphoproteomics on cell lines

Protein extraction and digestion

Parental (N = 4) and gilteritinib early (N = 4/ligand) and late (N = 4/ligand) resistant cell lines were washed three times with PBS to remove any trace of fetal bovine serum, pelleted, and flash frozen. All samples were processed in 3 batches of 22 samples. Fresh lysis buffer was prepared for each batch containing 8 M urea (Sigma-Aldrich Inc.), 50 mM Tris pH 8.0, 75 mM sodium chloride, 1 mM ethylenediamine tetra-acetic acid, 2 µg/mL Aprotinin (Sigma-Aldrich Inc.), 10 µg/mL Leupeptin (Roche, Pleasanton, CA), 1 mM PMSF in EtOH, 10 mM sodium fluoride, 1% of

phosphatase inhibitor cocktail 2 and 3 (Sigma-Aldrich Inc.), 20 μM PUGNAc, and 0.01 U/μL Benzonase. After adding 500 μL of chilled lysis buffer, the samples were vortexed for 10 seconds and then placed in thermomixer set for 15 minutes at 4°C and 800 rpm. The lysis step was repeated by vortexing samples for an additional 10 seconds and incubating for 15 minutes utilizing the same settings. After incubation, the samples were centrifuged for 10 minutes at 4°C and 18000 rcf to remove cell debris. Following centrifugation, the protein supernatant was transferred to a fresh tube. A BCA assay (ThermoFisher Scientific Inc.) was performed on the supernatant to determine protein yield.

Protein concentrations were normalized based on the BCA assay before the entire sample was reduced with 5 mM dithiothreitol (DTT) (Sigma-Aldrich Inc.) for 1 hour at 37°C and 800 rpm. Reduced cysteines were alkylated with 10 mM iodoacetamide (Sigma-Aldrich Inc.) for 45 minutes at 25°C and 800 rpm in the dark. The sample was diluted four-fold with 50 mM Tris HCl pH 8.0 and then initially digested with Lys-C (Wako Chemicals, Richmond, VA) at a 1:20 enzyme:substrate ratio, followed by an incubation for 2 hours at 25°C, shaking at 800 rpm. Following the initial digest, trypsin (Promega, Madison, WI) was added at a 1:20 enzyme:substrate ratio, followed by a 14-hour incubation set at 25°C and 800 rpm. The sample was quenched by adding formic acid (FA) to 1% and centrifuged for 15 minutes at 1500 rcf to remove any remaining cell debris. The peptides were desalted using a C18 solid phase extraction (SPE) cartridge (Waters Sep-Pak, Milford, MA). Global samples were vialed at 0.1 μg/μL and remaining peptides were pooled with previously cleaned peptides from previous experiment and aliquoted for TMT isobaric labeling (ThermoFisher Scientific Inc.).

TMT labeling

The samples were divided into four tandem mass tag-11 (TMT-11) plex sets, each with approximately 3 mg of total peptides. After drying down, each sample was reconstituted with 50 mM HEPES, pH 8.5 to a concentration of 5 μg/μL. Each isobaric tag aliquot was dissolved in 250

µL anhydrous acetonitrile to a final concentration of 20 µg/µL. The tag was added to the sample at a 1:1 peptide:isobaric label ratio and incubated in thermomixer for 1 hour at 25°C and 400 rpm and then diluted to 2.5 mg/mL with 50 mM HEPES pH 8.5, 20% acetonitrile (ACN). Finally, the reaction was quenched with 5% hydroxylamine and incubated for 15 minutes at 25°C and 400 rpm. The samples were then combined per each plex set and concentrated in a speed-vac before a final C18 SPE cleanup. Each 11-plex experiment was fractionated into 96 fractions by basic pH reversed phase liquid chromatography (bRPLC) separation, followed by concatenation into 12 global fractions for MS analysis[473, 474].

Phosphopeptide enrichment using immobilized metal affinity chromatography (IMAC)

Six samples per plex were created by concatenation from the 12 global TMT fractions. Fe^{3+}-NTA-agarose beads were freshly prepared for phosphopeptide enrichment using the Ni-NTA-agarose beads (Qiagen Inc.). Sample peptides were reconstituted to a 0.5 µg/µL concentration with 80% ACN, 0.1% TFA and incubated with 40 µL of the bead suspension for 30 minutes at RT in a thermomixer set at 800 rpm. After incubation the beads were washed with 100 µL 80% ACN, 0.1% TFA and 50 µL 1% FA to remove any non-specific binding. Phosphopeptides were eluted off beads with 210 µL 500 mM K_2HPO_4, pH 7.0 directly onto C18 stage tips and eluted from C18 material with 60 µL 50% ACN, 0.1% FA. Samples were dried in speed-vac concentrator and reconstituted with 12 µL of 3% ACN, 0.1% FA.

Liquid Chromatography (LC) coupled to tandem MS analysis

Proteomic fractions were separated using a Waters nano-Aquity UPLC system (Waters Inc.) equipped with a in-house 75 um I.D. x 25 cm length C18 column packed with 1.9 um ReproSil-Pur 120 C18-AQ (Dr. Maisch GmbH). A 100-minute gradient of 95% mobile phase A (0.1% (v/v) formic acid in water) to 19% mobile phase B (0.1% (v/v) FA in ACN) was applied to each fraction. The system was coupled to a Thermo Orbitrap Fusion Lumos mass spectrometer for MS/MS analysis. MS Spectra were collected from 350 to 1800 m/z at a mass resolution setting of 60,000.

A top speed method was used for the collection of MS^2 spectra at a mass resolution of 50K. An isolation window of 0.7 m/z was used for higher energy collision dissociation (HCD), singly charged species were excluded, and the dynamic exclusion window was 45 seconds.

TMT global proteomics data processing

All 60 Thermo.raw files were processed using mzRefinery to correct for mass calibration errors, and then spectra were searched with MS-GF+ v9881[475-477] to match against the RefSeq human protein sequence database downloaded on June 29, 2018 (hg38; 41,734 proteins), combined with 264 contaminants (e.g., trypsin, keratin). A partially tryptic search was carried out with a ± 20 ppm parent tolerance, allowed for isotopic error in precursor ion selection, and searched a decoy database composed of the forward and reversed protein sequences. MS-GF+ considered static carbamidomethylation (+57.0215 Da) on Cys residues and TMT modification (+229.1629 Da) on the peptide N terminus and Lys residues, and dynamic oxidation (+15.9949 Da) on Met residues. The resulting peptide identifications were filtered to a 1% false discovery rate at the unique peptide level. A sequence coverage minimum of 6 per 1000 amino acids was used to maintain a 1% FDR at the protein level after rollup by parsimonious inference.

The intensities TMT 11 reporter ions were extracted using MASIC software[478]. Extracted intensities were then linked to peptide-spectrum matches passing the confidence thresholds described above by scan number. The reporter ion intensities from different scans and different bRPLC fractions corresponding to the same gene were grouped. Relative protein abundance was calculated as the ratio of sample abundance to reference channel abundance using the summed reporter ion intensities from peptides that could be uniquely mapped to a gene. The relative abundances were log2 transformed and zero-centered for each gene to obtain final relative abundance values.

TMT phosphoproteomics data processing

The 30.raw files generated from enriched IMAC fractions were used for phosphopeptide identification as in the global proteome data analysis described above with an additional dynamic

phosphorylation (+79.9663 Da) modification on Ser, Thr, or Tyr residues. The phosphoproteome data were further processed with the Ascore algorithm[479] for phosphorylation site localization, and the top-scoring assignments were reported. For phosphoproteomic datasets, the quantitative data were not summarized by protein, but analyzed at the peptide sequence level. Because all peptides are labeled simultaneously, all technical biases upstream of labeling are assumed to be identical between global and phosphoproteomics datasets. Thus, to account for sample-specific biases in the phosphoproteome analysis, we applied the same correction factors derived from median-centering of the global proteomic dataset for normalization.

Data visualization, KSEA, & CausalPath analyses

PCA visualization was carried out using custom R scripts and packages from the Bioconductor project[480]. Plots were created using all proteins (phosphopeptides for phospho) with abundance ratios measured across all samples in the dataset. We used the Kinase Substrate Enrichment Analysis (KSEAapp) R package to infer kinase activity changes between early and late resistant MOLM14 and MV4;11 cells and their parental cell lines[440, 441]. We selected those kinases with significantly ($p < 0.05$) altered activity for visualization in Figure 5. Our analysis can be found on GitHub.

CausalPath was used to identify potential cause-effect relations between proteomic changes (global and phospho) by matching those changes with the signaling relations in pathway databases and checking the compatibility of the change directions with prior information in a site-specific manner. Readouts were compared using a T-test with 0.1 FDR threshold that was determined by the Benjamini-Hochberg method[442]. The data label randomization feature of CausalPath was used to detect activated and inhibited proteins (0.1 FDR) based on the enrichment of their effects on the downstream network. Network diagrams were generated via ChiBE[481, 482].

Cell cycle analysis

For each parental or gilteritinib resistant MOLM14 cell line, 1e6 cells were fixed in ice-cold 70% ethanol on ice for 20 minutes, washed in cold FACS buffer, and then stained with anti-Ki67 (BioLegend Inc, San Diego, CA) for 45 minutes on ice. After staining, cells were washed twice in FACS buffer and resuspended in FACS buffer containing 0.5 mg/mL PI dye. Cells were examined on BD LSRFortessa flow cytometer (BD Biosciences, San Jose, CA) and the results were analyzed in FlowJo version 9.

Targeted proteomics on AML patient samples

$CD33^+$ and $CD34^+$ leukemic blast cell isolation

All clinical specimens utilized in this study were collected with informed consent from patients with AML according to the Beat AML clinical trial protocol approved by the Western IRB and local institutional IRBs (Study of Biomarker-Based Treatment of Acute Myeloid Leukemia, NCT01728402, Dr. Traer is PI of S8 arm). Newly diagnosed elderly AML patients with activating FLT3 mutations were treated with gilteritinib as single agent for a month. If the percentage of leukemia cells remained < 5% in their marrow after 1 month, patients could continue gilteritinib monotherapy. Patients with > 5% leukemia cells in their marrow had decitabine added to their therapy. Frozen mononuclear cells from paired pre-treatment and on-gilteritinib treatment (early resistant) samples (N = 12) were thawed with DNase I (100 µg/mL; Stem Cell Technologies Inc., Cambridge, MA) and counted. $CD33^+$ and $CD34^+$ isolation was performed using EasySep Human CD33 and CD34 Positive Selection II Kits (Stem Cell Technologies Inc.) using the manufacturer's protocol. Following isolation, samples were counted and flash frozen for targeted proteomics.

Protein digestion

The samples were processed in a single batch to minimize technical variance. The digestion was carried out as described above for MOLM14 and MV4;11 cell line proteomics with the following modifications. The samples were lysed using 100 µL of chilled lysis buffer, and after incubation, placed in a magnetic rack to capture the magnetic beads before transferring the

supernatant to new tubes. Peptide yield was determined by BCA assay (ThermoFisher Scientific Inc.), and 0.5 µg/µL aliquots were prepared for heavy peptide spike-in.

Stable isotope-labeled peptides

Proteotypic peptides for the target proteins were selected for targeted proteomics analysis based on well-accepted criteria[483], and the corresponding crude heavy stable isotope-labeled peptides were synthesized with $^{13}C/^{15}N$ on C-terminal lysine or arginine (New England Peptide, Gardner, MA). The heavy peptides were dissolved individually in 15% ACN and 0.1% FA at a concentration of 2 mM and used for creating a peptide mixture with a final concentration of 5 pmol/µL for each peptide.

Selected reaction monitoring (SRM) assay development

The heavy peptides in the peptide mixture were evaluated for peptide response and fragmentation pattern using LC-SRM. For each peptide, transition settings were as follows: (1) precursor charges: 2, 3 and 4; (2) ion charges: 1, 2 and 3; (3) ion type: y; and (4) m/z window: 250-1500. Transition lists were generated with optimal collision energy values by Skyline software (Version 20.1)[484]. LC-SRM was then used to evaluate all heavy peptides for stability of peptide retention time, reliable heavy peptides identification, transition interferences, and endogenous peptide detectability. In the end, 3 transitions per peptide were selected for the final assay configuration for targeted quantitation of a total of 244 peptides of the 123 target proteins. **Supplemental Table 6** provides a list of all 123 targets studied.

LC-SRM

The digested patient samples were reconstituted in 2% ACN/0.1% FA and spiked with 5 fmol/µL heavy peptides for a final concentration of 0.25 µg/µL, and 2 µL of the resulting samples were analyzed by LC-SRM using a Waters nanoACQUITY UPLC system (Waters Inc.) coupled to a Thermo Scientific TSQ Altis triple quadrupole mass spectrometer (ThermoFisher Scientific Inc.). A 100 µm i.d. × 10 cm, BEH 1.7-µm C18 capillary column (Waters Inc.) was operated at a temperature of 44 ºC. The mobile phases were (A) 0.1% FA in water and (B) 0.1% FA in ACN.

The peptide samples were separated at a flow rate of 400 nL/min using a 110-min gradient profile as follows (min:%B): 7:1, 9:6, 40:13, 70:22, 80:40, 85:95, 93:50, 94:95 and 95:1. The parameters of the triple quadruple instrument were set with 0.7 fwhm Q1 and Q3 resolution, and 1.2 s cycle time. Data were acquired in time-scheduled SRM mode (retention time window: 15 min).

Data analysis and visualization

SRM data were analyzed using the Skyline software (Version 20.1)[484]. The total peak area ratios of endogenous light peptides and their heavy isotope-labeled internal standards (i.e., L/H peak area ratios) were exported for quantitation[485]. Peak detection and integration were carried out according to two criteria: (1) same retention time and (2) similar peak area ratios for the transitions. All data were manually inspected to ensure correct retention time, peak detection and accurate integration. After median centering normalization and student t-test, the significantly expressed proteins (N = 52) were determined by filtering with permutation-based false discovery rate control ($q < 0.05$)[484]. These normalized data were used for generation of heatmap and network diagram shown in **Figure 7B-C**.

Ex vivo inhibitor sensitivity assay with primary AML samples

S8 clinical trial patients treated at Oregon Health and Science University (Study of Biomarker-Based Treatment of Acute Myeloid Leukemia, NCT01728402, Dr. Traer is PI of S8 arm) were also consented to local research protocol and these samples were used for *ex vivo* treatments in Figure 7 (IRB 4422). Frozen mononuclear cells from paired pre-treatment and on-gilteritinib treatment (early resistant) AML patient samples (N = 4 pairs) were thawed with HS-5 stromal conditioned medium and DNase I (100 µg/mL; Stem Cell Technologies Inc.). To remove dead cells, Ficoll gradient centrifugation was utilized and cells were thereafter cultured overnight in HS-5 stromal conditioned media supplemented with StemRegenin 1 (500 nM) and UM729 (1 µM, Stem Cell Technologies Inc.)[486].

Isolated $CD33^+$ and $CD34^+$ cells were seeded into 384-well assay plates at 1,000 cells/well in 50:50 stromal conditioned media and RPMI-1640 media supplemented with fetal bovine serum (10%), L-glutamine, penicillin-streptomycin and antimycotic. Gilteritinib and AZD2811 were distributed in a 7-point concentration series ranging from 10 μM to 0.004 μM as single agents or in combination. The final concentration of DMSO was ≤ 0.1% in all wells. After 72 hours, viability was inferred with MTS reagent as described above (read times: 3 and 6 hours). Raw absorbance values were adjusted to a reference blank value, and then used to determine cell viability (normalized to untreated control wells to produce cell viability estimates). GraphPad Prism 8 was used to model dose-specific, normalized cell viability values with 4-parameter logistic regression curves to determine IC_{50}s.

Supplemental Tables

Table 1: MOLM14 & MV4;11 parental cell lines & gilteritinib resistant cultures					
Culture Name (Replicate #)	Whole Exome Sequencing (WES)	CRISPR/Cas9 Screening	Metabolomics	Proteomics & Phosphoproteomics	Small-Molecule Inhibitor Screening
MOLM14 Parental (R-1)	X		X	X	X
MOLM14 Parental (R-2)			X	X	
MOLM14 Parental (R-3)			X	X	
MOLM14 Parental (R-4)			X	X	
MOLM14 Parental with 48 hr GILT (R-1)			X		
MOLM14 Parental with 48 hr GILT (R-2)			X		
MOLM14 Parental with 48 hr GILT (R-3)			X		
MOLM14 Parental with 48 hr GILT (R-4)			X		
MOLM14 Parental with 48 hr GILT + FGF2 (R-1)			X		
MOLM14 Parental with 48 hr GILT + FGF2 (R-2)			X		
MOLM14 Parental with 48 hr GILT + FGF2 (R-3)			X		
MOLM14 Parental with 48 hr GILT + FGF2 (R-4)			X		
MOLM14 Parental with 48 hr GILT + FL (R-1)			X		
MOLM14 Parental with 48 hr GILT + FL (R-2)			X		
MOLM14 Parental with 48 hr GILT + FL (R-3)			X		
MOLM14 Parental with 48 hr GILT + FL (R-4)			X		
MOLM14 FGF2 Early (R-1)			X	X	
MOLM14 FGF2 Early (R-2)			X	X	
MOLM14 FGF2 Early (R-3)			X	X	
MOLM14 FGF2 Early (R-4)		X	X	X	X
MOLM14 FL Early (R-1)			X	X	
MOLM14 FL Early (R-2)			X	X	
MOLM14 FL Early (R-3)			X	X	
MOLM14 FL Early (R-4)		X	X	X	X
MOLM14 FGF2 Late (R-1)	X		X	X	
MOLM14 FGF2 Late (R-2)	X		X	X	
MOLM14 FGF2 Late (R-3)	X		X	X	
MOLM14 FGF2 Late (R-4)	X	X	X	X	X
MOLM14 FL Late (R-1)	X		X	X	
MOLM14 FL Late (R-2)	X		X	X	
MOLM14 FL Late (R-3)	X		X	X	
MOLM14 FL Late (R-4)	X	X	X	X	X
MV4;11 Parental (R-1)	X			X	
MV4;11 Parental (R-2)				X	
MV4;11 Parental (R-3)				X	
MV4;11 Parental (R-4)				X	
MV4;11 Parental (R-5)				X	
MV4;11 FGF2 Early (R-1)				X	
MV4;11 FGF2 Early (R-2)				X	
MV4;11 FGF2 Early (R-3)				X	
MV4;11 FL Early (R-1)				X	
MV4;11 FL Early (R-2)				X	
MV4;11 FL Early (R-3)				X	
MV4;11 FL Early (R-4)				X	
MV4;11 FGF2 Late (R-1)	X			X	
MV4;11 FGF2 Late (R-2)	X			X	
MV4;11 FGF2 Late (R-3)	X			X	
MV4;11 FL Late (R-1)	X			X	
MV4;11 FL Late (R-2)	X			X	
MV4;11 FL Late (R-3)	X			X	
MV4;11 FL Late (R-4)	X			X	

Supplemental Table 1: List of all MOLM14 and MV4;11 parental cell lines and early (ligand-dependent) and late (ligand-independent) gilteritinib resistant cultures generated and used in the different orthogonal approaches (whole exome sequencing, CRISPR/Cas9, metabolomics, proteomics & phosphoproteomics, and small-molecule inhibitor screening). All extended resistant cultures were maintained in 100 nM of gilteritinib and all early resistant cultures were additionally supplemented with 10 ng/mL of FGF2 or FL. When possible four biological replicates (R1-4) per cell line were generated. "X" indicates if a particular culture was used for a given assay.

Table 2: *Ex vivo* drug efficacy on late (ligand independent) gilteritinib resistant MOLM14 cultures

Late Gilteritinib Resistant Cultures:			FGF2 Early R-4: IC_{50} (nM)			FL Early R-4: IC_{50} (nM)			FGF2 Early R-4: AUC%*			FL Early R-4: AUC%*		
Inhibitor	**# of Expo. Plates**	**Concen. range (nM)**	Mono.	+ Gilt.	CR†	Mono.	+ Gilt.	CR†	Mono.	+ Gilt.	CR†	Mono.	+ Gilt.	CR†
Gilteritinib (FLT3)	**10**	**2 – 100**	**46.3**	**63.0‡**	**NA**	**47.5**	**48.3‡**	**NA**	**69.6 %**	**68.3‡ %**	**NA**	**70.4 %**	**68.6‡ %**	**NA**
Taselisib (PI3Kα)	3	2 – 100	100.0	17.4	0.27	91.6	15.7	0.25	76.5 %	55.7 %	0.79	68.7 %	51.7 %	0.75
Selumetinib (MEK1/2)	4	2 – 100	100.0	21.4	0.48	100.0	22.1	0.54	86.9 %	61.3 %	0.85	84.2 %	60.4 %	0.91
Trametinib (MEK1/2)	3	2 – 100, 0.2 – 10¥	10	19.2	0.88¥	10	30.4	0.54¥	72.1 %	55.8 %	0.80	76.3 %	57.1 %	0.80

Supplemental Table 2: Summary of IC_{50} values and area under the curve (AUC) for small-molecule inhibitor studies in late gilteritinib resistant MOLM14 cultures. Data presented in Figure 3F-I and Supplemental Figure 4. IC_{50} and AUC% values are medians and "Mono." refers to inhibitor monotherapy. AUC%* = area under the curve, as a percentage of the maximum possible AUC with log_{10} concentration (nM) on the x-axis and plate-normalized cell viability percentage on the y-axis. CR† = median Combination Ratio for the IC_{50} or the AUC%, calculated by dividing the IC_{50}/AUC% of the drug combination by the IC_{50}/AUC% of the more effective single agent (Gilteritinib or the non-Gilteritinib drug) for each plate and then taking the median. ‡There were 6 (not 10) experiment plates involving a double dose series of Gilteritinib. ¥Trametinib was plated at a higher dose range (2 – 100 nM) for one experiment and a 10-fold lower dose range (0.2 – 10 nM) for two experiments. Only the higher dose experiment was considered for the IC_{50} CR since this dose range matched the range used for Gilteritinib on the same plates. Each experiment of late Gilteritinib resistance included in this table had at least two same-plate replicates (range 2-5) for each drug. The IC_{50} and AUC were derived from a linear piecewise curve fitted to the replicate-averaged, normalized viability percentages for the 7 dose points.

Supplemental Table 3: Level of all metabolites detected following short-term (48 hour) and long-term gilteritinib treatment. Data presented in Figure 4D-E and Supplemental Figure 7. This table is not included in the dissertation due to size constraints but will be published with the final manuscript.

Table 4: *Ex vivo* drug efficacy on early (ligand dependent) gilteritinib resistant MOLM14 cultures

Early Gilteritinib Resistant Cultures:			**FGF2 Early R-4: IC_{50} (nM)**			**FL Early R-4: IC_{50} (nM)**			**FGF2 Early R-4: AUC%***			**FL Early R-4: AUC%***		
Inhibitor	**# of Expo. Plates**	**Concen. range (nM)**	Mono.	+ Gilt.	CR†	Mono.	+ Gilt.	CR†	Mono.	+ Gilt.	CR†	Mono.	+ Gilt.	CR†
Gilteritinib (FLT3)	**8**	**1 – 1000**	**60.3**	**26.1**	**NA**	**82.9**	**40.8**	**NA**	**58.9 %**	**49.1 %**	**NA**	**60.0 %**	**50.3 %**	**NA**
AZD2811 (AURKB)	5	1 – 1000	7.1	4.1	0.69	8.5	7.0	0.82	34.1 %	20.4 %	0.67	42.2 %	27.9 %	0.65
MLN8054 (AURKA)	2	1 – 1000	728.9	59.7	0.89	851.2	78	0.85	93.4 %	60.0 %	0.97	93.2 %	59.6 %	0.99
MLN8237 (AURKA)	2	1 – 1000	45.7	22.8	0.51	63.2	29.3	0.46	65.4 %	45.9 %	0.75	64.6 %	47.5 %	0.79
VX-680 (AURKA)	2	1 – 1000	36.6	19.3	0.55	38.9	22.3	0.59	58.8 %	42.7 %	0.74	57.5 %	42.4 %	0.74
KW-2449 (AURKC)	2	1 – 1000	365.4	55.2	0.82	468.6	81.2	0.87	79.3 %	57.9 %	0.94	83.3 %	59.4 %	0.98

Supplemental Table 4: Summary of IC_{50} values and area under the curve (AUC) for small-molecule inhibitor studies in early gilteritinib resistant MOLM14 cultures. Data presented in Figure 6D-E and Supplemental Figure 14A-H. IC_{50} and AUC% values are medians and "Mono." refers to inhibitor monotherapy. AUC%* = area under the curve, as a percentage of the maximum possible AUC with log10 concentration (nM) on the x-axis and plate-normalized cell viability percentage on the y-axis. CR† = median Combination Ratio for the IC_{50} or the AUC%, calculated by dividing the IC_{50}/AUC% of the equimolar drug combination by the IC_{50}/AUC% of the more effective single agent (Gilteritinib or the non-Gilteritinib drug) for each plate and then taking the median. Each experiment of early Gilteritinib resistance included in this table had same-plate triplicates for each drug. The IC50 and AUC were derived from a linear piecewise curve fitted to the triplicate-averaged, normalized viability percentages for the 7 dose points.

Table 5: Available Patient Information						
Patient ID	**Gender**	**Karotype**	**FLT3**	**Other genetic abnormalities***	**Blasts Cycle 1 (response)***	**Blasts Cycle 2**
5009	Male	Monosomy 7	ITD AR 0.92	WT1 Splice site 1002-1G>A 45.15%	5-20% blasts (PR)	2%
5017	Male	normal	ITD AR 0.10	TET2 M695fs*17 46.37%	50% (PD)	
5029	Female	normal	ITD AR 0.23		2% (CRi)	9%
5087	Male	normal	ITD AR 0.24	NPM1 W288fs*12 12.36% TET2 R1516* 13.71%	10% (SD)	
5104	Male	normal	ITD AR 0.18		40% (SD)	
5145	Male	normal	ITD AR 0.69	WT1 T377fs*73 22.79% WT1 R369fs*7 41.28%	4% (CRi)	8%
5155	Female	normal	ITD AR 0.47	DNMT3A Q696fs*9 38.87% IDH1 R132H 41.24% NPM1 W288fs*12 29.28%	(PD)	
5174	Male	ring chr 8	ITD AR 0.41 FLT3 N841T 5.07% FLT3 Y842C 1.13%	NPM1 W288fs*12 31.73%	40% (SD)	
5180	Male	normal	ITD AR 0.28 FLT3 E444V 21.36%		92% (PD)	
5186	Male	normal	ITD AR 0.06 FLT3 D835Y 1.69%		10% (SD)	
5210	Male	normal	ITD AR 0.21 FLT3 V491L 19.41% FLT3 N676S 2.82%	NPM1 W288fs*12 33.81% TET2 M1522R 47.96% WT1 R462Q 4.10%	2% (MLFS)	
5273	Female	normal	ITD AR 0.55 FLT3 N151S 49.03%	DNMT3A R882H 46.80% DNMT3A T835A 49.12%	3% (CRi)	

* Response assessed as per Cheson *et al.* JCO 2003. In order of response from best to worst: CR = complete response; CRi = complete response with incomplete hematologic recovery; MLFS = morphologically-free leukemia state (<5% blasts); PR = >50% reduction in blasts but 5-20% blasts in marrow with hematologic recovery; SD = stable disease; PD = progressive disease; AR = Allelic Ratio

Supplemental Table 5: Available clinical information on patients from AML gilteritinib trial (trial is ongoing and full results will be reported separately). The following patient samples from the LLS Beat AML gilteritinib trial (NCT03013998, S8 sub-study) were analyzed by targeted proteomic panel using pre-treatment (PT) samples and early resistant (ER) samples after either 1 to 2 months of gilteritinib monotherapy (samples used for ER are highlighted in blue). As part of the trial screening and assignment, a rapid genetics screen was performed within one week using cytogenetics and Foundation medicine panel focused on targetable mutations for the trial. Mutated FLT3 patients (ITD and TKD mutations) were eligible for gilteritinib monotherapy and had an initial bone marrow biopsy to evaluation response after one cycle (28 days). Patients were eligible to continue gilteritinib monotherapy if they had at least partial response (PR) or better. Blast percentages were reported by study sites, and/or by clinical response. If they did not achieve PR, they were eligible to receive gilteritinib + decitabine. PD = Progressive Disease; SD = Stable Disease. AR = Allelic Ratio. This table was prepared by Elie Traer.

Supplemental Table 6 - Targeted proteomics panel
ABCD1
ACAA1
ACAA2
ACADM
ACADVL
ACAT1
ACAT2
ACOT2
ACOT8
ACSF2
ACSL1
ACSL4
ACSL5
ACSS2
ADIPOR1
AFP
AKR1C1
AKT1
ALDH1A3
ALDH7A1
AMBRA
ANAPC1
ANAPC4
APOM
ARID1A
ARID1B
ARID2
ARID4B
ASF1A
ASF1B
ATF4
ATP5F1C
AURKA
AURKB
BAD
BARD1
BAX
BCL2

BECN1
BRAF
BUB1B
CBL
CCNB1
CCNB2
CCND3
CCNT2
CD36
CDK1
CDK2
CDK4
CDK5
CDK6
CDK7
CDK9
CENPU
CHEK1
CHMP4C
CPT1A
CPT1C
CPT2
CRAT
CTGF
CYBB
DNMT1
DNMT3A
DOT1L
E2F3
ETNK2
FABP4
FABP5
FASN
FLT3
GSK3B
HIPK2
KAT5
KRAS
LAMTOR4

LIG1
MAP2K1
MAP2K2
MAP2K3
MAP2K4
MAP2K5
MAP2K6
MAP2K7
MAP3K8
MAPK11
MAPK12
MAPK14
MAPK4
MAPK7
MAPK8
MAPK9
MAPKAPK3
MCAK
MCL1
MCM3
MCM7
MTOR
NEK6
NRAS
PABPC1
PDPK1
PIM1
PIM2
PPARA
PPARG
PRKAA1
PRKAA2
PRKAB1
PRKCA
PTPN11
PTPN12
RAF1
RARA
RXRA

RXRB
SGK1
SPRY3
SRC
STIL
TXNRD1
ZBTB7A

Supplemental Table 6: Targeted Proteomics Panel. 123 proteins were included in this panel based upon significant CRISPR/Cas9, CausalPath, KSEA, and small-molecule inhibitor screening data from resistant cell cultures. In addition, related-proteins in the signaling pathways were also selected for analysis. For example, if CausalPath suggested that expression of CPT1A was increased in early resistance, we also selected CPT1B, CPT1C, and CPT2 in our targeted analysis since these proteins function within a signaling family.

Table 7a: Sanger Sequencing Primers

Gene	Mutation	Forward Primer Sequence (5'→3')	Tm (°C)	Reverse Primer Sequence (5'→3')	Tm (°C)
FLT3	F691L/N701K	ACCCACAGACTTCACGGTGCCT	62.13	TCAGCAGAGAACCAAGCCCTCC	60.31
NRAS	G12D/G12S	GCATAGTGTTCGGCTTTGGG	59.55	AGTCTCGCTACTATGGCCTG	58.68
	G13D	AGGATCAGGTCAGCGGGCTACC	61.87	GCGGGGGTCCTTCCATTTGGTG	62.04
	Q61H	ACTCTGGTTCCAAGTCATTCCCA	57.45	TGAACTTCCCTCCCTCCCTGCC	61.7

Table 7b: Site-Directed Mutagenesis Primers

Gene	Amino Acid Change	Forward Primer Sequence (5'→3')	Tm (°C)	Reverse Primer Sequence (5'→3')	Tm (°C)
NRAS	G12D	GCTTTTCCCAACACCATCTGCTCCAAC CACCAC	80.38	GTGGTGGTTGGAGCAGATGGTGTTGGG AAAAGC	80.38
	G12S	CTTTTCCCAACACCACTTGCTCCAACC ACCACC	80.38	GGTGGTGGTTGGAGCAAGTGGTGTTGG GAAAAG	80.38

Supplemental Table 7: List of all Sanger sequencing (a) and site-directed mutagenesis (b) primers used in this study.

Table 8: Antibodies used in this study						
Target	**Antibody Product #**	**Vendor**	**Clone**	**Species**	**Antibody Dilution**	**Predicted Size (kDa)**
Phospho-Akt (Ser473)	9271	Cell Signaling		Rb	1:1000	60
Akt	9272	Cell Signaling		Rb	1:1000	60
Phospho-p44/42 MAPK (Erk1/2) (Thr202/Tyr204)	9101	Cell Signaling		Rb	1:1000	42, 44
p44/42 MAPK (Erk1/2)	9102	Cell Signaling		Rb	1:1000	42, 44
Phospho-Stat5 (Tyr694)	9351	Cell Signaling		Rb	1:250	90
Total Stat5	25656	Cell Signaling	D3N2B	Rb	1:1000	90
Phospho-FLT3 (Tyr589/591)	3464	Cell Signaling	30D4	Rb	1:1000	160
Phospho-FLT3 (Tyr842)	4577	Thermo Fisher	10A8	Rb	1:1000	160
Phospho-FLT3 (Tyr969)	3463	Cell Signaling	C24D9	Rb	1:1000	160
Total FLT3	3462	Cell Signaling	8F2	Rb	1:1000	130, 160
FGFR1	9740	Cell Signaling	D8E4	Rb	1:1000	92, 120, 145
FGF2	SC-79	Santa Cruz		Rb	1:500	20
FL	AB52648	ABCAM	EP1140Y	Rb	1:500	26
GAPDH	AM4300	Thermo Fisher	6C5	Ms	1:5000	39
IRDye 800CW Goat anti-Rabbit IgG	926-32211	LiCOR		Rb	1:15000	-
IRDye 680RD Goat anti-Mouse IgG	926-68070	LiCOR		Ms	1:15000	-

Supplemental Table 8: List of all antibodies used in this study.

Table 9: CRISPR sgRNAs		
Target Gene	**Guide Number**	**Sequence (5'→3')**
Non-Targeting (NT)	1	GGAGATATCAATCCTCCCGC
ACOT7	1	CCTCGAGGTGCCTCCTGTTG
ACOT7	2	CATTGCAACAGCCAGAACG
ACOX1	1	CACTCGCAGCCAGCGTTATG
ACOX1	2	CGCAGCCAGCGTTATGAGG
AURKA	1	TGAGTCACGAGAACACGTTT
AURKA	2	TAGGCTACAGCTCCAGTTGG
AURKB	1	GGGCACTTACGTTAAGATGT
AURKB	2	GGCAGGGTGCTCAGGCCAGA
AURKC	1	TCTCAATTTCCCGGCGCAGC
AURKC	2	TTTCAAAGTCATCGACTGTG
CCND1	1	CGAAGGTCTGCGCGTGTTTG
CCND1	2	CATTTGAAGTAGGACACCG
CENPU	1	CTGATGTCTCAAGCATTGGC
CPT1A	1	GCCAAGATCGACCCCTCGTT
CPT1C	1	CACATAATTGGACGCCCACC
CPT1C	2	TTAGTACCTGGAGTCGGTC
CPT2	1	CTTTAACCTCATTATCGCCA
CPT2	2	CAACGGAGTCTCGAGCAGAT
ELOVL5	1	AGTCGAAGGATCAGTTCGTG
ELOVL5	2	GTGTTTGTTACAGTCCAAA
ETNK2	1	GACCCGGACGACATCCTTCC
FOLH1	1	TGTGCATCATAGTATCCAAT
FOLH1	2	CGTGGAATTGCAGAGGCTGT
GNA13	1	CTTCGACCAGCGCGCGCGCG
GNA13	2	CATTCCTTGGGCTGCCATG
MAP3K7	1	AGAGCCTGATGACTCGTTGT
NDC80	1	CTCACGTTTGAGGGGTATAG
NDC80	2	GATCCCGGAATAGTCAACT
NEK6	1	TCACGCCGGGTGATGCACCG
NEK6	2	CCTGCATGCCAGCCTCACGA
NRAS	1	AGAAAACAAGTGGTTATAGA
PHGDH	1	TTTCTGCTTCAGGACTGTGA
PHGDH	2	TGGACGAAGGCGCCCTGCTC
PIK3CD	1	GCGCGAAAGTCGTTCACTTC
PMS1	1	AATCTGATGACGACTTGTTA
PMS1	2	ATACAACAAATTGACCCCA
PSMA3	1	ACTTGAAAAACTCTTCCGTC
PSMA3	2	GGTCTTACAGTGTGAATGA
PLTP	1	TGAGCAGGACCGTCCCTGCG
PLTP	2	ATGGGGAGTCAATCACTGC
RAP2C	1	CCCCTCCGTGCTGGAAATTC
RAP2C	2	CTACCGCAAAGAGATCGAAG

SAMHD1	1	GCTTAGTTATATCCAGCGAT
SCLY	1	TCCCCCCTATCATCTTCGCG
SERINC4	1	CTATTATGCAGCTGTGCCCG
SERINC4	2	ATGCTGTAGAATCCTAGGG
SGPL1	1	TAATTGCATGGAGTGTCGTG
SGPL1	2	GCAGACGCCTTCTGGCAAG
SMAD4	1	AACTCTGTACAAAGACCGCG
SMAD4	2	GGATTAACACTGCAGAGTAA
SMC4	1	ACCCTCATCGTGTTCAGTC
STIL	1	TAGCATGACGATAAGCAAGT

Supplemental Table 9: List of single guides tested in CRISPR/Cas validation studies.

Acknowledgements

We are extremely thankful to our patients for their time and precious tissue samples. We also thank Stephen Christy for organization of patient sample accrual, Setareh Sharzehi, Jack Sumner, Massively Parallel Sequencing Shared Resource, and Flow Cytometry core, and Francesca Cendali (University of Colorado) for technical support. The authors also thank Stephen E. Kurtz and TingTing Liu for helpful discussions and Robert L. Raffai (UC San Francisco) for critical review of the manuscript. AZD2811 was kindly provided by AstraZeneca. This work was supported by the American Cancer Society (MRSG-17-040-01-LIB) to E.T., the Clinical Proteomics Tumor Analysis Consortium (CPTAC; U01CA214116 and U24CA210955), the Drug Sensitivity and Resistance Network (DRSN; U54CA224019), and the Cancer Target Discovery and Development Network (CTD^2; U01CA217862) from the National Cancer Institute to K.D.R., B.J.D., T.L., and J.W.T. Additional funding was provided by the Howard Hughes Medical Institute, The Leukemia & Lymphoma Society, and the National Cancer Institute grant (R01CA214428) awarded to B.J.D. Portions of the proteomics research were performed using the Environmental Molecular Sciences Laboratory, a national scientific user facility sponsored by the Department of Energy's Office of Biological and Environmental Research that is located at the Pacific Northwest National laboratory (PNNL). S.K.J. is supported by the ARCS Scholar Foundation, The Paul & Daisy Soros Fellowship, and the National Cancer Institute (F30CA239335). T.N. is supported by the National Cancer Institute (R50CA251708). E.T. is supported by grants from the Leukemia & Lymphoma Society, Hildegard Lamfrom Physician Scientist Award, American Cancer Society, Cancer Early Detection Advanced Research Center, and the National Cancer Institute (U54CA224019). J.W.T. received grants from the V Foundation for Cancer Research, Gabrielle's Angel Foundation for Cancer Research, Mark Foundation for Cancer Research, Silver Family Foundation, and the National Cancer Institute (R01CA183947). A.D. acknowledges support from the Boettcher Webb-Waring Investigator Award, National Institute of General and Medical Sciences (RM1GM131968),

and National Heart, Lung, and Blood Institute (R01HL146442, R01HL149714, R01HL148151, and R21HL150032). A.D. and J.A.R., on behalf of the University of Colorado School of Medicine Metabolomics Facility, acknowledge shared resource support from the National Cancer Institute (P30CA046934).

Author Contributions

Study supervision: E. Traer

Conception and design: S.K. Joshi, T. Nechiporuk, P.D. Piehowski, J.A. Reisz, T. Liu, E. Traer

Development of methodology: S.K. Joshi, T. Nechiporuk, D. Bottomly, P.D. Piehowski, J.A. Reisz, Y.T. Wang, O. Babur, E. Demir, A. D'Alessandro, T. Liu, S.K. McWeeney, K.D. Rodland, E. Traer

Acquisition of data: S.K. Joshi, T. Nechiporuk, P.D. Piehowski, J.A. Reisz, J. Pittsenbarger, Y.T. Wang, J.R. Hansen, M.A. Gritsenko, C. Hutchinson, K.K. Weitz, T. L. Fillmore, J.E. McDermott, T. Liu, E Traer

Analysis and interpretation of data (e.g., statistical analysis, biostatistics, computational analysis): S.K. Joshi, T. Nechiporuk, D. Bottomly, P.D. Piehowski, J.A. Reisz, A. Kaempf, S.J.C. Gosline, Y.T. Wang, J. Moon, C.F. Tsai, A. A. Schepmoes, T. Shi, O.A. Arshad, J.E. McDermott, O. Babur, K. Watanabe-Smith, E. Demir, A. D'Alessandro, T. Liu, C.E. Tognon, J.W. Tyner, S.K. McWeeney, K.D. Rodland, B.J. Druker, E. Traer

Writing, review, & editing of the manuscript: S.K. Joshi, T. Nechiporuk, D. Bottomly, P.D. Piehowski, J.A. Reisz, J. Pittsenbarger, A. Kaempf, S.J.C. Gosline, Y.T. Wang, J.R. Hansen, M.A. Gritsenko, C. Hutchinson, K.K. Weitz, J. Moon, T. L. Fillmore, C.F. Tsai, A. A. Schepmoes, T. Shi, O.A. Arshad, J.E. McDermott, O. Babur, K. Watanabe-Smith, E. Demir, A. D'Alessandro, T. Liu, C.E. Tognon, J.W. Tyner, S.K. McWeeney, K.D. Rodland, B.J. Druker, E. Traer

Development of prioritization framework to assist in rigor and reproducibility: D. Bottomly, A. Kaempf, S.J.C. Gosline, S.K. McWeeney

PART IV:
Discussion & Future Directions

9 *Summary, perspective, & future directions*

"Don't let yourself be. Find something new to try, something to change. Count how often it succeeds and how often it doesn't. Write about it. Ask a patient or a colleague what they think about it. See if you can keep the conversation going."

— Atul Gawande

Leukemia is a dynamic disease that culminates from the concurrent dysregulation of multiple cellular processes. While the work presented in this dissertation is heavily focused on the dysregulation of RTKs, it is the interplay of several intrinsic and extrinsic modes of activation and/or resistance that orchestrate the development and progression of leukemia. Moreover, these intrinsic and extrinsic processes are broadly applicable to all cancers. In fact, our characterization of NTRK mutations in part II of this dissertation stems from the success of Trk inhibitors in solid malignancies[82]. The persistence of residual AML cells as examined in part III relies on extrinsic microenvironmental signaling and is applicable across a wide range of malignancies[153]. In this chapter, I briefly summarize our findings presented in the previous chapters, highlight concepts that I found intriguing, and accordingly suggest future directions. As I discuss below, the integration of genomic and transcriptomic information provided by single cell technologies will allow us to further dissect signaling mechanisms of intrinsic and extrinsic activation and resistance and, thereby facilitate the development of more-effective personalized therapies.

Intrinsic activation: Activating NTRK, ERBB2, and FLT3 mutations in hematologic neoplasms

Summary

Advances in molecular diagnostics and clinical sequencing technologies have paved the discovery of both new and known drivers of tumorigenesis. In part II of this dissertation, I described our discovery and characterization of oncogenic NTRK, ERBB2, and FLT3 mutations in hematologic malignancies. Although mutations in NTRK and ERBB2 are extremely rare (<1%) in liquid tumors, the availability of FDA-approved inhibitors that directly target them is a cause for excitement. Cells transformed by NTRK and ERBB2 mutations demonstrated robust sensitivity to FDA-approved Trk and ErbB2 inhibitors, respectively[487, 488]. While most treatment strategies focus on targeting well-known drivers of cancer, our work emphasizes the need to consider noncanonical activators which could be equally valuable in guiding treatment strategies. And for that reason, rigorous *in vitro* characterization, while laborious in nature, is necessary to determine if a given mutation has functional relevance. The activating mutations we report for NTRK and ERBB2 all fall outside the tyrosine kinase domain and exhibit oncogenic potential, debunking the common myth that mutations outside the tyrosine kinase domain are of minimal significance.

While intrinsic activation of RTKs can contribute to the initial malignancy as noted above with NTRK and ERBB2, it can also manifest resistance. Through *in vitro* characterization, we identified $FLT3^{N701K}$ as an activating mutation that confers resistance to the type I inhibitor gilteritinib. Similar to the FLT3 gatekeeper mutation F691L, N701K also sterically hinders the binding of gilteritinib, acting as a noncanonical gatekeeper. The N701K mutation showed minimal sensitivity to type I inhibitors midostaurin and crenolanib. It was strikingly more sensitive to the type II inhibitor quizartinib, suggesting that TKI class switching could serve as a promising avenue to mitigate development of gilteritinib resistance. The use of type I FLT3 inhibitors following the acquisition of resistance to type II inhibitors is a well-established approach to overcome resistance. However,

what makes the case with the N701K mutation interesting is acquired sensitivity to a type II inhibitor following development of resistance to a type I inhibitor, which is a largely underappreciated concept.

Perspective & future directions

Our work reiterates that functional characterization of oncogenic mutations is extremely informative in deciphering the genomic underpinnings of malignancies as it brings us closer towards the promise of delivering personalized cancer care. The availability of cell-based models (Ba/F3, NIH3T3, etc.) allows for rigorous yet rapid screening and prioritization of oncogenic mutations. However, this approach cannot be used as a standalone as these prioritized mutations often coexist in the presence of other known or unknown disease drivers, collectively culminating in the observed disease phenotype. For that reason, it is imperative that we examine both the functional relevance of a given mutation in the context of other genomic alterations and the structural change it may educe.

Although it was necessary for us to assess the oncogenicity of each NTRK and ERBB2 mutation separately, it does not fully recapitulate the underlying biology in the patients we prioritized. Chapter 4 of this dissertation discusses our characterization of the NTRK2^{R458G} mutation in a patient with CML[487]. This patient also harbored a BCR-ABL1^{T315I} mutation and exhibited insensitivity to known CML TKIs ponatinib, imatinib, dasatinib, and nilotinib. While we speculate that NTRK2^{R458G} may serve as a bypass resistance mutation in this setting, we are unable to conclude that from our solo assessment of NTRK2^{R458G}. Indeed, preliminary work from our lab has observed decreased sensitivity to ABL inhibitor treatment in BCR-ABL1^{T315I} cells engineered to co-express NTRK2^{R458G} (Eide *et al.*, unpublished). Future studies should consider the interplay of these and other mutations to understand the overall disease landscape. In the case of NTRKs, our recent work and that of others has shown that a loss of TP53 induces aberrant

activation of Trks[145, 251], further underscoring the value of studying genomic interactions in parallel. The order of mutation acquisition and/or co-occurrence could also enhance our understanding of the disease biology. For example, NTRK2^{R458G} could be a mutation that is accrued later in disease relative to BCR-ABL1^{T315I} based on the loss of response to CML TKIs that was observed. However, this is merely a speculation. Keeping with this, the resolution offered by single cell technologies could be informative here. Such technologies can resolve the co-occurrence of mutations, provide a greater appreciation for the clonal complexity in cancer cells, and trace the evolution/pre-existence of mutations.

The resultant structural changes that a mutation can introduce to RTKs can influence their function, regulation, and interactions with the neighboring environment. A major challenge in appreciating structural alterations is the unavailability of crystallized structures. For most RTKs, crystallized structures are available only for the tyrosine kinase domain. As our work demonstrates, mutations that arise outside the kinase domain can equally herald malignancy. There is a need to comprehend the structural impact of such mutations. Given the unavailability of a crystallized structure of the TrkB juxtamembrane domain, we were unable to fully appreciate the underlying biological changes brought forward by the R458G mutation. Using a molecular dynamics stimulation, we were able to hypothesize that a mutation in the juxtamembrane domain at residue 458 causes the TrkB receptor to adopt a new conformation that alters its interaction with the neighboring lipid nanoclusters of the cell membrane. As discussed in chapter 2, interactions with the neighboring lipid environment, prevents unwarranted RTK activity by maintaining the inhibitory switch of the juxtamembrane domain in place[34]. Future studies focused on characterizing activating or resistance mutations should examine structural alterations. Similar to advances in deep sequencing technologies to detect genomic changes, advances in protein crystallization reveal that modeling structural changes no longer seems to be a monumental undertaking. An artificial intelligence network developed by Google AI offshoot DeepMind has brought a tool that can predict protein 3D structure from its amino acid sequence[489]. One can

speculate that such technology will enhance our interpretation of a protein's function, its interactions with downstream effectors, predict the effect of structural modifications brought by genomic mutations, and importantly inform drug discovery efforts.

Extrinsic activation: The AML microenvironment catalyzes a step-wise evolution to gilteritinib resistance

Summary

In this section I summarize our examination of gilteritinib resistance from chapter 8 as our investigation on quizartinib resistance from chapter 7 provided the necessary framework.

Targeted kinase inhibitors have revolutionized oncology treatment, but the development of resistance limits their durability. In acute myeloid leukemia (AML), activating mutations in FLT3 are the most common genetic abnormality, found in >30% of AML patients. Multiple FLT3 inhibitors have been developed to target FLT3 in AML, including the drug gilteritinib, which is a potent FLT3 inhibitor recently approved by the FDA. However, AML patients only respond to gilteritinib for approximately six months due to the emergence of drug resistance. While gilteritinib efficiently eliminates peripheral blasts in the blood, residual blasts in the bone marrow microenvironment are able to survive, protected by cytokines and growth factors. Persistence of these residual cells represents "early resistance" to treatment. How these cells adapt to survive in the marrow microenvironment remains unclear. Over time, resistant subclones resume growth and lead to relapsed disease, often through the acquisition of intrinsic resistance mutations, what we term "late resistance."

In our study, we utilized a stepwise *in vitro* model that charts the temporal evolution of early to late gilteritinib resistance. Experimentally, we recapitulated early resistance with exogenous

microenvironmental ligands, FGF2 and FL, that allow cells to become resistant to gilteritinib in a ligand-dependent manner, without the need for resistance mutations. Once the ligands are removed, the cells became transiently sensitive to gilteritinib again, but eventually there was a clonal expansion of NRAS resistance mutations that drove late, intrinsic resistance. To understand the mechanisms of evolution from early to late resistance, we used a comprehensive approach that includes whole exome sequencing, CRISPR/Cas9 screening, proteomics/phosphoproteomics, metabolomics, and small-molecule inhibitor screening.

Early resistance is characterized by slowly dividing cells and metabolic reprogramming, particularly with respect to lipid metabolism. Early resistant cultures also became uniquely dependent on Aurora kinase B (AURKB) for survival. We then validated these pathways using primary AML cells from patients treated with gilteritinib and found that early resistant cells, protected in the marrow microenvironment, demonstrated reduced cell cycle and alterations in lipid metabolism. Primary early resistant AML cells also became dependent on AURKB signaling, and were exquisitely sensitive to the combination of AURKB inhibitors and gilteritinib. In contrast, late resistant cells were characterized by an expansion of pre-existing NRAS mutant subclones, which became the primary driver of late resistance. Despite the expansion of NRAS mutations, metabolic reprogramming continued to evolve in late resistance with further dependence upon lipid metabolism. The timeframe and expansion of late NRAS mutations observed in our model is analogous to the acquisition of NRAS resistance mutations in gilteritinib-treated AML patients[164].

The strength of our data derives from the complementary approaches that converge to reveal the biology underlying early and late resistance and how closely it recapitulates resistance in AML patients. Our work strongly supports the notion that resistance is a non-stochastic process, which was nicely captured by our use of a two-step model that is clinically relevant. While mutagenesis screens are informative in identifying mutations that confer resistance, they are unable to depict the order of events and bottlenecks that precede the establishment of full resistance. Our approach allowed us to define a unique vulnerability to AURKB inhibitors in early resistance. By

targeting early resistance, it may be possible to thwart the expansion of late resistant NRAS clones and improve the durability of FLT3 inhibitors.

Perspective & future directions

It is often thought that resistance is simply manifested by the acquisition of sequential intrinsic genomic alterations. However, there is accumulating evidence that resistance also leverages extrinsic signaling processes that occur concomitantly with intrinsic processes[153]; they are not mutually exclusive and should be studied in parallel. Notably, our work on understanding gilteritinib resistance provides a greater appreciation for extrinsic signaling (1) as a mode of RTK activation and (2) as a mediator of resistance and persistence disease. While most studies in AML resistance have focused on defining intrinsic mutations that signify disease relapse[40, 137, 164, 182], our work shifts the paradigm and emphasizes the need to understand the biology of residual (persistent) AML cells that form the basis of relapse with the goal of improving the success of FDA-approved therapies. Residual cells are protected by extrinsic survival signals purveyed by the tumor microenvironment among other mechanisms. Previous treatment approaches to addressing resistance have centered on the sequential use of single inhibitors or inhibitor combinations to target intrinsic signaling pathways as determined from the mutational profile of a patient at relapse[137, 164]. A focus on targeting residual disease may circumvent or delay the development of full resistance, thereby moving away from our conventional '**reactive**' strategy of combating resistance and disease relapse to adopting a more '**proactive**' approach in monitoring and intercepting earlier in the disease course. Albeit, this requires knowledge of the underlying biology that characterizes persistent or early resistant AML cells. To this end, our work and that of others has begun to define the fundamental properties of these cells that can be therapeutically exploited.

I believe we were successful in the answering the initial question that we set out to investigate: what confers gilteritinib resistance and what combinatorial strategy can be used to prevent or

delay the development of resistance? In relation to Stephen Paget's "soil and seed" hypothesis, our work heavily focused on defining the persistent 'seed' cells that bring about resistance[86]. Equally important, our findings provided insight on the plausible role of the marrow microenvironment 'soil' in nurturing these persistent AML cells. Given these findings, I am now interested in further exploring the following two directions (**Figure 1**).

1. *Performing a comprehensive examination of the stromal microenvironment to identify other protective factors that communicate with leukemia cells and confer resistance. An understanding of the pathological stromal landscape will enable development of therapies that abrogate these protective signaling pathways to improve treatment outcomes.*

2. *Defining metabolic dependencies of leukemia cells to reveal pharmacologically actionable targets that can be exploited in the clinic. Given that recent studies[464, 490] have suggested that metabolomic reprogramming may emanate from the stromal microenvironment, the nutritional role of AML stroma should be explored.*

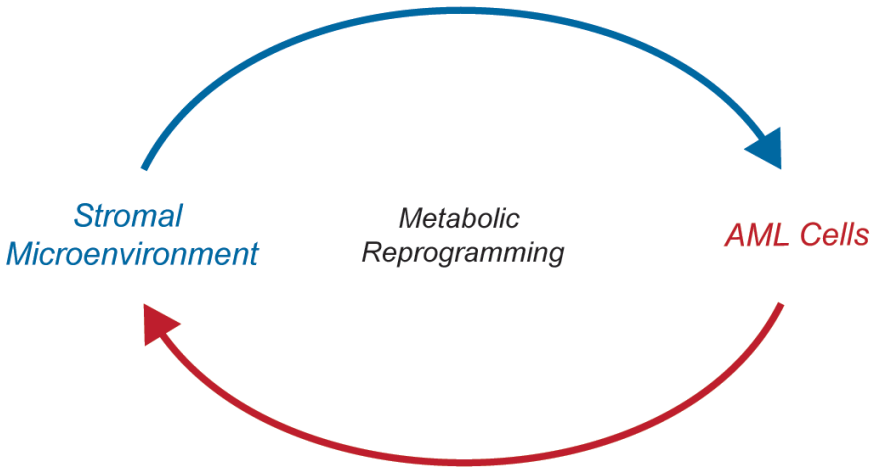

Figure 1: Schematic highlighting the importance exploring the crosstalk between AML cells and stromal microenvironment. Apart from protection facilitated by growth factors or cytokines, the microenvironment may also provide nutritional support to AML cells.

While I limit my discussion below to AML, these concepts apply to both liquid and solid tumors. I also acknowledge that such ideas would need to be developed further and focused for purposes of grant applications. However, I broadly discuss these ideas below as I believe that a comprehensive understanding of the stromal microenvironment and metabolism are needed before delving deeper into specific pathways to gain a full appreciation of the landscape that contributes to the AML phenotype. Where appropriate, I also include unpublished data to support these ideas.

(i) Resolving heterogeneity of the dynamic stromal microenvironment

The tumor microenvironment, in particular the crosstalk between leukemia cells and bone marrow mesenchymal stromal cells, has been implicated to be critical for both cancer development and drug resistance. Particularly, previous work from our laboratory[106, 396] and that of others[108, 117, 190-194, 490] has shown that mesenchymal stromal cells found within the AML microenvironment contribute significantly to the development of drug resistance by upregulating survival pathways and/or providing nutritional support to leukemia cells. In parallel to leukemia cells, our work suggests that the stromal microenvironment is also dynamically changing. Yet, this idea seems to be under investigated. No published study thus far has examined heterogeneity among mesenchymal stromal cells and how it could contribute to AML initiation, progression, and development of drug resistance. Insight into the pathological stromal landscape could guide the development of therapeutics to overcome microenvironmentally-mediated resistance.

Single-cell RNA-sequencing provides one promising approach to resolve the heterogeneity of the stromal microenvironment as evidenced from the work of Tikhonova *et al.*[491] and Severe *et al.*[492] who characterized AML stroma using elegant mouse models. However, a major limitation of single-cell RNA-sequencing on fresh patient samples is the inability to capture a sufficient number of stromal cells due to the size constraints (diameter of ~ 50 microns) of the current microfluidics technology offered by 10X Genomics. Given that stromal cells can be cultured on plastic for weeks

before undergoing senescence, this provides another promising avenue to study heterogeneity of stroma over time in a patient. However, the major challenge in pursuing this approach is our limited understanding of what surface markers and internal proteins constitute stromal cells. As discussed in Chapter 2 of this dissertation, in 2006 the International Society for Cellular Therapy defined mesenchymal stromal cells as having the following three markers among other criteria: CD73, CD90, and CD105[118]. Despite this definition, an in-depth understanding of stromal biology in the context of AML is warranted.

Given the cost of single-cell RNA-Sequencing and other limitations (cell size, viability, etc.), deconvolution of bulk RNA-sequencing data has emerged as a promising method to digitally dissect heterogeneity among bulk populations of cells[493]. With respect to studying how AML stroma changes over time, deconvolution could serve as a first step to unmask the heterogeneity among stromal subsets and mitigate the challenges posed by single-cell technologies. Deciphering the subpopulations of stromal cells may reveal other extrinsic, non-genetic factors that may support cancer growth or underpin resistance to cancer therapies at different stages of disease (**Figure 2**). Another method to study the contribution of the stromal microenvironment entails examining its direct communication with leukemia cells. Such cell-to-cell communication can now be inferred using computational tools such as CellPhoneDB, CellChat, ICELLNET, and etc. that use a collated list of known ligand-receptor interactions to reveal aspects of disease biology[494].

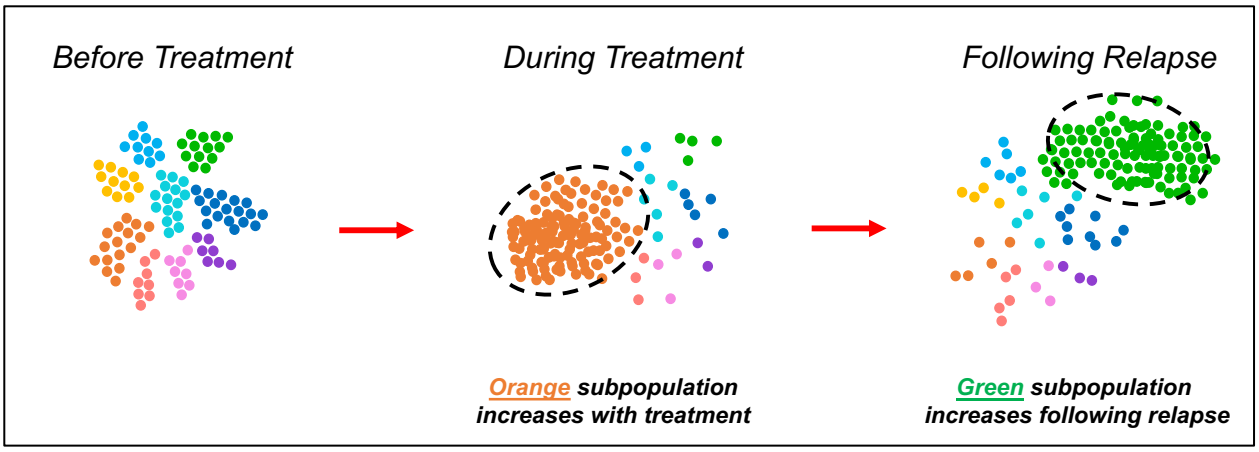

Figure 2: Successful cataloging of stromal subpopulations could provide insight on the dynamic reprogramming that occurs within the stromal microenvironment during the disease process. Different colored dots represent stromal subpopulations.

(ii) Metabolic reprogramming

While most cancer research has largely focused on defining genomic alterations (mutated oncogenes or tumor suppressors) that cause tumorigenesis, an interest in understanding how cancer cells hijack cellular metabolism to support their proliferation and survival has garnered interest in the last decade. However, it would be appropriate to say that the association of metabolism and cancer has been long known and exploited, yet its complexity has been difficult to study. In fact, the backbone of most chemotherapy regimens consists of inhibitors such as cytarabine, 5-fluorouracil, 6-mercaptopurine, etc. that target metabolic constituents[495]. For that reason, it is predictable that targeting metabolic dependencies could be of therapeutic utility. In the past decade, multiple studies have identified various metabolic processes that may have gone awry in the setting of AML. In **Table 1** and **Figure 3**, to my knowledge, I provide a comprehensive list of these studies. Many studies in AML have focused on the importance of glucose[496-498] as the preferred energy source owing to the observation made by Otto Warburg in 1927 that cancer cells upregulate glycolysis under aerobic conditions, also known as the Warburg effect[499, 500]. However, more recent studies have brought to light that de novo AML cells have a dependency upon redox

metabolism[451, 501] or oxidative phosphorylation (OXPHOS)[451, 456, 457, 502-504], challenging the assumptions of the Warburg theory. In respect to OXPHOS, several studies have revealed the importance of amino acids (glutamine, arginine, serine)[452, 457, 503, 505-507], vitamins[463], nucleotides[508], and fatty acids[502, 509-515] as reliable sources of energy for AML cells. Importantly, the source of OXPHOS can also differ in the context of resistance[146-148, 451] (**Figure 3**).

Table 1:			
Model	**Metabolism Pathway**	**Citation**	**Year**
AML cell lines	Glycolysis	Samudio *et al.*, Cancer Res., 2008. PMID: 18593920	2008
AML patient blasts	Glycolysis	Chen *et al.*, Blood, 2014. PMID: 25006128	2014
AML mouse model	Glycolysis	Wang *et al.*, Cell, 2014. PMID: 25215489	2014
AML cell lines	Glycolysis	Chen *et al.*, Cancer Cell, 2016. PMID: 27746145	2016
AML patient blasts, cell lines, xenograft	Glycolysis	Ju *et al.*, Leukemia, 2017. PMID: 28194038	2017
AML patient blasts, cell lines, xenograft	Glycolysis	Poulain *et al.*, Leukemia, 2017. PMID: 28280275	2017
AML patient blasts and cell lines	Glycolysis	Zhang *et al.*, J Cell BioChem., 2018. PMID: 29663500	2018
AML blasts from patients, cell lines	Glycolysis	Robinson *et al.*, Cancer Res., 2019. PMID: 31862780	2019
AML patient blasts, cell lines, xenograft	Glycolysis	Qing *et al.*, Mol Cell., 2021. PMID: 33434505	2021
AML patient blasts and cell lines	Oxidative phosphorylation	Skrtic *et al.*, Cancer Cell, 2011. PMID: 22094260	2011
AML patient blasts and cell lines	Oxidative phosphorylation	Chan *et al.*, Nat Med., 2015. PMID: 25599133	2015
AML patient blasts and cell lines	Oxidative phosphorylation	Cole *et al.*, Cancer Cell, 2015. PMID: 26058080	2015
AML patient blasts	Oxidative phosphorylation	Liyanage *et al.*, Blood, 2017. PMID: 28283480	2017
AML patient blasts and cell lines	Oxidative phosphorylation	Molina *et al.*, Nat Med., 2018. PMID: 29892070	2018
AML patient blasts and cell lines	Oxidative phosphorylation	Baccelli *et al.*, Cancer Cell, 2019. PMID: 31287994	2019
Resistant AML patient LSCs	Oxidative phosphorylation	Pei *et al.*, Cancer Discov., 2020. PMID: 31974170	2020
AML patient LSCs and blasts	Oxidative phosphorylation	Presti *et al.*, Blood Adv., 2021.	2021
AML patient LSCs	Amino acid metabolism	Lagadinou *et al.*, Cell Stem Cell, 2013. PMID: 23333149	2013
AML cell lines	Amino acid metabolism	Willems *et al.*, Blood, 2013. PMID: 24014241	2013
AML patient blasts and cell lines	Amino acid metabolism	Mussai *et al.*, Blood, 2015. PMID: 25710880	2015
AML patient blasts and cell lines	Amino acid metabolism	Jacque *et al.*, Blood, 2015. PMID: 26186940	2015
AML cell lines	Amino acid metabolism	Gregory *et al.*, Exp Hematol., 2018. PMID: 28947392	2018

AML patient LSCs	Amino acid metabolism	Jones *et al.*, Cancer Cell, 2018. PMID: 30423294	2018
AML cell lines	Amino acid metabolism	Ni *et al.*, Nat Metab., 2019. PMID: 31535081	2019
AML cell lines and xenograft	Amino acid metabolism	Jeong *et al.*, Cancer Metab., 2021. PMID: 33357456	2021
AML cell lines and mouse model	Amino acid metabolism	Bjelosevic *et al.*, Cancer Discov., 2021. PMID: 33436370	2021
AML patient blasts and cell lines	Fatty acid oxidation/lipid metabolism	Sriskanthadevan *et al.*, Blood, 2015. PMID: 25631767	2015
AML patient blasts and cell lines	Fatty acid oxidation/lipid metabolism	Ricciardi *et al.*, Blood, 2015. PMID: 26276667	2015
AML patient LSCs	Fatty acid oxidation/lipid metabolism	Ye *et al.*, Cell Stem Cell, 2016. PMID: 27374788	2016
AML patient blasts and cell lines	Fatty acid oxidation/lipid metabolism	German *et al.*, Mol Cell, 2016. PMID: 27635760	2016
AML patient blasts	Fatty acid oxidation/lipid metabolism	Shi *et al.*, EBioMedicine, 2016. PMID: 27916548	2016
AML patient blasts and cell lines	Fatty acid oxidation/lipid metabolism	Shafat *et al.*, Blood, 2017. PMID: 28049638	2017
AML patient blasts and cell lines	Fatty acid oxidation/lipid metabolism	Tabe *et al.*, Cancer Res., 2017. PMID: 28108519	2017
AML patient blasts and cell lines	Fatty acid oxidation/lipid metabolism	Farge *et al.*, Cancer Discov., 2017. PMID: 28416471	2017
Resistant AML patient LSCs	Fatty acid oxidation/lipid metabolism	Stevens *et al.*, Nat Cancer, 2020. PMID: N/A	2020
AML mouse model	Nucleotide metabolism	Sykes *et al.*, Cell, 2016. PMID: 27641501	2016
AML mouse model of residual disease	Nucleotide metabolism	van Gastal *et al.*, Cell Metab., 2020. PMID: 32763164	2020
AML mouse model	Vitamin metabolism	Chen *et al.*, Cancer Cell, 2020. PMID: 31935373	2020
Resistant AML patient LSCs	Vitamin metabolism	Jones *et al.*, Cell Stem Cell, 2020. PMID: 32822582	2020
AML patient LSCs	Redox metabolism	Pei *et al.*, J Biol Chem., 2013. PMID: 24089526	2013
AML cell lines	Redox metabolism	Gregory *et al.*, Proc Natl Acad Sci U.S.A., 2016. PMID: 27791036	2016
AML mouse model	Redox metabolism	Forte *et al.*, Cell Metab., 2020. PMID: 32966766	2020

Table 1: Comprehensive list of all studies focused on defining the metabolic source in the setting of AML. Studies are grouped by metabolic pathways and are color coded as follows: glycolysis (green), oxidative phosphorylation (orange), amino acid metabolism (blue), fatty acid oxidation/lipid metabolism (teal), nucleotide metabolism (yellow), vitamin metabolism (purple), and redox metabolism (red). The table also provides information on the model used to study metabolism (*in vitro* cell lines, *ex vivo* patient samples, and/or *in vivo* animal models).

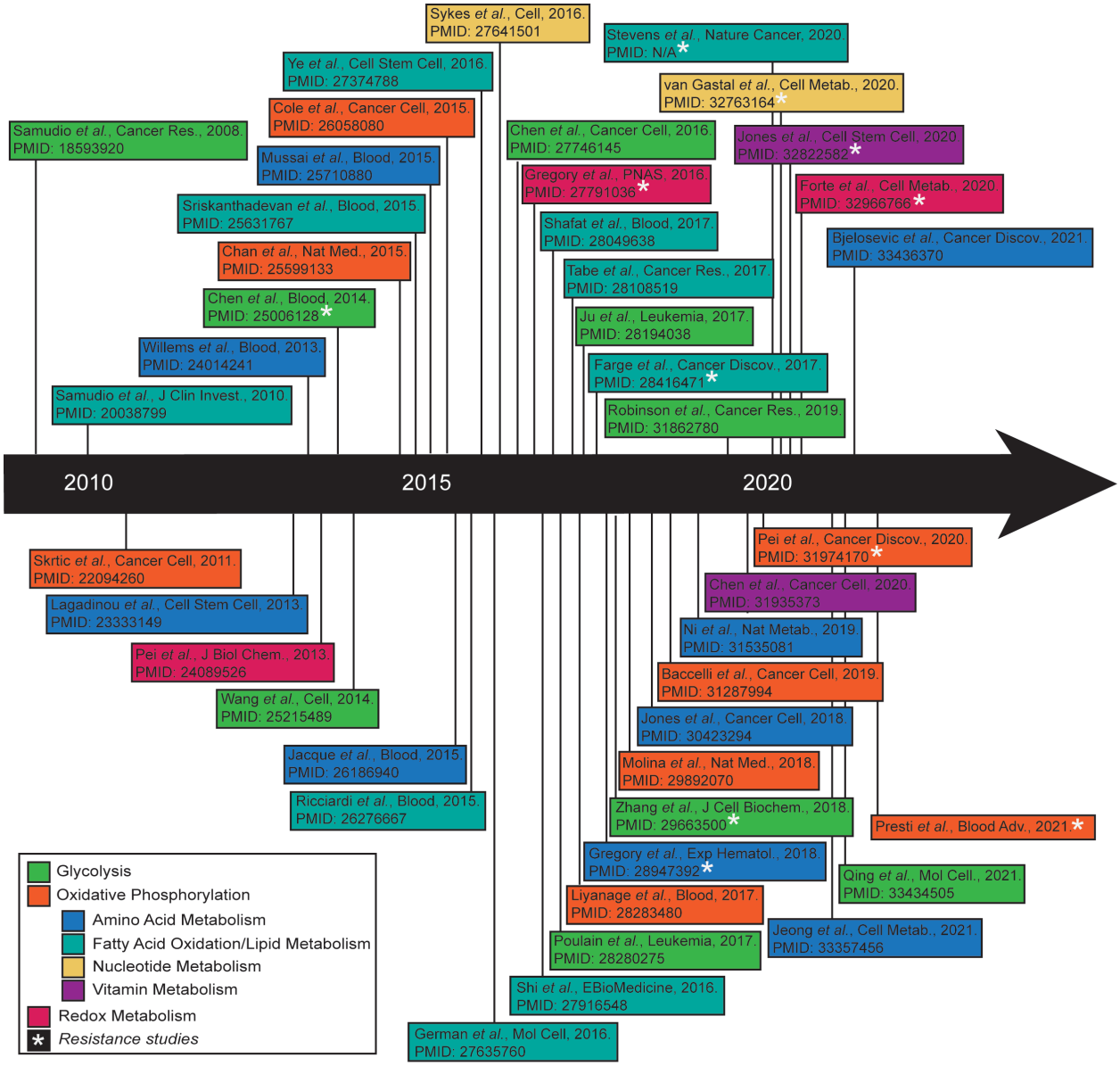

Figure 3: Timeline of key advances relating to the metabolic profiling of AML cells. Different pre-clinical models (*ex vivo* patient cells, *in vitro* cell lines, and *in vivo* mouse studies) have revealed the underlying metabolic heterogeneity of AML. Asterisk (*) indicates studies where the source of metabolism is altered in the setting of drug resistance. Different metabolic pathways are color coded as follows: glycolysis (green), oxidative phosphorylation (orange), amino acid metabolism (blue), fatty acid oxidation/lipid metabolism (teal), nucleotide metabolism (yellow), vitamin metabolism (purple), and redox metabolism (red).

While many studies, including our own, have shown the predilection for lipid metabolism as a preferred energy source of resistant AML cells, a full understanding of the molecular details that guide this process remain largely undefined. In 2010, for the first time, Samudio *et al.* reported that AML cells oxidize fatty acids for energy production, survival, and chemoresistance[502]. Inhibition of fatty acid oxidation (FAO) in their cell line model facilitated Bak/Bax oligomerization and apoptosis. This work has been further strengthened by subsequent studies that detail the importance of inhibiting FAO with etomoxir or ST1326, which prevent the entry of fatty acids into the mitochondria by blocking activity of carnitine palmitoyl transferase 1 (CPT1)[146, 509, 512]. Loss in expression of prolyl hydroxylase 3 (PHD3)[511] or upregulation of the scavenger receptor[510], CD36 have also been shown to promote FAO in AML cells, potentially serving as biomarkers to identify patients who may benefit from FAO inhibitors. In our two-step model of gilteritinib resistance, we saw that AML resistant cells switched from glucose to lipid metabolism, which began in early resistance and continued into late resistance. The switch in energy source was permanent in contrast to other studies[490], suggesting that AML resistant cells become reprogrammed over time and develop a metabolic memory. An increase in lipid metabolism was also confirmed in residual AML cells from patients on gilteritinib. Our unpublished data suggests that lipid metabolism may result from the crosstalk between leukemia cells and neighboring stromal cells. It may be the case that fatty acids are provided by the stromal microenvironment. Transcriptomic analyses of stromal samples from AML patients on gilteritinib show an abundance of retinoic acid receptor responder protein 2 (RARRES2) expression which is linked to FAO (**Figure 4 & 5**). The crosstalk of AML cells and the neighboring RARRES2^{+} stroma needs to be further studied. Although the basic aspects of these findings remain to be elucidated, targeting FAO could serve as a fruitful strategy in a subset of patients.

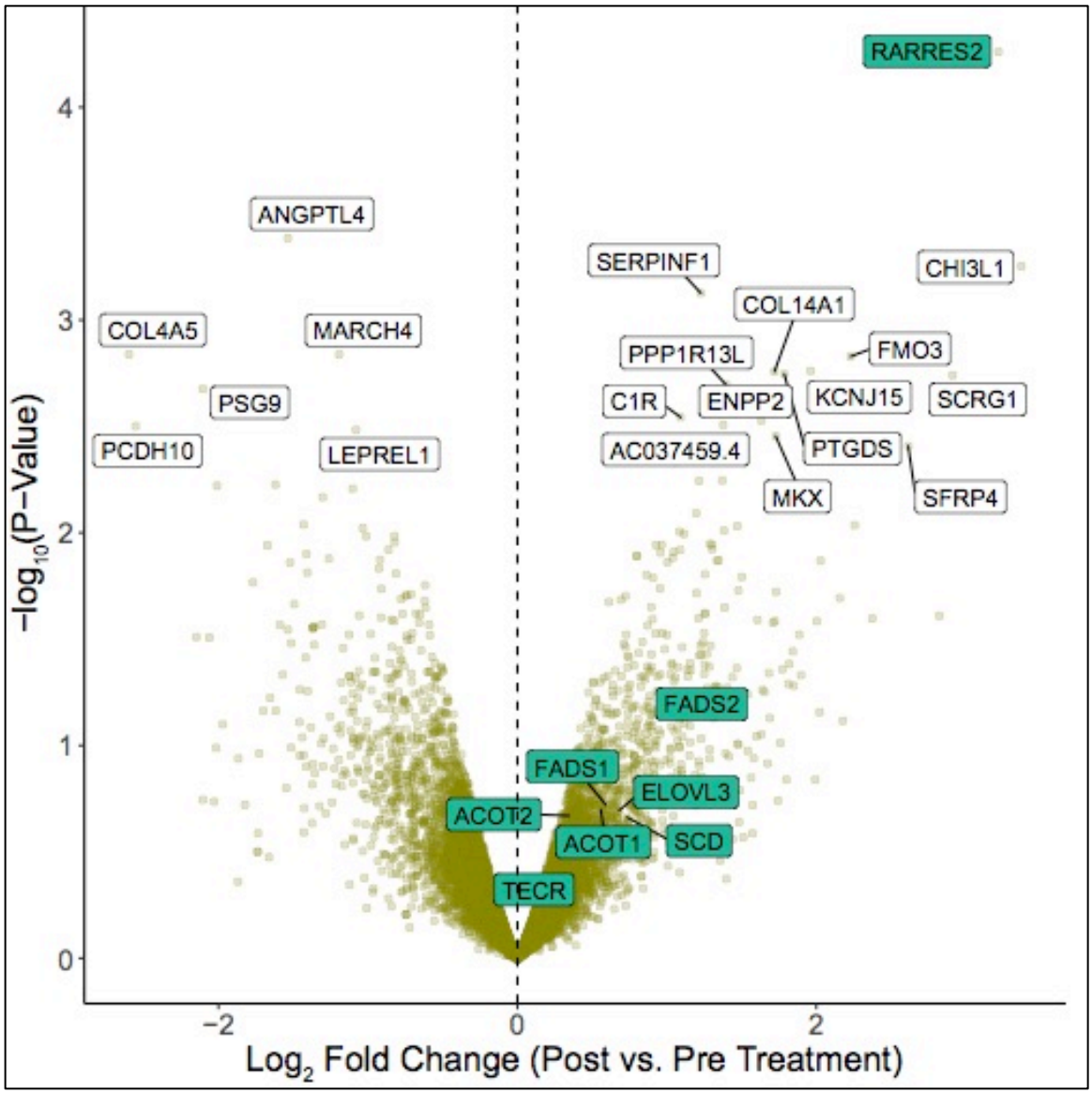

Figure 4: Enrichment of lipid metabolism genes in AML stromal cells following gilteritinib treatment. Alignments were performed using Kallisto[516] and summarized to the gene level using `tximport`[517]. Paired t-tests (comparing pre. vs post-gilteritinib) were carried out using the limma-trend methodology[518]. Genes are displayed in terms of $\log_2$ fold-change (x-axis) and raw p-value (y-axis). Genes in teal are part of lipid metabolism. This volcano plot was prepared by Daniel Bottomly.

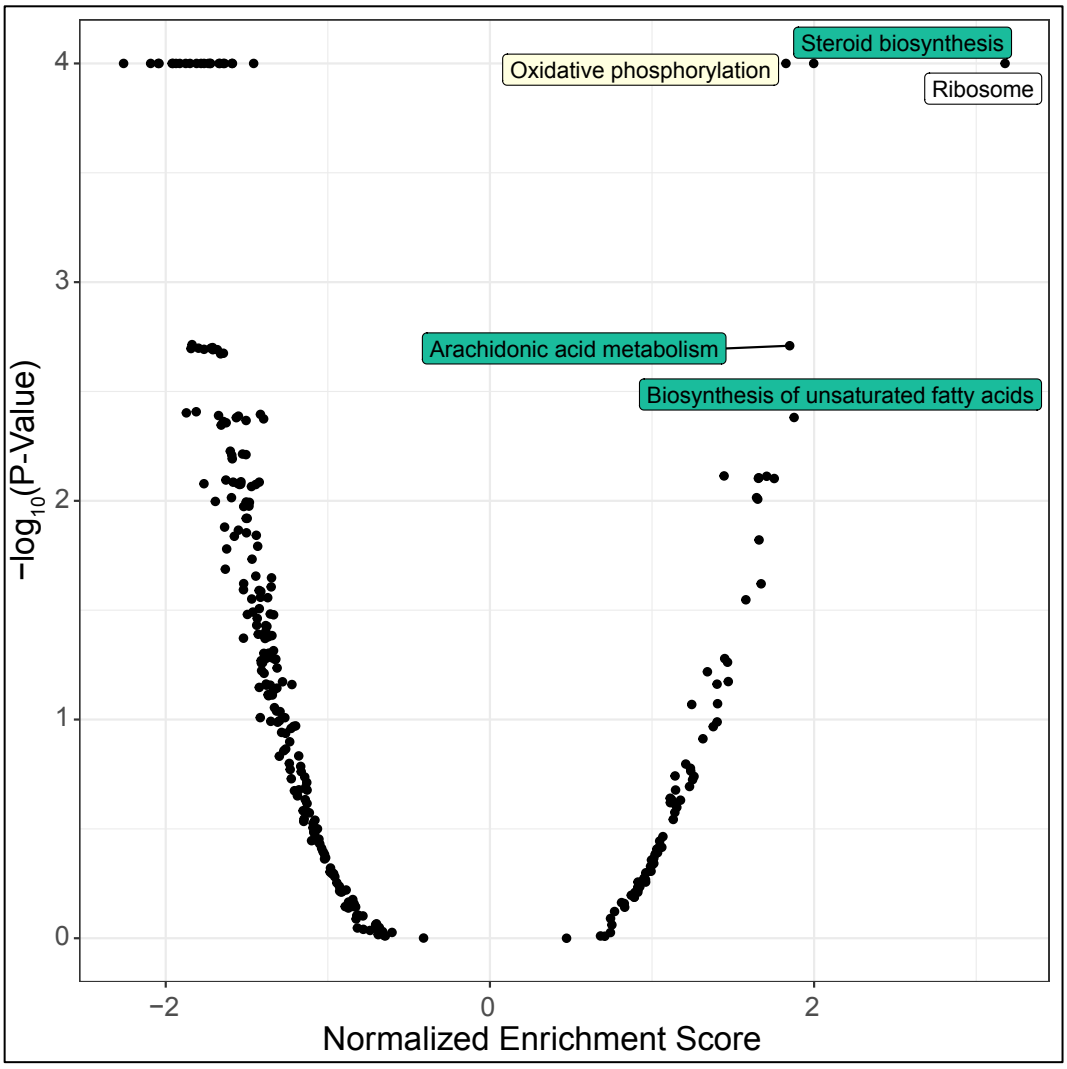

Figure 5: Enrichment of lipid metabolism signature in AML stromal cells following gilteritinib treatment. Pathway enrichment was assessed using the GSEA functionality in WebGestaltR[519] with KEGG[520] pathways based on the paired t-statistic. This volcano plot was prepared by Daniel Bottomly.

Additionally, from our current findings, it is difficult to conclude if the shift to lipid metabolism is a cause or consequence of gilteritinib resistance. Our current CRISPR/Cas9 profiling suggests that lipid metabolism contributes to resistance as we did not observe a single gene or pathway dependency. One approach to fully answering this question could be attempting to create gilteritinib resistant cell lines with MOLM14 cells after knocking out or knocking down the lipid metabolism machinery to assess its contribution to conferring resistance. If lipid metabolism is a driver of resistance, its downregulation should prevent or delay the development of resistance in long-term culture.

Recent work from Stevens *et al.* and our analysis of Beat AML (**Figure 6**) have also suggested a possible correlation between NRAS mutations and lipid metabolism[146]. To this end, detailed metabolomic and lipidomic analyses following knock-out of NRAS or stable expression of NRAS mutations could be of great value in understanding if a causal relationship between NRAS and lipid metabolism exists.

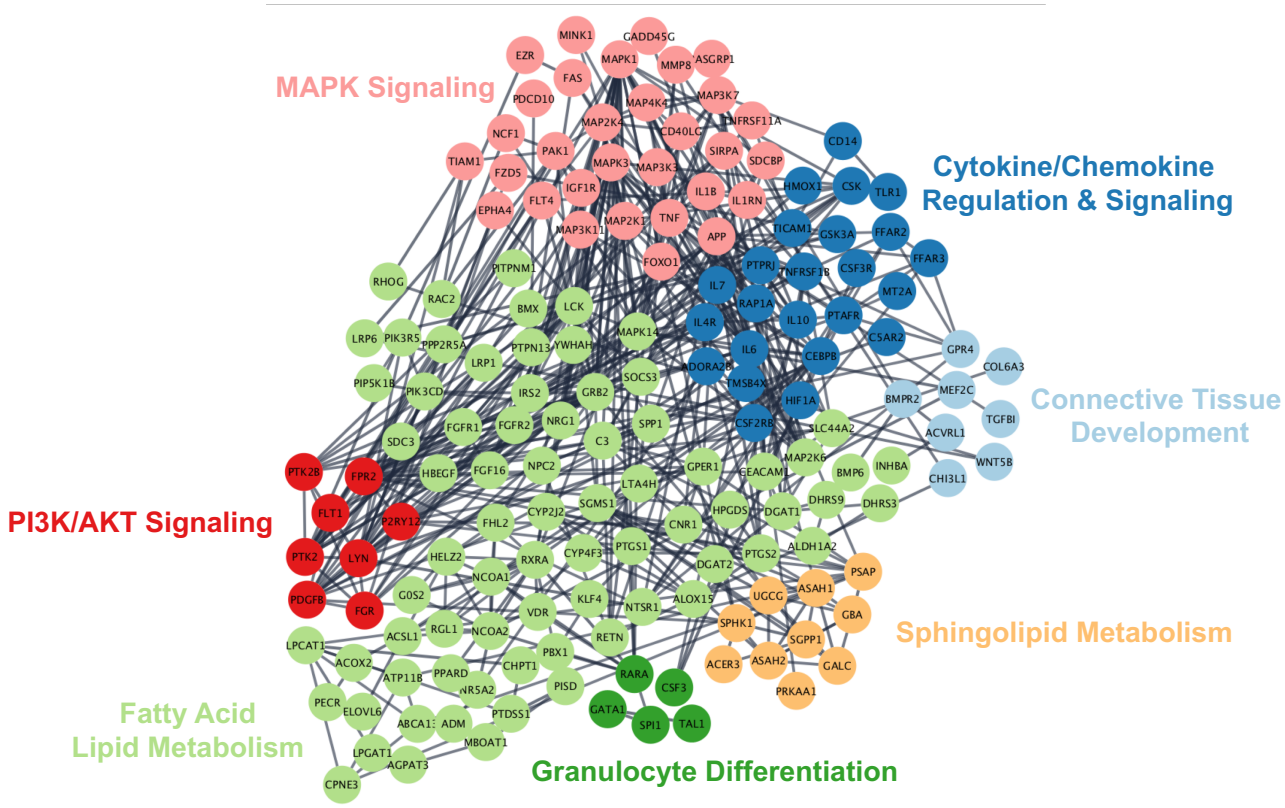

Figure 6: Transcriptional analysis of patients with NRAS mutations from BeatAML show an enrichment of genes involved in fatty acid and sphingolipid metabolism. Correlative analysis was performed with patients with FLT3 mutations (n = 108) versus patients with NRAS mutations (n = 65). Pathway determination was performed with WebGestalt (FDR ≤ 0.05) and visualized through Cytoscape[446].

All in all, the work presented in this dissertation illustrates that intrinsic and extrinsic activation of RTKs can initiate and sustain the growth of leukemia cells. Rigorous testing of intrinsic mutations in NTRK2/3, ERBB2, and FLT3 steered the identification of new oncogenic targets. Protective factors secreted by marrow stromal cells can promote the growth of leukemia cells via sustained activation of FLT3 signaling, thereby thwarting the depth of current treatment modalities. Understanding the interplay of intrinsic and extrinsic activation of RTKs may yield improved therapeutic strategies that target leukemia cells more effectively.

References

1. Laurenti, E. and B. Gottgens, *From haematopoietic stem cells to complex differentiation landscapes.* Nature, 2018. **553**(7689): p. 418-426. PMC6555401
2. Jagannathan-Bogdan, M. and L.I. Zon, *Hematopoiesis.* Development, 2013. **140**(12): p. 2463-7. PMC3666375
3. Pinho, S. and P.S. Frenette, *Haematopoietic stem cell activity and interactions with the niche.* Nat Rev Mol Cell Biol, 2019. **20**(5): p. 303-320. PMC6483843
4. Kaushansky, K., *Lineage-specific hematopoietic growth factors.* N Engl J Med, 2006. **354**(19): p. 2034-45.
5. Lyengar, V. and A. Shimanovsky, *Leukemia*, in *StatPearls*. 2020: Treasure Island (FL).
6. Davis, A.S., A.J. Viera, and M.D. Mead, *Leukemia: an overview for primary care.* Am Fam Physician, 2014. **89**(9): p. 731-8.
7. Siegel, R.L., K.D. Miller, and A. Jemal, *Cancer statistics, 2019.* CA Cancer J Clin, 2019. **69**(1): p. 7-34.
8. Clarke, R.T., A. Van den Bruel, C. Bankhead, C.D. Mitchell, B. Phillips, and M.J. Thompson, *Clinical presentation of childhood leukaemia: a systematic review and meta-analysis.* Arch Dis Child, 2016. **101**(10): p. 894-901.
9. Riley, R.S., D. Williams, M. Ross, S. Zhao, A. Chesney, B.D. Clark, et al., *Bone marrow aspirate and biopsy: a pathologist's perspective. II. interpretation of the bone marrow aspirate and biopsy.* J Clin Lab Anal, 2009. **23**(5): p. 259-307. PMC6648980
10. Dohner, H., D.J. Weisdorf, and C.D. Bloomfield, *Acute Myeloid Leukemia.* N Engl J Med, 2015. **373**(12): p. 1136-52.
11. Tyner, J.W., C.E. Tognon, D. Bottomly, B. Wilmot, S.E. Kurtz, S.L. Savage, et al., *Functional genomic landscape of acute myeloid leukaemia.* Nature, 2018. **562**(7728): p. 526-531. PMC6280667

12. Fletcher, L., S.K. Joshi, and E. Traer, *Profile of Quizartinib for the Treatment of Adult Patients with Relapsed/Refractory FLT3-ITD-Positive Acute Myeloid Leukemia: Evidence to Date.* Cancer Manag Res, 2020. **12**: p. 151-163. PMC6955578
13. Druker, B.J., S. Tamura, E. Buchdunger, S. Ohno, G.M. Segal, S. Fanning, et al., *Effects of a selective inhibitor of the Abl tyrosine kinase on the growth of Bcr-Abl positive cells.* Nat Med, 1996. **2**(5): p. 561-6.
14. Druker, B.J., *Perspectives on the development of imatinib and the future of cancer research.* Nat Med, 2009. **15**(10): p. 1149-52.
15. Carter, J.L., K. Hege, J. Yang, H.A. Kalpage, Y. Su, H. Edwards, et al., *Targeting multiple signaling pathways: the new approach to acute myeloid leukemia therapy.* Signal Transduct Target Ther, 2020. **5**(1): p. 288.
16. Roskoski, R., Jr., *Properties of FDA-approved small molecule protein kinase inhibitors: A 2020 update.* Pharmacol Res, 2020. **152**: p. 104609.
17. Manning, G., D.B. Whyte, R. Martinez, T. Hunter, and S. Sudarsanam, *The protein kinase complement of the human genome.* Science, 2002. **298**(5600): p. 1912-34.
18. Lemmon, M.A. and J. Schlessinger, *Cell signaling by receptor tyrosine kinases.* Cell, 2010. **141**(7): p. 1117-34. PMC2914105
19. Robinson, D.R., Y.M. Wu, and S.F. Lin, *The protein tyrosine kinase family of the human genome.* Oncogene, 2000. **19**(49): p. 5548-57.
20. Schlessinger, J., *Receptor tyrosine kinases: legacy of the first two decades.* Cold Spring Harb Perspect Biol, 2014. **6**(3). PMC3949355
21. Ullrich, A. and J. Schlessinger, *Signal transduction by receptors with tyrosine kinase activity.* Cell, 1990. **61**(2): p. 203-12.
22. Ward, C.W., M.C. Lawrence, V.A. Streltsov, T.E. Adams, and N.M. McKern, *The insulin and EGF receptor structures: new insights into ligand-induced receptor activation.* Trends Biochem Sci, 2007. **32**(3): p. 129-37.

23. Clayton, A.H., M.L. Tavarnesi, and T.G. Johns, *Unligated epidermal growth factor receptor forms higher order oligomers within microclusters on A431 cells that are sensitive to tyrosine kinase inhibitor binding.* Biochemistry, 2007. **46**(15): p. 4589-97.

24. Nagy, P., J. Claus, T.M. Jovin, and D.J. Arndt-Jovin, *Distribution of resting and ligand-bound ErbB1 and ErbB2 receptor tyrosine kinases in living cells using number and brightness analysis.* Proc Natl Acad Sci U S A, 2010. **107**(38): p. 16524-9. PMC2944731

25. Hubbard, S.R., *Structural analysis of receptor tyrosine kinases.* Prog Biophys Mol Biol, 1999. **71**(3-4): p. 343-58.

26. Bazan, J.F., *Structural design and molecular evolution of a cytokine receptor superfamily.* Proc Natl Acad Sci U S A, 1990. **87**(18): p. 6934-8. PMC54656

27. Kobe, B. and J. Deisenhofer, *The leucine-rich repeat: a versatile binding motif.* Trends Biochem Sci, 1994. **19**(10): p. 415-21.

28. Reuther, G.W., Q.T. Lambert, M.A. Caligiuri, and C.J. Der, *Identification and characterization of an activating TrkA deletion mutation in acute myeloid leukemia.* Mol Cell Biol, 2000. **20**(23): p. 8655-66. PMC86471

29. Stern, D.F., M.P. Kamps, and H. Cao, *Oncogenic activation of p185neu stimulates tyrosine phosphorylation in vivo.* Mol Cell Biol, 1988. **8**(9): p. 3969-73. PMC365461

30. Watanabe-Smith, K., C. Tognon, J.W. Tyner, J.P. Meijerink, B.J. Druker, and A. Agarwal, *Discovery and functional characterization of a germline, CSF2RB-activating mutation in leukemia.* Leukemia, 2016. **30**(9): p. 1950-3. PMC5014660

31. Weiner, D.B., J. Liu, J.A. Cohen, W.V. Williams, and M.I. Greene, *A point mutation in the neu oncogene mimics ligand induction of receptor aggregation.* Nature, 1989. **339**(6221): p. 230-1.

32. Zenatti, P.P., D. Ribeiro, W. Li, L. Zuurbier, M.C. Silva, M. Paganin, et al., *Oncogenic IL7R gain-of-function mutations in childhood T-cell acute lymphoblastic leukemia.* Nat Genet, 2011. **43**(10): p. 932-9.

33. Hubbard, S.R., *Juxtamembrane autoinhibition in receptor tyrosine kinases.* Nat Rev Mol Cell Biol, 2004. **5**(6): p. 464-71.

34. Hedger, G., M.S. Sansom, and H. Koldso, *The juxtamembrane regions of human receptor tyrosine kinases exhibit conserved interaction sites with anionic lipids.* Sci Rep, 2015. **5**: p. 9198. PMC4361843

35. Abd Halim, K.B., H. Koldso, and M.S.P. Sansom, *Interactions of the EGFR juxtamembrane domain with PIP2-containing lipid bilayers: Insights from multiscale molecular dynamics simulations.* Biochim Biophys Acta, 2015. **1850**(5): p. 1017-1025. PMC4547087

36. Chavent, M., D. Karia, A.C. Kalli, J. Domanski, A.L. Duncan, G. Hedger, et al., *Interactions of the EphA2 Kinase Domain with PIPs in Membranes: Implications for Receptor Function.* Structure, 2018. **26**(7): p. 1025-1034 e2. PMC6039763

37. Griffith, J., J. Black, C. Faerman, L. Swenson, M. Wynn, F. Lu, et al., *The structural basis for autoinhibition of FLT3 by the juxtamembrane domain.* Mol Cell, 2004. **13**(2): p. 169-78.

38. Mol, C.D., D.R. Dougan, T.R. Schneider, R.J. Skene, M.L. Kraus, D.N. Scheibe, et al., *Structural basis for the autoinhibition and STI-571 inhibition of c-Kit tyrosine kinase.* J Biol Chem, 2004. **279**(30): p. 31655-63.

39. Nolen, B., S. Taylor, and G. Ghosh, *Regulation of protein kinases; controlling activity through activation segment conformation.* Mol Cell, 2004. **15**(5): p. 661-75.

40. Smith, C.C., Q. Wang, C.S. Chin, S. Salerno, L.E. Damon, M.J. Levis, et al., *Validation of ITD mutations in FLT3 as a therapeutic target in human acute myeloid leukaemia.* Nature, 2012. **485**(7397): p. 260-3. PMC3390926

41. Azam, M., M.A. Seeliger, N.S. Gray, J. Kuriyan, and G.Q. Daley, *Activation of tyrosine kinases by mutation of the gatekeeper threonine.* Nat Struct Mol Biol, 2008. **15**(10): p. 1109-18. PMC2575426

42. Taylor, S.S. and A.P. Kornev, *Protein kinases: evolution of dynamic regulatory proteins.* Trends Biochem Sci, 2011. **36**(2): p. 65-77. PMC3084033

43. Cowan-Jacob, S.W., W. Jahnke, and S. Knapp, *Novel approaches for targeting kinases: allosteric inhibition, allosteric activation and pseudokinases.* Future Med Chem, 2014. **6**(5): p. 541-61.

44. Fabbro, D., S.W. Cowan-Jacob, and H. Moebitz, *Ten things you should know about protein kinases: IUPHAR Review 14.* Br J Pharmacol, 2015. **172**(11): p. 2675-700. PMC4439867

45. Mohammadi, M., J. Schlessinger, and S.R. Hubbard, *Structure of the FGF receptor tyrosine kinase domain reveals a novel autoinhibitory mechanism.* Cell, 1996. **86**(4): p. 577-87.

46. Shewchuk, L.M., A.M. Hassell, B. Ellis, W.D. Holmes, R. Davis, E.L. Horne, et al., *Structure of the Tie2 RTK domain: self-inhibition by the nucleotide binding loop, activation loop, and C-terminal tail.* Structure, 2000. **8**(11): p. 1105-13.

47. Roskoski, R., Jr., *The role of small molecule Flt3 receptor protein-tyrosine kinase inhibitors in the treatment of Flt3-positive acute myelogenous leukemias.* Pharmacol Res, 2020. **155**: p. 104725.

48. Pettersen, E.F., T.D. Goddard, C.C. Huang, G.S. Couch, D.M. Greenblatt, E.C. Meng, et al., *UCSF Chimera--a visualization system for exploratory research and analysis.* J Comput Chem, 2004. **25**(13): p. 1605-12.

49. Wagner, M.J., M.M. Stacey, B.A. Liu, and T. Pawson, *Molecular mechanisms of SH2- and PTB-domain-containing proteins in receptor tyrosine kinase signaling.* Cold Spring Harb Perspect Biol, 2013. **5**(12): p. a008987. PMC3839611

50. Ostman, A. and F.D. Bohmer, *Regulation of receptor tyrosine kinase signaling by protein tyrosine phosphatases.* Trends Cell Biol, 2001. **11**(6): p. 258-66.

51. Amit, I., A. Citri, T. Shay, Y. Lu, M. Katz, F. Zhang, et al., *A module of negative feedback regulators defines growth factor signaling.* Nat Genet, 2007. **39**(4): p. 503-12.

52. Rodrigues, G.A. and M. Park, *Oncogenic activation of tyrosine kinases.* Curr Opin Genet Dev, 1994. **4**(1): p. 15-24.

53. Croce, C.M., *Oncogenes and cancer.* N Engl J Med, 2008. **358**(5): p. 502-11.

54. Vogelstein, B., N. Papadopoulos, V.E. Velculescu, S. Zhou, L.A. Diaz, Jr., and K.W. Kinzler, *Cancer genome landscapes.* Science, 2013. **339**(6127): p. 1546-58. PMC3749880

55. Bell, D.W., *Our changing view of the genomic landscape of cancer.* J Pathol, 2010. **220**(2): p. 231-43. PMC3195356

56. Weinstein, I.B. and A.K. Joe, *Mechanisms of disease: Oncogene addiction--a rationale for molecular targeting in cancer therapy.* Nat Clin Pract Oncol, 2006. **3**(8): p. 448-57.

57. Weinstein, I.B., *Cancer. Addiction to oncogenes--the Achilles heal of cancer.* Science, 2002. **297**(5578): p. 63-4.

58. Downward, J., Y. Yarden, E. Mayes, G. Scrace, N. Totty, P. Stockwell, et al., *Close similarity of epidermal growth factor receptor and v-erb-B oncogene protein sequences.* Nature, 1984. **307**(5951): p. 521-7.

59. Wang, Z., P.A. Longo, M.K. Tarrant, K. Kim, S. Head, D.J. Leahy, et al., *Mechanistic insights into the activation of oncogenic forms of EGF receptor.* Nat Struct Mol Biol, 2011. **18**(12): p. 1388-93. PMC3230693

60. Bell, D.W., I. Gore, R.A. Okimoto, N. Godin-Heymann, R. Sordella, R. Mulloy, et al., *Inherited susceptibility to lung cancer may be associated with the T790M drug resistance mutation in EGFR.* Nat Genet, 2005. **37**(12): p. 1315-6.

61. Harari, D. and Y. Yarden, *Molecular mechanisms underlying ErbB2/HER2 action in breast cancer.* Oncogene, 2000. **19**(53): p. 6102-14.

62. Smith, C.C., C. Zhang, K.C. Lin, E.A. Lasater, Y. Zhang, E. Massi, et al., *Characterizing and Overriding the Structural Mechanism of the Quizartinib-Resistant FLT3 "Gatekeeper" F691L Mutation with PLX3397.* Cancer Discov, 2015. **5**(6): p. 668-79. PMC4522415

63. Heinrich, M.C., C.L. Corless, G.D. Demetri, C.D. Blanke, M. von Mehren, H. Joensuu, et al., *Kinase mutations and imatinib response in patients with metastatic gastrointestinal stromal tumor.* J Clin Oncol, 2003. **21**(23): p. 4342-9.

64. Carraway, K.L., 3rd and C. Sweeney, *EGF receptor activation by heterologous mechanisms.* Cancer Cell, 2002. **1**(5): p. 405-6.

65. Tanaka, H. and T. Watanabe, *Mechanisms Underlying Recurrent Genomic Amplification in Human Cancers.* Trends Cancer, 2020. **6**(6): p. 462-477. PMC7285850

66. Vogt, N., S.H. Lefevre, F. Apiou, A.M. Dutrillaux, A. Cor, P. Leuraud, et al., *Molecular structure of double-minute chromosomes bearing amplified copies of the epidermal growth factor receptor gene in gliomas.* Proc Natl Acad Sci U S A, 2004. **101**(31): p. 11368-73. PMC509208

67. Kuwahara, Y., C. Tanabe, T. Ikeuchi, K. Aoyagi, M. Nishigaki, H. Sakamoto, et al., *Alternative mechanisms of gene amplification in human cancers.* Genes Chromosomes Cancer, 2004. **41**(2): p. 125-32.

68. Dutt, A., A.H. Ramos, P.S. Hammerman, C. Mermel, J. Cho, T. Sharifnia, et al., *Inhibitor-sensitive FGFR1 amplification in human non-small cell lung cancer.* PLoS One, 2011. **6**(6): p. e20351. PMC3110189

69. Reis-Filho, J.S., P.T. Simpson, N.C. Turner, M.B. Lambros, C. Jones, A. Mackay, et al., *FGFR1 emerges as a potential therapeutic target for lobular breast carcinomas.* Clin Cancer Res, 2006. **12**(22): p. 6652-62.

70. Nowell, P.C., *The minute chromosome (Phl) in chronic granulocytic leukemia.* Blut, 1962. **8**: p. 65-6.

71. Rowley, J.D., *Letter: A new consistent chromosomal abnormality in chronic myelogenous leukaemia identified by quinacrine fluorescence and Giemsa staining.* Nature, 1973. **243**(5405): p. 290-3.

72. de Klein, A., A.G. van Kessel, G. Grosveld, C.R. Bartram, A. Hagemeijer, D. Bootsma, et al., *A cellular oncogene is translocated to the Philadelphia chromosome in chronic myelocytic leukaemia.* Nature, 1982. **300**(5894): p. 765-7.

73. Daley, G.Q., R.A. Van Etten, and D. Baltimore, *Induction of chronic myelogenous leukemia in mice by the P210bcr/abl gene of the Philadelphia chromosome.* Science, 1990. **247**(4944): p. 824-30.

74. Heisterkamp, N., G. Jenster, J. ten Hoeve, D. Zovich, P.K. Pattengale, and J. Groffen, *Acute leukaemia in bcr/abl transgenic mice.* Nature, 1990. **344**(6263): p. 251-3.

75. Sato, Y., S.K. Bohlander, H. Kobayashi, S. Reshmi, Y. Suto, E.M. Davis, et al., *Heterogeneity in the breakpoints in balanced rearrangements involving band 12p13 in hematologic malignancies identified by fluorescence in situ hybridization: TEL (ETV6) is involved in only one half.* Blood, 1997. **90**(12): p. 4886-93.

76. Rabbitts, T.H., *Chromosomal translocations in human cancer.* Nature, 1994. **372**(6502): p. 143-9.

77. Mertens, F., B. Johansson, T. Fioretos, and F. Mitelman, *The emerging complexity of gene fusions in cancer.* Nat Rev Cancer, 2015. **15**(6): p. 371-81.

78. Schram, A.M., M.T. Chang, P. Jonsson, and A. Drilon, *Fusions in solid tumours: diagnostic strategies, targeted therapy, and acquired resistance.* Nat Rev Clin Oncol, 2017. **14**(12): p. 735-748.

79. Davare, M.A. and C.E. Tognon, *Detecting and targetting oncogenic fusion proteins in the genomic era.* Biol Cell, 2015. **107**(5): p. 111-29. PMC5837291

80. Joshi, S.K., M.A. Davare, B.J. Druker, and C.E. Tognon, *Revisiting NTRKs as an emerging oncogene in hematological malignancies.* Leukemia, 2019.

81. Drilon, A., C. Jenkins, S. Iyer, A. Schoenfeld, C. Keddy, and M.A. Davare, *ROS1-dependent cancers - biology, diagnostics and therapeutics.* Nat Rev Clin Oncol, 2020.

82. Cocco, E., M. Scaltriti, and A. Drilon, *NTRK fusion-positive cancers and TRK inhibitor therapy.* Nat Rev Clin Oncol, 2018. **15**(12): p. 731-747.

83. Krystal, G.W., S.J. Hines, and C.P. Organ, *Autocrine growth of small cell lung cancer mediated by coexpression of c-kit and stem cell factor.* Cancer Res, 1996. **56**(2): p. 370-6.

84. Esposito, I., J. Kleeff, S.C. Bischoff, L. Fischer, P. Collecchi, M. Iorio, et al., *The stem cell factor-c-kit system and mast cells in human pancreatic cancer.* Lab Invest, 2002. **82**(11): p. 1481-92.

85. Lee, J.O., H. Yang, M.M. Georgescu, A. Di Cristofano, T. Maehama, Y. Shi, et al., *Crystal structure of the PTEN tumor suppressor: implications for its phosphoinositide phosphatase activity and membrane association.* Cell, 1999. **99**(3): p. 323-34.

86. Paget, S., *The distribution of secondary growths in cancer of the breast. 1889.* Cancer Metastasis Rev, 1989. **8**(2): p. 98-101.

87. Fidler, I.J. and G. Poste, *The "seed and soil" hypothesis revisited.* Lancet Oncol, 2008. **9**(8): p. 808.

88. Spill, F., D.S. Reynolds, R.D. Kamm, and M.H. Zaman, *Impact of the physical microenvironment on tumor progression and metastasis.* Curr Opin Biotechnol, 2016. **40**: p. 41-48. PMC4975620

89. Liu, Q., H. Zhang, X. Jiang, C. Qian, Z. Liu, and D. Luo, *Factors involved in cancer metastasis: a better understanding to "seed and soil" hypothesis.* Mol Cancer, 2017. **16**(1): p. 176. PMC5712107

90. Brantley-Sieders, D., S. Schmidt, M. Parker, and J. Chen, *Eph receptor tyrosine kinases in tumor and tumor microenvironment.* Curr Pharm Des, 2004. **10**(27): p. 3431-42.

91. Wiesner, C., S.M. Nabha, E.B. Dos Santos, H. Yamamoto, H. Meng, S.W. Melchior, et al., *C-kit and its ligand stem cell factor: potential contribution to prostate cancer bone metastasis.* Neoplasia, 2008. **10**(9): p. 996-1003. PMC2517645

92. Kaplan, R.N., R.D. Riba, S. Zacharoulis, A.H. Bramley, L. Vincent, C. Costa, et al., *VEGFR1-positive haematopoietic bone marrow progenitors initiate the pre-metastatic niche.* Nature, 2005. **438**(7069): p. 820-7. PMC2945882

93. Kinoshita, K., K. Nakagawa, J. Hamada, Y. Hida, M. Tada, S. Kondo, et al., *Imatinib mesylate inhibits the proliferation-stimulating effect of human lung cancer-associated stromal fibroblasts on lung cancer cells.* Int J Oncol, 2010. **37**(4): p. 869-77.

94. Gialeli, C., D. Nikitovic, D. Kletsas, A.D. Theocharis, G.N. Tzanakakis, and N.K. Karamanos, *PDGF/PDGFR signaling and targeting in cancer growth and progression: Focus on tumor microenvironment and cancer-associated fibroblasts.* Curr Pharm Des, 2014. **20**(17): p. 2843-8.

95. Agerstam, H., C. Karlsson, N. Hansen, C. Sanden, M. Askmyr, S. von Palffy, et al., *Antibodies targeting human IL1RAP (IL1R3) show therapeutic effects in xenograft models of acute myeloid leukemia.* Proc Natl Acad Sci U S A, 2015. **112**(34): p. 10786-91. PMC4553807

96. Carey, A., D.K.t. Edwards, C.A. Eide, L. Newell, E. Traer, B.C. Medeiros, et al., *Identification of Interleukin-1 by Functional Screening as a Key Mediator of Cellular Expansion and Disease Progression in Acute Myeloid Leukemia.* Cell Rep, 2017. **18**(13): p. 3204-3218. PMC5437102

97. Hosseini, M.M., S.E. Kurtz, S. Abdelhamed, S. Mahmood, M.A. Davare, A. Kaempf, et al., *Inhibition of interleukin-1 receptor-associated kinase-1 is a therapeutic strategy for acute myeloid leukemia subtypes.* Leukemia, 2018.

98. Weisberg, E., R.D. Wright, D.W. McMillin, C. Mitsiades, A. Ray, R. Barrett, et al., *Stromal-mediated protection of tyrosine kinase inhibitor-treated BCR-ABL-expressing leukemia cells.* Mol Cancer Ther, 2008. **7**(5): p. 1121-9. PMC4034541

99. Lotem, J. and L. Sachs, *Hematopoietic cytokines inhibit apoptosis induced by transforming growth factor beta 1 and cancer chemotherapy compounds in myeloid leukemic cells.* Blood, 1992. **80**(7): p. 1750-7.

100. Abdul-Aziz, A.M., M.S. Shafat, T.K. Mehta, F. Di Palma, M.J. Lawes, S.A. Rushworth, et al., *MIF-Induced Stromal PKCbeta/IL8 Is Essential in Human Acute Myeloid Leukemia.* Cancer Res, 2017. **77**(2): p. 303-311.

101. Abdul-Aziz, A.M., M.S. Shafat, Y. Sun, C.R. Marlein, R.E. Piddock, S.D. Robinson, et al., *HIF1alpha drives chemokine factor pro-tumoral signaling pathways in acute myeloid leukemia.* Oncogene, 2018. **37**(20): p. 2676-2686.

102. Gallipoli, P., F. Pellicano, H. Morrison, K. Laidlaw, E.K. Allan, R. Bhatia, et al., *Autocrine TNF-alpha production supports CML stem and progenitor cell survival and enhances their proliferation.* Blood, 2013. **122**(19): p. 3335-9. PMC3953090

103. Fleischman, A.G., K.J. Aichberger, S.B. Luty, T.G. Bumm, C.L. Petersen, S. Doratotaj, et al., *TNFalpha facilitates clonal expansion of JAK2V617F positive cells in myeloproliferative neoplasms.* Blood, 2011. **118**(24): p. 6392-8. PMC3236121

104. Yang, X., A. Sexauer, and M. Levis, *Bone marrow stroma-mediated resistance to FLT3 inhibitors in FLT3-ITD AML is mediated by persistent activation of extracellular regulated kinase.* Br J Haematol, 2014. **164**(1): p. 61-72. 4076672

105. Lisovsky, M., S.E. Braun, Y. Ge, H. Takahira, L. Lu, V.G. Savchenko, et al., *Flt3-ligand production by human bone marrow stromal cells.* Leukemia, 1996. **10**(6): p. 1012-8.

106. Traer, E., J. Martinez, N. Javidi-Sharifi, A. Agarwal, J. Dunlap, I. English, et al., *FGF2 from Marrow Microenvironment Promotes Resistance to FLT3 Inhibitors in Acute Myeloid Leukemia.* Cancer Res, 2016. **76**(22): p. 6471-6482. PMC5290120

107. Traer, E., N. Javidi-Sharifi, A. Agarwal, J. Dunlap, I. English, J. Martinez, et al., *Ponatinib overcomes FGF2-mediated resistance in CML patients without kinase domain mutations.* Blood, 2014. **123**(10): p. 1516-24. PMC3945862

108. Zeng, Z., Y.X. Shi, I.J. Samudio, R.Y. Wang, X. Ling, O. Frolova, et al., *Targeting the leukemia microenvironment by CXCR4 inhibition overcomes resistance to kinase inhibitors and chemotherapy in AML.* Blood, 2009. **113**(24): p. 6215-24. PMC2699240

109. Schelker, R.C., S. Iberl, G. Muller, C. Hart, W. Herr, and J. Grassinger, *TGF-beta1 and CXCL12 modulate proliferation and chemotherapy sensitivity of acute myeloid leukemia cells co-cultured with multipotent mesenchymal stromal cells.* Hematology, 2017: p. 1-9.

110. Hu, X., S. Mei, W. Meng, S. Xue, L. Jiang, Y. Yang, et al., *CXCR4-mediated signaling regulates autophagy and influences acute myeloid leukemia cell survival and drug resistance.* Cancer Lett, 2018. **425**: p. 1-12.

111. Zhao, C., J. Blum, A. Chen, H.Y. Kwon, S.H. Jung, J.M. Cook, et al., *Loss of beta-catenin impairs the renewal of normal and CML stem cells in vivo.* Cancer Cell, 2007. **12**(6): p. 528-41. PMC2262869

112. Jacamo, R., Y. Chen, Z. Wang, W. Ma, M. Zhang, E.L. Spaeth, et al., *Reciprocal leukemia-stroma VCAM-1/VLA-4-dependent activation of NF-kappaB mediates chemoresistance.* Blood, 2014. **123**(17): p. 2691-702. PMC3999754

113. Macanas-Pirard, P., R. Broekhuizen, A. Gonzalez, C. Oyanadel, D. Ernst, P. Garcia, et al., *Resistance of leukemia cells to cytarabine chemotherapy is mediated by bone marrow stroma, involves cell-surface equilibrative nucleoside transporter-1 removal and correlates with patient outcome.* Oncotarget, 2017. **8**(14): p. 23073-23086. PMC5410286

114. Dierks, C., R. Beigi, G.R. Guo, K. Zirlik, M.R. Stegert, P. Manley, et al., *Expansion of Bcr-Abl-positive leukemic stem cells is dependent on Hedgehog pathway activation.* Cancer Cell, 2008. **14**(3): p. 238-49.

115. Zhao, C., A. Chen, C.H. Jamieson, M. Fereshteh, A. Abrahamsson, J. Blum, et al., *Hedgehog signalling is essential for maintenance of cancer stem cells in myeloid leukaemia.* Nature, 2009. **458**(7239): p. 776-9. PMC2946231

116. Folgiero, V., L. Cifaldi, G. Li Pira, B.M. Goffredo, L. Vinti, and F. Locatelli, *TIM-3/Gal-9 interaction induces IFNgamma-dependent IDO1 expression in acute myeloid leukemia blast cells.* J Hematol Oncol, 2015. **8**: p. 36. PMC4404691

117. Ruvolo, P.P., V.R. Ruvolo, J.K. Burks, Y. Qiu, R.Y. Wang, E.J. Shpall, et al., *Role of MSC-derived galectin 3 in the AML microenvironment.* Biochim Biophys Acta, 2018. **1865**(7): p. 959-969. PMC5936474

118. Dominici, M., K. Le Blanc, I. Mueller, I. Slaper-Cortenbach, F. Marini, D. Krause, et al., *Minimal criteria for defining multipotent mesenchymal stromal cells. The International Society for Cellular Therapy position statement.* Cytotherapy, 2006. **8**(4): p. 315-7.

119. Worthley, D.L., Y. Si, M. Quante, M. Churchill, S. Mukherjee, and T.C. Wang, *Bone marrow cells as precursors of the tumor stroma.* Exp Cell Res, 2013. **319**(11): p. 1650-6. PMC4097986

120. Agarwal, P. and R. Bhatia, *Influence of Bone Marrow Microenvironment on Leukemic Stem Cells: Breaking Up an Intimate Relationship.* Adv Cancer Res, 2015. **127**: p. 227-52.

121. Chen, Y., R. Jacamo, Y.X. Shi, R.Y. Wang, V.L. Battula, S. Konoplev, et al., *Human extramedullary bone marrow in mice: a novel in vivo model of genetically controlled hematopoietic microenvironment.* Blood, 2012. **119**(21): p. 4971-80. PMC3367899

122. Xiao, P., L. Sandhow, Y. Heshmati, M. Kondo, T. Bouderlique, M. Dolinska, et al., *Distinct roles of mesenchymal stem and progenitor cells during the development of acute myeloid leukemia in mice.* Blood Adv, 2018. **2**(12): p. 1480-1494.

123. Geyh, S., M. Rodriguez-Paredes, P. Jager, C. Khandanpour, R.P. Cadeddu, J. Gutekunst, et al., *Functional inhibition of mesenchymal stromal cells in acute myeloid leukemia.* Leukemia, 2016. **30**(3): p. 683-91.

124. Druker, B.J., F. Guilhot, S.G. O'Brien, I. Gathmann, H. Kantarjian, N. Gattermann, et al., *Five-year follow-up of patients receiving imatinib for chronic myeloid leukemia.* N Engl J Med, 2006. **355**(23): p. 2408-17.

125. Henderson, C.A., Jr., *Imatinib: the promise of a "magic bullet" for cancer fulfilled.* J Med Assoc Ga, 2003. **92**(1): p. 12-4, 22.

126. Dar, A.C. and K.M. Shokat, *The evolution of protein kinase inhibitors from antagonists to agonists of cellular signaling.* Annu Rev Biochem, 2011. **80**: p. 769-95.

127. Gavrin, L.K. and E. Saiah, *Approaches to discover non-ATP site kinase inhibitors.* MedChemComm, 2013. **4**(1): p. 41-51.

128. Vijayan, R.S., P. He, V. Modi, K.C. Duong-Ly, H. Ma, J.R. Peterson, et al., *Conformational analysis of the DFG-out kinase motif and biochemical profiling of structurally validated type II inhibitors.* J Med Chem, 2015. **58**(1): p. 466-79. PMC4326797

129. Cocco, E., J.E. Lee, S. Kannan, A.M. Schram, H.H. Won, S. Shifman, et al., *TRK xDFG mutations trigger a sensitivity switch from type I to II kinase inhibitors.* Cancer Discov, 2020.

130. Romond, E.H., E.A. Perez, J. Bryant, V.J. Suman, C.E. Geyer, Jr., N.E. Davidson, et al., *Trastuzumab plus adjuvant chemotherapy for operable HER2-positive breast cancer.* N Engl J Med, 2005. **353**(16): p. 1673-84.

131. Franklin, M.C., K.D. Carey, F.F. Vajdos, D.J. Leahy, A.M. de Vos, and M.X. Sliwkowski, *Insights into ErbB signaling from the structure of the ErbB2-pertuzumab complex.* Cancer Cell, 2004. **5**(4): p. 317-28.

132. Pirker, R., J.R. Pereira, A. Szczesna, J. von Pawel, M. Krzakowski, R. Ramlau, et al., *Cetuximab plus chemotherapy in patients with advanced non-small-cell lung cancer (FLEX): an open-label randomised phase III trial.* Lancet, 2009. **373**(9674): p. 1525-31.

133. Gibson, T.B., A. Ranganathan, and A. Grothey, *Randomized phase III trial results of panitumumab, a fully human anti-epidermal growth factor receptor monoclonal antibody, in metastatic colorectal cancer.* Clin Colorectal Cancer, 2006. **6**(1): p. 29-31.

134. Vermorken, J.B., R. Mesia, F. Rivera, E. Remenar, A. Kawecki, S. Rottey, et al., *Platinum-based chemotherapy plus cetuximab in head and neck cancer.* N Engl J Med, 2008. **359**(11): p. 1116-27.

135. Kawase, T., T. Nakazawa, T. Eguchi, H. Tsuzuki, Y. Ueno, Y. Amano, et al., *Effect of Fms-like tyrosine kinase 3 (FLT3) ligand (FL) on antitumor activity of gilteritinib, a FLT3 inhibitor, in mice xenografted with FL-overexpressing cells.* Oncotarget, 2019. **10**(58): p. 6111-6123. PMC6817455

136. Marine, J.C., S.J. Dawson, and M.A. Dawson, *Non-genetic mechanisms of therapeutic resistance in cancer.* Nat Rev Cancer, 2020. **20**(12): p. 743-756.

137. Zhang, H., S. Savage, A.R. Schultz, D. Bottomly, L. White, E. Segerdell, et al., *Clinical resistance to crenolanib in acute myeloid leukemia due to diverse molecular mechanisms.* Nat Commun, 2019. **10**(1): p. 244. PMC6335421

138. Hanker, A.B., M.R. Brewer, J.H. Sheehan, J.P. Koch, G.R. Sliwoski, R. Nagy, et al., *An Acquired HER2(T798I) Gatekeeper Mutation Induces Resistance to Neratinib in a Patient with HER2 Mutant-Driven Breast Cancer.* Cancer Discov, 2017. **7**(6): p. 575-585. PMC5457707

139. Gorre, M.E., M. Mohammed, K. Ellwood, N. Hsu, R. Paquette, P.N. Rao, et al., *Clinical resistance to STI-571 cancer therapy caused by BCR-ABL gene mutation or amplification.* Science, 2001. **293**(5531): p. 876-80.

140. Drilon, A., *TRK inhibitors in TRK fusion-positive cancers.* Ann Oncol, 2019. **30**(Suppl_8): p. viii23-viii30. PMC6859818

141. Pao, W., V.A. Miller, K.A. Politi, G.J. Riely, R. Somwar, M.F. Zakowski, et al., *Acquired resistance of lung adenocarcinomas to gefitinib or erlotinib is associated with a second mutation in the EGFR kinase domain.* PLoS Med, 2005. **2**(3): p. e73. PMC549606

142. Kobayashi, S., H. Ji, Y. Yuza, M. Meyerson, K.K. Wong, D.G. Tenen, et al., *An alternative inhibitor overcomes resistance caused by a mutation of the epidermal growth factor receptor.* Cancer Res, 2005. **65**(16): p. 7096-101.

143. Somwar, R., N.E. Hofmann, B. Smith, I. Odintsov, M. Vojnic, I. Linkov, et al., *NTRK kinase domain mutations in cancer variably impact sensitivity to type I and type II inhibitors.* Commun Biol, 2020. **3**(1): p. 776. PMC7745027

144. Yu, H.A., M.E. Arcila, N. Rekhtman, C.S. Sima, M.F. Zakowski, W. Pao, et al., *Analysis of tumor specimens at the time of acquired resistance to EGFR-TKI therapy in 155 patients with EGFR-mutant lung cancers.* Clin Cancer Res, 2013. **19**(8): p. 2240-7. PMC3630270

145. Nechiporuk, T., S.E. Kurtz, O. Nikolova, T. Liu, C.L. Jones, A. D'Alessandro, et al., *The TP53 Apoptotic Network is a Primary Mediator of Resistance to BCL2 inhibition in AML Cells.* Cancer Discov, 2019.

146. Stevens, B.M., C.L. Jones, D.A. Pollyea, R. Culp-Hill, A. D'Alessandro, A. Winters, et al., *Fatty acid metabolism underlies venetoclax resistance in acute myeloid leukemia stem cells.* Nature Cancer, 2020.

147. Jones, C.L., B.M. Stevens, D.A. Pollyea, R. Culp-Hill, J.A. Reisz, T. Nemkov, et al., *Nicotinamide Metabolism Mediates Resistance to Venetoclax in Relapsed Acute Myeloid Leukemia Stem Cells.* Cell Stem Cell, 2020.

148. Pei, S., D.A. Pollyea, A. Gustafson, B.M. Stevens, M. Minhajuddin, R. Fu, et al., *Monocytic Subclones Confer Resistance to Venetoclax-Based Therapy in Patients with Acute Myeloid Leukemia.* Cancer Discov, 2020. **10**(4): p. 536-551. PMC7124979

149. Zhang, H., Y. Nakauchi, T. Köhnke, M. Stafford, D. Bottomly, R. Thomas, et al., *Integrated analysis of patient samples identifies biomarkers for venetoclax efficacy and combination strategies in acute myeloid leukemia.* Nature Cancer, 2020. **1**(8): p. 826-839.

150. Wilson, T.R., J. Fridlyand, Y. Yan, E. Penuel, L. Burton, E. Chan, et al., *Widespread potential for growth-factor-driven resistance to anticancer kinase inhibitors.* Nature, 2012. **487**(7408): p. 505-9. PMC3724525

151. Terai, H., K. Soejima, H. Yasuda, S. Nakayama, J. Hamamoto, D. Arai, et al., *Activation of the FGF2-FGFR1 autocrine pathway: a novel mechanism of acquired resistance to gefitinib in NSCLC.* Mol Cancer Res, 2013. **11**(7): p. 759-67.

152. Ware, K.E., T.K. Hinz, E. Kleczko, K.R. Singleton, L.A. Marek, B.A. Helfrich, et al., *A mechanism of resistance to gefitinib mediated by cellular reprogramming and the acquisition of an FGF2-FGFR1 autocrine growth loop.* Oncogenesis, 2013. **2**: p. e39. PMC3641357

153. Shen, S., S. Vagner, and C. Robert, *Persistent Cancer Cells: The Deadly Survivors.* Cell, 2020. **183**(4): p. 860-874.

154. Sharma, S.V., D.Y. Lee, B. Li, M.P. Quinlan, F. Takahashi, S. Maheswaran, et al., *A chromatin-mediated reversible drug-tolerant state in cancer cell subpopulations.* Cell, 2010. **141**(1): p. 69-80. PMC2851638

155. Hata, A.N., M.J. Niederst, H.L. Archibald, M. Gomez-Caraballo, F.M. Siddiqui, H.E. Mulvey, et al., *Tumor cells can follow distinct evolutionary paths to become resistant to epidermal growth factor receptor inhibition.* Nat Med, 2016. **22**(3): p. 262-9. PMC4900892

156. Shah, K.N., R. Bhatt, J. Rotow, J. Rohrberg, V. Olivas, V.E. Wang, et al., *Aurora kinase A drives the evolution of resistance to third-generation EGFR inhibitors in lung cancer.* Nat Med, 2019. **25**(1): p. 111-118. PMC6324945

157. Banelli, B., E. Carra, F. Barbieri, R. Wurth, F. Parodi, A. Pattarozzi, et al., *The histone demethylase KDM5A is a key factor for the resistance to temozolomide in glioblastoma.* Cell Cycle, 2015. **14**(21): p. 3418-29. PMC4825557

158. Echeverria, G.V., Z. Ge, S. Seth, X. Zhang, S. Jeter-Jones, X. Zhou, et al., *Resistance to neoadjuvant chemotherapy in triple-negative breast cancer mediated by a reversible drug-tolerant state.* Sci Transl Med, 2019. **11**(488). PMC6541393

159. Walens, A., J. Lin, J.S. Damrauer, B. McKinney, R. Lupo, R. Newcomb, et al., *Adaptation and selection shape clonal evolution of tumors during residual disease and recurrence.* Nat Commun, 2020. **11**(1): p. 5017. PMC7539014

160. Kumar, B., M. Garcia, L. Weng, X. Jung, J.L. Murakami, X. Hu, et al., *Acute myeloid leukemia transforms the bone marrow niche into a leukemia-permissive microenvironment through exosome secretion.* Leukemia, 2018. **32**(3): p. 575-587.

161. Szczepanski, M.J., M. Szajnik, A. Welsh, T.L. Whiteside, and M. Boyiadzis, *Blast-derived microvesicles in sera from patients with acute myeloid leukemia suppress natural killer cell function via membrane-associated transforming growth factor-beta1.* Haematologica, 2011. **96**(9): p. 1302-9. PMC3166100

162. Man, C.H., T.K. Fung, C. Ho, H.H. Han, H.C. Chow, A.C. Ma, et al., *Sorafenib treatment of FLT3-ITD(+) acute myeloid leukemia: favorable initial outcome and mechanisms of subsequent nonresponsiveness associated with the emergence of a D835 mutation.* Blood, 2012. **119**(22): p. 5133-43.

163. Rosenberg, M.W., K. Watanabe-Smith, J.W. Tyner, C.E. Tognon, B.J. Druker, and U. Borate, *Genomic markers of midostaurin drug sensitivity in FLT3 mutated and FLT3*

wild-type acute myeloid leukemia patients. Oncotarget, 2020. **11**(29): p. 2807-2818. PMC7381100

164. McMahon, C.M., T. Ferng, J. Canaani, E.S. Wang, J.J.D. Morrissette, D.J. Eastburn, et al., *Clonal Selection with RAS Pathway Activation Mediates Secondary Clinical Resistance to Selective FLT3 Inhibition in Acute Myeloid Leukemia.* Cancer Discov, 2019. **9**(8): p. 1050-1063.

165. Tarver, T.C., J.E. Hill, L. Rahmat, A.E. Perl, E. Bahceci, K. Mori, et al., *Gilteritinib is a clinically active FLT3 inhibitor with broad activity against FLT3 kinase domain mutations.* Blood Adv, 2020. **4**(3): p. 514-524. PMC7013266

166. Friedman, R., *The molecular mechanism behind resistance of the kinase FLT3 to the inhibitor quizartinib.* Proteins, 2017. **85**(11): p. 2143-2152.

167. Smith, C.C., K. Lin, A. Stecula, A. Sali, and N.P. Shah, *FLT3 D835 mutations confer differential resistance to type II FLT3 inhibitors.* Leukemia, 2015. **29**(12): p. 2390-2. PMC4675689

168. Smith, C.C., A. Paguirigan, G.R. Jeschke, K.C. Lin, E. Massi, T. Tarver, et al., *Heterogeneous resistance to quizartinib in acute myeloid leukemia revealed by single-cell analysis.* Blood, 2017. **130**(1): p. 48-58. PMC5501146

169. Challier, C., C.C. Uphoff, J.W. Janssen, and H.G. Drexler, *Differential expression of the ufo/axl oncogene in human leukemia-lymphoma cell lines.* Leukemia, 1996. **10**(5): p. 781-7.

170. Neubauer, A., A. Fiebeler, D.K. Graham, J.P. O'Bryan, C.A. Schmidt, P. Barckow, et al., *Expression of axl, a transforming receptor tyrosine kinase, in normal and malignant hematopoiesis.* Blood, 1994. **84**(6): p. 1931-41.

171. Rochlitz, C., A. Lohri, M. Bacchi, M. Schmidt, S. Nagel, M. Fopp, et al., *Axl expression is associated with adverse prognosis and with expression of Bcl-2 and CD34 in de novo*

acute myeloid leukemia (AML): results from a multicenter trial of the Swiss Group for Clinical Cancer Research (SAKK). Leukemia, 1999. **13**(9): p. 1352-8.

172. Park, I.K., A. Mishra, J. Chandler, S.P. Whitman, G. Marcucci, and M.A. Caligiuri, *Inhibition of the receptor tyrosine kinase Axl impedes activation of the FLT3 internal tandem duplication in human acute myeloid leukemia: implications for Axl as a potential therapeutic target.* Blood, 2013. **121**(11): p. 2064-73. 3596966

173. Park, I.K., B. Mundy-Bosse, S.P. Whitman, X. Zhang, S.L. Warner, D.J. Bearss, et al., *Receptor tyrosine kinase Axl is required for resistance of leukemic cells to FLT3-targeted therapy in acute myeloid leukemia.* Leukemia, 2015. **29**(12): p. 2382-9.

174. Lee, L.Y., D. Hernandez, T. Rajkhowa, S.C. Smith, J.R. Raman, B. Nguyen, et al., *Preclinical studies of gilteritinib, a next-generation FLT3 inhibitor.* Blood, 2017. **129**(2): p. 257-260. PMC5234222

175. Dumas, P.Y., C. Naudin, S. Martin-Lanneree, B. Izac, L. Casetti, O. Mansier, et al., *Hematopoietic niche drives FLT3-ITD acute myeloid leukemia resistance to quizartinib via STAT5- and hypoxia- dependent up-regulation of AXL.* Haematologica, 2019.

176. Li, L., T. Osdal, Y. Ho, S. Chun, T. McDonald, P. Agarwal, et al., *SIRT1 activation by a c-MYC oncogenic network promotes the maintenance and drug resistance of human FLT3-ITD acute myeloid leukemia stem cells.* Cell Stem Cell, 2014. **15**(4): p. 431-446. PMC4305398

177. Fiskus, W., S. Sharma, J. Qi, B. Shah, S.G. Devaraj, C. Leveque, et al., *BET protein antagonist JQ1 is synergistically lethal with FLT3 tyrosine kinase inhibitor (TKI) and overcomes resistance to FLT3-TKI in AML cells expressing FLT-ITD.* Mol Cancer Ther, 2014. **13**(10): p. 2315-27. PMC4185220

178. Heidel, F., F.K. Solem, F. Breitenbuecher, D.B. Lipka, S. Kasper, M.H. Thiede, et al., *Clinical resistance to the kinase inhibitor PKC412 in acute myeloid leukemia by mutation of Asn-676 in the FLT3 tyrosine kinase domain.* Blood, 2006. **107**(1): p. 293-300.

179. Sato, T., X. Yang, S. Knapper, P. White, B.D. Smith, S. Galkin, et al., *FLT3 ligand impedes the efficacy of FLT3 inhibitors in vitro and in vivo.* Blood, 2011. **117**(12): p. 3286-93. 3069670

180. Baker, S.D., E.I. Zimmerman, Y.D. Wang, S. Orwick, D.S. Zatechka, J. Buaboonnam, et al., *Emergence of polyclonal FLT3 tyrosine kinase domain mutations during sequential therapy with sorafenib and sunitinib in FLT3-ITD-positive acute myeloid leukemia.* Clin Cancer Res, 2013. **19**(20): p. 5758-68. PMC3878304

181. Smith, C.C., E.A. Lasater, K.C. Lin, Q. Wang, M.Q. McCreery, W.K. Stewart, et al., *Crenolanib is a selective type I pan-FLT3 inhibitor.* Proc Natl Acad Sci U S A, 2014. **111**(14): p. 5319-24. PMC3986131

182. Zimmerman, E.I., D.C. Turner, J. Buaboonnam, S. Hu, S. Orwick, M.S. Roberts, et al., *Crenolanib is active against models of drug-resistant FLT3-ITD-positive acute myeloid leukemia.* Blood, 2013. **122**(22): p. 3607-15. PMC3837509

183. Ben-Batalla, I., A. Schultze, M. Wroblewski, R. Erdmann, M. Heuser, J.S. Waizenegger, et al., *Axl, a prognostic and therapeutic target in acute myeloid leukemia mediates paracrine crosstalk of leukemia cells with bone marrow stroma.* Blood, 2013. **122**(14): p. 2443-52.

184. Hou, P., C. Wu, Y. Wang, R. Qi, D. Bhavanasi, Z. Zuo, et al., *A Genome-Wide CRISPR Screen Identifies Genes Critical for Resistance to FLT3 Inhibitor AC220.* Cancer Res, 2017. **77**(16): p. 4402-4413. PMC5559306

185. Javidi-Sharifi, N., J. Martinez, I. English, S.K. Joshi, R. Scopim-Ribeiro, S.K. Viola, et al., *FGF2-FGFR1 signaling regulates release of Leukemia-Protective exosomes from bone marrow stromal cells.* Elife, 2019. **8**. PMC6363389

186. Damnernsawad, A., T. Nechiporuk, D. Bottomly, S.E. Kurtz, C.A. Eide, S.K. McWeeney, et al., *Genome-Wide CRISPR Screening Identifies MAPK and Mtorc Pathways As*

Regulators of Sorafenib Resistance in Acute Myeloid Leukemia. Blood, 2019. **134**(Supplement_1): p. 2557-2557.

187. Dhillon, A.S., S. Hagan, O. Rath, and W. Kolch, *MAP kinase signalling pathways in cancer.* Oncogene, 2007. **26**(22): p. 3279-90.

188. Samatar, A.A. and P.I. Poulikakos, *Targeting RAS-ERK signalling in cancer: promises and challenges.* Nat Rev Drug Discov, 2014. **13**(12): p. 928-42.

189. Hong, A., M. Piva, S. Liu, W. Hugo, S.H. Lomeli, V. Zoete, et al., *Durable Suppression of Acquired MEK Inhibitor Resistance in Cancer by Sequestering MEK from ERK and Promoting Anti-Tumor T-cell Immunity.* Cancer Discov, 2020.

190. Kornblau, S.M., P.P. Ruvolo, R.Y. Wang, V.L. Battula, E.J. Shpall, V.R. Ruvolo, et al., *Distinct protein signatures of acute myeloid leukemia bone marrow-derived stromal cells are prognostic for patient survival.* Haematologica, 2018.

191. Raaijmakers, M.H., S. Mukherjee, S. Guo, S. Zhang, T. Kobayashi, J.A. Schoonmaker, et al., *Bone progenitor dysfunction induces myelodysplasia and secondary leukaemia.* Nature, 2010. **464**(7290): p. 852-7. PMC3422863

192. Tabe, Y. and M. Konopleva, *Advances in understanding the leukaemia microenvironment.* Br J Haematol, 2014. **164**(6): p. 767-78. PMC4381431

193. Xia, B., C. Tian, S. Guo, L. Zhang, D. Zhao, F. Qu, et al., *c-Myc plays part in drug resistance mediated by bone marrow stromal cells in acute myeloid leukemia.* Leuk Res, 2015. **39**(1): p. 92-9.

194. Spaeth, E.L., A.M. Labaff, B.P. Toole, A. Klopp, M. Andreeff, and F.C. Marini, *Mesenchymal CD44 expression contributes to the acquisition of an activated fibroblast phenotype via TWIST activation in the tumor microenvironment.* Cancer Res, 2013. **73**(17): p. 5347-59. PMC3767181

195. Weisberg, E., Q. Liu, E. Nelson, A.L. Kung, A.L. Christie, R. Bronson, et al., *Using combination therapy to override stromal-mediated chemoresistance in mutant FLT3-*

positive AML: synergism between FLT3 inhibitors, dasatinib/multi-targeted inhibitors and JAK inhibitors. Leukemia, 2012. **26**(10): p. 2233-44. PMC4054699

196. Ayala, F., R. Dewar, M. Kieran, and R. Kalluri, *Contribution of bone microenvironment to leukemogenesis and leukemia progression.* Leukemia, 2009. **23**(12): p. 2233-41. PMC4313556

197. Hui, L. and Y. Chen, *Tumor microenvironment: Sanctuary of the devil.* Cancer Lett, 2015. **368**(1): p. 7-13.

198. Stirewalt, D.L. and J.P. Radich, *The role of FLT3 in haematopoietic malignancies.* Nat Rev Cancer, 2003. **3**(9): p. 650-65.

199. Ghiaur, G. and M. Levis, *Mechanisms of Resistance to FLT3 Inhibitors and the Role of the Bone Marrow Microenvironment.* Hematol Oncol Clin North Am, 2017. **31**(4): p. 681-692. PMC5512588

200. Weisberg, E., Q. Liu, X. Zhang, E. Nelson, M. Sattler, F. Liu, et al., *Selective Akt inhibitors synergize with tyrosine kinase inhibitors and effectively override stroma-associated cytoprotection of mutant FLT3-positive AML cells.* PLoS One, 2013. **8**(2): p. e56473. 3578845

201. Druker, B.J., C.L. Sawyers, H. Kantarjian, D.J. Resta, S.F. Reese, J.M. Ford, et al., *Activity of a specific inhibitor of the BCR-ABL tyrosine kinase in the blast crisis of chronic myeloid leukemia and acute lymphoblastic leukemia with the Philadelphia chromosome.* N Engl J Med, 2001. **344**(14): p. 1038-42.

202. Joensuu, H., *Adjuvant treatment of GIST: patient selection and treatment strategies.* Nat Rev Clin Oncol, 2012. **9**(6): p. 351-8.

203. Rutkowski, P., M. Van Glabbeke, C.J. Rankin, W. Ruka, B.P. Rubin, M. Debiec-Rychter, et al., *Imatinib mesylate in advanced dermatofibrosarcoma protuberans: pooled analysis of two phase II clinical trials.* J Clin Oncol, 2010. **28**(10): p. 1772-9. PMC3040044

204. Mathisen, M.S., S. O'Brien, D. Thomas, J. Cortes, H. Kantarjian, and F. Ravandi, *Role of tyrosine kinase inhibitors in the management of Philadelphia chromosome-positive acute lymphoblastic leukemia.* Curr Hematol Malig Rep, 2011. **6**(3): p. 187-94. PMC4201047

205. Scott, L.J., *Larotrectinib: First Global Approval.* Drugs, 2019.

206. *Larotrectinib OK'd for Cancers with TRK Fusions.* Cancer Discov, 2019. **9**(1): p. 8-9.

207. Drilon, A., T.W. Laetsch, S. Kummar, S.G. DuBois, U.N. Lassen, G.D. Demetri, et al., *Efficacy of Larotrectinib in TRK Fusion-Positive Cancers in Adults and Children.* N Engl J Med, 2018. **378**(8): p. 731-739. PMC5857389

208. *Larotrectinib Has Antitumor Activity in TRK(+) Pediatric Solid Tumors.* Cancer Discov, 2018. **8**(6): p. OF17.

209. *Entrectinib OK'd for Cancers with NTRK Fusions, NSCLC.* Cancer Discov, 2019. **9**(10): p. OF2.

210. Amatu, A., A. Sartore-Bianchi, and S. Siena, *NTRK gene fusions as novel targets of cancer therapy across multiple tumour types.* ESMO Open, 2016. **1**(2): p. e000023. PMC5070277

211. Tognon, C., M. Garnett, E. Kenward, R. Kay, K. Morrison, and P.H. Sorensen, *The chimeric protein tyrosine kinase ETV6-NTRK3 requires both Ras-Erk1/2 and PI3-kinase-Akt signaling for fibroblast transformation.* Cancer Res, 2001. **61**(24): p. 8909-16.

212. Calella, A.M., C. Nerlov, R.G. Lopez, C. Sciarretta, O. von Bohlen und Halbach, O. Bereshchenko, et al., *Neurotrophin/Trk receptor signaling mediates C/EBPalpha, -beta and NeuroD recruitment to immediate-early gene promoters in neuronal cells and requires C/EBPs to induce immediate-early gene transcription.* Neural Dev, 2007. **2**: p. 4. PMC1796876

213. Martin-Zanca, D., S.H. Hughes, and M. Barbacid, *A human oncogene formed by the fusion of truncated tropomyosin and protein tyrosine kinase sequences.* Nature, 1986. **319**(6056): p. 743-8.

214. Greco, A., C. Miranda, and M.A. Pierotti, *Rearrangements of NTRK1 gene in papillary thyroid carcinoma.* Mol Cell Endocrinol, 2010. **321**(1): p. 44-9.

215. Brzezianska, E., M. Karbownik, M. Migdalska-Sek, D. Pastuszak-Lewandoska, J. Wloch, and A. Lewinski, *Molecular analysis of the RET and NTRK1 gene rearrangements in papillary thyroid carcinoma in the Polish population.* Mutat Res, 2006. **599**(1-2): p. 26-35.

216. Vaishnavi, A., M. Capelletti, A.T. Le, S. Kako, M. Butaney, D. Ercan, et al., *Oncogenic and drug-sensitive NTRK1 rearrangements in lung cancer.* Nat Med, 2013. **19**(11): p. 1469-1472. PMC3823836

217. Wu, G., A.K. Diaz, B.S. Paugh, S.L. Rankin, B. Ju, Y. Li, et al., *The genomic landscape of diffuse intrinsic pontine glioma and pediatric non-brainstem high-grade glioma.* Nat Genet, 2014. **46**(5): p. 444-450. PMC4056452

218. Tognon, C., S.R. Knezevich, D. Huntsman, C.D. Roskelley, N. Melnyk, J.A. Mathers, et al., *Expression of the ETV6-NTRK3 gene fusion as a primary event in human secretory breast carcinoma.* Cancer Cell, 2002. **2**(5): p. 367-76.

219. Frattini, V., V. Trifonov, J.M. Chan, A. Castano, M. Lia, F. Abate, et al., *The integrated landscape of driver genomic alterations in glioblastoma.* Nat Genet, 2013. **45**(10): p. 1141-9. PMC3799953

220. Drilon, A., G. Li, S. Dogan, M. Gounder, R. Shen, M. Arcila, et al., *What hides behind the MASC: clinical response and acquired resistance to entrectinib after ETV6-NTRK3 identification in a mammary analogue secretory carcinoma (MASC).* Ann Oncol, 2016. **27**(5): p. 920-6. PMC4843186

221. Drilon, A., S. Siena, S.I. Ou, M. Patel, M.J. Ahn, J. Lee, et al., *Safety and Antitumor Activity of the Multitargeted Pan-TRK, ROS1, and ALK Inhibitor Entrectinib: Combined Results from Two Phase I Trials (ALKA-372-001 and STARTRK-1).* Cancer Discov, 2017. **7**(4): p. 400-409. PMC5380583

222. Okamura, R., A. Boichard, S. Kato, J.K. Sicklick, L. Bazhenova, and R. Kurzrock, *Analysis of NTRK Alterations in Pan-Cancer Adult and Pediatric Malignancies: Implications for NTRK-Targeted Therapeutics.* JCO Precis Oncol, 2018. **2018**. PMC6329466

223. Skalova, A., T. Vanecek, R. Sima, J. Laco, I. Weinreb, B. Perez-Ordonez, et al., *Mammary analogue secretory carcinoma of salivary glands, containing the ETV6-NTRK3 fusion gene: a hitherto undescribed salivary gland tumor entity.* Am J Surg Pathol, 2010. **34**(5): p. 599-608.

224. Nagasubramanian, R., J. Wei, P. Gordon, J.C. Rastatter, M.C. Cox, and A. Pappo, *Infantile Fibrosarcoma With NTRK3-ETV6 Fusion Successfully Treated With the Tropomyosin-Related Kinase Inhibitor LOXO-101.* Pediatr Blood Cancer, 2016. **63**(8): p. 1468-70. PMC5074243

225. Bishop, J.A., R. Yonescu, D. Batista, S. Begum, D.W. Eisele, and W.H. Westra, *Utility of mammaglobin immunohistochemistry as a proxy marker for the ETV6-NTRK3 translocation in the diagnosis of salivary mammary analogue secretory carcinoma.* Hum Pathol, 2013. **44**(10): p. 1982-8. PMC3779501

226. Halalsheh, H., M.B. McCarville, M. Neel, M. Reynolds, M.C. Cox, and A.S. Pappo, *Dramatic bone remodeling following larotrectinib administration for bone metastasis in a patient with TRK fusion congenital mesoblastic nephroma.* Pediatr Blood Cancer, 2018. **65**(10): p. e27271.

227. Davis, J.L., C.M. Lockwood, C.M. Albert, K. Tsuchiya, D.S. Hawkins, and E.R. Rudzinski, *Infantile NTRK-associated Mesenchymal Tumors.* Pediatr Dev Pathol, 2018. **21**(1): p. 68-78.

228. Vaishnavi, A., A.T. Le, and R.C. Doebele, *TRKing down an old oncogene in a new era of targeted therapy.* Cancer Discov, 2015. **5**(1): p. 25-34. PMC4293234

229. Ardini, E., R. Bosotti, A.L. Borgia, C. De Ponti, A. Somaschini, R. Cammarota, et al., *The TPM3-NTRK1 rearrangement is a recurring event in colorectal carcinoma and is associated with tumor sensitivity to TRKA kinase inhibition.* Mol Oncol, 2014. **8**(8): p. 1495-507. PMC5528583

230. Kheder, E.S. and D.S. Hong, *Emerging Targeted Therapy for Tumors with NTRK Fusion Proteins.* Clin Cancer Res, 2018. **24**(23): p. 5807-5814.

231. Euhus, D.M., C.F. Timmons, and G.E. Tomlinson, *ETV6-NTRK3--Trk-ing the primary event in human secretory breast cancer.* Cancer Cell, 2002. **2**(5): p. 347-8.

232. Knezevich, S.R., D.E. McFadden, W. Tao, J.F. Lim, and P.H. Sorensen, *A novel ETV6-NTRK3 gene fusion in congenital fibrosarcoma.* Nat Genet, 1998. **18**(2): p. 184-7.

233. Leeman-Neill, R.J., L.M. Kelly, P. Liu, A.V. Brenner, M.P. Little, T.I. Bogdanova, et al., *ETV6-NTRK3 is a common chromosomal rearrangement in radiation-associated thyroid cancer.* Cancer, 2014. **120**(6): p. 799-807. PMC3947712

234. Golub, T.R., G.F. Barker, M. Lovett, and D.G. Gilliland, *Fusion of PDGF receptor beta to a novel ets-like gene, tel, in chronic myelomonocytic leukemia with t(5;12) chromosomal translocation.* Cell, 1994. **77**(2): p. 307-16.

235. Papadopoulos, P., S.A. Ridge, C.A. Boucher, C. Stocking, and L.M. Wiedemann, *The novel activation of ABL by fusion to an ets-related gene, TEL.* Cancer Res, 1995. **55**(1): p. 34-8.

236. Wai, D.H., S.R. Knezevich, T. Lucas, B. Jansen, R.J. Kay, and P.H. Sorensen, *The ETV6-NTRK3 gene fusion encodes a chimeric protein tyrosine kinase that transforms NIH3T3 cells.* Oncogene, 2000. **19**(7): p. 906-15.

237. Carroll, M., M.H. Tomasson, G.F. Barker, T.R. Golub, and D.G. Gilliland, *The TEL/platelet-derived growth factor beta receptor (PDGF beta R) fusion in chronic myelomonocytic leukemia is a transforming protein that self-associates and activates*

PDGF beta R kinase-dependent signaling pathways. Proc Natl Acad Sci U S A, 1996. **93**(25): p. 14845-50. PMC26224

238. Jousset, C., C. Carron, A. Boureux, C.T. Quang, C. Oury, I. Dusanter-Fourt, et al., *A domain of TEL conserved in a subset of ETS proteins defines a specific oligomerization interface essential to the mitogenic properties of the TEL-PDGFR beta oncoprotein.* EMBO J, 1997. **16**(1): p. 69-82. PMC1169615

239. Tognon, C.E., C.D. Mackereth, A.M. Somasiri, L.P. McIntosh, and P.H. Sorensen, *Mutations in the SAM domain of the ETV6-NTRK3 chimeric tyrosine kinase block polymerization and transformation activity.* Mol Cell Biol, 2004. **24**(11): p. 4636-50. PMC416412

240. Golub, T.R., G.F. Barker, S.K. Bohlander, S.W. Hiebert, D.C. Ward, P. Bray-Ward, et al., *Fusion of the TEL gene on 12p13 to the AML1 gene on 21q22 in acute lymphoblastic leukemia.* Proc Natl Acad Sci U S A, 1995. **92**(11): p. 4917-21. PMC41818

241. Hoglund, M., B. Johansson, J. Pedersen-Bjergaard, P. Marynen, and F. Mitelman, *Molecular characterization of 12p abnormalities in hematologic malignancies: deletion of KIP1, rearrangement of TEL, and amplification of CCND2.* Blood, 1996. **87**(1): p. 324-30.

242. De Braekeleer, E., N. Douet-Guilbert, F. Morel, M.J. Le Bris, A. Basinko, and M. De Braekeleer, *ETV6 fusion genes in hematological malignancies: a review.* Leuk Res, 2012. **36**(8): p. 945-61.

243. Zhou, F. and B. Chen, *Acute myeloid leukemia carrying ETV6 mutations: biologic and clinical features.* Hematology, 2018. **23**(9): p. 608-612.

244. Eguchi, M., M. Eguchi-Ishimae, A. Tojo, K. Morishita, K. Suzuki, Y. Sato, et al., *Fusion of ETV6 to neurotrophin-3 receptor TRKC in acute myeloid leukemia with t(12;15)(p13;q25).* Blood, 1999. **93**(4): p. 1355-63.

245. Setoyama, M., A. Tojo, F. Nagamura, S. Asano, M. Ishimae, M. Eguchi, et al., *A unique translocation of the TEL gene in a case of acute myelogenous leukemia with inv(12)(p13q15).* Blood, 1998. **92**(4): p. 1454-5.

246. Eguchi, M., M. Eguchi-Ishimae, A. Green, T. Enver, and M. Greaves, *Directing oncogenic fusion genes into stem cells via an SCL enhancer.* Proc Natl Acad Sci U S A, 2005. **102**(4): p. 1133-8. PMC545834

247. Kralik, J.M., W. Kranewitter, H. Boesmueller, R. Marschon, G. Tschurtschenthaler, H. Rumpold, et al., *Characterization of a newly identified ETV6-NTRK3 fusion transcript in acute myeloid leukemia.* Diagn Pathol, 2011. **6**: p. 19. PMC3063188

248. Taylor, J., D. Pavlick, A. Yoshimi, C. Marcelus, S.S. Chung, J.F. Hechtman, et al., *Oncogenic TRK fusions are amenable to inhibition in hematologic malignancies.* J Clin Invest, 2018. **128**(9): p. 3819-3825. PMC6118587

249. Tomasson, M.H., Z. Xiang, R. Walgren, Y. Zhao, Y. Kasai, T. Miner, et al., *Somatic mutations and germline sequence variants in the expressed tyrosine kinase genes of patients with de novo acute myeloid leukemia.* Blood, 2008. **111**(9): p. 4797-808. PMC2343607

250. Li, Z., G. Beutel, M. Rhein, J. Meyer, C. Koenecke, T. Neumann, et al., *High-affinity neurotrophin receptors and ligands promote leukemogenesis.* Blood, 2009. **113**(9): p. 2028-37. PMC2651014

251. Iacobucci, I., J. Wen, M. Meggendorfer, J.K. Choi, L. Shi, S.B. Pounds, et al., *Genomic subtyping and therapeutic targeting of acute erythroleukemia.* Nat Genet, 2019. **51**(4): p. 694-704.

252. Lamballe, F., P. Tapley, and M. Barbacid, *trkC encodes multiple neurotrophin-3 receptors with distinct biological properties and substrate specificities.* EMBO J, 1993. **12**(8): p. 3083-94. PMC413573

253. Liu, Q., J. Schwaller, J. Kutok, D. Cain, J.C. Aster, I.R. Williams, et al., *Signal transduction and transforming properties of the TEL-TRKC fusions associated with t(12;15)(p13;q25) in congenital fibrosarcoma and acute myelogenous leukemia.* EMBO J, 2000. **19**(8): p. 1827-38. PMC302017

254. Forghieri, F., M. Morselli, L. Potenza, M. Maccaferri, L. Pedrazzi, A. Paolini, et al., *Chronic eosinophilic leukaemia with ETV6-NTRK3 fusion transcript in an elderly patient affected with pancreatic carcinoma.* Eur J Haematol, 2011. **86**(4): p. 352-5.

255. Pemovska, T., M. Kontro, B. Yadav, H. Edgren, S. Eldfors, A. Szwajda, et al., *Individualized systems medicine strategy to tailor treatments for patients with chemorefractory acute myeloid leukemia.* Cancer Discov, 2013. **3**(12): p. 1416-29.

256. Roberts, K.G., Y. Li, D. Payne-Turner, R.C. Harvey, Y.L. Yang, D. Pei, et al., *Targetable kinase-activating lesions in Ph-like acute lymphoblastic leukemia.* N Engl J Med, 2014. **371**(11): p. 1005-15. PMC4191900

257. Roberts, K.G., L.J. Janke, Y. Zhao, A. Seth, J. Ma, D. Finkelstein, et al., *ETV6-NTRK3 induces aggressive acute lymphoblastic leukemia highly sensitive to selective TRK inhibition.* Blood, 2018. **132**(8): p. 861-865. PMC6107883

258. Roberts, K.G., Z. Gu, D. Payne-Turner, K. McCastlain, R.C. Harvey, I.M. Chen, et al., *High Frequency and Poor Outcome of Philadelphia Chromosome-Like Acute Lymphoblastic Leukemia in Adults.* J Clin Oncol, 2017. **35**(4): p. 394-401. PMC5455698

259. Wang, Y., S. Miller, D. Roulston, D. Bixby, and L. Shao, *Genome-Wide Single-Nucleotide Polymorphism Array Analysis Improves Prognostication of Acute Lymphoblastic Leukemia/Lymphoma.* J Mol Diagn, 2016. **18**(4): p. 595-603.

260. Alessandri, A.J., S.R. Knezevich, J.A. Mathers, K.R. Schultz, and P.H. Sorensen, *Absence of t(12;15) associated ETV6-NTRK3 fusion transcripts in pediatric acute leukemias.* Med Pediatr Oncol, 2001. **37**(4): p. 415-6.

261. Diamond, E.L., B.H. Durham, J. Haroche, Z. Yao, J. Ma, S.A. Parikh, et al., *Diverse and Targetable Kinase Alterations Drive Histiocytic Neoplasms.* Cancer Discov, 2016. **6**(2): p. 154-65. PMC4744547

262. Chalmers, Z.R., S.M. Ali, R.S. Ohgami, P.V. Campregher, G.M. Frampton, R. Yelensky, et al., *Comprehensive genomic profiling identifies a novel TNKS2-PDGFRA fusion that defines a myeloid neoplasm with eosinophilia that responded dramatically to imatinib therapy.* Blood Cancer J, 2015. **5**: p. e278. PMC4349257

263. Sigal, D.S., M.S. Bhangoo, J.A. Hermel, D.C. Pavlick, G. Frampton, V.A. Miller, et al., *Comprehensive genomic profiling identifies novel NTRK fusions in neuroendocrine tumors.* Oncotarget, 2018. **9**(88): p. 35809-35812. PMC6254675

264. Campbell, P.J., P.J. Stephens, E.D. Pleasance, S. O'Meara, H. Li, T. Santarius, et al., *Identification of somatically acquired rearrangements in cancer using genome-wide massively parallel paired-end sequencing.* Nat Genet, 2008. **40**(6): p. 722-9. PMC2705838

265. Watson, F.L., M.A. Porcionatto, A. Bhattacharyya, C.D. Stiles, and R.A. Segal, *TrkA glycosylation regulates receptor localization and activity.* J Neurobiol, 1999. **39**(2): p. 323-36.

266. Coulier, F., R. Kumar, M. Ernst, R. Klein, D. Martin-Zanca, and M. Barbacid, *Human trk oncogenes activated by point mutation, in-frame deletion, and duplication of the tyrosine kinase domain.* Mol Cell Biol, 1990. **10**(8): p. 4202-10. PMC360953

267. Meyer, J., M. Rhein, B. Schiedlmeier, O. Kustikova, C. Rudolph, K. Kamino, et al., *Remarkable leukemogenic potency and quality of a constitutively active neurotrophin receptor, deltaTrkA.* Leukemia, 2007. **21**(10): p. 2171-80.

268. Arevalo, J.C., B. Conde, B.L. Hempstead, M.V. Chao, D. Martin-Zanca, and P. Perez, *TrkA immunoglobulin-like ligand binding domains inhibit spontaneous activation of the receptor.* Mol Cell Biol, 2000. **20**(16): p. 5908-16. PMC86068

269. Arevalo, J.C., B. Conde, B.I. Hempstead, M.V. Chao, D. Martin-Zanca, and P. Perez, *A novel mutation within the extracellular domain of TrkA causes constitutive receptor activation.* Oncogene, 2001. **20**(10): p. 1229-34.

270. Tacconelli, A., A.R. Farina, L. Cappabianca, G. Desantis, A. Tessitore, A. Vetuschi, et al., *TrkA alternative splicing: a regulated tumor-promoting switch in human neuroblastoma.* Cancer Cell, 2004. **6**(4): p. 347-60.

271. Kaebisch, A., S. Brokt, U. Seay, J. Lohmeyer, U. Jaeger, and H. Pralle, *Expression of the nerve growth factor receptor c-TRK in human myeloid leukaemia cells.* Br J Haematol, 1996. **95**(1): p. 102-9.

272. Labouyrie, E., P. Dubus, A. Groppi, F.X. Mahon, J. Ferrer, M. Parrens, et al., *Expression of neurotrophins and their receptors in human bone marrow.* Am J Pathol, 1999. **154**(2): p. 405-15. PMC1849993

273. Kermani, P., D. Rafii, D.K. Jin, P. Whitlock, W. Schaffer, A. Chiang, et al., *Neurotrophins promote revascularization by local recruitment of TrkB+ endothelial cells and systemic mobilization of hematopoietic progenitors.* J Clin Invest, 2005. **115**(3): p. 653-63. PMC1051987

274. Vega, J.A., O. Garcia-Suarez, J. Hannestad, M. Perez-Perez, and A. Germana, *Neurotrophins and the immune system.* J Anat, 2003. **203**(1): p. 1-19. PMC1571144

275. Maroder, M., D. Bellavia, D. Meco, M. Napolitano, A. Stigliano, E. Alesse, et al., *Expression of trKB neurotrophin receptor during T cell development. Role of brain derived neurotrophic factor in immature thymocyte survival.* J Immunol, 1996. **157**(7): p. 2864-72.

276. Mulloy, J.C., V. Jankovic, M. Wunderlich, R. Delwel, J. Cammenga, O. Krejci, et al., *AML1-ETO fusion protein up-regulates TRKA mRNA expression in human CD34+ cells, allowing nerve growth factor-induced expansion.* Proc Natl Acad Sci U S A, 2005. **102**(11): p. 4016-21. PMC554792

277. Herbrich, S.M., S. Kannan, R.M. Nolo, M. Hornbaker, J. Chandra, and P.A. Zweidler-McKay, *Characterization of TRKA signaling in acute myeloid leukemia.* Oncotarget, 2018. **9**(53): p. 30092-30105. PMC6059018

278. Peng, W.M., L. Maintz, J.P. Allam, U. Raap, I. Gutgemann, J. Kirfel, et al., *Increased circulating levels of neurotrophins and elevated expression of their high-affinity receptors on skin and gut mast cells in mastocytosis.* Blood, 2013. **122**(10): p. 1779-88.

279. Yang, M., K. Huang, G. Busche, A. Ganser, and Z. Li, *Activation of TRKB receptor in murine hematopoietic stem/progenitor cells induced mastocytosis.* Blood, 2014. **124**(7): p. 1196-7.

280. Yang, M., Z. Pan, K. Huang, G. Busche, F. Feuerhake, A. Chaturvedi, et al., *Activation of TRKA receptor elicits mastocytosis in mice and is involved in the development of resistance to KIT-targeted therapy.* Oncotarget, 2017. **8**(43): p. 73871-73883. PMC5650308

281. O'Hare, T., M.W. Deininger, C.A. Eide, T. Clackson, and B.J. Druker, *Targeting the BCR-ABL signaling pathway in therapy-resistant Philadelphia chromosome-positive leukemia.* Clin Cancer Res, 2011. **17**(2): p. 212-21.

282. Ren, R., *Mechanisms of BCR-ABL in the pathogenesis of chronic myelogenous leukaemia.* Nat Rev Cancer, 2005. **5**(3): p. 172-83.

283. Cowan-Jacob, S.W., V. Guez, G. Fendrich, J.D. Griffin, D. Fabbro, P. Furet, et al., *Imatinib (STI571) resistance in chronic myelogenous leukemia: molecular basis of the underlying mechanisms and potential strategies for treatment.* Mini Rev Med Chem, 2004. **4**(3): p. 285-99.

284. Gu, T.L., L. Popova, C. Reeves, J. Nardone, J. Macneill, J. Rush, et al., *Phosphoproteomic analysis identifies the M0-91 cell line as a cellular model for the study of TEL-TRKC fusion-associated leukemia.* Leukemia, 2007. **21**(3): p. 563-6.

285. Chen, S., S. Nagel, B. Schneider, H. Dai, R. Geffers, M. Kaufmann, et al., *A new ETV6-NTRK3 cell line model reveals MALAT1 as a novel therapeutic target - a short report.* Cell Oncol (Dordr), 2018. **41**(1): p. 93-101.

286. Tognon, C.E., B. Rafn, N.M. Cetinbas, T. Kamura, G. Trigo, B. Rotblat, et al., *Insulin-like growth factor 1 receptor stabilizes the ETV6-NTRK3 chimeric oncoprotein by blocking its KPC1/Rnf123-mediated proteasomal degradation.* J Biol Chem, 2018. **293**(32): p. 12502-12515. PMC6093223

287. Tapley, P., F. Lamballe, and M. Barbacid, *K252a is a selective inhibitor of the tyrosine protein kinase activity of the trk family of oncogenes and neurotrophin receptors.* Oncogene, 1992. **7**(2): p. 371-81.

288. Fabbro, D., S. Ruetz, S. Bodis, M. Pruschy, K. Csermak, A. Man, et al., *PKC412--a protein kinase inhibitor with a broad therapeutic potential.* Anticancer Drug Des, 2000. **15**(1): p. 17-28.

289. Weisberg, E., C. Boulton, L.M. Kelly, P. Manley, D. Fabbro, T. Meyer, et al., *Inhibition of mutant FLT3 receptors in leukemia cells by the small molecule tyrosine kinase inhibitor PKC412.* Cancer Cell, 2002. **1**(5): p. 433-43.

290. Chi, H.T., B.T. Ly, Y. Kano, A. Tojo, T. Watanabe, and Y. Sato, *ETV6-NTRK3 as a therapeutic target of small molecule inhibitor PKC412.* Biochem Biophys Res Commun, 2012. **429**(1-2): p. 87-92.

291. Shaw, A.T., D.W. Kim, K. Nakagawa, T. Seto, L. Crino, M.J. Ahn, et al., *Crizotinib versus chemotherapy in advanced ALK-positive lung cancer.* N Engl J Med, 2013. **368**(25): p. 2385-94.

292. Taipale, M., I. Krykbaeva, L. Whitesell, S. Santagata, J. Zhang, Q. Liu, et al., *Chaperones as thermodynamic sensors of drug-target interactions reveal kinase inhibitor specificities in living cells.* Nat Biotechnol, 2013. **31**(7): p. 630-7. PMC3774174

293. Tognon, C.E., A.M. Somasiri, V.E. Evdokimova, G. Trigo, E.E. Uy, N. Melnyk, et al., *ETV6-NTRK3-mediated breast epithelial cell transformation is blocked by targeting the IGF1R signaling pathway.* Cancer Res, 2011. **71**(3): p. 1060-70.

294. Thress, K., T. Macintyre, H. Wang, D. Whitston, Z.Y. Liu, E. Hoffmann, et al., *Identification and preclinical characterization of AZ-23, a novel, selective, and orally bioavailable inhibitor of the Trk kinase pathway.* Mol Cancer Ther, 2009. **8**(7): p. 1818-27.

295. Rolfo, C., R. Ruiz, E. Giovannetti, I. Gil-Bazo, A. Russo, F. Passiglia, et al., *Entrectinib: a potent new TRK, ROS1, and ALK inhibitor.* Expert Opin Investig Drugs, 2015. **24**(11): p. 1493-500.

296. Smith, K.M., P.C. Fagan, E. Pomari, G. Germano, C. Frasson, C. Walsh, et al., *Antitumor Activity of Entrectinib, a Pan-TRK, ROS1, and ALK Inhibitor, in ETV6-NTRK3-Positive Acute Myeloid Leukemia.* Mol Cancer Ther, 2018. **17**(2): p. 455-463.

297. Fuse, M.J., K. Okada, T. Oh-Hara, H. Ogura, N. Fujita, and R. Katayama, *Mechanisms of Resistance to NTRK Inhibitors and Therapeutic Strategies in NTRK1-Rearranged Cancers.* Mol Cancer Ther, 2017. **16**(10): p. 2130-2143.

298. Konicek, B.W., A.R. Capen, K.M. Credille, P.J. Ebert, B.L. Falcon, G.L. Heady, et al., *Merestinib (LY2801653) inhibits neurotrophic receptor kinase (NTRK) and suppresses growth of NTRK fusion bearing tumors.* Oncotarget, 2018. **9**(17): p. 13796-13806. PMC5862616

299. O'Hare, T., D.K. Walters, E.P. Stoffregen, T. Jia, P.W. Manley, J. Mestan, et al., *In vitro activity of Bcr-Abl inhibitors AMN107 and BMS-354825 against clinically relevant imatinib-resistant Abl kinase domain mutants.* Cancer Res, 2005. **65**(11): p. 4500-5.

300. Apperley, J.F., *Part I: mechanisms of resistance to imatinib in chronic myeloid leukaemia.* Lancet Oncol, 2007. **8**(11): p. 1018-29.

301. Larrosa-Garcia, M. and M.R. Baer, *FLT3 Inhibitors in Acute Myeloid Leukemia: Current Status and Future Directions.* Mol Cancer Ther, 2017. **16**(6): p. 991-1001. PMC5600895

302. Russo, M., S. Misale, G. Wei, G. Siravegna, G. Crisafulli, L. Lazzari, et al., *Acquired Resistance to the TRK Inhibitor Entrectinib in Colorectal Cancer.* Cancer Discov, 2016. **6**(1): p. 36-44.

303. Drilon, A., R. Nagasubramanian, J.F. Blake, N. Ku, B.B. Tuch, K. Ebata, et al., *A Next-Generation TRK Kinase Inhibitor Overcomes Acquired Resistance to Prior TRK Kinase Inhibition in Patients with TRK Fusion-Positive Solid Tumors.* Cancer Discov, 2017. **7**(9): p. 963-972. PMC5581710

304. Drilon, A., S.I. Ou, B.C. Cho, D.W. Kim, J. Lee, J.J. Lin, et al., *Repotrectinib (TPX-0005) Is a Next-Generation ROS1/TRK/ALK Inhibitor That Potently Inhibits ROS1/TRK/ALK Solvent- Front Mutations.* Cancer Discov, 2018. **8**(10): p. 1227-1236.

305. Gatalica, Z., J. Xiu, J. Swensen, and S. Vranic, *Molecular characterization of cancers with NTRK gene fusions.* Mod Pathol, 2019. **32**(1): p. 147-153.

306. Chetty, R., *Neurotrophic tropomyosin or tyrosine receptor kinase (NTRK) genes.* J Clin Pathol, 2019.

307. Yamada, K. and T. Nabeshima, *Brain-derived neurotrophic factor/TrkB signaling in memory processes.* J Pharmacol Sci, 2003. **91**(4): p. 267-70.

308. Indo, Y., M. Tsuruta, Y. Hayashida, M.A. Karim, K. Ohta, T. Kawano, et al., *Mutations in the TRKA/NGF receptor gene in patients with congenital insensitivity to pain with anhidrosis.* Nat Genet, 1996. **13**(4): p. 485-8.

309. Tessarollo, L., P. Tsoulfas, D. Martin-Zanca, D.J. Gilbert, N.A. Jenkins, N.G. Copeland, et al., *trkC, a receptor for neurotrophin-3, is widely expressed in the developing nervous system and in non-neuronal tissues.* Development, 1993. **118**(2): p. 463-75.

310. Nakagawara, A., *Trk receptor tyrosine kinases: a bridge between cancer and neural development.* Cancer Lett, 2001. **169**(2): p. 107-14.

311. Huang, E.J. and L.F. Reichardt, *Neurotrophins: roles in neuronal development and function.* Annu Rev Neurosci, 2001. **24**: p. 677-736. PMC2758233

312. Lamballe, F., R. Klein, and M. Barbacid, *The trk family of oncogenes and neurotrophin receptors.* Princess Takamatsu Symp, 1991. **22**: p. 153-70.

313. Al-Salama, Z.T. and S.J. Keam, *Entrectinib: First Global Approval.* Drugs, 2019.

314. Warmuth, M., S. Kim, X.J. Gu, G. Xia, and F. Adrian, *Ba/F3 cells and their use in kinase drug discovery.* Curr Opin Oncol, 2007. **19**(1): p. 55-60.

315. Kelley, L.A., S. Mezulis, C.M. Yates, M.N. Wass, and M.J. Sternberg, *The Phyre2 web portal for protein modeling, prediction and analysis.* Nat Protoc, 2015. **10**(6): p. 845-58. PMC5298202

316. Tyner, J.W., M.W. Deininger, M.M. Loriaux, B.H. Chang, J.R. Gotlib, S.G. Willis, et al., *RNAi screen for rapid therapeutic target identification in leukemia patients.* Proc Natl Acad Sci U S A, 2009. **106**(21): p. 8695-700. PMC2680429

317. Tyner, J.W., W.F. Yang, A. Bankhead, 3rd, G. Fan, L.B. Fletcher, J. Bryant, et al., *Kinase pathway dependence in primary human leukemias determined by rapid inhibitor screening.* Cancer Res, 2013. **73**(1): p. 285-96. PMC3537897

318. Maxson, J.E., J. Gotlib, D.A. Pollyea, A.G. Fleischman, A. Agarwal, C.A. Eide, et al., *Oncogenic CSF3R mutations in chronic neutrophilic leukemia and atypical CML.* N Engl J Med, 2013. **368**(19): p. 1781-90. PMC3730275

319. Edwards, D.K.t., K. Watanabe-Smith, A. Rofelty, A. Damnernsawad, T. Laderas, A. Lamble, et al., *CSF1R inhibitors exhibit antitumor activity in acute myeloid leukemia by blocking paracrine signals from support cells.* Blood, 2019. **133**(6): p. 588-599. PMC6367650

320. Lek, M., K.J. Karczewski, E.V. Minikel, K.E. Samocha, E. Banks, T. Fennell, et al., *Analysis of protein-coding genetic variation in 60,706 humans.* Nature, 2016. **536**(7616): p. 285-91. PMC5018207

321. Maxson, J.E., S.B. Luty, J.D. MacManiman, M.L. Abel, B.J. Druker, and J.W. Tyner, *Ligand independence of the T618I mutation in the colony-stimulating factor 3 receptor (CSF3R) protein results from loss of O-linked glycosylation and increased receptor dimerization.* J Biol Chem, 2014. **289**(9): p. 5820-7. PMC3937653

322. White, S.H. and W.C. Wimley, *Hydrophobic interactions of peptides with membrane interfaces.* Biochim Biophys Acta, 1998. **1376**(3): p. 339-52.

323. Jones, D.T., W.R. Taylor, and J.M. Thornton, *A model recognition approach to the prediction of all-helical membrane protein structure and topology.* Biochemistry, 1994. **33**(10): p. 3038-49.

324. Nugent, T. and D.T. Jones, *Transmembrane protein topology prediction using support vector machines.* BMC Bioinformatics, 2009. **10**: p. 159. PMC2700806

325. Kall, L., A. Krogh, and E.L. Sonnhammer, *A combined transmembrane topology and signal peptide prediction method.* J Mol Biol, 2004. **338**(5): p. 1027-36.

326. Buchan, D.W., F. Minneci, T.C. Nugent, K. Bryson, and D.T. Jones, *Scalable web services for the PSIPRED Protein Analysis Workbench.* Nucleic Acids Res, 2013. **41**(Web Server issue): p. W349-57. PMC3692098

327. Tsirigos, K.D., C. Peters, N. Shu, L. Kall, and A. Elofsson, *The TOPCONS web server for consensus prediction of membrane protein topology and signal peptides.* Nucleic Acids Res, 2015. **43**(W1): p. W401-7. PMC4489233

328. Sonnhammer, E.L., G. von Heijne, and A. Krogh, *A hidden Markov model for predicting transmembrane helices in protein sequences.* Proc Int Conf Intell Syst Mol Biol, 1998. **6**: p. 175-82.

329. Krogh, A., B. Larsson, G. von Heijne, and E.L. Sonnhammer, *Predicting transmembrane protein topology with a hidden Markov model: application to complete genomes.* J Mol Biol, 2001. **305**(3): p. 567-80.

330. Jones, D.T., *Improving the accuracy of transmembrane protein topology prediction using evolutionary information.* Bioinformatics, 2007. **23**(5): p. 538-44.

331. Jones, D.T., *Protein secondary structure prediction based on position-specific scoring matrices.* J Mol Biol, 1999. **292**(2): p. 195-202.

332. Kall, L., A. Krogh, and E.L. Sonnhammer, *Advantages of combined transmembrane topology and signal peptide prediction--the Phobius web server.* Nucleic Acids Res, 2007. **35**(Web Server issue): p. W429-32. PMC1933244

333. Wybenga-Groot, L.E., B. Baskin, S.H. Ong, J. Tong, T. Pawson, and F. Sicheri, *Structural basis for autoinhibition of the Ephb2 receptor tyrosine kinase by the unphosphorylated juxtamembrane region.* Cell, 2001. **106**(6): p. 745-57.

334. Maeda, R., T. Sato, K. Okamoto, M. Yanagawa, and Y. Sako, *Lipid-Protein Interplay in Dimerization of Juxtamembrane Domains of Epidermal Growth Factor Receptor.* Biophys J, 2018. **114**(4): p. 893-903. PMC5984969

335. Maxson, J.E., S.B. Luty, J.D. MacManiman, J.C. Paik, J. Gotlib, P. Greenberg, et al., *The Colony-Stimulating Factor 3 Receptor T640N Mutation Is Oncogenic, Sensitive to JAK Inhibition, and Mimics T618I.* Clin Cancer Res, 2016. **22**(3): p. 757-64. PMC4738027

336. Maxson, J.E., M.A. Davare, S.B. Luty, C.A. Eide, B.H. Chang, M.M. Loriaux, et al., *Therapeutically Targetable ALK Mutations in Leukemia.* Cancer Res, 2015. **75**(11): p. 2146-50. PMC4453002

337. Xiang, Z., Y. Zhao, V. Mitaksov, D.H. Fremont, Y. Kasai, A. Molitoris, et al., *Identification of somatic JAK1 mutations in patients with acute myeloid leukemia.* Blood, 2008. **111**(9): p. 4809-12. PMC2343608

338. Kelley, L.A., R.M. MacCallum, and M.J. Sternberg, *Enhanced genome annotation using structural profiles in the program 3D-PSSM.* J Mol Biol, 2000. **299**(2): p. 499-520.

339. Team, R.C. *R: A language and environment for statistical computing.* . 2018; Available from: https://www.R-project.org/.

340. Team, R. *RStudio: Integrated Development for R.* 2016; Available from: http://www.rstudio.com/.

341. Wickham, H. *tidyverse: Easily Install and Load the 'Tidyverse'. R package version 1.2.1.* . 2017; Available from: https://CRAN.R-project.org/package=tidyverse

342. Slowikowski, K. *ggrepel: Automatically Position Non-Overlapping Text Labels with 'ggplot2'. R package version 0.8.0.* 2018; Available from: https://CRAN.R-project.org/package=ggrepel.

343. Hadley Wickham, J.B., *readxl: Read Excel Files. R package version 1.1.0.* . 2018.

344. Firke, S. *janitor: Simple Tools for Examining and Cleaning Dirty Data. R package version 1.1.1.* . 2018; Available from: https://CRAN.R-project.org/package=janitor.

345. Chang, W., *extrafont: Tools for using fonts. R package version 0.17.* . 2014.

346. Wickham, H. *scales: Scale Functions for Visualization. R package version 1.0.0.* . 2018; Available from: https://CRAN.R-project.org/package=scales.

347. Pedersen, T.L. *patchwork: The Composer of ggplots. R package version 0.0.1.* . 2017; Available from: https://github.com/thomasp85/patchwork.

348. Endres, N.F., R. Das, A.W. Smith, A. Arkhipov, E. Kovacs, Y. Huang, et al., *Conformational coupling across the plasma membrane in activation of the EGF receptor.* Cell, 2013. **152**(3): p. 543-56. PMC3718647

349. Perkins, A., J.L. Phillips, N.I. Kerkvliet, R.L. Tanguay, G.H. Perdew, S.K. Kolluri, et al., *A Structural Switch between Agonist and Antagonist Bound Conformations for a Ligand-Optimized Model of the Human Aryl Hydrocarbon Receptor Ligand Binding Domain.* Biology (Basel), 2014. **3**(4): p. 645-69. PMC4280506

350. Iqbal, N. and N. Iqbal, *Human Epidermal Growth Factor Receptor 2 (HER2) in Cancers: Overexpression and Therapeutic Implications.* Mol Biol Int, 2014. **2014**: p. 852748. PMC4170925

351. Olayioye, M.A., R.M. Neve, H.A. Lane, and N.E. Hynes, *The ErbB signaling network: receptor heterodimerization in development and cancer.* EMBO J, 2000. **19**(13): p. 3159-67. PMC313958

352. Slamon, D.J., W. Godolphin, L.A. Jones, J.A. Holt, S.G. Wong, D.E. Keith, et al., *Studies of the HER-2/neu proto-oncogene in human breast and ovarian cancer.* Science, 1989. **244**(4905): p. 707-12.

353. Burstein, H.J., *The distinctive nature of HER2-positive breast cancers.* N Engl J Med, 2005. **353**(16): p. 1652-4.

354. Basso, A.D., D.B. Solit, P.N. Munster, and N. Rosen, *Ansamycin antibiotics inhibit Akt activation and cyclin D expression in breast cancer cells that overexpress HER2.* Oncogene, 2002. **21**(8): p. 1159-66. PMC3221005

355. Holbro, T., R.R. Beerli, F. Maurer, M. Koziczak, C.F. Barbas, 3rd, and N.E. Hynes, *The ErbB2/ErbB3 heterodimer functions as an oncogenic unit: ErbB2 requires ErbB3 to drive breast tumor cell proliferation.* Proc Natl Acad Sci U S A, 2003. **100**(15): p. 8933-8. PMC166416

356. Nagano, M., S. Kohsaka, T. Ueno, S. Kojima, K. Saka, H. Iwase, et al., *High-Throughput Functional Evaluation of Variants of Unknown Significance in ERBB2.* Clin Cancer Res, 2018. **24**(20): p. 5112-5122.

357. Ruschoff, J., W. Hanna, M. Bilous, M. Hofmann, R.Y. Osamura, F. Penault-Llorca, et al., *HER2 testing in gastric cancer: a practical approach.* Mod Pathol, 2012. **25**(5): p. 637-50.

358. Chiosea, S.I., L. Williams, C.C. Griffith, L.D. Thompson, I. Weinreb, J.E. Bauman, et al., *Molecular characterization of apocrine salivary duct carcinoma.* Am J Surg Pathol, 2015. **39**(6): p. 744-52.

359. Heinmoller, P., C. Gross, K. Beyser, C. Schmidtgen, G. Maass, M. Pedrocchi, et al., *HER2 status in non-small cell lung cancer: results from patient screening for enrollment to a phase II study of herceptin.* Clin Cancer Res, 2003. **9**(14): p. 5238-43.

360. Lynch, T.J., D.W. Bell, R. Sordella, S. Gurubhagavatula, R.A. Okimoto, B.W. Brannigan, et al., *Activating mutations in the epidermal growth factor receptor underlying responsiveness of non-small-cell lung cancer to gefitinib.* N Engl J Med, 2004. **350**(21): p. 2129-39.

361. Paez, J.G., P.A. Janne, J.C. Lee, S. Tracy, H. Greulich, S. Gabriel, et al., *EGFR mutations in lung cancer: correlation with clinical response to gefitinib therapy.* Science, 2004. **304**(5676): p. 1497-500.

362. Engelman, J.A., P.A. Janne, C. Mermel, J. Pearlberg, T. Mukohara, C. Fleet, et al., *ErbB-3 mediates phosphoinositide 3-kinase activity in gefitinib-sensitive non-small cell lung cancer cell lines.* Proc Natl Acad Sci U S A, 2005. **102**(10): p. 3788-93. PMC553328

363. Slamon, D.J., B. Leyland-Jones, S. Shak, H. Fuchs, V. Paton, A. Bajamonde, et al., *Use of chemotherapy plus a monoclonal antibody against HER2 for metastatic breast cancer that overexpresses HER2.* N Engl J Med, 2001. **344**(11): p. 783-92.

364. Deeks, E.D., *Neratinib: First Global Approval.* Drugs, 2017. **77**(15): p. 1695-1704.

365. Lin, N.U., E.P. Winer, D. Wheatley, L.A. Carey, S. Houston, D. Mendelson, et al., *A phase II study of afatinib (BIBW 2992), an irreversible ErbB family blocker, in patients with HER2-positive metastatic breast cancer progressing after trastuzumab.* Breast Cancer Res Treat, 2012. **133**(3): p. 1057-65. PMC3387495

366. Bottomly, D., B. Wilmot, J.W. Tyner, C.A. Eide, M.M. Loriaux, B.J. Druker, et al., *HitWalker: variant prioritization for personalized functional cancer genomics.* Bioinformatics, 2013. **29**(4): p. 509-10. PMC3570211

367. Collins, D., W. Jacob, J.M. Cejalvo, M. Ceppi, I. James, M. Hasmann, et al., *Direct estrogen receptor (ER) / HER family crosstalk mediating sensitivity to lumretuzumab and pertuzumab in ER+ breast cancer.* PLoS One, 2017. **12**(5): p. e0177331. PMC5426757

368. Goss, G.D., E. Felip, M. Cobo, S. Lu, K. Syrigos, K.H. Lee, et al., *Association of ERBB Mutations With Clinical Outcomes of Afatinib- or Erlotinib-Treated Patients With Lung Squamous Cell Carcinoma: Secondary Analysis of the LUX-Lung 8 Randomized Clinical Trial.* JAMA Oncol, 2018. **4**(9): p. 1189-1197. PMC6143014

369. Clark, T.A., A.C. Schweitzer, T.X. Chen, M.K. Staples, G. Lu, H. Wang, et al., *Discovery of tissue-specific exons using comprehensive human exon microarrays.* Genome Biol, 2007. **8**(4): p. R64. PMC1896007

370. Sadeghi, A. and H. Frohlich, *Steiner tree methods for optimal sub-network identification: an empirical study.* BMC Bioinformatics, 2013. **14**: p. 144. PMC3674966

371. Roskoski, R., Jr., *Small molecule inhibitors targeting the EGFR/ErbB family of protein-tyrosine kinases in human cancers.* Pharmacol Res, 2019. **139**: p. 395-411.

372. Choi, Y., Y.S. Ko, J. Park, Y. Choi, Y. Kim, J.S. Pyo, et al., *HER2-induced metastasis is mediated by AKT/JNK/EMT signaling pathway in gastric cancer.* World J Gastroenterol, 2016. **22**(41): p. 9141-9153. PMC5107595

373. Han, J.S. and D.L. Crowe, *Jun amino-terminal kinase 1 activation promotes cell survival in ErbB2-positive breast cancer.* Anticancer Res, 2010. **30**(9): p. 3407-12.

374. Meshinchi, S., D.L. Stirewalt, T.A. Alonzo, Q. Zhang, D.A. Sweetser, W.G. Woods, et al., *Activating mutations of RTK/ras signal transduction pathway in pediatric acute myeloid leukemia.* Blood, 2003. **102**(4): p. 1474-9.

375. Robichaux, J.P., Y.Y. Elamin, R.S.K. Vijayan, M.B. Nilsson, L. Hu, J. He, et al., *Pan-Cancer Landscape and Analysis of ERBB2 Mutations Identifies Poziotinib as a Clinically Active Inhibitor and Enhancer of T-DM1 Activity.* Cancer Cell, 2019. **36**(4): p. 444-457 e7.

376. Greulich, H., B. Kaplan, P. Mertins, T.H. Chen, K.E. Tanaka, C.H. Yun, et al., *Functional analysis of receptor tyrosine kinase mutations in lung cancer identifies oncogenic extracellular domain mutations of ERBB2.* Proc Natl Acad Sci U S A, 2012. **109**(36): p. 14476-81. PMC3437859

377. Yun, C.H., T.J. Boggon, Y. Li, M.S. Woo, H. Greulich, M. Meyerson, et al., *Structures of lung cancer-derived EGFR mutants and inhibitor complexes: mechanism of activation and insights into differential inhibitor sensitivity.* Cancer Cell, 2007. **11**(3): p. 217-27. PMC1939942

378. Maxson, J.E., M.L. Abel, J. Wang, X. Deng, S. Reckel, S.B. Luty, et al., *Identification and Characterization of Tyrosine Kinase Nonreceptor 2 Mutations in Leukemia through Integration of Kinase Inhibitor Screening and Genomic Analysis.* Cancer Res, 2016. **76**(1): p. 127-38. PMC4703549

379. Szklarczyk, D., J.H. Morris, H. Cook, M. Kuhn, S. Wyder, M. Simonovic, et al., *The STRING database in 2017: quality-controlled protein-protein association networks, made broadly accessible.* Nucleic Acids Res, 2017. **45**(D1): p. D362-D368. PMC5210637

380. Carvalho, B.S. and R.A. Irizarry, *A framework for oligonucleotide microarray preprocessing.* Bioinformatics, 2010. **26**(19): p. 2363-7. PMC2944196

381. Irizarry, R.A., B. Hobbs, F. Collin, Y.D. Beazer-Barclay, K.J. Antonellis, U. Scherf, et al., *Exploration, normalization, and summaries of high density oligonucleotide array probe level data.* Biostatistics, 2003. **4**(2): p. 249-64.

382. De Kouchkovsky, I. and M. Abdul-Hay, *'Acute myeloid leukemia: a comprehensive review and 2016 update'.* Blood Cancer J, 2016. **6**(7): p. e441. PMC5030376

383. Perl, A.E., G. Martinelli, J.E. Cortes, A. Neubauer, E. Berman, S. Paolini, et al., *Gilteritinib or Chemotherapy for Relapsed or Refractory FLT3-Mutated AML.* N Engl J Med, 2019. **381**(18): p. 1728-1740.

384. Miller, C.A., J. McMichael, H.X. Dang, C.A. Maher, L. Ding, T.J. Ley, et al., *Visualizing tumor evolution with the fishplot package for R.* BMC Genomics, 2016. **17**(1): p. 880. PMC5100182

385. McKenna, A., M. Hanna, E. Banks, A. Sivachenko, K. Cibulskis, A. Kernytsky, et al., *The Genome Analysis Toolkit: a MapReduce framework for analyzing next-generation DNA sequencing data.* Genome Res, 2010. **20**(9): p. 1297-303. PMC2928508

386. Li, H., *Aligning sequence reads, clone sequences and assembly contigs with BWA-MEM.* 2013.

387. McLaren, W., L. Gil, S.E. Hunt, H.S. Riat, G.R. Ritchie, A. Thormann, et al., *The Ensembl Variant Effect Predictor.* Genome Biol, 2016. **17**(1): p. 122. PMC4893825

388. Karczewski, K.J., L.C. Francioli, G. Tiao, B.B. Cummings, J. Alföldi, Q. Wang, et al., *The mutational constraint spectrum quantified from variation in 141,456 humans.* bioRxiv, 2020: p. 531210.

389. Weisberg, E., R. Barrett, Q. Liu, R. Stone, N. Gray, and J.D. Griffin, *FLT3 inhibition and mechanisms of drug resistance in mutant FLT3-positive AML.* Drug Resist Updat, 2009. **12**(3): p. 81-9. PMC4472331

390. Traer, E., R. MacKenzie, J. Snead, A. Agarwal, A.M. Eiring, T. O'Hare, et al., *Blockade of JAK2-mediated extrinsic survival signals restores sensitivity of CML cells to ABL inhibitors.* Leukemia, 2012. **26**(5): p. 1140-3. PMC3960073

391. Colmone, A., M. Amorim, A.L. Pontier, S. Wang, E. Jablonski, and D.A. Sipkins, *Leukemic cells create bone marrow niches that disrupt the behavior of normal hematopoietic progenitor cells.* Science, 2008. **322**(5909): p. 1861-5.

392. Manshouri, T., Z. Estrov, A. Quintas-Cardama, J. Burger, Y. Zhang, A. Livun, et al., *Bone marrow stroma-secreted cytokines protect JAK2(V617F)-mutated cells from the effects of a JAK2 inhibitor.* Cancer Res, 2011. **71**(11): p. 3831-40. PMC4067142

393. Paggetti, J., F. Haderk, M. Seiffert, B. Janji, U. Distler, W. Ammerlaan, et al., *Exosomes released by chronic lymphocytic leukemia cells induce the transition of stromal cells into cancer-associated fibroblasts.* Blood, 2015. **126**(9): p. 1106-17. PMC4560344

394. Huang, J.C., S.K. Basu, X. Zhao, S. Chien, M. Fang, V.G. Oehler, et al., *Mesenchymal stromal cells derived from acute myeloid leukemia bone marrow exhibit aberrant cytogenetics and cytokine elaboration.* Blood Cancer J, 2015. **5**: p. e302. PMC4450324

395. Huan, J., N.I. Hornick, N.A. Goloviznina, A.N. Kamimae-Lanning, L.L. David, P.A. Wilmarth, et al., *Coordinate regulation of residual bone marrow function by paracrine trafficking of AML exosomes.* Leukemia, 2015. **29**(12): p. 2285-95. PMC4834971

396. Javidi-Sharifi, N., E. Traer, J. Martinez, A. Gupta, T. Taguchi, J. Dunlap, et al., *Crosstalk between KIT and FGFR3 Promotes Gastrointestinal Stromal Tumor Cell Growth and Drug Resistance.* Cancer Res, 2015. **75**(5): p. 880-91. PMC4348216

397. Itkin, T., A. Ludin, B. Gradus, S. Gur-Cohen, A. Kalinkovich, A. Schajnovitz, et al., *FGF-2 expands murine hematopoietic stem and progenitor cells via proliferation of stromal cells, c-Kit activation, and CXCL12 down-regulation.* Blood, 2012. **120**(9): p. 1843-55.

398. Zhao, M., J.T. Ross, T. Itkin, J.M. Perry, A. Venkatraman, J.S. Haug, et al., *FGF signaling facilitates postinjury recovery of mouse hematopoietic system.* Blood, 2012. **120**(9): p. 1831-42. PMC3433089

399. Steringer, J.P., H.M. Muller, and W. Nickel, *Unconventional secretion of fibroblast growth factor 2--a novel type of protein translocation across membranes?* J Mol Biol, 2015. **427**(6 Pt A): p. 1202-10.

400. Zacherl, S., G. La Venuta, H.M. Muller, S. Wegehingel, E. Dimou, P. Sehr, et al., *A direct role for ATP1A1 in unconventional secretion of fibroblast growth factor 2.* J Biol Chem, 2015. **290**(6): p. 3654-65. PMC4319031

401. Berardi, A.C., A. Wang, J. Abraham, and D.T. Scadden, *Basic fibroblast growth factor mediates its effects on committed myeloid progenitors by direct action and has no effect on hematopoietic stem cells.* Blood, 1995. **86**(6): p. 2123-9.

402. Avraham, H., N. Banu, D.T. Scadden, J. Abraham, and J.E. Groopman, *Modulation of megakaryocytopoiesis by human basic fibroblast growth factor.* Blood, 1994. **83**(8): p. 2126-32.

403. Roecklein, B.A. and B. Torok-Storb, *Functionally distinct human marrow stromal cell lines immortalized by transduction with the human papilloma virus E6/E7 genes.* Blood, 1995. **85**(4): p. 997-1005.

404. Zarrinkar, P.P., R.N. Gunawardane, M.D. Cramer, M.F. Gardner, D. Brigham, B. Belli, et al., *AC220 is a uniquely potent and selective inhibitor of FLT3 for the treatment of acute myeloid leukemia (AML).* Blood, 2009. **114**(14): p. 2984-92. PMC2756206

405. Trudel, S., S. Ely, Y. Farooqi, M. Affer, D.F. Robbiani, M. Chesi, et al., *Inhibition of fibroblast growth factor receptor 3 induces differentiation and apoptosis in t(4;14) myeloma.* Blood, 2004. **103**(9): p. 3521-8.

406. Guagnano, V., P. Furet, C. Spanka, V. Bordas, M. Le Douget, C. Stamm, et al., *Discovery of 3-(2,6-dichloro-3,5-dimethoxy-phenyl)-1-{6-[4-(4-ethyl-piperazin-1-yl)-phenylamin o]-pyrimidin-4-yl}-1-methyl-urea (NVP-BGJ398), a potent and selective inhibitor of the fibroblast growth factor receptor family of receptor tyrosine kinase.* J Med Chem, 2011. **54**(20): p. 7066-83.

407. Bianchi, G., A. Banfi, M. Mastrogiacomo, R. Notaro, L. Luzzatto, R. Cancedda, et al., *Ex vivo enrichment of mesenchymal cell progenitors by fibroblast growth factor 2.* Exp Cell Res, 2003. **287**(1): p. 98-105.

408. Coutu, D.L., M. Francois, and J. Galipeau, *Inhibition of cellular senescence by developmentally regulated FGF receptors in mesenchymal stem cells.* Blood, 2011. **117**(25): p. 6801-12.

409. Zhou, M., R.L. Sutliff, R.J. Paul, J.N. Lorenz, J.B. Hoying, C.C. Haudenschild, et al., *Fibroblast growth factor 2 control of vascular tone.* Nat Med, 1998. **4**(2): p. 201-7. PMC3850292

410. Parmar, A., S. Marz, S. Rushton, C. Holzwarth, K. Lind, S. Kayser, et al., *Stromal niche cells protect early leukemic FLT3-ITD+ progenitor cells against first-generation FLT3 tyrosine kinase inhibitors.* Cancer Res, 2011. **71**(13): p. 4696-706.

411. Peinado, H., M. Aleckovic, S. Lavotshkin, I. Matei, B. Costa-Silva, G. Moreno-Bueno, et al., *Melanoma exosomes educate bone marrow progenitor cells toward a pro-metastatic phenotype through MET.* Nat Med, 2012. **18**(6): p. 883-91. PMC3645291

412. Filipazzi, P., M. Burdek, A. Villa, L. Rivoltini, and V. Huber, *Recent advances on the role of tumor exosomes in immunosuppression and disease progression.* Semin Cancer Biol, 2012. **22**(4): p. 342-9.

413. Marlein, C.R., L. Zaitseva, R.E. Piddock, S.D. Robinson, D.R. Edwards, M.S. Shafat, et al., *NADPH oxidase-2 derived superoxide drives mitochondrial transfer from bone marrow stromal cells to leukemic blasts.* Blood, 2017. **130**(14): p. 1649-1660.

414. Moschoi, R., V. Imbert, M. Nebout, J. Chiche, D. Mary, T. Prebet, et al., *Protective mitochondrial transfer from bone marrow stromal cells to acute myeloid leukemic cells during chemotherapy.* Blood, 2016. **128**(2): p. 253-64.

415. Proia, P., G. Schiera, M. Mineo, A.M. Ingrassia, G. Santoro, G. Savettieri, et al., *Astrocytes shed extracellular vesicles that contain fibroblast growth factor-2 and vascular endothelial growth factor.* Int J Mol Med, 2008. **21**(1): p. 63-7.

416. Choi, J.S., H.I. Yoon, K.S. Lee, Y.C. Choi, S.H. Yang, I.S. Kim, et al., *Exosomes from differentiating human skeletal muscle cells trigger myogenesis of stem cells and provide*

biochemical cues for skeletal muscle regeneration. J Control Release, 2016. **222**: p. 107-15.

417. Schafer, T., H. Zentgraf, C. Zehe, B. Brugger, J. Bernhagen, and W. Nickel, *Unconventional secretion of fibroblast growth factor 2 is mediated by direct translocation across the plasma membrane of mammalian cells.* J Biol Chem, 2004. **279**(8): p. 6244-51.

418. Perez-Torres, M., B.L. Valle, N.J. Maihle, L. Negron-Vega, R. Nieves-Alicea, and E.M. Cora, *Shedding of epidermal growth factor receptor is a regulated process that occurs with overexpression in malignant cells.* Exp Cell Res, 2008. **314**(16): p. 2907-18.

419. Sanderson, M.P., S. Keller, A. Alonso, S. Riedle, P.J. Dempsey, and P. Altevogt, *Generation of novel, secreted epidermal growth factor receptor (EGFR/ErbB1) isoforms via metalloprotease-dependent ectodomain shedding and exosome secretion.* J Cell Biochem, 2008. **103**(6): p. 1783-97. PMC4922250

420. Amorim, M., G. Fernandes, P. Oliveira, D. Martins-de-Souza, E. Dias-Neto, and D. Nunes, *The overexpression of a single oncogene (ERBB2/HER2) alters the proteomic landscape of extracellular vesicles.* Proteomics, 2014. **14**(12): p. 1472-9.

421. Thery, C., L. Zitvogel, and S. Amigorena, *Exosomes: composition, biogenesis and function.* Nat Rev Immunol, 2002. **2**(8): p. 569-79.

422. Sato, N., Y. Hattori, D. Wenlin, T. Yamada, T. Kamata, T. Kakimoto, et al., *Elevated level of plasma basic fibroblast growth factor in multiple myeloma correlates with increased disease activity.* Jpn J Cancer Res, 2002. **93**(4): p. 459-66. PMC5927008

423. Chesi, M., L.A. Brents, S.A. Ely, C. Bais, D.F. Robbiani, E.A. Mesri, et al., *Activated fibroblast growth factor receptor 3 is an oncogene that contributes to tumor progression in multiple myeloma.* Blood, 2001. **97**(3): p. 729-36.

424. Aguayo, A., H. Kantarjian, T. Manshouri, C. Gidel, E. Estey, D. Thomas, et al., *Angiogenesis in acute and chronic leukemias and myelodysplastic syndromes.* Blood, 2000. **96**(6): p. 2240-5.

425. Aguayo, A., H.M. Kantarjian, E.H. Estey, F.J. Giles, S. Verstovsek, T. Manshouri, et al., *Plasma vascular endothelial growth factor levels have prognostic significance in patients with acute myeloid leukemia but not in patients with myelodysplastic syndromes.* Cancer, 2002. **95**(9): p. 1923-30.

426. Bieker, R., T. Padro, J. Kramer, M. Steins, T. Kessler, S. Retzlaff, et al., *Overexpression of basic fibroblast growth factor and autocrine stimulation in acute myeloid leukemia.* Cancer Res, 2003. **63**(21): p. 7241-6.

427. Schindelin, J., I. Arganda-Carreras, E. Frise, V. Kaynig, M. Longair, T. Pietzsch, et al., *Fiji: an open-source platform for biological-image analysis.* Nat Methods, 2012. **9**(7): p. 676-82. PMC3855844

428. Sanjana, N.E., O. Shalem, and F. Zhang, *Improved vectors and genome-wide libraries for CRISPR screening.* Nat Methods, 2014. **11**(8): p. 783-784. PMC4486245

429. Agarwal, A., C.A. Eide, A. Harlow, A.S. Corbin, M.J. Mauro, B.J. Druker, et al., *An activating KRAS mutation in imatinib-resistant chronic myeloid leukemia.* Leukemia, 2008. **22**(12): p. 2269-72.

430. Wang, A. and H. Zhong, *Roles of the bone marrow niche in hematopoiesis, leukemogenesis, and chemotherapy resistance in acute myeloid leukemia.* Hematology, 2018. **23**(10): p. 729-739.

431. Konopleva, M., Y. Tabe, Z. Zeng, and M. Andreeff, *Therapeutic targeting of microenvironmental interactions in leukemia: mechanisms and approaches.* Drug Resist Updat, 2009. **12**(4-5): p. 103-13. PMC3640296

432. Konopleva, M., S. Konoplev, W. Hu, A.Y. Zaritskey, B.V. Afanasiev, and M. Andreeff, *Stromal cells prevent apoptosis of AML cells by up-regulation of anti-apoptotic proteins.* Leukemia, 2002. **16**(9): p. 1713-24.

433. Battula, V.L., P.M. Le, J.C. Sun, K. Nguyen, B. Yuan, X. Zhou, et al., *AML-induced osteogenic differentiation in mesenchymal stromal cells supports leukemia growth.* JCI Insight, 2017. **2**(13). PMC5499365

434. Melgar, K., M.M. Walker, L.M. Jones, L.C. Bolanos, K. Hueneman, M. Wunderlich, et al., *Overcoming adaptive therapy resistance in AML by targeting immune response pathways.* Sci Transl Med, 2019. **11**(508). PMC6985905

435. Dhillon, S., *Gilteritinib: First Global Approval.* Drugs, 2019. **79**(3): p. 331-339.

436. Ye, K., M.H. Schulz, Q. Long, R. Apweiler, and Z. Ning, *Pindel: a pattern growth approach to detect break points of large deletions and medium sized insertions from paired-end short reads.* Bioinformatics, 2009. **25**(21): p. 2865-71. PMC2781750

437. Kolde, R., S. Laur, P. Adler, and J. Vilo, *Robust rank aggregation for gene list integration and meta-analysis.* Bioinformatics, 2012. **28**(4): p. 573-80. PMC3278763

438. Mertins, P., L.C. Tang, K. Krug, D.J. Clark, M.A. Gritsenko, L. Chen, et al., *Reproducible workflow for multiplexed deep-scale proteome and phosphoproteome analysis of tumor tissues by liquid chromatography-mass spectrometry.* Nat Protoc, 2018. **13**(7): p. 1632-1661. PMC6211289

439. Piehowski, P.D., V.A. Petyuk, R.L. Sontag, M.A. Gritsenko, K.K. Weitz, T.L. Fillmore, et al., *Residual tissue repositories as a resource for population-based cancer proteomic studies.* Clin Proteomics, 2018. **15**: p. 26. PMC6074037

440. Casado, P., J.C. Rodriguez-Prados, S.C. Cosulich, S. Guichard, B. Vanhaesebroeck, S. Joel, et al., *Kinase-substrate enrichment analysis provides insights into the heterogeneity of signaling pathway activation in leukemia cells.* Sci Signal, 2013. **6**(268): p. rs6.

441. Wiredja, D.D., M. Koyuturk, and M.R. Chance, *The KSEA App: a web-based tool for kinase activity inference from quantitative phosphoproteomics.* Bioinformatics, 2017. **33**(21): p. 3489-3491. PMC5860163

442. Babur, Ö., A. Luna, A. Korkut, F. Durupinar, M.C. Siper, U. Dogrusoz, et al., *Causal interactions from proteomic profiles: molecular data meets pathway knowledge.* bioRxiv, 2018: p. 258855.

443. Bertran-Alamillo, J., V. Cattan, M. Schoumacher, J. Codony-Servat, A. Gimenez-Capitan, F. Cantero, et al., *AURKB as a target in non-small cell lung cancer with acquired resistance to anti-EGFR therapy.* Nat Commun, 2019. **10**(1): p. 1812. PMC6472415

444. Su, G., A. Kuchinsky, J.H. Morris, D.J. States, and F. Meng, *GLay: community structure analysis of biological networks.* Bioinformatics, 2010. **26**(24): p. 3135-3137.

445. Szklarczyk, D., A.L. Gable, D. Lyon, A. Junge, S. Wyder, J. Huerta-Cepas, et al., *STRING v11: protein–protein association networks with increased coverage, supporting functional discovery in genome-wide experimental datasets.* Nucleic Acids Research, 2018. **47**(D1): p. D607-D613.

446. Shannon, P., A. Markiel, O. Ozier, N.S. Baliga, J.T. Wang, D. Ramage, et al., *Cytoscape: a software environment for integrated models of biomolecular interaction networks.* Genome Res, 2003. **13**(11): p. 2498-504. PMC403769

447. Sharma, S.V. and J. Settleman, *Oncogene addiction: setting the stage for molecularly targeted cancer therapy.* Genes Dev, 2007. **21**(24): p. 3214-31.

448. Lantermann, A.B., D. Chen, K. McCutcheon, G. Hoffman, E. Frias, D. Ruddy, et al., *Inhibition of Casein Kinase 1 Alpha Prevents Acquired Drug Resistance to Erlotinib in EGFR-Mutant Non-Small Cell Lung Cancer.* Cancer Res, 2015. **75**(22): p. 4937-48.

449. Sosa, M.S., P. Bragado, and J.A. Aguirre-Ghiso, *Mechanisms of disseminated cancer cell dormancy: an awakening field.* Nat Rev Cancer, 2014. **14**(9): p. 611-22. PMC4230700

450. Bradeen, H.A., C.A. Eide, T. O'Hare, K.J. Johnson, S.G. Willis, F.Y. Lee, et al., *Comparison of imatinib mesylate, dasatinib (BMS-354825), and nilotinib (AMN107) in an N-ethyl-N-nitrosourea (ENU)-based mutagenesis screen: high efficacy of drug combinations.* Blood, 2006. **108**(7): p. 2332-8. PMC1895563

451. Gregory, M.A., A. D'Alessandro, F. Alvarez-Calderon, J. Kim, T. Nemkov, B. Adane, et al., *ATM/G6PD-driven redox metabolism promotes FLT3 inhibitor resistance in acute myeloid leukemia.* Proc Natl Acad Sci U S A, 2016. **113**(43): p. E6669-E6678. PMC5086999

452. Gregory, M.A., T. Nemkov, J.A. Reisz, V. Zaberezhnyy, K.C. Hansen, A. D'Alessandro, et al., *Glutaminase inhibition improves FLT3 inhibitor therapy for acute myeloid leukemia.* Exp Hematol, 2018. **58**: p. 52-58. PMC5815916

453. Gallipoli, P., G. Giotopoulos, K. Tzelepis, A.S.H. Costa, S. Vohra, P. Medina-Perez, et al., *Glutaminolysis is a metabolic dependency in FLT3(ITD) acute myeloid leukemia unmasked by FLT3 tyrosine kinase inhibition.* Blood, 2018. **131**(15): p. 1639-1653. PMC6061932

454. Ye, H., M. Minhajuddin, A. Krug, S. Pei, C.H. Chou, R. Culp-Hill, et al., *The hepatic microenvironment uniquely protects leukemia cells through induction of growth and survival pathways mediated by LIPG.* Cancer Discov, 2020.

455. Savino, A.M., S.I. Fernandes, O. Olivares, A. Zemlyansky, A. Cousins, E.K. Markert, et al., *Metabolic adaptation of acute lymphoblastic leukemia to the central nervous system microenvironment depends on stearoyl-CoA desaturase.* Nature Cancer, 2020. **1**(10): p. 998-1009.

456. Lagadinou, E.D., A. Sach, K. Callahan, R.M. Rossi, S.J. Neering, M. Minhajuddin, et al., *BCL-2 inhibition targets oxidative phosphorylation and selectively eradicates quiescent human leukemia stem cells.* Cell Stem Cell, 2013. **12**(3): p. 329-41. PMC3595363

457. Jones, C.L., B.M. Stevens, A. D'Alessandro, J.A. Reisz, R. Culp-Hill, T. Nemkov, et al., *Inhibition of Amino Acid Metabolism Selectively Targets Human Leukemia Stem Cells.* Cancer Cell, 2018. **34**(5): p. 724-740 e4. PMC6280965

458. Zhao, B., J.C. Sedlak, R. Srinivas, P. Creixell, J.R. Pritchard, B. Tidor, et al., *Exploiting Temporal Collateral Sensitivity in Tumor Clonal Evolution.* Cell, 2016. **165**(1): p. 234-246. PMC5152932

459. Lin, K.H., J.C. Rutter, A. Xie, B. Pardieu, E.T. Winn, R.D. Bello, et al., *Using antagonistic pleiotropy to design a chemotherapy-induced evolutionary trap to target drug resistance in cancer.* Nat Genet, 2020. **52**(4): p. 408-417. PMC7398704

460. Tricker, E.M., C. Xu, S. Uddin, M. Capelletti, D. Ercan, A. Ogino, et al., *Combined EGFR/MEK Inhibition Prevents the Emergence of Resistance in EGFR-Mutant Lung Cancer.* Cancer Discov, 2015. **5**(9): p. 960-971. PMC4824006

461. Smida, M., F. Fece de la Cruz, C. Kerzendorfer, I.Z. Uras, B. Mair, A. Mazouzi, et al., *MEK inhibitors block growth of lung tumours with mutations in ataxia-telangiectasia mutated.* Nat Commun, 2016. **7**: p. 13701. PMC5150652

462. Morgillo, F., C.M. Della Corte, A. Diana, C.D. Mauro, V. Ciaramella, G. Barra, et al., *Phosphatidylinositol 3-kinase (PI3Kalpha)/AKT axis blockade with taselisib or ipatasertib enhances the efficacy of anti-microtubule drugs in human breast cancer cells.* Oncotarget, 2017. **8**(44): p. 76479-76491. PMC5652721

463. Chen, C.C., B. Li, S.E. Millman, C. Chen, X. Li, J.P.t. Morris, et al., *Vitamin B6 Addiction in Acute Myeloid Leukemia.* Cancer Cell, 2020. **37**(1): p. 71-84 e7. PMC7197326

464. Forte, D., M. Garcia-Fernandez, A. Sanchez-Aguilera, V. Stavropoulou, C. Fielding, D. Martin-Perez, et al., *Bone Marrow Mesenchymal Stem Cells Support Acute Myeloid*

Leukemia Bioenergetics and Enhance Antioxidant Defense and Escape from Chemotherapy. Cell Metab, 2020.

465. Tzelepis, K., H. Koike-Yusa, E. De Braekeleer, Y. Li, E. Metzakopian, O.M. Dovey, et al., *A CRISPR Dropout Screen Identifies Genetic Vulnerabilities and Therapeutic Targets in Acute Myeloid Leukemia.* Cell Rep, 2016. **17**(4): p. 1193-1205. PMC5081405

466. Martin, M., *Cutadapt removes adapter sequences from high-throughput sequencing reads.* 2011, 2011. **17**(1): p. 3.

467. Langmead, B. and S.L. Salzberg, *Fast gapped-read alignment with Bowtie 2.* Nat Methods, 2012. **9**(4): p. 357-9. PMC3322381

468. Li, W., H. Xu, T. Xiao, L. Cong, M.I. Love, F. Zhang, et al., *MAGeCK enables robust identification of essential genes from genome-scale CRISPR/Cas9 knockout screens.* Genome Biol, 2014. **15**(12): p. 554. PMC4290824

469. Nemkov, T., K.C. Hansen, and A. D'Alessandro, *A three-minute method for high-throughput quantitative metabolomics and quantitative tracing experiments of central carbon and nitrogen pathways.* Rapid Commun Mass Spectrom, 2017. **31**(8): p. 663-673. PMC5364945

470. Nemkov, T., J.A. Reisz, S. Gehrke, K.C. Hansen, and A. D'Alessandro, *High-Throughput Metabolomics: Isocratic and Gradient Mass Spectrometry-Based Methods.* Methods Mol Biol, 2019. **1978**: p. 13-26.

471. Reisz, J.A., C. Zheng, A. D'Alessandro, and T. Nemkov, *Untargeted and Semi-targeted Lipid Analysis of Biological Samples Using Mass Spectrometry-Based Metabolomics.* Methods Mol Biol, 2019. **1978**: p. 121-135.

472. Gehrke, S., S. Rice, D. Stefanoni, R.B. Wilkerson, T. Nemkov, J.A. Reisz, et al., *Red Blood Cell Metabolic Responses to Torpor and Arousal in the Hibernator Arctic Ground Squirrel.* J Proteome Res, 2019. **18**(4): p. 1827-1841. PMC7219541

473. Wang, Y., F. Yang, M.A. Gritsenko, Y. Wang, T. Clauss, T. Liu, et al., *Reversed-phase chromatography with multiple fraction concatenation strategy for proteome profiling of human MCF10A cells.* Proteomics, 2011. **11**(10): p. 2019-26. PMC3120047

474. Dou, Y., E.A. Kawaler, D. Cui Zhou, M.A. Gritsenko, C. Huang, L. Blumenberg, et al., *Proteogenomic Characterization of Endometrial Carcinoma.* Cell, 2020. **180**(4): p. 729-748 e26. PMC7233456

475. Gibbons, B.C., M.C. Chambers, M.E. Monroe, D.L. Tabb, and S.H. Payne, *Correcting systematic bias and instrument measurement drift with mzRefinery.* Bioinformatics, 2015. **31**(23): p. 3838-40. PMC4653383

476. Kim, S. and P.A. Pevzner, *MS-GF+ makes progress towards a universal database search tool for proteomics.* Nat Commun, 2014. **5**: p. 5277. PMC5036525

477. Kim, S., N. Gupta, and P.A. Pevzner, *Spectral probabilities and generating functions of tandem mass spectra: a strike against decoy databases.* J Proteome Res, 2008. **7**(8): p. 3354-63. PMC2689316

478. Monroe, M.E., J.L. Shaw, D.S. Daly, J.N. Adkins, and R.D. Smith, *MASIC: a software program for fast quantitation and flexible visualization of chromatographic profiles from detected LC-MS(/MS) features.* Comput Biol Chem, 2008. **32**(3): p. 215-7. PMC2487672

479. Beausoleil, S.A., J. Villen, S.A. Gerber, J. Rush, and S.P. Gygi, *A probability-based approach for high-throughput protein phosphorylation analysis and site localization.* Nat Biotechnol, 2006. **24**(10): p. 1285-92.

480. Gentleman, R.C., V.J. Carey, D.M. Bates, B. Bolstad, M. Dettling, S. Dudoit, et al., *Bioconductor: open software development for computational biology and bioinformatics.* Genome Biol, 2004. **5**(10): p. R80. PMC545600

481. Babur, O., U. Dogrusoz, E. Demir, and C. Sander, *ChiBE: interactive visualization and manipulation of BioPAX pathway models.* Bioinformatics, 2010. **26**(3): p. 429-31. PMC2815657

482. Babur, O., U. Dogrusoz, M. Cakir, B.A. Aksoy, N. Schultz, C. Sander, et al., *Integrating biological pathways and genomic profiles with ChiBE 2.* BMC Genomics, 2014. **15**: p. 642. PMC4131037

483. Lange, V., P. Picotti, B. Domon, and R. Aebersold, *Selected reaction monitoring for quantitative proteomics: a tutorial.* Mol Syst Biol, 2008. **4**: p. 222. PMC2583086

484. MacLean, B., D.M. Tomazela, N. Shulman, M. Chambers, G.L. Finney, B. Frewen, et al., *Skyline: an open source document editor for creating and analyzing targeted proteomics experiments.* Bioinformatics, 2010. **26**(7): p. 966-8. PMC2844992

485. Tyanova, S., T. Temu, P. Sinitcyn, A. Carlson, M.Y. Hein, T. Geiger, et al., *The Perseus computational platform for comprehensive analysis of (prote)omics data.* Nat Methods, 2016. **13**(9): p. 731-40.

486. Pabst, C., J. Krosl, I. Fares, G. Boucher, R. Ruel, A. Marinier, et al., *Identification of small molecules that support human leukemia stem cell activity ex vivo.* Nat Methods, 2014. **11**(4): p. 436-42.

487. Joshi, S.K., K. Qian, W.H. Bisson, K. Watanabe-Smith, A. Huang, D. Bottomly, et al., *Discovery and characterization of targetable NTRK point mutations in hematologic neoplasms.* Blood, 2020. **135**(24): p. 2159-2170. PMC7290093

488. Joshi, S.K., J.M. Keck, C.A. Eide, D. Bottomly, E. Traer, J.W. Tyner, et al., *ERBB2/HER2 mutations are transforming and therapeutically targetable in leukemia.* Leukemia, 2020. **34**(10): p. 2798-2804. PMC7515826

489. Senior, A.W., R. Evans, J. Jumper, J. Kirkpatrick, L. Sifre, T. Green, et al., *Improved protein structure prediction using potentials from deep learning.* Nature, 2020. **577**(7792): p. 706-710.

490. van Gastel, N., J.B. Spinelli, A. Sharda, A. Schajnovitz, N. Baryawno, C. Rhee, et al., *Induction of a Timed Metabolic Collapse to Overcome Cancer Chemoresistance.* Cell Metab, 2020. **32**(3): p. 391-403 e6.

491. Tikhonova, A.N., I. Dolgalev, H. Hu, K.K. Sivaraj, E. Hoxha, A. Cuesta-Dominguez, et al., *The bone marrow microenvironment at single-cell resolution.* Nature, 2019. **569**(7755): p. 222-228. PMC6607432

492. Severe, N., N.M. Karabacak, K. Gustafsson, N. Baryawno, G. Courties, Y. Kfoury, et al., *Stress-Induced Changes in Bone Marrow Stromal Cell Populations Revealed through Single-Cell Protein Expression Mapping.* Cell Stem Cell, 2019. **25**(4): p. 570-583 e7. PMC6778015

493. Aran, D., Z. Hu, and A.J. Butte, *xCell: digitally portraying the tissue cellular heterogeneity landscape.* Genome Biol, 2017. **18**(1): p. 220. PMC5688663

494. Armingol, E., A. Officer, O. Harismendy, and N.E. Lewis, *Deciphering cell-cell interactions and communication from gene expression.* Nat Rev Genet, 2020. PMC7649713

495. Peters, G.J., C.L. van der Wilt, C.J. van Moorsel, J.R. Kroep, A.M. Bergman, and S.P. Ackland, *Basis for effective combination cancer chemotherapy with antimetabolites.* Pharmacol Ther, 2000. **87**(2-3): p. 227-53.

496. Samudio, I., M. Fiegl, T. McQueen, K. Clise-Dwyer, and M. Andreeff, *The warburg effect in leukemia-stroma cocultures is mediated by mitochondrial uncoupling associated with uncoupling protein 2 activation.* Cancer Res, 2008. **68**(13): p. 5198-205. PMC2562568

497. Chen, W.L., J.H. Wang, A.H. Zhao, X. Xu, Y.H. Wang, T.L. Chen, et al., *A distinct glucose metabolism signature of acute myeloid leukemia with prognostic value.* Blood, 2014. **124**(10): p. 1645-54. PMC5726328

498. Wang, Y.H., W.J. Israelsen, D. Lee, V.W.C. Yu, N.T. Jeanson, C.B. Clish, et al., *Cell-state-specific metabolic dependency in hematopoiesis and leukemogenesis.* Cell, 2014. **158**(6): p. 1309-1323. PMC4197056

499. Warburg, O., F. Wind, and E. Negelein, *The Metabolism of Tumors in the Body.* J Gen Physiol, 1927. **8**(6): p. 519-30. PMC2140820

500. Warburg, O., *On the origin of cancer cells.* Science, 1956. **123**(3191): p. 309-14.

501. Pei, S., M. Minhajuddin, K.P. Callahan, M. Balys, J.M. Ashton, S.J. Neering, et al., *Targeting aberrant glutathione metabolism to eradicate human acute myelogenous leukemia cells.* J Biol Chem, 2013. **288**(47): p. 33542-58. PMC3837103

502. Samudio, I., R. Harmancey, M. Fiegl, H. Kantarjian, M. Konopleva, B. Korchin, et al., *Pharmacologic inhibition of fatty acid oxidation sensitizes human leukemia cells to apoptosis induction.* J Clin Invest, 2010. **120**(1): p. 142-56. PMC2799198

503. Willems, L., N. Jacque, A. Jacquel, N. Neveux, T.T. Maciel, M. Lambert, et al., *Inhibiting glutamine uptake represents an attractive new strategy for treating acute myeloid leukemia.* Blood, 2013. **122**(20): p. 3521-32. PMC3829119

504. Chan, S.M., D. Thomas, M.R. Corces-Zimmerman, S. Xavy, S. Rastogi, W.J. Hong, et al., *Isocitrate dehydrogenase 1 and 2 mutations induce BCL-2 dependence in acute myeloid leukemia.* Nat Med, 2015. **21**(2): p. 178-84. PMC4406275

505. Mussai, F., S. Egan, J. Higginbotham-Jones, T. Perry, A. Beggs, E. Odintsova, et al., *Arginine dependence of acute myeloid leukemia blast proliferation: a novel therapeutic target.* Blood, 2015. **125**(15): p. 2386-96. PMC4416943

506. Jacque, N., A.M. Ronchetti, C. Larrue, G. Meunier, R. Birsen, L. Willems, et al., *Targeting glutaminolysis has antileukemic activity in acute myeloid leukemia and synergizes with BCL-2 inhibition.* Blood, 2015. **126**(11): p. 1346-56. PMC4608389

507. Ni, F., W.M. Yu, Z. Li, D.K. Graham, L. Jin, S. Kang, et al., *Critical role of ASCT2-mediated amino acid metabolism in promoting leukaemia development and progression.* Nat Metab, 2019. **1**(3): p. 390-403. PMC6750232

508. Sykes, D.B., Y.S. Kfoury, F.E. Mercier, M.J. Wawer, J.M. Law, M.K. Haynes, et al., *Inhibition of Dihydroorotate Dehydrogenase Overcomes Differentiation Blockade in Acute Myeloid Leukemia.* Cell, 2016. **167**(1): p. 171-186 e15. PMC7360335

509. Ricciardi, M.R., S. Mirabilii, M. Allegretti, R. Licchetta, A. Calarco, M.R. Torrisi, et al., *Targeting the leukemia cell metabolism by the CPT1a inhibition: functional preclinical effects in leukemias.* Blood, 2015. **126**(16): p. 1925-9.

510. Ye, H., B. Adane, N. Khan, T. Sullivan, M. Minhajuddin, M. Gasparetto, et al., *Leukemic Stem Cells Evade Chemotherapy by Metabolic Adaptation to an Adipose Tissue Niche.* Cell Stem Cell, 2016. **19**(1): p. 23-37. PMC4938766

511. German, N.J., H. Yoon, R.Z. Yusuf, J.P. Murphy, L.W. Finley, G. Laurent, et al., *PHD3 Loss in Cancer Enables Metabolic Reliance on Fatty Acid Oxidation via Deactivation of ACC2.* Mol Cell, 2016. **63**(6): p. 1006-20. PMC5040345

512. Shi, J., H. Fu, Z. Jia, K. He, L. Fu, and W. Wang, *High Expression of CPT1A Predicts Adverse Outcomes: A Potential Therapeutic Target for Acute Myeloid Leukemia.* EBioMedicine, 2016. **14**: p. 55-64. PMC5161445

513. Shafat, M.S., T. Oellerich, S. Mohr, S.D. Robinson, D.R. Edwards, C.R. Marlein, et al., *Leukemic blasts program bone marrow adipocytes to generate a protumoral microenvironment.* Blood, 2017. **129**(10): p. 1320-1332.

514. Tabe, Y., S. Yamamoto, K. Saitoh, K. Sekihara, N. Monma, K. Ikeo, et al., *Bone Marrow Adipocytes Facilitate Fatty Acid Oxidation Activating AMPK and a Transcriptional Network Supporting Survival of Acute Monocytic Leukemia Cells.* Cancer Res, 2017. **77**(6): p. 1453-1464. PMC5354955

515. Farge, T., E. Saland, F. de Toni, N. Aroua, M. Hosseini, R. Perry, et al., *Chemotherapy-Resistant Human Acute Myeloid Leukemia Cells Are Not Enriched for Leukemic Stem Cells but Require Oxidative Metabolism.* Cancer Discov, 2017. **7**(7): p. 716-735. PMC5501738

516. Bray, N.L., H. Pimentel, P. Melsted, and L. Pachter, *Near-optimal probabilistic RNA-seq quantification.* Nat Biotechnol, 2016. **34**(5): p. 525-7.

517. Soneson, C., M.I. Love, and M.D. Robinson, *Differential analyses for RNA-seq: transcript-level estimates improve gene-level inferences.* F1000Res, 2015. **4**: p. 1521. PMC4712774

518. Law, C.W., Y. Chen, W. Shi, and G.K. Smyth, *voom: Precision weights unlock linear model analysis tools for RNA-seq read counts.* Genome Biol, 2014. **15**(2): p. R29. PMC4053721

519. Liao, Y., J. Wang, E.J. Jaehnig, Z. Shi, and B. Zhang, *WebGestalt 2019: gene set analysis toolkit with revamped UIs and APIs.* Nucleic Acids Res, 2019. **47**(W1): p. W199-W205. PMC6602449

520. Aoki-Kinoshita, K.F. and M. Kanehisa, *Gene annotation and pathway mapping in KEGG.* Methods Mol Biol, 2007. **396**: p. 71-91.